

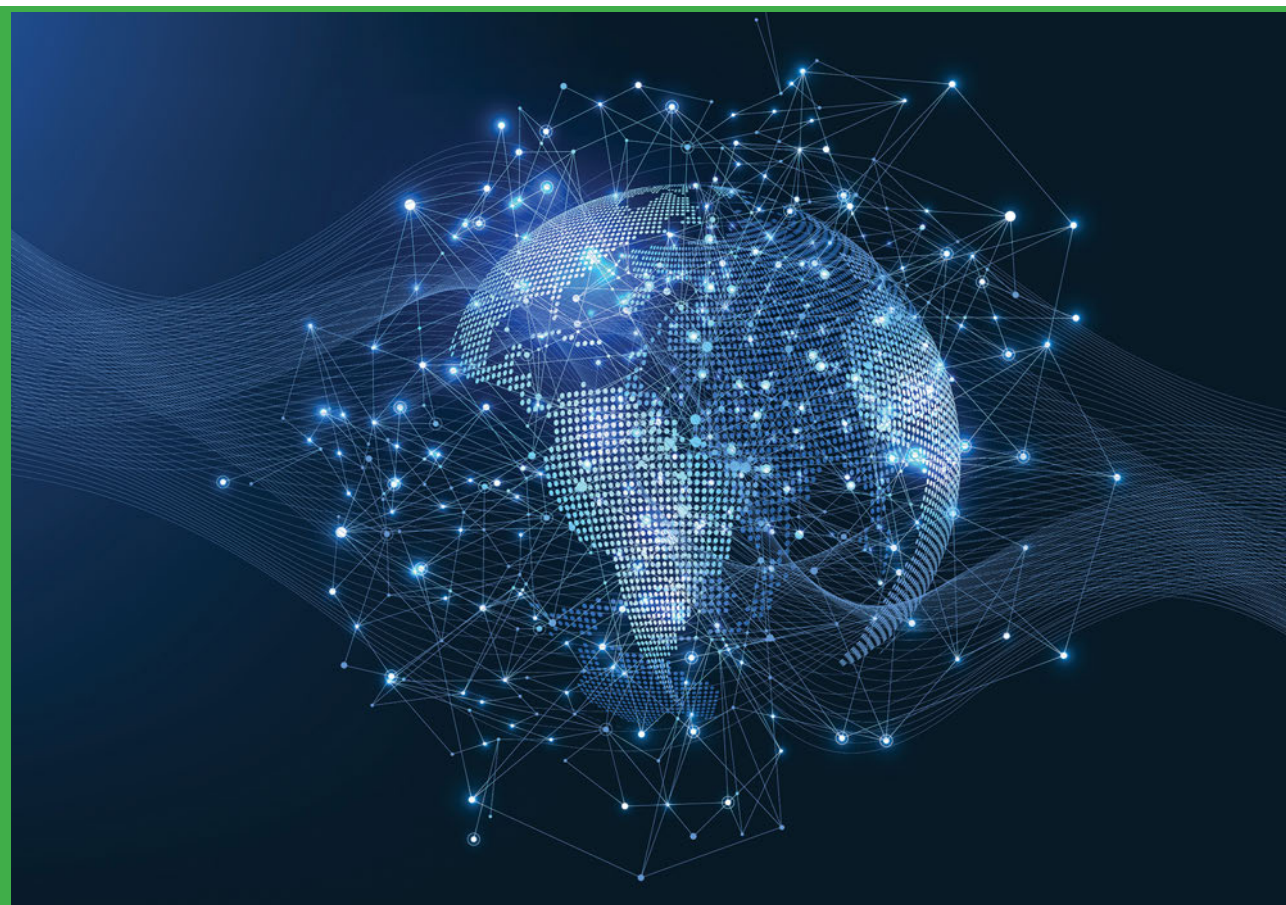


RIGA TECHNICAL
UNIVERSITY

Toms Salgals

**DEVELOPMENT AND ASSESSMENT
OF A SPECTRALLY EFFICIENT HYBRID
OPTICAL COMMUNICATION SYSTEMS**

Doctoral Thesis



RTU Press
Riga 2022

RIGA TECHNICAL UNIVERSITY

Faculty of Electronics and Telecommunications
Institute of Telecommunications

Toms Salgals

Doctoral Student of the Study Programme “Telecommunications”

**DEVELOPMENT AND ASSESSMENT OF SPECTRALLY
EFFICIENT HYBRID OPTICAL COMMUNICATION SYSTEMS**

Doctoral Thesis

Scientific supervisors:

Professor Dr. sc. ing. SANDIS SPOLĪTIS

Associate Professor Dr. sc. ing. OSKARS OZOLIŅŠ

Riga 2022

Salgals, T. Development and assessment of a spectrally efficient hybrid optical communication systems. Doctoral Thesis. Riga: RTU Press, 2022. 246 pp.

Published in accordance with the decision of the Promotion Council
“P- 08” of 03. May 2022,
Minutes No. 12.

This work has been supported by the European Social Fund within Project No. 8.2.2.0/20/I/008 «Strengthening of PhD students and academic personnel of Riga Technical University and BA School of Business and Finance in the strategic fields of specialization» of the Specific Objective 8.2.2 «To Strengthen Academic Staff of Higher Education Institutions in Strategic Specialization Areas» of the Operational Programme «Growth and Employment».

The research was supported by Doctoral Grant programme of Riga Technical University.

**NATIONAL
DEVELOPMENT
PLAN 2020**



EUROPEAN UNION
European Social
Fund

I N V E S T I N G I N Y O U R F U T U R E

DOCTORAL THESIS PROPOSED TO RIGA TECHNICAL UNIVERSITY FOR THE PROMOTION TO THE SCIENTIFIC DEGREE OF DOCTOR OF SCIENCE

To be granted the scientific degree of Doctor of Science (Ph. D.), the present Doctoral Thesis has been submitted for the defense at the open meeting of RTU Promotion Council on 9 September 2022 at the Faculty of Electronics and Telecommunications of Riga Technical University (RTU), 12 Azenes Str., Room 201.

OFFICIAL REVIEWERS

Dr. sc. ing. *Jaime Rodrigo Navarro*
Casa Systems, Inc., Spain

Leading Researcher *Dr. sc. ing. Giuseppe Rizzelli*
Politecnico di Torino, Italy

Professor *Dr. sc. ing. Dmitrijs Pikuļins*
Riga Technical University

DECLARATION OF ACADEMIC INTEGRITY

I hereby declare that the Doctoral Thesis submitted for the review to Riga Technical University for the promotion to the scientific degree of Doctor of Science (Ph. D.) is my own. I confirm that this Doctoral Thesis had not been submitted to any other university for the promotion to a scientific degree.

The Doctoral Thesis has been prepared as thematically united collection of scientific publications. It comprises 13 scientific articles and publications in conference proceedings proceeding from the 30 author's existing works indexed in SCOPUS, WoS, and IEEE databases. Publications are written in English and are published in SCOPUS, WoS, IEEE databases, their total volume/number of pages is 246 pages.

ACKNOWLEDGMENTS

I would like to express my gratitude to everyone who contributed to the Thesis and were directly involved as colleagues, supervisors or co-authors, to my family, and those who provided assistance and support in possible and impossible novel ideas.

Specifically, I thank my supervisors Professor Sandis Spolītis for knowledge and skills, scientific support and each-day supervising which always resulted in many hours in the lab, Associate Professor Oskars Ozoliņš for opening doors and showing new opportunities, and Director of the Institute of Telecommunications (IT) of the Faculty of Electronics and Telecommunications (FET) Professor Vjačelsavs Bobrovs for his trust, belief, support, and guidance throughout these years.

I thank to all my colleagues and co-authors across the globe; it was and is an honor and pleasure to work with you, especially those whom have become friends, who will always support and in spite of everything will be ready to move forward to reach new incomprehensible mountain peaks even higher than Everest.

Finally, the biggest thank you goes to my family and friends for the day-to-day support and faith in my strength.

Thank you! Paldies!

Toms Salgals

LIST OF ABBREVIATIONS

**Skaitliskie sākuma sāsinājumi / Numerical initial abbreviations*

3G – *Third Generation* – trešās paaudzes mobilie sakari

4G – *Fourth Generation* – ceturtais paaudzes mobilie sakari

5G – *Fifth Generation* – piektās paaudzes mobilie sakari

A

AEQ – *Adaptive equalization* – adaptīvā ekvalizācija

AON – *Active optical network* – aktīvs optiskais tīkls

APD – *Avalanche Photodiode* – lavīnfotodiode

ARoF – *Analog Radio-over-Fiber* – analogais radio caur šķiedru

ASE – *Amplified Spontaneous Emission* – pastiprināta spontāna emisija

ASI – *Institute of Astronomy and Spectroscopy* – Atomfizikas un spektroskopijas institūts

AWG – *Arrayed Waveguide Grating* – sakārtots viļņvadu režģis (viļņvadu masīva režģis)

B

B2B – *Back-to-back* – tiešā savienojumā

BBU – *Base-band unit* – mobilo sakaru raidītāju bloks

BER – *Bit-Error-Rate* – bitu kļūdu attiecība

BPF – *Bandpass Filter* – Joslas Filtrs

BS – *Base Station* – bāzes stacija

BW – *Bandwidth* – josla

C

CAM – *Microscope camera* – mikroskopa kamera

C-Band – *Conventional Band* – tradicionālais diapazons (josla)

CD – *Chromatic Dispersion* – hromatiskā dispersija

CEPT – *Committee of the European Conference of Postal and Telecommunications Administrations* – Eiropas telekomunikāciju pārvalžu konferences komiteja

CO – *Central Office* – centrālais offīss

CPRI – *Common Public Radio Interface* – kopēja publiskā radio saskarne

C-RAN – *Cloud/Centralized Radio Access Networks* – Centralizēti radio piekļuves tīkli

CRU – *Clock recovery unit* – Takts signāla atjaunošanas bloks

CW – *Continuous Wave (Laser)* – nepārtrauktā viļņa starojuma (lāzera avots)

D

DAC – *Digital-to-analog converter* – digitāla uz analogu signālu pārveidotājs

DB – *Duobinary* – duobinārais

DC – *Direct current* – līdzstrāva

*DC – *Data centers* – Datu centri

DCF – *Dispersion Compensating Fiber* – Dispersiju kompensējoša šķiedra

DCM – *Dispersion Compensating Module* – disperijas kompensācijas modulis

DCI – *Data Center Interconnection* - Datu centra savstarpēja savienošana

De-MUX – *De-multiplexer* – demultipleksors (atblīvētājs pēc viņa garuma)

DFE – *Linear decision-feedback equalizer* - lineārs signāla uz priekšu vērtais atsauksmes elements

DMD – *Differential Mode Delay* – diferenciālā modu aizture

DSA – *Digital signal analyzer* – Digitālais signālu analizators

DSO – *Digital Storage Oscilloscope* – ciparu signālu osciloskops

DSP – *Digital Signal Processing* – ciparu signālu apstrāde

DTU – *Denmark Technical University* – Dānijas Tehniskā universitāte

DWDM – *Dense Wavelength Division Multiplexing* – augsta blīvuma optiskās sistēmas

E

EA- *Electrical Broadband amplifier* – elektriskais platjoslas pastiprinātājs

EAWG – *Electrical Arbitrary Waveform Generator* – elektrisks patvaļīgas formas signālu ģenerators

ED – *Envelope detector* – signāla apliecējas uztvērēja diodes modulis

EDB – *Electrical Duobinary* – elektriskais duobinārais

EDFA – *Erbium-Doped Fiber Amplifier* – ar erbija legētas šķiedras pastiprinātājs

EPON – *Ethernet Passive Optical Network* – Ethernet Pasīvais Optiskais Tīkls

F

FBG – *Fiber Bragg Grating* – šķiedras Brega režģis

FB – *feedback* – lēmumu atgriezeniskās saite

FBT – *Feed-back tap* - lēmumu atgriezeniskās saites elements

FEC – *Forward Error Correction* – turpvērstā kļūdu labošana

FF-feed-forward - signāla uz priekšu vērstā atsauksmes saite

*FFT – *Fast-Fourier-Transform* – ātrā-Furjē-transformācija

FFT – *Feed-forward taps* – signāla uz priekšu vērtais atsauksmes elements

FOTS – *Fiber optical Transmission systems* – Šķiedru optiskās pārraides sistēmas

FPGA – *Field-programmable gate array* – Programmējamais loģiskais masīvs

FTTA – *fiber-to-the-antenna* – šķiedra līdz antenai

FTTx – *Fiber to the x* – šķiedra līdz (punktam) x

FTTH – *Fiber to the Home* – šķiedra līdz mājai

FSPL – *Free-Space-Loss* – pārraides pamatzudumi brīvā telpā

FSR – *Free spectral range* – Brīvais spektra diapazons

FWHM – *Full width at half maximum* – Pilns platumums līdz pusei maksimālā

FWM – *Four wave Mixing* – četru viļņu mijiedarbe

H

HD-FEC – *Hard-Decision Forward error-correction code* - Spēcīga lēmuma turpvērstās kļūdas labošanas kods

HPC – *High-performance computing* - Augstas veiktspējas skaitļošana

HS-PON – *High-speed Passive Optical Network* – Ātrgaitas pasīvais optiskais tīkls

I

IEEE – *Institute of Electrical and Electronics Engineers* – Elektrotehnikas un elektronikas inženieru institūts

IF – *Intermediate Frequency* – starpfrekvence

IL – *Insertion Loss* – Ienestie Zudumi
IM – *Intensity Modulation* – intensitātes modulācija
IM-DD – *Intensity Modulation Direct Detection* – intensitātes modulācija ar tiešo uztveršanu
IoT – *Internet of Things* – lietu internets
IP – *Internet Protocol* – interneta protokols
IPF-RAN – *Institute of Applied Physics of the Federal Research Center of the Russian Academy of Sciences* – Krievijas Zinātņu akadēmijas Federālā pētniecības centra Lietišķās fizikas institūts
ISI – *Intersymbol interference* – starpsimbolu interference
ITU – *International Telecommunication Union* – Starptautiskā Telekomunikāciju apvienība
ITU-T – *International Telecommunication Unit* – Telecommunication Standardization Sector - starptautiskā Telekomunikāciju Savienība - Telekomunikācijas Standartu Sektors

K

KOH – *Potassium hydroxide* – Kālija hidroksīds
KTH – *Royal Swedish Technical University* – Zveidrijas Karaliskā Tehniskā universitāte
KPI – *Key performance indicators* – Galvenie veiktspējas rādītāji

L

LCoS – *Liquid crystal on silicon* – Šķidrie kristāli uz silikona
LD – *Light source* – gaismas avots
LNA – *Low Noise broadband Amplifier* – Zema trokšņa līmeņa platjoslas pastiprinātājs
LO – *Local Oscillator* – šaurjoslas nepārtraukta optiskā starojuma lokālā oscilatora lāzera avots
LPF – *Low-pass filter* – zemfrekvenču elektriskais filtrs
LSBs – *Least significant bits* – vismazāk nozīmīgie biti
LTE – *Long Term Evolution* – starptautisko mobilo telekomunikāciju sistēma LTE
LU – *University of Latvia* – Latvijas universitāte

M

MCF – *Multi Core Fiber* – daudzkodolu optiskā šķiedra
MIMO – *Multiple-input-multiple-output* – vairāk ieejas un vairāk izejas
MSBs – *Most significant bits* – nozīmīgāko bitu secība
MUX – *Multiplexer* – multipleksors (blīvētājs)
MZM – *Mach-Zehnder Modulator* – Maha-Zendera modulators

N

NF – *Noise Factor* – ienesto trokšņu rādītājs
NG – *Next-generation* – nākamā paaudze
NG-PON – *Next Generation Passive Optical Network* – Nākamās paaudzes pasīvais optiskais tīkls
NG-PON2 – *40-Gigabit-capable Passive Optical Network* – 40 Gigabitu pasīvais optiskais tīkls
NOE – *Nonlinear Optical Effects* – nelineārie optiskie efekti
NRZ – *Non Return to-Zero* – bez atgriešanās pie nulles līnijas kods
NRZ-OOK – *Non-Return-to-Zero On-Off Keying* – intensitātes manipulācija ar kodēšanu bez atgriešanās pie nulles
NZ-DSF – *Non-zero dispersion-shifted fiber* – Šķiedra ar nobīdīto nulles dispersiju

O

OB – *Optical budget* – optiskās jaudas budžets
OBPF – *Optical Band Pass Filter* – optiskais joslas filtrs
ODN – *Optical Distribution Network* – optiskās sadales tīkls
O/E/O – *Optical-to-Electrical-to-Optical* – opto-elektriskā-optiskā (pārveide)
OFC – *Optical frequency comb* – Optiskās frekvences ķemme
OLT – *Optical line terminal* – optiskās līnijas terminālis (gala iekārta)
ONT – *Optical Network terminal* – optiskā tīkla terminālis/galiekārta
ONU – *Optical Network Unit* – optiskā tīkla iekārta
OOK – “*On-Off*” *Keying* – “ieslēgt-izslēgt” manipulācija (signāla intensitātes modulācijas formāts)
OPB – *Optical Power Budget* – optiskais jaudas budžets
OSA – *Optical Spectrum Analyzer* – optiskais spektra analizators
OSNR – *Optical Signal-to-Noise Ratio* – optiskā signāls-troksnis attiecība
OTDR – *Optical Time Domain Reflectometer* – optiskā laika apgabala reflektometrs

P

P2P – *Point-to-Point* – punkts-punkts topoloģija
PAM – *Pulse-Amplitude Modulation* – impulsa amplitūdas modulācija
PAM-M – *Multi-level Pulse amplitude modulation* – daudzlīmeņu impulsa amplitūdas modulācija
PC – *Polarization Controller* – polarizācijas kontrolieris
PD – *Photo-detector* – fotodetektors
PDFA – *Praeseodymium-Doped Fiber Amplifier* - ar prazeodīmu leģētu šķiedru pastiprinātājs
PIN – *Photodiode* – Positive-Intrinsic-Negative (photodiode) – PIN fotodiode
PM – *Power meter* – jaudas mērītājs
PON – *Passive Optical Network* – Pasīvais optiskais tīkls
PRBS – *Pseudorandom Binary Sequence* – pseido-gadījuma bitu secība
PSU – *Power supply units* – Barošanas bloki

Q

QAM – *Quadrature Amplitude Modulation* - amplitūdas kvadrātūmodelēšana
QoT – *Quality of transmission* – Pārraidis kvalitāte
QPSK – *Quadrature Phase-Shift Keying* – kvadrātūras fāzes manipulācija

R

RAN – *Radio Access Network* – radio piekļuves tīkls
RF – *Radio Frequency* – radio frekvence
RoF – *Radio-over-Fiber* – radio caur šķiedru
ROP – *Received optical power* – Uztvertās optiskās jaudas līmenis
RRU – *Remote radio unit* - tālvadības radio vienība
RT – *Remote Terminal* – attālinātais terminālis
Rx – *Receiver* – uztvērējs
RU – *Radio unit* – bāzes stacijas uztvērēja bloks
RZ – *Return-to-Zero* – ar atgriešanos pie nulles līnijas kods

S

SC-SMF – *Single-core single-mode optical fiber* – viena kodola vienmodas optiskā šķiedra
SAD – *Symmetrical Adaptive Decorrelation* – simetriski adaptīvā bitu aiztures tehnika
SDM – *Spatial-division multiplexing* – telpdales (telpiskā) blīvēšana
SMCF – *Single mode Multicore fiber* – vienmodas daudzkodolu optiskā šķiedra
SNR – *Signal to Noise Ratio* – signāls-troksnis attiecība
SOA – *Semiconductor optical amplifier* – pusvadītāju optiskais pastiprinātājs
SMF – *Single Mode Fiber* – vienmodas optiskā šķiedra
SSMF – *Standart Single Mode Fiber* – standarta vienmodas optiskā šķiedra

T

TI – Institute of Telecommunications – Telekomunikāciju institūts
TWDM-PON – *Time Wavelength Division Multiplexed PON* – laukdales-viļņgarumdales blīvēts pasīvais optiskais tīkls
Tx – *Transmitter* – raidītājs

V

VDC – *Volts of direct current* – līdzstrāvas spriegums
VoD – *Video on Demand* – Video pēc Pieprasījuma

W

WDM – *Wavelength Division Multiplexing* – viļņgarumdales blīvēšana
WDM-PON – *Wavelength Division Multiplexed Passive Optical Network* – viļņgarumdales blīvēts pasīvais optiskais tīkls
WGM – *whispering gallery mode* – čukstošās galerijas režīms
WGMR – *Whispering Gallery Mode Resonator* – Čukstošās galerijas modu rezonators
WSS – *Wavelength Selective Switch* – pēc viļņa garuma selektīvs optiskais slēdzis
WS-WDM-PON – *wavelength-selected WDM-PON* – viļņa garuma selektīvais WDM-PON
WR-WDM-PON – *wavelength-routed WDM-PON* – viļņa garuma maršrutēts WDM-PON

V

VOA – *Variable optical attenuator* – pārskrūvojams optiskais vājinātājs
VR – *Virtual and augmented reality* – virtuālā un paplašinātā realitāte

X

XG-PON (10G-PON) – *10 Gigabit Passive Optical Network* – 10 Gigabitu pasīvais optiskais tīkls

Z

ZDW – *Zero Dispersion Wavelength* – nulles dispersijas viļņa garums

CONTENTS

1	GENERAL OVERVIEW OF THE THESIS	12
1.1	Introduction	12
1.2	The aim and theses of the dissertation	13
1.3	The main key tasks of the Doctoral Thesis	14
1.4	Research Methods	15
1.5	Scientific novelty and main results	15
1.6	Structure of the thesis.....	18
1.7	Publications and approbation of the Thesis	18
2	MAIN RESULTS OF THE DOCTORAL THESIS	25
2.1	Assessment and evolution of WDM fiber optical communication system directions.	26
3	APPLICATION AND EVALUATION OF THE SPECTRALLY EFFICIENT MODULATION FORMATS SUSTAINABLE TO INCREASE THE PERFORMANCE OF WDM-PON TRANSMISSION SYSTEMS.....	28
3.1	Application of NRZ, PAM-4 and EDB modulation formats for PON networks	28
3.2	Evaluation of PAM-4 coding format application in 10G WDM-PON transmission systems	30
3.3	Evaluation of 4-PAM, EDB and NRZ modulation formats performance in WDM-PON optical access transmission system with a data transmission speed of 20 Gbit/s per wavelength	33
3.4	Evaluation of spectrally efficient transmission of IM/DD 10G PON with data rates up to 56 Gbit/s per wavelength using alternative multilevel modulation formats	36
4	IMPACT ASSESSMENT OF THE USED OPTICAL TRANSMISSION ENVIRONMENT FOR THE RECEIVED SIGNAL QUALITY TO DEVELOP A HIGH-SPEED SPECTRALLY EFFICIENT WDM-PON BROADBAND TRANSMISSION SYSTEM	44
4.1	Realization of WDM-PON fiber optic transmission system for performance evaluation depending on the data transmission rate up to 32 Gbit / s per channel and the total optical line length.....	44
4.2	Comparison of the performance of an experimental 40 km long DWDM-PON 4-channel transmission system with a total transmission rate of up to 160 Gbit / s depending on the applied DCF and FBG dispersion compensation methods and data transmission speed in the channel	50
4.3	The combined solution of space-division multiplexed (SDM) and wavelength division multiplexed (WDM) technologies to implement a spectrally efficient high-speed fiber optic transmission system	57
5	DEVELOPMENT AND EVALUATION OF SPECTRALLY EFFICIENT NEXT-GENERATION MOBILE OPTICAL SYSTEMS FOR MILLIMETER-WAVE RADIO SIGNAL TRANSMISSION	62

5.1 Research and analysis of the application of Radio over Fiber (ROF) in the solution of future mobile communication systems.....	62
5.2 Performance evaluation in a simulated environment of NRZ-OOK modulated ARoF-WDM PON transmission system with 2.5 Gbit/s data rate per channel depending on the used upconversion of optical signals.....	64
5.3 Evaluation of spectrally efficient AR oF-WDM PON transmission system in a simulation environment using PAM-4 modulation format providing data transmission speed up to 5 Gbit/s in the channel.	69
5.4 Evaluation of 2.5 Gbit/s NRZ modulated signal transmission in RoF real-time transmission system where signal upconversion is realized by two separately connected CW laser sources.....	75
5.5 Evaluation of 2.5 Gbaud/s NRZ and PAM-4 modulated signal transmission in RoF real-time transmission system where signal upconversion is realized by one CW laser sources	79
5.6 Development of hybrid ARoF-WDM-PON communication system with data transmission speeds of 10 Gbit/s per channel for broadband internet service and up to 2.5 Gbit/s per channel for 28 GHz (ka-band) millimeter wave signal transmission.	85
6 IMPLEMENTATION OF SPECTRALLY EFFICIENT WDM TRANSMISSION SYSTEM WITH SILICA MICROSPHERE (SiO₂) WGMR-BASED KERR-OFC LIGHT SOURCE. ..	91
6.1 Whispering Gallery Mode (WGM) based optical frequency comb sources (OFC) and its application in telecommunications.....	91
6.2 Experimentally designed setup and characteristics of silica microsphere WGMR-based Kerr-OFC light source for application in optical communications.....	92
6.2.1 Characteristics of silica microsphere WGMR-based Kerr-OFC light source.	92
6.2.2 Experimentally designed setup and characteristics of silica microsphere WGMR-based Kerr-OFC light source	
	96
6.3 Evaluation of received signal quality for WDM-PON communication system with data transmission speed in the channel up to 10 Gbit/s per λ using OFC as a light source.....	100
6.4 Evaluation of received signal quality for DCI communication system with data transmission speed in the channel up to 50 Gbit/s per λ using OFC as a light source.....	105
CONCLUSIONS.....	110
BIBLIOGRAPHY.....	113
SUPPLEMENTS.....	129

1 GENERAL OVERVIEW OF THE THESIS

1.1 Introduction

The rapid growth of Internet traffic requires the improvement of telecommunications network infrastructure by increasing data transmission speed [1]. Passive optical access networks (PONs) are one of the most popular low-cost optical networks. Standardized PON network solutions already have a number of improvements related to data transfer speeds for end-users. In order to obtain spectrally efficient data transmission, the infrastructure of PON networks is provided using a wavelength division multiplexing (WDM) technology [2].

The demand for large-scale data transmission is growing exponentially due to the implementation of new technologies (e.g. Internet of Things (IoT), 4K / 8K television, virtual and augmented reality (VR), etc.). For the enormously growing number of end-users who requires more bandwidth, the solution is spatial division multiplexing (SDM) technology for new fiber optical communication systems [3]–[4]. Multicore fiber is being explored as a new solution to meet the growing data traffic in optical networks [5]. A single-core single-mode optical fiber is limited by the possible data rate and is limited by the amplifier bandwidth and nonlinear optical effects (NOE) [6].

The solution to the improvement of telecommunication systems is to improve the optical communication lines, which use non-return-to-zero (NRZ) modulation formats. Instead of using multi-stage pulse-amplitude modulation, abbreviated as “*PAM-M or M-PAM*”, where several bits are encoded at one signal level. The multi-level pulse amplitude modulation (PAM-M) modulation format is relatively easy to implement, offers a relatively easy trade-off between performance and the level of complexity of its implementation, and can provide a cost-effective solution for telecom service providers [7].

The traditional mobile radio access network (RAN), which combines baseband signal processing and radio functions in each base station, is used in the long-term evolution (LTE) solution in fourth-generation (4G) mobile technology as well as third-generation (3G) mobile technology. The next, fifth-generation (5G) mobile technology must provide at least 10 times higher data rates, spectral efficiency, and energy efficiency than current 3G, 4G / LTE mobile technologies. The technical requirements for fifth-generation 5G technology can be met by wavelength division multiplexed fiber-optic passive access networks (WDM-PONs) based on a centralized optical data network architecture, as well as the use of higher radio frequency bands, such as millimetre-wave (24 –86 GHz) frequency band [8].

Therefore, to ensure faster data transmission, it is necessary to create an architecture of a new solution for optical access communication systems, ensuring improvement of performance, functionality and capacity. The widely used fiber optic WDM-PON system can be technologically transformed into a hybrid Analog Radio-over-Fiber (ARoF)-WDM-PON system without the need to replace existing network elements, simply by integrating the mobile transmitter unit (BBU) and mobile base station receiver unit (RU) into the existing WDM-PON communication systems without changing the rest of the broadband Internet network architecture and optical line terminals

(OLT), as well as optical network terminals (ONT). Within the research framework carried out in this PhD, the architecture of a hybrid ARoF-WDM-PON transmission system capable of providing optical signal transmission for broadband internet services and 28 GHz (ka-band) millimeter-wave signal transmission over single single-mode fiber (SMF), following 40 Gigabit Passive Optical Network (NG-PON2) requirements, was developed.

The low-cost concept, which can provide an attractive solution for the development of hybrid optical communication systems combining broadband Internet and mobile fiber transmission, is considered a solution for the architecture of the next generation (NG) PON network. Kerr optical frequency combs (OFCs) using different types of whispering gallery mode microresonators (WGMRs) have already shown different applications, and in particular, their applications in fiber optic communication systems replacing laser light sources at specific wavelengths [9]. In addition, OFC generators are used in technologies such as optical clocks [10], ultra-stable microwave generation [11], applications requiring accurate optical frequency reference, spectroscopy [12], sensors [13], quantum applications [14], and optical communications [15], etc. The application of WGMR-OFC light sources in WDM fiber optic communication systems covers application scenarios ranging from short reach, such as data center interconnection (DCI) to access layer fiber optic networks [9], [16]. The Kerr OFC comb generators, which are physically implemented on silica microsphere resonators or micro-rods, demonstrate a new technological solution capable of providing an attractive solution for telecommunication fiber optic networks with low implementation costs and energy efficiency.

1.2 The aim and theses of the dissertation

Summarizing the above-mentioned facts about the directions of development of mobile communications and fiber optic transmission systems, the following **aim of the Doctoral Thesis is proposed:**

Experimentally develop hybrid fiber optical wavelength division multiplexed communication system solutions and evaluate their performance with spectrally efficient intensity modulation formats.

To achieve the aim set, the following theses were put forward:

1. In high-speed PON (HS-PON) transmission systems using 10 Gigabit PON (XG-PON) components, the maximum transmission distance in the optical C-band with a bit error rate $BER \geq 1 \times 10^{-3}$ can be realized using electric duobinary (EDB) modulation format, while the PAM-4 multilevel modulation format can achieve the maximum transmission speed per λ .
2. 5 Gbit/s PAM-4 gross-rate transmission over a joint 20 km optical fiber and at least 3 meter mm-Wave wireless link can be achieved with $BER \geq 1 \times 10^{-3}$ threshold by using heterodyne detection and photonic up-conversion technique in 28 GHz Ka-band having 2.5 GHz analog bandwidth.
3. The transmission of 2.5 Gbit/s NRZ-OOK modulated 28 GHz mm-wave radio signals and 10 Gbit/s NRZ-OOK modulated optical signals per optical channel via 20 km optical fiber in

hybrid ARoF-WDM-PON communication system can be realized using wavelength-routed WDM-PON architecture (WR-WDM-PON) for channel interval (ΔF) > 100 GHz, whereas wavelength-selected WDM-PON architecture (WS-WDM-PON) must be used for $\Delta F \leq 50$ GHz.

4. The newly generated harmonics of the silica microsphere whispering-gallery-mode resonator (WGMR)-based Kerr-OFC light source can be used in WDM-PON communication systems with 10 Gbit/s data rate per λ without adaptive equalization, while in DCI data transmission systems adaptive equalization is required at data rates up to 50 Gbit/s per λ .

1.3 The main key tasks of the Doctoral Thesis

To achieve the set goal of the dissertation and to prove the proposed theses, it is necessary to perform the following **key tasks**:

1. Evaluate the use of multilevel PAM-M and EDB intensity modulation formats in mathematical modeling environment to increase the maximum transmission distance in 10 Gigabit PON communication systems with intensity modulation and direct detection (IM/DD) without exceeding the BER $\geq 1 \times 10^{-3}$ of the received signal.
2. Experimentally and in a mathematical modeling environment evaluate the effect of chromatic dispersion (CD) and its compensation methods for increasing the maximum transmission distance in NRZ-OOK and PAM-4 modulated IM/DD WDM-PON communication systems with data transmission speeds up to 40 Gbit/s per λ , without exceeding the BER $\geq 1 \times 10^{-3}$ of the received signal.
3. Experimentally evaluate the application of spectrally efficient PAM-4, PAM-8, and EDB modulation formats to increase the data transmission speed up to 56 Gbit/s per λ with and without the use of adaptive equalization in high-speed PON (HS-PON) IM/DD transmission systems using 10 Gigabit PON (XG-PON) components and without exceeding BER $\geq 1 \times 10^{-3}$.
4. Experimentally evaluate the application of a combined solution of spatial (SDM) and wavelength division multiplexing (WDM) technologies in a 7-core single-mode multi core fiber (SMCF) for the development of a spatially multiplexed NRZ-OOK modulated 2.5 Gbit/s per λ fiber optical IM/DD communication system.
5. Experimentally and in mathematical modeling environment evaluate the application of heterodyne detection and 28 GHz mm-wave radio signal photonic up-conversion technique, providing transmission of 2.5 Gbit/s NRZ-OOK modulated and spectrally efficient up to 5 Gbit/s PAM-4 modulated signals over a joint 20 km optical fiber and at least 3 meter mm-wave wireless link.
6. Experimentally and in a mathematical modeling environment, develop and evaluate a hybrid ARoF-WDM-PON transmission system capable of providing the principle of backhaul operation for 2.5 Gbit/s NRZ-OOK modulated 28 GHz mm-wave radio signal and 10 Gbit/s

NRZ-OOK modulated optical signal transmission per channel through a 20 km fiber optical line.

7. Experimentally develop silica microsphere whispering-gallery-mode resonator WGMR-based Kerr-OFC as a multi-wavelength light source capable of providing an optical frequency comb in the C-band, where the number of newly generated harmonics corresponds to 2^n (n – integer number) used in ITU-T G.694.1 FOTS solutions, and evaluate their application for the transmission of NRZ-OOK modulated signals in such IM/DD systems with data transmission speeds up to 50 Gbit/s λ .

1.4 Research Methods

To perform the tasks outlined in the Doctoral Thesis and to analyze the problems, mathematical calculations, numerical simulations, and experimental measurements have been used. Numerical simulations were implemented in RSoft OptSim and VPI Design Suite simulation software, which are based on the nonlinear Schrödinger equation using the Split-Step method, the Fourier transform, and the Monte Carlo method for estimating the bit-error-rate (BER).

The spectra and power of the electrical and optical signals were used to evaluate the quality of optical signals in the simulation environment and experimental implementations. The quality of the received electrical signals was evaluated using bit error rate BER and eye diagrams. In the implementation of experimental systems, in some cases the quality of electrical signals received in real-time measurements was evaluated by the quality (Q-factor), from which the bit error rate BER of the transmitted signal was calculated, as well as in some cases offline digital signaling processing (DSP) was performed in MatLab computing environment for adaptive post-equalization and processing of the obtained results.

Scientific experiments described in the Doctoral Thesis and their results were carried out at the Institute of Telecommunications (TI) of Riga Technical University (RTU), Institute of Astronomy and Spectroscopy (ASI) of the University of Latvia (LU), Danish Technical University (DTU) in Denmark, and at the Department of Applied Physics of Royal Swedish Technical University (KTH) in close collaboration with the Swedish research institute RISE Acreo in Sweden and using video calls for online experiment measurements during the COVID-19 pandemic (digital laboratory work called “Zoom-lab”) in close collaboration with the Institute of Applied Physics of the Federal Research Center of the Russian Academy of Sciences (IPF-RAN) in Russia.

1.5 Scientific novelty and main results

Novel achievements of the Doctoral Thesis are as follows:

1. The most suitable intensity modulation formats (NRZ, PAM-4, PAM-8, EDB) for NG-PON2, XG-PON/HS-PON transmission systems depending on their application have been determined, as well as the application of NRZ and PAM-4 modulation formats in ARoF has been evaluated in WDM transmission systems for the transmission of 28 GHz (ka-band) millimeter wave radio signals, providing the principle of backhaul operation.

2. Factors influencing the BER and transmission distance of the received signal in the wavelength division multiplexed IM/DD PON and ARoF topology transmission systems (*dispersion, application of intensity modulation formats*) were evaluated, as a result in a mathematical simulation environment and experimental realization the methods of the received signal quality improvements were analyzed and improved.
3. The combined application of space division (SDM) and wavelength division multiplexing (WDM) technologies to increase the data rate of multi-core single-mode (SMCF) fiber in the development of NG spectrally efficient spatially capacitive IM/DD PON and RoF communication systems have been evaluated, and the factors (*crosstalk, differential mode delay*) influencing the received signal quality have been identified for multicore optical fiber.
4. The available up-conversion techniques of optical signals to 28 GHz (ka-band) millimeter wave radio signals in the RoF solution has been evaluated, and the hybrid ARoF-WDM-PON communication system has been experimentally developed for 2.5 Gbit/s NRZ and 5Gbit/s PAM-4 modulated data per channel transmission of 28 GHz (ka-band) millimeter-wave radio signals, providing the principle of backhaul operation via 20 km of SMF fiber.
5. Under the requirements of NG-PON2 (ITU-T G.989.3) recommendation, a hybrid ARoF-WDM-PON communication system has been experimentally developed and evaluated in mathematical simulation environment showing capable transmission of NRZ modulated data transmission speed up to 10 Gbit/s per channel for the internet broadband transmission and of up to 2.5 Gbit/s per channel transmission for a 28 GHz (ka-band) millimeter-wave signal transmission over a 40 km SMF fiber optic line.
6. A new innovative whispering-gallery-mode resonator WGMR-based Kerr-OFC light source based on silicon microspheres (SiO₂) has been developed, where with the newly generated harmonic of the light source: WDM-PON communication system solutions can transmit data at speed in the channel of up to 10 Gbit/s without AEQ, while applying for DCI system solutions it is possible to perform data transmission with data transmission speed in the channel up to 50 Gbit/s with use of AEQ.
7. A new innovative silicon microsphere and/or micro-rod whispering-gallery-mode resonator WGMR-based Kerr-OFC has been developed as a multi-wave light source, where the number of generated harmonics corresponds to $2n$ (n – integer number) used in FOTS solutions, and the inter-channel spacing between newly generated harmonics corresponds to ITU-T G.694.1, which is capable for use in communication system transmitting NRZ modulated signals at data rates up to 50 Gbit/s per λ .

The Practical Value of the Doctoral thesis:

1. A patent developed in Latvia: “*Hybrid fiber optic access system for transmission of millimeter-wave radio signals through a fiber*”, No. (P-19-73).

2. A patent application has been developed in Latvia “A multi-wave light source for data transmission in fiber optical telecommunication systems developed on a silica microrod resonator” (submitted patent application).
3. At the Institute of Telecommunications of RTU ETF have been developed a new NRZ modulated up to 2.5 Gbit/s and spectrally efficient PAM-4 modulated up to 5 Gbit/s per channel ARoF-WDM PON communication system model for the transmission of 28 GHz millimeter-wave radio signals through a 20 km fiber, (*is proposed for further experimental research*).
4. At the Institute of Telecommunications of RTU ETF have been experimentally developed and evaluated in mathematical simulation environment a new M-PAM modulated hybrid ARoF-WDM-PON communication system model capable for transmission of NRZ modulated data transmission with speed up to 10 Gbit/s per channel for the internet broadband transmission and of up to 2.5 Gbit/s per channel transmission for a 28 GHz (ka-band) millimeter-wave signal over a 40 km SMF fiber optic line, (*is proposed for further experimental research*).
5. At the Institute of Telecommunications of RTU ETF have been developed a new 4-channel 100 GHz spaced NRZ modulated dense wavelength division multiplexed (DWDM-PON) transmission system model able to provide a total data transmission with a total speed of 160 Gbit/s by using a symmetrical adaptive decorrelation (SAD) for channel separation in the optical C-band over 40 km using a symmetrical adaptive decorrelation, (*is proposed for further experimental research*).
6. At the Institute of Telecommunications of RTU ETF have been developed a new innovative silicon microsphere and/or micro-rod whispering-gallery-mode resonator WGMR-based Kerr-OFC light source, which is capable for use in communication system transmitting NRZ modulated signals at data rates up to 50 Gbit/s per λ , (*is proposed for further experimental research*).

The results obtained in the dissertation were used:

- In PostDoc project “Next Generation High Speed Fiber Optic Access Systems (NG-FAST)” No. 1.1.1.2/VIAA/1/16/044
- ERAF project “Development of optical frequency comb generator based on a whispering gallery mode microresonator and its applications in telecommunications (WCOMB)” No. 1.1.1.1/18/A/155
- ERAF project “Ring-Resonator Modulators for Optical Interconnects (RINGO)”, No. 1.1.1.1/21/A/052

1.6 Structure of the thesis

The dissertation is prepared as a thematically unified set of publications on development and evaluation of a spectrally efficient hybrid optical communication systems and their elements.

1.7 Publications and approbation of the Thesis

The results of the Doctoral Thesis are presented in 13 scientific articles and in publications in conference proceeding indexed in SCOPUS, WoS, and IEEE databases. The author has altogether 30 publications. The Latvian patent has been granted for the technology “*Hybrid Fiber Optic Access System for the Transmission of Millimeter Wave Radio Signals Through Fiber*”, developed within the framework of this work. The developed technology “*A multi-wave light source for data transmission in fiber optical telecommunication systems developed on a silica microrod resonator*” within the framework of the Thesis has been submitted to the Patent Office for consideration in order to apply for the Latvian state patent.

The results of the Doctoral Thesis have been presented at 13 international scientific conferences:

1. International conference Photonics West 2021 Digital Forum. Presentation: I. Brice, K. Grundstein, A. Sedulis, **T. Salgals**, S. Politis, V. Bobrov, and J. Alnis, “*Frequency comb generation in whispering gallery mode microsphere resonators*”, March 6–11, 2021.
2. 64th International Conference for Students of Physics and Natural Sciences – Open Readings 2021. Presentation: K. Draguns, I. Brice, **T. Salgals**, and J. Alnis, “*Dispersion Engineering of Whispering Gallery Mode Resonators for Frequency Comb Generation and Telecommunication Applications*,” March 16–19, 2021.
- 4th International conference “Quantum Optics and Photonics 2021”, online Zoom, April 22–23, 2021. Presentations:
 3. I. Brice, **T. Salgals**, V. Bobrovs, R. Viter, and J. Alnis, “*Whispering gallery mode silica microsphere resonator applications for biosensing and communications*”.
 4. **T. Salgals**, J. Alnis, R. Murnieks, I. Brice, J. Porins, A. V. Andrianov, E. A. Anashkina, S. Politis, and V. Bobrovs, “*Microsphere-based OFC-WGMR multi-wavelength source and its applications in telecommunications*”.
5. Photonics & Electromagnetics Research Symposium (PIERS 2019), China, Xiamen, 17–20 December 2019. Presentation: **T. Salgals**, A. Ostrovskis, A. Ipatovs, V. Bobrovs, and S. Politis, “*Hybrid ARoF-WDM PON Infrastructure for 5G Millimeter-wave Interface and Broadband Internet Service*”.
6. 60th RTU International Scientific and Technical Conference, October 15, 2019. Presentation: “*Cost-effective high-speed up to 32 Gbit/s WDM-PON next generation access network performance analysis*”.

7. 60th RTU International Scientific and Technical Conference, October 15, 2019). Presentation: “*Evaluation of Optical Frequency Comb Generator Based on WGMR Microresonator and its Applications in FOTS*”.
8. RTUWO 2018 – Advance in Wireless and optical Communications. Presentation: „*Evaluation of 4-PAM, NRZ and Duobinary Modulation Formats Performance for Use in 20 Gbit/s DWDM-PON Optical Access System*”.
9. RTUWO 2018 – Advance in Wireless and optical Communications, Chair of Section “*Optical communications*”, Riga, Latvia, 2018.
10. 59th RTU International Scientific and Technical Conference, November 2018. Presentation: “*Evaluation and Development of Next Generation Spectrally Efficient Access Optical Networks*”.
11. 58th RTU Student Scientific and Technical Conference, June 2017. Presentation: “*Research and evaluation of the Next-generation spectrally efficient optical communication systems*”.
12. 58th RTU International Scientific and Technical Conference, October 2017. Presentation: “*Performance evaluation of PAM-4 modulation format in optical access networks*”.
13. 57th RTU International Scientific and Technical Conference, November 2016. Presentation: “*Evaluation of Dispersion and Nonlinear Effects in a 10 Gbit/s WDM Transmission System*”.

The results of the author's doctoral thesis are presented in 13 scientific articles and conference proceeding indexed in SCOPUS–, WoS, and IEEE databases:

- [PAPER-1] [T. Salgals](#), [S. Spolitis](#), S. Olonkins, and V. Bobrovs, "Investigation of 4-PAM modulation format for use in WDM-PON optical access systems," *2017 Progress In Electromagnetics Research Symposium – Spring (PIERS)*, pp. 2450–2454, St. Petersburg, Russia, May 22–25, (2017), DOI: [10.1109/PIERS.2017.8262162](https://doi.org/10.1109/PIERS.2017.8262162)
- [PAPER-2] [T. Salgals](#), L. Skladova, K. Vilcane, J. Braunfelds, and [S. Spolitis](#), "Evaluation of 4-PAM, NRZ and Duobinary Modulation Formats Performance for Use in 20 Gbit/s DWDM-PON Optical Access Systems," *2018 Advances in Wireless and Optical Communications (RTUWO)*, pp. 134–138, Riga, Latvia, Nov. 15–16, (2018), DOI: [10.1109/RTUWO.2018.8587887](https://doi.org/10.1109/RTUWO.2018.8587887)
- [PAPER-3] A. Udalcovs, [T. Salgals](#), L. Zhang, X. Pang, A. Djupsjöbacka, [S. Spolitis](#), V. Bobrovs, S. Popov, and [O. Ozolins](#), "Optical Power Budget of 25+ Gbps IM/DD PON with Digital Signal Post-Equalization," *Applied Sciences* 10(17), 6106, (2020), DOI: <https://doi.org/10.3390/app10176106>
- [PAPER-4] A. Korra, [T. Salgals](#), J. Porins, E. Kazoks, R. Miho, and [S. Spolitis](#), "Performance Analysis of Cost-efficient High-speed up to 32 Gbit/s WDM-PON Next-generation Access Network with Dispersion Compensation," *2019 Photonics & Electromagnetics Research Symposium – Spring (PIERS-Spring)*, pp. 2671–2678, Rome, Italy, June 17-20, (2019), DOI: [10.1109/PIERS-Spring46901.2019.9017854](https://doi.org/10.1109/PIERS-Spring46901.2019.9017854)

- [PAPER-5] [T. Salgals](#), A. Supe, V. Bobrovs, J. Porins, and [S. Spolitis](#), "Comparison of Dispersion Compensation Techniques for Real-Time up to 160 Gbit/s DWDM C-Band Transmission", *ELEKTRON ELEKTROTECH* 26(2), 85–93, (2020), DOI:[10.5755/j01.eie.26.2.25892](#)
- [PAPER-6] G. K. M. Hasanuzzaman, [S. Spolitis](#), [T. Salgals](#), J. Braunfelds, A. Morales, L. E. Gonzalez, S. Rommel, R. Puerta, P. Asensio, V. Bobrovs, S. Iezekiel, I. T. Monroy, "Performance Enhancement of Multi-Core Fiber Transmission Using Real-Time FPGA Based Pre-Emphasis", *Asia Communications and Photonics Conference (ACPC)*, Guangzhou, November 10–13, (2017), DOI: [10.1364/ACPC.2017.M2H.1](#)
- [PAPER-7] [T. Salgals](#), L. Skladova, J. Porins, V. Bobrovs, and [S. Spolitis](#), "Analog Radio-over-fiber WDM-PON Architecture for 5G Millimeter-wave Interface," *2019 Photonics & Electromagnetics Research Symposium – Spring (PIERS-Spring)*, pp. 2679–2686, Rome, Italy, June 17–20, (2019), DOI: [10.1109/PIERS-Spring46901.2019.9017431](#)
- [PAPER-8] [T. Salgals](#), I. Kurbatska, V. Bobrovs, and [S. Spolitis](#), "Research of PAM-4 Modulated WDM-PON Architecture for 5G Millimeter-wave Hybrid Photonics-wireless Interface," *2019 Photonics & Electromagnetics Research Symposium - Fall (PIERS – Fall)*, pp. 728–734, Xiamen, China, Dec. 17–20, (2019), DOI: [10.1109/PIERS-Fall48861.2019.9021846](#)
- [PAPER-9] [T. Salgals](#), A. Ostrovskis, A. Ipatovs, V. Bobrovs, and [S. Spolitis](#), "Hybrid ARoF-WDM PON Infrastructure for 5G Millimeter-wave Interface and Broadband Internet Service," *2019 Photonics & Electromagnetics Research Symposium – Fall (PIERS – Fall)*, pp. 2161–2168, Xiamen, China, Dec. 17–20, (2019), DOI: [10.1109/PIERS-Fall48861.2019.9021479](#)
- [PAPER-10] E. A. Anashkina, V. Bobrovs, [T. Salgals](#), I. Brice, J. Alnis, and A. V. Andrianov, "Kerr Optical Frequency Combs With Multi-FSR Mode Spacing in Silica Microspheres," *IEEE Photon. Technol. Lett.* 33(9), 453–456, (2021), DOI: [10.1109/LPT.2021.3068373](#)
- [PAPER-11] E. A. Anashkina, M. P. Marisova, [T. Salgals](#), J. Alnis, I. Lyashuk, G. Leuchs, [S. Spolitis](#), V. Bobrovs, and A. V. Andrianov, "Optical Frequency Combs Generated in Silica Microspheres in the Telecommunication C-, U-, and E-Bands", *Photonics* 8(9), 345, (2021), DOI: [10.3390/photonics8090345](#)
- [PAPER-12] [T. Salgals](#), J. Alnis, R. Murnieks, I. Brice, J. Porins, A. V. Andrianov, E. A. Anashkina, [S. Spolitis](#), and V. Bobrovs, "Demonstration of a fiber optical communication system employing a silica microsphere-based OFC source," *Opt. Express* 29(7), 10903-10913, (2021), DOI: [10.1364/OE.419546](#)
- [PAPER-13] [T. Salgals](#), J. Alnis, [O. Ozolins](#), A.V. Andrianov, E. Anashkina, I. Brice, R. Berkis, X. Pang, A. Udalcovs, J. Porins, [S. Spolitis](#), and V. Bobrovs, "Silica microsphere WGMR-based Kerr-OFC light source and its application for high-speed IM/DD

short-reach optical interconnects”, *Applied Sciences* 12(9), 4722, (2022), DOI: [10.3390/app12094722](https://doi.org/10.3390/app12094722)

During the elaboration of the author's doctoral thesis, the author in general published 25 original scientific articles and conference proceedings (published in SCOPUS, WoS, IEEE databases).

- [Published-1] X. Pang, T. Salgals, H. Louchet, D. Che, M. Gruen, Y. Matsui, T. Dippon, R. Schatz, M. Joharifar, B. Krüger, L. Zhang, Y. Fan, A. Udalcovs, X. Yu, S. Spolitis, V. Bobrovs, S. Popov, O. Ozolins, "200 Gb/s Unamplified IM/DD Transmission over 20-km SMF with an O-band Low-Chirp Directly Modulated Laser, " *European Conference and Exhibition on Optical Communication (ECOC)*, September 21, (2022) (Accepted Post-deadline paper)
- [Published-2] O. Ozolins, T. Salgals, H. Louchet, M. Joharifar, R. Schatz, DiChe, Yasuhiro Matsui, M. Gruen, T. Dippon, F. Pittala, B. Krüger, Y.Fan, A. Udalcovs, U. Westergren, L. Zhang, X. Yu, S. Spolitis, V. Bobrovs, S. Popov, and X. Pang, "Error-Free 108 Gbps On-Off Keying Link for Optical Interconnect Applications," *European Conference and Exhibition on Optical Communication (ECOC)*, September 21, (2022) (Accepted Post-deadline paper)
- [Published-3] O. Ozolins, T. Salgals, H. Louchet, M. Joharifar, R. Schatz, D. Che, Y. Matsui, M. Gruen, T. Dippon, F. Pittala, B. Krüger, Y. Fan, A. Udalcovs, U. Westergren, Lu. Zhang, X. Yu, S. Spolitis, V. Bobrovs, S. Popov, and X. Pang, "High Baudrate Short-Reach Communication," *OptoElectronics and Communications Conference (OECC)*, pp. 1-3, Toyama, Japan, July 3-6, (2022), (Invited paper) [10.23919/OECC/PSC53152.2022.9850148](https://doi.org/10.23919/OECC/PSC53152.2022.9850148)
- [Published-4] A. Ostrovskis, K. Rubuls, T. Salgals, L. Skladova, V. Bobrovs and S. Spolitis, "Demonstration of Ka-band mm-wave ARoF signal transmission," *2022 International Conference Laser Optics (ICLO)*, 2022, pp. 1-1, [10.1109/ICLO54117.2022.9840183](https://doi.org/10.1109/ICLO54117.2022.9840183)
- [Published-5] T. Salgals, J. Alnis, O. Ozolins, A.V. Andrianov, E. Anashkina, I. Brice, R. Berkis, Z. Pang, A. Udalcovs, J. Porins, S. Spolitis, and V. Bobrovs, "Silica microsphere WGMR-based Kerr-OFC light source and its application for high-speed IM/DD short-reach optical interconnects”, *Applied Sciences* 12(9), 4722, (2022) DOI: [10.3390/app12094722](https://doi.org/10.3390/app12094722)
- [Published-6] O. Ozolins, T. Salgals, H. Louchet, M. Joharifar, R. Schatz, M. Gruen, T. Dippon, B. Krüger, D. Che, Y. Matsui, Y. Fan, A. Udalcovs, L. Zhang, X. Yu, S. Spolitis, V. Bobrovs, S. Popov, and X. Pang, "Optical Amplification-Free 200 Gbaud On-Off Keying Link for Intra-Data Center Communications," *Optical Fiber Communication (OFC)*, pp. 1-3, Th4A.6, San Diego, CA, US, March 10, (2022), (Accepted Post-Deadline paper), DOI: [10.1364/OFC.2022.Th4A.6](https://doi.org/10.1364/OFC.2022.Th4A.6)

- [Published-7] X. Pang, H. Dely, R. Schatz, D. Gacemi, M. Joharifar, **T. Salgals**, A. Udalcovs, Y.T. Sun, Y. Fan, L. Zhang, E. Rodriguez, **S. Spolitis**, V. Bobrovs, X. Yu, S. Lourduoss, S. Popov, **O. Ozolins**, A. Vasaneli, and C. Sirtori, "11 Gb/s LWIR FSO Transmission at 9.6 μm using a Directly-Modulated Quantum Cascade Laser and an Uncooled Quantum Cascade Detector," *Optical Fiber Communication (OFC)*, (Th4B.5), pp. 1-3, Th4B.5, San Diego, CA, US, March 10, (2022), (*Accepted Post-Deadline paper*), DOI: [OFC.2022.Th4B.5](https://doi.org/10.1364/OFC.2022.Th4B.5)
- [Published-8] M. Aleksejeva, I. Lyashuk, R. Kudojars, D. Prigunovs, D. Ortiz, J. Braunfelds, **T. Salgals**, **S. Spolitis**, and V. Bobrovs, "Research on Super-PON Communication System with FWM-based Comb Source," *2021 Photonics & Electromagnetics Research Symposium Proceedings (PIERS)*, Hangzhou, China, November 21-25, (2021), DOI: [10.1109/PIERS53385.2021.9694669](https://doi.org/10.1109/PIERS53385.2021.9694669)
- [Published-9] A. Ostrovskis, I. Kurbatska, **T. Salgals**, **S. Spolitis**, and V. Bobrovs, "The architecture of hybrid mm-wave ARoF Super-PON system for 5G implementation," *Optical Fiber Technology (OFT)* 67, 102697 (2021), DOI: [10.1016/j.yofte.2021.102697](https://doi.org/10.1016/j.yofte.2021.102697)
- [Published-10] E. A. Anashkina, V. Bobrovs, **T. Salgals**, I. Brice, J. Alnis, and A. V. Andrianov, "Kerr Optical Frequency Combs With Multi-FSR Mode Spacing in Silica Microspheres," *IEEE Photon. Technol. Lett.* 33(9), 453–456, (2021), DOI: [10.1109/LPT.2021.3068373](https://doi.org/10.1109/LPT.2021.3068373)
- [Published-11] **T. Salgals**, J. Alnis, R. Murnieks, I. Brice, J. Porins, A. V. Andrianov, E. A. Anashkina, **S. Spolitis**, and V. Bobrovs, "Demonstration of a fiber optical communication system employing a silica microsphere-based OFC source," *Opt. Express* 29(7), 10903-10913, (2021), DOI: [10.1364/OE.419546](https://doi.org/10.1364/OE.419546)
- [Published-12] E. A. Anashkina, M. P. Marisova, **T. Salgals**, J. Alnis, I. Lyashuk, G. Leuchs, **S. Spolitis**, V. Bobrovs, and A. V. Andrianov, "Optical Frequency Combs Generated in Silica Microspheres in the Telecommunication C-, U-, and E-Bands", *Photonics* 8(9), 345, (2021), DOI: [10.3390/photonics8090345](https://doi.org/10.3390/photonics8090345)
- [Published-13] I. Brice, K. Grundsteins, A. Sedulis, **T. Salgals**, **S. Spolitis**, V. Bobrovs, J. Alnis, "Frequency comb generation in whispering gallery mode silica microsphere resonators," *Proc. SPIE 11672, Laser Resonators, Microresonators, and Beam Control XXIII*, 1167213, (2021), DOI: [10.1117/12.2577148](https://doi.org/10.1117/12.2577148)
- [Published-14] **S. Spolitis**, R. Murnieks, L. Skladova, **T. Salgals**, A. V. Andrianov, M. P. Marisova, G. Leuchs, E. A. Anashkina, and V. Bobrovs, "IM/DD WDM-PON Communication System Based on Optical Frequency Comb Generated in Silica Whispering Gallery Mode Resonator," *IEEE Access* 9, 66335–66345, (2021), DOI: [10.1109/ACCESS.2021.3076411](https://doi.org/10.1109/ACCESS.2021.3076411)
- [Published-15] J. Braunfelds, U. Senkans, P. Skels, R. Janeliukstis, **T. Salgals**, D. Redka, I. Lyashuk, J. Porins, **S. Spolitis**, V. Haritonovs, V. Bobrovs, "FBG-Based Sensing

- for Structural Health Monitoring of Road Infrastructure," *Journal of Sensors* 2021, 1-11, (2021), DOI: [10.1155/2021/8850368](https://doi.org/10.1155/2021/8850368)
- [Published-16] J. Braunfelds, R. Murnieks, [T. Salgals](#), I. Brice, T. Sharashidze, I. Lyashuk, A. Ostrovskis, [S. Spolitis](#), J. Alnis, J. Poriņš, V. Bobrovs, "Frequency Comb Generation in WGM Microsphere Based Generators for Telecommunication Applications," *Quantum Electron.* 50(11), 1043–1049, (2020), DOI: [10.1070/QEL17409](https://doi.org/10.1070/QEL17409)
- [Published-17] E. A. Anashkina, M. P. Marisova, A. V. Andrianov, R. A. Akhmedzhanov, R. Murnieks, M. D. Tokman, L. Skladova, I. V. Oladyshkin, [T. Salgals](#), I. Lyashuk, A. Sorokin, [S. Spolitis](#), G. Leuchs, and V. Bobrovs, "Microsphere-Based Optical Frequency Comb Generator for 200 GHz Spaced WDM Data Transmission System," *Photonics* 7(3), 72, (2020), DOI: [10.3390/photonics7030072](https://doi.org/10.3390/photonics7030072)
- [Published-18] A. Udalcovs, [T. Salgals](#), L. Zhang, X. Pang, A. Djupsjöbacka, [S. Spolitis](#), V. Bobrovs, S. Popov, and [O. Ozolins](#), "Optical Power Budget of 25+ Gbps IM/DD PON with Digital Signal Post-Equalization," *Applied Sciences* 10(17), 6106, (2020), DOI: <https://doi.org/10.3390/app10176106>
- [Published-19] [T. Salgals](#), I. Kurbatska, V. Bobrovs and [S. Spolitis](#), "Research of PAM-4 Modulated WDM-PON Architecture for 5G Millimeter-wave Hybrid Photonics-wireless Interface," *2019 Photonics & Electromagnetics Research Symposium - Fall (PIERS - Fall)*, pp. 728-734, Xiamen, China, Dec. 17-20, (2019), DOI: [10.1109/PIERS-Fall48861.2019.9021846](https://doi.org/10.1109/PIERS-Fall48861.2019.9021846)
- [Published-20] [T. Salgals](#), A. Supe, V. Bobrovs, J. Porins, and [S. Spolitis](#), "Comparison of Dispersion Compensation Techniques for Real-Time up to 160 Gbit/s DWDM C-Band Transmission", *ELEKTRON ELEKTROTECH* 26(2), 85–93, (2020), DOI: [10.5755/j01.eie.26.2.25892](https://doi.org/10.5755/j01.eie.26.2.25892)
- [Published-21] R. Beļinskis, N. Bogdanovs, E. Petersons, A. Ipatovs and [T. Salgals](#), "Routing Algorithm for Wireless Sensor Network Considering Propagation Losses," *2019 Photonics & Electromagnetics Research Symposium - Fall (PIERS - Fall)*, pp. 3020-3026, Xiamen, China, Dec. 17-20, (2019), DOI: [10.1109/PIERS-Fall48861.2019.9021811](https://doi.org/10.1109/PIERS-Fall48861.2019.9021811)
- [Published-22] [T. Salgals](#), A. Ostrovskis, A. Ipatovs, V. Bobrovs and [S. Spolitis](#), "Hybrid ARoF-WDM PON Infrastructure for 5G Millimeter-wave Interface and Broadband Internet Service," *2019 Photonics & Electromagnetics Research Symposium - Fall (PIERS - Fall)*, pp. 2161-2168, Xiamen, China, Dec. 17-20, (2019), DOI: [10.1109/PIERS-Fall48861.2019.9021479](https://doi.org/10.1109/PIERS-Fall48861.2019.9021479)
- [Published-23] R. Beļinskis, N. Bogdanovs, E. Pētersons, A. Ipatovs and [T. Salgals](#), "Efficient Algorithm for Reliable Routing of Wireless Sensor Networks Considering Propagation Losses," *2019 Photonics & Electromagnetics Research Symposium -*

Spring (PIERS-Spring), pp. 3895-3901, Rome, Italy, June 17-20, (2019), DOI: [10.1109/PIERS-Spring46901.2019.9017312](https://doi.org/10.1109/PIERS-Spring46901.2019.9017312)

- [Published-24] **T. Salgals**, L. Skladova, J. Porins, V. Bobrovs and **S. Spolitis**, "Analog Radio-over-fiber WDM-PON Architecture for 5G Millimeter-wave Interface," *2019 Photonics & Electromagnetics Research Symposium - Spring (PIERS-Spring)*, , pp. 2679-2686, Rome, Italy, June 17-20, (2019), DOI: [10.1109/PIERS-Spring46901.2019.9017431](https://doi.org/10.1109/PIERS-Spring46901.2019.9017431)
- [Published-25] A. Korra, **T. Salgals**, J. Porins, E. Kazoks, R. Miho and **S. Spolitis**, "Performance Analysis of Cost-efficient High-speed up to 32 Gbit/s WDM-PON Next-generation Access Network with Dispersion Compensation," *2019 Photonics & Electromagnetics Research Symposium - Spring (PIERS-Spring)*, pp. 2671-2678, Rome, Italy, June 17-20, (2019), DOI: [10.1109/PIERS-Spring46901.2019.9017854](https://doi.org/10.1109/PIERS-Spring46901.2019.9017854)
- [Published-26] **T. Salgals**, L. Skladova, K. Vilcane, J. Braunfelds and **S. Spolitis**, "Evaluation of 4-PAM, NRZ and Duobinary Modulation Formats Performance for Use in 20 Gbit/s DWDM-PON Optical Access Systems," *2018 Advances in Wireless and Optical Communications (RTUWO)*, pp. 134-138, Riga, Latvia, Nov. 15-16, (2018), DOI: [10.1109/RTUWO.2018.8587887](https://doi.org/10.1109/RTUWO.2018.8587887)
- [Published-27] G.K.M. Hasanuzzaman, **S. Spolitis**, **T. Salgals**, J. Braunfelds, A. Morales, L. E. Gonzalez, S. Rommel, R. Puerta, P. Asensio, V. Bobrovs, S. Iezekiel, I. Tafur. Monroy, "Performance Enhancement of Multi-Core Fiber Transmission Using Real-Time FPGA Based Pre-Emphasis", *Asia Communications and Photonics Conference (ACP)*, Guangzhou, November 10-13, (2017), DOI: [10.1364/ACPC.2017.M2H.1](https://doi.org/10.1364/ACPC.2017.M2H.1)
- [Published-28] **T. Salgals**, **S. Spolitis**, S. Olonkins and V. Bobrovs, "Investigation of 4-PAM modulation format for use in WDM-PON optical access systems," *2017 Progress In Electromagnetics Research Symposium - Spring (PIERS)*, pp. 2450-2454, St. Petersburg, Russia, May 22-25, (2017), DOI: [10.1109/PIERS.2017.8262162](https://doi.org/10.1109/PIERS.2017.8262162)
- [Published-29] S. Olonkins, V. Bickovs, **T. Salgals**, V. Bobrovs, and G. Ivanovs, "Investigation of Dual-Pump FOPA Performance in a 4-Channel 40 Gbps WDM Transmission System", *Elektronika Ir Elektrotehnika*, 23(6), 85-89, (2017), DOI: [10.5755/j01.eie.23.6.19699](https://doi.org/10.5755/j01.eie.23.6.19699)

Chapter in the scientific monograph:

- [Published-1] **T. Salgals**, I. Kurbatska, **S. Spolitis**, V. Bobrovs and G. Ivanovs, "Research of M-PAM and Duobinary modulation formats for use in high-speed WDM-PON systems", IntechOpen, the world's leading publisher of Open Access books Built by scientists, for scientists, 'Telecommunication Systems', October (2018), DOI: [10.5772/intechopen.84600](https://doi.org/10.5772/intechopen.84600)

2 MAIN RESULTS OF THE DOCTORAL THESIS

The dissertation has been prepared as a thematically unified set of scientific publications. The results are presented in 13 scientific publications. The first chapter of the dissertation describes the topicality of the research, evaluates the aim and theses, describes the main tasks, research methodology and the structure of the work and the main results.

The second chapter of the dissertation describes the wavelength division multiplexed fiber optic communication systems, i.e., assessment of the development of passive optical access networks (PON) and data center interconnection (DCI).

The third chapter discusses the evaluation of the application of spectrally efficient multi-level pulse amplitude modulation formats to increase the performance of WDM-PON systems (*first contribution comes from [PAPER-1], [PAPER-2] and [PAPER-3]*).

In the fourth chapter, the evaluation of the received signal quality depending on the applied optical transmission environment for the implementation of a high-speed spectrally efficient WDM-PON broadband transmission system is performed. The analysis of the received signal quality under the influence of nonlinear optical effects (NOE) and chromatic dispersion (CD) is performed, as well as the application of space division multiplexing (SDM) technology for the implementation of a spectrally and spatially efficient wavelength division multiplexed optical communication system is evaluated (*contribution comes from [PAPER-4], [PAPER-5] and [PAPER-6]*).

The fifth chapter summarizes the application of the radio-over-fiber (RoF) as the solution for future cellular mobile communications, including the fifth-generation (5G and beyond) technological implementation solution. Within the framework of the dissertation, a spectrally efficient next-generation optical system for the transmission of millimeter-wave radio signals over fiber was experimentally developed for future cellular mobile communications as well as a new hybrid fiber optic transmission system architecture capable of broadband Internet data transmission and radio signal transmission over a single optical fiber was developed (*contribution comes from [PAPER-7], [PAPER-8], and [PAPER-9]*).

The sixth chapter describes the implementation of a new type of spectrally efficient WDM transmission with a new novel silica microsphere whispering-gallery-mode resonator WGMR-based Kerr-OFC multi-wave light source. At the moment, for the first time in the world, high-speed data transmission of experiments using harmonics generated of WGMR-based Kerr-OFC was demonstrated. The results of this world-class experiment are described in the publication where the first author and principal investigator is Tom Salgals - “*Demonstration of a fiber optical communication system employing a silica microsphere-based OFC source*”, Optics Express (Q1 Journal). The use of WGMR Kerr-OFC light sources for short reach, such as data center interconnection DCI, to transmit NRZ encoded signals at data rates up to 50 Gbit/s per wavelength is also substantiated and experimentally demonstrated a new record in the current field (*contribution comes from [PAPER-10], [PAPER-11], [PAPER-12], and 20*).

In Conclusions, the comparison and evaluation of the experimental and simulative results are performed, and the answers to the key tasks and theses set in the dissertation are given.

2.1 Assessment and evolution of WDM fiber optical communication system directions.

Optical fibers provide major connectivity in modern communication networks. Wireless and copper lines are used only in the vicinity of the wireless and wireline end-users and network element devices. The fiber connection between residences or commercial buildings to the access point is part of a passive optical network PON, which moves data at distances of up to 40 km from the service provider's central office. For the PON interface, the data rate in the field is up to 10 Gb/s. Technologies using the next-generation standard accommodate 40 Gb/s and are being deployed. The eventual introduction of 100-Gb/s capability is being discussed. The fiber connection between the remote radio head and the base station is standardized by a common public radio interface (CPRI), and the cable length can be up to about 25 km. As for the next-generation mobile front-haul links, such as the connection between the remote radio head and base station, wavelength-division multiplexing (WDM) needs to be considered to support the 10 times capacity increase of fifth-generation (5G) networks over the current 4G/LTE networks. Once end-user traffic is aggregated in the gateways to metropolitan networks, the traffic is transported by a DWDM optical link. A DWDM optical link can contain more than 100 wavelength channels in a single-mode optical fibre's 1550 nm optical wavelength range. There is also an ongoing discussion to introduce 1.6 Tbit/s connectivity for DWDM based on 2x800 Gbit/s links, which can travel up to 1000 km [17]. While the metropolitan network distance typically goes up to several hundred kilometres, a long-haul network may rely on a transoceanic link with more than 10,000 km between transceivers [18]. Optical links are moving to higher and higher transmission speeds while shrinking to shorter and shorter ranges where optical links are envisaged even at the chip scale. 1.6 Tbit/s transmitter for optical interconnects has been recently demonstrated by Intel Corporation [19].

In 2016 39% of a global data center, Internet protocol (IP) traffic was handled by 338 hyperscale data centers. This means that one hyperscale data center each day handles an average of ~20 PB of traffic [18]. The explosive growth of Internet Protocol IP traffic is driving data centers to the so-called "Zettabyte Era," as predicted by the Cisco Report that expects annual global IP traffic to reach over 4.8 zettabytes/year by 2022. For some applications, such as those on Facebook, the internal traffic may be several orders of magnitude greater. In addition to the internal traffic required to build web pages and search indices, relatively recent machine-learning applications are driving increasing amounts of both computation and traffic on the data center interconnection network [20]. As well, many applications are moving to cloud-based computing, where all data processing and calculations are performed within these data centers (supporting the so-called Edge computing approach) and end-users only receive the prepared output information [21].

Power and cost-efficient fiber optical access networks and short-range fiber optical links are one of the key technologies enabling bandwidth-hungry services like video on demand (VoD), high definition TV, and cloud computing supported by large scale high-performance computers and data centers. Such optical links typically use direct detection and on-off keying modulation (OOK) with non-return-to-zero NRZ line code. Today's challenge for optical access networks and

data centers is to increase the serial line rate of an NRZ link due to the physical bandwidth limitation of the photonic and electronic components like optical signal modulators and photodiodes. Solution for telecommunication infrastructure upgrade and alternative solution for the increase of the serial line rate of an NRZ link is to use multi-level signaling formats such as pulse-amplitude modulation (abbreviated as PAM-M or M-PAM), where multiple digital bits per symbol are encoded into M different signal amplitude levels. The 4 level PAM modulation format (PAM-4) is receiving significant attention because of its relative ease of implementation compared to higher-order modulation formats like quadrature phase-shift keying (QPSK), and m-ary quadrature amplitude modulation (m-QAM). It is clear that M-PAM offers a good tradeoff between performance and complexity. Usage of PAM-4 format is an effective way to double the data rate of the NRZ link. Previously PAM-4 modulation formats have been investigated with traditional electrical networks, but now researchers are focused on investigating PAM-4 and M-PAM modulation formats for optical access networks and data center interconnections. It must be noted that multi-level signaling also changes some rules used in NRZ coded transmission systems. For M-PAM systems, it is important to implement more complex (and precise) level threshold detection for signal inputs also signal-to-noise (SNR) requirements are higher than in case of NRZ. Eye time skew, amplitude compression in lower eye diagram eyes, intersymbol interference for M-PAM systems also is an issue. So, we can say that PAM-4 links are new science – still learning what impairments create errors in receivers. Significant efforts have been put on investigation of PAM-4 format in fiber optical transmission networks, however there are following aspects, which have not been studied or are studied insufficiently, highlighting the innovative level and novelty of this thesis. Therefore the much higher level PAM modulation techniques like 8-PAM, which can dramatically improve the spectral efficiency and available bitrate by using the bandwidth of already existing optical, electro-optical or electrical devices and minimal available channel spacing (which has a direct impact on the utilization of resources like optical spectrum), maximal available number of channels and maximal transmission distance (network reach) in dispersion compensated and non-compensated in M-PAM modulated WDM-PON optical access systems have been studied.

3 APPLICATION AND EVALUATION OF THE SPECTRALLY EFFICIENT MODULATION FORMATS SUSTAINABLE TO INCREASE THE PERFORMANCE OF WDM-PON TRANSMISSION SYSTEMS

3.1 Application of NRZ, PAM-4 and EDB modulation formats for PON networks

There are two main architectures for implementing fiber optical access networks - passive optical networks PONs and active optical networks (AONs). However, in most cases, PON is considered a more cost-efficient solution compared to AON [22]. Today's last standardized PON is NG-PON2 (ITU-T G.989). It defines time- and wavelength-division multiplexed PON (TWDM-PON) with four wavelengths of 10 Gb/s each as a main solution for NG-PON2 implementation. Furthermore, 8-channel point-to-point WDM-PON is considered an optional capability mainly intended for transporting mobile fronthaul [23], [24]. According to [24], further enhancements of PON standards have already been discussed, considering the increase in per-channel line rates from 10 to 25 Gbps. Moreover, the possibilities of increasing per-wavelength data rates to 40 Gbit/s have also been studied widely, for example, in [23]–[26]. In this regard, it is crucial to evaluate the capability of the WDM-PON transmission system in terms of the increase of the per-channel data rate.

It should be underlined that the utilization of the traditional non-return-to-zero NRZ modulation for high per-wavelength data rates may cause significant technical difficulties in terms of both transceiver bandwidth capability and fiber dispersion [27]–[28]. Several characteristics of the transmission system, such as resistance to chromatic and polarization mode dispersion, resistance to NOE, and required transceiver bandwidth, depending on the utilized modulation format. Consequently, the choice of modulation format significantly influences the performance reach, bit error ratio BER, capacity and receiver sensitivity of fiber optical access network [23], [27]–[28].

Some authors, e.g. in [29], evaluate the performance of modulation formats in terms of optical signal-to-noise ratio (optical SNR or OSNR). However, evaluation of OSNR is essential for the transmission systems where optical amplifiers are used. Like in [29] where PAM-4 is evaluated for the utilization in extended data center interconnects that require optical amplification. Moreover, in the DWDM transmission system, it is desirable to measure the OSNR of each channel separately [30]. Considering that the evaluation of OSNR is not crucial for non-amplified transmission systems, the BER is utilized as a sufficient characteristic of the received signal quality.

The four-level pulse amplitude modulation PAM-4 and electrical Duobinary EDB modulation formats have been extensively studied for the utilization in high data rate optical transmission systems. For example, in [23], authors evaluate the performance of the electrical EDB, optical ODB and PAM-4 for use in WDM-PON with 40 Gbit/s per-wavelength data rate. Their obtained results reveal that electrical DB and optical DB are power-efficient schemes for smaller transmission distances, e.g. 10 km. While PAM-4 demonstrates the best power budget and cost

efficiency for longer distances of around 20 km. Authors in [26] indicate 100 Gbit/s TWDM-PON with four 25 Gbit/s optical ODB channels, while authors in [25] demonstrate the feasibility of PAM-4 and electrical EDB in NG-PON with 28 Gbit/s per channel data rate. Nonetheless, authors in [31] report that the applying of NRZ is the most cost-efficient solution for the Ethernet PON (EPON) with 25 Gbit/s per wavelength data rate. Furthermore, authors in [32] demonstrate the feasibility of utilization of NRZ in TWDM-PON with 25 Gbit/s per-channel data rate and equalization. While according to [33], return-to-zero (RZ) has greater tolerance to the nonlinear optical effects NOE and consequently is less susceptible to inter-symbol interference (ISI).

All modulation formats under research are intensity modulation (IM) formats. In intensity modulation, the intensity of the lightwave carrier is changed in response to the digital data, keeping everything else fixed. That is, bit 1 is transmitted by the lightwave carrier with a particular intensity. To transmit 0, the intensity is changed to a minimum [34]. Utilizing non-return-to-zero on-fff keying (NRZ-OOK), the intensity remains constant over all bit period. NRZ-OOK also has the simplest configuration and setting of transmitters.

EDB is a partial response modulation format. For EDB, information is conveyed by the intensity levels $\{0,1\}$, in addition, π -phase shifts occur for 1-bits separated by an odd number of 0-bits. The spectrum of EDB is narrower than the spectrum of NRZ-OOK. However, direct-detection (square-law) receivers are utilized, the phase information is not used for detection. Instead, it shapes the spectrum to improve the tolerance of a format to specific propagation impairments. For DB modulated signals, the spectrum shaping ensures higher tolerance to CD and narrowband optical filtering [35]. PAM-4 is a multi-level amplitude modulation format. PAM-4 modulated signal has four levels, corresponding to binary symbols consisting from two bits – “00”, “01”, “10” and “11”. The main advantage of PAM-4 is higher spectral efficiency in comparison to one-level modulation formats [23], [36].

However, very few publications are available in the literature that evaluates the utilization of NRZ, PAM-4 and EDB for supporting different data rates keeping the same physical structure and key parameters of the transmission system. However, it would allow comparing the modulation formats in terms of the best performance for each per-wavelength data rate. In research done during the Doctoral thesis, the same parameters of the transmission system for each data rate (except data rate related) were used. That allows tracking the change in the performance of each modulation format caused by the utilization of the corresponding data rate. Thus, ensuring for each data rate the determination of the most suitable modulation format among the investigated ones. The current research evaluates four modulation formats – PAM-8, PAM-4, EDB and NRZ. During the research, all parameters of the transmission system’s elements remain the same, excluding the data rate related. The performance of investigated modulation formats (namely PAM-8, PAM-4, EDB, NRZ) was evaluated in terms of the impact of transmission distance, received power, and receiver bandwidth on the BER.

3.2 Evaluation of PAM-4 coding format application in 10G WDM-PON transmission systems

A simulation model was developed to evaluate the performance of PAM-4 modulation format use in current 10G WDM-PON optical access networks (see *Figure 1.*). Results displayed in the current report are obtained in industry and academy recognized Rsoft Optsim Optical Systems simulation software. In the current research step, the 4-channel 10 Gbaud/s (20 Gbit/s) PAM-4 modulated WDMPON access system with different channel spacing without chromatic dispersion CD compensation and compensation with fiber Bragg grating (FBG) dispersion compensation module (DCM) was investigated. The minimal allowable channel spacing was found, which directly impacts the utilization of resources like optical spectrum and maximal transmission distance for multichannel PAM-4 modulated WDM-PON transmission system operating at 10 Gbaud/s symbol rate.

The central office (CO) consists of an optical line terminal OLT with four transmitters (OLT_Tx). As it is shown in *Figure 1.*, each transmitter (OLT_Tx) consists of two electrical pseudo-random bit sequence (PRBS) data sources, two NRZ drivers, which encodes the data from data sources by using the non-return zero NRZ encoding technique and electrical coupler, which couples both electrical signal in one signal in such a way generating PAM-4 signal. The amplitude of the electrical signal generated by the second NRZ driver was twice larger than the amplitude of the first NRZ driver output signal. Coupled electrical PAM-4 signal with 4 different amplitude levels is filtered by an electrical lowpass filter and sent to an external Mach-Zehnder modulator (MZM). The light source continuous wavelength (CW) laser with a linewidth of 50MHz and output power of +3dBm is used. MZM has a 3 dB insertion loss and 20 dB extinction ratio. Optical signals from each transmitter are coupled together using an optical combiner with 1 dB loss. Next, chromatic dispersion pre-compensation by FBG DCM is realized for all channels before launching them into standard ITU-T G.652 single-mode fiber SMF span. An additional 3 dB attenuator is used to simulate FBG DCM's insertion loss. After transmission in the optical distribution network (ODN), all channels are separated by arrayed waveguide grating (AWG) filter (located in remote terminal (RT)), which insertion loss is 3.5 dB, channel spacing is 50 or 100 GHz, and 3-dB bandwidth is 20 GHz. The receiver side consists of users or optical network terminals ONTs.

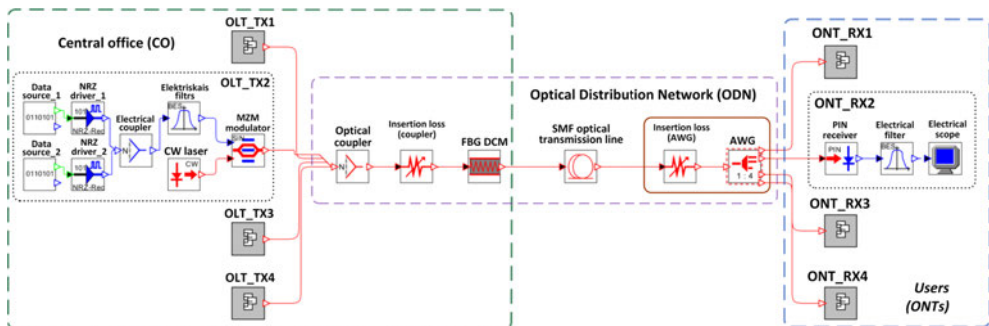


Figure 1. Simulation scheme of 10 Gbaud/s PAM-4 WDM-PON optical transmission system.

Each ONT receiver (ONT_RX) consists of a PIN photodiode (sensitivity is -19dBm for BER of 10^{-12}), electrical Bessel low-pass filter (3-dB bandwidth is 7.5 GHz), and electrical scope to evaluate the quality of the received signal (e.g., show bit pattern).

*The goal of this simulation model was to evaluate the performance and maximum reach as well as minimal channel spacing for PAM-4 modulated WDM-PON system with four 10 Gbaud/s (20 Gbit/s) channels, under the condition that it is still possible to achieve a bit error ratio (BER) of 10^{-3} [37]. The theoretical performance restores a 1.1×10^{-3} pre-FEC BER to a 10^{-12} post-FEC BER. As shown in **Figure 1**, the PAM-4 modulated WDM-PON simulation scheme consists of 4 channels. The central frequency is 193.1 THz and channel spacing is chosen 50 or 100 GHz, according to the ITU G.694.1 recommendation.*

The first investigated channel spacing was 100 GHz. As one can see in **Figure 2(a)** and **Figure 3(a)**, in back-to-back (B2B) configuration, the signal quality is very good, the eye is open and error-free transmission with 100 GHz channel spacing can be provided. After 59 km transmission (see **Figure 2(b)** and **Figure 3(b)**), which was the maximum transmission distance without dispersion compensation, the BER of the received signal was 7.5×10^{-4} . The BER of the received PAM-4 signal was estimated offline through built digital signal processing DSP algorithm in Matlab software. For extension of transmission distance by dispersion compensation, the FBG-DCM module in the simulation model was also implemented.

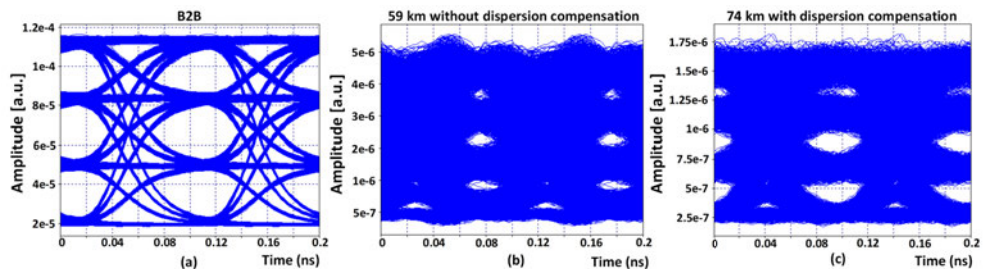


Figure 2. Eye diagrams of the received signal (a) after B2B transmission, (b) after 59km transmission without the use of DCM module and (c) after 74km transmission with dispersion compensation by FBG DCM unit for 4-channel 100 GHz spaced WDM-PON system with PAM-4 modulation format.

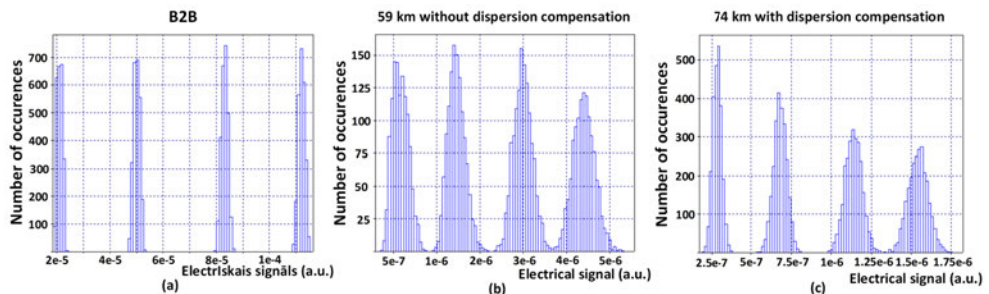


Figure 3. Histograms of the received signal (a) after B2B transmission, (b) after 59km transmission without the use of DCM module, and (c) after 74km transmission with dispersion compensation by FBG DCM unit for 4-channel 100 GHz spaced WDM-PON system with PAM-4 modulation format.

Using this dispersion compensation technique, the maximum achievable transmission distance was 74 km, where the BER of the received signal was 9×10^{-4} , please see *Figure 2(c)* and *Figure 3(c)*. As shown in *Figure 2.* and *Figure 3.* by using additional dispersion compensation with FBG, an extra 15 km or 25.4% of link length was gained.

As one can see in *Figure 4(a)* and *Figure 5(a)*, in B2B configuration, the signal quality for 50 GHz channel spacing also is very good, the eye is open, and error-free transmission can be provided. After 58 km transmission (see *Figure 4(b)* and *Figure 5(b)*), which was the maximum transmission distance without dispersion compensation, the BER of the received signal was 8×10^{-4} . The crosstalk between channels can explain the drop in BER performance; therefore, the eye diagrams and histograms of the received signal for the central channel (third channel), which showed the worst BER performance, are shown.

The same tunable FBG-DCM module was implemented to extend transmission distance by using dispersion compensation. Using this dispersion compensation technique, the maximum achievable transmission distance was 72 km, where the BER of the received signal was 5.5×10^{-4} , please see *Figure 4(c)* and *Figure 5(c)*. As shown in *Figure 4* and *Figure 5*, by using additional dispersion compensation, there were gained extra 14 km or 24% of link length by using FBG for CD compensation.

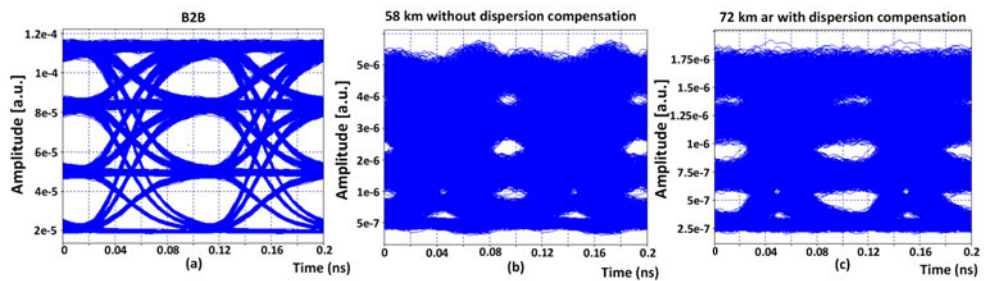


Figure 4. Eye diagrams of the received signal (a) after B2B transmission, (b) after 58km transmission without the use of DCM module and (c) after 72km transmission with dispersion compensation by FBG DCM unit for 4-channel 50 GHz spaced WDM-PON system with PAM-4 modulation format.

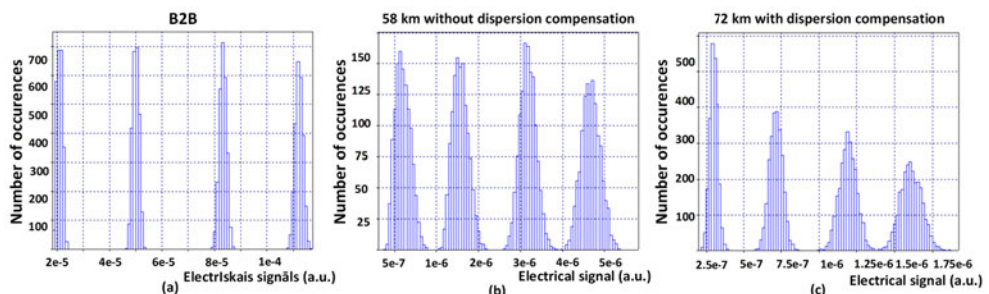


Figure 5. Histogram of the received signal (a) after B2B transmission, (b) after 58km transmission without the use of DCM module, and (c) after 72km transmission with dispersion compensation by FBG DCM unit for 4-channel 100 GHz spaced WDM-PON system with PAM-4 modulation format.

It was shown that maximal transmission distance with BER below FEC limit of 10^{-3} for 100 GHz spaced PAM-4 WDM-PON system can be increased by 15 km or 25.4% (from 59 to 74 km) if dispersion compensation with fiber Bragg grating FBG dispersion compensation module DCM is implemented. Moreover, in the case of 50 GHz channel spacing, which was minimal, ensuring BER $< 10^{-3}$, maximum transmission system reach can be increased by 14 km or 24% (from 58 to 72 km) by using additional dispersion compensation with FBG-DCM.

3.3 Evaluation of 4-PAM, EDB and NRZ modulation formats performance in WDM-PON optical access transmission system with a data transmission speed of 20 Gbit/s per wavelength

Instead of using widely used NRZ code with physical bandwidth limitations, an alternative solution to increase serial line rate is to use spectrally efficient multi-level signalling formats such as M-PAM, in our case PAM-4, where number 4 means different signal amplitude levels [38]. Another way to improve limited bandwidth capacity is using an electrical duobinary EDB modulation format. With this modulation format, transmission capacity will be increased by improving the bandwidth efficiency and reducing channel spacing [39]. As we know, Duobinary is a type of proficient multi-level modulation format and therefore is the area of interest due to its increased spectral efficiency. It is being used to increase the channel capacity by improving bandwidth utilization. The most important feature of this modulation format is usage for longer transmission distances without regeneration and high tolerance to chromatic dispersion influence [40].

Displayed results during this research are obtained by OptSim simulation software with the additional use of recognized numerical computing environment – Matlab software for BER estimation of received PAM-4 signals. At least 1024 simulated bits for all simulations to obtain a high accuracy level of bit error rate BER was chosen. Forward-error-correction (FEC) with 10^{-3} BER performance threshold allows the evaluation of the maximal transmission reach of the investigated transmission system [41].

To achieve *the goal - evaluate maximum transmission reach using different modulation formats: PAM-4, EDB and NRZ*, the 8-channel DWDM-PON simulation model was created. As shown in *Figure 6.*, a simulation scheme with different optical transmitters for the realization of each modulation format is shown. According to ITU-T G.694.1 DWDM frequency grid, the central frequency of 193.1 THz and channel spacing of 50 and 100 GHz is chosen for the simulation model. Therefore, the impact of crosstalk on investigated modulation formats was also evaluated. The optical line terminal OLT consists of eight transmitters (OLT_Tx) located in the central office CO. The first simulation model with PAM-4 modulation was performed with a 10 Gbaud/s symbol rate, providing 20 Gbit/s data rate per channel. PAM-4 signal is generated from two electrical data signals by coupling them, where one of them has a twice larger amplitude than the other. To obtain electrical data signals, two data sources with the same pseudo-random bit sequence PRBS and NRZ drivers for each electrical signal are used to generate two NRZ coded electrical signals with different amplitude levels.

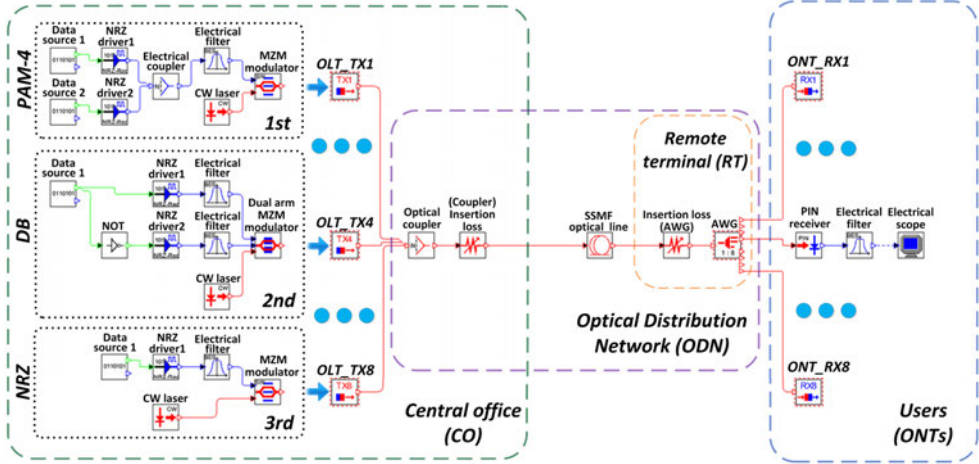


Figure 6. Simulation scheme of 8-channel PAM-4, EDB and NRZ modulated DWDM-PON optical transmission system with 20 Gbit/s transmission speed per channel.

Afterwards, both electrical signals are coupled with an electrical coupler and filtered with an electrical Bessel low-pass filter (3-dB bandwidth is 10 GHz) and sent to an external Mach-Zehnder modulator (MZM) [39].

The second simulation model with DB modulated transmission system was realized with a 20 Gbit/s data rate per channel. In simulation model data source element has one electrical output, where the output signal is divided into two electrical signals, where one of them is inverted by logical NOT element. Afterwards, output data signal and the inverted copy is sent to NRZ drivers, filtered by Bessel low-pass filters (3-dB bandwidth is 5 GHz), and passed to RF inputs of dual-arm Mach-Zehnder modulator, together forming the EDB transmitter [42].

The third simulation model is based on NRZ transmitter and realized with the same 20 Gbit/s data rate per channel as DB modulated transmission system. The transmitter consists of one NRZ driver with an electrical signal input of PRBS sequence and an NRZ coded output electrical signal. MZM provides electrical to the optical signal conversation of previously formed, and Bessel low-pass filter (3-dB bandwidth is 19 GHz) filtered electrical signal, passing from NRZ driver.

The following fixed parameters of optical and electrical elements was used in simulation models: continuous wavelength CW laser output power 6 dBm, extinction ratio 20 dB and 3 dB insertion loss of MZM, standard single-mode fiber SMF with dispersion coefficient 17 ps/(nm × km), dispersion slope 0.056 ps/nm² × km and 0.2 dB/km attenuation coefficient [43]. The bandwidth of electrical filters has been adjusted for optimal performance of each modulation format and have not been changed during research. As shown in **Figure 6.**, investigated transmission system model consists of eight channels coupled together using an optical coupler. ITU-T G.652 single-mode fiber is used for transmission in an optical distribution network ODN. After transmission in ODN, all channels are separated by demultiplexer based on arrayed waveguide grating AWG located in remote terminal RT, with an equal insertion loss of 3.5 dB for

all channels as mentioned before, simulations with various channel spacing of 50 or 100 GHz are obtained and analyzed for research of crosstalk impact. Each receiver of optical network terminal ONT consists of a 40 GHz PIN photodiode with sensitivity equal to -19 dBm at 10 Gbit/s reference bitrate, the dark current of 10 nA, and responsivity 0.8 A/W [44]. The optimal electrical bandwidth of the electrical low pass filter (LPF) was found. An electrical Bessel low-pass filter bandwidth was adopted for more successful system performance depending on the modulation format used. During the simulations Bessel LPF bandwidth of 15 GHz was chosen for PAM-4 modulated signals, 10 and 17 GHz for DB and NRZ modulated electrical signals, respectively. An electrical scope was used to measure received signal bit patterns quality, BER and eye diagrams.

The main target is to compare the performance of PAM-4, DB, NRZ modulated optical signals for use in DWDM-PON transmission system and to find out maximal network reach each particular modulation format. The BER threshold of 1×10^{-3} with assumed additional FEC for investigated transmission system was used to evaluate maximal achieved distance by each modulation format. BER of received PAM-4 signal was estimated offline through built digital signal processing DSP algorithm in Matlab software. In contrast, the BER of received DB and NRZ signals was estimated in the environment of OptSim simulation software by using a BER estimator based on statistical signal analysis.

The main results of our investigated transmission system performance are shown in *Figure 7*. During the simulations, it was observed that maximal achievable distance has minimal impact depending of chosen channel spacing 100 or 50 GHz, e.g. the impact of crosstalk on BER for all modulation formats was minor.

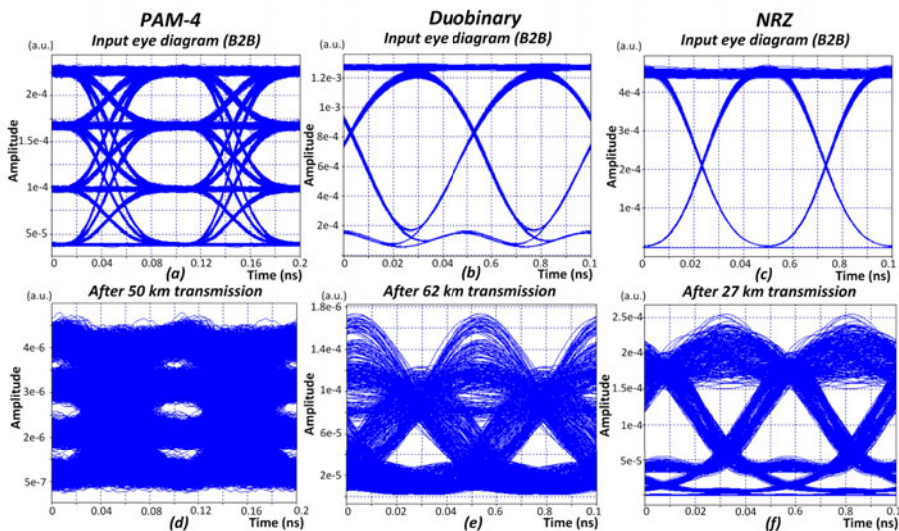


Figure 7. Eye diagrams of received (a) PAM4, (b) Duobinary and (c) NRZ signals after B2B measurement, and after maximal achieved transmission distance: (d) 50 km with PAM-4 modulated signal, (e) 56 km with DB modulated signal, (f) 27 km with NRZ modulated signal for 8-channel 50 GHz spaced DWDM-PON system operating at 20 Gbit/s bitrate.

Maximal reached transmission distance with 50 or 100 GHz channel spacing is almost the same for each modulation. However, higher spectral efficiency is achieved by 50 GHz spacing.

As one can see in *Figure 7(a-c)*, the signal quality of B2B measurements are good for all modulated signals providing error-free transmission with 50 GHz spacing. After transmission (see *Figure 7(e)*), the BER of the received EDB modulated signal was 3.7×10^{-4} with a maximum reached distance of 62 km. PAM-4 and NRZ modulation demonstrates (see *Figure 7(d)* and *Figure 7(f)*) 50 km and 27 km maximal transmission distance, where the BER of received signals was 5.8×10^{-4} and 3.1×10^{-4} , respectively. As one can see from results (*Figure 7.*), the largest network reach was provided by EDB modulation format, which extends the reach of optical network up to 62 km, ensuring $BER < 10^{-3}$. PAM-4 modulation format provided successful transmission over up to 50 km and NRZ up to 27 km long SSMF optical spans with BER below the defined threshold.

As shown by simulation results with narrowest 50 GHz channel spacing, the use of DB modulation format extends the reach of an optical link allowing to achieve maximal transmission distance of 62 km, ensuring $BER < 10^{-3}$ threshold. *PAM-4 modulation format demonstrated the second-best result ensuring the $BER < 10^{-3}$ at 50 km optical line length. EDB format allowed extending the maximum reach of an optical link by an extra 12 km or 19% compared to the four-level pulse amplitude modulation format. The worst system performance was shown by NRZ modulation format, demonstrating 27 km maximal reached transmission distance.* This can be explained by mainly the impact of chromatic dispersion. Investigated EDB and PAM-4 modulation formats showed the best performance in achieving the maximal distance of the optical transmission system, although comparatively spectral efficient PAM-4 modulation can provide higher data transmission speeds in fiber optical networks with limited bandwidth.

3.4 Evaluation of spectrally efficient transmission of IM/DD 10G PON with data rates up to 56 Gbit/s per wavelength using alternative multilevel modulation formats

As 10G PON systems are not capable of supporting future services, especially in the fifth generation 5G mobile networks, 25G is the next evolution step that must be taken [45]. However, it is unclear which means will be used to make it. Recent ITU-T recommendations for passive optical networks PONs, ITU-T G.9807.1 (symmetric 10G PON (XG(S)-PON)) and ITU-T G.989 (next-generation PON2 (NG-PON2)) describe transmission requirements for line rates of up to 40 Gbit/s per channel, while new recommendations for higher line rates (e.g., G.HSP.Req, G.HSP.comTC, G.HSP.50Gpmd, G.HSP.TWDMpmd) are under active development [46]–[48]. The enhancements being discussed for the next-generation PON standards include the increase in channel line rates from 10 to 25 Gbit/s [24]. Now, the 100G-EPON standard is still under development by the Institute of Electrical and Electronics Engineers (IEEE) P802.3ca Task Force. It is intended to scale up to 25 Gbit/s or 50 Gbit/s per single lane capacity while reusing the existing infrastructure of 10G-EPON [48]–[50]. Overall, the future PON is currently under development and standardization for future broadband network solutions beyond 10 Gbps [51]–[53]. The

evolution towards higher line rates is mainly driven by point-to-point (P2P) connections and wireless fronthaul, e.g., the next generation of mobile cellular networks (i.e., 5G and beyond 5G), where a 25 Gbps could be needed soon for either backhauling or new interfaces supporting the functional splits. The x-haul of these mobile cellular networks is expected to be centralized and based on a point-to-point P2P WDM-PON architecture [7], [46], [54]. However, due to cost considerations and commercial viability, it is desired to re-use some components from 10 Gbit/s transceivers operating in 10G PONs [55]. Bandwidth limitations from electrical and electro-optical components increase significantly due to the utilization of signals with higher line rates.

Nevertheless, such elements/components are crucial for component vendors as their re-use reduce development costs. For example, a cost of an optical line terminal OLT transmitter is about twice the cost of the receiver and modulator of the optical network unit (ONU), which represents the major part of the transceiver cost. Therefore, the operational capabilities of the bandwidth-limited transceivers have received considerable attention from component vendors, optical network operators, and research communities [23], [25], [32], [54]. The choice of a modulation format plays a critical role in the performance of HS-PON systems to provide the necessary line rate for the end-users [41]. It seems unreasonable that coherent technology for such relatively low rates could penetrate this market segment at this time, despite the potential sensitivity and optical power budget (OPB) improvements. Therefore, it is assumed that IM/DD formats will be used to deliver 25G or even 50G over a 20 km long single-mode fiber, i.e., the conventional PON configuration. For some applications, shorter fibers are also considered (e.g., 10–15 km when PON-based fronthauling solutions for 5G are on the table) but some require a substantially more extended reach (up to 40 km) [24], [54].

The desire for multi-level signaling formats such as Electrical Duobinary EDB and Pulse-Amplitude Modulation (PAM) have been preferred to their advantages in terms of simpler transmitter and receiver structure for HS-PONs. Coexistence with 10G PON technologies and reuse of the deployed optical distribution network ODN are among the main challenges for upgrading to new generation PON systems. Technically, it requires that the optical budget OPB, which determines the maximum tolerable optical loss between an optical line terminal OLT and an optical network unit ONU, must be compliant to E1 or E2 class. Firstly, optical amplifications can be performed to compensate for the sensitivity degradation, either with a praseodymium doped fiber amplifier (PDFA) as a booster in the OLT, or with a semiconductor optical amplifier (SOA) as a pre-amplifier in the ONU. The optical power budget of 35 dB is demonstrated in [53], [56], where both such optical amplifiers are used for the 25 Gbps PAM-4 downstream transmission. Although they achieve a higher optical power budget, the PDFA provides more than 10 dB gain. Furthermore, the attribution of digital post-equalization is not discussed. Digital equalization techniques, such as linear feed-forward (FF) equalizer or decision feedback (FB) equalizer, can help overcome the transceiver and link induced ISI.

This research part aims to bridge the knowledge gap by countifying the gain that digital signal post-equalization has on the optical power budget in IM/DD PONs with NRZ-OOK, EDB, PAM-4, and PAM-8 formats. In this research, is considered a PON architecture based on point-to-

multipoint passive optical power splitting in the ODN and focus on the downstream transmission at data rates above 25 Gbit/s over a single wavelength in the C-band. Furthermore, as the receiver's bandwidth is 8 GHz, it is investigated whether components intended for the 10G operation can be used for 25+ Gbps operation. This enables the full compatibility with XG(S)-PON and 10G-EPON and leads to smooth migration of customers to higher data rates in a cost-effective way.

The experimental setup of a 25+ Gbps IM/DD PON system is shown in *Figure 8*. It resembles a PON architecture based on point-to-multipoint passive optical power splitting in the outside distribution network. Downstream transmission at data rates above 25 Gbit/s over a single wavelength in the C-band is considered. It is fully compatible with XG(S)-PON and 10G-EPON, and thus, it enables smooth migration of customers to higher data rates without needing to change the ODN. Furthermore, the system's throughput can be increased by exploiting the WDM technique and adding new wavelengths as required. In the OLT, the output of a continuous-wave laser source CW operating at 1550 nm wavelength is connected to the dual-arm Mach-Zehnder modulator (MZM, Sumitomo, T.DEH1.5-40-ADC). An $S_1(t)$ input of the MZM, having a 3 dB bandwidth of 30 GHz, 9 dB insertion loss (IL), and 15 dB extinction ratio, is driven using analog waveforms from an arbitrary waveform generator (EAWG, Tektronix, AWG70001A) having 13 GHz analog bandwidth, up to 50 GSa/s sample rate and 8 bits vertical resolution. These waveforms are obtained using a $2^{15}-1$ long pseudo-random bit sequence (PRBS15) and bit-to-symbol (B2S) mapping performed in MATLAB prior to the digital-to-analog conversion (DAC). The electrical signal after the output of the AWG was linearly amplified by an electrical broadband amplifier (EA) and fed into the electrical RF input of one arm of the dual-drive MZM. The second arm was loaded with a 50-Ohm load. To optimize the BER performance, we adjusted a bias voltage of the MZM. In such a way, we impact the MZM's chirp parameter. This adjustment ensures the best possible performance in terms of the dispersion-tolerance, which directly impacts signal quality. Note that the modulator's chirp is a key factor enabling dynamic tunability of the transmission reach in IM/DD-based optical fiber links [57]. After the MZM, the modulated optical signal is coupled into the feeder fiber and transmitted over a 21 km long standard single-mode fiber SMF link. The input optical power of +4 dBm ensures the ODN compliance to the E1 (18–33 dB) power budget class for several modulation format alternatives. After the downstream transmission, the optical signal is passively split by a 1-to-N (1:N) optical power splitter. In an ONU, the split optical signal is pre-amplified by an SOA (Samsung Electronics, OA40B3A, InP/InGaAsP, 1550 nm) prior to the detection

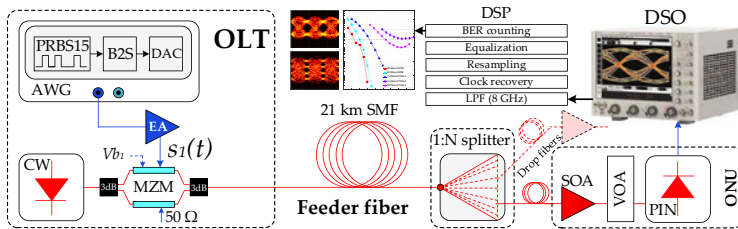


Figure 8. Experimental setup of the 25+ Gbps IM/DD PON system used for the power budget comparison.

The variable optical attenuator (VOA), placed before the receiver, is used to adjust the received optical power required for the OPB assessment and to protect it from overload. The receiver consists of a photodiode (PIN, Discovery, DSC-R409, 30 GHz, 0.7 A/W) and a digital storage oscilloscope (DSO, Agilent Technologies, DSOX93304Q, 33 GHz, 80 GSa/s). The DSO is used to limit the receiver's minus 3 dB bandwidth to 8 GHz using a 4th order Bessel–Thompson filter to digitize the received waveforms and store the digitized for further post-processing. The applied low-pass filtering LPF is imposed to emulate the bandwidth limitations at the receiver's Rx side, aiming to investigate whether components intended for the 10G operation can be used for higher line rates. The offline digital signal processing DSP module consists of clock recovery, resampling, linear post-equalization (if considered), and bit-error-rate BER estimation. The signal is post-equalized by a linear symbol-spaced equalizer that uses feed-forward and feedback taps to compensate for analog imperfections. For BER estimation, direct error counting is used. It relies on the bit-by-bit comparison of the transmitted and received bit sequences. More than 10^5 bits are available for the BER estimation at the receiver.

Here is reveal how the signal post-equalization impacts the achievable optical power budget of the IM/DD PON system. Before optical power budget analysis, the summarized analyses for the pros and cons of transceivers exploiting the modulation formats of the interest (see [Table 1](#)). Aspects are evaluated such as spectral efficiency of the modulation scheme, power consumption (as a line card must supply enough electrical power), transmission reach (considering an MZM with non-zero chirp factor), and simplicity of the transmitter and receiver (considering the complexity of the driving circuits and pre-/post- processing requirements).

Table 1.

Pros and cons of transceivers exploiting the considered intensity modulation direct detection (IM/DD) schemes.

Modulation Format	Spectral Efficiency	Transmission Reach	Power Consumption	Transmitter Simplicity	Receiver Simplicity
NRZ	-	-	+	++	++
EDB	+	++	-	-	-
PAM-4	++	++	--	--	--
PAM-8	+++	+	--	--	--

For the optical power budget assessment, the conventional BER curves show how pre-FEC BER values change with the received optical power. Two different pre-FEC BER criteria are considered: (i) a 7% overhead (OH) HD-FEC threshold of 3.8×10^{-3} and (ii) a 20% OH soft-decision (SD) FEC threshold of 2×10^{-2} . It is assumed that an FEC code can correct all errors for the pre-FEC BER below 3.8×10^{-3} .

[Figure 9](#). shows BER curves and eye diagrams for the 28 Gbaud OOK/EDB/PAM-4 and 14 Gbaud PAM-4/8 modulated signals in the IM/DD PON systems. First, the system performance without any post-equalization ([Figure 9\(a\)](#) and [Figure 9\(c\)](#)) is analyzed, and then, focus on improvements that the linear post-equalization offers ([Figure 9\(b\)](#) and [Figure 9\(d\)](#)) is obtained.

The optical power budget values (together with the corresponding values of the available power margin) obtained for all considered cases are summarized in *Table 2*. For the power margin calculation, the insertion loss of 4.4 dB for the feeder fiber, 17.3 dB for the 1:32 optical power splitter, and 2.2 dB for the drop fiber is assumed. A negative power margin (as for the 28 Gbaud PAM-4) means that the splitting ratio of 1:32 is not supported. Note that the average insertion loss of 1:16 splitter is at least 3 dB lower, which enables the 28 Gbaud PAM-4 alternative.

Table 2.

Optical power budget and available power margin for the explored alternatives and post-equalizer structures (number of FF and FB taps).

Signals	w/o	4-FF	9-FF&5-FB	43-FF&21-FB
28 Gbaud OOK	-	29 dB/5.1 dB	31 dB/7.1 dB	31 dB/7.1 dB
28 GBaud EDB	27 dB/3.1 dB	29 dB/5.1 dB	30 dB/6.1 dB	30 dB/6.1 dB
14 Gbaud PAM-4	26 dB/2.1 dB	27 dB/3.1 dB	27 dB/3.1 dB	27 dB/3.1 dB
14 Gbaud PAM-8	-	-	-	-
28 Gbaud PAM-4	-	-	22 dB/-1.9 dB	23 dB/-0.9 dB

In the configuration without the post-equalization, the HD-FEC requirements are met for two cases: (i) 28 Gbaud EDB and (ii) 14 Gbaud PAM-4. These signal formats allow achieving the HD-FEC requirements and the optical power budget of 27 dB and 26 dB, respectively. Even for the 14 Gaud PAM-8, the linearity is acceptable, and only a high signal-to-noise ratio SNR requirement hinders to reach the HD-FEC performance. A dispersion-induced power fading degrades the performance for the 28 Gbaud OOK and PAM-4, and chromatic dispersion compensation or signal equalization must be applied to reach the BER threshold of 3.8×10^{-3} . To test this, a linear equalizer whose structure consists of 43-FF&21-FB taps. The number of taps is chosen to maximally improve the system's performance by tackling the bandwidth limitations due to the receiver's side bandwidth and chromatic dispersion. Note that linear equalization using FF taps only is implemented to overcome bandwidth limitations and ISI, whereas FB taps are added to the structure to improve the performance in the presence of noise.

The results show that such post-equalization (43-FF&21-FB taps) significantly improve the BER performance, and thus, it enhances the optical power budget as compared to the previous case without the post-equalization. The optical power budget of the 14 Gbaud PAM-4 is increased by 1 dB. The corresponding value for the 28 Gbaud EDB is 3 dB. More importantly, the post-equalization enables more options of the modulation format alternatives. The HD-FEC requirement is met for the 28 Gbaud OOK and 28 Gbaud PAM-4 modulations. Moreover, the signal quality is so good that it allows achieving the optical power budget of 31 dB and 23 dB, respectively. Although the BER improvement is not enough to meet the HD-FEC requirements for the 14 Gbaud PAM-8 signals, its BER curve approaches to the threshold and a slight SNR improvement, e.g., using a nonlinear equalization, would aid in meeting this requirement. *Figure 9(d)* shows the corresponding eye diagrams captured for received optical power values that allow detecting signals with the BER below 3.8×10^{-3} or close to it as in the 14 Gbaud PAM-8 case.

Next and to better explore the impact that post-equalization has on the optical power budget and to emphasize its importance, was used three equalizer configurations and compare the OPB for each of them: (i) without post-equalizer, (ii) post-equalizer with only 4-FF taps, (iii) 9-FF&5-FB taps. **Figure 10.** presents the results for scenarios whose combination of data rates and modulation formats ensures line rates no higher than 28 Gbit/s—28 Gbaud OOK/EDB and 14 Gbaud PAM-4, while **Figure 11.** includes the 14 Gbaud PAM-8 and 28 Gbaud PAM-4. **Figure 10.** shows that an equalizer with just 9-FF&5-FB taps significantly improves the performance of the 28 Gbaud OOK system.

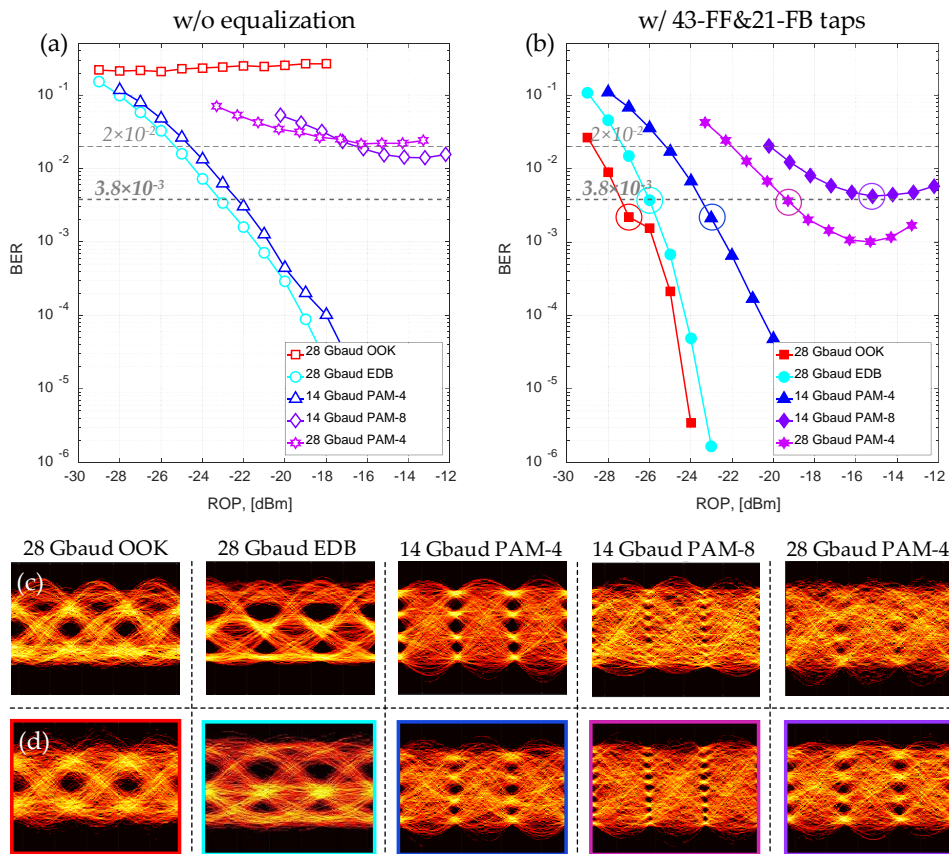


Figure 9. Quality of transmission (QoT) characteristics for the 28 Gbaud OOK, 28 Gbaud EDB, 14 Gbaud PAM-4, 14 Gbaud PAM-8, and 28 Gbaud PAM-4 signals in the IM/DD PON system: (a) BER vs. received optical power (ROP) before the digital post-equalization; (b) BER vs. ROP after the digital post-equalization employing 43-FF&21-FB taps; (c) eye diagrams captured in the ONU at the highest ROP and before the digital post-equalization; and (d) eye diagrams captured in the ONU and ROP values that ensure $BER < 3.8 \times 10^{-3}$ after the digital post-equalization.

The optical power budget is 29 dB, which is by 2 dB smaller as compared to the case with 43-FF&21-FB taps. Unfortunately, only FF taps are not able to provide the necessary improvement to meet the pre-FEC BER requirement. At -18 dBm of the received optical power, the BER approaches but does not cross the defined threshold. As for the 14 Gbaud PAM-4 and 28 Gbaud EDB, an equalizer with just 4-FF taps is enough to improve the performance and leads to a higher sensitivity—by 1 dB and by 3 dB, respectively. Using a more complex structure with more taps does not enhance the performance, and the optical power budget remains unchanged.

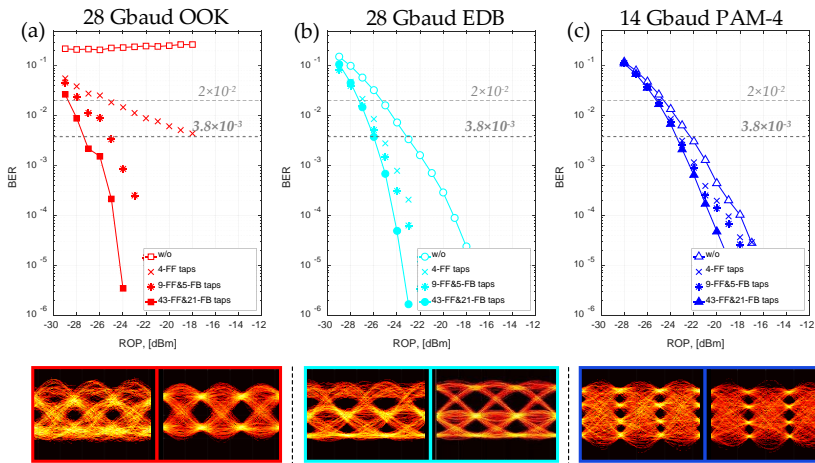


Figure 10. Plots of BER vs. ROP and post-equalizer structure for the (a) 28 Gbaud OOK, (b) 28 Gbaud EDB, and (c) 14 Gbaud PAM-4 signals accompanied by the corresponding eye diagrams captured in the ONU before and after digital post-equalization employing 43-FF&21-FB taps.

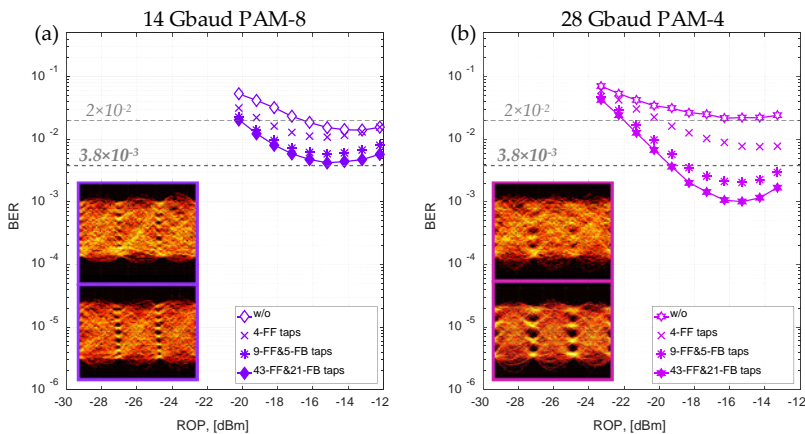


Figure 11. Plots of BER vs. ROP and post-equalizer structure for the (a) 14 Gbaud PAM-8 and (b) 28 Gbaud PAM-4 signals accompanied by the corresponding eye diagrams captured in the ONU before and after digital post-equalization employing 43-FF&21-FB taps.

Further, is explored two scenarios—14 Gbaud PAM-8 and 28 Gbaud PAM-4—ensuring a higher line rate (42 Gbps and 56 Gbps, respectively). *Figure 11(a)* shows results for the 8-level PAM signals, 14 Gbaud PAM-8, which was used to test the MZM driver linearity. The obtained eye diagrams evidence their good linearity as signal levels are equally distributed, but we see that the system is SNR limited as the upper and lower eyes are noisy. Therefore, applying even strong linear post-equalization (i.e., using 43-FF&21-FB taps) does not improve the quality significantly to fulfil the performance requirement, although the BER approaches the threshold of 3.8×10^{-3} . Finally, *Figure 11(b)* shows that the linear equalization with 9-FF&5-FB taps is sufficient to fulfil the HD-FEC BER requirements and reach the optical power budget of 22 dB for the 28 Gbaud PAM-4 alternative. A more complex structure of the equalizer does not provide significant improvements neither in terms of the signal quality nor in the optical power budget. The system is partially SNR limited. Insets in *Figure 11(b)* show the best eye diagrams for the configuration without the equalizer and with 43-FF&21-FB tap equalizer. The latter has a relatively large eye-opening. The fact that the BER threshold of 2×10^{-2} is met for all considered modulation format alternatives proves the viability of IM/DD formats to be used in HS-PON solutions delivering 25+ Gbit/s or even 50+ Gbit/s in commercial PONs if SNR improvement and modulator chirp management are achieved.

The obtained results show that (i) 10G PON component bandwidth is enough to achieve net-rates above 25 Gbit/s; (ii) linearity of the optoelectronic components allows operating them using schemes with multilevel modulation formats; and (iii) in combination with the digital signal post-equalization, the obtained optical power budget is compliant with E1 class (OPB = 18–33 dB). The 28 Gbaud EDB and 14 Gbaud PAM-4 schemes can be used in PONs even without any post-equalization. The signal quality is such that it fulfils the HD-FEC requirement and ensures a power margin of 3.1 dB. For the 28 Gbaud NRZ-OOK, an equalizer with FB taps is required; a 9-FF&5-FB tap equalizer helps to overcome ISI in the presence of noise, which leads to the optical power budget of 29 dB. Finally, data rates up to 56 Gbps can be supported by the PON employing the PAM-4 modulation. Although a 1:32 splitting ratio might not be feasible due to high insertion loss of such a splitter, it provides the optical power budget of 23 dB. Therefore, the considered IM/DD PON alternatives together with digital signal equalization has the potential to ensure the sustainability for future PONs with line rates well beyond 25 Gbit/s in the access segment of optical networks.

4 IMPACT ASSESSMENT OF THE USED OPTICAL TRANSMISSION ENVIRONMENT FOR THE RECEIVED SIGNAL QUALITY TO DEVELOP A HIGH-SPEED SPECTRALLY EFFICIENT WDM-PON BROADBAND TRANSMISSION SYSTEM

4.1 Realization of WDM-PON fiber optic transmission system for performance evaluation depending on the data transmission rate up to 32 Gbit / s per channel and the total optical line length

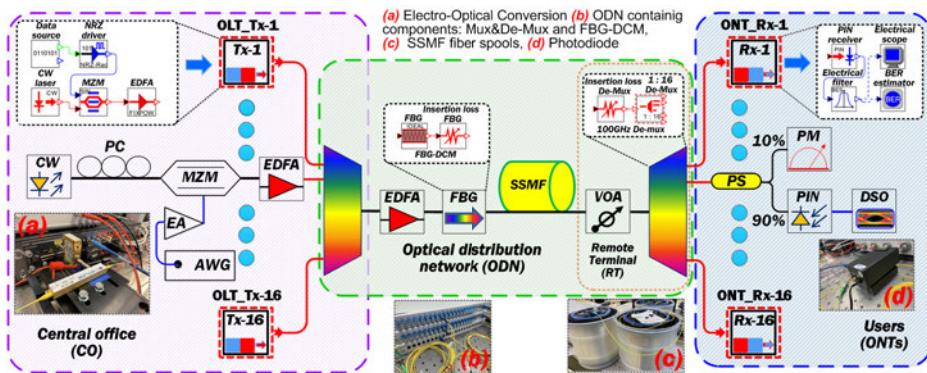
Third-generation fiber-to-the-x (FTTx) will introduce wavelength division multiplexing WDM technology to increase data rates up to 40 Gbit/s and coexist with current communication systems. WDM passive optical network WDM-PON based fiber-to-the-home (FTTH) system architecture together with the Next-generation passive optical network (NG-PON) can provide a solution related to nowadays problems with transmission capacity. It is expected that NG-PON systems will become more cost-efficient at high per-user data rates, providing different transmission speeds for end users based on the pay-as-you-grow approach.

Accordingly, wavelength division multiplexed passive optical access networks WDM-PONs can be the best solution to modern capacity-related problems and support high data rates providing large distance coverage between network nodes to keep up with the increasing demand traffic [3]–[4]. The wavelength division multiplexing WDM technique is a solution to deal with Internet traffic by using the bandwidth of optical fiber more effectively. It is considered a definitive solution for future telecommunication infrastructure upgrades, providing almost unlimited bandwidth to each subscriber. WDM-PON based fiber to the home FTTH system architecture can compete with the Next-generation passive optical network NG-PON solution related to current problems of transmission capacity [58]–[59].

Chromatic dispersion CD is a fundamental problem in optical transport networks [41]. The distortion of the signal leads to intersymbol interference, resulting in data losses and traffic interruption. In order to protect the signal from losses and affection of CD during transmission in optical fiber, appropriate technique by dispersion compensation based on fiber Bragg gratings FBG can save costs and meet the technical requirements needed to facilitate higher data rate optical transport network [60]. The main advantage of using fiber Bragg grating FBG dispersion compensation module DCM is low insertion loss and greater power capacity without introducing additional non-linear signal effects. They have become a key factor, along with erbium-doped fiber amplifiers (EDFAs) increasing broadband fiber optics transport networks [61]–[62]. The introduced system model is used to obtain the system performance for different operating data rates of up to 32 Gbit/s per downstream transmission channel. *The purpose of this research was to evaluate the performance of investigated 100 GHz spaced WDM-PON transmission system with the most often used transmission speeds of up to 32 Gbit/s per channel and obtain the maximum reach of the system with chromatic dispersion CD compensation, under the condition that it is still possible to achieve forward error correction pre-FEC BER of 1×10^{-3} .*

Firstly experimentally, single-channel passive optical network PON performance after 80 km transmission through standard single-mode fiber (SSMF) span, with additional use of implemented dispersion compensation module FBG-DCM, is shown. Secondly, the additional effect of crosstalk is obtained with a simulative-experimental model. The purpose of the experimental section was to observe experimental system physical parameters and the impact of used components. Therefore, the properly adjusted 16-channel WDM-PON transmission system model was created in the newest RSoft OptSim simulation software.

The experimental system part is represented in *Figure 12*. The output of the laser source with 8.49 dBm output power at $\lambda = 1552.605$ nm is connected to the Mach-Zehnder modulator MZM input. A polarization controller (PC) is placed before the MZM to reduce polarisation-dependent losses. An MZM (bias point 3.14 V) is driven at data rates of 10 Gbit/s up to 32 Gbit/s by a 2^9 long pseudo-random bit sequence (PRBS-9) non-return-to-zero NRZ signal from an electrical arbitrary waveform generator EAWG. The modulated output from the MZM is being amplified by fixed output power (fixed +10 dBm output power) erbium-doped EDFA. Then 100 GHz spaced arrayed waveguide grating AWG multiplexer filters out particular optical channels. The output of the multiplexer is connected to the input of the second EDFA with fixed +14 dBm output power and transmitted through 80 km long ITU-T G.652 rec. standard SMF section with additional CD pre-compensation by tunable FBG-DCM, which has 3 dB insertion loss at 1550 nm wavelength. After the ODN transmission part, the 100 GHz spaced AWG de-multiplexer is connected through a variable optical attenuator VOA. The output of the AWG de-multiplexer's central channel (193.1 THz) is connected to a 50 GHz photodiode PIN. The detected electrical signal is sent to a digital storage oscilloscope DSO to analyze the signal - display the eye diagrams, and perform BER measurements. Research is divided into two parts: 1st experimental part, where



CW: Continuous wavelength laser source, PC: polarization controller, MZM: Mach-Zehnder modulator, AWG: arbitrary waveform generator, EA: electrical amplifier, EDFA: erbium-doped fiber amplifier, FBG-DCM: fiber Bragg grating dispersion compensation module, SSMF: standard single mode fiber, VOA: variable optical attenuator, PS: power splitter, PM: optical power meter, PIN: photodiode, DSO: digital storage oscilloscope.

WDM-PON system parameters:

- 16 WDM channels
- NRZ coding
- CD compensation with FBG-DCM
- Channel spacing $\Delta f = 100$ GHz
- Optical line length $L = 40/80$ km and \geq (maximal achievable distance)
- Transmission speed per channel $R = 10, 20, 25, 28, 32$ Gbit/s

Figure 12. An experimental model of NRZ-OOK modulated up to 32 Gbit/s per channel WDM-PON optical transmission system.

we obtain limiting factors of physical parameters and impact of components used in WDM-PON designed transmission system model and 2nd part, investigation of the simulation model with improved system capacity up to 16 channels, allowing us to observe the effect of crosstalk and non-linear optical effects NOE [63]. As shown in *Figure 12*, the investigated WDM-PON simulation scheme consists of 16 channels. According to ITU-T G.694.1 rec., the channel spacing is chosen 100 GHz, and the central frequency of the middle channel is 193.1 THz ($\lambda = 1552.524$ nm), which is based on experimentally used one [64].

According to PON architecture, the proposed simulation model central office CO consists of an optical line terminal OLT with sixteen transmitters (OLT_Tx). Each particular OLT_Tx transmitter based on widely used NRZ line code consists of a data source element with 2⁹ long pseudo-random bit sequence PRBS9 connected to the NRZ driver. The coded electrical output signal is directly sent to MZM, converting electrical to the optical signal. Continuous wavelength CW laser with + 8.49 dBm output power was used for each transmitter. Optical signals from each OLT_Tx are coupled together using optical AWG multiplexer with 100 GHz channel spacing, 3.5 dB insertion loss at 1550 nm wavelength, and a 3-dB bandwidth of 80 GHz. Afterwards, coupled signals are amplified by fixed output power (fixed +14 dBm output) EDFA.

According to ITU-T G.989.2 Next-generation PON standard (NG-PON2) definition of optical distribution network ODN length, we have chosen 40 km and twice larger 80 km optical fiber transmission distances [46]. An ITU-T G.652 optical fiber SMF with 17 ps/(nm×km) dispersion coefficient and 0.2 dB/km insertion loss (at 1550 nm reference wavelength) was used in our research. CD pre-compensation by fiber Bragg grating-based dispersion compensation module (FBG-DCM) is realized for coupled channels before transmission through transmission fiber span. An additional attenuator with 3 dB attenuation is used to implement FBG-DCM insertion loss. After transmission through the SMF optical transmission line, all-optical channels are separated by AWG de-multiplexer located in remote terminal RT, with 100 GHz channel spacing, 3.5 dB insertion loss, and 3-dB bandwidth 80 GHz. The receiver consists of optical network terminals ONTs, where each receiver (ONT_Rx) consists of a 50 GHz PIN photodiode based on experimentally used one, with sensitivity equal to +4 dBm, dark current of 10 nA and responsivity

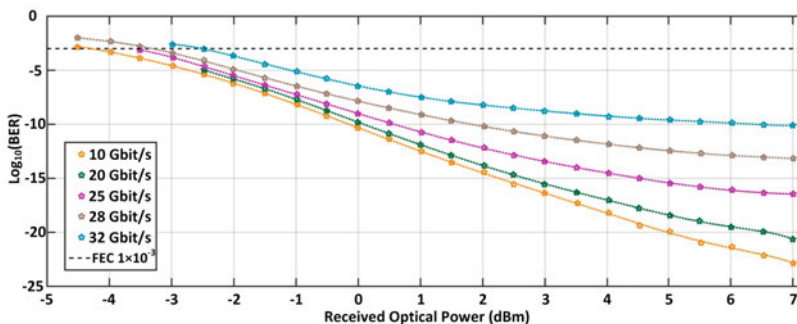


Figure 13. Comparison of experimentally measured BER versus received optical power for investigated single-channel PON transmission system with data rate of up to 32 Gbit/s with use of FBG-DCM module for ODN length of 80 km.

of 0.7 A/W [65]. The optimal 5-pole electrical Bessel low pass filter LPF bandwidth was found for each operating bitrate based on the most successful system performance. An electrical scope and BER estimator were used during simulations to measure received signal bit patterns quality. The *Figure 13*. shows experimentally obtained BER of the transmitted signal with data rate of up to 32 Gbit/s versus received optical power at PIN after 80 km transmission through ODN. The measured optical output power after transmission through 80 km ODN length varied from -4.5 to 7.1 dBm, where the BER of received NRZ-OOK signals was from 1.2×10^{-2} to 1.4×10^{-23} .

The obtained BER of the operating data rate of up to 32 Gbit/s for 100 GHz spaced 16-channel wavelength division multiplexed WDM-PON passive optical transmission system in response to received optical power at PIN receiver is shown in *Figure 14*. in two different scenarios – with 40 and 80 km of SMF fiber length.

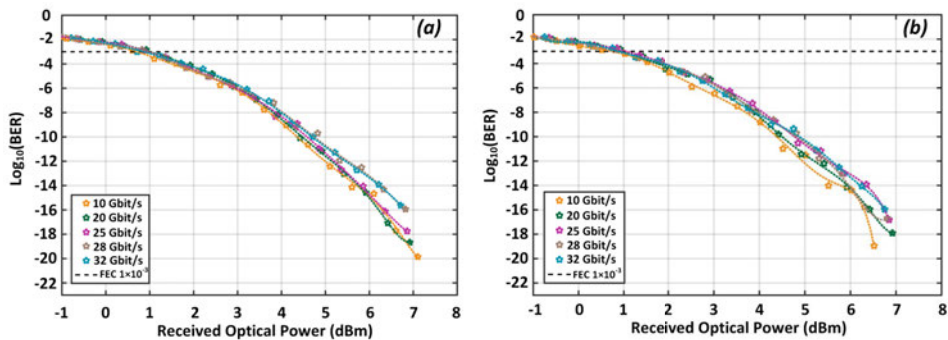


Figure 14. Comparison of measured BER versus received optical power with use of DCM module for ODN length of (a) 40 km and (b) 80 km for investigated 16-channel WDM-PON transmission system at operating bitrate up to 32 Gbit/s per channel.

Applying for shorter transmission distances of ODN part, it is possible to decrease impact of NOE effects in the optical fiber link. In the scenario with a shorter fiber link length (40 km), the gain of the second used EDFA was reduced to 8 dBm, respectively. The measured optical output power after transmission through the 40 km ODN part varied from -1.1 to 7.1 dBm, where the BER of received NRZ-OOK signals was from 2.2×10^{-2} to 5.2×10^{-20} (see *Figure 14(a)*). In the second scenario with 40 km SMF fiber ODN link in response to received optical power is shown in *Figure 14(b)*, where measured optical output power after transmission through 80 km ODN length varied from -1.1 to 7 dBm, where the BER of received signals was from 2.2×10^{-2} to 1.3×10^{-19} .

As shown in *Figure 15(a1-a5)*, in B2B configuration, the signal quality for all operating data rates is good, the eye is open, and error-free transmission is provided. After 80 km transmission in an experimental and simulative environment, the obtained simulative-experimental results are mainly similar (see *Figure 15(b)* and *Figure 15(c)*). Performance comparison for investigated 100 GHz spaced 16-channel WDM-PON transmission system with transmission of operating data rates per channel of up to 32 Gbit/s through ODN part, with different lengths of 40 and 80 km SMF fiber spans is shown in *Figure 16*.

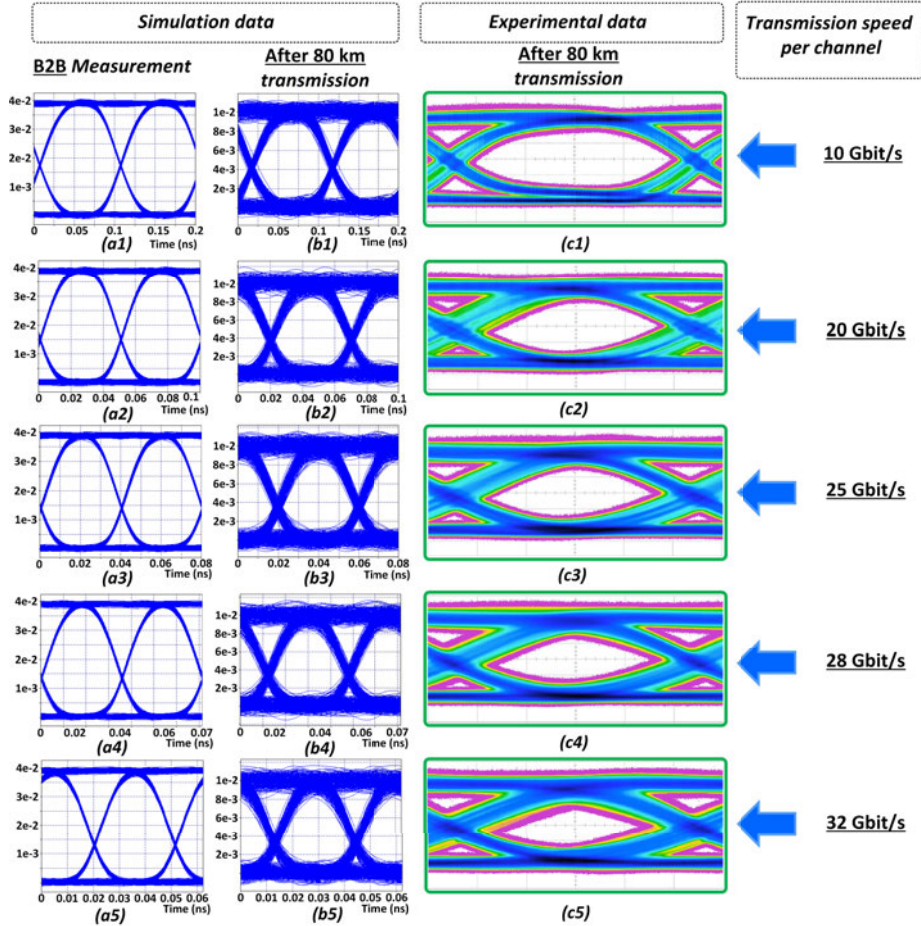


Figure 15. Eye diagrams of experimentally received signal: (a) after B2B transmission, (b) analyzed in OptSim simulation software environment after 80 km transmission with the use of FBG-DCM module and (c) after 80 km transmission with the use of FBG-DCM module for investigated PON transmission system with operating data rates of (1) 10 Gbit/s (2) 20 Gbit/s, (3) 25 Gbit/s, (4) 28 Gbit/s, (5) 32 Gbit/s per channel.

Additional losses in optical fiber line and effect of crosstalk and NOE on transmitted signals for longer distances of 80 km lead to performance decrease of 100 GHz spaced 16-channel WDM-PON transmission system, where the BER at operating 10 Gbit/s data rate per channel of the received signal (worst performing channel) was 1.3×10^{-19} (see **Figure 16(b1)**). After decreasing ODN length to 40 km the crosstalk and NOE effects are reduced significantly, where the BER of the channel with worst performance operating at 10 Gbit/s data rate was 5.2×10^{-20} (**Figure 16(a1)**). After transmission through ODN fiber length defined distances as 40 and 80 km, the BER at operating 32 Gbit/s data rate per channel of received signals was 1.1×10^{-14} and 1×10^{-14} (see in **Figure 16(a5)** and **Figure 16(b5)**).

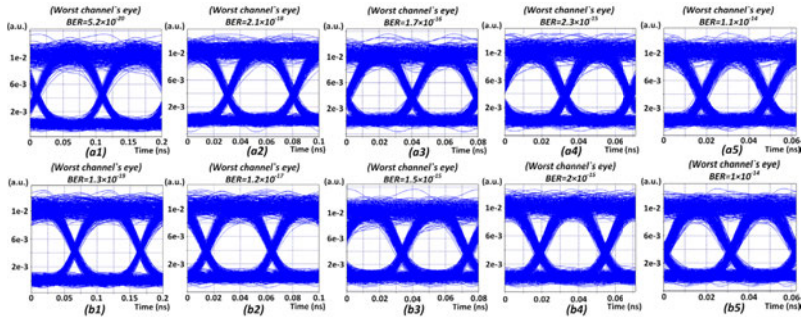


Figure 16. Eye diagrams of experimentally received signal with use of FBG-DCM module, (a) after 40 km transmission and (b) after 80 km transmission for investigated 16-channel WDM-PON transmission system at operating bitrate of: (1) 10 Gbit/s (2) 20 Gbit/s, (3) 25 Gbit/s, (4) 28 Gbit/s, (5) 32 Gbit/s per channel.

The purpose of this last section was to numerically evaluate the performance of NRZ-OOK modulated 100 GHz spaced 16-channel WDM-PON system together with implementation of dispersion compensation and find the maximum network reach per operating data rate. As mentioned before, the BER threshold in our investigated transmission system with assumed additional FEC is 10^{-3} . By using the FBG-DCM dispersion compensation technique, the maximum achievable transmission distance for the system operating at data rates of 25, 28, and 32 Gbit/s per channel was 105 km, where the BER of the received signal was 3.9×10^{-4} , 9.9×10^{-4} and 7.5×10^{-4} (see **Figure 17(c-e)**). As it is shown by simulation results with 10 Gbit/s operating data rate per channel for investigated 100 GHz spaced 16-channel WDM-PON transmission system, maximum achievable transmission distance was 109 km, where the BER of received signal was 8.1×10^{-4} , please see **Figure 17(a)**. The second-best result with 106 km maximal achieved transmission distance was with the operating data rate of 20 Gbit/s per channel, where the BER of received signal was 9.4×10^{-4} , please see **Figure 17(b)**.

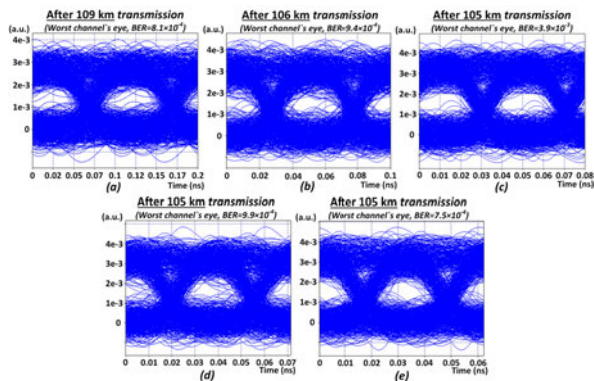


Figure 17. Eye diagrams of received signal after maximal achieved transmission distance with dispersion compensation by FBG-DCM module and operating bitrate of: (a) 10 Gbit/s (b) 20 Gbit/s, (c) 25 Gbit/s, (d) 28 Gbit/s, (e) 32 Gbit/s per channel for 4-channel 100 GHz spaced NRZ-OOK modulated WDM-PON transmission system.

4.2 Comparison of the performance of an experimental 40 km long DWDM-PON 4-channel transmission system with a total transmission rate of up to 160 Gbit / s depending on the applied DCF and FBG dispersion compensation methods and data transmission speed in the channel

With the massive deployment of coherent optical fiber transmission systems at 100 Gbit/s in backbone networks, the pressure has shifted to the metro networks. Intensity modulation with direct detection IM/DD transmission technique is preferred due to its advantages of low cost and easy implementation, where chromatic dispersion CD induced power fading is one of the key limiting factors in IM/DD transmission systems [66]–[69]. Chromatic dispersion CD is possible to compensate in both - optical or electrical domains. Depending on the optical domain dispersion profile, the effects of CD can be either removed locally by fiber Bragg grating FBG or can be compensated throughout the dispersion-compensating fiber DCF [66], [70].

In previous research, was concluded that intensity non-return-to-zero on-off keying NRZ-OOK modulation format, as well four-level amplitude modulation PAM-4 modulation format, which has higher spectral efficiency and potentially can provide higher data transmission speeds in fiber optical networks with limited bandwidth, are still affected with the chromatic dispersion CD, which is one of the main distance-limiting factors [41], [71].

The main purpose of this research is to evaluate the performance of experimentally developed dense wavelength division multiplexed DWDM transmission system and compare the most often commercially used CD compensation techniques such as CD compensation based on dispersion compensation fibers (DCF) and compensation based on fiber Bragg grating FGB dispersion compensation module DCM. The experimental 4-channel DWDM optical transmission system model is used to evaluate system effectiveness for different bitrates of up to 40 Gbit/s per wavelength and compare widely used techniques of CD post-compensation in terms of received signal quality, e.g. bit-error-ratio BER and eye diagrams.

The experimental system is shown in *Figure 18*. The output of four continuous-wave CW laser sources with channel spacing of 100 GHz with related 10 dBm output power for each particular source are coupled together by a 100 GHz spaced arrayed waveguide grating AWG multiplexer[64]. Polarization controllers (PC's) are placed before the multiplexer to reduce each laser source's polarisation-dependent loss. The output of AWG is connected to the input of the external Mach-Zehnder modulator MZM. An MZM (bias point 3.14 V) is driven at bitrates from 20 Gbit/s up to 40 Gbit/s by a 2^{11} long pseudo-random bit sequence (PRBS11) non-return-to-zero NRZ signal from an electrical arbitrary waveform generator EAWG.

The modulated output from the MZM is connected to the de-correlation module through a monitoring splitter (PS1) for measurements of the optical spectrum. The output of the de-correlation module with four separated and delayed WDM channels is amplified by the first erbium-doped fiber amplifier EDFA with fixed output power (+23 dBm) and transmitted through 40 km long ITU-T G.652 standard SSMF fiber span with dispersion coefficient 17.15 ps/(nm × km), dispersion slope 0.096 ps/nm² and 0.27 dB/km attenuation coefficient (at $\lambda=1550$ nm reference wavelength).

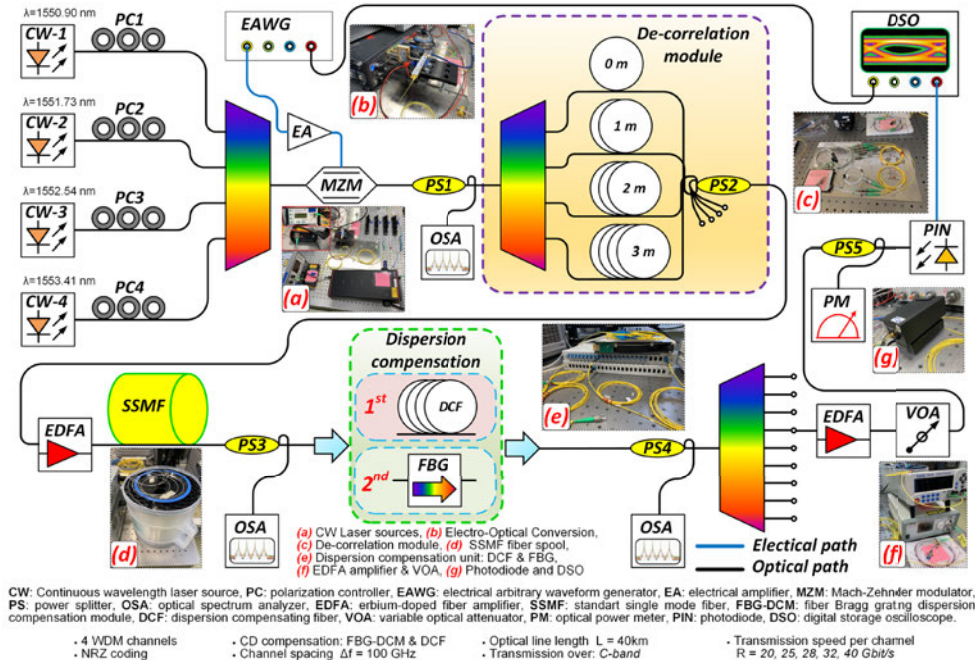


Figure 18. Experimental setup for comparison of the effectiveness of dispersion compensation techniques in 4-channel NRZ-OOK modulated DWDM optical transmission system with a total transmission capacity of up to 160 Gbit/s.

The monitoring splitters (PS3) after transmission through SMF fiber before dispersion CD post-compensation and (PS4) after CD post-compensation for optical spectrum measurements are also used. The CD post-compensation is consecutively investigated by using:

- Tunable fiber Bragg grating dispersion compensation module FBG-DCM, which has 3.5 dB insertion loss at $\lambda=1550$ nm wavelength, dispersion coefficient of -680 ps/(nm \times km);
- Dispersion compensation fiber (DCF) spool with a length of 5.684 km, which has 4.75 dB insertion loss (at $\lambda=1550$ nm reference wavelength) with dispersion coefficient of -686.76 ps/nm/km and -2.48 ps/nm² dispersion slope was used as well.

After transmission through SSMF fiber span and CD post-compensation, the 100 GHz spaced AWG de-multiplexer is connected to the second EDFA with fixed +10 dBm output power. The output of EDFA amplifier is connected to 50 GHz photodiode PIN with sensitivity equal to +4 dBm for BER of 10^{-12} , the dark current of 10 nA and responsivity of 0.8 A/W through a variable optical attenuator VOA for measurements of received signal bit patterns quality (e.g. eye diagrams) and BER [65].

To increase the capacity of the experimental communication system, the number of WDM channels was increased by implementing a symmetrical adaptive decorrelation SAD method [72],

[73]. MZM modulator used experimental transmission system is driven at bitrates from 20 Gbit/s up to 40 Gbit/s by a $2^{11}-1$ long pseudo-random bit sequence NRZ signal from an electrical arbitrary waveform generator EAWG. The output of four laser sources with a spacing of 100 GHz are coupled together by AWG multiplexer and sent to the MZM input. After MZM output, four 100 GHz spaced modulated optical channels are being separated with the de-correlation module, which consists of (1) 100 GHz spaced AWG de-multiplexer (De-MUX), (2) SMF optical fiber spans with different lengths, and (3) optical coupler (see [Figure 19](#)). After separation of modulated optical signals, the optical SMF fiber spans with different lengths are used for time delay, where 1-meter long optical fiber span is used for the second channel, 2 and 3-meters long SMF spans are used for third and fourth separated WDM channels.

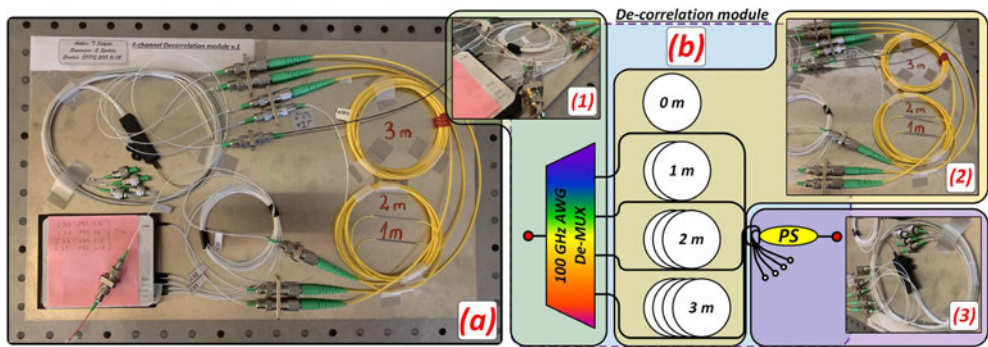


Figure 19. Setup of de-correlation module: (a) experimentally created, (b) schematics of channel separation principle, where such as optical components are used: (1) 100 GHz spaced AWG de-multiplexer, (2) SMF optical fiber spans, (3) 1×8 optical coupler.

The first output of AWG DE-MUX is connected directly to the coupler. After each optical channel has been de-correlated, all channels are combined by an optical coupler for further data transmission. Each transmitted bit length of the optical fiber according to the used bitrate is calculated by the following equation where SMF fiber core refraction index is 1.4682 at $\lambda=1550$ nm wavelength:

$$L = T \times \left(\frac{c}{n_g} \right) \times 100 \quad (1)$$

where, L – fiber length for 1 bit (cm);

T – bit duration (s);

c – light speed in vacuum (km/s);

n_g – optical fiber effective group index of refraction;

According to the bitrate (from 20 Gbit/s up to 40 Gbit/s) of the NRZ-OOK signal, the optical path length of 1 bit is shown in [Table 3](#)..

Table 3.

Optical path length for 1 bit of transmission

Bitrate (Gbit/s)	20	25	28	32	40
Fiber length for 1 bit transmission (cm)	1,02	0,81	0,72	0,63	0.51

Each separated modulated NRZ-OOK signal based on the used de-correlation technique accordingly by the used bitrate per channel with PRBS11 sequence has constant bitstream delay, please see **Table 4.**

Table 4.

PRBS11 delay in bits for transmission system by use of the de-correlation technique

Experimentally used bitrate Gbit/s						
Bitrate (Gbit/s)		20	25	28	32	40
PRBS delay (bits)	CH2	98	122	137	157	196
% of total PRBS length		5%	6%	7%	8%	10%
PRBS delay (bits)	CH3	196	245	274	313	392
% of total PRBS length		10%	12%	13%	15%	19%
PRBS delay (bits)	CH4	294	367	411	470	587
% of total PRBS length		14%	18%	20%	23%	29%

To determine the exact dispersion coefficient for the standard single-mode optical fiber used in the experimental part and determine the necessary length of DCF fiber spool for total accumulated dispersion compensation, CD measurements for SSMF fiber span were performed. Optical domain (OTDR) measurements for standard single-mode optical fiber span was also prepared to clarify the optical link section match of experimental 4-channel 100 GHz spaced NRZ modulated DWDM system according to ITU-T G.989.2 definition of optical distribution network ODN length. In experimental optical transmission system, second EDFA was used in terms to satisfy input optical power level of high power InGaAs 50 GHz PIN photoreceiver under high-speed up to 40 Gbit/s WDM transmission systems conditions, where post-amplification is not required, as PIN photo receivers neither avalanche photodiode (APD) with a much lower input power level are used [65]. According to OTDR verified measurements, the length for experimentally used SSMF fiber span is 42.13 km with 11.49 dB total insertion loss. The experimentally measured SMF fiber span chromatic dispersion coefficient and total chromatic dispersion depending on bandwidth in telecommunication S, C and L transmission bands are shown in **Figure 20(a)** and **Figure 20(b)**. As shown in **Figure 20.**, the standard single-mode optical fiber span measured dispersion coefficient and total dispersion at reference wavelength $\lambda=1550$ nm is 17.15 ps/(nm × km) and 688.71 ps/nm at dispersion slope of 0.096 ps/nm². The most suitable DCF optical fiber span was selected to perform accumulated dispersion compensation. Afterwards, after the most appropriate choice, optical domain OTDR measurements was prepared to the latest calculate achieved the maximum DWDM system's optical link sections length.

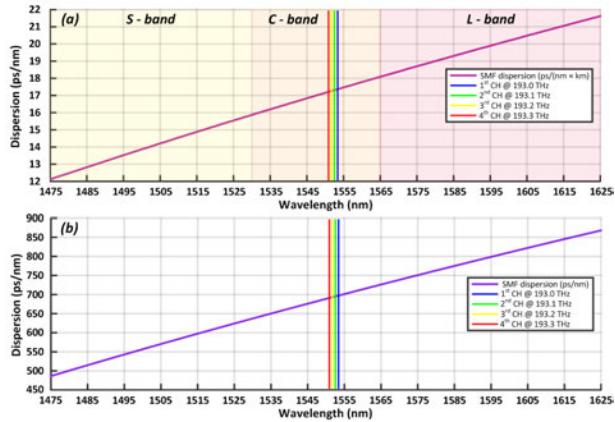


Figure 20. Experimentally measured SMF fiber span: (a) chromatic dispersion coefficient and (b) total chromatic dispersion depending on bandwidth and used wavelength.

According to verified OTDR measurements, it was concluded that the length of the experimentally used dispersion compensating fiber spool is 5.68 km with 4.75 dB total insertion loss of 0.83 dB/km. Experimentally obtained dispersion compensating fiber spool CD coefficient and total chromatic dispersion depending on bandwidth in telecommunication S, C and L transmission bands are shown in *Figure 21(a)* and *Figure 21(b)*. As shown in *Figure 21.*, the DCF fiber spool measured dispersion coefficient and total dispersion at reference wavelength $\lambda=1550$ nm is -123.06 ps / (nm \times km) and -697.82 ps/nm at -2.48 ps/nm² dispersion slope. DCF fiber gives the opportunity to increase the length of our 4-channel 100 GHz spaced DWDM optical transmission system for an additional 45.68 km or extra 13.5 % and achieved that the maximum DWDM system's link length of 47.81 km.

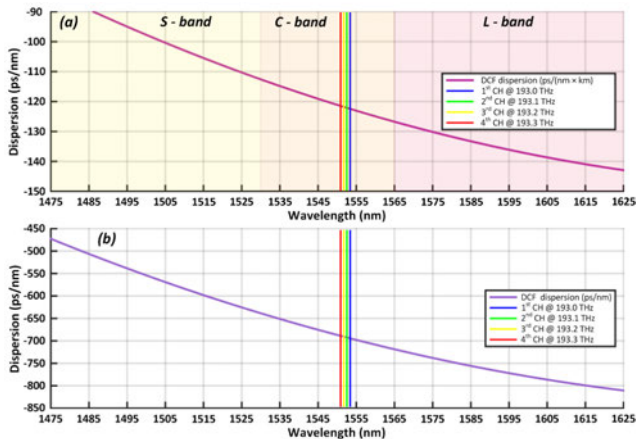


Figure 21. Experimentally measured DCF fiber spool: (a) chromatic dispersion coefficient and (b) total chromatic dispersion depending on bandwidth and used wavelength.

The 4-channel 100 GHz spaced NRZ modulated and de-correlated optical signals spectrum before launching into a 40 km long SSMF fiber span of DWDM optical transmission system which is driven by one Mach-Zehnder modulator MZM and operating at a bitrate up to 40 Gbit/s per channel are shown in *Figure 22.* Applying for the use of DCF post-compensation for 4-channel 100 GHz spaced NRZ modulated DWDM transmission system, the received optical signals are mainly affected by NOE effects. The reason for that is the input optical power of a DCF fiber which exceeds a certain value optical power density in the fiber core. It becomes excessively high because the effective cross-sectional area of the fiber is only $A_{\text{eff}}=20 \mu\text{m}^2$, triggering the nonlinear polarization of fiber materials. As shown in *Figure 23.*, the experimentally received signal after 40 km transmission trough SSMF optical fiber link with dispersion compensation by (a) fiber Bragg grating dispersion compensation module FBG-DCM and (b) by dispersion compensation fiber DCF for investigated NRZ modulated 4-channel 100 GHz spaced DWDM optical transmission system at operating bitrates of up to 40 Gbit/s per channel is good, eye is open and error-free transmission is provided. Performance comparison was demonstrated for 4-channel 100 GHz spaced NRZ modulated DWDM transmission system at operating total capacity up to 160 Gbit/s over 40 km SSMF fiber optical link, with different dispersion-compensating techniques.

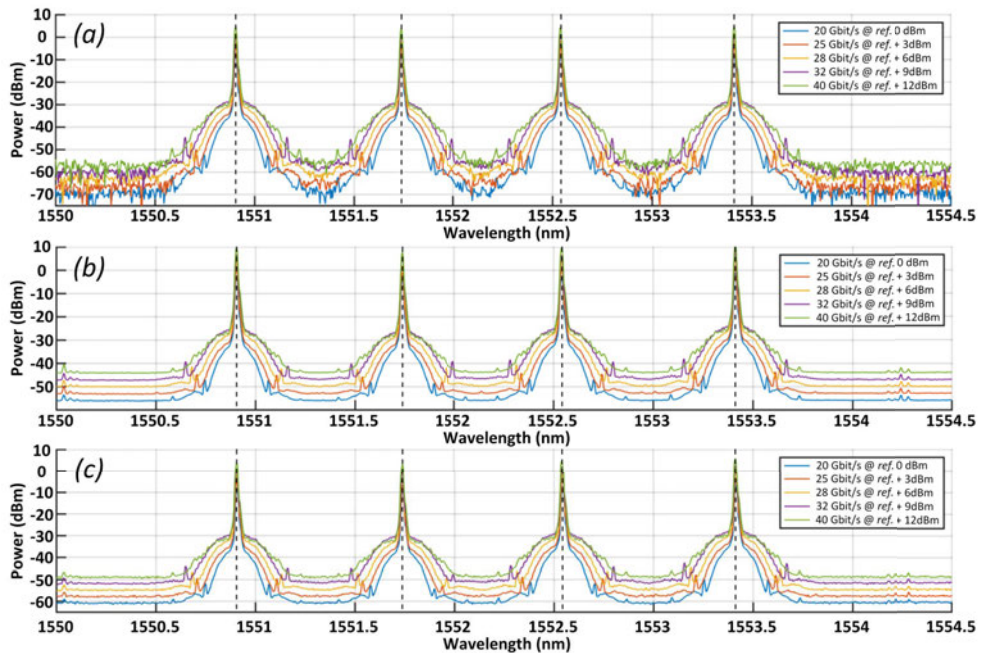


Figure 22. Optical spectra: (a) after B2B transmission through SSMF fiber, (b) after 40 km transmission through SSMF fiber and (c) after 40 km transmission through SSMF fiber with use of dispersion compensation by DCF for multiplexed 4-channel NRZ modulated DWDM optical transmission system at bitrates of up to 40 Gbit/s per channel.

Additional insertion losses in dispersion-compensating optical fiber DCF line and affection of NOE on transmitted signals lead to performance decrease of experimental 4-channel 100 GHz spaced DWDM optical transmission system, where the BER at operating 20 Gbit/s and 40 Gbit/s bitrate per channel of received signal was 5.8×10^{-2} and 1.27×10^{-5} due optical power level on PIN photoreceiver -1.65 dBm and +2.36 dBm (see *Figure 23(b1)* and *Figure 23(b5)*). After decreasing total optical link length by replacing DCF and applying for fiber Bragg grating tunable DCM module the NOE effects are reduced significantly, where the BER of operating at 20 Gbit/s and 40 Gbit/s bitrates per channel was 5×10^{-2} and 2.45×10^{-5} due optical power level on PIN photoreceiver -0.21 dBm and 3.3 dBm (see *Figure 23(a1)* and *Figure 23(a5)*). As shown in *Figure 23(a)* and *Figure 23(b)* sections, comparison depending on bitrate per channel from 20 Gbit/s up to 40 Gbit/s, with previously discussed dispersion compensation techniques implementation into experimental 4-channel DWDM optical transmission system, according to systems performance, the received signal quality is shown (e.g. eye diagrams of received bit patterns).

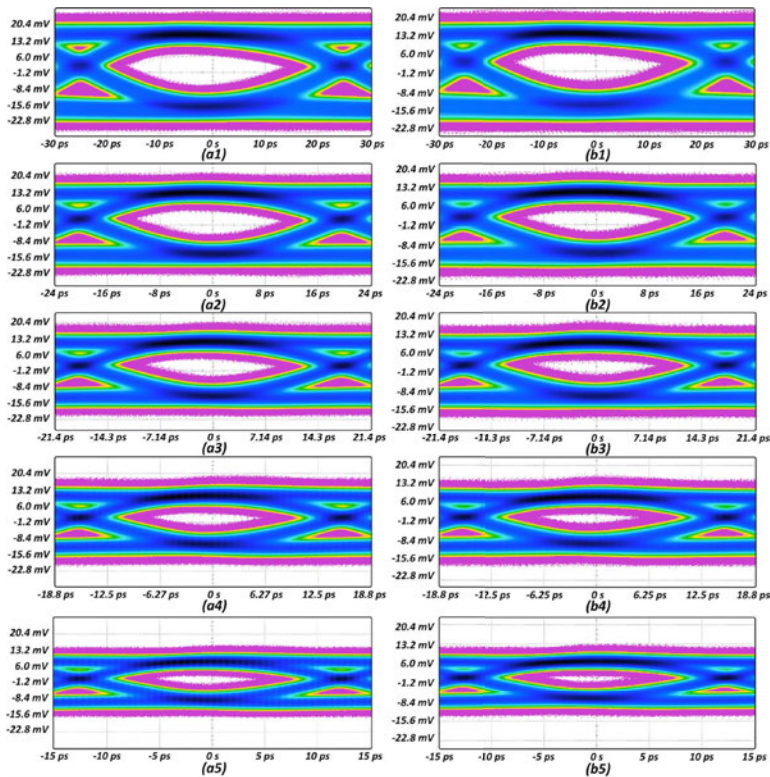


Figure 23. Eye diagrams of the experimentally received signal after 40 km transmission through SSMF fiber with dispersion compensation by (a1-a5) fiber Bragg grating dispersion compensation module FBG-DCM, (b1-b5) dispersion compensation fiber DCF for investigated NRZ-OOK modulated 4-channel 100 GHz spaced DWDM optical transmission system at bitrates of: (1) 20 Gbit/s, (2) 25 Gbit/s, (3) 28 Gbit/s, (4) 32 Gbit/s and (5) 40 Gbit/s per channel.

4.3 The combined solution of space-division multiplexed (SDM) and wavelength division multiplexed (WDM) technologies to implement a spectrally efficient high-speed fiber optic transmission system

Today's widely used single-core single-mode optical fiber (SC-SMF) is already close to its fundamental capacity of 100 Tbit/s, limited by amplifier bandwidth and non-linear noise. The single-mode multicore optical fiber (SMCF) solution offer space-division- multiplexing compaction SDM technology application. The multicore optical fiber (MCF) technology is also being considered for microwave photonics applications such as multi-cavity optoelectronic oscillators [74], and signal processing [75], since it offers identical mechanical and environmental conditions for all parallel cores. MCFs have also been implemented in fibre-wireless links such as a full-duplex, 802.11ac-compliant, 3×3 Multiple-Input Multiple-Output (MIMO) system using 7-core fiber [76], and Centralized Radio Access Networks (C-RANs) [77].

The experimentally developed setup for a 7-channel optical transmission system with a data transmission speed of 2.5 Gbit/s per λ using the NRZ-OOK modulation format via the new generation 2 km long SMCF optical fiber with seven cores, please see in *Figure 24*. The implementation of the experimental optical transmission system was performed at the Technical University of Denmark DTU using the existing equipment of the DTU. An experimental 7-channel optical transmission system using one 2 km long SMCF optical fiber was developed in the laboratory. The experimental setup includes a 2 km long 7- core MCF with 4 upstream transmission channels through (cores 0,1,3,5) and 3 downstream transmission channels trough (cores 2,4,6). The transmission system used a single laser light source with a central wavelength of 1500.12 nm and output power of 12 dBm, connected to a Y-type (50:50) optical power splitter. The output of each splitter was connected to one of the two used optical inputs of the MZM-1 and MZM-2 optical modulators. Before using optical modulators for the transmission system, the operating quadrature BIAS points of the modulator were clarified.

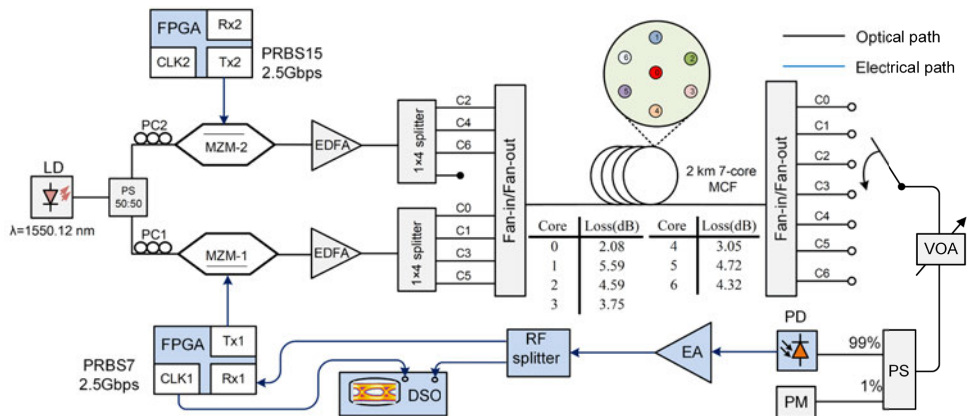


Figure 24. Block diagram of the developed fiber optic 2.5 Gbit/s per λ NRZmodulated transmission system with 7 core SMCF fiber.

Curves were created to determine the modulator operating BIAS point from the optical power level at the modulator output and the DC power supply output voltage. The operating voltage point is determined by finding the minimum and maximum of the sinusoidal function and calculating the two voltages' average, resulting in a working point in the linear region.

The characteristics of the MZM-1 Fujitsu 10G modulator are shown in *Figure 25*. Optimum DC power supply output voltage was determined for the MZM-1 Fujitsu 10G modulator. The minimum voltage point has a minimum of 4.2 V and a maximum of 9.8 V. Calculating the average value of both voltages - 7 V, results in a working point in the linear range. The minimum 2.2 V and maximum 4.6 V operating voltage points were set for the MZM-2 Covega 10G modulator. Calculating the average value of both voltages - 4.7 V, results in a working point in the linear range. Adjustable polarization controllers (PC1, PC2) were used to reduce the polarization between the laser light source and the modulators.

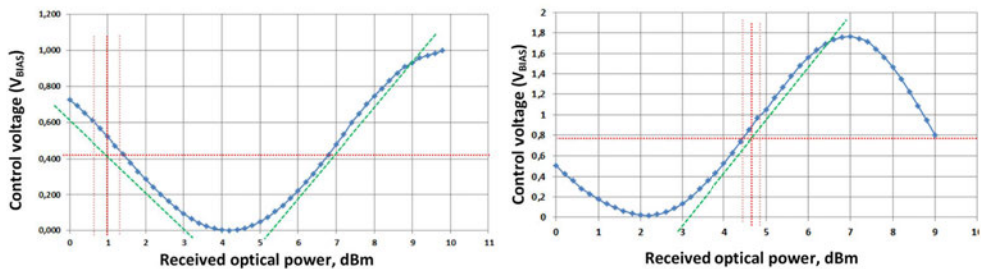


Figure 25. The characteristic curve of (a) Fujitsu 10G and (b) Covega 10G modulator received optical power versus DC source output voltage.

The Field Programmable Gate Arrays (FPGA, Altera Stratix V FPGA) module containing 7 transmitter channels was used to generate an electrical NRZ signal with a pseudo-random bit sequence PRBS. For the MZM-1 modulator, the electrical RF signal was generated with the PRBS7 pseudo-random bit sequence, for the MZM-2 modulator, the electrical RF signal is generated with the PRBS15. Using the option of the Altera Stratix V FPGA module to detect and evaluate the signal BER value, the quality of the received signals was evaluated throughout the experiment. The FPGA module also supports obtaining an eye diagram for the received signal. However, the module's output with an external clock signal was connected to the DSO Agilent 86100A digital oscilloscope during the experiment. After the 10 HGz PIN photodiode, the electrical signal was divided by RF splitter to evaluate the BER by dividing one output to the receiving part of the FPGA. The other output was connected to the DSO to evaluate the signal quality according to the eye diagram and opening.

The modulated optical signal for each modulator: MZM-1, MZM-2 was divided into four channels using two 1x4 optical splitters. EDFA amplifiers were connected in the switching phase between the 1x4 optical power splitters and the output of each modulator. The outputs of the 1x4 optical power splitter were connected to a spliced SMCF 2 km long fiber (FAN-IN) core coupler inputs. For the MZM-1 modulator, the electrical RF signal is generated with the PRBS 7; for the MZM-2 modulator, the electrical RF signal is generated with the PRBS15. The optical signal with

the PRBS7 from the MZM-1 modulator after the 1x4 splitter was decorrelated and fed through the input of (FAN-IN) core coupler to the respective SMCF 2 km long optical fiber cores (0, 1, 3, 5). An optical signal with a PRBS15 from the MZM-2 modulator was applied to the SMCF fiber cores (2, 4, 6). As shown in *Figure 26.*, the 7-core SMCF with FAN-IN and FAN-OUT was used during the experiment.

The transmitted optical signals are received at the corresponding core for each SMCF fiber core using a (FAN-OUT) core coupler. A tunable optical attenuator VAO was connected to the corresponding core output by using a (FAN-OUT) core coupler. The output of the tunable attenuator was divided using an optical power splitter (1% to 99%), where at 1% output, the optical power meter (PM, HEWLET 8583A) was connected, and at 99% output PIN photodiode (PD, AMONICS 10G) was connected. An additional 26dB broadband RF signal amplifier was connected at PD output. The received RF signal had to be amplified because the signal generated at the output of the FPGA module had too low a voltage value (400 mV-pp). The electrical signal after the EA was split by an RF splitter, connected to the DSO and FPGA for real-time BER estimation.

The laser light source (LD, COBRITE DX1) and the high-sensitivity optical power meter (PM, HEWLET 8583A) were used to measure the loss and crosstalk impact of each 7-core SMCF fiber core. The attenuation introduced by each core of 2 km SMCF was measured by connecting a laser light source with a certain optical output power to each individual core. The power meter at the other end of the SMCF fiber core was used to determine the optical power level and calculate the input and output power difference (see *Table 5.*).

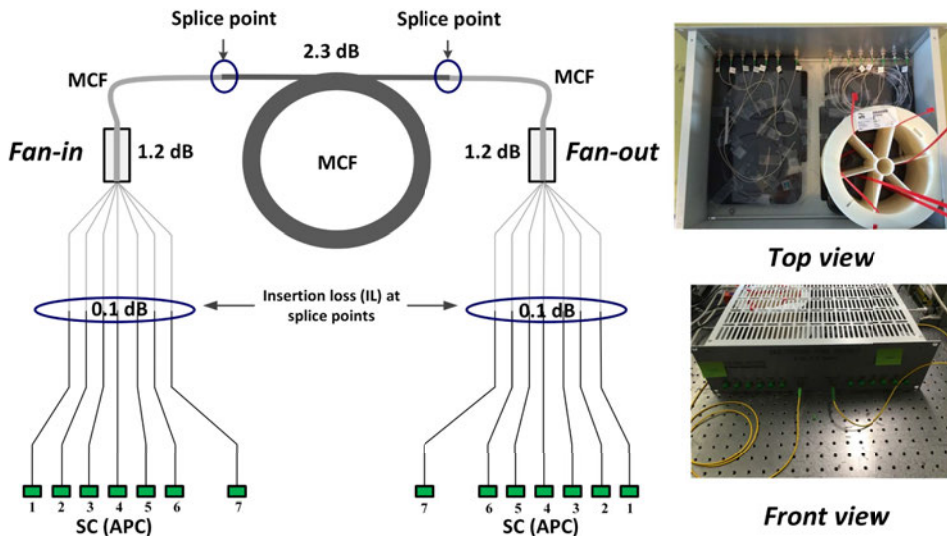


Figure 26. The 7-core MCF fiber used in the experiment with spliced (FAN-IN, FAN-OUT) core couplers.

Table 5.

Attenuation per each core of a 2 km long 7-core SMCF optical fiber

Fiber core number, (No)	Attenuation, (dB)
0	2,08
1	5,59
2	4,59
3	3,75
4	3,05
5	4,72
6	4,32

From the obtained data shown in **Table 5**, it can be concluded that the attenuation introduced by the SMCF optical fiber is 5 to 10 times higher than for the standart single-mode SMF fiber (0.2 dB/km @ $\lambda = 1550$ nm), which is explained by the introduced attenuation at splicing places of the SMCF fiber together with the FAN-IN and FAN-OUT transitions.

The effect of each SMCF fiber core crosstalk was also measured using the light source LD and power meter PM. The results were summarized in a 7x7 crosstalk effect matrix. To measure the effect of crosstalk, a light source was connected to each MCF fiber core, and the output power of all other existing MCF fiber cores was measured. The effect of crosstalk on cores of different locations was determined by measuring and analysing the results, see **Table 6**.

Table 6.

2 km 7 core SMCF fiber core crosstalk 7x7 matrix

		Output / to core						
		C0	C1	C2	C3	C4	C5	C6
Input from the core	C0	-	-38,4	-41,4	-46,1	-36,8	-39,0	-40,00
	C1	-49,3	-	-40,0	-43,7	-48,4	-39,4	-45,7
	C2	-35,0	-54,9	-	-44,2	-64,0	-54,5	-52,5
	C3	-39,7	-56,2	-43,0	-	-44,5	-47,2	-60,5
	C4	-37,1	-51,4	-50,0	-45,5	-	-62,0	-42,5
	C5	-44,0	-37,5	-52,3	-46,7	-54,6	-	-39,0
	C6	-40,3	-58,2	-58,0	-47,1	-41,5	-34,7	-
Overall impact		-32,0	-34,7	-36,2	-37,6	-34,8	-32,2	-35,0

The **Figure 27(a)** shows the measured pair-wise power coupling between all 7 cores. The total crosstalk (summation of each core contribution) is shown in **Figure 27(b)**. The central core (core 0) exhibits the highest crosstalk as expected, and other outer cores (1,2,4,6) have roughly equal crosstalk where core 3 and core 5 are much lower and higher than the other outer cores, respectively.

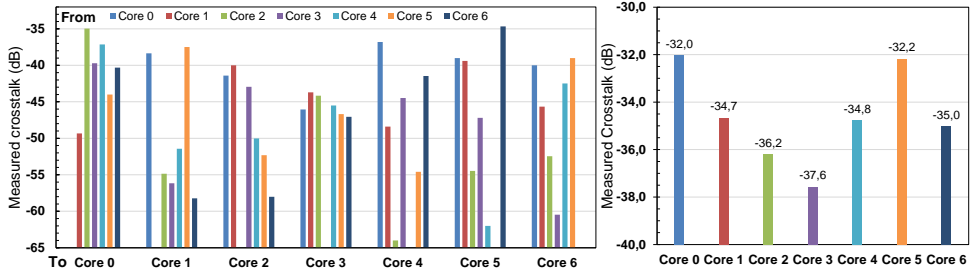


Figure 27. (a) Measured pairwise crosstalk between cores and (b) measured total crosstalk per core.

The obtained BER of core-0 in response to received optical power at photodiode PD is shown in Figure 28. in two different scenarios, with and without signal pre-emphasis for mitigation of signal distortions. Applying the FPGA pre-emphasis option it is possible to reduce the effect of distortions in each core, and the BER is far below the forward error correction FEC limit, as shown in Figure 28(a) and Figure 28 (b). The measured optical output power of core 0 after 2 km MCF transmission varied from -12.55 to -4.35 dBm, where the 2.5 Gbps NRZ-OOK signal's BER without equalization was from 1.4×10^{-2} to 8.7×10^{-7} , but with equalization, it varied from 2.6×10^{-4} to 5.1×10^{-7} , as shown in Figure 28(a). Eye diagrams of the received signal without any signal equalization and with the use of FPGA equalization are shown in Figure 28(c) and Figure 28(d).

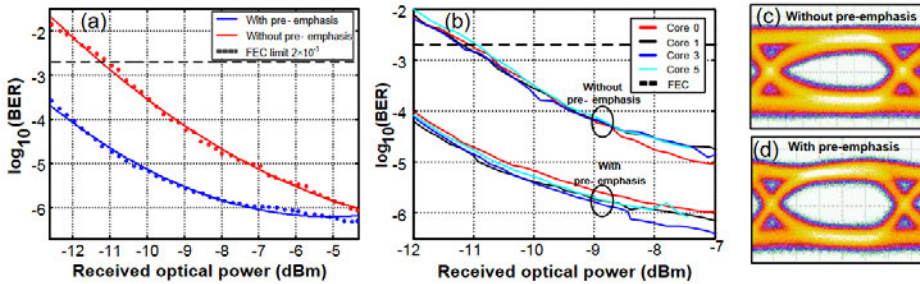


Figure 28. Comparison of measured BER versus received optical power of a 2.5 Gbps NRZ-OOK signal with and without FPGA equalization enabled (a) for central MCF core (core 0) (b) central core 0 and outer cores 1, 3 and 5. Eye pattern of the received 2.5 Gbps signal (c) without equalization and (d) with FPGA equalization for central MCF core 0.

5 DEVELOPMENT AND EVALUATION OF SPECTRALLY EFFICIENT NEXT-GENERATION MOBILE OPTICAL SYSTEMS FOR MILLIMETER-WAVE RADIO SIGNAL TRANSMISSION

5.1 Research and analysis of the application of Radio over Fiber (ROF) in the solution of future mobile communication systems

The fifth-generation 5G mobile communications will greatly impact different use cases such as stadiums, hospitals, railway stations, homes, and businesses using conventional wireless access technology [78]–[80]. 5G will feature data transmissions up to tens of gigabits, ultra-low latency, and high-reliability communication. On the one hand, this will change and significantly improve several different applications like the Internet of Things IoT, augmented and virtual reality VR, and super high-resolution video streaming (4K/8K) [78]–[80]. On the other hand, 5G technology still needs to satisfy stringent key performance indicators (KPIs) such as higher bandwidth and data-rate per user, increased number of connected devices, lower energy consumption, and reduced end-to-end latency [8], [80]–[82].

Considering the required capabilities of 5G and beyond 5G mobile radio communication networks and their techniques, an optical fiber can be considered as the primary complement for 5G/beyond 5G fronthaul and backhaul networking [83]–[84]. As the passive optical network PON is a cost-efficient, mature, and the most widespread access architecture being deployed worldwide with even more recent massive deep fiber installations near end-user premises it is clear that the convergence of both technologies (here meaning radio signal transmission and light-guide systems (fiber optical communication systems) is a natural process [85]–[87].

The Electronic Communications Committee of the European Conference of Postal and Telecommunications Administrations (CEPT) has recently harmonized the first bands for 5G applications [88]. These bands are 3.4 - 3.8 GHz (sub-6 GHz band) and 24.25 - 27.5 GHz (so-called 26 GHz band). Furthermore, the CEPT has identified the 26 GHz band for early European harmonization as it provides over 3 GHz of contiguous spectrum and more favorable propagation than the higher frequency bands also under consideration. In addition to the 26 GHz band, the 28 GHz band has emerged as the second most important band for 5G networks [79]. Currently, the research and development of the 5G mobile systems at the higher frequencies, e.g. 28 GHz band, has been considered for urban areas and communication between vehicles [89]. These unlicensed or slightly licensed millimeter-wave (mm-Wave) frequency bands are very attractive for future 5G mobile radio communication networks. Therefore, to achieve ultra-high capacity and bring ubiquitous high-bitrate wireless connectivity per mobile user, the cost-effective hybrid photonics-wireless mm-wave interface communication systems are required, where wireless transmission on millimeter-wave bands can be realized [90]. According to ITU-T G. 9803 rec. describing radio-over-fiber RoF systems, the PON network is desired for mobile fronthaul of latest 5G mobile systems with functions to provide the connection between the baseband units BBU pool and radio units RU. As shown in *Figure 29.*, mobile fronthaul of 5G and beyond 5G systems over wavelength-division multiplexed passive optical access network PON can be realized using a

centralized/cloud radio access network C-RAN architecture. As shown in *Figure 29.*, low latency and high capacity WDM optical access network providing optical fiber connectivity near or very close to the antenna premises such as fiber-to-the-antenna (FTTA), can be a preferable and cost-effective solution for the 5G transport [83], [91]. Passive optical access networks are considered feasible solutions for the cost-effective integration of C-RAN and transmit both intermediate radio frequency (IF) and baseband signals by a single or multiple wavelengths per optical channel over a single fiber in a cost-efficient way into the already deployed fiber infrastructure. As mentioned before, in terms of the access network, mobile fronthaul are based on FTTA links with optical fibers deployed very close to the antenna [83].

Traditionally widely used PON network architecture can be technologically modified to radio-over-fiber RoF link for 5G mobile communications, which is seamlessly integrated into the PON segment, leaving the existing optical distribution network ODN part unchanged [82]. Additionally, the analog mm-wave radio over fiber RoF as one of the promising solutions is considered for the latest 5G mobile systems by transmitting intermediate signals (used for generation of mm-wave RF signals in the receiver side) through the fronthaul optical link [8]. Instead, to applying for more advanced modulation formats like multi-level quadrature amplitude modulation (M-QAM) and duobinary (DB), the M-PAM, where M is abbreviated as different signal amplitude levels, offers a simple way to enhance the spectral efficiency and at least double the bitrate per wavelength using the same optical bandwidth [92]–[93]. Accordingly, the 4-level pulse amplitude modulation format (PAM-4) attracted much attention to its relative ease of implementation which offers a good trade-off between performance and complexity allowing to double the bit rate in the channel without doubling the necessary bandwidth, if compared to the NRZ-OOK link [41], [92]–[93]. In connection with this, the high-speed PAM-4 -based optical link for the common public radio interface (CPRI) in mobile fronthaul is still discussed [71].

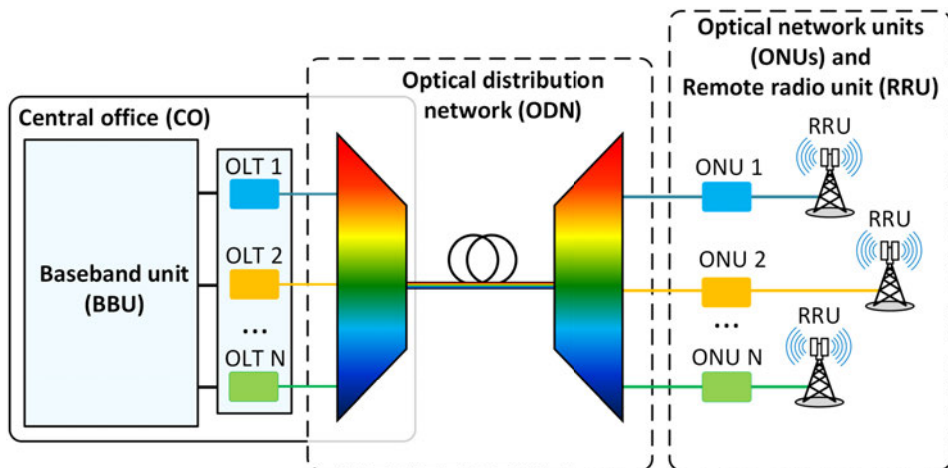


Figure 29. Centralized mobile fronthaul over wavelength-division multiplexed passive optical access network PON.

5.2 Performance evaluation in a simulated environment of NRZ-OOK modulated A-RoF-WDM PON transmission system with 2.5 Gbit/s data rate per channel depending on the used upconversion of optical signals

The fifth generation 5G currently is the latest generation of cellular mobile communications. Infrastructure for 5G needs to deliver solutions, architectures, technologies, and standards for the next decade's ubiquitous 5G communication infrastructures. Traditional radio access networks RANs, which combines baseband processing and radio functions at each physical base station, are also used in long-term evolution LTE cellular 4G generation technology [94]. 5G is still under research and discussion, but it is already known that baseband processing for many cells will be centralized and stands for Cloud RAN or Centralized RAN (C-RAN) with benefits of improved performance and cost reductions as a result of pooling resources. Enabling C-RAN for the 5G front-haul architecture will evolve it into a more complex network, where additional costs of the increase in capacity requirements can be reduced. The basic front-haul is assumed to run over a common public radio interface CPRI, processed in the Base-band units BBU and sent to the remote radio head (RRH). Nowadays, it is being considered that 5G wireless communications will use the backhaul section of existing optical fiber links between remote radio units (RRU) and BBUs located in the central office CO side [95]–[96]. Compared to the spectrum below 6 GHz used for mobile communications, millimeter waves have enormous available bandwidths. Millimeter wave is a promising candidate to address the capacity demands of 5G. Integrated backhaul for 5G millimeter wave could be placed easily in urban areas, without additional effort, cost for wired backhaul and connection to the core network [97]. Currently, research and development of the 5G mobile systems at the higher frequency, such as 28 GHz band, has been considered for urban areas and vehicular communications [98]. Two possible RF bands of 6 GHz and ka-band of 28 GHz are considered for 5G spectrum [98]–[99]. With PON's segment, the radio-over-fiber RoF provides a unique solution for fiber optical infrastructure, which can be the next step for 5G wireless transmission implementation, ensuring energy saving and cost reduction [100]. However, it is known that these solutions have mainly impact from linear (e.g. chromatic dispersion CD) and non-linear (e.g. nonlinear optical effects NOE) impairments for each sub-carrier signals in fiber optical links that is the main distance-limiting factor for the high-frequency transmission [41], [60], [62], [101]. Several novel schemes are investigated during the last decade, allowing transmitting 28 GHz radio frequency (RF) carriers through optical modulation techniques for analog radio-over-fiber A-RoF links.

The goal of this simulation model was to evaluate the performance and maximum reach for investigated A-RoF WDM-PON transmission system with four 2.5 Gbit/s NRZ-OOK modulated channels, where BBUs are implemented in CO allowing transporting of intermediate frequencies along existing fiber optical distribution network ODN under condition that it is still possible to achieve pre-forward error correction pre-FEC BER of 10^{-3} or lower. Displayed are obtained by OptSim simulation software. Additional use of Matlab software was performed to display estimated results of received signals. As shown in **Figure 30.**, the investigated A-RoF WDM-PON optical transmission system model consists of 4 channels operating at 2.5 Gbit/s bitrate each.

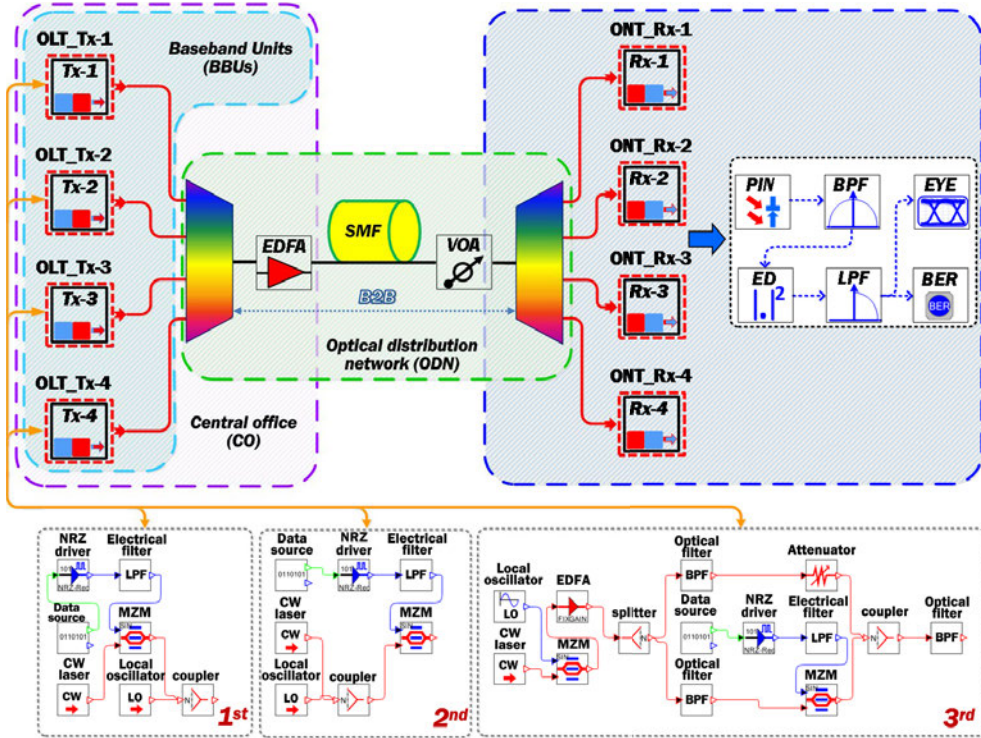


Figure 30. Simulation scheme of 4-channel 2.5 Gbit/s per channel NRZ-OOK modulated A-RoF WDM-PON optical transmission system with investigated A-RoF transmitters: (1st) using one laser source as LO, (2nd) use of two coupled light sources and (3rd) use of the sinusoidal signal generator as LO for generation of 28 GHz mm-wave signal.

According to ITU-T G.964.1 rec., dense WDM architecture with 100 GHz channel spacing and 193.1 THz central frequency is chosen [64]. Baseband units BBUs pool in proposed model architecture is integrated into WDM-PON central office CO side, which consists of optical line terminal OLT. CO includes optical line terminal OLT with four transmitters (OLT-Tx) modified for A-RoF system data containing 28 GHz carrier frequencies generation [46].

Electrical pseudo-random bit sequence PRBS data source and NRZ driver, which encodes the logical data form by using the non-return to zero NRZ technique, are directly sent to low-pass filter LPF with 3 GHz 3-dB bandwidth in such a way generating widely used on-off keying non-return to zero NRZ-OOK modulated signal for all investigated system types of A-RoF implementation [102].

Three possible A-RoF system types for a different generation of mm-wave inside transmitters (Tx) of simulation environment model is investigated:

- The simulation model of the first A-RoF transmitter was designed using two continuous wavelength CW light sources with a linewidth of 50 MHz each, where one

of them with an output power of +10 dBm is directly connected to intensity Mach-Zehnder modulator MZM. The second light source operates as local oscillator (LO) and is used for the generation of intermediate frequency (tone) with an output power of +2.6 dBm. Such an output power of a second CW laser is set to ensure equal power level of both optical tones afterwards being coupled by a power coupler. The frequency spacing between both above-mentioned lasers is set to be 28 GHz, accordingly enabling to generate 28 GHz (ka-band) mm-wave (detailed illustration, please see in *Figure 31*). By homodyne up-conversion, channel interval between two laser sources are equal for necessary mm-wave generation, in this case for 28 GHz ka-band intermediate frequency generation.

Optical mm-Wave (24 GHz – 300 GHz) generation principle:

- Optical receiver receives an optical data signal at one frequency and tunable LO signal at another
- RF signal is generated through heterodyne photonic up-conversion on a photodiode
- frequency spacing between these two signals is equal to the desired mm-Wave frequency
- 26.5 - 28 GHz (Ka-band)

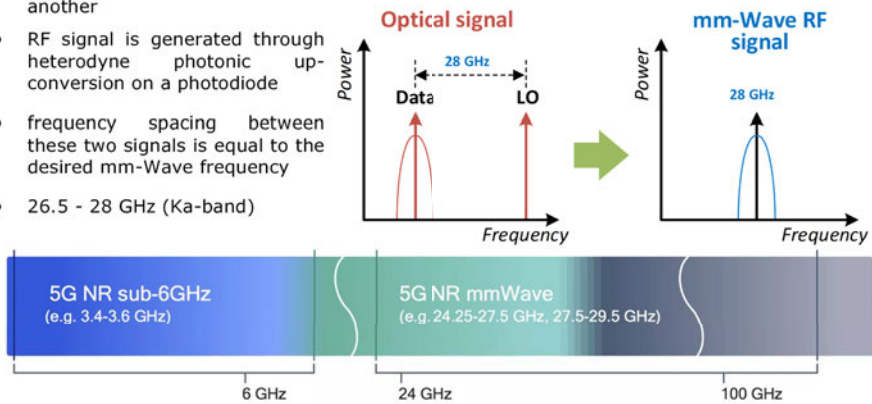


Figure 31. Optical mm-Wave generation by the homodyne up-conversion principle.

The inter-channel frequency difference of the first data modulated optical carrier (F_1) and second local oscillator optical carrier (F_{LO1}) is equal to the necessary mm-wave radio frequency RF for transmitting wireless signals at the receiver side. By transmitting the two carrier signals F_1 and F_{LO1} with an appropriate inter-channel interval through the ODN, providing backbone routing network operation, an uplink conversion of the transmitted signal to a carrier frequency IF is performed by a broadband semiconductor photodiode PIN within a single optical channel. Here $IF = F_{LO1} - F_1$, enabling the direct wireless transmission of data between remote base station radio units RU as well as multiple-input and multiple-output MIMO antennas [103], [104], [105].

- **The second A-RoF transmitter** for WDM-PON optical transmission system was realized by use of two separately coupled continuous wavelength light sources with 28 GHz channel interval between two channels with a related output power level of 10 dBm and sent to external MZM. In such a way, both optical tones are modulated in this scenario.

- **Third A-RoF transmitter realization** for intermediate frequency generation is more complex, CW laser source with 10 dBm output power is directly connected to first MZM, which has 3 dB insertion loss and 20 dB extinction ratio modulator BIAS point is adjusted at its zero point. Sinusoidal signal generator with 14 GHz sinusoidal electrical signal (half of proposed IF frequency) is directly connected to first MZM electrical signal input. The output of the first MZM with two 28 GHz spaced optical tones are amplified with an EDFA amplifier and divided by a 50% percent optical power splitter with 3.5 dB insertion loss. Afterwards, each tone is filtered out by a variable optical band-pass filter (BPF) with 20 GHz 3-dB bandwidth for each optical signal. The second optical signal is attenuated accordingly to the first modulated signal optical power level after MZM to ensure equal related power level for both optical signals. Finally, both optical signals are coupled together and prepared for transmission in fiber optical part.

Optical signals from each OLT-Tx are coupled together using arrayed waveguide grating AWG multiplexer with 3.5 dB insertion loss and 100 GHz channel interval where 3-dB bandwidth is 40 GHz. An optical signal pre-amplification by an erbium-doped amplifier EDFA with optimized gain accordingly to each A-RoF implementation type is realized before launching coupled optical signals into ITU-T G.652 rec. single-mode optical fiber SMF span, with 0.02 dB/km attenuation and 17 ps/nm/km dispersion coefficients at 1550 nm reference wavelength. An additional variable optical attenuator VOA is used to obtain BER in terms of received optical power. After transmission through ODN, intermediate frequency optical signals are separated by AWG demultiplexer with 3.5 dB insertion loss, 100 GHz channel interval, and 40 GHz 3-dB bandwidth, located in optical network terminals ONTs. After optical-to-electrical conversion, the electrical data containing RF signals are sent throughout a remote radio unit RRU. The next containing step is to produce mm-wave transmission between multiple-input and multiple-output MIMO antennas.

The receiver side consists of optical network terminals ONTs. Each ONT receiver (ONT-Rx) consists of a PIN photoreceiver with 50 GHz 3-dB electrical bandwidth with a sensitivity level of +4 dBm for BER of 10^{-12} and a dark current of 5 nA and responsivity of 0.65 A/W [106]. Electrical Bessel band-pass filter BPF with 3 GHz 3-dB electrical bandwidth tuned to 28 GHz central frequency is used for each containing channel carrier frequency pre-filtering. Filtered intermediate frequency signal down-conversion is realized by homodyne signal processing technique using passive Schottky diode-based envelope detector (ED) with video-bandwidth 28 GHz [107]. Afterwards received modulated baseband signal is filtered by an electrical Bessel low-pass filter LPF with 3 GHz 3-dB electrical bandwidth. The scope and BER estimator based on statistical signal analysis was used to measure the received signal e.g., showing bit pattern and bit-error-rate BER. Received signal with worst BER performance for the middle channel, where the highest impact of crosstalk is observed in displayed results are shown.

The 4-channel 100 GHz spaced signals spectrum of each channel in B2B and after 20 km transmission for investigated ARoF WDM-PON optical transmission system are shown in *Figure 32.*

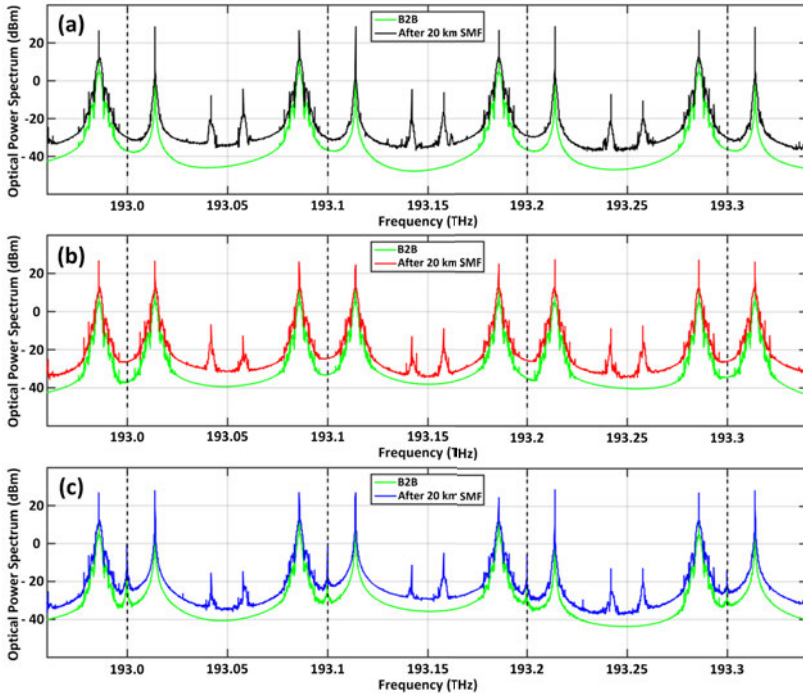


Figure 32. Optical spectrum of multiplexed 4-channel WDM-PON system before B2B and after 20 km transmission through ODN, for photonic up-conversion and generation of single 2.5 Gbit/s NRZ modulated 28 GHz carrier by different A-RoF implementation: (a) using one laser source as LO, (b) using two coupled light sources, (c) using sinusoidal signal generator as LO.

The obtained BER of each A-RoF transmitter in response to received optical power at PIN photoreceiver is shown in **Figure 33**. Results are obtained in two different scenarios, with 20 and 40 km ODN fiber length.

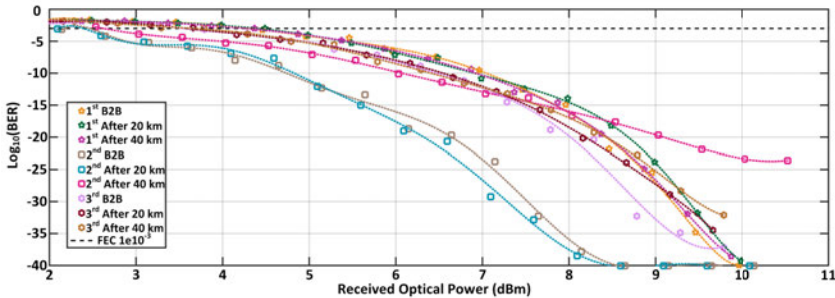


Figure 33. Comparison of measured BER after ED versus received optical power for 2.5 Gbit/s NRZ-OOK signals depending of A-RoF implementation realization type and use of photonics up-conversion method for 28 GHz carrier frequency.

In B2B the signal quality for all implemented A-RoF transmitter types is good, the eye is open and error-free transmission of investigated WDM-ROF system with 100 GHz channel spacing can be provided.

Accordingly, to Next-generation PON standards (NG-PON2), ITU-T G.989.2 ODN fiber distance classes with a defined length of 20 and 40 km with equal differential optical path loss of a maximum 8 dB for the designed simulation model was chosen. By increasing the length of the distribution network up to 40 km, after transmission, the BER of received signals with the use of 2nd implemented A-RoF transmitter was 2.6×10^{-22} . Additional losses in optical fiber line and CD effect after increasing length show the relevance of WDM-PON transmission systems performance reduction, where the BER of implemented 1st and 3rd A-RoF transmitter after received signals was 2.9×10^{-37} and 7.2×10^{-31} .

According to ITU-T G.989.2 recommendation, the specified valid optical link distances is up to 40 km, but it is also possible to support longer distances, which may require the usage of extenders. Therefore, the transmission distance of fiber optical link section was extended up to 60 km. After extending the link section, that maximal possible reached distance for 2nd implemented A-RoF transmitter was 57 km with the BER of 3.6×10^{-4} , please see [Figure 34\(b\)](#). As shown in [Figure 34\(a\)](#) and [Figure 34\(c\)](#) with 1st implemented A-RoF transmitter using one laser source as LO and 3rd implemented A-RoF transmitter with use of the sinusoidal signal generator as LO, the BER of received signal was 3.3×10^{-4} and 5.1×10^{-4} , with maximum reached distance of 65 and 63 km, respectively.

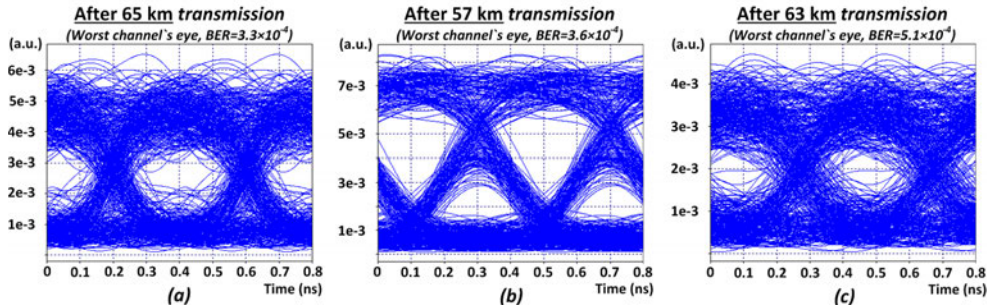


Figure 34. Eye diagrams of received 28 GHz carrier signal after ED detection by A-RoF implementation (a) after 65 km transmission using one laser source as LO, (b) after 57 km use two coupled light sources and (c) after 63 km use of sinusoidal wave generator as LO for 4-channel 100 GHz spaced WDM-PON transmission system with 2.5 Gbit/s transmission speed per channel

5.3 Evaluation of spectrally efficient AR oF-WDM PON transmission system in a simulation environment using PAM-4 modulation format providing data transmission speed up to 5 Gbit/s in the channel.

For research of millimeter-wave (mm-wave) hybrid photonics-wireless access system, the *VPI Photonics Design Suite* software was used. Here was designed and simulated 8-channel 2.5 Gbaud per channel PAM-4 modulated WDM-PON optical transmission system with embedded analog

mm-wave RoF transmission of 28 GHz mm-wave signal for 5G mm-wave hybrid photonics-wireless interface, as it is shown in *Figure 35.*

The goal of this hybrid photonics-wireless analog mm-wave RoF-WDM-PON system simulation model was to evaluate the performance and system reach up to 40 km according to NG-PON2 link section requirements, under the condition that it is still possible to achieve pre-forward error correction (pre-FEC) BER level of 1×10^{-3} or lower [108]. According to RoF ITU-T G.9803. recommendation, in investigated 8-channel analog mm-wave RoF-WDM-PON transmission system, depicted in *Figure 35.*, the baseband units BBUs are located in the service provider's central office CO, allowing to transport intermediate frequencies IF over the optical front-haul network, and lastly performing signal up-conversion in radio units RUs located at the receiver side of the base station (BS) [109].

Here for the generation of an mm-wave signal, on the receiver side, was used the simplest realization scheme - two coupled laser sources (CW1 and CW2), which both were modulated with the same data. As it is shown in *Figure 35.*, passive optical access network PON architecture, standardized to NG-PON2 requirements, can be technologically transformed into an analog mm-wave RoF-WDM-PON transmission system through the RoF segment integration. The proposed analog mm-wave RoF-WDM-PON transmission system designed to transmit intermediate frequencies IF over commercially used fiber optical network is a perspective solution for the latest fifth-generation (5G/5G+) cellular mobile communication network. According to the fundamental PONs architecture, the frequency grid according to ITU-T G.694.1 rec (dense WDM systems) is chosen for investigated 8-channel hybrid analog mm-wave RoF-WDM-PON system, where the central frequency is anchored on 193.1 THz and channel spacing is 50 or 100 GHz [64]. As it is shown in *Figure 35.*, the CO includes OLT with 8 transmitters modified as RoF transmitters (ROF_Tx) and designed for heterodyne analog mm-wave RoF system, where 28 GHz intermediate frequencies are generated.

Each ROF_Tx transmitter based on heterodyne up-conversion technique by using two separately coupled continuous wave CW laser sources, with 28 GHz frequency difference for

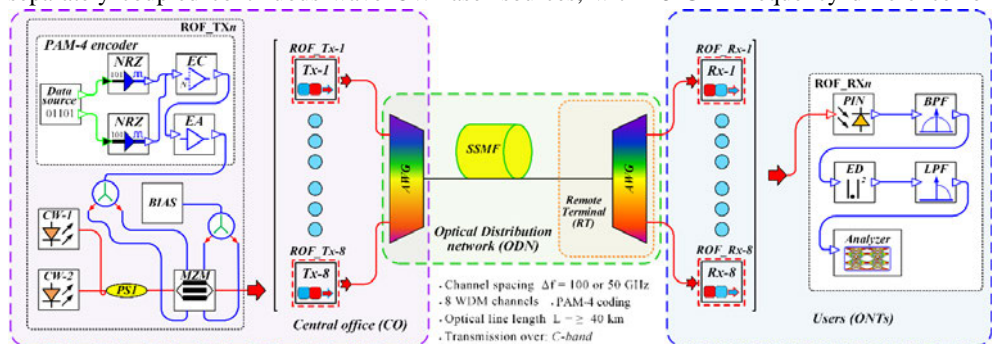


Figure 35. Simulation scheme of 8-channel 2.5 Gbaud per channel PAM-4 modulated analog RoF WDM-PON optical access system where 28 GHz mm-wave signal transmission for 5G the mm-wave hybrid photonics-wireless interface is realized.

necessary mm-wave generation (e.g. 28 GHz (Ka-band)) with +9 dBm output power is directly connected to differential Mach-Zehnder modulator MZM resulting in +3.5 dBm optical transmitter average output power [103], [104].

The parameters of the MZM, including S_{21} frequency response, are set according to the Photline MX-LN-10 intensity modulator [110], [111]. The modulation of both optical signals is ensured as follows. Both arms of the differential MZM are driven by the same electrical PAM-4 signal, while bias voltage with opposite signs is ensured. The electrical PAM-4 signal is provided by dividing pseudo-random bit sequence PRB) from PRBS generator into two subsequences (sequence of most significant bits (MSBs) and the sequence of least significant bits (LSBs) with a bit rate of 2.5 Gbit/s each and generating electrical NRZ signals with appropriate amplitude levels. The NRZ signals are then combined into one PAM-4 signal with a data rate of 5 Gbit/s (2.5 Gbaud /s), amplified by an electrical amplifier whose parameters are set according to the technical specification of the SHF 100 BP amplifier [112]. All optical signals from each ROF_Tx transmitter are coupled together by using an arrayed waveguide-grating AWG multiplexer.

The optical signal at the output of the multiplexer for 100 GHz and 50 GHz channel spacing is shown in *Figure 36(a)* and *Figure 36(b)*. As it is shown in *Figure 36.*, each physical optical channel of AWG contains two optical signals with 28 GHz spacing, which are further used for the generation of mm-wave signals in the receiver side through the photonic upconversion process on the photodiode.

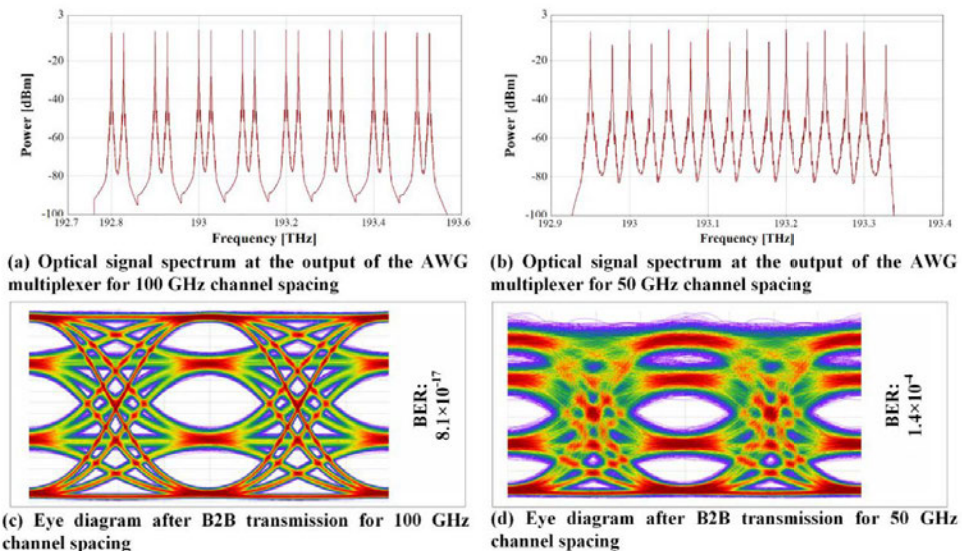


Figure 36. Optical spectra of multiplexed 8-channel hybrid photonics analog RoF WDM-PON access system with (a) 100 GHz and (b) 50 GHz channel spacing and (c) received down-converted 2.5 Gbaud PAM-4 modulated 28 GHz mm-wave signal eye diagram after B2B transmission with 100 GHz channel spacing and (d) received down-converted 2.5 Gbaud PAM-4 modulated 28 GHz mm-wave signal eye diagram after B2B transmission with 50 GHz channel spacing.

At the receiver side, the signal is demultiplexed utilizing AWG demultiplexer, which corresponds to wavelength-routed WDM-PON WR-WDM-PON architecture. The 3-dB bandwidth of each channel of AWGs was set to 75 GHz for 100 GHz channel spacing and 35 GHz for 50 GHz channel spacing [113], [114]. Optical signals are transmitted through the ODN link section in the optical C-band via ITU-T G.652 standard-compliant single-mode optical fiber (SSMF).

The receiver side consists of optical network terminals ONTs, where each ONT receiver (ROF_Rx) consists of a photoreceiver PIN with 3-dB bandwidth of 36 GHz, the sensitivity of -18 dBm at a bitrate of BER of 10^{-12} , the dark current of 1 nA and responsivity of 0.7 A/W [64]. Pre-filtering of the received electrical signal after PIN is realized by the electrical band-pass filter BPF, which has a 28 GHz central frequency and 5 GHz 3-dB electrical bandwidth. Finally, down-conversion is realized by the envelope detector, which is emulated multiplying the signal by itself and filtering it using a low-pass Bessel filter with a 3-dB bandwidth of 2.5 GHz [107], [115]–[117].

The eye diagrams for the received and down-converted 100 GHz and 50 GHz spaced 2.5 Gbaud PAM-4 modulated 28 GHz mm-wave signal for B2B transmission are shown in *Figure 36(c)* and *Figure 36(d)*. The spectrum of electrical radio signal on the output of 36 GHz PIN photodiode, and after filtering by 28 GHz BPF filter with 5 GHz 3-dB bandwidth is shown in *Figure 37*. As shown in *Fig. Figure 37(b)*, the signal's baseband part is suppressed by the 28 GHz passband filter. Of course, the signal after the PIN receiver can be split (e.g. by using RF power divider), and then one of the outputs can be filtered by a low-pass filter, therefore enabling access to the transmitted data in the ONU, before further transmission in RF domain through antenna operating in the mm-Wave band, e.g. K/Ka-band.

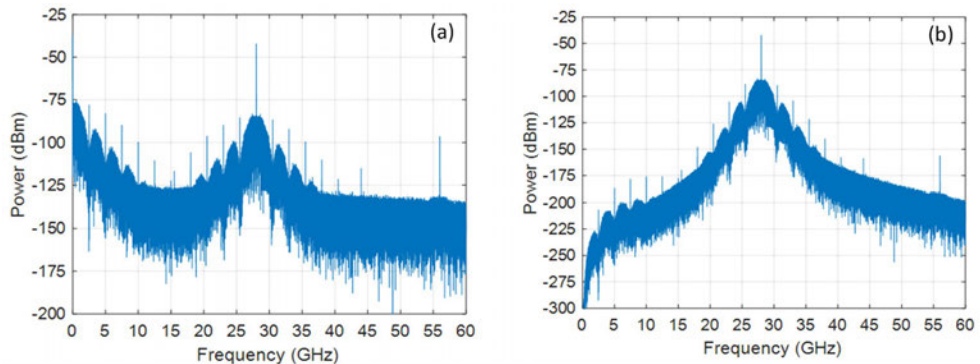


Figure 37. Electrical RF signal spectrum (a) on the output of PIN photodiode, and (b) after filtering by 28 GHz BPF filter with 5 GHz 3-dB bandwidth.

However, to obtain received signal quality, the down-conversion from RF frequency (28 GHz) to baseband by using the bandpass filter and envelope detector, as it should be realized in hybrid analog mm-wave RoF optical access systems, after receiving the transmitted RF signal, e.g. 28 GHz, is shown.

The feasibility of the designed hybrid photonics-wireless system is verified by the performance indicators as pre-forward-error-correction pre-FEC BER threshold $BER \leq 10^{-3}$ and eye diagrams of received and down-converted mm-wave radio signal. The obtained results of the worst-performing channel for transmission distances of up to 40 km over SMF ODN section for PAM-4 modulated 8-channel analog mm-wave RoF-WDM-PON transmission system with 100 GHz channel spacing is shown in *Figure 38*.

After transmission through 20 km of ODN, including SSMF fiber, the BER is significantly lower than the FEC threshold, where the BER of received signals was 4×10^{-8} . While after 40 km transmission through ODN the BER of received signals was 2.8×10^{-3} , which is slightly above the FEC threshold. That means that it is technically challenging to ensure such transmission distance, and more comprehensive future research on the limits of the transmission system parameters for the implementation of such a long transmission distance (40 km) is desirable.

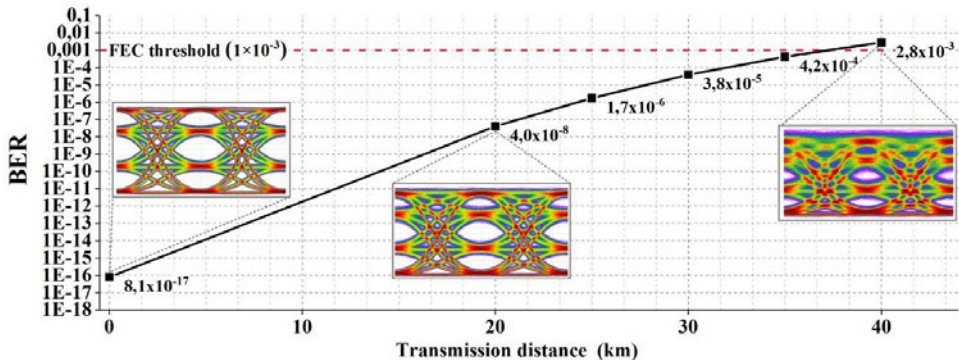


Figure 38. BER versus transmission distance for down-converted 2.5 Gbaud PAM-4 modulated 28 GHz mm-wave signal after analog mm-wave RoF-WDM-PON transmission over 20 and 40 km SSMF ODN distances. Insets show the received down-converted PAM-4 signal eye diagrams after B2B, 20 and 40 km transmission over SSMF for 2.5 Gbaud symbol rate with 100 GHz spacing.

Further, the utilization of twice narrower - 50 GHz channel spacing was investigated. The optical spectrum of the 2.5 Gbaud PAM-4 modulated signal at the output of AWG de-multiplexer (original signal) and after AWG de-multiplexer (after transmission over 20 km ODN link section) for hybrid photonics analog mm-wave RoF-WDM-PON system obtained by use of AWG's with 50 GHz channel spacing and 3-dB bandwidth of the 35 GHz is shown at *Figure 39*. While the eye diagram of the received signal and corresponding BER is shown at the inset of *Figure 39*. As one can see in *Figure 39*. (inset), with the 50 GHz channel spacing, it is not possible to ensure transmission with BER below the FEC threshold for investigated 2.5 Gbaud PAM-4 modulated 8-channel analog mm-wave RoF-WDM-PON transmission system even for 20 km long SSMF.

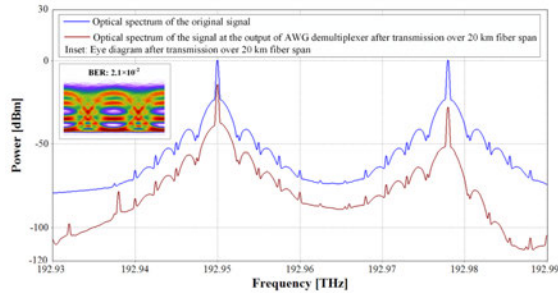


Figure 39. Optical spectra of the worst performing channel containing two 2.5 Gbaud PAM-4 modulated and 50 GHz spaced optical signals at the output of RoF transmitter (launched optical signal) and on the output of AWG demultiplexer after transmission over 20 km SMF fiber span. Insets show the corresponding eye diagram of the 2.5 Gbaud mm-wave signal received and down-converted after 20 km transmission.

In this case, the BER of received and down-converted 28 GHz mm-wave PAM-4 modulated signal is 2.1×10^{-2} . It is worth to mention that even for B2B transmission the demonstrated BER is slightly below defined BER threshold 1.4×10^{-4} , see **Figure 36(d)**. This drop in the BER performance with applying the narrow (50 GHz) channel spacing can be explained by the small cut-off frequency passband (3-dB bandwidth is 35 GHz) of commercially used AWG multiplexer/de-multiplexer. Respectively, the signal at IF frequency is considerably affected by the bandwidth (3-dB bandwidth is 35 GHz) of 50 GHz spaced AWGs, as it is situated at 28 GHz inter-channel spacing relative to the main (baseband) frequency. The described effect can be observed by comparing the spectrums of the original and de-multiplexed signals, as shown in **Figure 39**. That is also confirmed with the relatively high BER value obtained for B2B transmission (see **Figure 36(d)**).

Proposed 8-channel 2.5 Gbaud PAM-4 modulated analog mm-wave RoF-WDM-PON optical transmission system with 100 GHz channel spacing is capable of providing transmission through ODN over SSMF fiber for at least 20 km with BER significantly smaller than FEC threshold (BER is 4×10^{-8}), while after 40 km transmission the BER of received and the down-converted mm-wave signal was 2.8×10^{-3} , which is slightly above FEC threshold. That means that it is technically difficult to ensure such a transmission distance of 40 km with the use of 100 GHz channel interval commercial AWG. The use of 50 GHz channel spacing for such a hybrid system is limited. It is not possible to implement 50 GHz channel interval utilizing commercial AWG where 3-dB bandwidth is 35 GHz and, consequently, WR-WDM-PON architecture, due to the low cut-off frequency passband of AWG multiplexer/de-multiplexer, which leads to the considerable cut-off of the 28 GHz intermediate frequency IF signal.

As a result, was concluded that WR-WDM-PON architecture can be successfully utilized for the generation and transmission of 2.5 Gbaud PAM-4 modulated mm-wave signal ensuring channel spacing of 100 GHz, however for smaller channel spacing, e.g. 50 GHz and smaller, the use of wavelength-selective switch (WSS) with a tunable bandwidth and low roll-off (known as the steepness of a transfer function with frequency, measured in dB/decade) should be used to provide good channel isolation.

5.4 Evaluation of 2.5 Gbit/s NRZ modulated signal transmission in RoF real-time transmission system where signal upconversion is realized by two separately connected CW laser sources

For proof of concept for prior obtained simulation results, the first built setup in RTU TI laboratory was a hybrid mm-wave RoF optical access system model with two separately coupled continuous wave CW laser sources, where one of them was modulated by a 10 GHz MZM modulator and driven with 2.5 Gbits/s (2.5 Gbaud /s) NRZ signal (PRBS15 pattern), as it is shown in *Figure 42*. The experimental setup shows the transmission of RF 28 GHz mm-wave intermediate frequency IF signal (as the laser 1 has a central frequency of 193.1 THz and laser 2 has a central frequency of 193.128 THz, forming the intermediate frequency of 28 GHz) over the optical access system and also show is further transmission over the 28 GHz radio frequency, which is hard to model in the simulation environment.

Major technical parameters of each component are shown on the respective component, as shown in *Figure 42*. It is worth noting that, due to the availability of different components which does not perfectly match the technical parameters components used in simulation model (as the simulation model was first and it was used to predict the overall operation of the system and the impact of separate optical, electro-optical or electrical components).

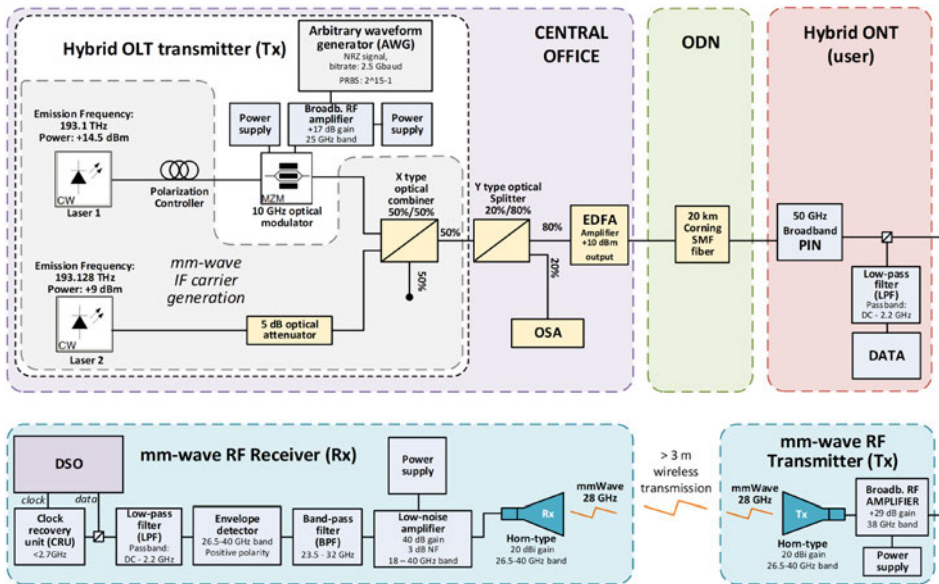


Figure 40. The first experimental setup of 2.5Gbit/s NRZ-OOK modulated 28 GHz mm-wave hybrid analog mm-wave RoF optical access system with RF transmission distance of at least 3 meters.

In optical distribution network ODN is used a 20 km ITU-T G.652 standard single-mode optical fiber with attenuation coefficient of 0.2 dB/km and dispersion coefficient of 16 ps/nm/km at 1550 nm reference wavelength. As for the optical receiver, was used a 50 GHz broadband PIN

photoreceiver, which realized the photonic up-conversion process, where the RF signal is generated. As it is shown in *Figure 40.*, was not coupled both continuous wave CW laser sources and then modulated both (as it was done in the simulations), because in the laboratory, the central frequencies of both lasers are not perfectly stable, as it was in the simulation models of such a hybrid system. Therefore, it was assumed that if only one of the lasers is modulated by the data signal and then coupled with the other laser (which in this case works as a local oscillator – LO for the generation of mm-wave signal). Both laser sources were C-band narrowband laser sources with up to +16 dBm output and linewidth less than 100 kHz, where set the center frequency of 193.1 THz for Laser 1 and 193.128 THz for Laser 2, therefore defining that the central frequency IF of mm-wave RF signal will be 28 GHz. As shown in *Figure 40.*, the hybrid ONT part includes 50 GHz broadband PIN, where the output RF signal can be divided by RF divider and by using the lowpass filter, baseband signal (DC-2.2 GHz) can be filtered out. Another part of the RF signal in the mm-wave RF transmitter (Tx) is amplified by a 38 GHz and +29 dB gain broadband amplifier before being transmitted to the Ka-band (26.5 – 40 GHz) horn-type antenna with 20 dBi gain. In the first trial, the free space distance providing line of sight conditions was 3 meters, where the free space path loss (FSPL) of the transmitted 28 GHz signal was 30.93 dB. The transmitted mm-wave signal was received by the same type of Ka-band antenna and amplified by the 40 dB LNA (noise factor (NF) was 3 dB), to provide its further processing in mm-wave RF receiver Rx part. After amplification, the signal with 28 GHz central frequency was filtered by the band-pass filter and sent to the envelope detector with positive polarity, which realized the frequency downconversion of 28 GHz IF signal. The downconverted baseband 2.5 Gbit/s NRZ signal was then filtered by the DC-2.2 GHz low-pass filter and sent to DSO for the analysis of its quality and BER estimation. As it is shown in *Figure 40.*, for the BER evaluation of NRZ signal, the external clock from Anritsu clock recovery unit (CRU) is used. *Figure 41.* shows some insight into the realized hybrid mm-wave RoF optical access system model setup, with some key components.

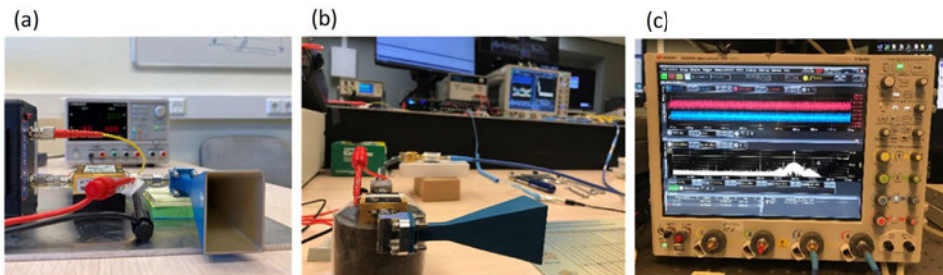


Figure 41. Some photos from our realized model of hybrid analog mm-wave RoF fiber optical access system: (a) 50 GHz PIN receiver with 40 GHz broadband amplifier, power supply, Ka mm-wave 20 dB gain horn-type antenna, (b) receiver part consisting of 20 dB gain horn-type Ka mm-wave antenna, low-noise amplifier, bandpass filter, envelope detector, low-pass filter and DSO (downconverted 2.5 Gbit/s NRZ signal), and (c) measured mm-wave RF signal on the output of 23.5 – 32 GHz band-pass filter, before envelope detector.

In the wireless part of the setup, was transmitted the 28 GHz RF signal (containing 2.5 Gbit/s NRZ data, PRBS15 (pattern length $2^{15}-1$), which is in line with proposed frequencies for 5G

applications. Initial transmission distance or distance between Tx and Rx mm-wave horn-type antennas was 3 meters, where the line of sight-propagation was ensured. On the 28 GHz frequency band, the wireless signal experienced very high attenuation or free space path loss FSPL (see [Figure 42.](#)), which was taken into account for the power budget calculation of hybrid optical access system.

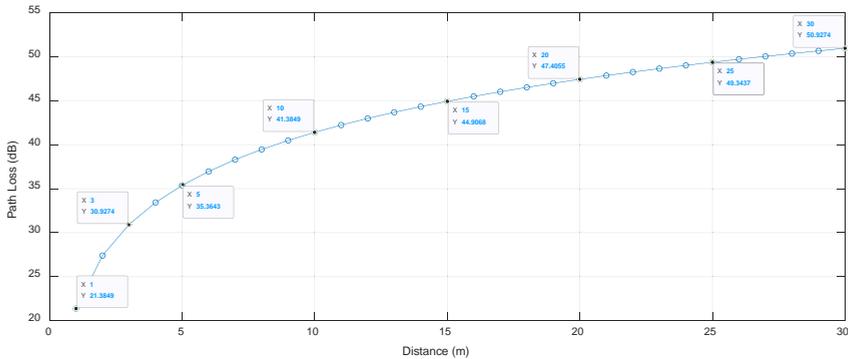


Figure 42. Calculated free space path loss (FSPL) of the transmitted 28 GHz signal versus the distance between Tx and Rx mm-wave antennas with 20 dBi gain each.

Despite the fact that was modulated only one of the laser sources (Laser 1), first tests with 2.5 Gbit/s NRZ-OOK signal showed that the RF signal at 28 GHz is non-stable as it has carrier instability of ± 80 MHz, as it can be also seen in [Figure 43.](#), where the carrier frequency is not exactly 28 GHz. Due to the mm-wave carrier frequency instability, these variations limit the spectrum-efficient 5G channel deployment. As one can see in [Figure 43.](#), the carrier frequency (see the spectrum on the right) is not stable and equal to 28 GHz as it should be. Also, from the eye diagram on the left, we can see the high noise impact (low SNR) as voltage variance the logical “1” and “0” levels, as well as the jitter, are relatively large, therefore pushing the eye to close. Observed the 28 GHz carrier frequency instability was due to the natural instability of laser sources used caused by the phase noise (please see [Figure 44.](#)), however, for 2.5 Gbit/s NRZ signal, as it is shown in [Figure 43.](#), was possible to provide error-free transmission over distances at least 3 meters, where line-of-sight conditions were provided. From the literature are know, that the basic concept of phase noise centers around frequency stability, or the characteristic of an oscillator to produce the same frequency over a specified time period [118]. In line with this, as shown in [Figure 44.](#), the output of a “single-frequency” laser is not perfectly monochromatic. Instead, it is experiencing some phase noise, i.e., fluctuations of the optical phase. This is very important when we used two laser sources for the generation of the mm-wave RF signals by using the photonic upconversion technique. If both laser sources have an unstable central frequency, the mm-wave frequency also is unstable – it is drifting. In the laboratory environment, was experienced ~ 80 MHz drift around the 28 GHz central mm-wave frequency, which resulted in the reduced eye opening and jitter of the recovered 2.5 Gbit/s NRZ signal.

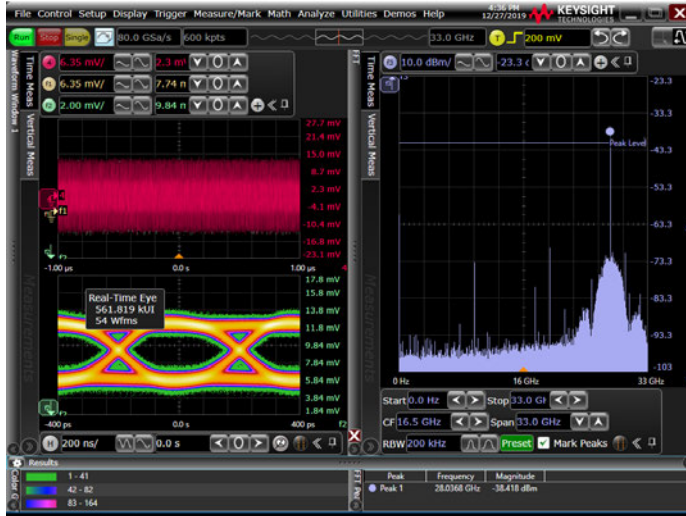


Figure 43. Real-time 2.5 Gbit/s NRZ signal eye diagram (obtained by Keysight DSO using in-built real-time envelope detector and DC-2.2 GHz low-pass filter).

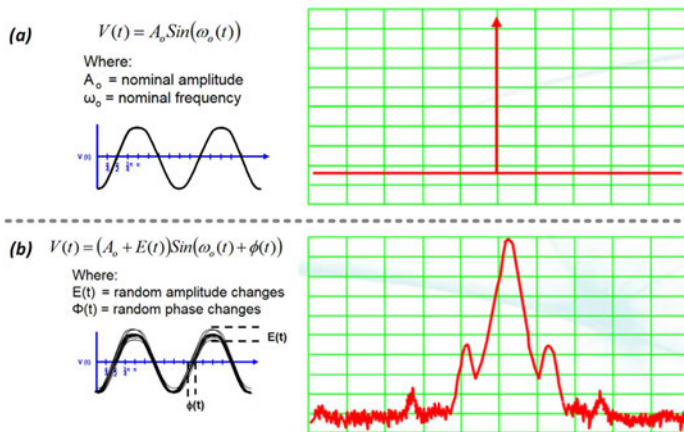


Figure 44. Comparison of (a) ideal signal and (b) real-world signal with random amplitude and phase changes [119].

However, for the PAM-4 signal instead of 2 logical signal levels, we have 4 levels, which have higher OSNR demands. With this experimental setup was observed that due to the IF carrier (28 GHz) frequency instability and therefore received waveform distortions caused by it, the error-free transmission was not possible (all three PAM-4 signal eyes were closed).

5.5 Evaluation of 2.5 Gbaud/s NRZ and PAM-4 modulated signal transmission in RoF real-time transmission system where signal upconversion is realized by one CW laser sources

To mitigate the problem of 28 GHz IF frequency instability caused by laser phase noise, the way how we generate the reference laser signals (data and LO) was changed. Instead of using two independent tunable optical narrowband laser sources, was used only one of them (laser 1, 193.1 THz central frequency), and through null-biased 40 GHz MZM modulator modulated it by the sinusoidal signal, which has a frequency equal to half of our expected mm-wave frequency (14 GHz), as it is shown in the second experimental setup, see *Figure 45.*, below.

As shown in *Figure 45.*, the significant difference between this experimental setup and the previous one is the mm-wave IF carrier generation part located in the hybrid OLT transmitter. As well, due to the optimization of the parameters (input power levels on different electrical and optical components, power budget optimization, signal polarization state (before both MZMs)), the transmission distance between both Ka-band antennas was increased up to 6 meters, limited by the dimensions of the laboratory facilities. However, power budget calculations showed that the transmission distance, keeping the line of sight conditions, can be increased also up to 150 meters.

For the generation of multiple correlated carriers, the 40 GHz MZM modulator was biased at its null point (V_p , around 2.7 VDC, as shown in *Figure 46.*) and driven with a 14 GHz sinusoidal signal ($V_{pp}=3.68$ V) from up to 31.8 GHz Anritsu RF/Microwave Signal Generator. In such a way, on the output of the first 40 GHz MZM modulator, three optical carriers with 14 GHz spacing between every one of them was obtained, where the spacing between the first and third major carrier is about 28 GHz, as it is shown below in the figure captured from the optical spectrum analyzer (see optical spectrum analyzer (OSA) e.g. OSA1 block in *Figure 45.*).

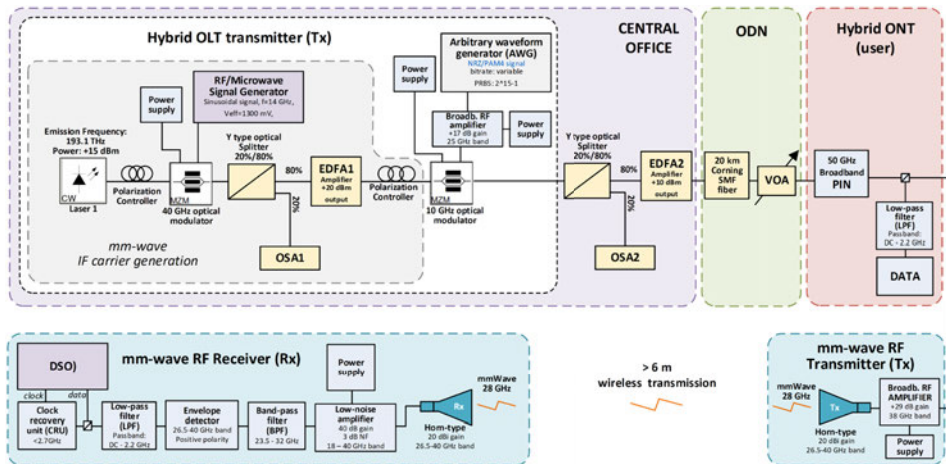


Figure 45. Second experimental setup of variable bitrate NRZ-OOK and PAM-4 modulated 28 GHz mm-wave hybrid analog mm-wave RoF optical access system with RF transmission distance of at least 6 meters.

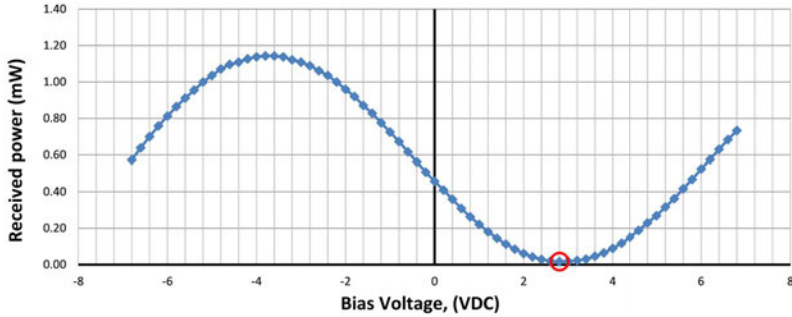


Figure 46. Measured Received Power VS Bias Voltage (linear MZM transfer function).

As one can see in Figure 47., the first and third generated carriers have the highest peak power (around -15 dBm (variation between both peak powers can be caused by the measurement error due to limited OSA wavelength resolution), while the carrier in the center is 3.32 dB lower (2.15 times lower) in power. By changing the power of the sinusoidal signal applied to the RF input of the MZM, was found a point ($V_{\text{eff}}=1.3$ V), where the power of the center carrier (which is not needed for our application and in the ideal case should be filtered off) has the lowest power if compared to neighbor carriers. Accordingly, after receiving such an optical signal with 3 carriers (as shown in Figure 47.) directly by the broadband 50 GHz PIN, on the output of this PIN, was received an electrical signal, which spectrum contains the baseband part and two carriers: one 14 GHz and one 28 GHz carrier.

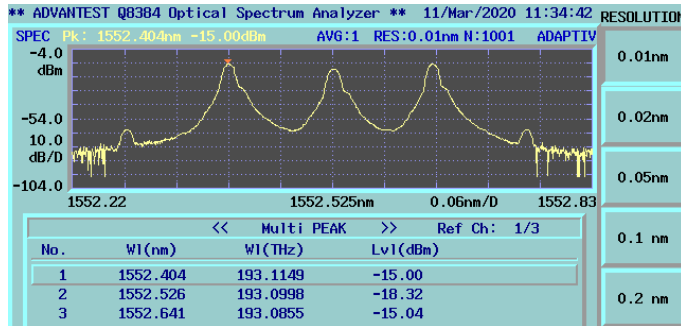


Figure 47. Measured optical spectrum on the output of the null-biased MZM modulator, driven by 14 GHz sinusoidal signal (0.01 nm resolution, 1001 points captured).

This, above mentioned, is shown also in the spectrum captured by 33 GHz DSO, see Figure 48.. To see the spectrum of the real-time waveform on the DSO's screen, a time-domain waveform should be converted into a frequency domain waveform through the Fast Fourier Transform (FFT) Magnitude math function, which creates a magnitude versus frequency waveform by using the well-known Fast Fourier Transform FFT. There, in the electrical spectrum of the signal received on the output of PIN, the 14 GHz carrier is generated due to the middle optical carrier component (shown in Figure 47. around 1552.526 nm or 193.0998 THz). As it is shown in Figure 47., the

central (middle) carrier is around 193.0998 THz, the first carrier is 193.1149 THz and the third carrier is 193.0855 THz. However, there is a measurement error due to the limited minimal resolution of our OSA (0.01 nm, which is a typical resolution for normal laboratory OSA). If it were possible to have an OSA with a much higher resolution, it will be possible to see that the central carrier is 193.1 THz, the third first carrier is around 193.086, and the first carrier is 193.114 THz. Of course, also the laser itself has a frequency drift, which can cause wavelength/frequency measurement error on the OSA. But, as all carriers are generated from one laser source then they are highly interrelated and the wavelength or frequency spacing between all of them stays fixed. Accordingly, the frequency spacing between the first and third carrier is 0.028 THz or 28 GHz.

Despite the fact, that we have this 14 GHz middle carrier in the electrical spectrum on the output of the broadband PIN, its negative impact on the waveform quality of transmitted mm-wave RF signal, which reduces the efficiency of heterodyning up-conversion process was identified as minimal, as subsequently it was naturally suppressed by our used horn-type mm-wave RF antennas (which have the passband of 26.5 to 40 GHz) and later by the limited passband of low noise broadband amplifier (LNA) (18 to 40 GHz bandwidth), filters (BPF, 23.5 to 32 GHz bandwidth), and envelope detector used.

In *Figure 48*, is shown the electrical signal (modulated, 2.5 Gbit/s NRZ-OOK, PRBS15) and its spectrum on the out of broadband PIN receiver. The primary focus in this image is on the spectrum (right part) – as we can see that the carrier signals are now stable in comparison to the first experimental setup. We can observe the 28 GHz carrier (27.9999 GHz) as well as the unneeded 14 GHz carrier (13.9999 GHz).



Figure 48. The captured waveform and its spectrum on the RF output of the broadband PIN receiver. *Left* – waveform of mixed baseband and modulated 2.5 Gbit/s NRZ-OOK signal on 14 GHz and 28 GHz carriers (to be amplified and further transmitted to mm-wave band antenna). *Right* - Spectrum of this waveform on the output of PIN receiver after 20 km transmission (captured by Keysight 33 GHz, 80 GSa/s DSO).

After the heterodyne up-conversion by the PIN, this signal was further sent to horn-type 20 dBi gain and 26.5 up to 40 GHz band antenna for the line-of-sight wireless transmission (6 meters were reached, limited by the space in the laboratory). According to the setup shown in *Figure 45.*, the 28 GHz mm-wave signal was received by the other horn-type (20 dBi gain, 26.5 up to 40 GHz band) antenna, then amplified by the LNA (40 dB gain, 18 to 40 GHz band), filtered by 23.5 to 32 GHz BPF to remove the unnecessary out-of-band noise and suppress spectral components, this signal is further directed to the 26.5 – 40 GHz envelope detector to downconvert the modulated 28 GHz mm-wave RF signal to baseband. After the downconverting, another signal filtering by DC to 2.2. GHz LPF is preferred to reject the out-of-band noise. Lastly, the received signal was captured by the 33 GHz 80 GSa/s advanced DSO for its further evaluation, as shown in *Figure 49.*

In the right part of *Figure 49.*, we can see the spectrum of received 2.5 Gbit/s NRZ signal, which occupies around 2.5 GHz. Also, as one can see in *Figure 49.*, the real-time eye diagram of transmitted and received 2.5 Gbit/s NRZ modulated signal is wide open, therefore it is clear that the error-free transmission ($BER < 10^{-9}$) can be provided with such a hybrid mm-wave fiber optical access-wireless system.

As the received signal quality in such an experimental setup was high, experiment was moved towards to higher level by changing of modulation format from NRZ to more demanding PAM4, keeping the same bitrate – 2.5 Gbit/s. As one can see in *Figure 50.*, all three eyes of the received PAM-4 signal are wide open, therefore meaning that **the error-free transmission ($BER < 10^{-9}$) can be provided.** The spectrum of received 2.5 Gbit/s PAM-4 signal occupies around 1.25 GHz of the frequency band.

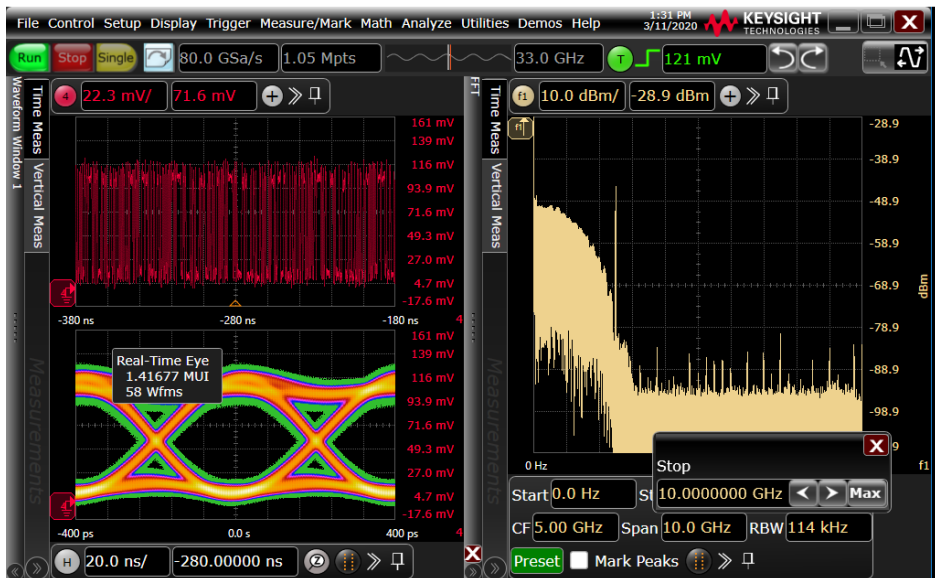


Figure 49. The captured waveform (red, up) of received and downconverted 2.5 Gbit/s NRZ modulated 28 GHz mm-wave RF signal, its eye diagram (left, bottom), and spectrum (right).

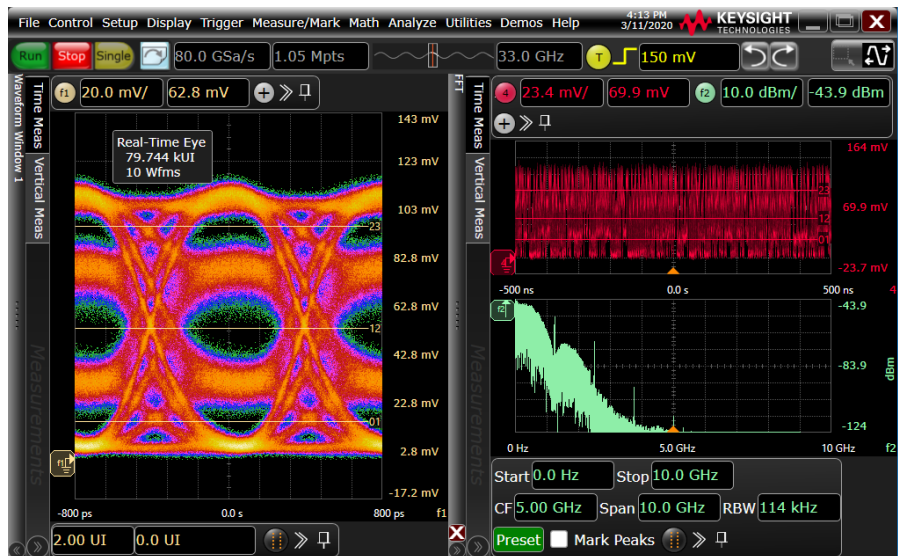


Figure 50. The captured waveform (red, up) of received and downconverted 2.5 Gbit/s (1.25 Gbaud) PAM-4 modulated 28 GHz mm-wave RF signal, its eye diagram (left, bottom), and spectrum (right, green).

Further, to test the limitations of experimental setup, the bitrate of our PAM-4 signal was increased from 2.5 Gbit/s (1.25 Gbaud) up to 5 Gbit/s (2.5 Gbaud), as one can see in Figure 51..

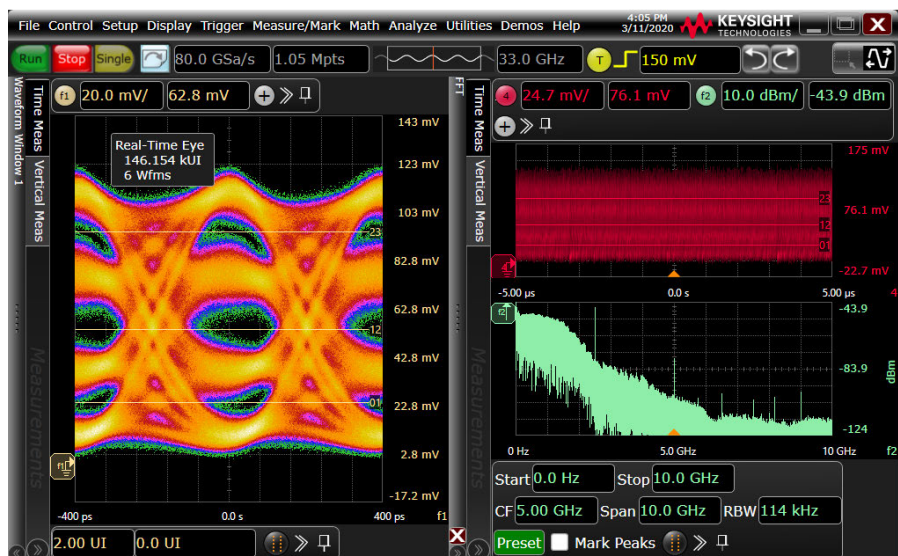


Figure 51. The captured waveform (red, up) of received and downconverted 5 Gbit/s (2.5 Gbaud) PAM-4 modulated 28 GHz mm-wave RF signal, its eye diagram (left, bottom), and spectrum (right, green).

As one can see in *Figure 52.*, the spectrum of received 5 Gbit/s PAM-4 signal occupies around 2.5 GHz of the baseband frequency band. From the results, we can see that the 2.5 Gbaud PAM-4 (5 Gbit/s) is the upper baudrate or bitrate limit of experimental PAM-4 modulated RoF access system technology, as the eye diagram tends to close. **However, as the eye is open, the error-free transmission ($BER < 10^{-9}$) can be provided.** With the increase of the bitrate, it is possible to see that the transmitted PAM-4 signal is more sensitive to amplitude noise, jitter, ISI, as well more filtering effects from the components used in the setup can be observed, e.g. LPF and others, which, of course, have limited bandwidth.

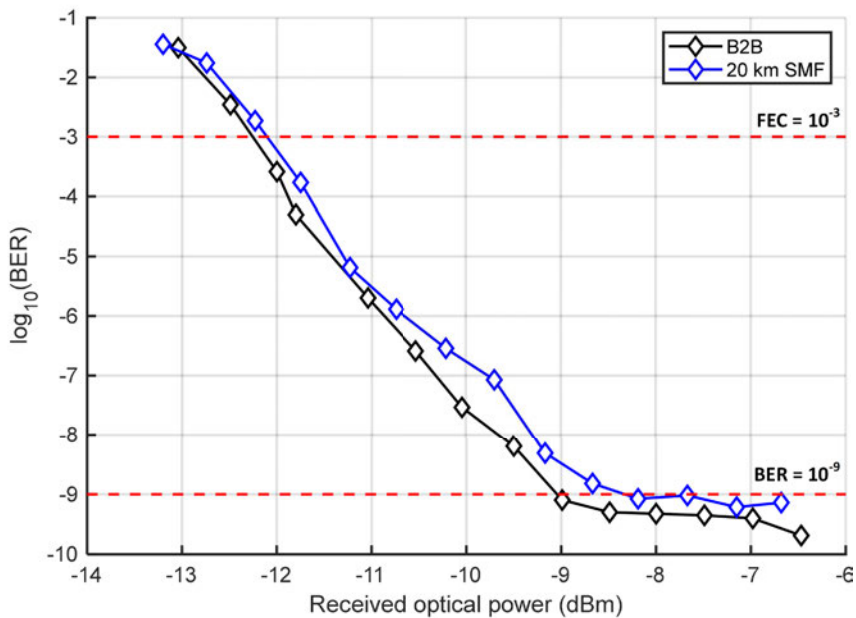


Figure 52. BER vs. received optical power (ROP) after (black line) B2B + 6 m wireless and (blue line) over 20 km SMF + 6 m wireless transmission of 5 Gbit/s (2.5 Gbaud) PAM-4 modulated 28 GHz mm-wave RF signal.

As one can see in *Figure 52.*, the B2B and 20 km SMF transmission performance for 28 GHz mm-wave signal is very similar. The measured power penalty is 0.16 dB at typical FEC threshold level (10^{-3}) and 0.73 dB at $BER 10^{-9}$, which can be accounted as negligible. From experimental results we can see, that proposed hybrid access technology is capable to optically transmit the intermediate frequency of 28 GHz (mm-wave) directly to the mm-wave antenna (in our case it was a horn-type 20 dBi antenna) over at least 20 km ITU-T G.652 optical fiber span and provide further wireless transmission in distances at least 6 meters, which can be further increased by optimizing the power budget of the system or by the introduction of new mm-wave RF components in the market.

5.6 Development of hybrid ARoF-WDM-PON communication system with data transmission speeds of 10 Gbit/s per channel for broadband internet service and up to 2.5 Gbit/s per channel for 28 GHz (ka-band) millimeter wave signal transmission.

In this chapter, the architecture of hybrid analog radio over fiber ARoF and next-generation NG wavelength division multiplexed passive optical network WDM-PON infrastructure for broadband internet services and the latest fifth-generation 5G cellular mobile communications is proposed. Investigated ARoF-WDM PON architecture is a trade-off between technology and cost for future 5G mobile cellular communications to meet the internet service requirements, allowing to increase system capacity ensuring higher spectral and energy efficiency. According to ITU-T G.9803 rec. it is proposed to implement analog radio over fiber ARoF into the passive optical network PON segment, coexisting with a 40-Gigabit-capable passive optical network (NG-PON2) supporting the international mobile telecommunication (IMT) systems over the fiber core network e.g., optical distribution network (ODN) [46], [109].

The goal is to design hybrid AROF-WDM-PON passive optical access communication system and evaluate the performance of such a data and radio signal transmission system, which implements baseband radio processing in a service provider's central office CO part, allows the effective provision of broadband internet and cellular data transmission between the service provider's CO and end-users. Developed and further investigated the 8-channel A-RoF-WDM-PON optical transmission system model is depicted in **Figure 53**. The widespread used passive optical access network (PON) architecture is technologically transformed into the AROF-WDM-PON transmission system without the need to replace existing network elements by integrating mobile radio transmitters of baseband units BBUs and the receiving radio unit RU parts of mobile base stations, leaving the traditional WDM-PON broadband architecture the same.

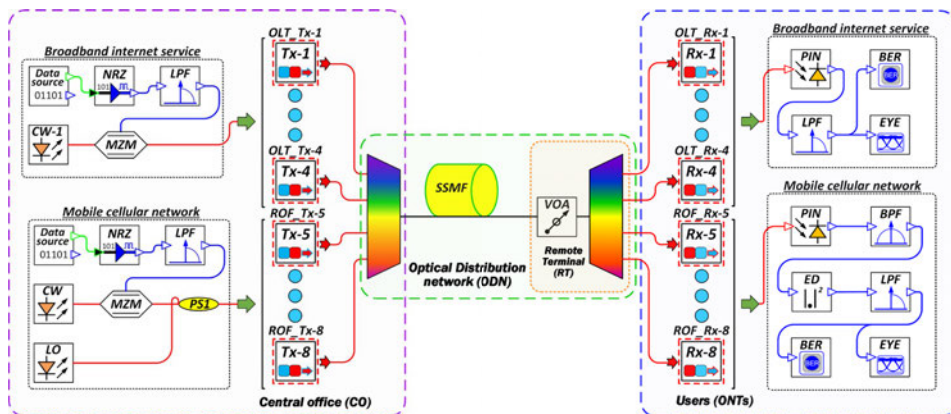


Figure 53. Simulation scheme of 8-channel hybrid ARoF-WDM PON transmission system which consists of two parts: (1st) 4-channel 10 Gbit/s per channel NRZ-OOK modulated signal transmission for broadband internet service and (2nd) 4-channel 2.5 Gbit/s per channel NRZ-OOK modulated multi-channel mobile cellular network - transmission of 28 GHz mm-wave signals for 5G mm-wave interface.

The hybrid AROF-WDM-PON system consists of cellular mobile and broadband internet transmission parts. The cellular mobile part consists of baseband units BBUs and mobile base station incoming receiver radio unit parts RUs, providing a radio signal transmission over fiber RoF, while the broadband internet transmission part consists of an optical line terminal OLT, which houses optical transmitters Tx and a receiver or optical network terminal ONT. Central office CO of our research model includes optical line terminal OLT, which consists of eight transmitters (OLT-Tx), where four of them are unchanged for commercial fiber optical broadband internet end-user data transmission and four of them are modified for A-RoF system data containing 28 GHz carrier frequencies (even more considered frequency bands depending on allocation of regional spectrum management) generation and transport of an intermediate frequencies through existing fiber optical distribution network ODN [109]. Due to management of frequency bands up to 28 GHz (Ka-band) in Europe, Japan, Korea, and Australia, as well as higher frequency bands in the US (≤ 72 GHz V-band), China (≤ 43.5 GHz V-band) are considered for deployment [8], [115], [119], [120].

Displayed results are obtained by the newest RSoft OptSim simulation software, the Matlab software was used to estimate obtained quality of the received signals, perform BER measurements and display them. For this research object the obtained performance of our investigated AROF-WDM-PON transmission system according to a commercially used BER threshold equal to 10^{-12} . Forward-error-correction FEC with a 10^{-3} BER performance threshold is shown to determine the system's performance and received signal capability after 20 and 40 km SSMF optical link transmission which is in line with NG-PON requirements [41]. According to ITU-T G.964.1 recommendation, dense WDM architecture with 50 GHz and 100 GHz channel spacing with 193.1 THz central frequency is chosen for investigated hybrid AROF-WDM-PON transmission system standardized to 40G PON (NG-PON2) requirements. As it is shown in *Figure 53.*, investigated 8-channel hybrid A-RoF-WDM-PON optical transmission system model consists of four channels operating at 2.5 Gbit/s for cellular mobile communication millimeter-wave (mm-wave) interface and four 10 Gbit/s channels for broadband internet connection.

The transmitter part of the cellular mobile communication mm-wave interface consists of baseband units (BBUs) integrated into the OLT of WDM-PON located on the CO side. According to the fundamental architecture of a typical RoF system for the case of downstream transmission, the CO includes OLT with four transmitters, where each of them has been modified to operate as RoF transmitter (ROF_Tx) designed for A-RoF system data containing 28 GHz intermediate frequencies IF generation. Trade-off radio communication service and requirements for the balance in radio signal frequency band, the necessary number of radio signals and optical path loss for various applications are achievable by investigated hybrid AROF-WDM-PON architecture taking into account ITU-T G. 9803 requirements [109]. Each of ARoF transmitters located in OLT for generation of mm-wave IF signal bases on homodyne up-conversion principle and is designed by using two continuous wave (CW) laser sources with a linewidth of 30 MHz, where one of them (with +8 dBm output power) is directly connected to intensity Mach-Zehnder modulator MZM [103], [105]. Second light source with channel spacing equal to necessary intermediate frequency

IF and mm-wave generation (in our case for 28 GHz (Ka-band)), by the inter-channel interval between two laser sources is operating as a local oscillator (LO) with a related output power of +1 dBm. The electrical pseudo-random bit sequence PRBS data source and non-return to zero NRZ driver encode the logical data into NRZ electrical signal [45], [93]. The MZM is driven at 2.5 Gbit/s bit rate by previously formed and Bessel low-pass filter (3-dB bandwidth is 3 GHz) filtered electrical NRZ signal.

The broadband internet transmitter part has an optical line terminal - OLT, which consists of four transmitters (OLT_Tx) located in a CO. Each OLT_Tx transmitter contains CW laser source (30 MHz linewidth, +9 dBm output power), which is directly connected to the intensity MZM modulator. The MZM is driven at 10 Gbit/s bit rate by previously formed and Bessel low-pass filter (3-dB bandwidth is 10 GHz) filtered electrical NRZ signal, passing from NRZ driver. MZM chirp factor, which guarantees the highest performances in terms of maximum achievable dispersion-tolerance in optical fiber links, was not observed. As a result, the transmitted optical signal was affected by the impact of chromatic dispersion CD, which leads to inter-symbol interference. In such a way, it performs E/O conversion using one single carrier (optical tone) for transmission through ODN [45], [103], [121].

The mean launch power of +4 dBm and optical budget (OB) depending on optical path loss within range of 18 to 33 dB is provided for ROF_Tx and OLT_Tx transmitter optical output signals of our investigated hybrid ARoF-WDM PON transmission system, which are compliant with the NG-PON2 defined E1 class optical distribution network ODN requirements [46], [109]. Optical signals from each RoF-Tx and OLT_Tx are coupled together by using arrayed waveguide grating AWG multiplexer with 3.5 dB insertion loss, and depending on the simulation model, 50 or 100 GHz channel interval (3-dB bandwidth is 30 GHz) is chosen. A single-mode optical fiber (SSMF) span with 0.2 dB/km attenuation and 16 ps/nm/km dispersion coefficients (at 1550 nm reference wavelength), according to ITU-T G.652 recommendation, is used for the ODN link sections with the length of 20 and 40 km [46]. After optical signal transmission through the ODN section, a variable optical attenuator VOA is used to obtain BER versus received optical power of the signal. After transmission through ODN and VOA, intermediate frequency IF and single-carrier are separated by AWG de-multiplexer located in the remote terminal RT. AWG de-multiplexer has 3.5 dB insertion loss, 30 GHz 3-dB bandwidth, and depending on the simulation model, it has 50 GHz or 100 GHz channel spacing.

The receiver side consists of optical network terminals (ONTs) divided into two parts: 1st for broadband internet service (channels 1 to 4) and 2nd for a cellular mobile network (channels 5 to 8). In the first scenario, each ONT receiver (ONT_Rx) of the broadband internet network consists of a semiconductor photoreceiver PIN with 50 GHz 3-dB bandwidth, the responsivity of 0.65 A/W, applicable to increase the total bitrate per wavelength up to 40 Gbit/s in line with ITU-T G.989.2 NG-PON2 requirements [46], [106]. After O/E conversion by PIN photoreceiver, received electrical signal is pre-filtering by electrical Bessel low-pass filter LPF with 9 GHz 3-dB electrical bandwidth. In the second part, designed for the cellular mobile network, each ONT receiver (ROF_Rx) consists of the same 50 GHz photoreceiver PIN applicable in both scenarios with ITU-

T G.989.2 [46]. After O/E conversion by PIN photoreceiver, pre-filtering of received electrical signal for each channel is realized by the electrical Bessel band-pass filter BPF, which is tuned to 28 GHz central frequency and has 28 GHz 3-dB electrical bandwidth. Afterward, homodyne down-conversion is realized by the homodyne signal processing technique using a passive Schottky diode-based envelope detector ED [107], [115], [117]. Received and down-converted modulated baseband signal is filtered by an electrical Bessel low-pass filter LPF with 3 GHz 3-dB electrical bandwidth.

Optical signal spectra after B2B and 20/40km long ODN fiber span transmission are shown, please see *Figure 54*. In this research simulation scheme was applied also narrower channel spacing, therefore the second investigated channel spacing was 50 GHz. Spectra of 8-channel 50 GHz spaced hybrid AROF-WDM-PON transmission system in B2B configuration and after transmission over 20 to 40 km long SSMF fiber spans is shown in *Figure 54(a)*, and *Figure 54(b)*.

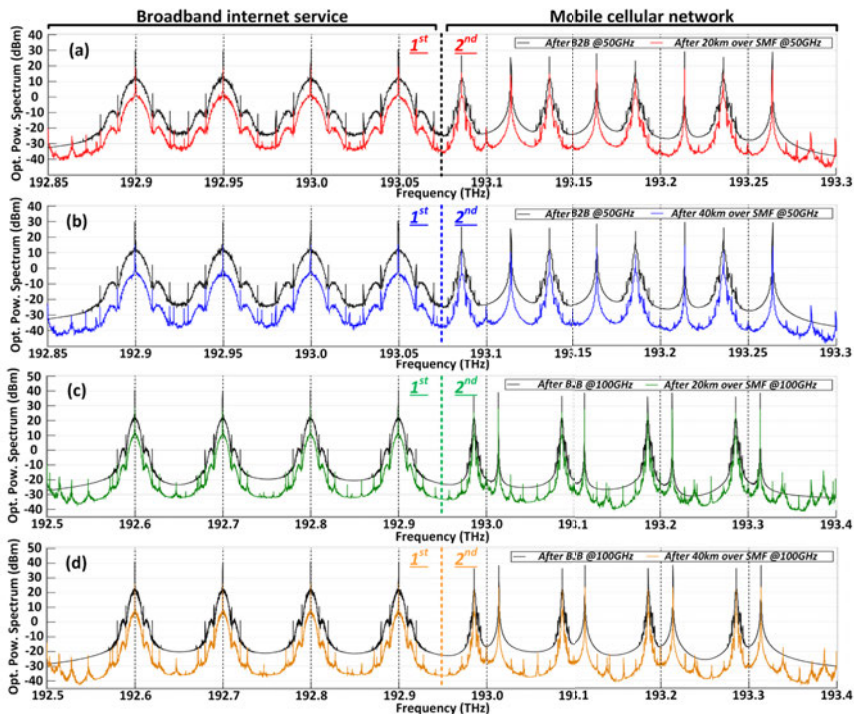


Figure 54. Optical spectra of multiplexed 8-channel hybrid AROF-WDM PON transmission which consists of two parts: (1st) 4-channel 10 Gbit/s per channel NRZ modulated signal transmission for broadband internet service and (2nd) 4-channel 2.5 Gbit/s per channel NRZ modulated 28 GHz mm-wave signal transmission before B2B and after transmission through (a) 20 km long ODN (50 GHz ch. spacing), (b) 40 km ODN (50 GHz ch. spacing), (c) 20 km ODN (100 GHz ch. spacing), and (d) 40 km ODN (100 GHz ch. spacing).

The obtained BER versus received optical power at PIN photoreceiver in two different scenarios with 50 and 100 GHz channel spacing for (1st) 10 Gbit/s (broadband internet) NRZ signal and (2nd)

down-converted 2.5 Gbit/s (28 GHz mm-wave 5G signal) after transmission over 20 to 40 km long ODN SSMF fiber span in 8-channel hybrid ARoF-WDM-PON transmission is shown in *Figure 55*.

As one can see in *Figure 56(b)* and *Figure 56(d)*, the signal quality after 20 and 40 km long ODN SSMF section transmission for cellular network mm-wave and end-user fiber optical broadband signal is good, the eye is open and error-free transmission is provided. After 40 km transmission through the ODN section over standard SSMF fiber, we conclude that received signal for broadband internet with 10 Gbit/s bitrate is mainly affected by the impact of crosstalk and chromatic dispersion.

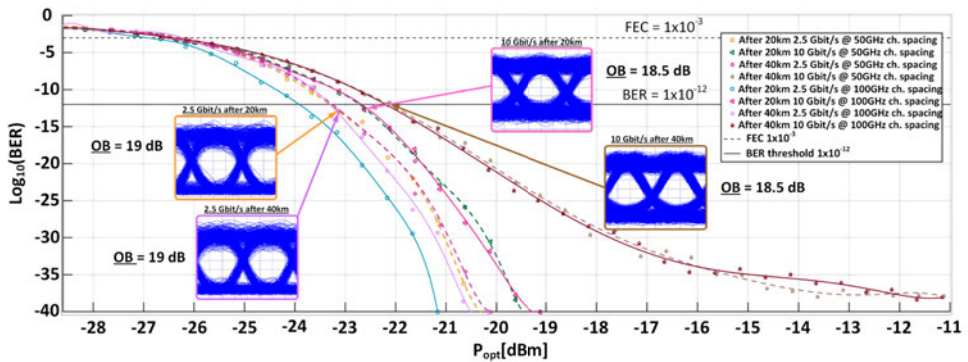


Figure 55. BER vs. received optical power for (1st) down-converted 2.5 Gbit/s (28 GHz mm-wave 5G signal) and (2nd) 10 Gbit/s (broadband internet) NRZ signal after hybrid ARoF-WDM PON transmission over 20 and 40 km SSMF fiber. Insets show the received signal eye diagrams after transmission over SSMF for 2.5 and 10 Gbit/s bitrates with 50 GHz ch. Spacing.

As one can see in *Figure 57(b)* and *Figure 57(d)* after transmission for our investigated 8-channel hybrid ARoF-WDM PON transmission system with 50 and 100 GHz channel spacing through 40 km ODN in 1st scenario for (broadband internet service) the NRZ signal operating at 10 Gbit/s bit rate per channel was mainly affected by CD, where the BER was 1.3×10^{-38} and 9.6×10^{-37} .

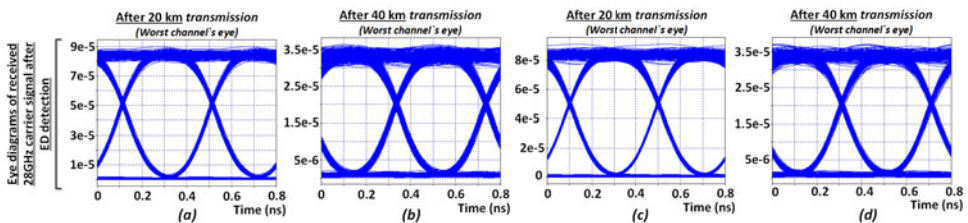


Figure 56. Eye diagrams of received 2.5 Gbit/s NRZ modulated 28 GHz mm-wave signal after ED detection: (a) after 20 km over SSMF transmission at 50 GHz spacing, (b) after 40 km over SSMF transmission at 50 GHz spacing, (c) after 20 km over SSMF transmission at 100 GHz spacing, (d) after 40 km over SSMF transmission at 100 GHz spacing for multiplexed 8-channel hybrid ARoF-WDM PON transmission system.

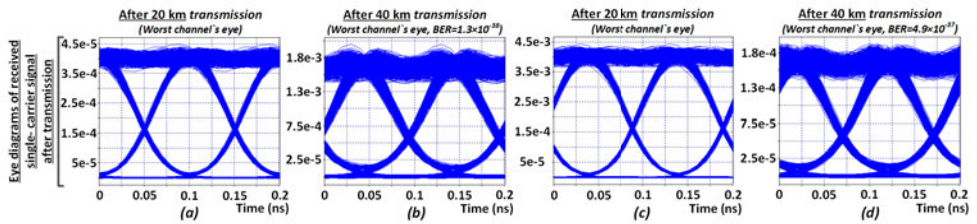


Figure 57. Eye diagrams of received 10 Gbit/s NRZ modulated broadband internet signal: (a) after 20 km over SSMF transmission at 50 GHz spacing, (b) after 40 km over SSMF transmission at 50 GHz spacing, (c) after 20 km over SSMF transmission at 100 GHz spacing, (d) after 40 km over SSMF transmission at 100 GHz spacing for multiplexed 8-channel hybrid ARoF-WDM PON transmission system.

According to obtained results, the proposed 8-channel ARoF-WDM-PON transmission system model can provide data transmission over an optical fiber distribution network with a length of up to 40 km with E1 class optical path loss using standardized ITU-T G.652 optical fiber as a signal transmission media.

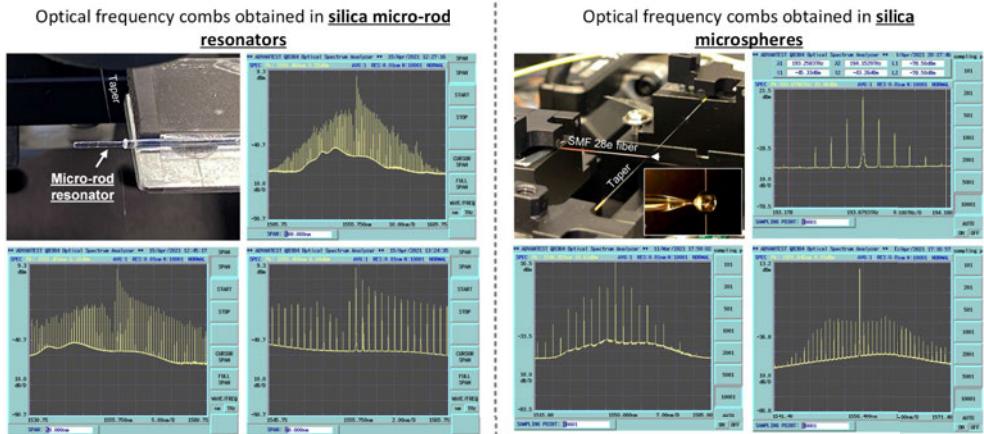
6 IMPLEMENTATION OF SPECTRALLY EFFICIENT WDM TRANSMISSION SYSTEM WITH SILICA MICROSPHERE (SiO₂) WGMR-BASED KERR-OFC LIGHT SOURCE.

6.1 Whispering Gallery Mode (WGM) based optical frequency comb sources (OFC) and its application in telecommunications.

Kerr optical frequency combs OFCs based on whispering-gallery-mode microresonator WGMR with a single laser source have already shown different applications and especially its application in fiber optical communication systems replacing multiple laser arrays [122]. Accurate timing, low phase noise, and the narrow linewidth of generated harmonics allow achieving the ultimate performance desired from an optical comb-based system. Besides this, OFC generators have applications in areas such as optical clocks [10], ultra-stable microwave generators [11], applications that require a precise and stable optical frequency distribution via long fiber [123], spectroscopy [12], sensing [13], quantum applications [14], optical communications [15], etc.

OFC sources for wavelength division multiplexed WDM systems cover use cases ranging from short reach fiber-optic links (e.g., as for data center interconnects DCI) to metro-access fiber-optic links interconnecting a large geographic areas [9], [16]. More specifically, the WGMR-based Kerr-OFC comb generators physically realized on silica microsphere demonstrate [9] a new concept that provides an attractive solution to intra-DCIs due to low cost and energy consumption. The data centers (DCs) are the foundation of Internet applications such as cloud computing, where Big Data storage and large-scale high-performance computing (HPC) take place. The intra-DCI devices and systems that rely on the sharing of computing resources require not only large capacity but, most importantly, high scalability and low energy consumption. Therefore, these requirements require new transmission technologies for short-reach communications [16], [124]. The main aspect of minimizing the expenses is the energy and spectral efficiency of the communication system. Both can be met by introducing an OFC generator [125] instead of laser arrays. From the energy efficiency (as well as spectral efficiency) perspective, it is better to use a single light source instead of several lasers. **Potentially cost-effective solutions for the realization of data transmission in optical WDM networks are OFC generation in silica whispering gallery mode resonator – microspheres manufactured from melted telecom fiber**, e.g. from Corning SMF 28e (ITU-T G.652) [9], [125]–[129], microtoroids **and resonators manufactured on the silica rod** [127]–[129], which is realized as the pumping of a high-quality (high-Q) optical resonator with Kerr nonlinearity using a single continuous-wave laser. When optimal conditions are met, the intracavity pump photons are redistributed via the four wave mixing (FWM) to the neighbouring cavity modes, thereby creating the so-called Kerr OFC. The exciting pump signal is launched into the Kerr-OFC resonator via a tapered fiber and an OFC is being generated at the output of this taper. The Kerr-OFC output spectrum for optical frequency comb obtained in silica **microspheres resonator manufactured from melted telecom fiber and OFC comb obtained in the silica rod**, please see in *Figure 58*. Kerr microresonator OFCs can achieve bandwidths of hundreds of nanometres covering different (e.g. E-, S-, C- and L-band) telecommunication bands. An OFC

source can produce the grid of equally spaced (according to ITU-T G. 694.1 recommendation) optical spectral lines (carriers) needed to sustain the data channels.



Micro-rod resonators can provide better comb stability over time and enable potential integration on-chip, while the production cost and complexity of silica microspheres is incomparably lower.

Figure 58. Optical frequency combs obtained in silica micro-rod and silica microspheres at RTU TI.

These comb lines are subsequently used as optical carriers for the data transmission using the intensity modulation direct detection IM/DD, where NRZ-OOK or a more complex PAM-4 modulation format can be applied.

In terms of these PhD author are capable of showing obtained and published results of silica microspheres for telecommunication applications; unfortunately, the micro-rod Kerr-OFC source results (used as a light source for the telecommunication applications) is under IPR during the ERDF project agreement!

It is important to note that at the moment, the project team is the only one in the world to experimentally demonstrate high-speed data transmission using harmonics generated in the silica microsphere. The results of this world-class experiment are described in the publication where first author and principal investigator is Tom Salgals - “*Demonstration of a fiber optical communication system employing a silica microsphere-based OFC source*”, Optics Express (Q1 Journal), 29, 10903-10913 (2021).

6.2 Experimentally designed setup and characteristics of silica microsphere WGMR-based Kerr-OFC light source for application in optical communications

6.2.1 Characteristics of silica microsphere WGMR-based Kerr-OFC light source.

Kerr optical frequency combs (OFC) based on whispering-gallery-mode microresonator (WGMR) with a single laser source have already shown different applications and especially its application in fiber optical communication systems replacing multiple laser arrays[122]. The main

aspect of minimizing the expenses is the energy and spectral efficiency of the communication system. Both can be met by introducing an OFC generator [125] instead of laser arrays. From the energy efficiency (as well as spectral efficiency) perspective, it is better to use a single light source instead of several lasers. It can provide a lower energy consumption while ensuring improved spectral efficiency and a stable frequency spacing between the OFC lines (carriers) thanks to the sustained strong phase relation between them [9], [125], [130]. Potentially cost-effective solutions for the realization of data transmission in optical WDM networks are OFC generation in silica whispering gallery mode resonator – microspheres manufactured from melted telecom fiber, e.g. from Corning SMF 28e (ITU-T G.652) [9], [125], [131], which is realized as the pumping of a high-quality (high Q factor) optical resonator with Kerr nonlinearity using a single continuous-wave CW laser. When optimal conditions are met, the intracavity pump photons are redistributed via the FWM to the neighbouring cavity modes, thereby creating the so-called Kerr OFC. The exciting pump signal is launched into the Kerr-OFC resonator via a tapered fiber and an OFC is being generated at the output of this taper.

In addition, besides being energy-efficient, conceptually simple and structurally robust, Kerr comb generators are very compact devices (to micrometric size) that can be integrated on a chip [132], [133]. Kerr microresonator OFCs can achieve bandwidths of hundreds of nanometres covering different (e.g. E-, S-, C- and L-band) telecommunication bands [134]. Extending OFCs to the L-band is also a straightforward solution for WDM-PONs when using the C-band is insufficient to satisfy the bandwidth demand. U-band laser sources are mainly used for network monitoring purposes, so their development and investigation is also required. For a more detailed description and illustration, please see author PAPER-10, where three experimental series on spectrally separated OFC generation in silica microspheres was observed:

- **OFC near the pump frequency in the C-band, the second Stokes OFC in the U-band and beyond, and the third anti-Stokes OFC in the E-band** (The gain coefficients and gain bandwidths for degenerate four-wave mixing FWM processes under the strong intraresonator CW field approximation was estimated).
- **By simply tuning the pump frequency via pump frequency in the 190-198 THz range attained, frequency tunable Raman OFCs and E-band OFCs and a C-band OFC were estimated.**
- **OFC when the the pump frequency was in the normal dispersion range – as a result was attained a Raman soliton-like spectrum without symmetric high-frequency sideband.**

An OFC source is capable of producing the grid of equally spaced (according to ITU-T G. 694.1 recommendation) optical spectral lines (carriers) needed to sustain the data channels. This advantage of the generation of several spectral lines applies also to WDM receivers, where an array of discrete local oscillators LO might be replaced by a single OFC. Such solutions are of importance for the fifth (and next) generations of mobile networks, where the optical signal down-conversion to millimeter wave (mm-wave) bands (e.g. Ka-band (26 –28 GHz)) by using a stable LO at the receiver side can be required as a part of the architectural solution [135]. Silica (SiO₂)

microspheres with diameter $D=170\ \mu\text{m}$ used for the Kerr-OFC were fabricated from a standard ITU-T G.652 single-mode telecommunication fiber by the melting method using a specially developed program for a commercially available optical fusion arc splicer.

During the manufacturing process, by changing the diameter of the fabricated silica microsphere, we can obtain an OFC with free spectral range (FSR, spacing between generated carriers) ranging from about 200 GHz (sphere $D=320\ \mu\text{m}$) [136] up to about 400 GHz (sphere $D=170\ \mu\text{m}$) [134]. In addition to the possibility of fine-tuning the coupling conditions between the resonator and tapered fiber, which is not possible for chip-based resonators with integrated waveguides, and, therefore can be considered to be a major advantage over other OFC technologies. Silica microsphere resonators also have advantages of fast and simple fabrication using commercially available fusion arc splicers, allowing the fabrication of silica microspheres with user-defined sphere diameter and high-quality factor ($Q \geq 10^7$) in a couple of minutes.

Most applications, especially silica microsphere-based Kerr-OFC, require the realization of the highest possible quality factor (so-called Q factor) microsphere resonators. It is important to mention that in regular laboratory conditions, the microsphere's Q factor deteriorates within a 1-h time scale in the open environment due to the deposition of nanoscale particles or water vapors to the microsphere surface. The Q factor of the microsphere is determined by several aspects such as intrinsic radiative (curvature) losses, scattering losses on residual surface inhomogeneities, losses introduced by surface contaminants and material losses [137]. For more detailed illustration (see *Figure 59.*), where newly fabricated and artificial degradation of the microsphere surface by water vapours is obtained using a scanning electron microscope (SEM, Hitachi S-4800) for $170\ \mu\text{m}$ silica microsphere resonators. Scanned sphere illustrations with a focused beam of electrons (captured at: 3kV (accelerating voltage), 4.0 mm (surface scale) @ $\times 400$ to 45.0k times and 2.9mm @ $\times 180k$ times) for a particular microsphere resonator after 100% humidity exposure (resonator has been in

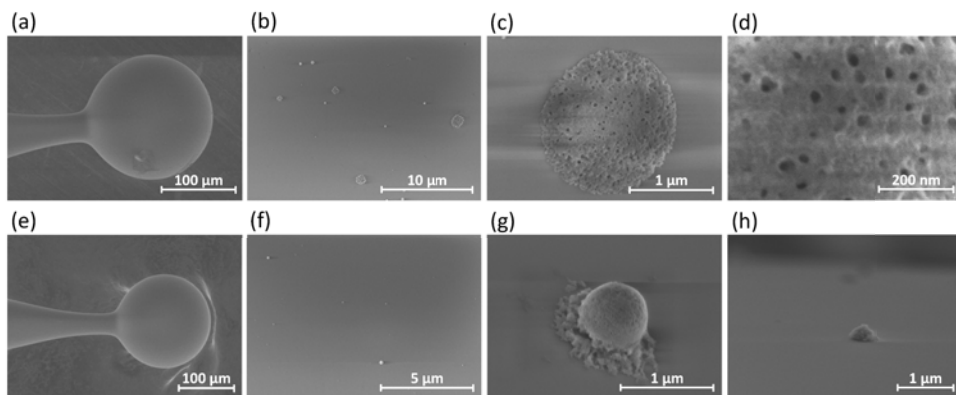


Figure 59. Illustration of $170\ \mu\text{m}$ SiO_2 microsphere resonator scans captured by SEM at 3 kV after artificial degradation by 100% humidity exposure: (a) 4.1 mm @ $\times 400$ times, (b) 4.0 mm @ $\times 5.00k$ times, (c) 4.0 mm @ $\times 45.0k$ times, (d) 2.9 mm @ $\times 180k$ times, and captured illustrations for newly fabricated $170\ \mu\text{m}$ SiO_2 microsphere: (e) 4.0 mm @ $\times 300$ times, (f) 4.0 mm @ $\times 10.0k$ times, (g) where evaporated silica from the arc fusion splicer discharge at 4.0 mm @ $\times 50.0k$ times, and (h) nanoscale particles at 4.0 mm @ $\times 30.0k$ times were observed.

humidity fog for 5 seconds) are shown in **Figure 59(a-d)**. The newly fabricated silica microsphere resonator obtained by the SEM (captured at: 3kV, 4.0mm @ x300 to 50.0k times), is shown in **Figure 59(e-h)**. White dots (see **Figure 59(f)**) – evaporated silica (cristobalite) from the arc fusion splicer discharge explain why the maximal Q factor of a newly fabricated microsphere is below 1×10^8 . We can observe that the evaporated silica dust from the arc fusion splicer (see **Figure 59(g)**) and nanoscale particles (see **Figure 59(h)**) are deposited on the surface of the silica microsphere.

It is important to note that during the experiment, by testing samples of fabricated microspheres, it is able to improve significantly the degraded 4 month-old microsphere (addicted by water vapours) Q factor from $Q = 2.0 \times 10^6$ (96 MHz full width at half maximum (FWHM) of the whispering gallery mode (WGM) resonance) to $Q = 4.4 \times 10^6$ (44 MHz FWHM of the WGM resonance) using a pure hydrogen (H) flame of a micro burner. Note that the Q factor of newly fabricated microsphere was 3.7×10^7 (5.2 MHz FWHM of the WGM resonance). The built up circulating intensity [138] was estimated to be 14 GW/cm^2 exceeding $\sim 1.0 \text{ GW/cm}^2$ [129] needed for OFC generation (see **Table 7**). No OFC was generated when it degraded below 2.0 GW/cm^2 . Microresonator with high Q factor can build up a significant internal circulating intensity when pumped with low laser power. The circulating intensity can be found [138]:

$$I_{circ} = \frac{P_{circ}}{A_{eff}} \quad (1)$$

where P_{circ} is internal circulating power and A_{eff} is the effective area of the mode area of the resonance. A_{eff} can be found by using simulations. As calculation parameters resonator radius, refraction index and resonance frequency at 1550 nm wavelength for fundamental mode were used. The P_{circ} in the silica microsphere WGMR can be found as [138]:

$$P_{circ} = P_{in} \frac{\lambda Q_{intr} K}{\pi^2 n R (K+1)^2} \quad (2)$$

where λ is the resonance wavelength, n is the refraction coefficient, R the microsphere radius, P_{in} the input power ($P_{in}=100 \text{ mW}$), K the coupling parameter, and Q_{intr} is the intrinsic Q-factor. Coupling parameter can be estimated using the transmission T at the resonance frequency [139]:

$$T = \left(\frac{1-K}{1+K} \right)^2 \text{ or } K = \frac{1 \pm \sqrt{T}}{1 \mp \sqrt{T}} \quad (3)$$

Table 7.

Results of characteristics calculations for 170 μm SiO_2 microsphere resonator vs. life cycle.

Life cycle	T	K	FWHM, MHz	Q	Q_{intr}	P_{circ} , W	I, GW/cm^2	Resulting OFC
Freshly fabricated	0.13	2.1	5.2	3.7×10^7	1.2×10^8	3327	13.8	yes
After 2 months	0.64	9.0	15.7	1.2×10^7	1.2×10^8	1458	6.0	yes
After 3.5 months	0.62	8.4	50	3.9×10^6	3.6×10^7	455	1.9	no
After 4 months	0.78	16.1	96	2.0×10^6	3.5×10^7	249	1.0	no
After 4 months (repaired by Hydrogen flame)	0.74	13.3	44	4.4×10^6	6.3×10^7	538	2.2	no

Several moisture and dust degradation methods of protection can be used to keep high Q factor of newly fabricated silica resonators, for instance, storage with ethanol drops or storage with dry nitrogen within hermetic enclosure boxes. The packaging technique utilized by UV-curable polymer for stabilizing both the microsphere and the tapered fiber could be preferred for long-term maintenance of silica microsphere WGMR-based Kerr-OFC light sources. While the use of a coating polymer significantly increases the stability of mechanical alignment between the microsphere and taper accompanied by a relatively low absorption and insertion loss of polymer packaging [140]. An additional solution to keep high Q factor for silica microresonators and taper satisfying coupling conditions and providing improved long-term frequency stability is packaging into modules that feature temperature control by integrated Peltier elements [141].

6.2.2 Experimentally designed setup and characteristics of silica microsphere WGMR-based Kerr-OFC light source

The setup used for the generation of WGMR-based Kerr-OFC is shown in *Figure 60(a)* and *Figure 60(c)*. Firstly, the tapered fiber for coupling the light into the silica microsphere was prepared.

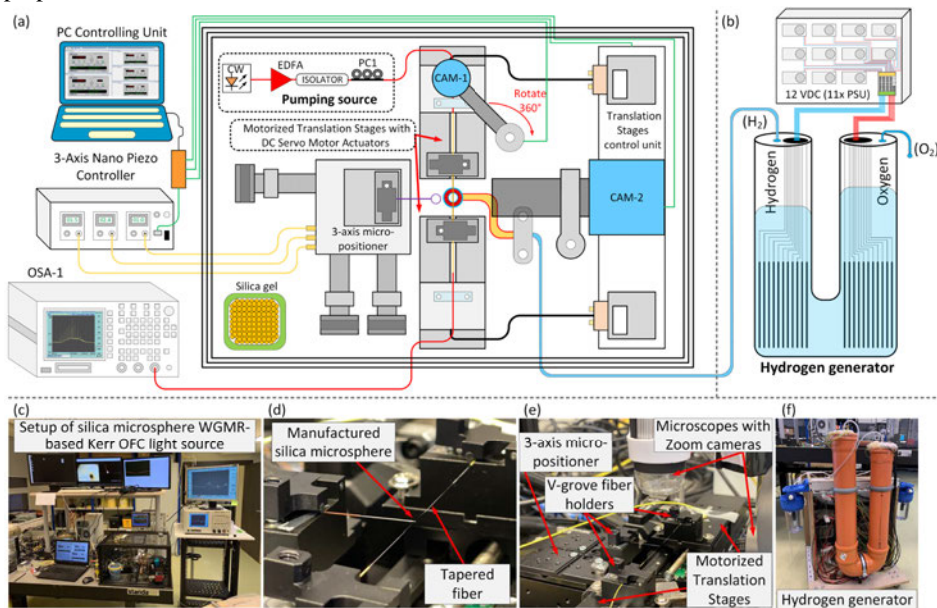


Figure 60. (a) Experimental setup illustrating the developed silica microsphere WGMR-based Kerr-OFC as light source for optical communications. (b) Schematic of a Hydrogen generator for pure generation of hydrogen (H_2) and oxygen (O_2) by electrolysis of water. (c) Captured setup of silica microsphere WGMR-based Kerr-OFC light source. (d) Tapered fiber and silica microsphere resonator positions inside of enclosure box for the dust and airflow prevention. (e) The 3-axis X, Y and Z micro-positioner stage with a built-in Piezo controller and compact motorized translation stages together with zoom microscopes used to monitor the position of the WGMR resonator. (f) Hydrogen generator for pure hydrogen and oxygen production.

The non-zero dispersion-shifted fiber (NZ-DSF) patch-cable compliant to ITU-T G.655 standard was used for the preparation of a tapered fiber pulling probe. In process of the tapered fiber fabrication procedure, the tapered fiber probe was formed from two separate cut parts of NZ-DSF compliant patch cable. The patch-cable fiber ends were cut using a fiber cleaver, cleaned and spliced together with a commercial arc fusion splicer (Sumitomo, T-71C) ensuring a low insertion loss ≤ 0.01 dB. As a result, the jacket and coating of connectorized patch-cable were removed in the region of 3.8 cm where it is intended for heat treatment.

In the process of the taper fiber fabrication procedure, the previously ruptured fiber was reused, broken ends were cut, spliced and performed as fiber region for pulling a tapered fiber. Clamps of V-groove fiber holders located on the 50 mm compact motorized translation stages with DC servo motor actuators (Thorlabs MTS50-Z8) were used to pull the tapered fiber in both directions with a constant speed of 100 $\mu\text{m/s}$ (see [Figure 60\(a\)](#) and [Figure 60\(e\)](#)). Several techniques can be used to form tapered fiber through thermal heating, for instance, a ceramic tube microheater(s) consisting of a heat-resistant wire that is approximately 22 mm in length and 19 mm inner diameter and placed within the ceramic [142]; another option would be micro burners driven by propane-butane (30% propane, 70% butane) gas flows [143] or by pure hydrogen (H_2) [144] providing a high-temperature ($\geq 1900^\circ\text{C}$) flame. The latter setup was used in experiments, specifically, a constant hydrogen flow of 50 ml/min from the hydrogen generator (see [Figure 60\(b\)](#)) was connected to a micro burner placed between compact motorized translation stages. For the generation of pure hydrogen, was used an in-house-built hydrogen generator (electrolyser) that operates by splitting the water into hydrogen and oxygen through the electrolysis. In order to preserve the hydrogen generator from overheating, the number of plates for cathode and anode is set to x11. Each plate was driven by 12 volts of direct current (VDC) (30 A) output voltage through 11x high-speed Schottky diodes barrier using a (220V~50 Hz 350 W) power supply units (PSU). As shown in [Figure 60\(b\)](#) and [Figure 60\(f\)](#) sets of 11 cathode and 11 anode plates are located in separate tubes ($D = 250$ mm) where the electrolysis interconnection between them was made by water and potassium hydroxide (KOH) electrolyte trough round tube transition.

For the micro burner, was used an in-house-built micro torch that consists of 9 cylindrical stainless-steel tubes of 0.9 mm inner diameter, allowing us to produce a low and wide flame of ~ 10 mm along the fiber axis [145]. The fiber position relative to the flame is a critical parameter, therefore, the micro torch stainless-steel tube position is sprightly adjusted to the fiber's mid-point. To sustain transmission, the tapered fiber needs to be pulled adiabatically not exceeding delineation angle [146]. Using a ~ 7 mm wide hydrogen flame we produced sub-wavelength nearly adiabatic tapers with an overall transmittance higher than 95%, as a very efficient adiabatic transfer from the single mode of the un-tapered fiber to the fundamental mode of the central part of the taper. The burning temperature of the hydrogen flame melted and softened the fiber slowly within the purified fiber section as a result of a tapered thicker section of 18 mm in length. It is important to mention that if the fiber ends are inclined (0.1 mrad) at the place of V-groove fiber holders, a curvature of 5 μm is intelligently formed in the melted place of the taper when the flame width is 1 mm. The angle exceeding 0.08 mrad is no longer good as the allowable adiabatic angle is between

0.02–0.05 mrad [147]. Due to rapid assembly, a flame wider than 1 mm was used. The mounting of the fiber holders on one optical axis is adjusted under a microscope. The 3-axis X, Y, and Z micro-positioner stages with the built-in piezo controller were used to align the microsphere with the tapered fiber at a place slightly thicker than the taper waist to achieve the critical coupling and minimize the coupler losses, see *Figure 60(d)* and *Figure 60(e)*. Side and top view microscope cameras (CAM) e.g. (CAM-1 and CAM-2) with 160x zoom lens (see *Figure 60(e)*) are used to monitor silica microsphere and tapered fiber positions to control the touchpoint of the resonator with the slightly thicker tapered fiber place to excite the fundamental mode of the microsphere. Silica microsphere and tapered fiber, including integrated and developed components for fiber tapering and microsphere positioning, are included in an enclosure box to protect it from dust and airflows. Humidity inside the enclosure box is reduced and maintained at the levels below 20% using a silica gel desiccant. The enclosure box together with pumping source components are located on a vibration isolation system breadboard table to minimize the impact of external low frequency vibrations.

The setup used for the characterization of the taper fiber (see *Figure 61.*) consists of InGaAs switchable gain amplified photo-detector PD $\lambda=800 - 1700$ nm (Thorlabs, PDA20CS2) connected with a digital signal analyzer (DSA) used to record the received electrical signal in time and to monitor the transmission spectra from the adiabatically tapered fiber for an overall transmittance analysis used also in further telecom data transmission.

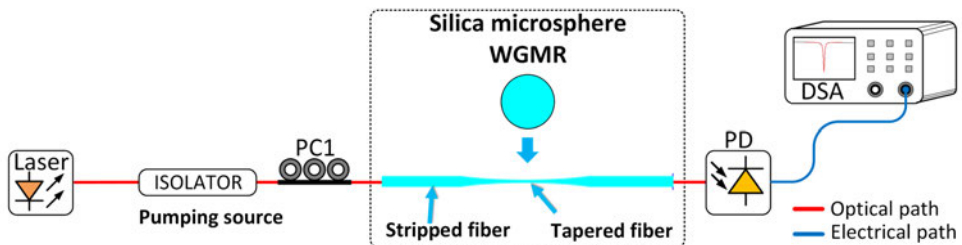


Figure 61. Experimental setup used for the characterization of the tapered fiber and silica microsphere.

A tunable $\lambda=1550$ nm laser (Thorlabs SFL1550P) with a narrow linewidth of 50 kHz and 10 dBm output optical power is connected via a polarization controller PC1 and used for the transmission spectra measurements. The transmission spectrum was monitored during the tapering process to determine when it returns to the single-mode operation state (see *Figure 62(a)*).

Calculations show that the hot zone's width of exponentially puller tapered fiber should be at least 7 mm long to satisfy the adiabaticity criteria at the middle of the pulling range and to maintain high final transmission [146]. Calculations of pulled length of tapered fiber hot zone to one side from center versus fiber diameter at taper section, please see *Figure 62(b)*. The setup shown in *Figure 61.* also, was used to determine the Q factor of silica microsphere and to identify the best coupling condition region between the microsphere and tapered fiber used in the OFC generation. The measured Q factor of the microsphere used for the OFC comb generation and further telecom data transmission is 3.7×10^7 (5.2 MHz FWHM of the WGM resonance), please see *Figure 62(c)*.

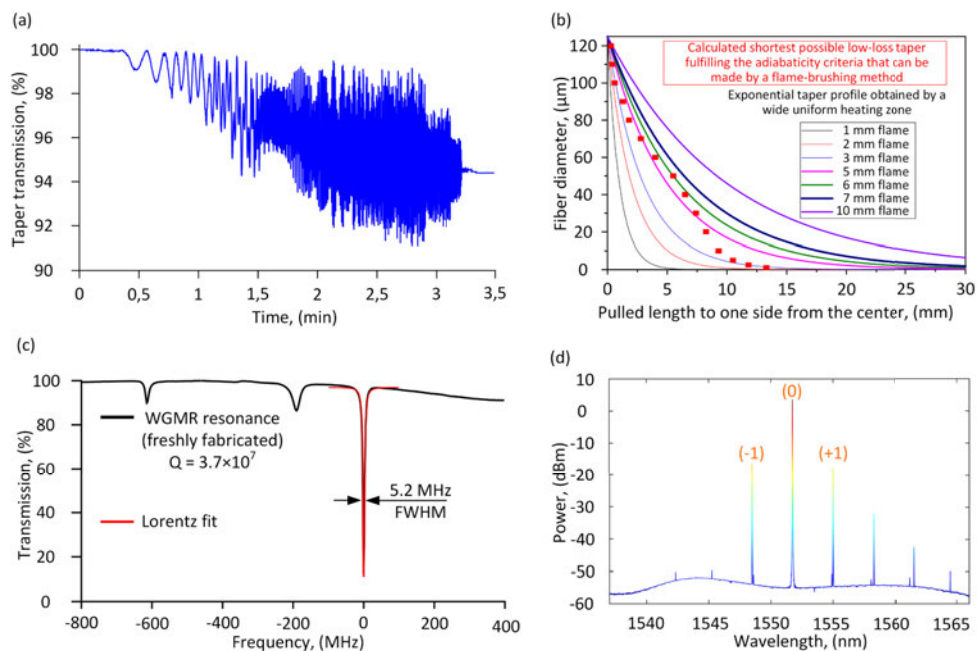


Figure 62. The characterization of the tapered fiber and its coupling conditions with the silica microsphere: (a) spectra of the adiabatically tapered fiber recorded for the overall transmittance analysis and (b) the calculations of pulled one side fiber length at hot zone from center versus fiber diameter at tapered section. (c) Experimentally observed (from the microsphere excited by the tapered fiber) WGM resonances of the Kerr-OFC at optical C-band used for the Q factor calculation and (d) optical spectra of the generated silica microsphere WGMR-based Kerr-OFC comb source.

The pumping source for the Kerr-OFC generation consists of an optical continuous wavelength CW laser source (Agilent 81989A) with a linewidth of 100 kHz and +6 dBm optical output power at $\lambda=1551.737$ nm that is directly connected to a fixed output power (up to +23 dBm) erbium-doped fiber amplifier EDFA. The dispersion for the fundamental WGMs was calculated by numerical solution of the characteristic equation as described in [136]. The calculated zero dispersion wavelength (ZDW) was 1545 nm, the microsphere was pumped in a slightly anomalous dispersion regime. The light coming from the EDFA is passed through an optical isolator and PC1 to prevent the back-scattering and to control the polarization state of the amplified signal before coupling it into the microsphere through the tapered fiber providing further stability of the resulting OFC. An optical spectrum analyzer (OSA-1, Advantest Q8384) with 0.01 nm resolution and 1001 sampling points is used to detect the current wavelengths of the OFC carriers and to observe the power of generated comb carriers (-1), (+1) and pumping source (Figure 62(d)). The power instability and power distribution stability over the wavelength of the generated OFC comb carriers was not measured during this research. The generated comb carriers (-1) and (+1) over 10 hours have a different performance within about a 3-dB margin, please see [9]. OFC generation was

initiated by hard bumping the pump fiber which translated to abrupt changes in the pump power coupled to the microsphere (optical power kick method [148]). The process was not 100% successful, so that several attempts were needed to attain OFC generation. First was generated an OFC with a single-FSR mode spacing of 0.4 THz, which corresponds to the theoretical FSR estimation (see *Figure 62(d)*). Secondly, by changing the relative position between the microsphere and the taper, was obtained an OFC with 2-FSR mode spacing of 0.8 THz with the spectrum. Also was tested the long-term stability of these both possible OFCs for 5 h by using 170 μm silica microsphere; the corresponding almost constant spectra as functions of time are shown in *Figure 63(g)* and *Figure 63(h)* for mode spacings of 1-FSR and 2-FSR. The recording time of 5 h for each measurement is shown in *Figure 63(g-h)* was chosen to obtain them in one day.

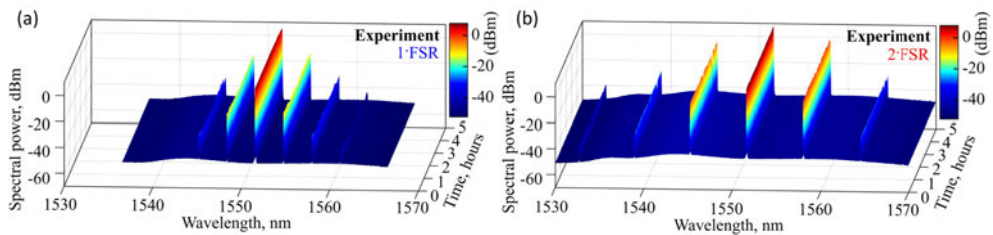


Figure 63. Silica microsphere-based Kerr-OFC output spectra as functions of time with (a) 1-FSR mode spacing (b) and 2-FSR mode spacing.

6.3 Evaluation of received signal quality for WDM-PON communication system with data transmission speed in the channel up to 10 Gbit/s per λ using OFC as a light source

In this chapter are shown first successful experimental demonstration of data transmission based on OFC generated light source in microsphere resonator which has not been previously demonstrated. Experimentally for the first time present designed silica microsphere whispering-gallery-mode microresonator (WGMR) OFC as a C-band light source where 400 GHz spaced carriers provide data transmission of up to 10 Gbps NRZ-OOK modulated signals over the standard ITU-T G.652 telecom fiber span of 20 km in length. *This research reports the first successful demonstration of experimental 2.5 and 10 Gbps non-return to zero NRZ on-off keying (OOK) WDM system based on optical carriers generated in fabricated silica microsphere resonator.* The setup for the generation of WGMR-OFC and the realized WDM communication system is shown in *Figure 64.* First, OFC generation was initiated by search for stable combs on an optical spectrum analyzer by tuning external cavity CW semiconductor laser in wavelength steps of 10 pm and bumping light source output fiber. As shown in *Figure 64.*, an optical spectrum analyzer (OSA) with 0.01 nm resolution is used to measure OFC performance over 10 hours period (see *Figure 65(b)*) and power stability and power distribution stability over the wavelength of the OFC carriers. After OFC generation the carriers (-1) and (+1) are similar but one can be a few dBm more intense than the other if multiple solitons are circling inside the resonator. Was observed that the comb lines (-1) and (+1) have a different performance where power instability over a 10-

hour period is within about a 3 dB margin due to the impact of resonator ability to support multiple spatial modes. The optical carriers $\lambda = 1549$ nm depicted as (-1) and $\lambda = 1555$ nm depicted as (+1) are used to demonstrate NRZ-OOK modulated 2.5 Gbps and 10 Gbps data transmission (see *Figure 65(a)*).

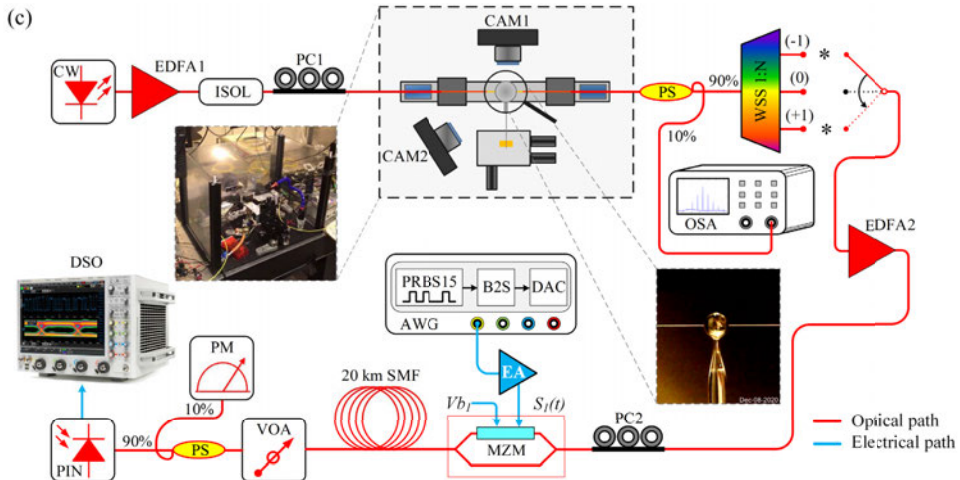


Figure 64. Experimental setup of the designed silica microsphere WGMR-OFC as a light source where 400 GHz spaced carriers provide NRZ-OOK modulated 2.5 and 10 Gbps data transmission over 20 km SMF fiber. Insets show tapered fiber and silica microsphere resonator positions of coupling conditions and WGMR-OFC reduced humidity and dust prevention cover box.

As shown in *Figure 64.*, the generated OFC signal is sent to the wavelength selective switch (WSS) used to filter out one optical carrier (-1) or (+1) at a time. The realization of an experimental setup corresponds to wavelength-selective (WS) fiber optical communication system architecture. Fully ITU flexible grid G.694.1 compliant WSS with dynamic channel width control provided by liquid crystal on silicon (LCoS) switching technology is set for 400 GHz OFCs channel spacing, where output optical channels bandwidth is 25 GHz (4×6.25 GHz). The filtered output (-1) or (+1) carrier is amplified with EDFA2 pre-amplifier to the necessary optical power level. A polarization controller PC2 is placed after EDFA2 to reduce the polarization-dependent loss. Bitrates of 2.5 Gbps and 10 Gbps by a 2^{15} long pseudo-random bit sequence PRBS15 NRZ signal from 65 GSa/s and 25 GHz analog bandwidth arbitrary waveform generator AWG are modulated onto the optical carrier signal (-1) or (+1) using the Mach-Zehnder intensity modulator MZM with an extinction ratio of 20 dB. Then the modulated signal is transmitted over 20 km of standard single-mode optical fiber SMF, variable optical attenuator VOA, and detected with 10 GHz photoreceiver PIN, which sensitivity is equal to -18 dBm at BER of 10^{-10} and overload power 0 dBm for BER of 10^{-13} . An optical coupler (coupling ratio 10/90) and a power meter are used before PIN to monitor the optical power level falling on the PIN receiver. An 80 GSa/s and 33 GHz analog bandwidth digital storage oscilloscope DSO is used to sample the received electrical signal, filter

it with an 8 GHz low-pass filter LPF in case of 10 Gbps and 2.3 GHz LPF in the case of 2.5 Gbps data transmission to measure the quality of the received signal (e.g., eye diagrams, waveform), and estimate its BER. The represented BER values are calculated from the DSO's estimated Q-factor values of the captured NRZ signal real-time eye diagrams.

The impact of the pump signal polarization state on the spectral purity of generated OFC carriers was also assessed. An additional experimental measurement scheme was built for this purpose, as shown in *Figure 65(c)*. For this measurement, the optical heterodyning process of two optical carriers, where the frequency difference or intermediate frequency IF between them generates the desired carrier on the output of high-speed photodiode, is used [70]. RF peaks around DC can be masked by a photodetector flicker noise and low-frequency technical noise. For that reason, main focus is on higher frequencies, which allows to better evaluate the spectral purity of generated OFC carriers. For the polarization measurement, to prevent the IF frequency instability caused by laser phase noise was used (+1) WGMR-OFC optical carrier which is fed into an optical input of MZM modulator and modulated by the 2 GHz sinusoidal signal originating from a high-stability microwave signal generator (see *Figure 65(c)*). Bias voltage V_{b1} of MZM is set to 3.33 VDC, which is near to its null-bias point. In such a way three optical carriers spaced by 2 GHz are obtained on the output of the 40 GHz analog bandwidth MZM.

The frequency spacing between the first and third carriers is 4 GHz. By changing the power of the 2 GHz sinusoidal signal applied to the $S_1(t)$ RF input of the MZM, an optimal RF drive voltage ($V_{\text{eff}} = 1.2$ V) ensuring almost equal peak powers of generated RF carriers is found. The first RF peak located at DC is not seen in *Figure 66*, as the DC blocker was attached to the electrical output of the PIN receiver.

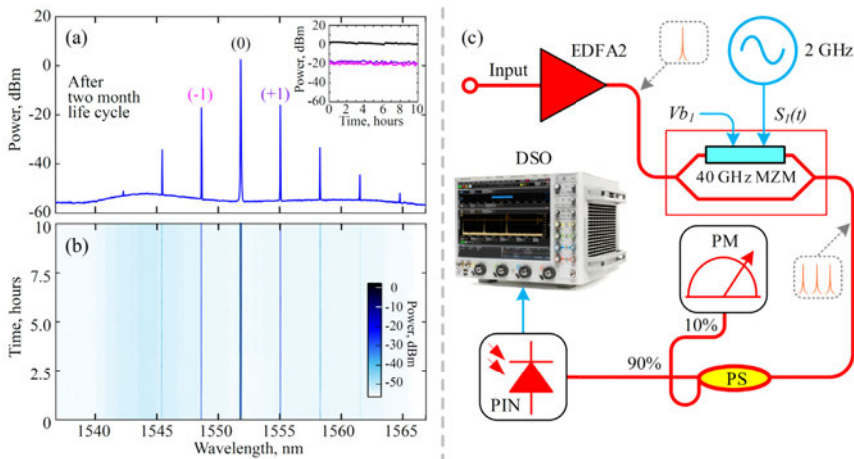


Figure 65. Measured OFC performance over a 10-hour period: (a) optical spectrum with inset representing captured power stability, and (b) power distribution stability over the wavelength. (c) The experimental measurement setup, where one WGMR-OFC optical carrier (+1) is fed into an MZM modulator driven by a 2 GHz sinusoidal tone to assess the impact of optical signal polarization on the spectral purity of generated optical carriers.

Accordingly, after directly receiving such an optical signal by the 10 GHz high-speed PIN photoreceiver, the optical heterodyne up-conversion process occurs. As a result, on the RF output of this PIN receiver, the electrical signal containing the DC-filtered baseband part and two RF carriers (2 GHz and 4 GHz) is generated. The 4 GHz RF tone originates from the heterodyning process of two outer optical carriers, while the 2 GHz RF tone originates from two neighboring optical carriers.

The effect of polarization is observed at three different scenarios; (1) polarization state with large amplitude modulation, (2) intermediate state, (3) polarization optimized for lowest amplitude modulation by adjusting PC1 before WGMR-OFC, see *Figure 66(a-c)*. Microsphere pump light polarization is adjusted by PC1 to minimize 27.92 MHz amplitude self-modulation of comb lines. Fast photodiode measure (+1) comb line to offset spectrum towards higher frequencies. The implemented heterodyne beating method enables to observe the effect of OFC input light polarization on the spectral purity of generated carriers. By the pump source first, and second polarization states, the generation of higher-order sub-carrier signals for 2 GHz and 4 GHz IF frequencies are observed, which lead to deterioration of the quality of data signal, see *Figure 66(a)* and *Figure 66(b)*.

An optimized polarization state, when the CW pump laser polarization coincides with the principal axes of the polarization, shows the best result and guarantees that equal amounts of optical power split to both the X/Y polarization states, see *Figure 66(c)* [149]. An optimized polarization state was set for the lowest amplitude modulation of PC1 during the data transmission of 2.5 and 10 Gbps NRZ-OOK modulated data over B2B and 20 km SMF transmission in both cases using (-1) or (+1) optical carriers. As shown in *Figure 66(d)*, the waveform fluctuations with

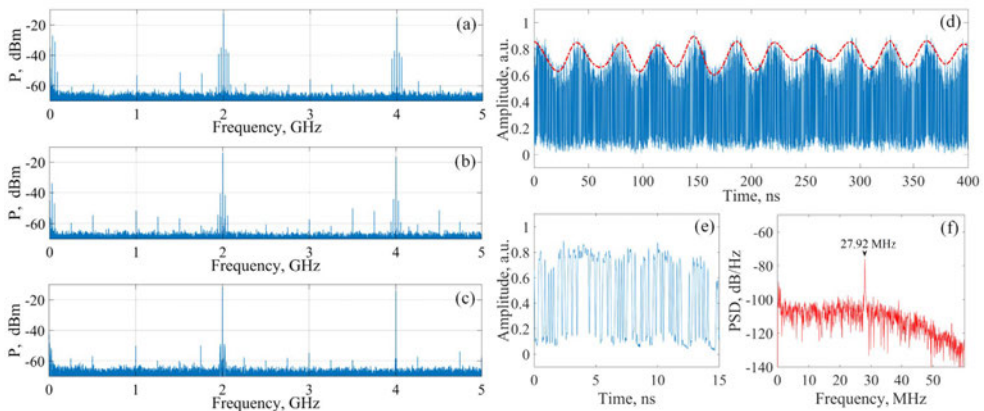


Figure 66. Measured effect of polarization, by received electrical signal IF after optical heterodyne up-conversion on photodiode in different polarization states: (a) polarization state with large amplitude modulation, (b) intermediate state, and (c) the optimized polarization state for lowest amplitude modulation showing the highest spectral purity of the generated OFC optical carrier. (d) Part of the received and normalized 10 Gbps NRZ-OOK signal waveform after 20 km transmission with applied upper envelope function, highlighting the periodic waveform fluctuations, (e) 15 ns insight of the normalized waveform showing received bit sequence, and (f) power spectral density of the calculated envelope signal.

periodic nature are observed on the captured data signal waveforms. After 2.5 and 10 Gbps data transmission, we estimate that the period of these fluctuations for (+1) OFC optical carrier is 35.82 ns or 27.92 MHz in frequency, as it is confirmed by the spectral analysis of the applied upper envelope signal, see [Figure 66\(e\)](#) and [Figure 66\(f\)](#).

It should be noted that the fluctuations on the lowest part of the waveform are optically suppressed by intentionally adjusting the bias point of MZM closer to its null-point. For (-1) harmonic, the same fluctuations period is observed. As observed during the experimental measurements, a periodic intensity modulation often appears on the comb lines, always having the same frequency for the particular resonator.

This process has been previously studied in [150] where it was shown that mechanically driven oscillations occur due to radiation pressure force which subsequently causes microsphere deformation. COMSOL Multiphysics calculations shows that for a silica microsphere with a diameter of 170 μm this resonance frequency corresponds to the strongest mechanical resonance of 27 ± 1 MHz, see [Figure 67](#).

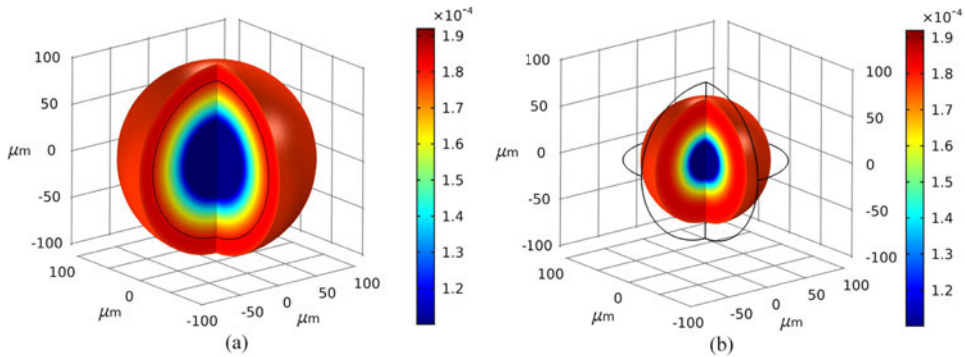


Figure 67. COMSOL simulation of mechanical oscillations at nm scale for silica microsphere of 170 μm in diameter indicating the strongest eigenfrequency at about 27 ± 1 MHz that can be excited by a radiation pressure causing periodic detuning from resonance and back manifesting as an amplitude modulation of comb lines, where (a) represents microsphere at its diameter maximal expansion, and (b) represents the diameter maximal contraction.

For a better visual representation, the deformation in simulation is exaggerated 100 000 times. The black surrounding line indicates the unperturbed microsphere size. Color scale represents the absolute value of deformation in micrometers.

It was observed that an amplitude modulation depth of less than 30% is deteriorating telecom data demodulation. By adjusting the polarization of the CW pump light, it is possible to reduce this amplitude modulation, see [Figure 66\(a-c\)](#). This reduction in amplitude modulation could be explained by the sideband cooling/heating effect of the mechanical resonance [151].

The performance indicators as eye diagrams and BER values of the received signal verify the feasibility of the fiber optical WGMR-OFC based transmission system. The worst-performing data channel based on the BER value is with the wavelength of 1549 nm, depicted as a carrier (-1), see [Figure 65\(a\)](#). The BER of received 2.5 Gbps and 10 Gbps NRZ-OOK signals after 20 km transmission is 5.58×10^{-7} and 1.58×10^{-6} , see [Figure 68\(b\)](#) and [Figure 68\(d\)](#). The best performing

data channel based on the BER is the one with a wavelength of 1555 nm, denoted as a carrier (+1). In this case, the BER of received 2.5 Gbps and 10 Gbps NRZ-OOK signals after 20 km transmission is 1.39×10^{-15} and 3.64×10^{-10} , please see *Figure 68(a)* and *Figure 68(c)*.

The error-free transmission is established during the experiment in both cases of 2.5 and 10 Gbps data rates for OFC comb pump source operating at 1552 nm wavelength. It allows to use WGMR-OFC as a light source where 400 GHz spaced carriers provide 2.5 and 10 Gbps NRZ modulated data transmission over 20 km SMF fiber. Captured signals eye diagrams see in *Figure 68(a-d)*. The BER versus received average optical power measurements are preferred for WGMR-OFC carrier signals (-1) and (+1) at 2.5 and 10 Gbps data rates to fully evaluate the quality of transmission characteristics, see *Figure 68(e)*.

According to the NGPON2 requirements to measure the BER correlation diagrams the B2B transmission and a distance of 20 km was choosens for experimental light source validation. *Figure 68(e)* shows that the optical carrier denoted as (+1) provided the highest system performance, where the received optical power varies from -4 to -17.5 dBm, and the BER of 2.5 Gbps NRZ-OOK signal is in the range from 1.39×10^{-15} to 7.76×10^{-3} .

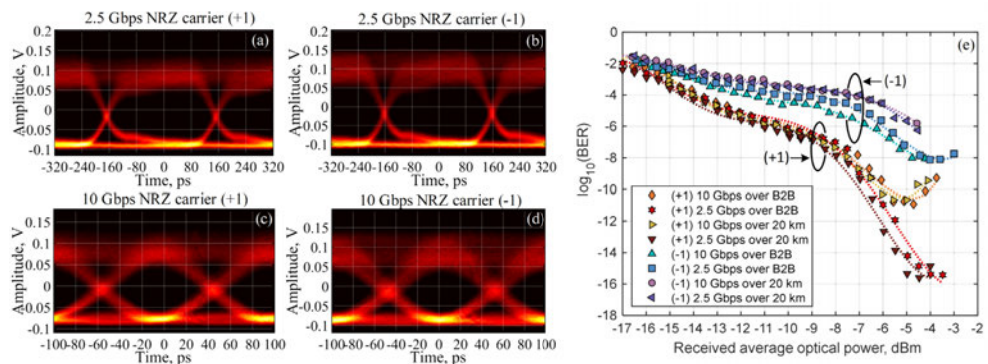


Figure 68. Eye diagrams of the received signal after 20 km transmission over SMF fiber at a data rate of 2.5 Gbps for (a) carrier “+1” and (b) carrier “-1”, and at a data rate of 10 Gbps for (c) carrier “+1” and (d) carrier “-1”, and (e) the plots of BER vs. average received optical power in B2B and after 20 km transmission of the NRZ-OOK modulated signal with bitrates of 2.5 and 10 Gbps for “+1” and “-1” carriers.

As one can see in *Figure 68*, BER curves bending upwards are observed at relatively high detected power levels for WGMR-OFC comb carrier (+1) at 10 Gbps B2B and 10 Gbps 20 km transmission, as well as for (-1) carrier at 2.5 Gbps B2B transmission. It could be explained by detector saturation, nonlinear optical processes in the resonator or transmission fiber.

6.4 Evaluation of received signal quality for DCI communication system with data transmission speed in the channel up to 50 Gbit/s per λ using OFC as a light source

The data centers DCs are the foundation of Internet applications such as cloud computing, where Big Data storage and large-scale high-performance computing HPC take place. The intra-

DCI devices and systems that rely on the sharing of computing resources require not only large capacity but, most importantly, high scalability and low energy consumption. Therefore, these requirements require new transmission technologies for short-reach communications [16], [124]. For telecommunication purposes, more specifically, the WGMR-based Kerr-OFC comb generators physically realized on silica microsphere demonstrate a new concept able to provide an attractive solution to intra-DCIs due to low cost and energy consumption. In this chapter, an experimental demonstration of a silica microsphere WGMR-based Kerr OFC light source with 400 GHz spaced carriers and its use for data transmission employing low-cost and low-complexity intensity modulation direct detection IM/DD schemes. Using the non-return to zero NRZ on-off keying OOK modulation format, data rates up to 50 Gbps/λ can be used for data transmission over 2 km single-mode fiber SMF link. Digital equalization techniques, such as a linear equalizer with feed-forward FF and feedback FB taps, are used to improve the signal quality due to different system's distortions, including the bandwidth limitations, optical to electrical (O/E) and electrical to optical (E/O) conversions, and the link induced inter-symbol interference ISI. Finally, an insight into possible alternative technologies for intra-datacenter interconnects and investigate their limitations through transmission experiments are provided.

The experimental setup is shown in *Figure 69*. The silica microsphere WGMR-based Kerr-OFC light source (i.e. Kerr-OFC) output 400 GHz spaced optical carriers at the following wavelengths: $\lambda=1548.485$ nm depicted as (-1), $\lambda=1554.992$ nm depicted as (+1), and the pumping source at $\lambda=1551.737$ nm depicted as (0) and having the highest achieved peak power levels are used to demonstrate NRZ-OOK modulated data up to 50 Gbps/λ over 2 km SMF link. As shown in *Figure 69*, the generated OFC carriers are sent to an optical band-pass filter (OBPF, Santec, OTF-350) having a 3-dB bandwidth of 75 GHz. The OBPF is used to filter out one of the three optical carriers.

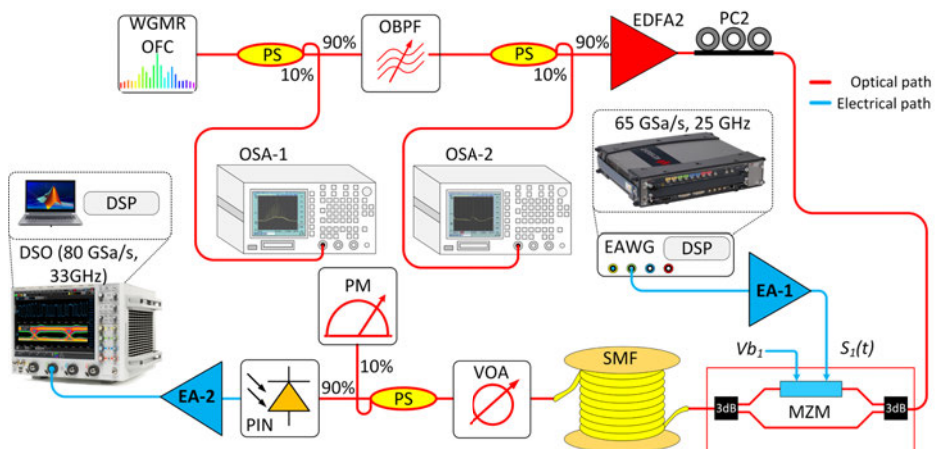


Figure 69. Experimental demonstration of the IM/DD optical interconnect relying on the in-house-built silica microsphere WGMR-based Kerr-OFC as a light source generating 400 GHz spaced optical carriers that are used for up to 50 Gbps/λ NRZ-OOK modulated signal transmission over a 2 km long SMF link.

An optical coupler with 10/90 coupling ratio is used to capture the output carrier spectrum using OSA-2. It is done for monitoring purposes and to determine wavelengths and optical peak powers of carriers that are later used for data transmission. The filtered optical carrier is amplified by a pre-amplifier (EDFA2) that fixes the output power level for each OFC carrier.

A polarization controller (PC2) is placed before the intensity Mach-Zehnder modulator (MZM, Photline, MX-LN40) to reduce the polarization-dependent loss. The high-speed NRZ signal is generated offline using a $2^{15}-1$ long pseudorandom binary sequence PRBS. The signal is up-sampled and filtered using a root-raised-cosine (RRC) filter having a roll-off factor of 1. At the next pre-processing stage, frequency domain pre-equalization up to 30 GHz is used to compensate amplitude-frequency distortions and limited bandwidth (BW) of a 65 GSa/s electrical arbitrary waveform generator (EAWG, Keysight M9502A, 25 GHz). The response of an end-to-end system calibration for optical back-to-back (OB2B) configuration is shown in *Figure 70*.

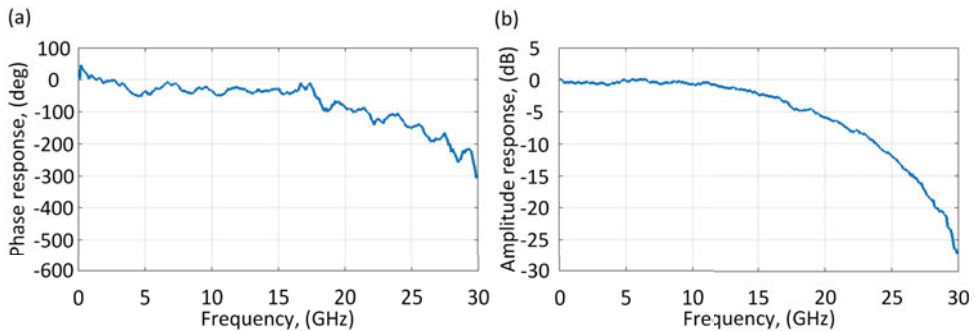


Figure 70. End-to-end system calibration using the EAWG for the OB2B configuration: (a) phase response and (b) amplitude response.

The high-speed NRZ signal is loaded to the EAWG, pre-equalized and transmitted. The generated output electrical signals are amplified by an electrical amplifier (EA1, 38 GHz, 29 dB gain) and fed into the $S_1(t)$ input of the MZM with null chirp factor and having 40 GHz 3 dB bandwidth, 20 dB extinction ratio and 9 dB insertion loss. To ensure the best possible BER performance, is adjusted a bias voltage V_{b1} of the MZM to 3.8 V. After the MZM, the modulated optical signal is transmitted over a 2 km long SMF link and passed through a variable optical attenuator VOA located before a photoreceiver for the power control. The photoreceiver module (PIN, Lab Buddy, DSC10H-39) consists of high optical power 50 GHz InGaAs photodiode with the 3 dB bandwidth of 50 GHz, the sensitivity of +4 dBm at BER of 10^{-12} and responsivity 0.5 A/W. An optical coupler with 10/90 coupling ratio and a power meter are used before the PIN to monitor the optical power level at the receiver. After optical-to-electrical conversion the electrical signal is amplified by an electrical amplifier (EA-2, 25 GHz, 16 dB gain). Thereafter, the signal is captured by a digital storage oscilloscope (DSO, Keysight DSAZ334A, 80 GSa/s, 33 GHz). The sampled signal is processed offline using the digital signal processing DSP consisting of a low-pass filter LPF, clock recovery, resampling, linear post-equalization based on a symbol-spaced

adaptive decision-feedback equalizer (DFE) and bit error rate BER counter. The BER values are obtained using the bit-by-bit comparison between the transmitted and received bit sequences.

Using the prior described experimental setup a fair comparison was made, showing the performance limits in terms of achievable data rates for short-reach optical interconnect applications. The goal is to achieve the data rate as high as possible even up to 60 Gbps/ λ in the system that uses the implemented Kerr-OFC generated optical carriers for carrying IM/DD data. The received and sampled signal is processed offline after the reception, using a DSP routine that consists of a low-pass filter LPF, a maximum variance timing recovery, post-equalization, and BER counter. The LPF has a bandwidth of 0.6 times the Baud rate. That value was identified using the results data shown in [Figure 71](#). It ensures the best possible performance after further processing. In such a case, the BER as a function of the LPF_{BW}/Baud rate from 0.4 to 0.8 for NRZ-OOK signals was obtained.

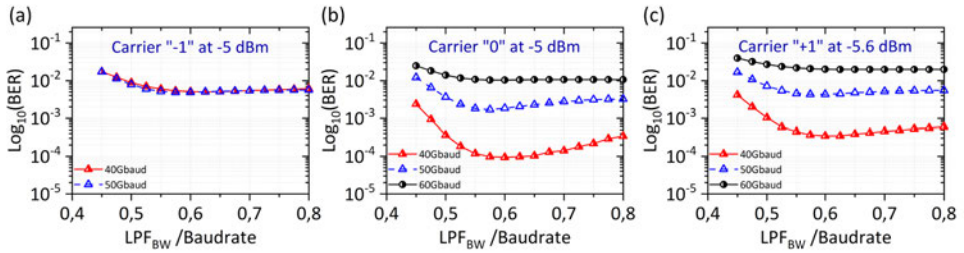


Figure 71. BER versus LPF_{BW}/Baud rate for the IM/DD communication system operating on 400 GHz spaced carriers generated by microsphere Kerr-OFC: (a) $\lambda=1548.485$ depicted as carrier “-1” (b) $\lambda=1551.737$ depicted as carrier “0” and (c) $\lambda=1554.992$ depicted as carrier “+1” provide NRZ-OOK signals up to 60 Gbps/ λ .

The post-equalization was used to improve signal quality; therefore, a DFE configuration with 33 feed-forward taps FFT and 15 feedback taps FBT, as well as 16 taps are used as a reference. The adaptive DFE helps to overcome the inter-symbol interference ISI in presence of noise. The initial weights of the equalizer are obtained using the training data with the normalized least-mean-square (NLMS) algorithm before applying other data. A total number of 1.2 million bits are used for BER counting. First, the system performance without the post-equalization was analyzed; afterwards, main focus was on improvements that the linear post-equalization can offer. The hard-decision forward error correction HD-FEC with 7% overheads (OH) with pre-FEC BER threshold at 5×10^{-3} was considered as signal quality threshold [152]. For received signal quality analysis was preferred conventional BER curves showing how pre-FEC BER values change with the received optical power (ROP). For result analysis was assumed that all errors can be corrected for the pre-FEC BER below that threshold. As one can see in [Figure 72\(a\)](#), the worst-performing (based on the BER value) data channel is the carrier (-1) at 1548.485 nm, yet, it is capable to provide the maximum bitrate of 50 Gbps. In this sub-figure, the 60 Gbps curve is not shown because due to extremely poor BER performance, i.e., a way beyond defined pre-FEC BER threshold of 5×10^{-3} .

The best performing (based on the BER) data channel is the pumping source carrier with a wavelength of 1551.737 nm depicted as a carrier (0). Without the post-equalization, the received

40 Gbaud and 50 Gbaud NRZ-OOK signals are mostly below the 7% HD-FEC limit for the Kerr-OFC generated carriers (-1), (0), and (+1), see **Figure 72(a-c)**. In those cases, the main limitations are a relatively low effective bandwidth of the electrical components, ISI and the implementation penalty itself. In order to achieve higher data-rates, a dispersion-induced power fading must be reduced and signal equalization must be applied to reach the BER threshold of 5×10^{-3} . Therefore, linear equalizer (structure consists of 33-FF&15-FB taps) was chosen. The number of taps is chosen in a way to maximally improve the performance by tackling the bandwidth limitations of electrical components and chromatic dispersion. The results show that such post-equalization significantly improves the BER performance compared to the previous case without the post-equalization. As one can see in **Figure 72(d-f)**, the post-equalization can significantly improve the signal quality for the Kerr-OFC generated carriers (-1), (0), and (+1) or even enable new modulation format alternatives. With the linear post-equalization (33-FF&15-FB taps), the BER performance is significantly improved for carrier (+1), which allows us to achieve the BER floor below the 7% HD-FEC limit for NRZ-OOK signals at 60 Gbaud. **Figure 72(g-i)** show the corresponding eye diagrams captured for modulated carriers (-1), (0), and (+1) at -10 dBm received optical power (ROP) that allows detecting signals with the BER below 5×10^{-3} at 40 Gbaud.

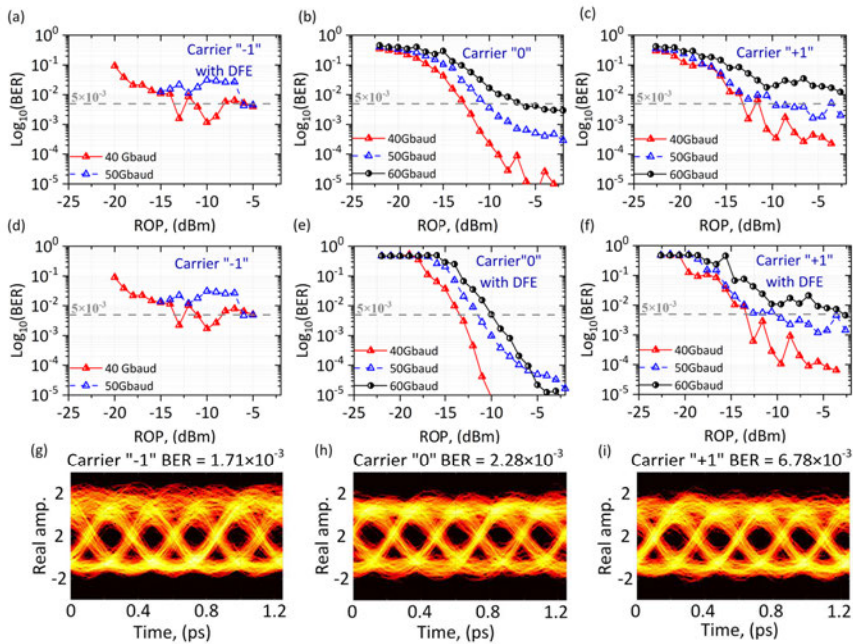


Figure 72. BER versus ROP for the IM/DD communication system where the Kerr-OFC light source carriers “-1”, “0” and “+1” can be used for NRZ-OOK signals transmission with baudrates up to (a) 50 Gbaud (b) 60 Gbaud and (c) 50 Gbaud without any post-equalization. If the post-equalizer with 33-FF&15-FB taps is used, the BER is significantly improved for carriers “-1”, “0” and “+1” up to (d) 50 Gbaud (e) 60 Gbaud and (f) 60 Gbaud. Received signal eye diagrams for carriers: (g) “-1”, (h) “0” and (i) “+1” captured at ROP of -10 dBm in the 40 Gbaud case.

CONCLUSIONS

- [1] To increase the data transmission distance above 27 km, WDM-PON transmission systems with 50 GHz inter-channel interval need to be replaced by NRZ-OOK with multi-level modulation formats (PAM-4, EDB) to ensure transmission reach up to 50 or 62 km, where EDB modulation format applications have 19% better transmission reach than spectrally efficient (10 Gbaud/s) PAM-4, which is explained by the distance between PAM-4 signal levels due to the effect of chromatic dispersion and SNR.
- [2] By evaluating the dispersion compensation methods for NG-PON2 ITU-T G.989.3 compliant WDM-PON transmission system, it is possible to provide a transmission distance of 40 km for an NRZ-OOK modulated signal with a data transmission rate from 20 to 40 Gbit/s per λ in the (C-band) range compliant FBG-DCM without exceeding the limit of the received signal ($BER \geq 1 \times 10^{-3}$) even with 3 dB less received signal power than in the case of DCF, significant effects on BER (2-5 BER steps at 20 and 40 Gbit/s transmission speed) arise under the influence of NOE.
- [3] To increase the data rate in HS-PON transmission systems, evaluating the performance provided by the intensity modulation (NRZ, PAM-4, PAM-8, EDB) after 20 km of transmission, it was concluded that at a data rate of 28 Gbit/s per λ not exceeding $BER \geq 1 \times 10^{-3}$ limit value without AEQ can be achieved using 28 Gbaud/s (NRZ, EDB) and 14 Gbaud/s (PAM-4) signal modulation, while 42 Gbit/s per λ and 56 Gbit/s per λ data transmission not exceeding $BER \geq 1 \times 10^{-3}$ threshold can be provided by use of adaptive equalization by constellation of feed-forward (FF) and feedback (FB) taps using 14 Gbaud/s (PAM-8) and 28 Gbaud/s (PAM-4) signal modulation.
- [4] Based on the experimental results and the information gathered in the dissertation, it can be concluded that SMCF fibers are suitable for short-distance (≤ 10 km) data transmission in data center interconnection (DCI) solutions. In the combined solution of SDM-WDM technologies - in the implementation of a 7-core SMCF fiber spectrally efficient spatially capacitive IM/DD PON communication system, the factors influencing the transmission of 2.5 Gbit/s (NRZ) coded signals are unequal input losses, the optical power of the received signal in the core (~ 8.2 dB IL difference) is significantly affected by the BER of each signal received in the core. For the implementation of A-RoF communication systems in the combined solution of SDM-WDM technology - SMCF optical fibers are applicable in case if one SMCF fiber core is used for transmission within optical channel and intermediate frequency IF. Due to the high differential mode delay (DMD) (in the case of two separate cores of the same MCF fiber), will result in the degradation of the received signal due to the time delay.
- [5] In the realization of ARoF-WDM-PON optical transmission systems with intensity modulation (NRZ, PAM-4) for the transmission of millimeter wave radio signals provided by the uplink conversion technique, the BER value of the least received signal can be achieved using heterodyne transmission and detection techniques. Primarily for the RoF transmitter RoF transmitter using one CW light source at the central emission frequency of the required

optical band area (according to ITU-G694.1) and a sinusoidal electrical signal generator as LO, where RF is half of the proposed IF frequency for the generation of the mm-wave signal. By secondary filtering the obtained F_n carrier frequency and performing (NRZ, PAM-4) modulation by combining F_n and F_{LO} in one optical channel. Using one CW laser light source in a circuit where the electrical signal generator is used as LO, the two generated optical carrier signals F_n and F_{LO} with appropriate frequency interval for the IF-generated mm-wave signal are resistant to λ non-uniformly induced oscillations depending on temperature changes (carrier instability of ± 80 MHz), as well as low phase noise is provided, therefore limiting the use of phase modulation for the transmission of a millimeter wave radio signal. If both laser sources have an unstable central frequency, the mm-wave frequency also is unstable – it is drifting.

- [6] In the hybrid ARoF-WDM-PON communication system for the transmission of 10 Gbit/s per channel (NRZ) modulated optical signals and 2.5 Gbaud (NRZ, PAM-4) modulated 28 GHz (ka-band) millimeter wave radio signals with data transmission speed in the channel up to 5 Gbit/s through 20 km long SMF fiber line, the main factors influencing the hybrid systems performance are chromatic dispersion CD, transmission system amplitude frequency characteristics, as well as basic free space transmission FSPL. A 28 GHz (ka-band) mm-wave IF radio signal cannot be implemented in ARoF-WDM-PON with a 50 GHz inter-channel interval using commercial AWG (significant effect on BER $\leq 1 \times 10^{-3}$), where 3-dB bandwidth is 35 GHz, so the WR-WDM-PON architecture results in significant filtering of the 28 GHz IF signal due to the AWG multiplexer/de-multiplexer cut-off frequency passband. As a result, the WR-WDM-PON architecture can be used for 2.5 Gbaud/s (NRZ, PAM-4) modulated 28 GHz mm-wave signal, as well as 10 Gbaud/s (PAM-4) modulated broadband Internet signals at the 100 GHz inter-channel spacing, but with a smaller bandwidth interval (according to ITU-T G.694.1) such as 50 GHz and less, are technically feasible using a wavelength selective optical switch WSS.
- [7] Potentially cost-effective solutions for the realization of data transmission in optical WDM networks are OFC generation in silica WGMR – microspheres manufactured from melted telecom fiber, e.g. from Corning SMF 28e (ITU-T G.652), which is realized as the pumping of a high-quality (high Q factor) optical resonator with Kerr nonlinearity using a single continuous-wave (CW) laser. Kerr microresonator OFCs can achieve bandwidths of hundreds of nanometres covering different (e.g. E-, S-, C- and L-band) telecommunication bands. An OFC source is capable of producing the grid of equally spaced (according to ITU-T G. 694.1 recommendation) optical spectral lines (carriers) needed to sustain the data channels. This advantage of the generation of several spectral lines applies also to WDM receivers, where an array of discrete local oscillators (LO) might be replaced by a single OFC. Such solutions are of importance for the fifth (and next) generations of mobile networks, where the optical signal down-conversion to millimeter wave (mmWave) bands (e.g. Ka-band (26–28 GHz)) by using a stable LO at the receiver side can be required as a part of the architectural solution. Silica microsphere based OFC sources for wavelength division multiplexed (WDM) systems cover

use cases ranging from short reach fiber-optic links (e.g., as for data center interconnects (DCI)) to metro-access fiber-optic links interconnecting large geographic areas.

During PhD thesis, based on the literature analysis, for the first time was present designed 170 μm silica microsphere WGMR-based Kerr-OFC as a C-band light source where 400 GHz spaced carriers provide data transmission of up to 10 Gbps NRZ modulated signals without AEQ over the standard ITU-T G.652 telecom fiber span of 20 km in length, which is suitable for IM/DD XG-PON transmission systems architecture.

Designed novel light source also have the potential to demonstrate a new low-cost concept enabling an attractive solution for intra-datacenter interconnects (DCI), therefor can provide low-cost and low-complexity IM/DD scheme for transmission of NRZ-OOK modulated signals at baudrates up to 50 Gbps/ λ over 2 km SMF link. **Such high data rates in terms of data transmission speed for silica microsphere WGMR-based Kerr-OFC light sources is a data transmission rate record of 50 Gbps per λ .** The obtained results show that pre- and post-equalization e.g. AEQ techniques allow to overcome the ISI and help to recover the signal from distortions caused by limited bandwidth and therefore enabling higher data-rate alternatives to intra-DCIs. For a proof-of-concept in both cases experiments was performed with two newly generated OFC carriers (FSR of 400GHz) having the highest peak optical power level.

Lower FSR between comb carriers can be achieved by using a WGMR with a larger diameter. To obtain 200 GHz spacing, one can use $\sim 330 \mu\text{m}$ diameter silica microsphere. To obtain standard 100 GHz spacing, one can use $\sim 660 \mu\text{m}$ diameter silica resonator. For operating with 100 GHz mode spacing, microspheres may be not a very optimal choice due to excitation of WGMs from not the fundamental mode family, so using silica microrod may be beneficial for this purpose. Moreover, when using larger WGMRs compared 170 μm , the effective field areas of the fundamental modes will be larger, so the nonlinear Kerr coefficient γ will be smaller. The nonlinear processes leading to OFC generation depend on $\gamma \times P_{\text{pump}}$, so the pump power P_{pump} should be increased, which means that the power in each harmonic will grow too.

BIBLIOGRAPHY

- [1] The Zettabyte Era — Trends and Analysis Cisco, see online: <https://www.cisco.com/c/en/us/solutions/executive-perspectives/annual-internet-report/index.html>
- [2] J. L. Wei, K. Grobe, and H. Griesser, "High speed next generation passive optical networks: performance, cost, and power dissipation," *2016 Progress in Electromagnetic Research Symposium (PIERS)*, pp. 4856-4857, Shanghai, China, 8-11 Aug (2016), DOI: [10.1109/PIERS.2016.7735774](https://doi.org/10.1109/PIERS.2016.7735774)
- [3] Bobrovs, V., A. Udalcovs, and G. Ivanovs, "Power efficiency vs. spectral efficiency and trans-mission distance in 2.5-10-40 Gbps backbone optical networks," *2014 6th International Symposium on Communications, Control and Signal Processing (ISCCSP)*, pp. 202–205, Athens, Greece, May 21–23, (2014), DOI: [10.1109/ISCCSP.2014.6877850](https://doi.org/10.1109/ISCCSP.2014.6877850)
- [4] S. Spolitis, V. Bobrovs, S. Berezins, and G. Ivanovs, "Optimal design of spectrally sliced ASE seeded WDM-PON system," *2012 15th International Telecommunications Network Strategy and Planning Symposium (NETWORKS)*, pp. 1–5, Rome, Italy, Oct. 15–18, (2012), DOI: [10.1109/NETWORKS.2012.6381687](https://doi.org/10.1109/NETWORKS.2012.6381687)
- [5] B. Zhu, T. F. Taunay, M. Fishteyn, X. Liu, S. Chandrasekhar, M. F. Yan, J. M. Fini, E. M. Monberg, and F. V. Dimarcello, "112-Tb/s Space-division multiplexed DWDM transmission with 14-b/s/Hz aggregate spectral efficiency over a 768-km seven-core fiber," *Opt. Express* 19(17), 16665 (2011), DOI: <https://doi.org/10.1364/OE.19.016665>
- [6] K. Saitoh and S. Matsuo, "Multicore Fiber Technology," *J. Lightwave Technol.* 34(1), 55–66 (2016), DOI: [10.1109/JLT.2015.2466444](https://doi.org/10.1109/JLT.2015.2466444)
- [7] C. Xiong, D. M. Gill, J. E. Proesel, J. S. Orcutt, W. Haensch, and W. M. J. Green, "Monolithic 56 Gb/s silicon photonic pulse-amplitude modulation transmitter," *Optica* 3(10), 1060 (2016), DOI: <https://doi.org/10.1364/OPTICA.3.001060>
- [8] K. Zeb, X. Zhang, and Z. Lu, "High Capacity Mode Division Multiplexing Based MIMO Enabled All-Optical Analog Millimeter-Wave Over Fiber Fronthaul Architecture for 5G and Beyond," *IEEE Access* 7, 89522–89533 (2019), DOI: [10.1109/ACCESS.2019.2926276](https://doi.org/10.1109/ACCESS.2019.2926276)
- [9] T. Salgals, J. Alnis, R. Murnieks, I. Brice, J. Porins, A. V. Andrianov, E. A. Anashkina, S. Spolitis, and V. Bobrovs, "Demonstration of a fiber optical communication system employing a silica microsphere-based OFC source," *Opt. Express* 29, 10903-10913 (2021), DOI: [10.1364/OE.419546](https://doi.org/10.1364/OE.419546)
- [10] A. D. Ludlow, M. M. Boyd, J. Ye, E. Peik, and P. O. Schmidt, "Optical atomic clocks," *Rev. Mod. Phys.* 87, 637–701 (2015), DOI: [10.1103/RevModPhys.87.637](https://doi.org/10.1103/RevModPhys.87.637)

- [11] D. Kwon, I. Jeon, W. K. Lee, M. S. Heo, and J. Kim, "Generation of multiple ultrastable optical frequency combs from an all-fiber photonic platform," *Science Advances* 6, (2020), DOI: [10.1126/sciadv.aax4457](https://doi.org/10.1126/sciadv.aax4457)
- [12] F. Adler, M. J. Thorpe, K. C. Cossel, and J. Ye, "Cavity-enhanced direct frequency comb spectroscopy: Technology and applications," *Annu. Rev. Anal. Chem.* 3, 175–205 (2010), DOI: [10.1146/annurev-anchem-060908-155248](https://doi.org/10.1146/annurev-anchem-060908-155248)
- [13] P. Guay, N. B. Hébert, V. Michaud-Belleau, D. G. Lancaster, and J. Genest, "Free-running optical frequency combs for remote sensing," *Optical Sensors and Sensing Congress (ES, FTS, HISE, Sensors)*, OSA Technical Digest, (2019), DOI: [10.1364/ES.2019.ETu3A.6](https://doi.org/10.1364/ES.2019.ETu3A.6)
- [14] H. H. Lu, A. M. Weiner, P. Lougovski, and J. M. Lukens, "Quantum Information Processing With Frequency-Comb Qudits," *IEEE Photonics Technology Letters*, vol. 31, no. 23, 1858-1861, (2019), DOI: [10.1109/LPT.2019.2942136](https://doi.org/10.1109/LPT.2019.2942136)
- [15] J. Pfeifle, V. Brasch, M. Lauermaun, Y. Yu, D. Wegner, T. Herr, K. Hartinger, P. Schindler, J. Li, D. Hillerkuss, R. Schmogrow, C. Weimann, R. Holzwarth, W. Freude, J. Leuthold, T. J. Kippenberg, and C. Koos, "Coherent terabit communications with microresonator Kerr frequency combs," *Nature Photon* 8(5), 375–380 (2014), DOI: [10.1038/nphoton.2014.57](https://doi.org/10.1038/nphoton.2014.57)
- [16] D. Kong, H. Xin, K. Kim, Y. Liu, L. K. Oxenløwe, P. Dong, and Hao Hu, "Intra-Datacenter Interconnects With a Serialized Silicon Optical Frequency Comb Modulator," *J. Lightwave Technol.* 38, 4677-4682, (2020), DOI: [10.1109/JLT.2020.2996410](https://doi.org/10.1109/JLT.2020.2996410)
- [17] H. Sun, M. Torbatian, M. Karimi, R. Maher, S. Thomson, M. Tehrani, Y. Gao, A. Kumpera, G. Soliman, A. Kakkar, M. Osman, Z. A. El-Sahn, C. Doggart, W. Hou, S. Sutarwala, Y. Wu, M. R. Chitgarha, V. Lal, H.-S. Tsai, S. Corzine, J. Zhang, J. Osenbach, S. Buggaveeti, Z. Morbi, M. I. Olmedo, I. Leung, X. Xu, P. Samra, V. Dominic, S. Sanders, M. Ziari, A. Napoli, B. Spinnler, K.-T. Wu, and P. Kandappan, "800G DSP ASIC Design Using Probabilistic Shaping and Digital Sub-Carrier Multiplexing," *J. Lightwave Technol.* 38(17), 4744–4756 (2020), DOI: [10.1109/JLT.2020.2996188](https://doi.org/10.1109/JLT.2020.2996188)
- [18] N. Kaneda, "Optimizing Optical Interconnects: Digital Predistortion and Postequalization Techniques in Optical Communications," *IEEE Microwave* 20(5), 98–114 (2019), DOI: [10.1109/MMM.2019.2898023](https://doi.org/10.1109/MMM.2019.2898023)
- [19] S. Fathololoumi, D. Hui, S. Jadhav, J. Chen, K. Nguyen, M. N. Sakib, Z. Li, H. Mahalingam, S. Amiralizadeh, N. N. Tang, H. Potluri, M. Montazeri, H. Frish, R. A. Defrees, C. Seibert, A. Krichevsky, J. K. Doylend, J. Heck, R. Venables, A. Dahal, A. Awujoola, A. Vardapetyan, G. Kaur, M. Cen, V. Kulkarni, S. S. Islam, R. L. Spreitzer,

- S. Garag, A. C. Alduino, R. Chiou, L. Kamyab, S. Gupta, B. Xie, R. S. Appleton, S. Hollingsworth, S. McCargar, Y. Akulova, K. M. Brown, R. Jones, D. Zhu, T. Liljeberg, and L. Liao, "1.6 Tbps Silicon Photonics Integrated Circuit and 800 Gbps Photonic Engine for Switch Co-Packaging Demonstration," *J. Lightwave Technol.* 39(4), 1155–1161 (2021), DOI: [10.1109/JLT.2020.3039218](https://doi.org/10.1109/JLT.2020.3039218)
- [20] Q. Cheng, M. Bahadori, M. Glick, S. Rumley, and K. Bergman, "Recent advances in optical technologies for data centers: a review," *Optica* 5(11), 1354 (2018), DOI: <https://doi.org/10.1364/OPTICA.5.001354>
- [21] Cisco Ltd. Jason Deign, "Edge computing can ease the burden for data centers", See online:<https://newsroom.cisco.com/c/r/newsroom/en/us/a/y2019/m10/edge-computing-can-ease-the-burden-for-data-centers.html>
- [22] M. Forzati, A. Bianchi, J. Chen, K. Grobe, B. Lannoo, C. M. Machuca, J.-C. Point, B. Skubic, S. Verbrugge, E. Weis, L. Wosinska, and D. Breuer, "Next-Generation Optical Access Seamless Evolution: Concluding Results of the European FP7 Project OASE," *J. Opt. Commun. Netw.* 7(2), 109 (2015), DOI: [10.1364/JOCN.7.000109](https://doi.org/10.1364/JOCN.7.000109)
- [23] J. L. Wei, K. Grobe, C. Sanchez, E. Giacomidis, and H. Griesser, "Comparison of cost- and energy-efficient signal modulations for next generation passive optical networks," *Opt. Express* 23(22), 28271 (2015), DOI: [10.1364/OE.23.028271](https://doi.org/10.1364/OE.23.028271)
- [24] D. Nettet, "PON Roadmap [Invited]," *J. Opt. Commun. Netw.* 9(1), A71 (2016), DOI: [10.1364/JOCN.9.000A71](https://doi.org/10.1364/JOCN.9.000A71)
- [25] J. L. Wei, K. Grobe, C. Sanchez, E. Giacomidis, and H. Griesser, "Comparison of cost- and energy-efficient signal modulations for next generation passive optical networks," *Opt. Express* 23(22), 28271 (2015), DOI: <https://doi.org/10.1364/OE.23.028271>
- [26] Y. Zhicheng, L. Shengping, C. Ning, L. Xiang, "Demonstration of high-performance cost-effective 100-Gb/s TWDM-PON using 4x 25-Gb/s optical Duobinary channels with 16-GHz APD and receiver-side post-equalization," *European Conference on Optical Communication (ECOC)*, Sept. 27 - Oct. 1, (2015), DOI: [10.1109/ECOC.2015.7341627](https://doi.org/10.1109/ECOC.2015.7341627)
- [27] C. Sun, S. H. Bae, and H. Kim, "Transmission of 28-Gb/s Duobinary and PAM-4 Signals Using DML for Optical Access Network," *IEEE Photon. Technol. Lett.* 29(1), 130–133 (2017), DOI: [10.1109/LPT.2016.2629623](https://doi.org/10.1109/LPT.2016.2629623)
- [28] J. L. Wei, K. Grobe, C. Wagner, E. Giacomidis, and H. Griesser, "40 Gb/s Lane Rate NG-PON using Electrical/Optical Duobinary, PAM-4 and Low Complex Equalizations," *Optical Fiber Communication Conference*, (2016), DOI: [10.1364/OFC.2016.Tu3C.5](https://doi.org/10.1364/OFC.2016.Tu3C.5)
- [29] B. Teipen, N. Eiselt, A. Dochhan, H. Griesser, M. Eiselt, and J.-P. Elbers, "Investigation of PAM-4 for extending reach in data center interconnect applications," *2015 17th*

- International Conference on Transparent Optical Networks (ICTON)*, pp. 1-4. Budapest, Hungary, July 5-9 ,(2015), DOI: [10.1109/ICTON.2015.7193371](https://doi.org/10.1109/ICTON.2015.7193371)
- [30] Agilent Technologies, "Making OSNR measurements in a modulated DWDM signal environment, pp. 1-26, see online: <https://docplayer.net/19987871-Making-osnr-measurements-in-a-modulated-dwdm-signal-environment.html>
- [31] X. Miao, M. Bi, Y. Fu, L. Li, and W. Hu, "Experimental Study of NRZ, Duobinary, and PAM-4 in O-Band DML-Based 100G-EPON," *IEEE Photon. Technol. Lett.* 29(17), 1490–1493 (2017), DOI: [10.1109/LPT.2017.2731372](https://doi.org/10.1109/LPT.2017.2731372)
- [32] H. Ji, W. Hu, L. Yi, Z. Li, L. Xue, X. Li, Q. Yang, S. Wang, Y. Yang, and S. Yu, "Field Demonstration of a Real-Time 100-Gb/s PON Based on 10G-Class Optical Devices," *J. Lightwave Technol.* 35(10), 1914–1921 (2017), DOI: [10.1109/JLT.2016.2633482](https://doi.org/10.1109/JLT.2016.2633482)
- [33] V. Bobrovs, J. Porins, G. Ivanovs, "Influence of nonlinear optical effects on the NRZ and RZ modulation signals in WDM systems," *Electronics and Electrical Engineering*, vol. 4(76), pp. 55–58, (2007), DOI: [10.5755/J01.EEE.76.4.10719](https://doi.org/10.5755/J01.EEE.76.4.10719)
- [34] L. N. Binh, "Advanced Digital Optical Communications. Second Edition", July 27, 2017 by CRC Press, 937 Pages (2015), DOI: [ISBN 9781138749542](https://doi.org/ISBN%209781138749542)
- [35] P. J. Winzer and R.-J. Essiambre, "Advanced Optical Modulation Formats," *Proc. IEEE* 94(5), 952–985 (2006), DOI: [10.1109/JPROC.2006.873438](https://doi.org/10.1109/JPROC.2006.873438)
- [36] H. Zhang, B. Jiao, Y. Liao, G. Zhang, "PAM4 Signaling for 56G Serial Link Applications - A Tutorial", Jan. 19-21, (2016), See online: <https://www.xilinx.com/publications/events/designcon/2016/slides-pam4signalingfor56gserial-zhang-designcon.pdf>
- [37] D. Brunina, S. Porto, A. Jain, C. P. Lai, C. Antony, N. Pavarelli, M. Rensing, G. Talli, P. Ossieur, P. O'Brien, and P. D. Townsend, "Analysis of Forward Error Correction in the Upstream Channel of 10Gb/s Optically Amplified TDM-PONs," *Optical Fiber Communication Conference*, 1–3, Los Angeles, CA, (2015), DOI: [10.1364/OFC.2015.Th4H.3](https://doi.org/10.1364/OFC.2015.Th4H.3)
- [38] Y. Wang, W. Gai and L. Tang, "A novel 40-Gb/S PAM4 transmitter with power-efficient pre-emphasis", *IEEE International Conference on Solid-State and Integrated Circuit Technology (ICSICT)*, pp. 1-3, Guilin, China, Oct. 28-31, (2014), DOI: [10.1109/ICSICT.2014.7021357](https://doi.org/10.1109/ICSICT.2014.7021357)
- [39] R. Kaur and S. Dewra, "Duobinary Modulation Format for Optical System- A Review," *International Journal of Advanced Research in Electrical, Electronics and Instrumentation Engineering (IJAREEIE)* 03(08), 11039–11046 (2014), DOI: [10.15662/ijareeie.2014.0308012](https://doi.org/10.15662/ijareeie.2014.0308012)

- [40] F. Qamar, M. K. Islam, S. Z. Ali Shah, R. Farhan, and M. Ali, "Secure Duobinary Signal Transmission in Optical Communication Networks for High Performance & Reliability," *IEEE Access* 5, 17795–17802 (2017), DOI: [10.1109/ACCESS.2017.2752002](https://doi.org/10.1109/ACCESS.2017.2752002)
- [41] **T. Salgals**, S. Spolitis, S. Olonkins and V. Bobrovs, "Investigation of 4-PAM modulation format for use in WDM-PON optical access systems," *2017 Progress In Electromagnetics Research Symposium - Spring (PIERS)*, 2017, pp. 2450-2454, St. Petersburg, Russia, (2017), DOI: [10.1109/PIERS.2017.8262162](https://doi.org/10.1109/PIERS.2017.8262162)
- [42] I. Kurbatska, S. Spolitis, V. Bobrovs, A. Alsevska, and G. Ivanovs, "Performance comparison of modulation formats for 10 Gbit/s WDM-PON systems," *2016 Advances in Wireless and Optical Communications (RTUWO)*, pp.51-54, Riga, Latvia, Nov. 3-4 (2016), DOI: [10.1109/RTUWO.2016.7821854](https://doi.org/10.1109/RTUWO.2016.7821854)
- [43] ID Photonics GmbH., "CoBrite MX1 – Laser," Technical Specification, pp. 1-4., (2017), see online: [https://www.id-photonics.com/images/stories/PDF/Data sheet CBDX1-x-x-xx.pdf](https://www.id-photonics.com/images/stories/PDF/Data_sheet_CBDX1-x-x-xx.pdf)
- [44] Optilab "40 GHz Linear InGaAs PIN Photodetector," Technical Specification, pp 1-4, (2016), See online: <https://www.optilab.com/products/pd-40b>
- [45] A. Korra, T. Salgals, J. Porins, E. Kazoks, R. Miho and S. Spolitis, "Performance Analysis of Cost-efficient High-speed up to 32 Gbit/s WDM-PON Next-generation Access Network with Dispersion Compensation," *2019 Photonics & Electromagnetics Research Symposium - Spring (PIERS-Spring)*, pp. 2671-2678, Rome, Italy, June 17–20, (2019), DOI: [10.1109/PIERS-Spring46901.2019.9017854](https://doi.org/10.1109/PIERS-Spring46901.2019.9017854)
- [46] ITU-T Recommendation G.989.2, "Digital sections and digital line system – Optical line systems for local and access networks–40-Gigabit-capable passive optical networks 2 (NG-PON2): Physical media dependent (PMD) layer specification", pp. 1–122, (2019), See online: https://www.itu.int/rec/dologin_pub.asp?lang=e&id=T-REC-G.989.2-201902-I!!PDF-E&type=items
- [47] ITU-T Recommendation G.9807.1., "Access Networks–Optical Line Systems for Local and Access Networks, 10-Gigabit-Capable Symmetric Passive Optical Network (XGS-PON)," see online: https://www.itu.int/rec/dologin_pub.asp?lang=e&id=T-REC-G.9807.1-202010-I!Amd2!PDF-E&type=items
- [48] ITU-T PON Standards-Progress and Recent Activities Q2/SG15, (accessed on 30 July 2020). See online: https://www.itu.int/en/ITU-T/studygroups/2017-2020/15/Documents/OFC2018-2-Q2_v5.pdf
- [49] P. Li, L. Yi, L. Xue and W. Hu, "56 Gbps IM/DD PON based on 10G-Class Optical Devices with 29 dB Loss Budget Enabled by Machine Learning," *2018 Optical Fiber*

- Communications Conference and Exposition (OFC)*, pp. 1-3, San Diego, CA, USA, 11–15 March (2018), DOI: [10.1364/OFC.2018.M2B.2](https://doi.org/10.1364/OFC.2018.M2B.2)
- [50] ITU-T standards. LS–High Speed PON Liaison to IEEE P802.3ca, (accessed on 30 July 2020). See online: http://www.ieee802.org/3/minutes/mar18/incoming/ITU_SG15-LS-95_to_IEEE_802d3.pdf
- [51] P. Torres-Ferrera, H. Wang, V. Ferrero, R. Mercinelli, and R. Gaudino, "Towards 50 Gb/s in High-Speed PON: Optimization of Modulation Formats Using Pre-Chirping," *2018 20th International Conference on Transparent Optical Networks (ICTON)*, Bucharest, Romania, 1–5 July, (2018), DOI: [10.1109/ICTON.2018.8473857](https://doi.org/10.1109/ICTON.2018.8473857)
- [52] P. Torres-Ferrera, V. Ferrero, M. Valvo, and R. Gaudino, "Impact of the Overall Electrical Filter Shaping in Next-Generation 25 and 50 Gb/s PONs," *J. Opt. Commun. Netw.* 10(5), 493 (2018), DOI: [10.1364/JOCN.10.000493](https://doi.org/10.1364/JOCN.10.000493)
- [53] S. Barthomeuf, F. Saliou, L. Anet Neto, P. Chanclou, and D. Erasme, "TDM-PON PAM Downstream Transmission for 25 Gbit/s and Beyond," *Photonics* 5(4), 45 (2018), DOI: [10.3390/photonics5040045](https://doi.org/10.3390/photonics5040045)
- [54] G. N. Liu, L. Zhang, T. Zuo, and Q. Zhang, "IM/DD Transmission Techniques for Emerging 5G Fronthaul, DCI, and Metro Applications," *J. Lightwave Technol.* 36(2), 560–567 (2018), DOI: [10.1109/JLT.2018.2793313](https://doi.org/10.1109/JLT.2018.2793313)
- [55] R. Lin, J. Van Kerrebrouck, X. Pang, M. Verplaetse, O. Ozolins, A. Udalcovs, L. Zhang, L. Gan, M. Tang, S. Fu, R. Schatz, U. Westergren, S. Popov, D. Liu, W. Tong, T. De Keulenaer, G. Torfs, J. Bauwelinck, X. Yin, and J. Chen, "Real-time 100 Gbps/core NRZ and EDB IM/DD transmission over multicore fiber for intra-datacenter communication networks," *Opt. Express* 26(8), 10519 (2018), DOI: [10.1364/OE.26.010519](https://doi.org/10.1364/OE.26.010519)
- [56] S. Barthomeuf, F. Saliou, L. A. Neto, P. Chanclou, and D. Erasme, "High Optical Budget 25Gbit/s PON with PAM4 and Optically Amplified O Band Downstream Transmission," *2018 European Conference on Optical Communication (ECOC)*, pp. 1-3 Rome, Italy, Sept 23-27, (2018), DOI: [10.1109/ECOC.2018.8535434](https://doi.org/10.1109/ECOC.2018.8535434)
- [57] D. Zou, F. Li, Z. Li, W. Wang, Q. Sui, Z. Cao, and Z. Li, "100G PAM-6 and PAM-8 Signal Transmission Enabled by Pre-Chirping for 10-km Intra-DCI Utilizing MZM in C-band," *J. Lightwave Technol.* 38(13), 3445–3453, (2020), DOI: [10.1109/JLT.2020.2973902](https://doi.org/10.1109/JLT.2020.2973902)
- [58] Y. C. Chung, "High-speed coherent WDM PON for next-generation access network," *2013 15th International Conference on Transparent Optical Networks (ICTON)*, pp. 1-4, Cartagena, Spain, 23-27 June (2013), DOI: [10.1109/ICTON.2013.6602825](https://doi.org/10.1109/ICTON.2013.6602825)

- [59] A. Hodzic, B. Konrad, and K. Petermann, "Prechirp in NRZ-based 40-Gb/s single-channel and WDM transmission systems," *IEEE Photon. Technol. Lett.* 14(2), 152–154 (2002), DOI: [10.1109/68.980479](https://doi.org/10.1109/68.980479)
- [60] V. Bobrovs, A. Udalcovs, S. Spolitis, and G. Ivanovs, "Schemes for Compensation of Chromatic Dispersion in Combined HDWDM Systems," *Latvian Journal of Physics and Technical Sciences* 48(5), (2011), DOI:<https://doi.org/10.2478/v10047-011-0033-6>
- [61] V. Duendorfs, S. Spolitis, and V. Bobrovs, "Comparison of dispersion compensation methods for 40Gbit/s WDM-PON transmission systems," *2017 Progress In Electromagnetics Research Symposium - Spring (PIERS)*, pp. 2431-2436, St. Petersburg Russia, 22-25 May, (2017), DOI: [10.1109/PIERS.2017.8262159](https://doi.org/10.1109/PIERS.2017.8262159)
- [62] S. Olonkins, S. Spolitis, I. Lyashuk, and V. Bobrovs, "Cost effective WDM-AON with multicarrier source based on dual-pump FOPA," *2014 6th International Congress on Ultra Modern Telecommunications and Control Systems and Workshops (ICUMT)*, pp. 23-28, St. Petersburg, Russia, Oct. 6-8, (2014), DOI: [10.1109/ICUMT.2014.7002073](https://doi.org/10.1109/ICUMT.2014.7002073)
- [63] R. Maharjan, I. Lavrinovica, A. Supe, and J. Porins, "Minimization of FWM effect in nonlinear optical fiber using variable channel spacing technique," *2016 Advances in Wireless and Optical Communications (RTUWO)*, pp. 1-4, Riga, Latvia, 3-4 Nov, (2016), DOI: [10.1109/RTUWO.2016.7821844](https://doi.org/10.1109/RTUWO.2016.7821844)
- [64] ITU-T Recommendation G.694.1, "Transmission media and optical systems characteristics –Characteristics of optical systems: Spectral grids for WDM applications: DWDM frequency grid", pp. 7–12, (2012), See online: https://www.itu.int/rec/dologin_pub.asp?lang=e&id=T-REC-G.694.1-202010-I!!PDF-E&type=items
- [65] Discovery Semiconductors Inc., "High Optical Power Handling InGaAs Photodiodes to 50 GHz," Technical Specification, pp 1-4, (2003), See online: https://www.discoverysemi.com/Product_Pages/DSC10H_20H.php
- [66] K. Keykhosravi, M. Secondini, G. Durisi, E. Agrell, "How to Increase the Achievable Information Rate by Per-Channel Dispersion Compensation," *J. Lightwave Technol.* 37, 2443-2451, (2019), DOI: <https://doi.org/10.1109/JLT.2019.2907311>
- [67] R. K. Ahmed and H. A. Mahmood, "Performance analysis of PAM intensity modulation based on dispersion compensation fiber technique for optical transmission system," *2018 1st International Scientific Conference of Engineering Sciences - 3rd Scientific Conference of Engineering Science (ISCES)*, pp. 126-130, Diyala Iraq, Jan. 10-11 (2018), DOI: [10.1109/ISCES.2018.8340540](https://doi.org/10.1109/ISCES.2018.8340540)
- [68] X. Sun, M. Yang, and I. B. Djordjevic, "Real-Time FPGA-Based Rate Adaptive LDPC Coding for Data Center Networks and PONs," *2018 European Conference on Optical*

- Communication (ECOC)*, pp. 1-3, Rome, Italy, Sept. 23-27, (2018), DOI: [10.1109/ECOC.2018.8535131](https://doi.org/10.1109/ECOC.2018.8535131)
- [69] ITU-T Recommendation G.709/Y, "Transmission systems and media digital systems and networks –Global information infrastructure, internet protocol aspects and Next-generation networks, internet of things and smart cities", pp. 1–89, (2016), See online: https://www.itu.int/rec/dologin_pub.asp?lang=e&id=T-REC-G.709-200912-S!!PDF-E&type=items
- [70] T. Salgals, I. Kurbatska, V. Bobrovs and S. Spolitis, "Research of PAM-4 Modulated WDM-PON Architecture for 5G Millimeter-wave Hybrid Photonics-wireless Interface," *2019 Photonics & Electromagnetics Research Symposium - Fall (PIERS - Fall)*, pp. 728-734, Xiamen, China, Dec 17-20, (2019), DOI: [10.1109/PIERS-Fall48861.2019.9021846](https://doi.org/10.1109/PIERS-Fall48861.2019.9021846)
- [71] F. Lu, M. Xu, L. Cheng, J. Wang, S. Shen, H. J. Cho, and G.-K. Chang, "Adaptive Digitization and Variable Channel Coding for Enhancement of Compressed Digital Mobile Fronthaul in PAM-4 Optical Links," *J. Lightwave Technol.* 35(21), 4714–4720 (2017), DOI: [10.1109/JLT.2017.2749567](https://doi.org/10.1109/JLT.2017.2749567)
- [72] E. Tangdiongga, N. Calabretta, P. C. W. Sommen, and H. J. S. Dorren, "WDM monitoring technique using adaptive blind signal separation," *IEEE Photon. Technol. Lett.* 13(3), 248–250 (2001), DOI: [10.1109/68.914336](https://doi.org/10.1109/68.914336)
- [73] Z. Tao, W. Yan, L. Dou, L. Li, S. Oda, T. Hoshida, J. C. Rasmussen, "The Impact of DWDM Channel De-correlation Method in Optical PSK Coherent Transmission Experiment", *2009 35th European Conference on Optical Communication (ECOC)*, pp. 1-2, Vienna, Austria, Sept. 20-24, (2009), See online: <https://ieeexplore.ieee.org/document/5287420?arnumber=5287420>
- [74] S. García and I. Gasulla, "Multi-cavity optoelectronic oscillators using multicore fibers," *Opt. Express* 23(3), 2403, (2015), DOI: [10.1364/OE.23.002403](https://doi.org/10.1364/OE.23.002403)
- [75] I. Gasulla, J. Lloret, J. Sancho, S. Sales, and J. Capmany, "Recent Breakthroughs in Microwave Photonics," *IEEE Photonics J.* 3(2), 311–315, (2011), DOI: [10.1109/JPHOT.2011.2130517](https://doi.org/10.1109/JPHOT.2011.2130517)
- [76] Y. F. Yuting Fan, J. L. Jianqiang Li, Y. L. Yi Lei, M. T. Ming Tang, F. Y. Feifei Yin, Y. D. Yitang Dai, and K. X. and Kun Xu, "Full-duplex transmission of IEEE 802.11ac-compliant MIMO WLAN signals over a 2-km 7-core fiber," *Chin. Opt. Lett.* 15(1), 010011–010015, (2017), DOI: [10.3788/COL201715.010011](https://doi.org/10.3788/COL201715.010011)
- [77] J. M. Galve, I. Gasulla, S. Sales, and J. Capmany, "Reconfigurable Radio Access Networks Using Multicore Fibers," *IEEE J. Quantum Electron.* 52(1), 1–7, (2016), DOI: [10.1109/JQE.2015.2497244](https://doi.org/10.1109/JQE.2015.2497244)

- [78] J. S. Wey and J. Zhang, "Passive Optical Networks for 5G Transport: Technology and Standards," *J. Lightwave Technol.* 37(12), 2830–2837, (2019), DOI: [10.1109/JLT.2018.2856828](https://doi.org/10.1109/JLT.2018.2856828)
- [79] GSM association (GSMA), "Study on socio-economic benefits of 5G services provided in mmWave bands," research report, available online, pp. 1-64, December, (2018), See online: <https://www.gsma.com/spectrum/wp-content/uploads/2019/10/mmWave-5G-benefits.pdf>
- [80] N. Argyris, G. Giannoulis, K. Kanta, N. Iliadis, C. Vagionas, S. Papaioannou, G. Kalfas, D. Apostolopoulos, C. Caillaud, H. Debregeas, N. Pleros, and H. Avramopoulos, "A 5G mmWave Fiber-Wireless IFoF Analog Mobile Fronthaul Link With up to 24-Gb/s Multiband Wireless Capacity," *J. Lightwave Technol.* 37(12), 2883–2891, (2019), DOI: [10.1109/JLT.2019.2897109](https://doi.org/10.1109/JLT.2019.2897109)
- [81] H. Li, X. Li, M. Luo, and S. Yu, "Digital Mobile Fronthaul Employing Enhanced Noise Shaping Based Pulse Code Modulation with Nonuniform Quantizer," *2018 European Conference on Optical Communication (ECOC)*, pp. 1-3, Rome, Italy, Sept. 23-27, (2018), DOI: [10.1109/ECOC.2018.8535173](https://doi.org/10.1109/ECOC.2018.8535173)
- [82] R. Noorani, L. Yi, P. Li, and W. Hu, "Demonstration of 25 Gbit/s PAM4 Hybrid Photonic-Wireless Transmission," *Asia Communications and Photonics Conference (ACPC)*, pp. 1-3., Guangzhou, China, Nov. 10-13, (2017), DOI: [10.1364/ACPC.2017.S3C.6](https://doi.org/10.1364/ACPC.2017.S3C.6)
- [83] I. A. Alimi, A. L. Teixeira, and P. P. Monteiro, "Toward an Efficient C-RAN Optical Fronthaul for the Future Networks: A Tutorial on Technologies, Requirements, Challenges, and Solutions," *IEEE Commun. Surv. Tutorials* 20(1), 708–769, (2018), DOI: [10.1109/COMST.2017.2773462](https://doi.org/10.1109/COMST.2017.2773462)
- [84] P. Chanclou, L. Anet Neto, K. Grzybowski, Z. Tayq, F. Saliou, and N. Genay, "Mobile Fronthaul Architecture and Technologies: A RAN Equipment Assessment [Invited]," *J. Opt. Commun. Netw.* 10(1), A1 (2017), DOI: [10.1364/JOCN.10.0000A1](https://doi.org/10.1364/JOCN.10.0000A1)
- [85] A. Weissberger, IEEE Communications Society, Technology Blog, May 28, (2017), See online: <http://techblog.comsoc.org/2017/05/>
- [86] A. Jurado-Navas, T. R. Raddo, J. M. Garrido-Balsells, B.-H. V. Borges, J. J. V. Olmos, and I. T. Monroy, "Hybrid optical CDMA-FSO communications network under spatially correlated gamma-gamma scintillation," *Opt. Express* 24(15), 16799, (2016), DOI: [10.1364/OE.24.016799](https://doi.org/10.1364/OE.24.016799)
- [87] L. Galdino, T. R. Raddo, A. L. Sanches, L. H. Bonani, and E. Moschim, "Performance comparison of hybrid 1-D WDM/OCDMA and 2-D OCDMA towards future access network migration scenario," *2012 14th International Conference on Transparent*

Optical Networks (ICTON), pp. 1-4, July 2-5, (2012), DOI: [10.1109/ICTON.2012.6254425](https://doi.org/10.1109/ICTON.2012.6254425)

- [88] The Electronic Communications Committee (ECC) of the European Conference of Postal and Telecommunications Administrations (CEPT), "Spectrum for wireless broadband – 5G", March, (2019), See online: <https://ec.europa.eu/research/participants/documents/downloadPublic/TVVxMGY5bGliUVZxSVRJMG5McDFIQWZGeE1SZI1wVzNZNmc4aGxveXIVVk9nZjBOTGdGenVBPT0=/attachment/VFEyQTO4M3ptUWRnN1h3NmN2ci9uR3R2a2pPYmxUQIA>
- [89] P. Marsch, O. Bulakci, O. Queseth, and M. Boldi, "5G system design - architectural and functional considerations and long term research," *Wiley*, (2018), See online: <https://www.wiley.com/enus/5G+System+Design%3A+Architectural+and+Functional+Considerations+and+Long+Term+Research-p-9781119425120>
- [90] K. Zeb, Z. G. Lu, J. R. Liu, P. J. Poole, M. Rahim, G. Pakulski, Y. X. Mao, C. Y. Song, and X. Zhang, "Experimental Demonstration of Photonic MMW-over Fiber System for Next Generation Access Networks," *2019 Photonics North (PN)*, pp. 1-1, Quebec City, QC, Canada, May 21-23, (2019), DOI: [10.1109/PN.2019.8819583](https://doi.org/10.1109/PN.2019.8819583)
- [91] E. Harstead, D. Van Veen, V. Houtsma, and P. Dom, "Technology Roadmap for Time Division Multiplexed Passive Optical Networks (TDM PONs)," *J. Lightwave Technol.*, 1–1 (2018), DOI: [10.1109/JLT.2018.2881933](https://doi.org/10.1109/JLT.2018.2881933)
- [92] W. Zhou, P. Gou, K. Wang, M. Kong, X. Li, L. Zhao, Z. Zhu, and J. Yu, "PAM-4 Wireless Transmission based on Look-up-table Pre-distortion and CMMA Equalization at V-band," *Optical Fiber Communication Conference (OFC)*, pp. 1-3, San Diego, CA, USA, March 11-15, (2018), DOI: <https://doi.org/10.1364/OFC.2018.Th2A.60>
- [93] **T. Salgals**, L. Skladova, K. Vilcane, J. Braunfelds and S. Spolitis, "Evaluation of 4-PAM, NRZ and Duobinary Modulation Formats Performance for Use in 20 Gbit/s DWDM-PON Optical Access Systems," *2018 Advances in Wireless and Optical Communications (RTUWO)*, pp.134-138, Riga Latvia, Nov 15-16, (2018), DOI: [10.1109/RTUWO.2018.8587887](https://doi.org/10.1109/RTUWO.2018.8587887)
- [94] C. Liu, J. Wang, L. Cheng, M. Zhu, and G.-K. Chang, "Key Microwave-Photonics Technologies for Next-Generation Cloud-Based Radio Access Networks," *J. Lightwave Technol.* 32(20), 3452–3460, (2014), DOI: [10.1109/JLT.2014.2338854](https://doi.org/10.1109/JLT.2014.2338854)
- [95] M. Jaber, M. A. Imran, R. Tafazolli, and A. Tukmanov, "5G Backhaul Challenges and Emerging Research Directions: A Survey," *IEEE Access* 4, 1743–1766, (2016), DOI: [10.1109/ACCESS.2016.2556011](https://doi.org/10.1109/ACCESS.2016.2556011)
- [96] M. Gapeyenko, V. Petrov, D. Moltchanov, S. Andreev, N. Himayat, and Y. Koucheryavy, "Flexible and Reliable UAV-Assisted Backhaul Operation in 5G

- mmWave Cellular Networks," *IEEE J. Select. Areas Commun.* 36(11), 2486–2496, (2018), DOI: [10.1109/JSAC.2018.2874145](https://doi.org/10.1109/JSAC.2018.2874145)
- [97] B. Panzner, "Scheduling conflicts in wireless in-band backhaul for 5G millimeter wave communications," *2016 IEEE Conference on Computer Communications Workshops (INFOCOM WKSHPS)*, pp. 1-2, San Francisco, CA, USA, April 10-14, (2016), DOI: [10.1109/INFCOMW.2016.7562055](https://doi.org/10.1109/INFCOMW.2016.7562055)
- [98] K. Kawasaki, Y. Ito, H. Iwai, S. Nakano, Y. Suegara, M. Sibayama, M. Umehara, "Analysis of Diffraction Characteristics at 28GHz Band in a Vehicular Communication Environment", *2018 International Symposium on Antennas and Propagation (ISAP)*, pp. 1-2, Busan, Korea (South), Oct. 23-26, (2018), See online: <https://www.ieice.org/ken/paper/20180517713V/eng/>
- [99] Guan-yun Wang, Yuan-jian Liu, Shuang-de Li, Xiao-jun Zhang, and Zhi-peng Chen, "Study on the outdoor wave propagation at 28GHz by ray tracing method," *2016 IEEE International Conference on Microwave and Millimeter Wave Technology (ICMMT)*, pp 1-3, Beijing, China, June 5-8, (2016), DOI: [10.1109/ICMMT.2016.7761813](https://doi.org/10.1109/ICMMT.2016.7761813)
- [100] A.Liu, X. Wang, Q. Shao, T. Song, H. Yin, and N. Zhao, "A low cost structure of radio-over-fiber system compatible with WDM-PON," *2016 25th Wireless and Optical Communication Conference (WOCC)*, pp. 1-3, Chengdu, China, May 21-23, (2016), DOI: [10.1109/WOCC.2016.7506546](https://doi.org/10.1109/WOCC.2016.7506546)
- [101] G. Giannoulis, N. Argyris, N. Iliadis, G. Pouloupoulos, K. Kanta, D. Apostolopoulos, and H. Avramopoulos, "Analog Radio-over-Fiber Solutions for 5G Communications in the Beyond-CPRI Era," *2018 20th International Conference on Transparent Optical Networks (ICTON)*, pp. 1-5, Bucharest, Romania, July 1-5 (2018), DOI: [10.1109/ICTON.2018.8473886](https://doi.org/10.1109/ICTON.2018.8473886)
- [102] **T. Salgals**, I. Kurbatska, S. Spolitis, V. Bobrovs and G. Ivanovs, "Research of M-PAM and Duobinary modulation formats for use in high-speed WDM-PON systems", IntechOpen, the world's leading publisher of Open Access books Built by scientists, for scientists, 'Telecommunication Systems', pp. 1-18, 22 February, (2019), DOI: [10.5772/intechopen.84600](https://doi.org/10.5772/intechopen.84600)
- [103] **T. Salgals**, L. Skladova, J. Porins, V. Bobrovs and S. Spolitis, "Analog Radio-over-fiber WDM-PON Architecture for 5G Millimeter-wave Interface," *2019 Photonics & Electromagnetics Research Symposium - Spring (PIERS-Spring)*, 2019, pp. 1-7, Rome, Italy, June 17-20, (2019), DOI: [10.1109/PIERS-Spring46901.2019.9017431](https://doi.org/10.1109/PIERS-Spring46901.2019.9017431)
- [104] V. A. Thomas, M. El-Hajjar, and L. Hanzo, "Millimeter-Wave Radio Over Fiber Optical Upconversion Techniques Relying on Link Nonlinearity," *IEEE Commun. Surv. Tutorials* 18(1), 29–53, (2016), DOI: [10.1109/COMST.2015.2409154](https://doi.org/10.1109/COMST.2015.2409154)

- [105] A. T. Latunde, M. Milosavljevic, P. Kourtessis, J. Senior, "OQAM-OFDM RoF with IM-DD remote heterodyne 28 GHz upconversion for 5G millimeter RANs," *2016 18th International Conference on Transparent Optical Networks (ICTON)*, pp. 1-4, Trento, Italy, July 10-14, (2016), DOI: [10.1109/COMST.2015.2409154](https://doi.org/10.1109/COMST.2015.2409154)
- [106] Finisar "50 GHz DWDM Single High-speed Photodetector XPDV21x(RA)," *Technical Specification*, pp 1-5, (2015), See online: <https://ii-vi.com/product/50-ghz-dwdm-single-high-speed-photodetector/>
- [107] J. Hesler, Kai Hui, and T. Crowe, "Ultrafast millimeter-wave and THz envelope detectors for wireless communications," 2012 IEEE International Topical Meeting on Microwave Photonics, pp. 93-94, Noordwijk, Netherlands, Sept. 11-14, (2012), DOI: [10.1109/MWP.2012.6474063](https://doi.org/10.1109/MWP.2012.6474063)
- [108] X. Pang, O. Ozolins, S. Gaiarin, M. I. Olmedo, R. Schatz, U. Westergren, D. Zibar, S. Popov, G. Jacobsen, "Evaluation of High-Speed EML-based IM/DD links with PAM Modulations and Low-Complexity Equalization," ECOC 2016; 42nd European Conference on Optical Communication (ECOC), pp. 1-3, Dusseldorf, Germany, Sept. 18-22, (2016), See online: <https://ieeexplore.ieee.org/stamp/stamp.jsp?arnumber=7767750>
- [109] ITU-T Recommendation G.9803, "Transmission systems and media digital systems and networks – Access networks–*Optical line systems for local and access networks, internet of Radio over fibresystems*", pp. 1–50, (2018), See online: https://www.itu.int/rec/dologin_pub.asp?lang=e&id=T-REC-G.9803-201908-1!Amd1!PDF-E&type=items
- [110] S. Spolitis, I. Kurbatska, and V. Bobrovs, "Evaluation of the Impact of MZM Frequency Response on BER Performance of PAM-4 Modulated WDM-PON," 2019 Photonics & Electromagnetics Research Symposium - Spring (PIERS-Spring), pp. 2037-2042, Rome, Italy, (2019), DOI: [10.1109/PIERS-Spring46901.2019.9017581](https://doi.org/10.1109/PIERS-Spring46901.2019.9017581)
- [111] IXblue Photonics "MX-LN series 1550nm band Intensity Modulators," Technical Specification, pp. 1–6, (2019), See online: https://www.ixblue.com/wp-content/uploads/2022/02/MX-LN_SERIES.pdf
- [112] SHF Communication Technologies AG "Datasheet SHF 100 BP Broadband Amplifier" Technical Specification, pp. 1–12, (2016), See online: https://www.shf-communication.com/wp-content/uploads/datasheets/datasheet_shf_100bp.pdf
- [113] D. Breuer, E. Weis, S. Krauss, M. Dueser, "5G Converged Transport in Future Access Networks," *Broadband Coverage in Germany; 11. ITG-Symposium*, pp. 1-4, Berlin, Germany, March 29-30, (2017), See online: <https://ieeexplore.ieee.org/document/7948536>

- [114] C. Behrens, S. Krauß, E. Weis, and D. Breuer, "Technologies for Convergence of Fixed and Mobile Access: An Operator's Perspective [Invited]," *J. Opt. Commun. Netw.* 10(1), A37, (2017), DOI: [10.1364/JOCN.10.000A37](https://doi.org/10.1364/JOCN.10.000A37)
- [115] M. Yasir, M. Aldrigo, M. Dragoman, A. Dinescu, M. Bozzi, S. Iordanescu, and D. Vasilache, "Integration of Antenna Array and Self-Switching Graphene Diode for Detection at 28 GHz," *IEEE Electron Device Lett.* 40(4), 628–631, (2019), DOI: [10.1109/LED.2019.2899028](https://doi.org/10.1109/LED.2019.2899028)
- [116] C.-H. Li, M.-F. Wu, C.-H. Lin, and C.-T. Lin, "W-band OFDM RoF System with Simple Envelope Detector Down-Conversion," *Optical Fiber Communication Conference (OFC)*, pp. 1-3, Los Angeles, CA, USA, March 22-26, (2015), DOI: [10.1364/OFC.2015.W4G.6](https://doi.org/10.1364/OFC.2015.W4G.6)
- [117] Y. Zhou, G. Huang, S. Nam, B. S. Kim, "A novel wide-band envelope detector," 2008 IEEE Radio Frequency Integrated Circuits Symposium, pp. 219-222, Atlanta, GA, USA, June 15-17, (2008), DOI: [10.1109/RFIC.2008.4561422](https://doi.org/10.1109/RFIC.2008.4561422)
- [118] Agilent Technologies , Keysight - Phase Noise Measurement Methods and Techniques Presented by: Kay Gheen, Agilent Technologies, (2012), See online: https://www.keysight.com/upload/cmc_upload/All/PhaseNoise_webcast19Jul12.pdf
- [119] M. Kottkamp, A. Pandey, D. Raddino, A. Roessler, R. Stuhlaufth "5G New Radio Fundamentals, procedures, testing aspects", *Rohde & Schwarz*, pp. 1-462, July 1, (2019), See online: https://cdn.rohdeschwarz.com/fr/general_37/local_webpages/2019_demystifying_5g_and_ota/5G_NR_France_June2019_Fundamentals_procedures_TM_aspects_RS_France_June2019.pdf
- [120] A. Tikhomirov, E. Omelyanchuk, A. Semenova, "Recommended 5G frequency bands evaluation," *2018 Systems of Signals Generating and Processing in the Field of on Board Communications*, pp. 1-5, Moscow Russia, March 14-15, (2018), DOI: [10.1109/SOSG.2018.8350639](https://doi.org/10.1109/SOSG.2018.8350639)
- [121] P. Bravetti, G. Ghislotti, S. Balsamo, "Chirp-inducing mechanisms in Mach-Zehnder modulators and their effect on 10 Gb/s NRZ transmission studied using tunable-chirp single drive devices," *Journal of Lightwave Technology (JLT)*, pp. 605-611, Vol. 22, No. 2, March 30, (2004), DOI: [10.1109/JLT.2003.822676](https://doi.org/10.1109/JLT.2003.822676)
- [122] V. Torres-Company, and A. M. Weiner, "Optical frequency comb technology for ultra-broadband radio-frequency photonics," *Laser & Photonics Reviews* 8, 368-393, (2014), DOI: [10.1002/lpor.201300126](https://doi.org/10.1002/lpor.201300126)
- [123] K. Predehl, G. Grosche, S. M. F. Raupach, S. Droste, O. Terra, J. Alnis, Th. Legero, T. W. Hänsch, T. Udem, R. Holzwarth and H. Schnatz, "A 920-kilometer optical fiber link for frequency metrology at the 19th decimal place," *Science* 336, 441-444, (2012), DOI: [10.1126/science.1218442](https://doi.org/10.1126/science.1218442)

- [124] X. Pang, A. Udalcovs, R. Schatz, V. Bobrovs, G. Jacobsen, S. Popov, and O. Ozolins "Short Reach Communication Technologies for Client-Side Optics Beyond 400 Gbps," IEEE Photonics Technology Letters, 1-1, (2021), DOI: [10.1109/LPT.2021.3078255](https://doi.org/10.1109/LPT.2021.3078255)
- [125] S. Spolitis, R. Murnieks, L. Skladova, T. Salgals, A. V. Andrianov, M. P. Marisova, G. Leuchs, E. A. Anashkina, and V. Bobrovs, "IM/DD WDM-PON Communication System Based on Optical Frequency Comb Generated in Silica Whispering Gallery Mode Resonator," IEEE Access, 1-1, (2021), DOI: [10.1109/ACCESS.2021.3076411](https://doi.org/10.1109/ACCESS.2021.3076411)
- [126] T. J. Kippenberg, A. L. Gaeta, M. Lipson, and M. L. Gorodetsky, "Dissipative Kerr solitons in optical microresonators," Science 361(6402), (2018), DOI: [10.1126/science.aan8083](https://doi.org/10.1126/science.aan8083)
- [127] T. J. Kippenberg, A. L. Gaeta, M. Lipson, and M. L. Gorodetsky, "Dissipative Kerr solitons in optical microresonators," Science 361(6402), (2018), DOI: [10.1364/CLEO_SI.2020.SF2G.5](https://doi.org/10.1364/CLEO_SI.2020.SF2G.5)
- [128] S. Zhang, J. M. Silver, L. D. Bino, F. Copie, M. T. M. Woodley, G. N. Ghalanos, A. Svela, N. Moroney, and P. Del'Haye, "Microwatt-Level Soliton Frequency Comb Generation in Microresonators Using an Auxiliary Laser," Conference on Lasers and Electro-Optics(CLEO), pp. 1-2, May 5-10, (2019), DOI: [10.1364/CLEO_SI.2019.SF3H.5](https://doi.org/10.1364/CLEO_SI.2019.SF3H.5)
- [129] P. Del'Haye, A. Schliesser, O. Arcizet, T. Wilken, R. Holzwarth and T.J. Kippenberg, "Optical frequency comb generation from a monolithic microresonator, " Nature 450(7173), 1214–1217, (2007), DOI: [10.1038/nature06401](https://doi.org/10.1038/nature06401)
- [130] H. Hu, and L. K. Oxenløwe, "Chip-based optical frequency combs for high-capacity optical communications" Nanophotonics 10(5), 1367-1385, (2021), DOI: [10.1515/nanoph-2020-0561](https://doi.org/10.1515/nanoph-2020-0561)
- [131] R. Wu, V. R. Supradeepa, C. M. Long, D. E. Leaird, and A. M. Weiner, "Generation of very flat optical frequency combs from continuous-wave lasers using cascaded intensity and phase modulators driven by tailored radio frequency waveforms," Opt. Lett. 35(19), 3234 (2010), DOI: [10.1364/OL.35.003234](https://doi.org/10.1364/OL.35.003234)
- [132] Y. K. Chembo, "Kerr optical frequency combs: theory, applications and perspective", Nanophotonics 5(2), 214-230, (2016), DOI: [10.1515/nanoph-2016-0013](https://doi.org/10.1515/nanoph-2016-0013)
- [133] S. H. Lee, D. Y. Oh, Q.-F. Yang, B. Shen, H. Wang, K. Y. Yang, Y.-H. Lai, X. Yi, X. Li, and K. Vahala, "Towards visible soliton microcomb generation," Nat Commun 8(1), 1295, (2017), DOI: [10.1038/s41467-017-01473-9](https://doi.org/10.1038/s41467-017-01473-9)
- [134] E.A. Anashkina, M.P. Marisova, T. Salgals, J. Alnis, I. Lyashuk, G. Leuchs, S. Spolitis, V. Bobrovs, and A.V. Andrianov, "Optical Frequency Combs Generated in Silica Microspheres in the Telecommunication C-, U-, and E-Bands," Photonics 8(9), 345, (2021), DOI: [10.3390/photonics8090345](https://doi.org/10.3390/photonics8090345)

- [135] T. Salgals, A. Ostrovskis, A. Ipatovs, V. Bobrovs and S. Spolitis, "Hybrid ARoF-WDM PON Infrastructure for 5G Millimeter-wave Interface and Broadband Internet Service," *2019 Photonics & Electromagnetics Research Symposium - Fall (PIERS - Fall)*, pp. 1-8, Dec. 17-20, (2019), DOI: [10.1109/PIERS-Fall48861.2019.9021479](https://doi.org/10.1109/PIERS-Fall48861.2019.9021479)
- [136] E. A. Anashkina, M. P. Marisova, A. V. Andrianov, R. A. Akhmedzhanov, R. Murnieks, M. D. Tokman, L. Skladova, I. V. Oladyshkin, T. Salgals, I. Lyashuk, A. Sorokin, S. Spolitis, G. Leuchs, and V. Bobrovs, "Microsphere-Based Optical Frequency Comb Generator for 200 GHz Spaced WDM Data Transmission System," *Photonics* 7(3), 72, (2020), DOI: [10.3390/photonics7030072](https://doi.org/10.3390/photonics7030072)
- [137] M. L. Gorodetsky, A. A. Savchenkov, and V. S. Ilchenko, "Ultimate Q of optical microsphere resonators," *Opt. Lett.* 21(7), 453, (1996), DOI: [10.1364/OL.21.000453](https://doi.org/10.1364/OL.21.000453)
- [138] A. Kovach, D. Chen, J. He, H. Choi, A. H. Dogan, M. Ghasemkhani, H. Taheri, and A. M. Armani, "Emerging material systems for integrated optical Kerr frequency combs," *Adv. Opt. Photon.* 12(1), 135, (2020), DOI: [10.1364/AOP.376924](https://doi.org/10.1364/AOP.376924)
- [139] S. M. Spillane, T. J. Kippenberg, O. J. Painter, and K. J. Vahala, "Ideality in a Fiber-Taper-Coupled Microresonator System for Application to Cavity Quantum Electrodynamics," *Phys. Rev. Lett.* 91(4), 043902, (2003), DOI: [PhysRevLett.91.043902](https://doi.org/PhysRevLett.91.043902)
- [140] Wang, P.; Ding, M.; Murugan, G.S.; Bo, L.; Guan, C.; Semenova, Y.; Wu, Q.; Farrell, G.; Brambilla, G. Packaged, high-Q, microsphere-resonator-based add-drop filter. *Opt. Lett.* 39(17), 5208, (2014), DOI: [10.1364/OL.39.005208](https://doi.org/10.1364/OL.39.005208)
- [141] Suh, M.; Wang, C.Y.; Johnson, C.; Vahala, K.J. Directly pumped 10 GHz microcomb modules from low-power diode lasers. *Opt. Lett.*, 44(7), 1841, (2019), DOI: [10.1364/OL.44.001841](https://doi.org/10.1364/OL.44.001841)
- [142] Yu, J.; Lewis, E.; Farrell, G.; Wang, P. Compound Glass Microsphere Resonator Devices. *Micromachines* 9(7), 356, (2018), DOI: [10.3390/mi9070356](https://doi.org/10.3390/mi9070356)
- [143] Andrianov, A.V.; Anashkina, E.A. Single-mode silica microsphere Raman laser tunable in the U-band and beyond. *Results in Physics*, 17, 103084, (2020), DOI: [10.1016/j.rinp.2020.103084](https://doi.org/10.1016/j.rinp.2020.103084)
- [144] Svela, A.; Silver, J.; Del Bino, L.; Zhang, S.; Woodley, M.T.M.; Vanner, M.R.; Del'Haye, P. Coherent suppression of backscattering in optical microresonators, *Light Sci Appl* 9(1), 204, (2020), DOI: [10.1038/s41377-020-00440-2](https://doi.org/10.1038/s41377-020-00440-2)
- [145] Orucevic, F., Seguin, V.L.; Hare, J. Transmittance and near-field characterization of sub-wavelength tapered optical fibers. *Opt. Express* 15(21), 13624, (2007), DOI: [10.1364/OE.15.013624](https://doi.org/10.1364/OE.15.013624)

- [146] Nagai, R.; Aoki, T. Ultra-low-loss tapered optical fibers with minimal lengths. *Opt. Express* 22(23), 28427, (2014), DOI: [10.1364/OE.22.028427](https://doi.org/10.1364/OE.22.028427)
- [147] Tiecke, T.G.; Nayak, K.P.; Thompson, J.D.; Peyronel, T.; de Leon, N.P.; Vuletić, V.; Lukin, M.D. Efficient fiber-optical interface for nanophotonic devices. *Optica* 2(2), 70, (2015), DOI: [10.1364/OPTICA.2.000070](https://doi.org/10.1364/OPTICA.2.000070)
- [148] K. E. Webb, M. Erkintalo, S. Coen, and S. G. Murdoch, "Experimental observation of coherent cavity soliton frequency combs in silica microspheres," *Opt. Lett.* 41(20), 4613, (2016), DOI: [10.1364/OL.41.004613](https://doi.org/10.1364/OL.41.004613)
- [149] Q. Wang and Y. Yue, "Accurate and Rigorous Calibration of Intradyne Coherent Receiver Using Polarization-Multiplexed Signal Generated within Intradyne Coherent Transmitter," *Applied Sciences* 10(10), 3467, (2020), DOI: [10.3390/app10103467](https://doi.org/10.3390/app10103467)
- [150] R. Ma, A. Schliesser, P. Del'Haye, A. Dabirian, G. Anetsberger, and T. J. Kippenberg, "Radiation-pressure-driven vibrational modes in ultrahigh-Q silica microspheres," *Opt. Lett.* 32(15), 2200, (2007), DOI: [10.1364/OL.32.002200](https://doi.org/10.1364/OL.32.002200)
- [151] A. Schliesser, R. Rivière, G. Anetsberger, O. Arcizet, and T. J. Kippenberg, "Resolved-sideband cooling of a micromechanical oscillator," *Nature Phys* 4(5), 415–419, (2008), DOI: [10.1038/nphys939](https://doi.org/10.1038/nphys939)
- [152] Y. Jian, H.D. Pfister, K.R. Narayanan, R. Raghu, R. Mazahreh, "In Iterative hard-decision decoding of braided BCH codes for high-speed optical communication, " In Proceedings of the 2013 IEEE Global Communications Conference (GLOBECOM), (2013), DOI: [10.1109/GLOCOM.2013.6831429](https://doi.org/10.1109/GLOCOM.2013.6831429)

SUPPLEMENTS

PAPER-1: Investigation of 4-PAM modulation format for use in WDM-PON optical access systems

T. Salgals, **S. Spolitis**, S. Olonkins and V. Bobrovs, "Investigation of 4-PAM modulation format for use in WDM-PON optical access systems," *2017 Progress In Electromagnetics Research Symposium - Spring (PIERS)*, pp. 2450-2454, St. Petersburg, Russia, May 22-25, (2017), DOI: [10.1109/PIERS.2017.8262162](https://doi.org/10.1109/PIERS.2017.8262162)

Investigation of 4-PAM Modulation Format for Use in WDM-PON Optical Access Systems

Toms Salgals, Sandis Spolitis, Sergejs Olonkins, and Vjaceslavs Bobrovs
Institute of Telecommunications, Riga Technical University, Riga, Latvia

Abstract— In this paper, we investigate the performance of four level pulse amplitude modulation (PAM-4) format in fiber optical access networks. PAM-4 modulation format has higher spectral efficiency if compared to widespread used non-return-to zero (NRZ) line code and therefore potentially can provide higher data transmission speeds in fiber optical networks with limited bandwidth. When transmission speed is increased, chromatic dispersion (CD) can be the main distance-limiting factor for PAM-4 modulation format. For this reason in this paper we investigate maximal transmission distance with dispersion compensation and without dispersion compensation in 4-PAM modulated wavelength division multiplexed passive optical network (WDM-PON), as well as minimal available channel spacing. It is shown that dispersion compensation with fiber Bragg grating dispersion compensation module (FBG DCM) can improve the performance and maximal available reach of PAM-4 modulated optical signal by 25.4% or extra 15 km in length.

1. INTRODUCTION

The exponential growth of Internet data traffic and progress of Information and Communication Technology (ICT) sector pushes hard the telecommunication infrastructure for upgrading the transmission data rate [1]. Power and cost efficient fiber optical access networks and short-range fiber optical links are one of the key technologies enabling bandwidth hungry services like video on demand (VoD), high definition TV, and cloud computing supported by large scale high-performance computers and data centers. Such optical links typically use direct detection and on-off keying modulation (OOK) with non-return-to zero (NRZ) line code. Today's challenge for optical access networks and data centers is to increase the serial line rate of a NRZ link due to the physical bandwidth limitation of the photonic and electronic components like optical signal modulators and photodiodes [2].

Solution for telecommunication infrastructure upgrade and alternative solution for increase of the serial line rate of a NRZ link is to use multi-level signalling formats such as pulse-amplitude modulation (abbreviated as PAM-M or M-PAM), where multiple digital bits per symbol are encoded into M different signal amplitude levels. The 4 level PAM modulation format (PAM-4) is receiving significant attention because of its relative ease of implementation compared to higher-order modulation formats like quadrature phase-shift keying (QPSK), and m-ary quadrature amplitude modulation (m-QAM). It is clear that M-PAM offers a good trade-off between performance and complexity. Usage of PAM-4 format is effective way to double the data rate of NRZ link. Previously PAM-4 modulation formats have been investigated with traditional electrical networks [3, 4], but now researchers are focused on investigation of PAM-4 modulation format for optical access networks as well as data center interconnections [5].

In our research we investigate the 4-channel 10 Gbaud/s (20 Gbit/s) PAM-4 modulated WDM-PON access system with different channel spacing as well as without chromatic dispersion (CD) compensation and compensation with fiber Bragg grating (FBG) dispersion compensation module (DCM). In our research we found the minimal allowable channel spacing, which has a direct impact on the utilization of resources like optical spectrum, and maximal transmission distance for multichannel PAM-4 modulated WDM-PON transmission system operating at 10 Gbaud/s symbol rate.

2. SIMULATION SCHEME OF PAM-4 MODULATED WDM-PON TRANSMISSION SYSTEM

The goal of this simulation model was to evaluate the performance and maximum reach as well as minimal channel spacing for PAM-4 modulated WDM-PON system with four 10 Gbaud/s (20 Gbit/s) channels, under the condition that it is still possible to achieve a bit error ratio (BER) of 10^{-3} [6].

A widely used error correction code for 10-Gbit/s PONs is Reed Solomon (RS) (255,223) forward error correction (FEC) code. The theoretical performance restores a 1.1×10^{-3} pre-FEC BER to a

10^{-12} post-FEC BER. This relationship has led to the widely accepted practice of quoting physical-layer system performance at a pre-FEC BER of 1.1×10^{-3} or 10^{-3} in the PON standards [6, 7]. Therefore, in our research we use 10^{-3} as the BER performance threshold.

As one can see in Fig. 1, PAM-4 modulated WDM-PON simulation scheme consists of 4 channels. The central frequency is 193.1 THz and channel spacing is chosen 50 or 100 GHz, according to the ITU G.694.1 recommendation. Transmission performance for WDM-PON system with narrower channel spacing like 25 and 37.5 GHz also was realized, however the performance of these systems was above our defined BER threshold, quality of received signal was low and therefore these results are not included in our paper.

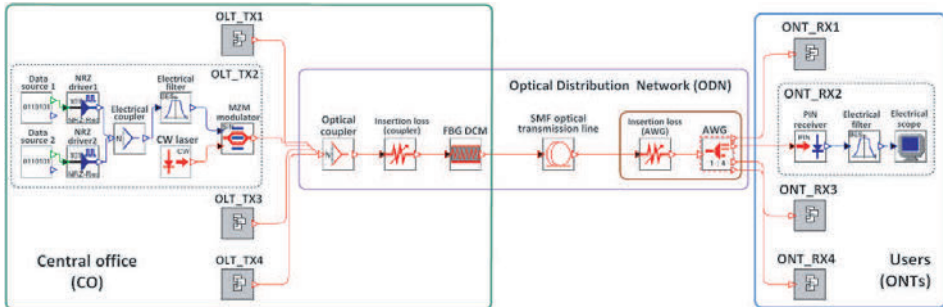


Figure 1: Simulation scheme of 10 Gbaud/s PAM-4 WDM-PON optical transmission system.

Central office (CO) consists of optical line terminal (OLT) with four transmitters (OLT_Tx). As it is shown in the Fig. 1, each transmitter (OLT_Tx) in consists of two electrical pseudo-random bit sequence (PRBS) data sources, two NRZ drivers, which encodes the data from data sources by using the non-return zero (NRZ) encoding technique and electrical coupler, which couples both electrical signal in one signal in such a way generating PAM-4 signal. The amplitude of electrical signal, generated by the second NRZ driver was twice larger than the amplitude of the first NRZ driver output signal. Coupled electrical PAM-4 signal with 4 different amplitude levels is filtered by electrical lowpass filter and send to external Mach-Zehnder modulator. As the light source continuous wavelength (CW) laser with linewidth of 50 MHz and output power of +3 dBm is used. MZM has 3 dB insertion loss and 20 dB extinction ratio.

Optical signals from each transmitter are coupled together by using optical combiner with 1 dB loss. Next, chromatic dispersion pre-compensation by FBG DCM is realized for all channels before launching them into standard ITU-T G.652 single mode fiber (SMF) span. Additional 3 dB attenuator is used for simulation of FBG DCM's insertion loss. After transmission in optical distribution network (ODN), all channels are separated by arrayed waveguide grating (AWG) filter (located in remote terminal (RT)), which insertion loss is 3.5 dB, channel spacing is 50 or 100 GHz and 3-dB bandwidth is 20 GHz. Receiver side consists of users or optical network terminals (ONTs). Each ONT receiver (ONT_RX) consists of PIN photodiode (sensitivity is -19 dBm for BER of 10^{-12}), electrical Bessel low-pass filter (3-dB bandwidth is 7.5 GHz), and electrical scope to evaluate the quality of received signal (e.g., show bit pattern).

3. RESULTS AND DISCUSSION

The purpose of this section was to numerically evaluate the performance of PAM-4 modulated WDM-PON system together with dispersion compensation and find the maximum network reach of this system. As mentioned before, the BER threshold for our investigated transmission system is 10^{-3} (it is assumed that additional FEC is used).

The first investigated channel spacing was 100 GHz. As one can see in Figs. 2(a) and 3(a), in B2B configuration the signal quality is very good, eye is open and error-free transmission with 100 GHz channel spacing can be provided. After 59 km transmission (see Figs. 2(b) and 3(b)), which was the maximum transmission distance without dispersion compensation, the BER of received signal was 7.5×10^{-4} . The BER of received PAM-4 signal was estimated offline through our built digital signal processing (DSP) algorithm in Matlab software. For extension of transmission distance by dispersion compensation we implemented FBG DCM module. By using this dispersion

compensation technique, the maximum achievable transmission distance was 74 km, where BER of received signal was 9×10^{-4} , please see Figs. 2(c) and 3(c). As one can see in Figs. 2 and 3, by using additional dispersion compensation with FBG, extra 15 km or 25.4% of link length was gained.

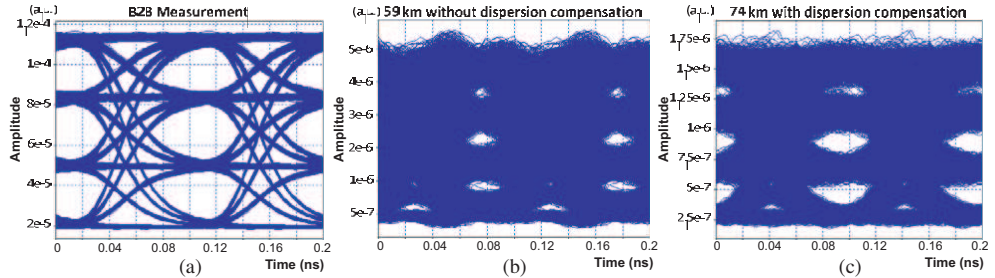


Figure 2: Eye diagrams of received signal (a) after B2B transmission, (b) after 59 km transmission without use of DCM module and (c) after 74 km transmission with dispersion compensation by FBG DCM unit for 4-channel 100 GHz spaced WDM-PON system with PAM-4 modulation format.

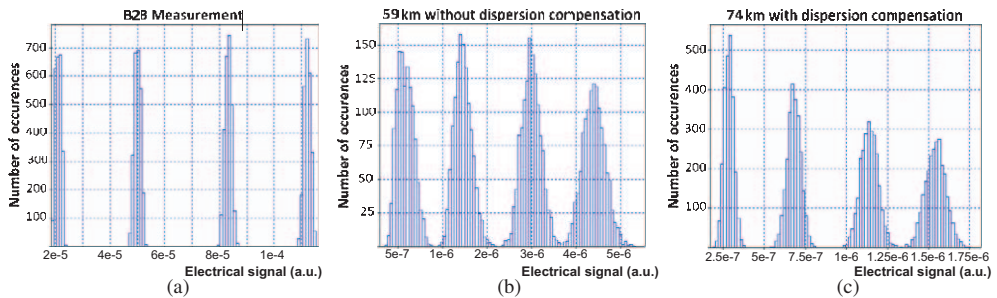


Figure 3: Histograms of received signal (a) after B2B transmission, (b) after 59 km transmission without use of DCM module, and (c) after 74 km transmission with dispersion compensation by FBG DCM unit for 4-channel 100 GHz spaced WDM-PON system with PAM-4 modulation format.

The second investigated channel spacing was 50 GHz. In our research we tried also narrower channel spacing like 37.5 GHz, but already in B2B configuration (without optical transmission line) BER of received signal was above our defined BER pre-FEC threshold (BER value was 2×10^{-3}) and error-free transmission with this channel spacing was not possible. Therefore we conclude that for PAM-4 modulated WDM-PON system, the minimal channel spacing for 10 Gbaud/s symbol rate is 50 GHz.

As one can see in Figs. 4(a) and 5(a), in B2B configuration the signal quality for 50 GHz channel spacing is also very good, eye is open and error-free transmission can be provided. After 58 km transmission (see Figs. 4(b) and 5(b)), which was the maximum transmission distance without dispersion compensation, the BER of received signal was 8×10^{-4} . The drop in BER performance can be explained by the crosstalk between channels, therefore in our research we show the eye diagrams and histograms of received signal for the middle channel (third channel), which showed the worst BER performance.

For extension of transmission distance by use of dispersion compensation, we implemented the same tunable FBG DCM module. By using this dispersion compensation technique, the maximum achievable transmission distance was 72 km, where BER of received signal was 5.5×10^{-4} , please see Figs. 4(c) and 5(c).

As one can see in Figs. 4 and 5, by using additional dispersion compensation, there were gained extra 14 km or 24% of link length by using FBG for CD compensation.

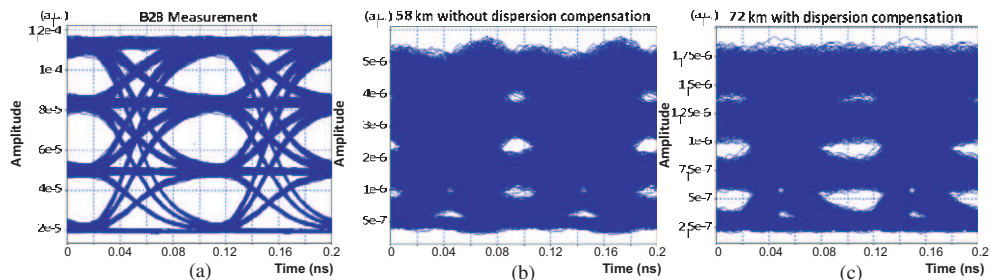


Figure 4: Eye diagrams of received signal (a) after B2B transmission, (b) after 58 km transmission without use of DCM module and (c) after 72 km transmission with dispersion compensation by FBG DCM unit for 4-channel 50 GHz spaced WDM-PON system with PAM-4 modulation format.

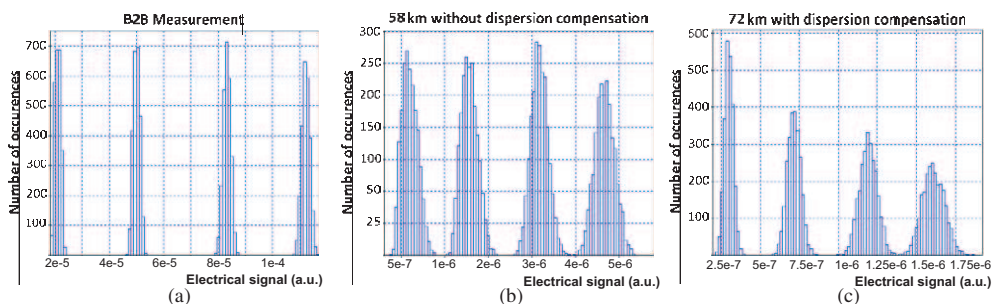


Figure 5: Histogram of received signal (a) after B2B transmission, (b) after 58 km transmission without use of DCM module, and (c) after 72 km transmission with dispersion compensation by FBG DCM unit for 4-channel 100 GHz spaced WDM-PON system with PAM-4 modulation format.

4. CONCLUSIONS

Chromatic dispersion (CD) limits transmission capacity when bit rates increase. Implementation of the efficient compensation solution may sufficiently extend the reach of optical link and improve the transmission quality. In this work we have realized and investigated the performance of 4-channel 50 GHz and 100 GHz spaced PAM-4 modulated WDM-PON system. Proposed system is realized in OptSim simulation environment and is based on ITU-T G.694.1 DWDM frequency grid, has four channels and is capable to provide data transmission over at least 72 km fiber span with transmission speed of 10 Gbaud/s (20 Gbit/s) per channel.

It was shown, that maximal transmission distance with BER below FEC limit of 10^{-3} for 100 GHz spaced PAM-4 WDM-PON system can be increased by 15 km or 25.4% (from 59 to 74 km) if dispersion compensation with fiber Bragg grating (FBG) dispersion compensation module (DCM) is implemented. And in case of 50 GHz channel spacing, which was the minimal channel spacing ensuring $\text{BER} < 10^{-3}$, maximum transmission system reach can be increased by 14 km or 24% (from 58 to 72 km) by using additional dispersion compensation with FBG DCM.

REFERENCES

1. Wei, J. L., K. Grobe, and H. Griesser, "High speed next generation passive optical networks: Performance, cost, and power dissipation," *Progress In Electromagnetic Research Symposium*, 4856–4857, Shanghai, China, August 8–11, 2016.
2. Reed, G. T., G. Mashanovich, F. Y. Gardes, and D. J. Thomson, "Silicon optical modulators," *Nature Photonics*, Vol. 4, No. 8, 518–526, 2010.
3. Nazemi, A., H. Kangmin, B. Catli, C. Delong, U. Singh, T. He, H. Zhi, Z. Bo, A. Momtaz, and C. Jun, "A 36 Gb/s PAM4 transmitter using an 8b 18 GS/s DAC in 28 nm CMOS," *ISSCC 2005 IEEE International Digest of Technical Papers Solid-State Circuits Conference*, 1–3, 2015.

4. Amirkhany, A., A. Abbasfar, J. Savoj, M. Jeeradit, B. Garlepp, R. T. Kollipara, V. Stojanovic, and M. Horowitz, “A 24 Gb/s software programmable analog multi-tone transmitter,” *IEEE Journal of Solid-State Circuits*, Vol. 43, No. 4, 999–1009, April 2008.
5. Xiong, C., D. M. Gill, J. E. Proesel, J. S. Orcutt, W. Haensch, and W. M. J. Green, “Monolithic 56 Gb/s silicon photonic pulse-amplitude modulation transmitter,” *Optica*, Vol. 3, 1060–1065, 2016.
6. Brunina, D., S. Porto, A. Jain, C. P. Lai, C. Antony, N. Pavarelli, M. Rensing, G. Talli, P. Ossieur, P. O’Brien, and P. D. Townsend, “Analysis of forward error correction in the upstream channel of 10 Gb/s optically amplified TDM-PONs,” *2015 Optical Fiber Communications Conference and Exhibition (OFC)*, 1–3, Los Angeles, CA, 2015.
7. ITU-T Recommendation G.984.2, *Gigabit-capable Passive Optical Networks (GPON): Physical Media Dependent (PMD) Layer Specification*, 25–29, 2011.

PAPER-2: Evaluation of 4-PAM, NRZ and Duobinary Modulation Formats Performance for Use in 20 Gbit/s DWDM-PON Optical Access Systems

T. Salgals, L. Skladova, K. Vilcane, J. Braunfelds and **S. Spolitis**, "Evaluation of 4-PAM, NRZ and Duobinary Modulation Formats Performance for Use in 20 Gbit/s DWDM-PON Optical Access Systems," *2018 Advances in Wireless and Optical Communications (RTUWO)*, pp. 134-138, Riga, Latvia, Nov. 15-16, (2018), DOI: [10.1109/RTUWO.2018.8587887](https://doi.org/10.1109/RTUWO.2018.8587887)

Evaluation of 4-PAM, NRZ and Duobinary Modulation Formats Performance for Use in 20 Gbit/s DWDM-PON Optical Access Systems

Toms Salgals, Laura Skladova, Klinta Vilcane, Janis Braunfelds and Sandis Spolitis

Institute of Telecommunications, Riga Technical University

Azenes street 12, Riga, Latvia

e-mail: {toms.salgals, laura.skladova, klinta.vilcane, janis.braunfelds, sandis.spolitis}@rtu.lv

Abstract— In this paper we compared performance of different modulation formats in 8-channel dense wavelength division multiplexed passive optical network (DWDM-PON). Higher spectral efficiency four-level pulse amplitude modulation (PAM-4) format operating at 10 Gbaud/s (20 Gbit/s) transmission speed per channel is compared to same bitrate non-return-to-zero (NRZ) and duobinary (DB) modulation formats in order analyze their performance in terms of maximal transmission distance and minimal channel spacing with pre-FEC BER $\leq 10^{-3}$. Through mathematical modelling it was found that the maximal achievable modulation distance of DB and spectrally efficient PAM-4 modulation formats in DWDM-PON system are 62 km and 50 km, respectively. It is numerically shown that DB modulation format has 19% better transmission reach than PAM-4 for 20 Gbit/s transmission systems.

Keywords— optical access, dense wavelength division multiplexed passive optical networks, PAM-4, duobinary, NRZ, NG-PON2

I. INTRODUCTION

Several coding methods have been proposed in the past and have become standards in telecommunication networks. Evolution from voice and text-based services to video streaming-based services meant, that demands of internet traffic of internet users have increased significantly. In result, broadband applications such as TV transmission, online gaming, live videos streaming, IPTV (Internet Protocol television), VOD (video on demand) and others require much higher bandwidth then ever [1].

Wavelength division multiplexed passive optical network (WDM-PON) can be the next generation solution for nowadays problems, which are related with transmission capacity [2]. As we know, passive optical networks (PONs) have been standardized to next-generation PON (NG-PON2, ITU-T G.989.2) standards and are now being deployed. At the moment, network operators are widely deploying time-division multiplexing (TDM) – based PONs in high-density urban areas, but wavelength division multiplexed (WDM) PONs are still in the stage of research and standardization [3]. For example, in Latvia, TDM based Gigabit-capable Passive Optical Networks (GPON) with bitrates up to 10 Gbit/s are widely deployed.

However, today's deployed wavelength-division multiplexed passive optical networks (WDM-PON) rely on fixed wavelength transmitters and are expected to become more cost-efficient at high per user data rates [4,5].

Important advantage of this technology is to set various channel spacing and use different modulation formats (increase spectral efficiency), at the same time and providing different transmission speeds for end user, based on pay-as-you-grow approach [6]. Therefore, DWDM-PON can be used in multiple channel optical fiber transmission systems to serve as many customers as possible at the same time increasing channel number and data-rate per channel [7,8].

Several modulation formats are investigated in this paper for use in PON transmission system – non-return to zero (NRZ), 4-level pulse-amplitude modulation (PAM-4) and Duobinary (DB). Mostly, in optical access networks typically direct detection on-off keying modulation (OOK) format with NRZ line code is used [9]. Alternative solution to increase serial line rate, instead of using widely used NRZ code with physical bandwidth limitations, is to use spectrally efficient multi-level signaling formats such as M-PAM, in our case PAM-4, where number 4 means different signal amplitude levels [10].

Another way to improve capacity of limited bandwidth is using Duobinary modulation format. With this modulation format transmission capacity will be increased by improving the bandwidth efficiency and reducing channel spacing [11]. As we know, Duobinary is type of proficient multi-level modulation format, and therefore is the area of interest due to its increased spectral efficiency. It is being used to increase the channel capacity by improving the bandwidth utilization. The most important feature of this modulation format is usage for longer transmission distances without regeneration and high tolerance to chromatic dispersion influence [12].

II. NUMERICAL ANALYSIS AND MEASUREMENT TECHNIQUE

Our research uses mathematical simulation method performed using OptSim simulation software. It is well known, that there exist two main effects, which affect optical signal: linear and non-linear. For non-linear effect studies the nonlinear Schrödinger equation is used, except in certain cases this equation can't be solved analytically. To solve this problem OptSim simulation software is used to simulate optical transmission systems. OptSim simulation software uses Time Domain Split-Step (TDSS) method to solve complex set of differential equations. That's why Split-Step method is used in most optical system simulation tools to perform the integration part of the fiber propagation equation [13].

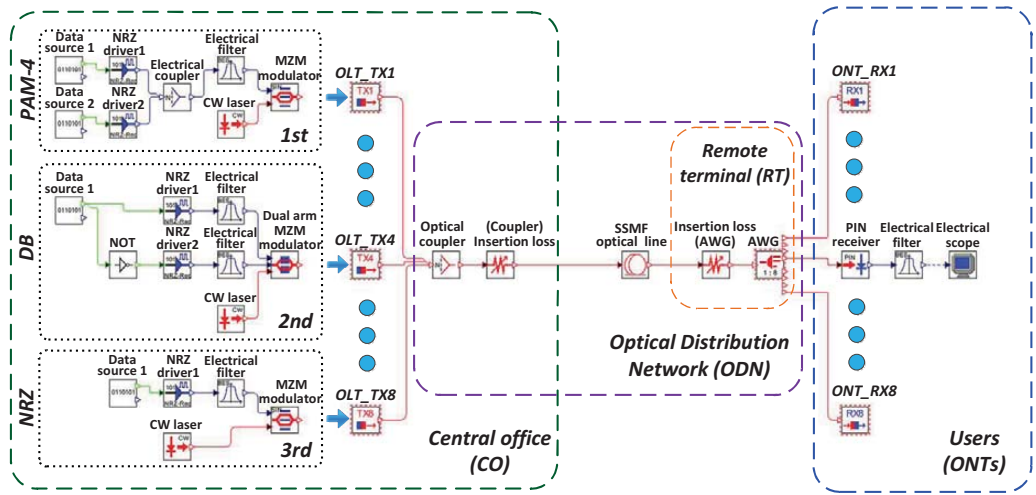


Fig. 1. Simulation scheme of 8-channel PAM-4, DB and NRZ modulated DWDM-PON optical transmission system with 20 Gbit/s transmission speed per channel.

Where $A(t,z)$ - optical field amplitude; L - linear operator responsible for dispersion and other linear effects; N - non-linear operator that accounts for the Kerr effect and other nonlinear effects (NOEs) [13].

Optical fiber length z is divided in Δz steps. Each step Δz consists of two half steps. First half step takes into account only linear effects, but second half step takes into account only non-linear effects. For best results it is importance to choose correct Δz value. If the value is too small, the time necessary to perform calculations will increase significantly, but if value is too large it will affect accuracy of the results. To achieve sufficient enough estimation accuracy, we have chosen the simulation of more than 1024 bits [13,14].

III. SIMULATION MODEL OF PAM-4, DB AND NRZ MODULATED WDM-PON TRANSMISSION SYSTEM.

Displayed results in this publication are obtained by newest OptSim simulation software with additional use of recognized numerical computing environment – Matlab software for BER estimation of received PAM-4 signals. In our case we chose at least 1024 simulated bits for all simulations to obtain high accuracy level of bit error rate (BER). In our research we used forward-error-correction (FEC) with 10^{-3} BER performance threshold, which allows us to evaluate maximal transmission reach of investigated transmission system (e.g. Reed Solomon (255, 239) code) [15].

To achieve the goal – evaluation of maximum transmission reach using different modulation formats: PAM-4, duobinary and NRZ, the 8-channel DWDM-PON simulation model was created. As one can see in Fig. 1, simulation scheme with different optical transmitters for realization of each modulation format are shown. According to ITU-T G.694.1 DWDM frequency with grid central frequency of 193.1 THz and channel spacing of 50 and 100 GHz is chosen for simulation model. Therefore, impact of crosstalk on investigated modulation formats was evaluated as well.

Optical line terminal (OLT) consists of eight transmitters (OLT_Tx) located in central office (CO). First simulation model with PAM-4 modulation was performed with 10 Gbaud/s symbol rate which provides 20 Gbit/s data rate per channel. PAM-4 signal is generated from two electrical data signals by coupling them, where one of them has twice larger amplitude than other. To obtain electrical data signals, two data sources with same pseudo-random bit sequence (PRBS) and NRZ drivers for each electrical signal are used to generate two NRZ coded electrical signals with different amplitude levels. Afterwards, both electrical signals are coupled with electrical coupler and filtered with electrical Bessel low-pass filter (3-dB bandwidth is 10 GHz) and send to external Mach-Zehnder modulator (MZM) [16].

Second simulation model with DB modulated transmission system was realized with 20 Gbit/s data rate per channel. In our simulation model data source element has one electrical output, where the output signal is divided in two electrical signals, where one of them is inverted by logical NOT element. Afterwards output data signal and inverted copy is sent to NRZ drivers, filtered by Bessel low-pass filters (3-dB bandwidth is 5 GHz), and passed to RF inputs of dual-arm Mach-Zehnder modulator, together forming the DB transmitter [17].

Our third simulation model is based on NRZ transmitter and realized with the same 20 Gbit/s data rate per channel as DB modulated transmission system. Transmitter consists of one NRZ driver with electrical signal input of PRBS sequence and form NRZ coded output electrical signal. MZM provides electrical to optical signal conversation of previously formed and Bessel low-pass filter (3-dB bandwidth is 19 GHz) filtered electrical signal, passing from NRZ driver.

The following fixed parameters of optical and electrical elements was used in our simulation models: continuous wavelength (CW) laser output power 6 dBm, extinction ratio 20 dB and 3 dB insertion loss of MZM, standard single mode fiber (SSMF) with dispersion coefficient 17 ps/(nm × km), dispersion slope 0.056 ps/nm² × km and 0.2 dB/km

attenuation coefficient [18]. Bandwidth of electrical filters has been adjusted for optimal performance of each modulation format and have not been changed during research. As one can see in Fig.1, our investigated model of transmission system consists of eight channels coupled together by using optical coupler with 1 dB insertion loss. ITU-T G.652 single mode fiber is used for transmission in optical distribution network (ODN). After transmission in ODN, all channels are separated by demultiplexer based on arrayed waveguide grating (AWG) located in remote terminal (RT), with equal insertion loss of 3.5 dB for all channels as mentioned before, simulations with various channel spacing of 50 or 100 GHz are obtained and analyzed for research of crosstalk impact. Each receiver of optical network terminal (ONT) consists of 40 GHz PIN photodiode with sensitivity equal -19 dBm at 10 Gbit/s reference bitrate, dark current of 10 nA and responsivity of 0.8 A/W [19]. The optimal electrical bandwidth of electrical low pass filter (LPF) was found. An electrical Bessel low-pass filter bandwidth was adopted for more successful system performance depending on the modulation format used. During the simulations Bessel LPF bandwidth of 15 GHz was chosen for PAM-4 modulated signals, and 10 and 17 GHz for DB and NRZ modulated electrical signals, respectively.

An electrical scope was used for measurements of received signal bit patterns quality, accordingly, BER and eye diagrams.

IV. RESULTS AND DISCUSSION

The main target of this work is to compare performance of PAM-4, DB, NRZ modulated optical signals for use in DWDM-PON transmission system and to find out maximal network reach for each particular modulation format.

The BER threshold of 10^{-3} with assumed additional FEC for our investigated transmission system was used to evaluate maximal achieved distance by each modulation format. BER of received PAM-4 signal was estimated offline through our built digital signal processing (DSP) algorithm in Matlab software, while BER of received DB

and NRZ signals was estimated in environment of OptSim simulation software by using BER estimator based on statistical signal analysis.

In our research we implemented different suitable dense channel spacing like 50 and 100 GHz for 8-channel DWDM-PON optical transmission system. During the simulations it was observed that maximal achievable distance has minimal impact depending of our chosen channel spacing, e.g. the impact of crosstalk on BER for all modulation formats was minor. As one can see in Fig. 2, results of maximal reached transmission distance with 50 or 100 GHz channel spacing are almost the same for each particular modulation. Therefore, we conclude that better signal quality and system performance are achieved with higher-100 GHz spacing. However, the higher spectral efficiency is achieved by 50 GHz spacing, therefore to evaluate performance of different modulation formats our results are shown for narrowest (50 GHz) channel spacing. Main results of our investigated transmission system performance are shown in Fig. 3. In our research we show eye diagrams of received signal for middle channel with highest crosstalk impact and worst BER performance.

As one can see in Figs 3(a), 3(b) and 3(c) the signal quality of B2B measurements are good for all modulated signals providing error free transmission with 50 GHz spacing. After transmission (see Fig. 3(e)) the BER of received DB modulated signal was 3.7×10^{-4} with maximum reached distance of 62 km.

PAM-4 and NRZ modulation shows (see Figs. 3(d) and 3(f)) 50 km and 27 km maximal transmission distance, where the BER of received signals was 5.8×10^{-4} and 3.1×10^{-4} , respectively.

As one can see from results (Fig. 3), the largest network reach was provided by DB modulation format, which extends the reach of optical network up to 62 km, in the same time ensuring $BER < 10^{-3}$. PAM-4 modulation format provided successful transmission over up to 50 km and NRZ up to 27 km long SSMF optical spans with BER below defined threshold.

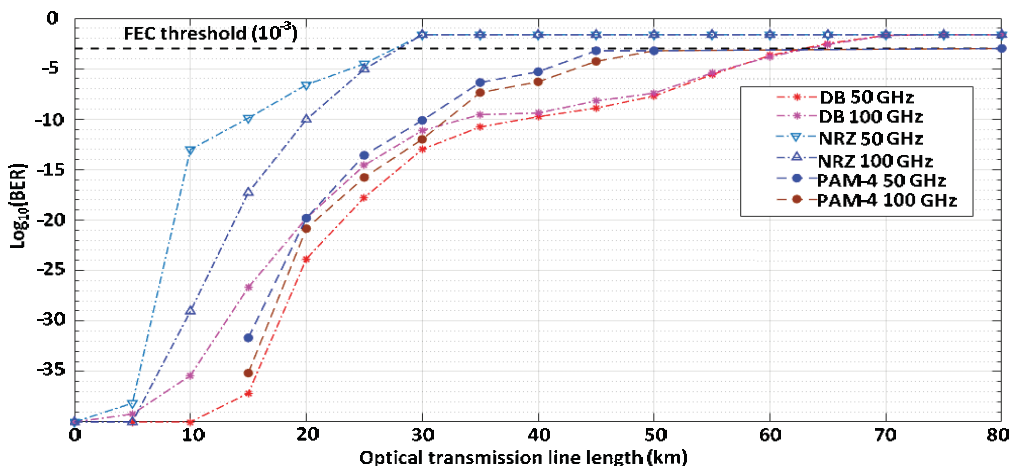


Fig. 2 Dependence of BER on the distance for the investigated PAM-4, DB and NRZ modulated WDM-PON optical transmission system.

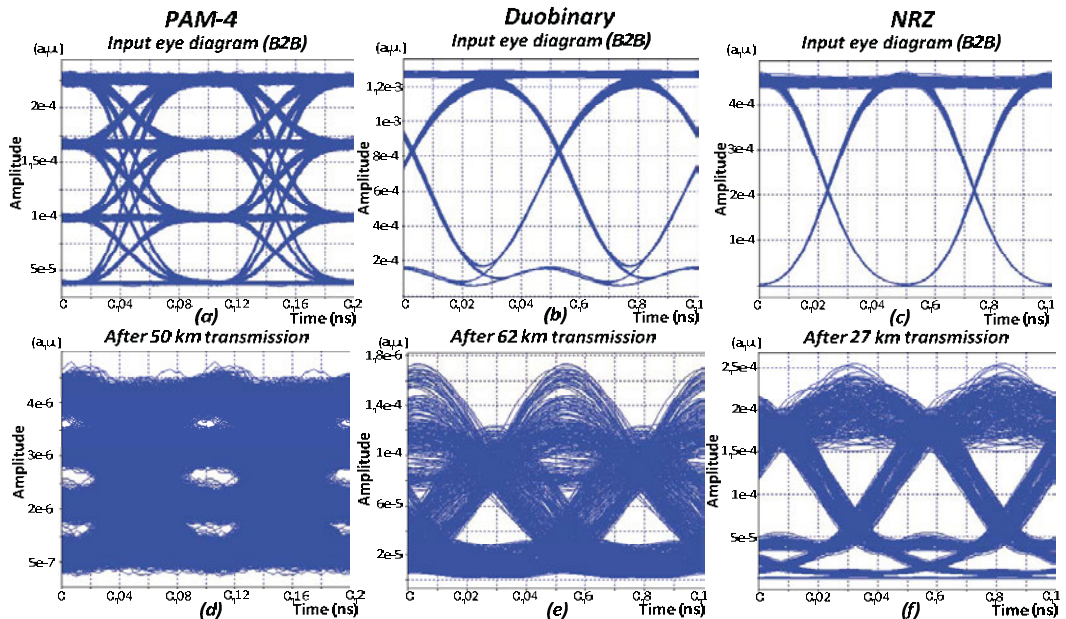


Fig. 3. Eye diagrams of received (a) PAM4, (b) Duobinary and (c) NRZ signals after B2B measurement, and after maximal achieved transmission distance: (d) 50 km with PAM-4 modulated signal, (e) 62 km with DB modulated signal, (f) 27 km with NRZ modulated signal for 8-channel 50 GHz spaced DWDM-PON system operating at 20 Gbit/s bitrate.

V. CONCLUSIONS

We have demonstrated performance comparison of PAM-4, DB and NRZ modulation formats for 8-channel DWDM-PON transmission system with 20 Gbit/s bitrate per channel. The model of our proposed system was realized in OptSim simulation software environment based on ITU-T G.694.1 rec. frequency grid and realized with 50 and 100 GHz channel spacing. The results are mainly shown for 50 GHz channel spacing as it provides higher spectral efficiency if compared to 100 GHz channel spacing. As it shown by simulation results with narrowest 50 GHz channel spacing the use of DB modulation format extends the reach of optical link allowing to achieve maximal transmission distance of 62 km ensuring $BER < 10^{-3}$ threshold.

Second best result was demonstrated by PAM-4 modulation format ensuring the $BER < 10^{-3}$ at 50 km optical line length. The use of DB format allowed extending the maximum reach of an optical link by extra 12 km or 19% in comparison to four-level pulse amplitude modulation format. The worst system performance was shown by NRZ modulation format demonstrating 27 km maximal reached transmission distance. This can be explained by mainly the impact of chromatic dispersion.

Our investigated DB and PAM-4 modulation formats showed best performance in achieving of maximal distance of optical transmission system, although, comparatively spectral efficient PAM-4 modulation can provide higher data transmission speeds in fiber optical networks with limited bandwidth.

VI. ACKNOWLEDGMENT

Development Fund within the Activity 1.1.1.2 “Post-doctoral Research Aid” of the Specific Aid Objective 1.1.1 “To increase the research and innovative capacity of scientific institutions of Latvia and the ability to attract external financing, investing in human resources and infrastructure” of the Operational Programme “Growth and Employment” (No. 1.1.1.2/VIAA/ 1/16/044).

REFERENCES

- [1] Q. H. Tran ; S. H. Yoo ; S. R. Moon and C.H. Lee, “A 2.5-Gb/s per channel DWDM-PON with a pulsed-ASE seed light source”, IEEE Photonics Conference (IPC), pp. 2, November 2015.
- [2] Jun-ichi Kani, F. Bourgart, A. Cui, A. Rafel, M. Campbell, R. Davey and S. Rodrigues, “Next-generation PON-part I: Technology roadmap and general requirements”, IEEE Communications Magazine, vol. 47, Issue: 11, pp. 43-49, November 2009.
- [3] R. Sanchez, J. A. Hernandez and D. Larrabeiti, “Troubleshooting PON networks effectively with carrier-grade ethernet and WDM-PON”, IEEE Communications Magazine, vol. 52, Issue: 2, February 2014.
- [4] C. Wagner, M. Eiselt, S. Zou, M. Lawin, B. Teipen, K. Grobe, J.J. Vegas Olmos and I. Tafur Monroy, “Wavelength-agnostic WDM-PON system”, IEEE International Conference on Transparent Optical Networks (ICTON), pp 1-4, August 2016.
- [5] J. Czékus, P. Megyesi, A. Mitscenkov and D. Mazroa, “Hardware cost and capacity analysis of future TDM- and WDM-PON access networks”, IEEE International Conference on Transparent Optical Networks (ICTON), pp. 1-4, August 2014.
- [6] A. Eira, J. Santos, J. Pedro and J. Pires, “Multi-objective design of survivable flexible-grid DWDM networks”, IEEE/OSA Journal of Optical Communications and Networking, vol. 6, Issue: 3, pp. 326 – 339, March 2014.
- [7] V. Kachhatiya and S. Prince, “Wavelength division multiplexing-dense wavelength division multiplexed passive optical network (WDM-DWDM-PON) for long reach terrain connectivity”, IEEE

- International Conference on Communication and Signal Processing (ICCSP), pp. 0104 – 0108, April 2016.
- [8] M.C. Cheng, C.T. Tsai, Y. Chi and G.R. Lin, "Direct QAM-OFDM Encoding of an L-band Master-to-Slave Injection-Locked WRC-FPLD Pair for 28×20 Gb/s DWDM-PON Transmission", *IEEE Journal of Lightwave Technology*, vol. 32, Issue: 17, pp. 2981 – 2988, July 2014.
- [9] M. Forzati, A. Berntson, J. Martensson, E. Pincemin and Paulette Gavignet, "NRZ-OOK transmission of 16×40 Gb/s over 2800 km SSMF using asynchronous phase modulation", *IEEE Conference on Lasers and Electro-Optics and 2008 Conference on Quantum Electronics and Laser Science*, pp. 1-2, July 2008.
- [10] Y. Wang, W. Gai and L. Tang, "A novel 40-Gb/S PAM4 transmitter with power-efficient pre-emphasis", *IEEE International Conference on Solid-State and Integrated Circuit Technology (ICSICT)*, pp. 1-3, October 2014.
- [11] R. Kaur and S. Dewra, "Duobinary Modulation Format for Optical System- A Review" *International Journal of Advanced Research in Electrical, Electronics and Instrumentation Engineering*, vol. 3, Issue 8, August 2014.
- [12] F. Qamar, M. K. Islam, S. Z. A. Shah, R. Farhan and M. Ali, "Secure Duobinary Signal Transmission in Optical Communication Networks for High Performance & Reliability", *IEEE Access*, vol. 5, pp. 17795 – 17802, September 2017.
- [13] Aleksejeva, M., Spolitis, S. Research on Dispersion Compensation Methods for WDM-PON Transmission Systems. In: *Proceedings of Advances in Wireless and Optical Communications (RTUWO 2016): Latvia, Riga, 3-4 November, 2016*. Riga: IEEE, 2016, pp.1-4.
- [14] S. Spolitis, V. Bobrovs, G. Ivanovs. Reach improvement of spectrum-sliced dense WDM-PON system., In *proceedings of 7th International Conference on Broadband, Wireless Computing, Communication and Applications, BWCCA 2012*, pp. 296-301.
- [15] T. Salgals, S. Spolitis, S. Olonkins and V. Bobrovs "Investigation of 4-PAM Modulation Format for Use in WDM-PON Optical Access Systems" *Progress in Electromagnetics Research Symposium (PIERS 2017)*, St. Petersburg, Russia, pp. 1-4.
- [16] Brunina D., S. Porto, A. Jain, C.P. Lai, C. Antony, N. Pavarelli, M. Rensing, G. Talli, P. Ossieur, P. O'Brien, and P.D. Townsend, "Analysis of forward error correction in the upstream channel of 10Gb/s optically amplified TDM-PONs," *2015 Optical Fiber Communications Conference and Exhibition (OFC)*, Los Angeles, CA, 2015, pp. 1-3.
- [17] I. Kurbatska, S. Spolitis, V. Bobrovs, A. Alševska and G. Ivanovs, Performance Comparison of Modulation Formats for 10 Gbit/s WDM-PON Systems. In: *2016 Advances in Wireless and Optical Communications (RTUWO 2016): Proceedings, Latvia, Riga, 3-4 November 2016*. Piscataway: IEEE, 2016, pp.51-54
- [18] ID Photonics GmbH., "CoBrite MX1 – Laser," *Technical Specification*, 2017, pp. 1-4.
- [19] Optilab "40 GHz Linear InGaAs PIN Photodetector," *Technical Specification*, 2016, pp 1-4.

PAPER-3: Optical Power Budget of 25+ Gbps IM/DD PON with Digital Signal Post-Equalization

A. Udalcovs, **T. Salgals**, L. Zhang, X. Pang, A. Djupsjöbacka, **S. Spolitis**, V. Bobrovs, S. Popov, and **O. Ozolins**, "Optical Power Budget of 25+ Gbps IM/DD PON with Digital Signal Post-Equalization," *Applied Sciences* 10(17), 6106, (2020), DOI: <https://doi.org/10.3390/app10176106>

Article

Optical Power Budget of 25+ Gbps IM/DD PON with Digital Signal Post-Equalization

Aleksejs Udalcovs ^{1,*}, Toms Salgals ^{2,3}, Lu Zhang ^{4,5}, Xiaodan Pang ⁶,
Anders Djupsjöbacka ¹, Sandis Spolitis ^{2,3}, Vjaceslavs Bobrovs ², Sergei Popov ⁶ and
Oskars Ozolins ^{1,6}

¹ Networks Unit, RISE Research Institutes of Sweden, 164 40 Kista, Sweden;
Anders.Djupsjobacka@ri.se (A.D.); Oskars.Ozolins@ri.se (O.O.)

² Institute of Telecommunications, Riga Technical University, 1048 Riga, Latvia; Toms.Salgals@rtu.lv (T.S.);
Sandis.Spolitis@rtu.lv (S.S.); Vjaceslavs.Bobrovs@rtu.lv (V.B.)

³ Communication Technologies Research Center, Riga Technical University, 1048 Riga, Latvia

⁴ College of Information Science and Electrical Engineering, Zhejiang University, Hangzhou 310027, China;
zhanglu1993@zju.edu.cn

⁵ Zhejiang Lab, Hangzhou 311121, China

⁶ School of Engineering Sciences, KTH Royal Institute of Technology, 100 44 Stockholm, Sweden;
xiaodan@kth.se (X.P.); sergeip@kth.se (S.P.)

* Correspondence: Aleksejs.Udalcovs@ri.se; Tel.: +46-10-228-40-85

Received: 31 July 2020; Accepted: 31 August 2020; Published: 2 September 2020



Abstract: While infrastructure providers are expanding their portfolio to offer sustainable solutions for beyond 10 Gbps in the access segment of optical networks, we experimentally compare several modulation format alternatives for future passive optical networks (PONs) aiming to deliver 25+ Gbps net-rates. As promising candidates, we consider the intensity modulation direct detection (IM/DD) schemes such as electrical duobinary (EDB) and 4-level and 8-level pulse amplitude modulations (PAM-4/8). They are more spectrally efficient than the conventional non-return-to-zero on-off-keying (NRZ-OOK) used in current 10G PONs. As we move to higher rates, digital equalization enhances the performance by smoothening the systems imperfection. However, the impact that such equalization has on the optical power budget remains unclear. Therefore, in this article, we fairly compare the optical power budget values of a time division multiplexed PON (TDM-PON) exploiting a linear digital signal equalization at the receiver side. We consider the conventional PON configuration (20 km of single-mode fiber (SMF), 1:N optical power splitting) with IM/DD and net-rates above 25 Gbps. Furthermore, we focus on a downstream transmission imposing the bandwidth limitations of 10G components using a digital filter before the detection. The obtained results show that the use of a digital post-equalization with 43 feed-forward (FF) and 21 feedback (FB) taps can significantly improve the signal quality enabling new alternatives and enhancing the optical power budget.

Keywords: digital post-equalization; electrical duobinary (EDB); intensity modulation direct detection (IM/DD); non-return-to-zero (NRZ); optical power budget; passive optical networks (PON); pulse amplitude modulation (PAM)

1. Introduction

An immense range of mobile and broadband services, such as Netflix, Spotify, etc., provoke an unprecedented growth of consumer-driven data consumption, which leads to an increase of bandwidth demands in fiber-optic access networks [1]. In this segment, passive optical networks (PON) together with a wavelength division multiplexing (WDM) and a time division multiplexing (TDM) technologies promote a pay-as-you-grow approach in the third generation fiber-to-the-x (FTTH)

systems. As 10G PON systems are not capable support future services, especially in the context of the fifth generation (5G) mobile networks, 25G is the next evolution step that must be taken [2]. However, it is not clear which means will be used to make it.

Recent ITU-T recommendations for passive optical networks (PONs), ITU-T G.9807.1 (symmetric 10G PON (XG(S)-PON)) and ITU-T G.989 (next-generation PON2 (NG-PON2)) describe transmission requirements for line rates of up to 40 Gbps per channel, while new recommendations for higher line rates (e.g., G.HSP.Req, G.HSP.comTC, G.HSP.50Gpmd, G.HSP.TWDMpmd) are under active development [3–5]. The enhancements being discussed for the next-generation PON standards include the increase in channel line rates from 10 to 25 Gbps [6]. Now, 100G-EPON standard is still under development by the IEEE P802.3ca Task Force. It is intended to scale up to 25 Gbps or 50 Gbps per single lane capacity while reusing the existing infrastructure of 10G-EPON [1,5,7]. Overall, the future PON is currently under development and standardization for future broadband network solutions beyond 10 Gbps [8–10]. The evolution towards higher line rates is mainly driven by point-to-point (P2P) connections and wireless fronthaul, e.g., the next generation of mobile cellular networks (i.e., 5G and beyond 5G), where a 25 Gbps could be needed soon for either backhauling or new interfaces supporting the functional splits. It is expected that the x-haul of these mobile cellular networks will be centralized and based on a point-to-point (PtP) WDM-PON architecture [3,11,12]. However, due to cost considerations and commercial viability, it is desired to re-use some of the components from 10 Gbps transceivers operating in 10G PONs [13]. Bandwidth limitations from electrical and electro-optical components increase significantly due to the utilization of signals with higher line rates. Nevertheless, such elements/components are crucial for component vendors as their re-use reduce development costs. For example, a cost of an optical line terminal (OLT) transmitter is about twice the cost of the receiver and modulator of the optical network unit (ONU), which represents the major part of the transceiver cost. Therefore, the operational capabilities of the bandwidth-limited transceivers have received considerable attention from component vendors, optical network operators, and research communities [9,14–16]. The choice of a modulation format plays a critical role in the performance of HS-PON systems to provide the necessary line rate for the end-users [17]. It seems unreasonable that coherent technology for such relatively low rates could penetrate this market segment at this time, despite the potential sensitivity and optical power budget (OPB) improvements. Therefore, we assume that IM/DD formats will be used to deliver 25G or even 50G over a 20 km long single-mode fiber, i.e., the conventional PON configuration. For some applications, shorter fibers are also considered (e.g., 10–15 km when PON-based fronthauling solutions for 5G are on the table) but some require a substantially longer reach (up to 40 km) [6,12].

Interestingly, when it comes to the physical (PHY) layer technology and its maturity, three abbreviations (except “NRZ”) are met the most often: “Duobinary”, “PAM—pulse amplitude modulation”, and “OFDM—orthogonal frequency division multiplexing”. The desire for multi-level signaling formats such as Duobinary and PAM have been preferred to their advantages in terms of simpler transmitter and receiver structure for HS-PONs. Therefore, they have become a key solution to provide a higher line rate and improve the bandwidth utilization, capacity, and spectral effectiveness [2,13,17–19]. However, they are also more sensitive to driver linearity and have higher sensitivity requirements, which impose additional restrictions and may limit the system’s reach. Coexistence with 10G PON technologies and reuse the deployed optical distribution network (ODN) are among the main challenges for upgrading to new generation PON systems. Technically, it requires that the optical budget (OPB), which determines the maximum tolerable optical loss between an optical line terminal (OLT) and an optical network unit (ONU), must be compliant to E1 or E2 class. However, with increased signal baudrates, impairments from both the transceivers and the fiber-link imposed constraints to fulfill the OPB requirement. Firstly, with a larger bandwidth, the receiver sensitivity can be degraded from a higher thermal noise level. Moreover, the bandwidth limitation from the optical and electrical components and the chromatic dispersion (CD) from the optical fiber channel induce more severe inter-symbol interference (ISI) [20,21]. Mitigation techniques from both the optical and the digital

domain can be used to maintain or even to improve the OPB level to enable a higher splitting ratio for an ODN, at a higher cost per customer provided equipment (CPE) [22–25]. Firstly, optical amplifications can be performed to compensate for the sensitivity degradation, either with a praseodymium doped fiber amplifier (PDFA) as a booster in the OLT, or with a semiconductor optical amplifier (SOA) as a pre-amplifier in the ONU. The optical power budget of 35 dB is demonstrated in [10,23], where both such optical amplifiers are used for the 25 Gbps PAM-4 downstream transmission. Although they achieve a higher optical power budget, the PDFA provides more than 10 dB gain. Furthermore, the attribution of digital post-equalization is not discussed. Digital equalization techniques, such as linear feed-forward (FF) equalizer or decision feedback (FB) equalizer, can help to overcome the transceiver and link induced ISI. Thus, they deserve the place in future PONs with spectral efficient modulation formats [10,22]. Such a study is performed in [22], where the advantages of electrical duobinary (EDB) schemes and signal post-equalization are discussed for the bandwidth-limited PON. Their results of optical back-to-back sensitivity as a function of the receiver's bandwidth show that (i) the EDB outperforms the conventional NRZ irrespective to the receiver's bandwidth, (ii) the EDB transmission is more dispersion tolerant as compared to the NRZ, and (iii) the NRZ seems unfeasible for the C-band operation, and, thus, the EDB or a multilevel format should be used. Although the extensive comparison between the EDB and the NRZ alternatives is made, the optical power budget considerations remain outside the scope.

This article aims to bridge the knowledge gap by countifying the gain that digital signal post-equalization has on the optical power budget in IM/DD PONs with NRZ-OOK, EDB, PAM-4, and PAM-8 formats. In this research, we consider a PON architecture based on point-to-multipoint passive optical power splitting in the ODN and focus on the downstream transmission at net-rates above 25 Gbps over a single wavelength in the C-band. Furthermore, as we limit the receiver's bandwidth to 8 GHz, we investigate whether components intended for the 10G operation can be used for 25+ Gbps operation. This enables the full compatibility with XG(S)-PON and 10G-EPON and leads to smooth migration of customers to higher net-rates in a cost-effective way. Our results show that even without any post-equalization, the 28 Gbaud EDB and the 14 Gbaud PAM-4 formats can be used for the downstream transmission allowing us to achieve the optical power budget of 26–27 dB. With the equalization, the corresponding numbers are 27–30 dB. A strong digital post-equalization, using the equalizer with 43-FF and 21-FB taps, enables the 28 Gbaud PAM-4 alternative. It ensures a bit-error-rate (BER) below a 7% hard-decision forward error correction (HD-FEC) threshold of 3.8×10^{-3} and a 23 dB optical power budget. The rest of the paper is organized as follows. Section 2 describes a configuration of the TDM-PON experimental setup used for a fair comparison of the selected IM/DD alternatives. Section 3 discusses the obtained results revealing the impact that signal equalization has on the achievable optical power budget in such PON systems. Finally, Section 4 briefly summarizes the research findings.

2. Experimental Setup and Principles

The experimental setup of a 25+ Gbps IM/DD PON system is shown in Figure 1. It resembles a PON architecture based on point-to-multipoint passive optical power splitting in the outside distribution network. We consider a downstream transmission at net-rates above 25 Gbps over a single wavelength in the C-band. It is fully compatible with XG(S)-PON and 10G-EPON, and thus, it enables smooth migration of customers to higher net-rates without needing to change the ODN. Furthermore, the system's throughput can be increased by exploiting the WDM technique and adding new wavelengths as required. Of course, such a solution requires the wavelength management. In the OLT, the output of a continuous-wave laser source (CW) operating at 1550 nm wavelength is connected to the input of the dual-arm Mach–Zehnder modulator (MZM, Sumitomo, T.DEH1.5-40-ADC). An $S_1(t)$ input of the MZM, having a 3 dB bandwidth of 30 GHz, 9 dB insertion loss, and 15 dB extinction ratio, is driven using analog waveforms from an arbitrary waveform generator (AWG, Tektronix, AWG70001A) having 13 GHz analog bandwidth, up to 50 GSa/s sample rate and 8 bits vertical

resolution. These waveforms are obtained using a $2^{15}-1$ long pseudo-random bit sequence (PRBS15) and bit-to-symbol (B2S) mapping performed in MATLAB prior to the digital-to-analog conversion (DAC). The electrical signal after the output of the AWG was linearly amplified by an electrical broadband amplifier (EA) and fed into the electrical RF input of one arm of the dual-drive MZM. The second arm was loaded with a 50-Ohm load. To optimize the BER performance, we adjusted a bias voltage of the MZM. In such a way, we impact the MZM's chirp parameter. This adjustment ensures the best possible performance in terms of the dispersion-tolerance, which has a direct impact on signal quality.

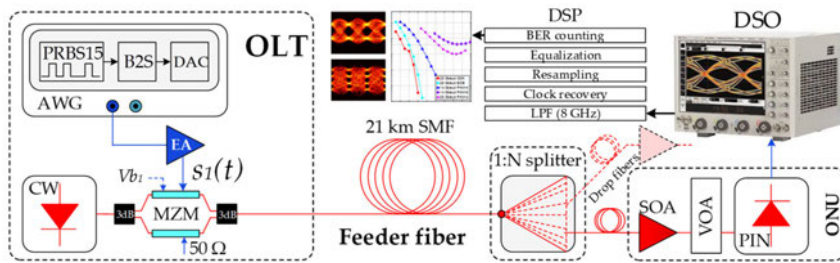


Figure 1. Experimental setup of the 25+ Gbps IM/DD PON system used for the power budget comparison: AWG—arbitrary waveform generator, B2S—bit-to-symbol mapping, CW—continuous wave laser, DAC—digital-to-analog converter, EA—electrical amplifier, MZM—Mach-Zehnder modulator, SMF—single-mode fiber, SOA—semiconductor optical amplifier, VOA—variable optical attenuator, PIN—(positive-intrinsic-negative) photodiode, DSO—digital storage oscilloscope, DSP—digital signal processing.

Note that the modulator's chirp is a key factor enabling dynamic tunability of the transmission reach in IM/DD-based optical fiber links [26]. After the MZM, the modulated optical signal is coupled into the feeder fiber and transmitted over a 21 km long standard single-mode fiber (SMF) link. The input optical power of +4 dBm ensures the ODN compliance to the E1 (18–33 dB) power budget class for several modulation format alternatives. After the downstream transmission, the optical signal is passively split by a 1-to-N (1:N) optical power splitter. In an ONU, the split optical signal is pre-amplified by a SOA (Samsung Electronics, OA40B3A, InP/InGaAsP, 1550 nm) prior to the detection. The variable optical attenuator (VOA), placed before the receiver, is used to adjust a received optical power required for the OPB assessment and to protect it from the overload. The receiver consists of a PIN photodiode (Discovery, DSC-R409, 30 GHz, 0.7 A/W) and a digital storage oscilloscope (DSO, Agilent Technologies, DSOX93304Q, 33 GHz, 80 GSa/s). The DSO is used to limit the receiver's minus 3 dB bandwidth to 8 GHz using a 4th order Bessel–Thompson filter, to digitize the received waveforms and to store the digitized for further post-processing. The applied low-pass filtering (LPF) is imposed to emulate the bandwidth limitations at the receiver's (Rx) side aiming to investigate whether components intended for the 10G operation can be used for higher line rates. The offline digital signal processing (DSP) module consists of clock recovery, resampling, linear post-equalization (if considered), and bit-error-rate (BER) estimation. The signal is post-equalized by a linear symbol-spaced equalizer that uses feed-forward and feedback taps to compensate for analog imperfections. For BER estimation, we use a direct error counting. It relies on the bit-by-bit comparison of the transmitted and received bit sequences. More than 10^5 bits are available for the BER estimation at the receiver.

3. Results and Discussion

In this section, we reveal how the signal post-equalization impacts the achievable optical power budget of the IM/DD PON system. Before moving to the optical power budget analysis, we summarize the pros and cons of transceivers exploiting the modulation formats of the interest (see Table 1). We judge aspects such as spectral efficiency of the modulation scheme, power consumption (as a line

card must supply enough electrical power), transmission reach (considering an MZM with non-zero chirp factor), and simplicity of the transmitter and receiver (considering the complexity of the driving circuits and pre-/post-processing requirements).

Table 1. Pros and cons of transceivers exploiting the considered intensity modulation direct detection (IM/DD) schemes.

Modulation Format	Spectral Efficiency	Transmission Reach	Power Consumption	Transmitter Simplicity	Receiver Simplicity
NRZ	–	–	+	++	++
EDB	+	++	–	–	–
PAM-4	++	++	--	--	--
PAM-8	+++	+	--	--	--

For the optical power budget assessment, we use the conventional BER curves showing how a pre-FEC BER values change with the received optical power. Two different a pre-FEC BER criteria are considered: (i) a 7% overhead (OH) HD-FEC threshold of 3.8×10^{-3} and (ii) a 20% OH soft-decision (SD) FEC threshold of 2×10^{-2} . If the first one is used as a benchmark for the performance and optical budget comparison, then the second one is mainly used for illustration purposes. We assume that all errors can be corrected by a FEC code for the pre-FEC BER below 3.8×10^{-3} , which leads to the background block error BBE = 0 and thus no service disruption. Additionally, we present eye diagrams so the reader could make the judgment about the signal quality in a such bandwidth-limited IM/DD PON solution.

Figure 2 shows BER curves and eye diagrams for the 28 Gbaud OOK/EDB/PAM-4 and 14 Gbaud PAM-4/8 modulated signals in the IM/DD PON systems. First, we analyze the system performance without any post-equalization (Figure 2a,c), and then, we focus on improvements that the linear post-equalization offers (Figure 2b,d). The optical power budget values (together with the corresponding values of the available power margin) obtained for all considered cases are summarized in Table 2. For the power margin calculation, we assume the insertion loss of 4.4 dB for the feeder fiber, 17.3 dB for the 1:32 optical power splitter, and 2.2 dB for the drop fiber. A negative power margin (as for the 28 Gbaud PAM-4) means that the splitting ratio of 1:32 is not supported. Note that the average insertion loss of 1:16 splitter is at least 3 dB lower, which enables the 28 Gbaud PAM-4 alternative.

Table 2. Optical power budget and available power margin for the explored alternatives and post-equalizer structures (number of FF and FB taps).

Signals	w/o	4-FF	9-FF&5-FB	43-FF&21-FB
28 Gbaud OOK	-	29 dB/5.1 dB	31 dB/7.1 dB	31 dB/7.1 dB
28 Gbaud EDB	27 dB/3.1 dB	29 dB/5.1 dB	30 dB/6.1 dB	30 dB/6.1 dB
14 Gbaud PAM-4	26 dB/2.1 dB	27 dB/3.1 dB	27 dB/3.1 dB	27 dB/3.1 dB
14 Gbaud PAM-8	-	-	-	-
28 Gbaud PAM-4	-	-	22 dB/−1.9 dB	23 dB/−0.9 dB

In the configuration without the post-equalization, the HD-FEC requirements are met for two cases: (i) 28 Gbaud EDB and (ii) 14 Gbaud PAM-4. These signal formats allow achieving the HD-FEC requirements and the optical power budget of 27 dB and 26 dB, respectively. Such performance could be considered as expected, but the level distribution between eyes in the eye diagrams shows evidence of driver’s linearity. Even for the 14 Gaud PAM-8, the linearity is acceptable, and only a high signal-to-noise ratio (SNR) requirement hinders to reach the HD-FEC performance. For the 28 Gbaud OOK and PAM-4, a dispersion-induced power fading degrades the performance, and chromatic dispersion compensation or signal equalization must be applied to reach the BER threshold of 3.8×10^{-3} . To test this, we have chosen a linear equalizer whose structure consists of 43-FF&21-FB taps.

The number of taps is chosen in a way to maximally improve the system’s performance by tackling the bandwidth limitations due to the receiver’s side bandwidth and chromatic dispersion. Further increase of the filter tap number does not improve BER values but only adds the complexity. Note that linear equalization using FF taps only is implemented to overcome bandwidth limitations and ISI, whereas FB taps are added to the structure to improve the performance in the presence of noise.

The results show that such post-equalization (43-FF&21-FB taps) significantly improve the BER performance, and thus, it enhances the optical power budget as compared to the previous case without the post-equalization. The optical power budget of the 14 Gbaud PAM-4 is increased by 1 dB. The corresponding value for the 28 Gbaud EDB is 3 dB. More importantly, the post-equalization enables more options of the modulation format alternatives. The HD-FEC requirement is met for the 28 Gbaud OOK and 28 Gbaud PAM-4 modulations. Moreover, the signal quality is so good that it allows achieving the optical power budget of 31 dB and 23 dB, respectively. Although the BER improvement is not enough to meet the HD-FEC requirements for the 14 Gbaud PAM-8 signals, its BER curve approaches to the threshold and a slight SNR improvement, e.g., using a nonlinear equalization, would aid in meeting this requirement. Figure 2d shows the corresponding eye diagrams captured for received optical power values that allow detecting signals with the BER below 3.8×10^{-3} or close to it as in the 14 Gbaud PAM-8 case.

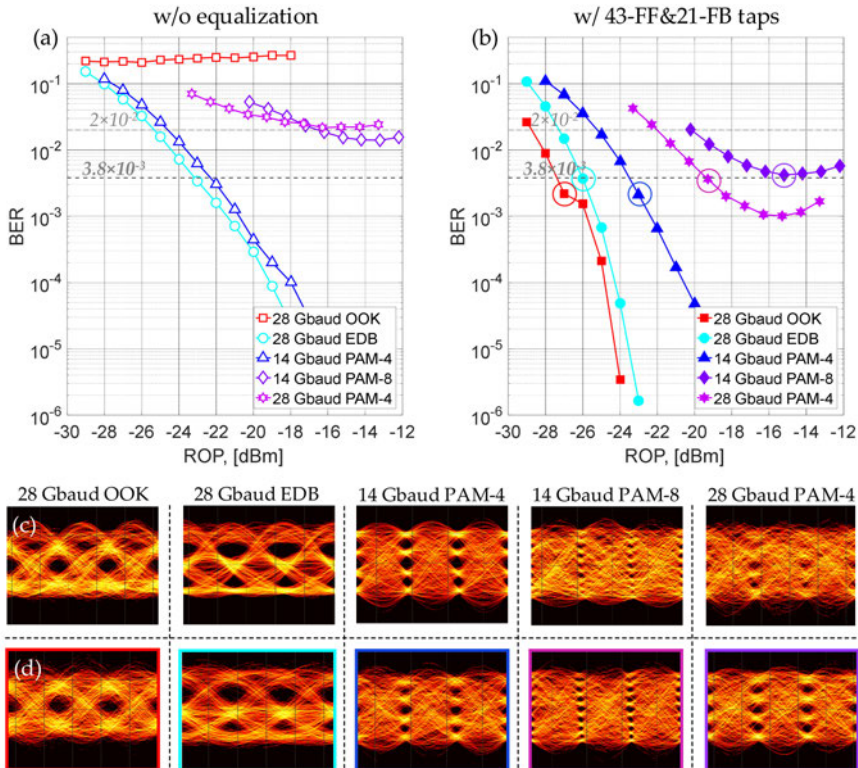


Figure 2. Quality of transmission (QoT) characteristics for the 28 Gbaud OOK, 28 Gbaud EDB, 14 Gbaud PAM-4, 14 Gbaud PAM-8, and 28 Gbaud PAM-4 signals in the IM/DD PON system: (a) BER vs. received optical power (ROP) before the digital post-equalization; (b) BER vs. ROP after the digital post-equalization employing 43-FF&21-FB taps; (c) eye diagrams captured in the ONU at the highest ROP and before the digital post-equalization; and (d) eye diagrams captured in the ONU and ROP values that ensure $BER < 3.8 \times 10^{-3}$ after the digital post-equalization.

Next and to better explore the impact that post-equalization has on the optical power budget and to emphasize its importance, we use three equalizer configurations and compare the OPB for each of them: (i) without post-equalizer, (ii) post-equalizer with only 4-FF taps, (iii) 9-FF&5-FB taps. The obtained results are benchmarked to the previous case, i.e., with the equalizer having 43-FF&21-FB taps. Figure 3 presents the results for scenarios whose combination of data rates and modulation formats ensures line rates no higher than 28 Gbps—28 Gbaud OOK/EDB and 14 Gbaud PAM-4, while Figure 4 includes the 14 Gbaud PAM-8 and 28 Gbaud PAM-4. The first is used to stress the bandwidth limitations of the system components and the second to test linearity of the MZM drivers and the system’s SNR.

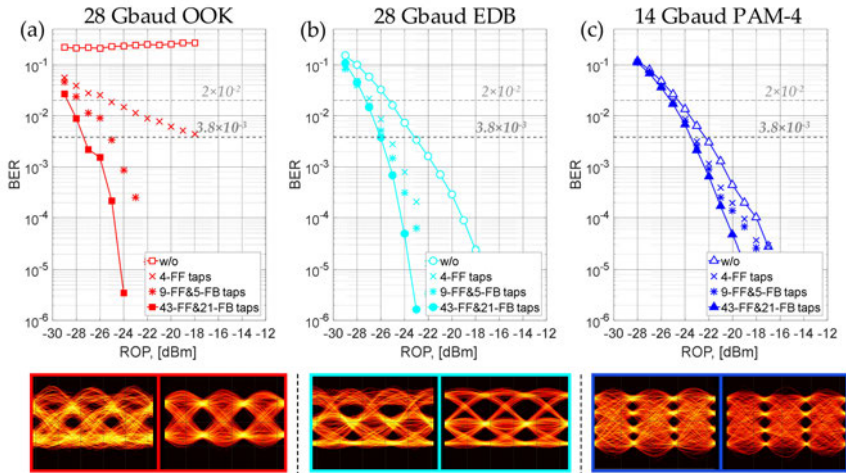


Figure 3. Plots of BER vs. ROP and post-equalizer structure for the (a) 28 Gbaud OOK, (b) 28 Gbaud EDB, and (c) 14 Gbaud PAM-4 signals accompanied by the corresponding eye diagrams captured in the ONU before and after digital post-equalization employing 43-FF&21-FB taps.

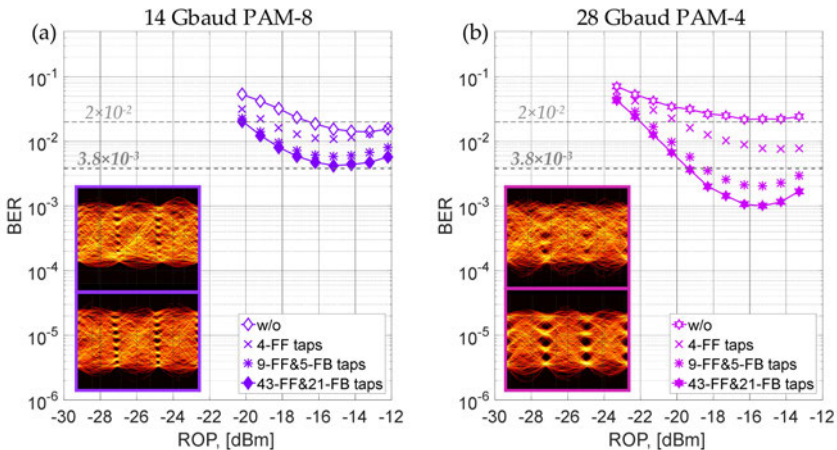


Figure 4. Plots of BER vs. ROP and post-equalizer structure for the (a) 14 Gbaud PAM-8 and (b) 28 Gbaud PAM-4 signals accompanied by the corresponding eye diagrams captured in the ONU before and after digital post-equalization employing 43-FF&21-FB taps.

Figure 3 shows that equalizer with just 9-FF&5-FB taps significantly improves the performance of the 28 Gbaud OOK system. The optical power budget is 29 dB, which is by 2 dB smaller as compared to the case with 43-FF&21-FB taps. Unfortunately, only FF taps are not able to provide the required improvement to meet the pre-FEC BER requirement. At -18 dBm of the received optical power, the BER approaches but not crosses the defined threshold. As for the 14 Gbaud PAM-4 and 28 Gbaud EDB, an equalizer with just 4-FF taps is enough to improve the performance and leads to a higher sensitivity—by 1 dB and by 3 dB, respectively. The use for a more complex structure with more taps does not enhance the performance, and the optical power budget remains unchanged.

Further, we explore two scenarios—14 Gbaud PAM-8 and 28 Gbaud PAM-4—ensuring a higher line rate (42 Gbps and 56 Gbps, respectively). Figure 4a shows results for the 8-level PAM signals, 14 Gbaud PAM-8, which was used to test the MZM driver linearity. The obtained eye diagrams evidence their good linearity as signal levels are equally distributed, but we see that the system is SNR limited as the upper and lower eyes are noisy. Therefore, applying even strong linear post-equalization (i.e., using 43-FF&21-FB taps) does not improve the quality significantly to fulfill the performance requirement although the BER approaches the threshold of 3.8×10^{-3} . Finally, Figure 4b shows that the linear equalization with 9-FF&5-FB taps is sufficient to fulfill the HD-FEC BER requirements and reach the optical power budget of 22 dB for the 28 Gbaud PAM-4 alternative. A more complex structure of the equalizer does not provide significant improvements neither in terms of the signal quality nor in the optical power budget. The system is a partially SNR limited. Insets in Figure 4b show the best eye diagrams for the configuration without the equalizer and with 43-FF&21-FB tap equalizer. The latter has a relatively large eye opening. The fact that the BER threshold of 2×10^{-2} is met for all considered modulation format alternatives proves the viability of IM/DD formats to be used in HS-PON solutions delivering 25+ Gbps or even 50+ Gbps in commercial PONs if SNR improvement and modulator chirp management are achieved.

4. Conclusions

The optical power budget is analyzed for the bandwidth-limited IM/DD PON exploiting the digital signal post-equalization at ONUs. We compare the optical power budget values and the available power margins for the conventional TDM-PON configuration (20 km long feeder fiber, 1:N passive optical power splitting before ONUs) with NRZ-OOK, EDB, PAM-4, and PAM-8 formats at net-rates above 25 Gbps. These signal formats are chosen thanks to their simplicity, the possibility to re-use some of the transceiver's elements (e.g., electrical drivers, amplifier, and photodiodes), and compatibility with the deployed PON infrastructure. We consider only a downstream transmission over a single wavelength in the C-band. To investigate whether components intended for the 10G operation can be used for 25+ Gbps operation, we limit the receiver's bandwidth to 8 GHz before the estimation of the optical power budget. The obtained results show that (i) 10G PON component bandwidth is enough to achieve net-rates above 25 Gbps; (ii) linearity of the optoelectronic components allows operating them using schemes with multilevel modulation formats; and (iii) in combination with the digital signal post-equalization, the obtained optical power budget is compliant with E1 class (OPB = 18–33 dB). More specifically, we reveal that the 28 Gbaud EDB and 14 Gbaud PAM-4 schemes could be used in PONs even without any post-equalization. The signal quality is such that it fulfills the HD-FEC requirement and ensures the power margin of 3.1 dB. For the 28 Gbaud NRZ-OOK, an equalizer with FB taps is required; a 9-FF&5-FB tap equalizer helps to overcome ISI in the presence of noise, which leads to the optical power budget of 29 dB. Finally, line-rates up to 56 Gbps can be supported by the PON employing the PAM-4 modulation. Although a 1:32 splitting ratio might not be feasible due to high insertion loss of such a splitter, it provides the optical power budget of 23 dB. Therefore, the considered IM/DD PON alternatives together with digital signal equalization has the potential to ensure the sustainability for future PONs with line rates well beyond 25 Gbps in the access segment of optical networks.

Author Contributions: Conceptualization, A.U. and L.Z.; methodology, A.U., A.D., S.P., and O.O.; software, A.U., L.Z., and X.P.; validation, T.S., S.S., and V.B.; formal analysis, T.S., S.S., and V.B.; investigation, A.D. and X.P.; resources, S.P. and O.O.; data curation, A.U.; writing—original draft preparation, A.U. and T.S.; writing—review and editing, A.U., T.S., L.Z., X.P., A.D., S.S., V.B., S.P., and O.O.; visualization, A.U.; supervision, O.O.; project administration, A.U.; funding acquisition, T.S., S.S., and O.O. All authors have read and agreed to the published version of the manuscript.

Funding: This work was supported by the ERDF-funded NG-FAST project (1.1.1.2/VIAA/1/16/044) within activity no. 1.1.1.2 Post-doctoral Research Aid, the Doctoral Grant programme of Riga Technical University in Latvia, the Swedish Research Council (Vetenskapsrådet) within the project PHASE (2016-04510) and the project (2019-05197), and the Fundamental Research Funds for the Central Universities (no. 2020QNA5012) in China.

Conflicts of Interest: The authors declare no conflict of interest.

References

- Li, P.; Yi, L.; Xue, L.; Hu, W. 56 Gbps IM/DD PON based on 10G-Class optical devices with 29 dB loss budget enabled by machine learning. In Proceedings of the Optical Fiber Communications Conference and Exposition (OFC), OSA Technical Digest, San Diego, CA, USA, 11–15 March 2018.
- Korra, A.; Salgals, T.; Porins, J.; Kazoks, E.; Miho, R.; Spolitis, S. Performance analysis of cost-efficient high-speed up to 32 Gbit/s WDM-PON next-generation access network with dispersion compensation. In Proceedings of the photonics & electromagnetics research symposium (PIERS–Spring), Rome, Italy, 17–20 June 2019; pp. 2671–2678.
- ITU-T Recommendation G.989.2. Digital Sections and Digital Line System—Optical Line Systems for Local and Access Networks—40-Gigabit-Capable Passive Optical Networks 2 (NG-PON2): Physical Media Dependent (PMD) Layer Specification. Available online: https://www.itu.int%2Frec%2Fdoclogin_pub.asp%3Fflang%3De%26id%3DT-REC-G.989.2-201902-!%PDF-E%26type%3Ditems&usg=AOvVaw2M98EzNwBbhxFce6LYjFRM (accessed on 2 September 2020).
- ITU-T Recommendation G.9807.1. Access Networks—Optical Line Systems for Local and Access Networks, 10-Gigabit-Capable Symmetric Passive Optical Network (XGS-PON). Available online: https://www.itu.int%2Frec%2Fdoclogin_pub.asp%3Fflang%3Ds%26id%3DT-REC-G.9807.2-201708-!%PDF-E%26type%3Ditems&usg=AOvVaw3kEProbTujyux1Kp3dCSFu (accessed on 2 September 2020).
- ITU-T PON Standards-Progress and Recent Activities Q2/SG15. Available online: https://www.itu.int/en/ITU-T/studygroups/2017-2020/15/Documents/OFC2018-2-Q2_v5.pdf (accessed on 30 July 2020).
- Nesbet, D. PON roadmap. *IEEE J. Opt. Commun. Netw.* **2017**, *9*, 71–76. [[CrossRef](#)]
- ITU-T standards. LS—High Speed PON Liaison to IEEE P802.3ca. Available online: http://www.ieee802.org/3/minutes/mar18/incoming/ITU_SG15-LS-95_to_IEEE_802d3.pdf (accessed on 30 July 2020).
- Torres-Ferrera, P.; Wang, H.; Ferrero, V.; Mercinelli, R.; Gaudino, R. Towards 50 Gb/s in high-speed PON: Optimization of modulation formats using pre-chirping. In Proceedings of the 20th International Conference on Transparent Optical Networks (ICTON), Bucharest, Romania, 1–5 July 2018.
- Torres-Ferrera, P.; Ferrero, V.; Valvo, M.; Gaudino, R. Impact of the Overall Electrical Filter Shaping in Next-Generation 25 and 50 Gb/s PONs. *IEEE J. Opt. Commun. Netw.* **2018**, *10*, 493–505. [[CrossRef](#)]
- Barthomeuf, S.; Saliou, F.; Neto, L.A.; Chanclou, P.; Erasme, D. TDM-PON PAM downstream transmission for 25 Gbit/s and beyond. *Photonics* **2018**, *5*, 45. [[CrossRef](#)]
- Zeb, K.; Zhang, X.; Lu, Z. High capacity mode division multiplexing based MIMO enabled all-optical analog millimeter-wave over fiber fronthaul architecture for 5G and beyond. *IEEE Access* **2019**, *7*, 89522–89533. [[CrossRef](#)]
- Liu, G.N.; Zhang, L.; Zuo, T.; Zhang, Q. IM/DD transmission techniques for emerging 5G fronthaul, DCI, and metro applications. *J. Lightw. Technol.* **2018**, *36*, 560–567. [[CrossRef](#)]
- Lin, R.; Van Kerrebrouck, J.; Pang, X.; Verplaetse, M.; Ozolins, O.; Udalcovs, A.; Zhang, L.; Gan, L.; Tang, M.; Fu, S.; et al. 100 Gbps/core NRZ and EDB IM/DD transmission over multicore fiber for intra-datacenter communication networks. *Opt. Express* **2018**, *26*, 10519–10526. [[CrossRef](#)] [[PubMed](#)]
- Wei, J.L.; Grobe, K.; Sanchez, C.; Giacomidis, E.; Griesser, H. Comparison of cost- and energy-efficient signal modulations for next generation passive optical networks. *Opt. Express* **2015**, *23*, 28271–28281. [[CrossRef](#)] [[PubMed](#)]

15. Wei, J.L.; Grobe, K.; Griesser, H. Cost-Efficient High-Speed Modulation for Next-Generation PONs. In Proceedings of the 16th ITG Symposium on Photonic Networks, VDE, Leipzig Germany, 7–8 May 2015.
16. Yi, L.; Ji, H.; Li, Z.; Li, X.; Li, C.; Yang, Q.; Xue, L.; Wang, X.; Wang, S.; Yang, Y.; et al. Field-trial of a real-time 100 Gb/s TWDM-PON based on 10G-Class optical devices. In Proceedings of the 42nd European Conference on Optical Communication (ECOC), Dusseldorf, Germany, 18–22 December 2016.
17. Salgals, T.; Spolitis, S.; Olonkins, S.; Bobrovs, V. Investigation of 4-PAM modulation format for use in WDM-PON optical access systems. In Proceedings of the Progress in Electromagnetics Research Symposium (PIERS), St. Petersburg, Russia, 22–25 May 2017.
18. Sun, X.; Yang, M.; Djordjevic, I.B. Real-time fpga-based rate adaptive LDPC coding for data center networks and PONs. In Proceedings of the European Conference on Optical Communication (ECOC), Rome, Italy, 23–27 September 2018.
19. Yi, L.; Li, P.; Liao, T.; Hu, W. 100Gb/s/λ IM-DD PON using 20G-Class optical devices by machine learning based equalization. In Proceedings of the European Conference on Optical Communication (ECOC), Rome, Italy, 23–27 September 2018.
20. Pang, X.; Ozolins, O.; Gaiarin, S.; Kakkar, A.; Rodrigo Navarro, J.; Olmedo, M.I.; Schatz, R.; Udalcovs, A.; Westergren, U.; Zibar, D.; et al. Experimental study of 1.55-μm EML-based optical IM/DD PAM-4/8 short reach systems. *IEEE Photonic Technol. Lett.* **2017**, *29*, 523–526. [[CrossRef](#)]
21. Zhang, K.; Zhuge, Q.; Xin, H.; Hu, W.; Plant, D.V. Performance comparison of DML, EML and MZM in dispersion-unmanaged short reach transmissions with digital signal processing. *Opt. Express* **2018**, *26*, 34288–34304. [[CrossRef](#)] [[PubMed](#)]
22. Torres-Ferrera, P.; Ferrero, V.; Mercinelli, R.; Gaudio, R. Experimental demonstration of DSP-assisted electrical duobinary optimization for high speed PON 25+ Gbps using 10 Gbps APD receiver. In Proceedings of the European Conference on Optical Communication (ECOC), Rome, Italy, 23–27 September 2018.
23. Barthelemy, S.; Saliou, F.; Neto, L.A.; Chanclou, P.; Erasme, D. High optical budget 25 Gbit/s PON with PAM4 and optically amplified O band downstream transmission. In Proceedings of the European Conference on Optical Communication (ECOC), Rome, Italy, 23–27 September 2018.
24. Harstead, E. 25G EPON PR20 Loss Budget. In Proceedings of the IEEE 802.3 Working Group Meeting, San Diego, CA, USA, July 2018. Available online: <http://docplayer.net/140523062-25g-epon-pr20-loss-budget-updated.html> (accessed on 30 July 2020).
25. Jackson, K.P.; Sanada, F.; Feng, H.; Takagi, T.; Tanaka, N.; Umeda, D.; Funada, T. PR30 Link Budget Considerations from a Component Perspective. In Proceedings of the IEEE P802.3ca 100G-EPON Task Force Meeting, New Orleans, LA, USA, 23–25 May 2017.
26. Zou, D.; Li, F.; Li, Z.; Wang, W.; Sui, Q.; Cao, Z.; Li, Z. 100G PAM-6 and PAM-8 signal transmission enabled by pre-chirping for 10-km intra-DCI utilizing MZM in C-Band. *J. Lightw. Technol.* **2020**, *38*, 3445–3453. [[CrossRef](#)]



PAPER-4: Performance Analysis of Cost-efficient High-speed up to 32 Gbit/s WDM-PON Next-generation Access Network with Dispersion Compensation

A. Korra, **T. Salgals**, J. Porins, E. Kazoks, R. Miho and **S. Spolitis**, "Performance Analysis of Cost-efficient High-speed up to 32 Gbit/s WDM-PON Next-generation Access Network with Dispersion Compensation," *2019 Photonics & Electromagnetics Research Symposium - Spring (PIERS-Spring)*, pp. 2671-2678, Rome, Italy, June 17-20, (2019), DOI: [10.1109/PIERS-Spring46901.2019.9017854](https://doi.org/10.1109/PIERS-Spring46901.2019.9017854)

Performance Analysis of Cost-efficient High-speed up to 32 Gbit/s WDM-PON Next-generation Access Network with Dispersion Compensation

Ambra Korra¹, Toms Salgals², Jurgis Porins²,
Edgars Kazoks², Rozeta Miho¹, and Sandis Spolitis²

¹Department of Electronics and Telecommunications, Polytechnic University of Tirana, Albania

²Institute of Telecommunications, Riga Technical University
Azenes Street 12, LV-1048, Riga, Latvia

Abstract— Third generation fiber-to-the-x (FTTx) will introduce wavelength division multiplexing (WDM) technology to increase data rates up to 40 Gbit/s, as well as coexist with current communication systems. WDM passive optical network (WDM-PON) based fiber-to-the-home (FTTH) system architecture together with the Next-generation passive optical network (NG-PON) can provide solution related to nowadays problems with transmission capacity. It is expected that NG-PON systems will become more cost-efficient at high per user data rates, providing different transmission speeds for end users, based on pay-as-you-grow approach. In this paper, our introduced system model is used to obtain WDM-PON system effectiveness for different data rates of up to 32 Gbit/s per downstream transmission channel. We created combined simulative-experimental WDM-PON transmission system model in environment of RSoft OptSim simulation software to compare the performance of non-return-to-zero (NRZ) on-off-keying (OOK) modulated PON transmission system versus transmission bitrate and distance. Results showed that proposed transmission system is capable to provide data transmission of up to 32 Gbit/s per channel with BER $< 10^{-3}$, if additional forward error correction (FEC) is used. Additionally, to increase the reach of investigated system, fiber Bragg grating-based dispersion compensation module (FBG-DCM) is implemented, therefore enabling full pre-compensation of chromatic dispersion.

1. INTRODUCTION

The newest technologies (e.g., 4K/8K television, virtual and augmented reality, etc.) and fast-growing number of end-users require higher bandwidth. Accordingly, wavelength division multiplexed passive optical access networks (WDM-PONs) can be offered as the best solution to modern capacity related problems and support high data rates providing large distance coverage between network nodes to keep up with the increasing demand of traffic [1, 2]. Wavelength division multiplexing (WDM) technique is a solution to deal with the Internet traffic by using the bandwidth of optical fiber more effectively. It is considered as a definitive solution for future telecommunication infrastructure upgrade, which is able to provide almost unlimited bandwidth to each subscriber. WDM-PON based fiber to the home (FTTH) system architecture can compete with the Next generation passive optical network (NG-PON) solution related to current problems of transmission capacity [3, 4].

It is critical to increase further the operating speed and maximal reach of WDM-PON in a cost-effective manner. The request for faster, low loss and cost-effective optical communication system must be fulfilled. Chromatic dispersion (CD) is a fundamental problem in optical transport networks [5]. The distortion of the signal leads to intersymbol interference, which eventually will result in data losses and traffic interruption. In order to protect the signal from losses and affection of CD during transmission in optical fiber, appropriate technique by dispersion compensation based on fiber Bragg gratings (FBG) can save costs as well as meet the technical requirements needed to facilitate higher data rate optical transport network [6]. The main advantage using fiber Bragg grating (FBG) dispersion compensation module (DCM) is low insertion loss and greater power capacity without introducing additional non-linear signal effects. They have become a key factor, along with EDFA amplifiers increasing the reach and capacity of broadband fiber optics transport networks [7, 8]. In this paper, our introduced system model is used to obtain the system performance for different operating data rates of up to 32 Gbit/s per downstream transmission channel. To fulfill Internet traffic requirements, using cost-effective solutions, the investigation of maximal transmission reach for higher data rates using fiber Bragg grating dispersion compensation module (FBG-DCM) is required [9]. We are going to compare the system performance of non-return-to

zero on-off keying (NRZ-OOK) modulated PON transmission system using erbium-doped fiber amplifier (EDFA) and (FBG-DCM), to provide sufficient input power at the photoreceiver in order to increase transmission distance by obtaining high system performance [10, 11].

2. EXPERIMENTAL NRZ-OOK MODULATED WDM-PON PASSIVE OPTICAL TRANSMISSION SYSTEM MODEL WITH DATA RATE UP TO 32 GBIT/S

The purpose of our research model was to evaluate performance of our investigated 100 GHz spaced WDM-PON transmission system with most often used transmission speeds of up to 32 Gbit/s per channel and obtain the maximum reach of the system with chromatic dispersion CD compensation, under condition that it is still possible to achieve forward error correction pre-(FEC) BER of 10^{-3} . In our previous research it is numerically shown that CD compensation can improve the performance and maximal available reach of WDM-PON system, therefore in our research we show results with FBG-DCM dispersion compensation technique [5]. Firstly we have experimentally shown single channel passive optical network (PON) performance after 80 km transmission through standard single-mode fiber (SSMF) span, with additional use of implemented dispersion compensation module FBG-DCM. Secondly additional effect of crosstalk is obtained with simulative-experimental model. The purpose of experimental section was to observe experimental system physical parameters and impact of used components, therefore properly adjusted 16-channel WDM-PON transmission system model was created in newest RSoft OptSim simulation software.

The experimental system part is represented in Fig. 1. The output of laser source with 8.49 dBm output power at $\lambda = 1552.605$ nm is connected to the Mach-Zehnder modulator (MZM) input. Polarization controller (PC) is placed before the MZM to reduce polarization dependent losses. An MZM (bias point 3.14 V) is driven at data rates of 10 Gbit/s up to 32 Gbit/s by a 2^9 long pseudo-random bit sequence (PRBS9) non-return-to-zero (NRZ) signal from electrical arbitrary waveform generator (AWG). The modulated output from the MZM is being amplified by fixed output power (fixed +10 dBm output power) erbium doped EDFA. Then 100 GHz spaced arrayed waveguide grating (AWG) multiplexer is used to filter out particular optical channel.

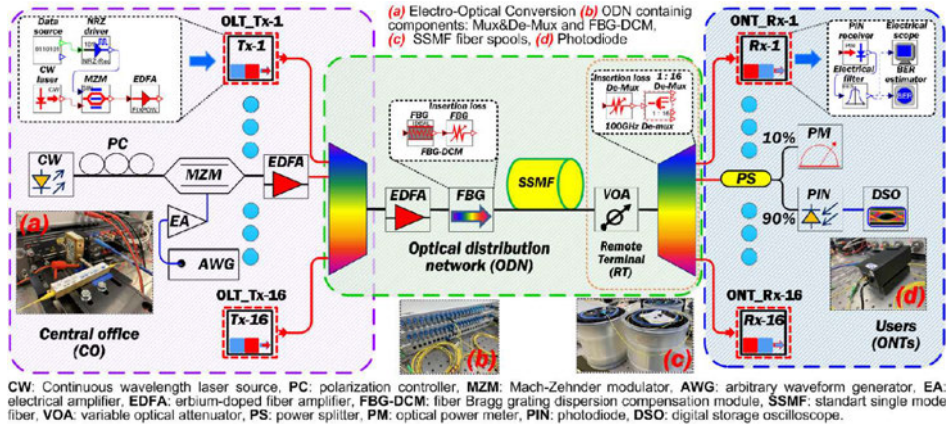


Figure 1. Experimental model of NRZ-OOK modulated up to 32 Gbit/s per channel WDM-PON optical transmission system.

The output of multiplexer is connected to the input of second EDFA with fixed +14 dBm output power and transmitted through 80 km long ITU-T G.652 rec. standard SMF section with additional CD pre-compensation by tunable FBG-DCM, which has 3 dB insertion loss at 1550 nm wavelength. After ODN transmission part the 100 GHz spaced AWG de-multiplexer is connected through a variable optical attenuator (VOA). Afterwards, the VOA is used to measure the system performance later show in figure 2 (BER versus received optical power). The output of AWG de-multiplexer's central channel (193.1 THz) is connected to 50 GHz photodetector (PIN). Detected

electrical signal is sent to a digital storage oscilloscope (DSO) to analyze signal — display the eye diagrams and perform BER measurements.

Investigated WDM-PON transmission system together with dispersion compensation was constructed to obtain effect of crosstalk in terms of transmission speed and maximum transmission reach for each appropriate operating data rate as well.

As one can see in Fig. 1 our investigated WDM-PON simulation scheme consists of 16 channels. The channel spacing according to ITU-T G.694.1 rec. is chosen 100 GHz and the central frequency of middle channel is 193.1 THz ($\lambda = 1552.524$ nm), which is based on experimentally used one [12].

According to PON architecture, our proposed simulation model central office (CO) consists of optical line terminal (OLT) with sixteen transmitters (OLT_Tx) as it is shown in the Fig. 1. Each particular OLT_Tx transmitter based on widely used NRZ line code consists of a data source element with 2^9 long pseudo random bit sequence (PRBS9) connected to NRZ driver. Coded electrical output signal is directly sent to MZM providing electrical to optical signal conversion. Continuous wavelength (CW) laser with +8.49 dBm output power was used for each particular transmitter.

Optical signals from each OLT_Tx are coupled together by using optical AWG multiplexer with 100 GHz channel spacing, 3.5 dB insertion loss at 1550 nm wavelength and 3-dB bandwidth of 80 GHz. Afterwards coupled signals are amplified by fixed output power (fixed +14 dBm output) EDFA.

According to ITU-T G.989.2 Next generation PON standard (NG-PON2) definition of optical distribution network ODN length, we have chosen 40 km and twice larger 80 km optical fiber transmission distances [13]. An ITU-T G.652 optical fiber SMF with 17 ps/(nm × km) dispersion coefficient and 0.2 dB/km insertion loss (at 1550 nm reference wavelength) was used in our research. CD pre-compensation by FBG-DCM is realized for coupled channels before launching them into transmission through transmission fiber span. Additional attenuator with 3 dB attenuation is used to implement FBG-DCM insertion loss.

After transmission through SMF optical transmission line, all optical channels are separated by AWG de-multiplexer located in remote terminal (RT), with 100 GHz channel spacing, 3.5 dB insertion loss and 3-dB bandwidth of 80 GHz.

Receiver consists of optical network terminals (ONTs), where each receiver (ONT_Rx) consists of 50 GHz PIN photodiode based on experimentally used one, with sensitivity equal to +4 dBm, dark current of 10 nA and responsivity of 0.7 A/W [14]. The optimal 5-pole electrical Bessel low pass filter (LPF) bandwidth was found for each operating bitrate based on the most successful system performance. An electrical scope and BER estimator was used during simulations for measurements of received signal bit patterns quality.

3. RESULTS AND DISCUSSION

The main purpose of this work is to evaluate maximum reach and performance of combined simulative-experimental developed WDM-PON system model as well as evaluate the impact of used optical, electro-optical and electrical components on the quality of transmitted signal in such a system. Our research is divided in two parts: 1st experimental part, where we obtain limiting factors of physical parameters and impact of components used in WDM-PON designed transmission system model and 2nd part, investigation of simulation model with improved system capacity up to 16 channels, allowing us to observe the effect of crosstalk and non-linear optical effects (NOE), etc. [15].

The Fig. 2 shows experimentally obtained BER of transmitted signal with bitrate of up to 32 Gbit/s versus received optical power at PIN after 80 km transmission through ODN. The measured optical output power after transmission through 80 km ODN length varied from -4.5 to 7.1 dBm, where the BER of received NRZ-OOK signals was from 1.2×10^{-2} to 1.4×10^{-23} .

In our research we used different operating data rates of up to 32 Gbit/s per channel for 100 GHz spaced 16-channel wavelength division multiplexed WDM-PON passive optical transmission system.

The obtained BER of operating data rate of up to 32 Gbit/s for 100 GHz spaced 16-channel WDM-PON transmission system in response to received optical power at PIN receiver is shown in Fig. 3 in two different scenarios — with 40 and 80 km of SMF fiber length. Applying for shorter transmission distances of ODN part we can decrease impact of NOE effects in optical fiber link. In scenario with shorter fiber link length (40 km), the gain of second used EDFA was reduced to 8 dBm respectively. The measured optical output power after transmission through 40 km ODN part varied from -1.1 to 7.1 dBm, where the BER of received NRZ-OOK signals was from 2.2×10^{-2}

to 5.2×10^{-20} , please see Fig. 3(a). In such a way second scenarios with 40 km SMF fiber ODN link in response to received optical power is shown in Fig. 3(b), where measured optical output power after transmission through 80 km ODN length varied from -1.1 to 7 dBm, where the BER of received signals was from 2.2×10^{-2} to 1.3×10^{-19} , respectively.

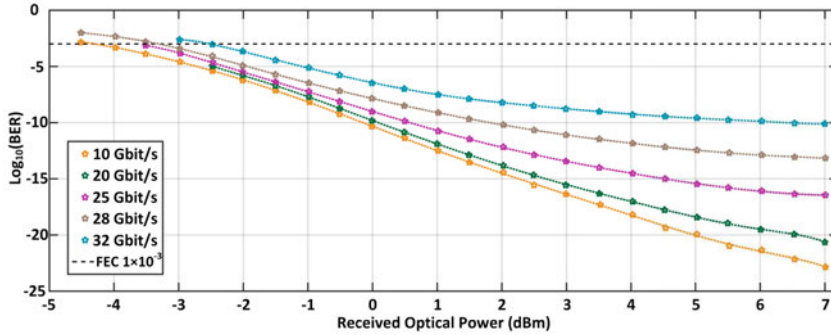


Figure 2. Comparison of experimentally measured BER versus received optical power for investigated single channel PON transmission system with bitrate of up to 32 Gbit/s with use of FBG-DCM module for ODN length of 80 km.

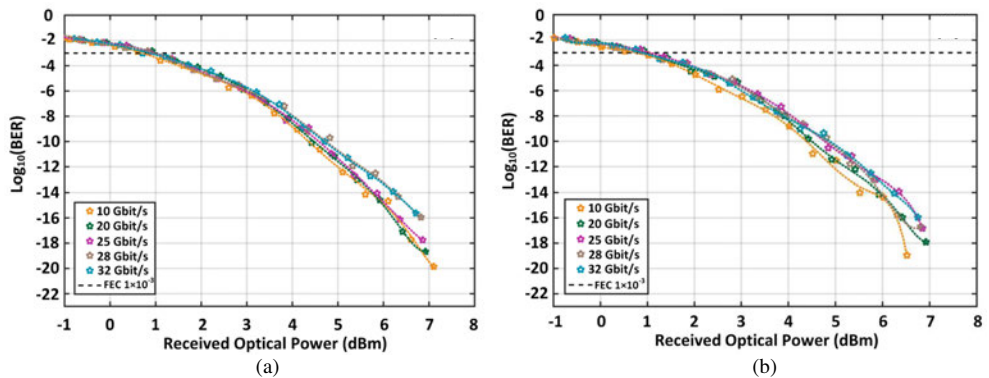


Figure 3. Comparison of measured BER versus received optical power with use of DCM module for ODN length of (a) 40 km and (b) 80 km for investigated 16-channel WDM-PON transmission system at operating bitrate up to 32 Gbit/s per channel.

As one can see in Figs. 4(a1), 4(a2), 4(a3), 4(a4) and 4(a5) in B2B configuration the signal quality for all operating data rates is good, eye is open and error-free transmission is provided. As one can see in Figs. 4(b) and 4(c), after 80 km transmission in experimental and simulative environment, the obtained simulative-experimental results are mainly similar, therefore we conclude that it is possible to increase system capacity up to 16 channels for evaluation of transmission system performance.

We have demonstrated performance comparison for investigated 100 GHz spaced 16-channel WDM-PON transmission system with transmission of operating data rates per channel of up to 32 Gbit/s through ODN part, with different lengths of 40 and 80 km SMF fiber spans, please see Fig. 5. Additional losses in optical fiber line and effect of crosstalk and NOE on transmitted signals for longer distances of 80 km lead to performance decrease of 100 GHz spaced 16-channel WDM-PON transmission system, where the BER at operating 10 Gbit/s data rate per channel of received signal (worst performing channel) was 1.3×10^{-19} , please see Fig. 5(b1). After decreasing ODN length to 40 km, from obtained results we conclude that crosstalk and NOE effects are reduced

significantly, where the BER of channel with worst performance operating at 10 Gbit/s data rate was 5.2×10^{-20} , please see Fig. 5(a1). As one can see in Figs. 5(a5) and 5(b5), after transmission through ODN fiber length defined distances as 40 and 80 km the BER at operating 32 Gbit/s data rate per channel of received signals was 1.1×10^{-14} and 1×10^{-14} , respectively.

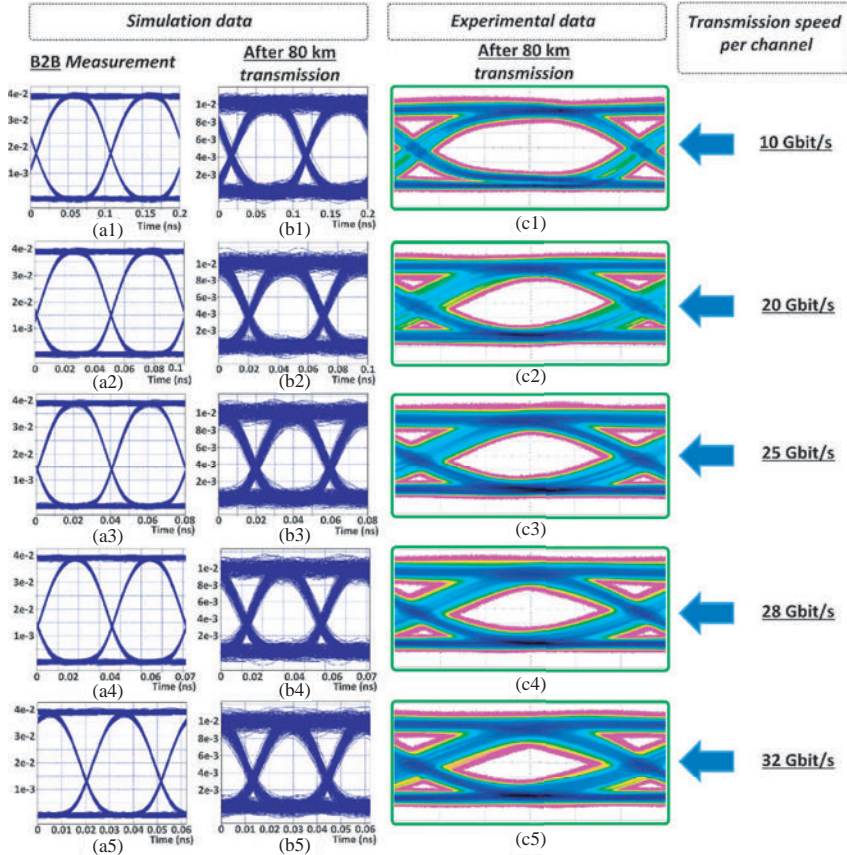


Figure 4. Eye diagrams of experimentally received signal: (a) after B2B transmission, (b) analyzed in OptSim simulation software environment after 80 km transmission with use of FBG-DCM module and (c) after 80 km transmission with use of FBG-DCM module for investigated PON transmission system with operating data rates of: (1) 10 Gbit/s (2) 20 Gbit/s, (3) 25 Gbit/s, (4) 28 Gbit/s, (5) 32 Gbit/s per channel.

The purpose of this last section was to evaluate numerically the performance of NRZ-OOK modulated 100 GHz spaced 16-channel WDM-PON system together with implementation of dispersion compensation and find the maximum network reach per each operating bitrate. As mentioned before, the BER threshold in our investigated transmission system with assumed additional FEC is 10^{-3} .

By using FBG-DCM dispersion compensation technique, the maximum achievable transmission distance for the system operating at bitrates of 25, 28 and 32 Gbit/s per channel was 105 km, where the BER of received signal was 3.9×10^{-4} , 9.9×10^{-4} and 7.5×10^{-4} , please see Figs. 6(c), 6(d) and 6(e). As it is shown by simulation results with 10 Gbit/s operating data rate per channel for investigated 100 GHz spaced 16-channel WDM-PON transmission system, maximum achievable transmission distance was 109 km, where the BER of received signal was 8.1×10^{-4} , please see Fig. 6(a). The second best result with 106 km maximal achieved transmission distance was with operating data rate of 20 Gbit/s per channel, where the BER of received signal was 9.4×10^{-4} , please see Fig. 6(b).

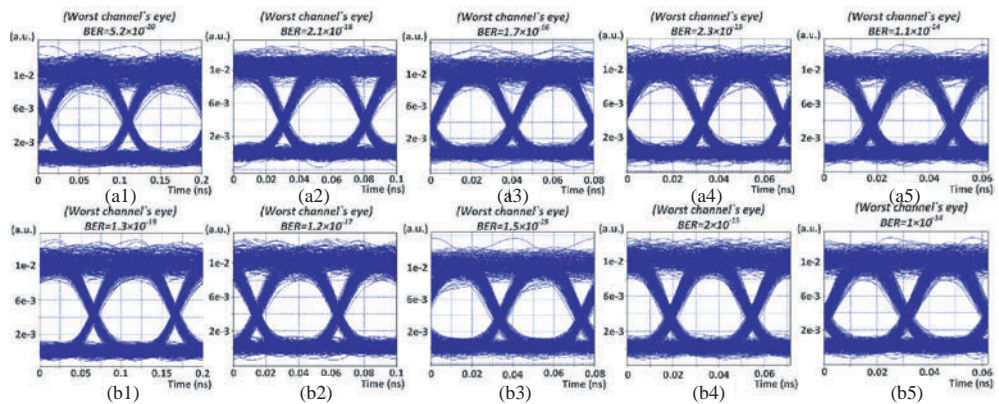


Figure 5. Eye diagrams of experimentally received signal with use of FBG-DCM module, (a) after 40 km transmission and (b) after 80 km transmission for investigated 16-channel WDM-PON transmission system at operating bitrate of: (1) 10 Gbit/s (2) 20 Gbit/s, (3) 25 Gbit/s, (4) 28 Gbit/s, (5) 32 Gbit/s per channel.

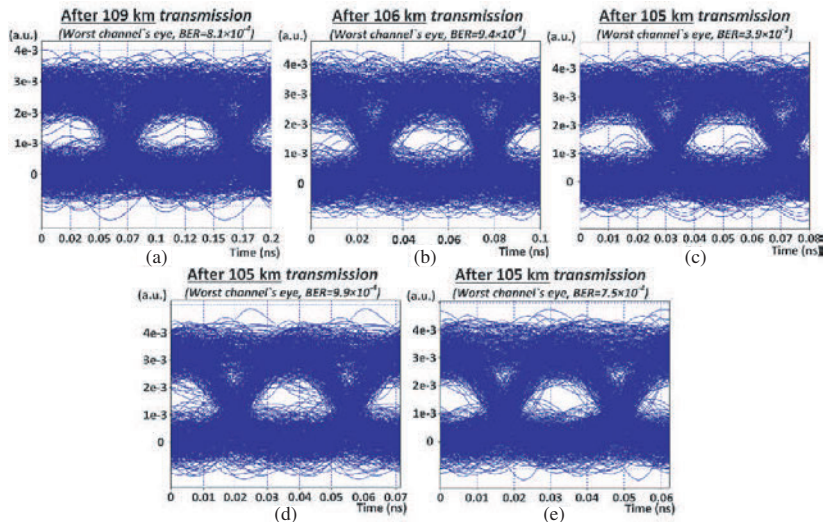


Figure 6. Eye diagrams of received signal after maximal achieved transmission distance with dispersion compensation by FBG-DCM module and operating bitrate of: (a) 10 Gbit/s (b) 20 Gbit/s, (c) 25 Gbit/s, (d) 28 Gbit/s, (e) 32 Gbit/s per channel for 4-channel 100 GHz spaced NRZ-OOK modulated WDM-PON transmission system.

4. CONCLUSIONS

Nowadays it is expected that WDM-PON will become more cost-efficient at high per user data rates. We have successfully demonstrated the operation of WDM-PON transmission system with most typical operating bitrates of up to 32 Gbit/s per channel, by using technical parameters from datasheets of optical, electro-optical and electrical system components. Afterwards, basis on experimental data, we developed extended 16-channel simulation model in RSoft OptSim simulation environment. Our investigated 100 GHz spaced 16-channel WDM-PON transmission system model is realized in simulation environment and established on traditionally used dense WDM frequency grid according to ITU-T G.694.1 recommendation. Initial ODN section is developed in line with Next-generation (NG-PON2) ITU-T G.989.2 requirements, therefore using the transmission optical

fiber span lengths of up to 40 km. Although, to test the system's capability, twice longer ODN fiber section experimentally was realized as well, with length of 80 km and finally implemented in our proposed 16-channel WDM-PON transmission system model, as well along with additional EDFA amplifier located in CO. It was shown that maximal achievable transmission distance with operating data rate of 32 Gbit/s per channel and use of FBG-DCM for dispersion compensation in 100 GHz spaced NRZ-OOK modulated 16-channel WDM-PON transmission system is 105 km, where the BER of received signal was 7.5×10^{-4} .

ACKNOWLEDGMENT

This work has been supported by the European Regional Development Fund within the Activity 1.1.1.2 "Post-doctoral Research Aid" of the Specific Aid Objective 1.1.1 "To increase the research and innovative capacity of scientific institutions of Latvia and the ability to attract external financing, investing in human resources and infrastructure" of the Operational Programme "Growth and Employment" (No. 1.1.1.2/VIAA/1/16/044).

REFERENCES

1. Bobrovs, V., A. Udalcovs, and G. Ivanovs, "Power efficiency vs. spectral efficiency and transmission distance in 2.5-10-40 Gbps backbone optical networks," *2014 6th International Symposium on Communications, Control and Signal Processing (ISCCSP)*, 202–205, ISBN: 978-1-4799-2890-3, Athens Greece, May 21–23, 2014.
2. Spolitis, S., V. Bobrovs, S. Berezins, and G. Ivanovs, "Optimal design of spectrally sliced ASE seeded WDM-PON system," *2012 15th International Telecommunications Network Strategy and Planning Symposium (NETWORKS)*, Art. No. 6381687, ISBN: 978-1-4673-1391-9, 1–5, Oct. 15–18, 2012.
3. Chung, Y. C., "High-speed coherent WDM PON for next-generation access network," *2013 15th International Conference on Transparent Optical Networks (ICTON)*, 1–4, ISBN: 978-1-4799-0683-3, ISSN: 2161-2064, Cartagena Spain, Jun. 23–27, 2013.
4. Hodzic, A., B. Konrad, and K. Petermann, "Prechirp in NRZ-based 40-Gb/s single-channel and WDM transmission systems," *IEEE Photonics Technology Letters*, Vol. 14, No. 2, 52–154, ISSN: 1941-0174, DOI: 10.1109/68.980479, Aug. 7, 2002.
5. Salgals, T., S. Spolitis, S. Olonkins, and V. Bobrovs "Investigation of 4-PAM modulation format for use in WDM-PON optical access systems," *2017 Progress In Electromagnetics Research Symposium — Spring (PIERS)*, 1–4, St Petersburg, Russia, May 22–25, 2017.
6. Bobrovs, V., A. Udalcovs, S. Spolitis, and G. Ivanovs, "Schemes for compensation of chromatic dispersion in combined HDWDM systems," *Latvian Journal of Physics and Technical Sciences*, Vol. 48 No. 5, 30–44, ISSN: 08688257, Jan. 1, 2011.
7. Dilendorfs, V., S. Spolitis, and V. Bobrovs, "Comparison of dispersion compensation methods for 40 Gbit/s WDM-PON transmission systems," *2017 Progress In Electromagnetics Research Symposium — Spring (PIERS)*, 2431–2436, St Petersburg, Russia, May 22–25, 2017.
8. Olonkins, S., S. Spolitis, I. Lyashuk, and V. Bobrovs, "Cost effective WDM-AON with multicarrier source based on dual-pump FOPA," *(2015) International Congress on Ultra Modern Telecommunications and Control Systems and Workshops*, 23–28, Art. no. 7002073, ISSN: 21570221, Jan. 6, 2015.
9. Spolitis, S., V. Bobrovs, and G. Ivanovs, "Reach improvement of spectrum-sliced dense WDM-PON system," *2012 Seventh International Conference on Broadband, Wireless Computing, Communication and Applications (BWCCA 2012)*, 296–301, Art. no. 6363072, ISBN: 978-1-4673-2972-9, Victoria BC Canada, Nov. 12–14, 2012.
10. Salgals, T., L. Skladova, K. Vilcane, J. Braunfelds, and S. Spolitis "Evaluation of 4-PAM, NRZ and duobinary modulation formats performance for use in 20 Gbit/s DWDM-PON optical access systems," *2018 Advances in Wireless and Optical Communications (RTUWO)*, ISBN: 978-1-5386-5558-0, 134–138, Riga Latvia, Nov. 15–16, 2018.
11. Salgals, T., I. Kurbatska, S. Spolitis, V. Bobrovs, and G. Ivanovs, "Research of M-PAM and duobinary modulation formats for use in high-speed WDM-PON systems," *Part of Book: Telecommunication Systems*, 1–18, DOI:10.5772/intechopen.84600, Feb. 22, 2019.
12. ITU-T Recommendation G.694.1, "Transmission media and optical systems characteristics — Characteristics of optical systems: Spectral grids for WDM applications: DWDM frequency grid," 7–12, 2012.

13. ITU-T Recommendation G.989.2, “Digital sections and digital line system — Optical line systems for local and access networks — 40-Gigabit-capable passive optical networks 2 (NG-PON2): Physical media dependent (PMD) layer specification,” 10–92, 2014.
14. Discovery Semiconductors Inc., “High optical power handling InGaAs photodiodes to 50 GHz,” Technical Specification, 1–4, 2003.
15. Maharjan, R., I. Lavrinovica, A. Supe, and J. Porins, “Minimization of FWM effect in nonlinear optical fiber using variable channel spacing technique,” *2016 Advances in Wireless and Optical Communications (RTUWO)*, 1–4, ISBN: 978-1-5090-1535-1, Riga Latvia, Nov. 3–4, 2016.

PAPER-5: Comparison of Dispersion Compensation Techniques for Real-Time up to 160 Gbit/s DWDM C-Band Transmission

T. Salgals, A. Supe, V. Bobrovs, J. Porins, and **S. Spolitis**, "Comparison of Dispersion Compensation Techniques for Real-Time up to 160 Gbit/s DWDM C-Band Transmission", *ELEKTRON ELEKTROTECH* 26(2), 85–93, (2020), DOI:[10.5755/j01.eie.26.2.25892](https://doi.org/10.5755/j01.eie.26.2.25892)

Comparison of Dispersion Compensation Techniques for Real-Time up to 160 Gbit/s DWDM C-Band Transmission

Toms Salgals^{1,2,*}, Andis Supe¹, Vjaceslavs Bobrovs¹, Jurgis Porins¹, Sandis Spolitis^{1,2}

¹*Institute of Telecommunications, Riga Technical University,*

Kalku st. 1, LV-1658, Riga, Latvia

²*Communication Technologies Research Center, Riga Technical University,*

Azenes st. 12, LV-1048, Riga, Latvia

toms.salgals@rtu.lv

Abstract—The exponential growth of data traffic related to the progress of newest technologies (e.g., 4K/8K live stream videos, virtual reality (VR) applications, etc.), new services, and a fast-growing number of end-users require higher bandwidth and increase of user bitrate, as a result pushing hard the telecommunication infrastructure for upgrading. Expected usage of more complex modulation formats in fiber optical link infrastructure for cellular network transmission and data center interconnections (DCI) are still affected with fundamental chromatic dispersion influence on the signal quality, which consequently increases bit error rate (BER). We experimentally demonstrate a real-time comparison of commercially used dispersion compensation techniques for 100 GHz spaced dense wavelength division multiplexed (DWDM) optical transmission system with a total transmission speed capacity of 160 Gbit/s.

Index Terms—Dense wavelength division multiplexing (DWDM); Chromatic dispersion (CD); Fiber Bragg grating dispersion compensation module (FBG-DCM); Dispersion compensation fiber (DCF); Non-return-to-zero on-off keying (NRZ-OOK).

I. INTRODUCTION

The newest technology trends being transformed by technology in a variety of ways of next-decade fulfilled by consumer-driven data consumption eventually lead to unprecedented pressures for fiber optical metro, i.e. long-haul networks. With the massive deployment of coherent optical fiber transmission systems at 100 Gbit/s in backbone networks, the pressure has shifted to the metro networks. Communication infrastructures of the next decade will be based on the integration of information and communication technologies (ICT) to optimize the efficiency of operations and large-scale deployment of connected and automated

mobility (CAM), cloud computing, wireless sensor networks, e.g., large scale next-generation cellular network coverage connections provide possibility in urban areas [1]–[3]. The evolution towards higher bitrates is mainly driven by the point-to-point (P2P) Fiber-to-the-home/building (FTTh/b) and wireless fronthaul, e.g., new mobile interfaces for fifth-generation (5G), where 25 Gbit/s could be needed soon for either backhauling or new functional split based interfaces [4]–[6].

Intensity modulation with direct detection (IM-DD) transmission technique is preferred due to its advantages of low cost and easy implementation, where chromatic dispersion (CD) induced power fading is one of the key limiting factors in IM/DD transmission systems [2], [7], [8], [9]. Chromatic dispersion CD is possible to compensate in the both optical and electrical domains. Depending on the optical domain dispersion profile, the effects of CD can be either removed locally by fiber Bragg grating (FBG) or can be compensated throughout the dispersion-compensating fiber (DCF) [3], [7].

In our previous research, we concluded that intensity non-return-to-zero on-off keying (NRZ-OOK) modulation format, as well as 4-level amplitude modulation PAM-4 modulation format, which has higher spectral efficiency and potentially can provide higher data transmission speeds in fiber optical networks with limited bandwidth, are still affected with the chromatic dispersion (CD), which is one of the main distance-limiting factors [10], [11]. In particular, the most common solution due to a cost-effective way is re-use the already developed and used commercially available components operating at 10 Gbit/s PONs (10G PON) technology for the desired NG-PONs at least increases bitrates for 25 Gbit/s either 40 Gbit/s per channel [12].

The main purpose of this work is to evaluate the performance of experimentally developed dense wavelength division multiplexed DWDM transmission system and compare the most often used CD compensation techniques. To protect signals and avoid dispersion effects during their transmission, two widely commercially implemented dispersion compensation techniques are experimentally shown: CD compensation based on fiber Bragg grating

Manuscript received 9 October, 2019; accepted 16 January, 2020.

This work has been supported by the European Regional Development Fund within the Activity 1.1.1.2 “Post-doctoral Research Aid” of the Specific Aid Objective 1.1.1 “To increase the research and innovative capacity of scientific institutions of Latvia and the ability to attract external financing, investing in human resources and infrastructure” of the Operational Programme “Growth and Employment” under Grant (No. 1.1.1.2/VIAA/1/16/044) and by the Riga Technical University’s Doctoral Grant programme.

(FGB) dispersion compensation module (DCM) and compensation based on dispersion compensation fibers (DCF). Finally, the influence of the nonlinear effects (NOE) causing signal distortion in DCF optical fiber is analysed [11], [13]. The experimental 4-channel DWDM optical transmission system model is used to evaluate system effectiveness for different bitrates of up to 40 Gbit/s per wavelength and compare widely used techniques of CD post-compensation in terms of received signal quality, e.g., bit-error-ratio (BER) and eye diagrams [14]. The total transmission capacity of the investigated DWDM system is up to 160 Gbit/s.

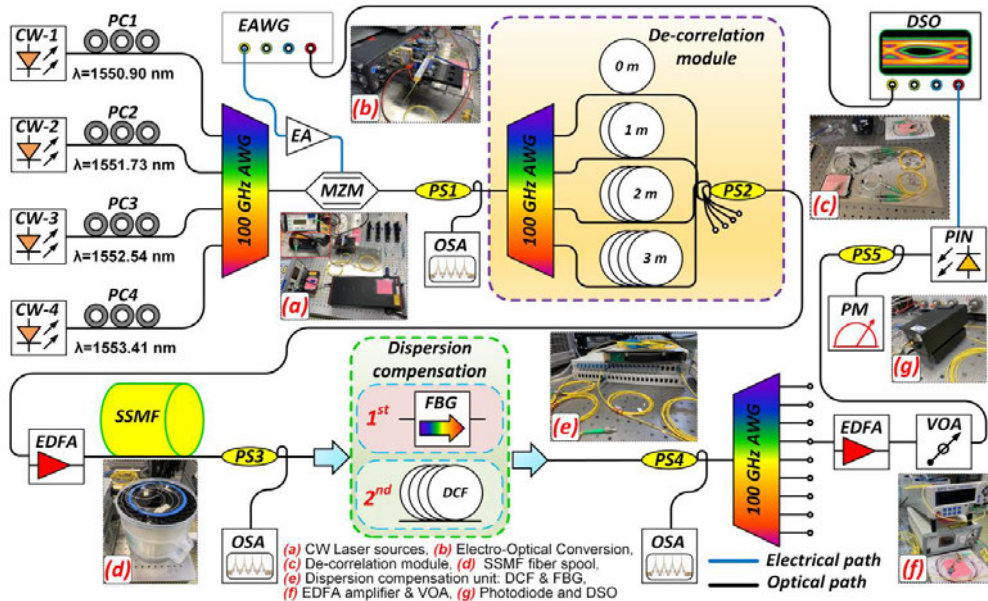
II. EXPERIMENTAL SETUP OF DWDM C-BAND TRANSMISSION SYSTEM

Through the development of experimental 100 GHz spaced dense WDM optical system, we compared most often used dispersion compensation CD techniques and obtained system performance indicators at operating bitrate of up to 40 Gbit/s per channel under the condition that is still possible to achieve BER threshold of 10^{-3} with the 7% Forward Error Correction (FEC) overhead [9], [11], [13].

Experimentally we have shown chromatic dispersion CD compensation technique's effectiveness with the use of implemented fiber Bragg grating dispersion compensation module (FBG-DCM) and dispersion compensating fiber (DCF) for 4-channel 100 GHz spaced dense NRZ-OOK modulated WDM optical transmission system after 40 km transmission through standard single-mode fiber (SSMF) span. A more detailed description of both techniques is

given in Section IV. The experimental system part is depicted in Fig. 1. The output of four continuous-wave (CW) laser sources with channel spacing of 100 GHz with related 10 dBm output power for each particular source are coupled together by 100 GHz spaced arrayed waveguide grating (AWG) multiplexer/de-multiplexer [15]. Polarization controllers (PCs) are placed before the multiplexer to reduce the polarization-dependent loss of each laser source. The output of AWG is connected to the input of the external Mach-Zehnder modulator (MZM). MZM (bias point 3.14 V) is driven at bitrates from 20 Gbit/s up to 40 Gbit/s by a 2^{11} long pseudo-random bit sequence (PRBS11) non-return-to-zero (NRZ) signal from Keysight M9502A electrical arbitrary waveform generator (EAWG).

The modulated output from the MZM is connected to the de-correlation module through a monitoring splitter (PS1) for measurements of the optical spectrum by Advantest Q8384 optical spectrum analyzer (OSA). A more detailed description of this module is given in Section III. The output of the de-correlation module with four separated and delayed WDM channels is amplified by the first erbium-doped fiber amplifier (EDFA) with fixed output power (+23 dBm) and transmitted through 40 km long ITU-T G.652 standard SSMF fiber span with dispersion coefficient 17.15 ps/(nm × km), dispersion slope 0.096 ps/nm², and 0.27 dB/km attenuation coefficient (at $\lambda = 1550$ nm reference wavelength). The monitoring splitters, (PS3) after transmission through SSMF fiber before dispersion CD post-compensation and (PS4) after CD post-compensation for optical spectrum measurements, are used as well.



CW: Continuous wavelength laser source, PC: polarization controller, EAWG: electrical arbitrary waveform generator, EA: electrical amplifier, MZM: Mach-Zehnder modulator, PS: power splitter, OSA: optical spectrum analyzer, EDFA: erbium-doped fiber amplifier, SSMF: standard single mode fiber, FBG-DCM: fiber Bragg grating dispersion compensation module, DCF: dispersion compensating fiber, VOA: variable optical attenuator, PM: optical power meter, PIN: photodiode, DSO: digital storage oscilloscope.

- 4 WDM channels
- CD compensation: FBG-DCM & DCF
- Optical line length $L = 40$ km
- Transmission speed per channel
- NRZ coding
- Channel spacing $\Delta\lambda = 100$ GHz
- Transmission over: C-band
- $R = 20, 25, 28, 32, 40$ Gbit/s

Fig. 1. Experimental setup for comparison of effectiveness of dispersion compensation techniques in 4-channel NRZ-OOK modulated DWDM optical transmission system with total transmission capacity of up to 160 Gbit/s.

The CD post-compensation is consecutively investigated by using:

1. *Tunable fiber Bragg grating dispersion compensation module FBG-DCM*, which has 3.5 dB insertion loss at $\lambda = 1550$ nm wavelength, dispersion coefficient of -680 ps/(nm \times km);
2. *Dispersion compensation fiber (DCF)* spool with a length of 5.684 km, which has 4.75 dB insertion loss (at $\lambda = 1550$ nm reference wavelength) with dispersion coefficient of -686.76 ps/nm/km, and -2.48 ps/nm² dispersion slope was used as well.

After transmission through SSMF fiber span and CD post-compensation, the 100 GHz spaced AWG de-multiplexer is connected to the second EDFA with fixed +10 dBm output power. The output of the EDFA amplifier is connected to 50 GHz photodiode (PIN) with sensitivity equal to +4 dBm for BER of 10^{-12} , the dark current of 10 nA and responsivity of 0.8 A/W through a variable optical attenuator (VOA). The received signal is sampled by Keysight DSAZ334A digital storage oscilloscope (DSO) with 33 GHz analogue bandwidth operating at 80 GSa/s for measurements of received signal bit patterns quality (e.g., eye diagrams) and BER [16].

III. WAVELENGTH DIVISION MULTIPLEXED (WDM) CHANNEL SEPARATION AND DELAY WITH THE USE OF A DE-CORRELATION TECHNIQUE

In our research, to increase the capacity of the experimental communication system and observe the effects of crosstalk, we increased the number of WDM channels by implementing a symmetrical adaptive de-correlation (SAD) method, which has also been used in other research works

[17]. MZM modulator used in our experimental transmission system is driven at bitrates from 20 Gbit/s up to 40 Gbit/s by a $2^{11}-1$ long pseudo-random bit sequence NRZ signal from an electrical arbitrary waveform generator (EAWG).

The outputs of four laser sources with a spacing of 100 GHz are coupled together by AWG multiplexer and sent to the MZM input. After MZM output, four 100 GHz spaced modulated optical channels are being separated with the de-correlation module, which consists of (1) (see Fig. 2) 100 GHz spaced AWG de-multiplexer, (2) (see Fig. 2) SMF optical fiber spans with different length, and (3) (see Fig. 2) optical coupler. After separation of modulated optical signals, the optical SMF fiber spans with different lengths are used for time delay, where 1 meter long optical fiber span is used for the second channel, 2 meters and 3 meters long SMF spans are used for third and fourth separated WDM channels, respectively. The first output of 100 GHz spaced AWG de-multiplexer is connected directly to the coupler. After each optical channel has been de-correlated, optical coupler for further data transmission combines all channels.

Each transmitted bit length of the optical fiber according to the used bitrate is calculated by the following equation, where SMF fiber core refraction index is 1.4682 at $\lambda = 1550$ nm wavelength

$$L = T \times \left(\frac{c}{n_g} \right) \times 100, \quad (1)$$

where L is fiber length for 1 bit (cm), T - bit duration (s), c - light speed in vacuum (km/s), and n_g - optical fiber effective group index of refraction.

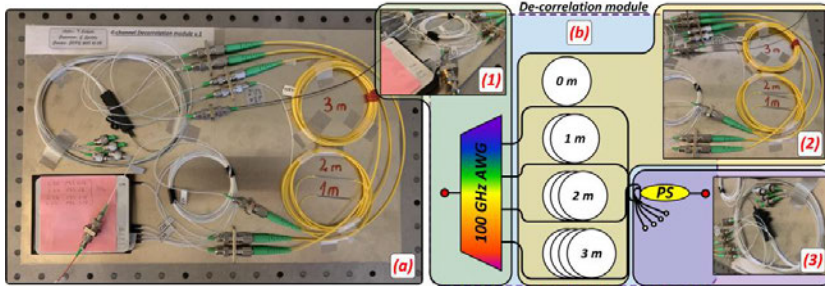


Fig. 2. Setup of de-correlation module: (a) experimentally created; (b) schematics of channel separation principle, where such optical components are used: (1) 100 GHz spaced AWG de-multiplexer, (2) SMF optical fiber spans, (3) 1×8 optical couplers.

According to the bitrate (from 20 Gbit/s up to 40 Gbit/s) of the NRZ-OOK signal, the optical path length of 1 bit is shown in Table I.

TABLE I. OPTICAL PATH LENGTH FOR 1 BIT OF TRANSMISSION.

Bitrate (Gbit/s)	20	25	28	32	40
Fiber length for 1 bit transmission (cm)	1,02	0,81	0,72	0,63	0.51

The each separated modulated NRZ-OOK signal based on the used de-correlation technique accordingly by the used bitrate per channel with PRBS11 sequence has a constant bit-stream delay (Table II).

TABLE II. PRBS11 DELAY IN BITS FOR TRANSMISSION SYSTEM BY USE OF DE-CORRELATION TECHNIQUE.

Experimentally used bitrate Gbit/s					
Bitrate (Gbit/s)	20	25	28	32	40
PRBS delay (bits)	98	122	137	157	196
% of total PRBS length	5 %	6 %	7 %	8 %	10 %
PRBS delay (bits)	196	245	274	313	392
% of total PRBS length	10 %	12 %	13 %	15 %	19 %
PRBS delay (bits)	294	367	411	470	587
% of total PRBS length	14 %	18 %	20 %	23 %	29 %

IV. EVALUATION OF CHOSEN DISPERSION COMPENSATION TECHNIQUES

Different chromatic dispersion CD compensation methods are used for wavelength division multiplexed (WDM) optical transmission networks, such as for passive optical access networks (PONs). The most commonly used CD compensation techniques for optical transmission networks are realized with Fiber Bragg grating (FBG), dispersion compensating fiber (DCF), electronic dispersion compensation (EDC), digital filters, and optical phase conjugator (OPC) [18]. Widely used FBG and DCF CD compensation methods are considered for comparison in our research. Implementation of FBG and DCF post-compensation in experimental DWDM 100 GHz spaced optical transmission system shows the relevance of system's performance depending on the used CD compensation technique.

Next-generation (NG) dense wavelength division multiplexed (DWDM) optical transmission systems will deal with the rising bandwidth needs of backbone optical transport networks. With the use of narrow spacing according to ITU-T G.654.2, the definition of flexible grids between wavelength bands will increase the number of optical channels and enable bitrates of several Terabits per second (Tbps) in a single optical fiber [4]. Nowadays, optical transmission systems are developed for laser-light wavelengths in the C-band, and later in the L-band leveraging the wavelengths with the lowest attenuation rates in optical fibers. The use of optical amplification methods is a key enabling technology for WDM systems, which might use many wavelengths at the same time. Several amplification methods are used for enhancing signals of WDM transmission systems. Therefore, widely erbium-doped fiber amplification EDFA technology is conventional for more common use in C-band (1530 nm to 1562 nm). Thereby, it is introduced in our investigated experimental 4-channel 100 GHz spaced NRZ modulated DWDM optical system [13]. Chromatic dispersion CD is a fundamental problem in optical networks related to broadening light pulses as they travel through the optical fiber. The propagation characteristics of each wavelength depend on the optical fiber glass refractive index of the medium and on the non-linearity of the propagation constant. Eventually, it will result in a distortion of the signal, which leads to inter-symbol interference (ISI) begin to overlap causing the bit error rate to increase. To protect the optical signals from the affection of CD during transmission in our investigated 4-channel 100 GHz spaced NRZ modulated DWDM optical system, the comparison of appropriate CD post-compensation techniques located at remote terminal (RT) section under NG-PON2 mentioned requirements are discussed [11], [14].

In the first scenario, we realize dispersion post-compensation based on fiber Bragg gratings (FBG) tunable dispersion compensation module (DCM) designed for use of compensation for all channels across the entire C-band enabling to apply for 100 GHz channel grid with the bandwidth of 100 GHz for current WDM channel. The main advantage is low insertion loss of 3.5 dB and greater power

capacity without introducing additional non-linear signal effects (NOE).

Secondly, we introduce dispersion post-compensation based on dispersion compensating fiber DCF, which is being used previously, as well as extensively used for optical fiber links operating at a 1550 nm band. The longer wavelengths will travel slower than the smaller wavelengths of the pulse in case of SMF fiber comparatively to dispersion compensating fiber manufactured for telecom wavelengths. In such a case of DCF, the longer wavelengths will travel faster than the shorter wavelengths and the pulse will tend to reshape itself into its original form. To determine the exact dispersion coefficient for the standard single-mode optical fiber used in the experimental part and find out the necessary length of DCF fiber spool for total accumulated dispersion compensation, we previously performed CD and optical time-domain (OTDR) measurements with EXFO FTB-500 for SSMF fiber span. We prepare OTDR measurements for experimentally used SMF fiber span to clarify the optical link section match of our experimental 4-channel 100 GHz spaced NRZ modulated DWDM system to ITU-T G.989.2 recommendation defined optical distribution network ODN length. In our experimental optical transmission system, the second EDFA was used in terms to satisfy the input optical power level of high power InGaAs 50 GHz PIN photoreceiver. In such case under high-speed up to 40 Gbit/s WDM transmission systems conditions, where post-amplification is not required, as PIN photo receiver's avalanche photodiode (APD) with a much lower input power level is used [16]. According to verified measurements, we conclude that the length of our experimentally used SSMF fiber span is 42.13 km with 11.49 dB total insertion loss. The obtained OTDR graphs of the results are not included in this paper. The experimentally measured SMF fiber span chromatic dispersion coefficient and total chromatic dispersion depending on bandwidth in telecommunication S, C, and L transmission bands (Fig. 3). As one can see in Fig. 3, the standard single-mode optical fiber span measured dispersion coefficient and total dispersion at reference wavelength $\lambda = 1550$ nm is 17.15 ps/(nm \times km) and 688.71 ps/nm at dispersion slope of 0.096 ps/nm², respectively.

The most suitable DCF optical fiber span was selected to perform the necessary accumulated dispersion compensation. Afterward, after the most appropriate choice, we prepare optical domain OTDR measurements to latest calculate achieved DWDM system's optical link sections length. According to verified OTDR measurements, we conclude that the length of our experimentally used dispersion compensating fiber spool is 5.68 km with 4.75 dB total insertion loss of 0.83 dB/km. Experimentally obtained dispersion compensating fiber spool CD coefficient and total chromatic dispersion depending on bandwidth in telecommunication S, C, and L transmission bands (Fig. 4). As one can see in Fig. 4, the DCF fiber spool measured dispersion coefficient and total dispersion at reference wavelength $\lambda = 1550$ nm is -123.06 ps/(nm \times km) and -697.82 ps/nm at -2.48 ps/nm² dispersion slope, respectively. DCF fiber gives us the opportunity to increase the length of our 4-channel 100 GHz spaced DWDM optical transmission

system for an additional 5.68 km or extra 13.5 % and 47.81 km. achieve the maximum DWDM system's link length of

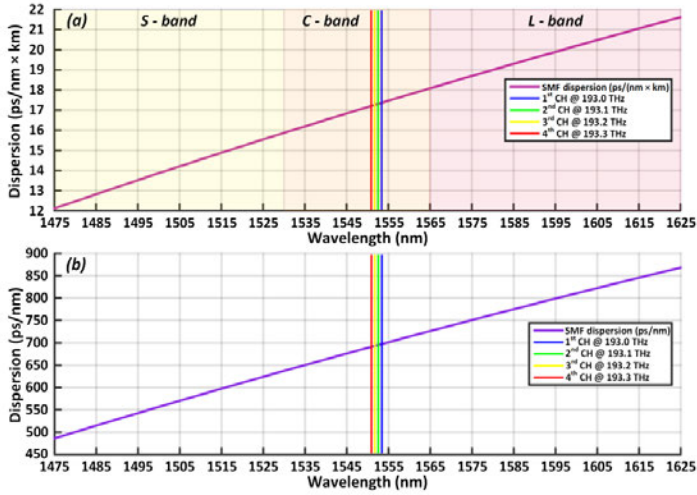


Fig. 3. Experimentally measured SMF fiber span: (a) chromatic dispersion coefficient and (b) total chromatic dispersion depending on bandwidth and wavelength used.

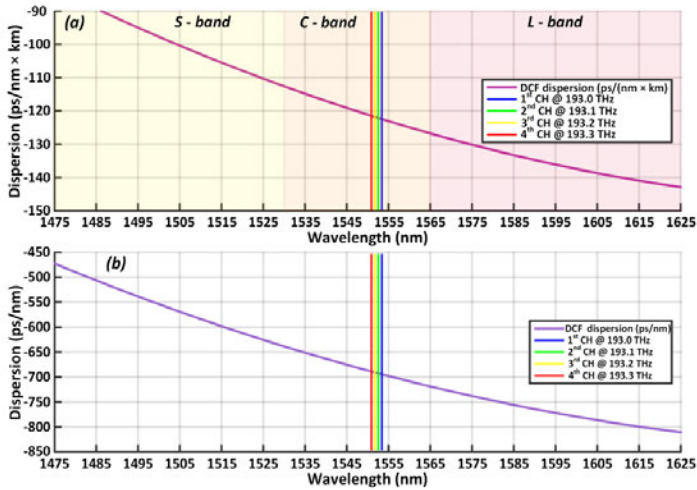


Fig. 4. Experimentally measured DCF fiber spool: (a) chromatic dispersion coefficient and (b) total chromatic dispersion depending on bandwidth and wavelength used.

V. RESULTS AND DISCUSSION

In our research, we implemented experimentally two different CD compensation techniques to observe the quality of the received signal and obtain limiting factors of physical parameters, the impact of used components, such as fiber Bragg grating dispersion compensation module (FBG-DCM) and widely used dispersion compensating fiber allowing us to observe additional non-linear optical effects (NOE).

According to next-generation (NG-PON2) ITU-T G.989.2 rec. requirements, we extend the SSMF link section up to 40 km [4]. Results are obtained in two different scenarios: 1st by use of fiber Bragg grating DCM and 2nd with the use of dispersion compensating fiber DCF for total dispersion

compensation of 688.71 ps/nm. Figure 5 shows experimentally obtained BER of transmitted NRZ-OOK signal with a bitrate from 20 Gbit/s up to 40 Gbit/s per channel versus received optical power at 50 GHz PIN photoreceiver. The measured optical output power after transmission through a 40 km fiber link section with FBG-DCM post-compensation varied from -0.21 dBm to 6.8 dBm, where the BER of received signal was from 5×10^{-2} to 1×10^{-10} . In such a way, the second scenario with DCF post-compensation, where measured optical output power after transmission through 47.81 km fiber link section (SMF + DCF length) varied from -1.65 dBm to 6.8 dBm, the BER of received signals was from 5.8×10^{-2} to 9.73×10^{-12} , respectively.

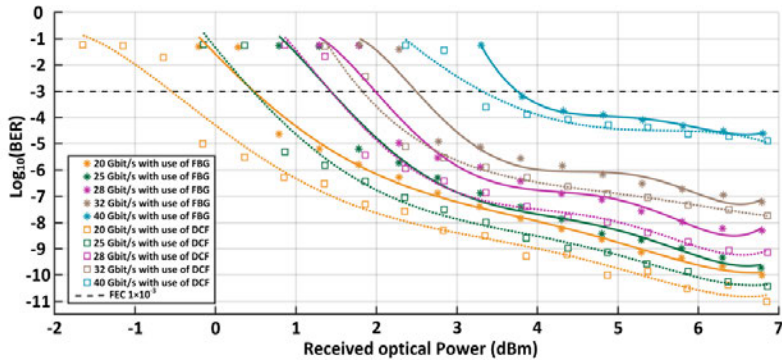


Fig. 5. Comparison of experimentally measured BER versus received optical power with use of: (1) fiber Bragg grating dispersion compensation module (FBG-DCM), (2) dispersion compensation fiber (DCF) depending of bitrate per channel for investigated 4-channel 100 GHz spaced DWDM optical transmission system.

As one can see in Fig. 6(a), the 4-channel 100 GHz spaced NRZ modulated and de-correlated optical signals spectrum before launching into a 40 km long SSMF fiber span of DWDM optical transmission system, which is driven by one Mach-Zehnder modulator MZM and operating at a bitrate up to 40 Gbit/s per channel, are shown. Ensuring difference of received optical signals firstly after transmission through 40 km long SSMF fiber span and secondly after use of DCF dispersion post-compensation for 4-channel 100 GHz spaced NRZ modulated and de-

correlated DWDM transmission system (Figs. 6(b) and 6(c)). We conclude that the optical spectrum after the FBG-DCM post-compensation module has only impact depending on FBG module physical bandwidth limitations with independent 3.5 dB insertion loss at the reference wavelength $\lambda = 1550$ nm. Therefore, optical signals spectrum after transmission through 40 km long optical fiber link section with the use of FBG-DCM post-compensation is not shown.

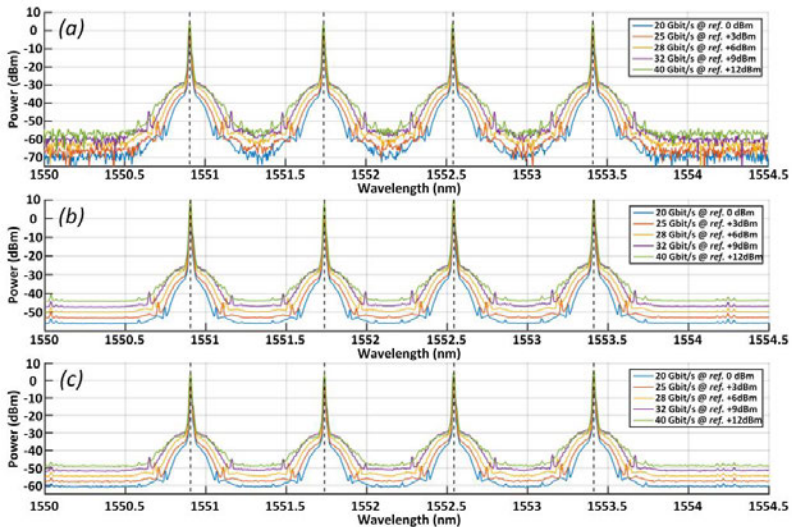


Fig. 6. Optical spectra: (a) after B2B transmission through SSMF fiber; (b) after 40 km transmission through SSMF fiber; (c) after 40 km transmission through SSMF fiber with use of dispersion compensation by DCF for multiplexed 4-channel NRZ modulated DWDM optical transmission system at bitrates of up to 40 Gbit/s per channel.

Therefore, we conclude that the optical spectrum after direct transmission through a 40 km SSMF fiber span and after transmission with the use of DCF post-compensation additionally extending the total length of the optical link section up to 47.81 km has significant changes. Applying for use of DCF post-compensation for our 4-channel 100 GHz spaced NRZ modulated DWDM transmission system, the

received optical signals are mainly affected by the impact of NOE effects. The Four-Wave Mixing (FWM) generating interactions between the information signals and the fiber medium occurs in the case of WDM systems, where the wavelength channel spacing is very close to each other. The reason for that is the input optical power of a DCF fiber, which exceeds a certain value optical power density in the

fiber core and becomes excessively high because the effective cross-sectional area of the fiber is only $A_{\text{eff}} = 20 \mu\text{m}^2$ triggering the non-linear polarization of fiber materials. Changes in the decrease of received optical power level before PIN photoreceiver applying for use of dispersion compensation fiber have explained by the impact due to fiber insertion loss 0.83 dB/km at the reference wavelength $\lambda = 1550 \text{ nm}$.

As one can see in Fig. 7, the experimentally received signal after 40 km transmission through SSMF optical fiber

link with dispersion compensation by (a) fiber Bragg grating dispersion compensation module (FBG-DCM) and (b) by dispersion compensation fiber (DCF) for investigated NRZ modulated 4-channel 100 GHz spaced DWDM optical transmission system at operating bitrates of up to 40 Gbit/s per channel is good, eye is open, and error-free transmission is provided. In our research, we show received signal with the worst BER performance for the 2nd channel, where the highest impact of crosstalk is observed compared to other WDM channels in the current transmission system.

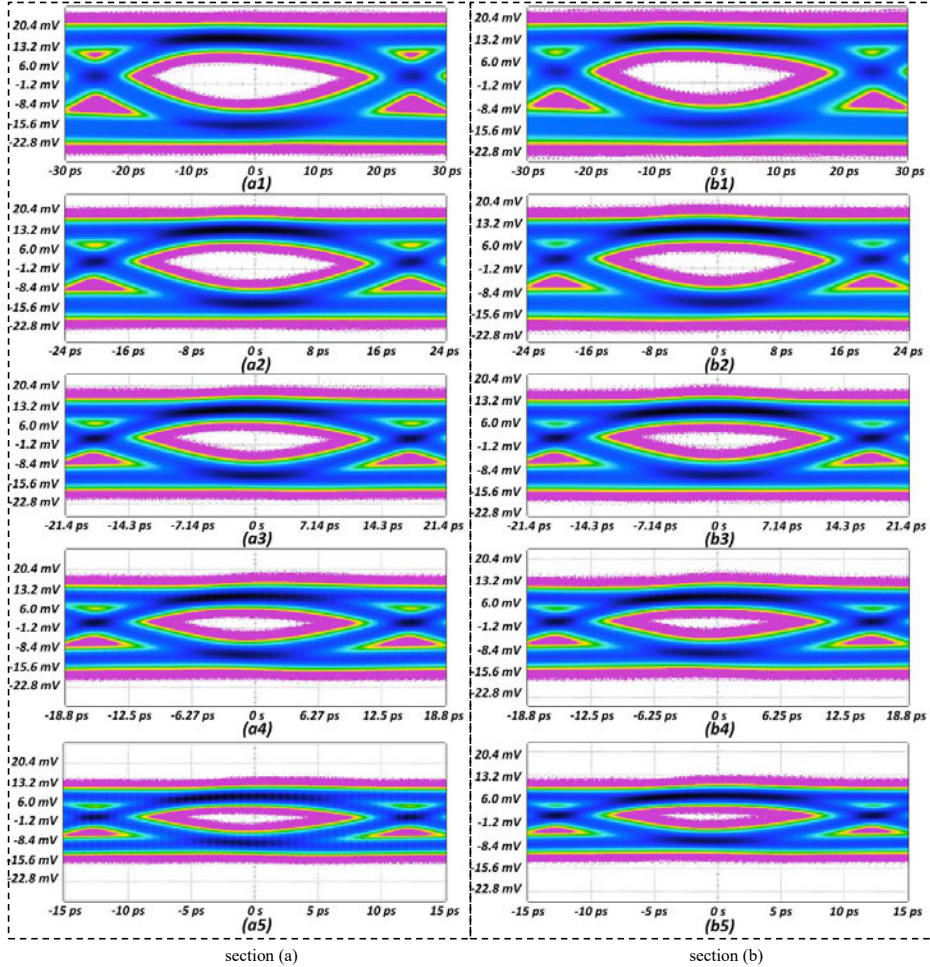


Fig. 7. Eye diagrams of experimentally received signal after 40 km transmission through SSMF fiber with dispersion compensation by (a1–a5) fiber Br

agg grating dispersion compensation module (FBG-DCM), (b1–b5) dispersion compensation fiber (DCF) for investigated NRZ-OOK modulated 4-channel 100 GHz spaced DWDM optical transmission system at bitrates of 20 Gbit/s, 25 Gbit/s, (3) 28 Gbit/s, (4) 32 Gbit/s, and (5) 40 Gbit/s per channel.

We have demonstrated performance comparison for 4-channel 100 GHz spaced NRZ modulated DWDM transmission system at operating total capacity up to 160 Gbit/s over 40 km SSMF fiber optical link with different dispersion-compensating techniques. Additional insertion losses in dispersion compensating optical fiber DCF line and affection of NOE on transmitted signals lead to performance decrease of our experimental 4-channel 100 GHz spaced DWDM optical transmission system, where the BER at

operating 20 Gbit/s and 40 Gbit/s bitrate per channel of received signal was 5.8×10^{-2} and 1.27×10^{-5} due to optical power level on PIN photoreceiver -1.65 dBm and $+2.36 \text{ dBm}$ (see Figs. 7(b1) and 7(b5)).

After decreasing total optical link length by replacing DCF and applying for fiber Bragg grating tunable DCM module, from obtained results, we conclude that NOE effects are reduced significantly, where the BER of operating at 20 Gbit/s and 40 Gbit/s bitrates per channel was 5×10^{-2}

and 2.45×10^{-5} due to optical power level on PIN photoreceiver -0.21 dBm and 3.3 dBm (see Figs. 7(a1) and 7(a5)). As one can see in Fig. 7, comparison depending on bitrate per channel from 20 Gbit/s up to 40 Gbit/s, with previously discussed dispersion compensation techniques implementation into our experimental 4-channel DWDM optical transmission system, according to systems performance, the received signal quality is shown (e.g., eye diagrams of received bit patterns).

VI. CONCLUSIONS

The newest technology of the next decade fulfilled by mobile and broadband services, e.g., large-scale latest-generation cellular network coverage inter-connections and data center interconnections (DCI), pushes hard communication infrastructures to be optimized and upgraded. Enabling the development of new technologies, the choice of dispersion compensation technique plays a critical role in high-speed fiber optical communication system performance and the possibility to provide and satisfy high demand bitrates for bandwidth-hungry end-users. Nowadays, the problems of transmission capacity and channel utilization are related to the correct choice of modulation format, which is a key to enable higher spectral efficiency and potentially provide higher data transmission speeds through fiber optical networks with limited bandwidth, where one of the physical main distance-limiting factors is chromatic dispersion, which leads to inter-symbol interference and distortion of the signal waveform.

The purpose of the experimental system created during this research was to compare the effectiveness of such a widely used chromatic dispersion compensation techniques like fiber Bragg grating dispersion compensation module (FBG-DCM) and dispersion compensating fiber (DCF). This comparison was performed by implementing both techniques into developed 4-channel DWDM transmission system allowing to provide high bitrate transmission over 40 km standard single-mode fiber line section reaching total WDM system capacity of 160 Gbit/s under the condition that is still possible to achieve commercial pre-FEC BER threshold 1×10^{-3} with 7 % FEC overhead being used.

Experimentally obtained data and implemented CD compensation techniques showed that with the significant increase of channel bitrate from 20 Gbit/s up to maximal achievable bitrate - 40 Gbit/s per channel the performance reduction was observed in 4-channel 100 GHz spaced DWDM optical transmission system.

Depending on NRZ-OOK modulated signal bitrate, the BER of the signal at the receiver at 20 Gbit/s and 40 Gbit/s bitrates varied from 5×10^{-2} to 1×10^{-10} and 5.8×10^{-2} to 9.73×10^{-12} with CD post-compensation by FBG-DCM and DCF, respectively. When the FBG-DCM post-compensation module was applied, we observed the negative filtering effect of channelized FBG, which has physical bandwidth limitations. Therefore, in our setup, DCF post-compensation extended the total length of the optical link section more than it was observed with FBG-DCM. Also, when DCF was used for CD compensation, we observed the signal degradation caused by NOE effects, such as FWM. In

addition to DCF fiber losses, which reduce the optical power output level, caused an adverse effect in terms of receiver sensitivity, which depends on the targeted BER level and the signal bitrate.

CONFLICTS OF INTEREST

The authors declare that they have no conflicts of interest.

REFERENCES

- [1] ITU-T Recommendation Y.Supp.29 to ITU-T Y.4250 series - series y: global information infrastructure, internet protocol aspects and next-generation networks, internet of things and smart cities: ITU-T Y.4250 series - Smart Sustainable Cities - "Multi-service infrastructure in new-development areas", pp. 4–27, 2016.
- [2] X. Sun, M. Yang, and I. B. Djordjevic, "Real-time FPGA-based rate adaptive LDPC coding for data center networks and PONs", in *Proc. of 2018 European Conference on Optical Communication (ECOC)*, Rome, Italy, Sept. 2018, pp. 1–3. DOI: 10.1109/ECOC.2018.8535131.
- [3] T. Salgals, I. Kurbatska, S. Spolitis, V. Bobrovs, and G. Ivanovs, "Research of M-PAM and duobinary modulation formats for use in high-speed WDM-PON systems", in *Telecommunication Systems: Principles and Applications of Wireless-Optical Technologies*. IntechOpen, Feb. 2019. DOI:10.5772/intechopen.84600.
- [4] ITU-T Recommendation G.989.2, "Digital sections and digital line system - Optical line systems for local and access networks-40-Gigabit-capable passive optical networks 2 (NG-PON2): Physical media dependent (PMD) layer specification", pp. 10–92, 2014.
- [5] K. Zeb, X. Zhang, and Z. Lu, "High capacity mode division multiplexing based MIMO enabled all-optical analog millimeter-wave over fiber fronthaul architecture for 5G and beyond", *IEEE Access*, vol. 7, pp. 89522–89533, 2019. DOI: 10.1109/ACCESS.2019.2926276.
- [6] G. N. Liu, L. Zhang, T. Zuo, and Q. Zhang, "IM/DD transmission techniques for emerging 5G fronthaul, DCI, and metro applications", *Journal of Lightwave Technology (JLT)*, vol. 36, no. 2, pp. 560–567, Jan. 2018. DOI: 10.1109/JLT.2018.2793313.
- [7] K. Keykhosravi, M. Secondini, G. Durisi, and E. Agrell, "How to increase the achievable information rate by per-channel dispersion compensation", *Journal of Lightwave Technology (JLT)*, vol. 37, no. 10, pp. 2443–2451, 2019. DOI: 10.1109/JLT.2019.2907311.
- [8] R. K. Ahmed and H. A. Mahmood, "Performance analysis of PAM intensity modulation based on dispersion compensation fiber technique for optical transmission system", in *Proc. of 2018 1st International Scientific Conference of Engineering Sciences - 3rd Scientific Conference of Engineering Science (ISCES)*, Diyala Iraq, Jan. 2018, pp. 126–130. DOI: 10.1109/ISCES.2018.8340540.
- [9] ITU-T Recommendation G.709/Y, "Transmission systems and media digital systems and networks - Global information infrastructure, internet protocol aspects and Next-generation networks, internet of things and smart cities", pp. 1–89, 2016.
- [10] F. Lu, M. Xu, L. Cheng, J. Wang, S. Shen, H. J. Cho, and G. Chan, "Adaptive digitization and variable channel coding for enhancement of compressed digital mobile fronthaul in PAM-4 optical links", *Journal of Lightwave Technology (JLT)*, vol. 35, no. 21, pp. 4714–4720, Nov. 2017. DOI: 10.1109/JLT.2017.2749567.
- [11] T. Salgals, S. Spolitis, S. Olonkins, and V. Bobrovs, "Investigation of 4-PAM modulation format for use in WDM-PON optical access systems", in *Proc. of Progress in Electromagnetics Research Symposium (PIERS 2017)*, St. Petersburg Russia, May 2017, p. 1–4. DOI: 10.1109/PIERS.2017.8262162.
- [12] R. Lin, J. V. Kerrebrouck, X. Pang, M. Verplaetse, O. Ozolins, A. Udalcovs, L. Zhang, L. Gan, M. Tang, S. Fu, R. Schatz, U. Westergren, S. Popov, D. Liu, W. Tong, T. D. Keulenaer, G. Torfs, J. Bauwelinck, X. Yin, and J. Chen, "Real-time 100 Gbps/core NRZ and EDB IM/DD transmission over multicore fiber for intradatacenter communication networks", *Opt. Express*, vol. 26, no. 8, pp. 10519–10526, 2018. DOI: 10.1364/OE.26.010519.
- [13] S. Olonkins, V. Bickovs, T. Salgals, V. Bobrovs, and G. Ivanovs, "Investigation of dual-pump FOPA performance in a 4-channel 40 Gbps WDM transmission system", *Elektronika ir Elektrotechnika*, vol. 23, no. 6, pp. 85–89, 2017. DOI: 10.5755/j01.eie.23.6.19699.
- [14] A. Korra, T. Salgals, J. Porins, E. Kazoks, R. Miho, and S. Spolitis, "Performance analysis of cost-efficient high-speed up to 32 Gbit/s WDM-PON next-generation access network with dispersion

- compensation”, in *Proc. of Progress in Electromagnetics Research Symposium (PIERS 2019)*, Rome, Italy, Jun. 2019, pp. 1–7. DOI: 10.1109/PIERS-Spring46901.2019.9017854.
- [15] ITU-T Recommendation G.694.1, “Transmission media and optical systems characteristics - Characteristics of optical systems: Spectral grids for WDM applications: DWDM frequency grid”, pp. 7–12, 2012.
- [16] Discovery Semiconductors Inc., High optical power handling InGaAs photodiodes to 50GHz, Technical Specification, 2003.
- [17] Z. Tao, W. Yan, L. Dou, L. Li, S. Oda, T. Hoshida, and J. C. Rasmussen, “The impact of DWDM channel de-correlation method in optical PSK coherent transmission experiment”, in *Proc. of 2009 35th European Conference on Optical Communication (ECOC)*, Vienna, Austria, Sep. 2009, pp. 1–2.
- [18] K. Nakshdeep and K. Gurmeet “Various dispersion compensation techniques for optical system: A survey”, *Open Journal of Communications and Software*, vol 1, no. 1, p. 1–10, May 2014. DOI: 10.15764/CS.2014.01006.

PAPER-6: Performance Enhancement of Multi-Core Fiber Transmission Using Real-Time FPGA Based Pre-Emphasis

G.K.M. Hasanuzzaman, **S. Spolitis**, **T. Salgals**, J. Braunfelds, A. Morales, L. E. Gonzalez, S. Rommel, R. Puerta, P. Asensio, V. Bobrovs, S. Iezekiel, I. Tafur. Monroy, "Performance Enhancement of Multi-Core Fiber Transmission Using Real-Time FPGA Based Pre-Emphasis", *Asia Communications and Photonics Conference (ACP)*, Guangzhou, November 10-13, (2017), DOI: [10.1364/ACPC.2017.M2H.1](https://doi.org/10.1364/ACPC.2017.M2H.1)

Performance Enhancement of Multi-Core Fiber Transmission Using Real-Time FPGA Based Pre-Emphasis

G.K.M. Hasanuzzaman^(1,3), S. Spolitis⁽²⁾, T. Salgals⁽²⁾, J. Braunfelds⁽²⁾, A. Morales⁽³⁾, L. E. Gonzalez⁽⁴⁾,
S. Rommel⁽³⁾, R. Puerta⁽³⁾, P. Asensio⁽³⁾, V. Bobrovs⁽²⁾, S. Iezekiel⁽¹⁾ and I. Tafur Monroy⁽⁵⁾

⁽¹⁾Microwave Photonics Research Laboratory, University of Cyprus, 1055 Latsia, Cyprus

⁽²⁾Institute of Telecommunications, Riga Technical University, LV-1048, Riga, Latvia

⁽³⁾Department of Photonics Engineering, Technical University of Denmark, 2800 Kgs. Lyngby, Denmark

⁽⁴⁾Departament de Física, Universidad del Valle, Cali, Colombia

⁽⁵⁾Department of Electrical Engineering, Technische Universiteit, 5600 Eindhoven, Netherlands

ghasan01@ucy.ac.cy, sandis.spolitis@rtu.lv

Abstract: We experimentally demonstrate pre-emphasis based performance for a 2 km long 7-core multicore fiber link. Simultaneous transmission below the FEC threshold is achievable for all cores by using signal equalization in a FPGA.

OCIS codes: (060.2270) Fiber characterization; (060.2360) Fiber optics links and subsystems.

1. Introduction

As single-core single-mode fiber (SC-SMF) approaches its fundamental limit of 100 Tbps due to limitations from amplifier bandwidth, nonlinear noise and fiber fuse phenomena [1], multicore fibers (MCFs) offer scaling of transmission capacity through space division multiplexing (SDM). Apart from data communications, MCF technology is also being considered for microwave photonics applications such as multi-cavity optoelectronic oscillators [2], and signal processing [3], since it offers identical mechanical and environmental conditions for all parallel cores. Several experimental results have been reported regarding the implementation of SDM in systems with MCFs, including 109 Tbps in a 7-core fiber [4], 112 Tbps in a 7-core fiber [5], 305 Tbps in a 19-core fiber [6], and 1.02 Pbps in a 12-core fiber [7]. Furthermore, MCFs have also been implemented in fiber-wireless links such as a full duplex, 802.11ac-compliant, 3×3 Multiple-Input Multiple-Output (MIMO) system using 7-core fiber [8], and Centralized Radio Access Networks (C-RANs) [9].

However, crosstalk between neighboring cores is a fundamental limitation of MCFs in SDM applications. Crosstalk fundamentally arises due to power coupling between the adjacent cores during signal propagation and can be determined from the structural parameters of MCFs. Imperfect splices and multicore erbium doped fiber amplifiers also affect crosstalk [10]. There are basically two known approaches for crosstalk reduction: (i) the first is to reduce the coupling coefficient between the cores in a homogeneous MCF, as in trench-assisted or hole-assisted MCFs [1]; (ii) the second approach is to introduce an intrinsic index difference between the adjacent cores, resulting in heterogeneous core MCFs. In addition to modified MCFs, offline digital signal processing (DSP) techniques and MIMO equalization [5,11], have been used to reduce the impact of crosstalk in strongly coupled 3-core MCFs. However, DSP introduces additional latency in the system which is undesirable in applications such as 5G networks [12].

In this paper we characterize a 2 km long 7-core MCF and experimentally demonstrate low-latency, FPGA-based real-time transmissions. By means of adaptive pre-emphasis, deterministic distortions due to the limited bandwidth of the link are compensated. Experimental results show that a 2.5 Gbps non-return-to-zero on-off-keying (NRZ-OOK) modulated signal in each core can be transmitted with a BER level below the FEC limit, enabling post-FEC error-free transmission.

2. Characterization of the Multi-Core Fiber

We characterized the crosstalk level and insertion loss of a 2 km 7-core MCF. To measure the pairwise crosstalk and insertion loss of the MCF fiber, we launched optical power from a laser diode to each one of the cores in turn and measured the output of each core with a high sensitivity optical power meter, thus obtaining a 7×7 coupling matrix. Fig. 1(a) shows the measured pair-wise power coupling between all 7 cores. The total crosstalk (summation of each core contribution) is shown in Fig. 1(b). The central core (core 0) exhibits the highest crosstalk as expected and other outer cores (1,2,4,6) have roughly equal crosstalk where core 3 and core 5 are much lower and higher than the other outer cores, respectively.

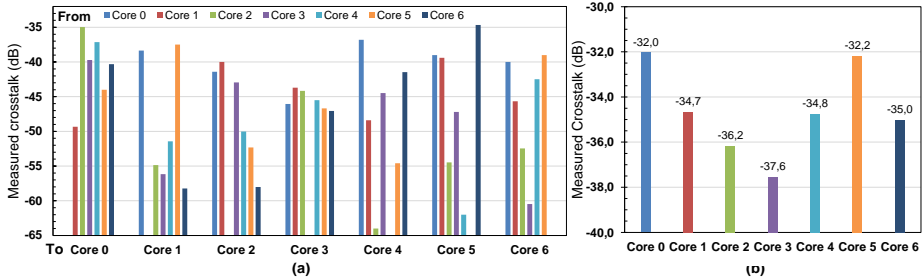


Fig. 1: (a) Measured pairwise crosstalk between cores and (b) measured total crosstalk per core.

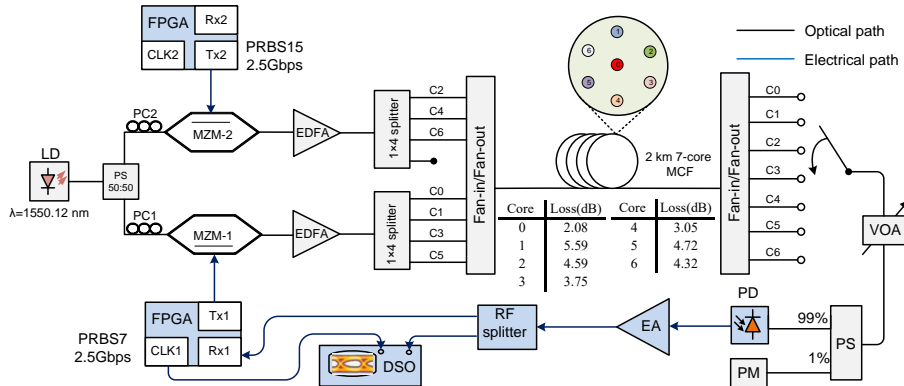


Fig. 2: Experimental setup for BER and eye diagrams measurements.

LD: laser diode, PS: power splitter, PC: polarization controller, MZM: Mach-Zehnder modulator, FPGA: field-programmable gate array, PRBS: pseudo-random binary sequence, EDFA: erbium-doped fiber amplifier, C: core, MCF: multicore optical fiber, VOA: variable optical attenuator, PM: optical power meter, PD: photodiode, EA: electrical amplifier, DSO: digital storage oscilloscope.

3. Experimental Setup

Fig. 2 shows the experimental setup for BER measurements and signal quality characterization, which includes a 2 km long 7-core MCF with 4 transmission channels (cores 0,1,3,5) and 3 interfering channels (cores 2,4,6). The output of the laser source is divided by a 50:50 power splitter to the input of two quadrature biased Mach-Zehnder modulators (MZMs): MZM-1 (bias point 1.2 V) and MZM-2 (bias point 4.6 V). Polarization controllers (PC1, PC2) are placed before the MZMs to reduce polarization dependent loss. An Altera Stratix V FPGA module that contains 7 transceiver channels is used to generate data streams and estimate the BER. MZM-1 and MZM-2 are modulated by 2.5 Gbps OOK signals generated from the FPGA module transmitters with PRBS7 and PRBS15 bit patterns, respectively. The modulated output from the MZMs is split by a 1x4 power splitter after being amplified by erbium-doped fiber amplifiers (EDFAs). The 1x4 splitter's outputs are connected to the inputs of the MCF's cores via a fan-in module. One of the MCF's outputs is connected to a photodetector through a variable optical attenuator (VOA) for BER measurements. The signal into adjacent outer cores is decorrelated by transmitting PRBS7 in cores 0,1,3,5 and PRBS15 in 2,4 and 6.

The detected electrical signal is then amplified by a 26 dB broadband RF amplifier and divided into two paths; one is connected to a digital storage oscilloscope (DSO) to display the eye diagram and the second is connected to the receiver part of the FPGA for BER estimation. During the experiments, the optical power of each core was kept nearly equal.

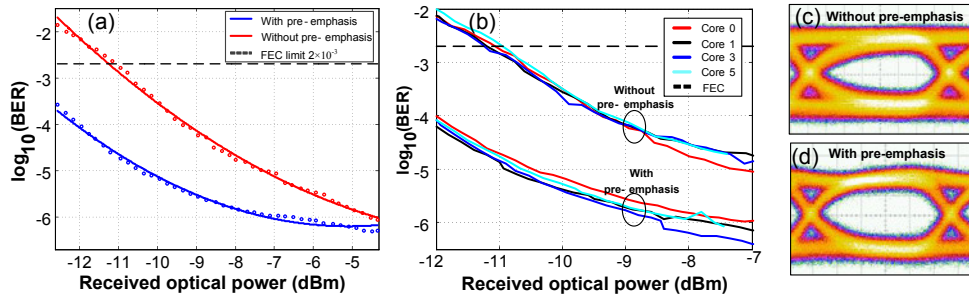


Fig.3: Comparison of measured BER versus received optical power of a 2.5 Gbps NRZ-OOK signal with and without FPGA equalization enabled (a) for central MCF core (core 0) (b) central core 0 and outer cores 1, 3 and 5. Eye pattern of the received 2.5 Gbps signal (c) without equalization and (d) with FPGA equalization for central MCF core 0.

4. Results and Discussion

The obtained BER of core-0 in response to received optical power at photodiode (PD) is shown in Fig. 3 in two different scenarios, with and without signal pre-emphasis for mitigation of signal distortions. Applying the FPGA pre-emphasis option we can reduce the effect of distortions in each core and the BER is far below the level of the forward error correction (FEC) limit as shown in Figs. 3(a) and 3(b). The measured optical output power of core 0 after 2 km MCF transmission varied from -12.55 to -4.35 dBm, where the 2.5 Gbps NRZ-OOK signal's BER without equalization was from 1.4×10^{-2} to 8.7×10^{-7} , but with equalization it varied from 2.6×10^{-4} to 5.1×10^{-7} , as shown in Fig. 3(a). Eye diagrams of the received signal without any signal equalization and with FPGA equalization are shown in Figs. 3(c) and 3(d).

5. Conclusions

Results show that by using FPGA pre-emphasis function the crosstalk is minimized and the BER value of received signals for each of seven MCF cores is reduced. Hence FPGA-based real-time multicore fiber technology is a viable solution for future high speed and high capacity communications.

6. Acknowledgements

This project has received funding from the European Union's Horizon 2020 research and innovation programme under the Marie Skłodowska-Curie grant agreement No 642355.

7. References

- [1] K. Saitoh and S. Matsuo, "Multicore Fiber Technology," *Journal of Lightwave Technology* 34, 55-66 (2016).
- [2] S. García and I. Gasulla, "Multi-cavity optoelectronic oscillators using multicore fibers," *Optics Express* 23, 2403 (2015).
- [3] I. Gasulla et al., "Recent Breakthroughs in Microwave Photonics," *IEEE Photonics Journal* 3, 311-315 (2011).
- [4] J. Sakaguchi et al., "109-Tb/s (7x97x172-Gb/s SDM/WDM/PDM) QPSK transmission through 16.8-km homogeneous multi-core fiber," *Proc. OFC, PDPB6*, Los Angeles (2011).
- [5] S. Randel et al., "MIMO-based Signal Processing of Spatially Multiplexed 112-Gb/s PDM-QPSK Signals using Strongly-Coupled 3-Core Fiber," *Proc. ECOC, Tu.5.B.1*, Geneva (2011).
- [6] J. Sakaguchi et al., "19-core fiber transmission of 19x100x172-Gb/s SDM-WDM-PDM-QPSK signals at 305Tb/s," *Proc. OFC, PDP5C.1*, Los Angeles (2012).
- [7] H. Takara et al., "1.01-Pb/s (12 SDM/222 WDM/456 Gb/s) Crosstalk-managed Transmission with 91.4-b/s/Hz Aggregate Spectral Efficiency," *Proc. ECOC, Th.3.C.1*, Amsterdam (2012).
- [8] Y. Fan et al., "Full-duplex transmission of IEEE 802.11ac-compliant MIMO WLAN signals over a 2-km 7-core fiber," *Chin. Opt. Lett.* 15, 010011- (2017).
- [9] J. Galve et al., "Reconfigurable Radio Access Networks Using Multicore Fibers," *IEEE Journal of Quantum Electronics* 52, 1-7 (2016).
- [10] T. Eriksson et al., "Experimental Investigation of Crosstalk Penalties in Multicore Fiber Transmission Systems," *IEEE Photonics Journal* 7, 1-7 (2015).
- [11] R. Ryf et al., "MIMO-Based Crosstalk Suppression in Spatially Multiplexed 3x56-Gb/s PDM-QPSK Signals for Strongly Coupled Three-Core Fiber," in *IEEE Photonics Technology Letters*, 23,1469-1471, (2011).
- [12] V. Bobrovskiy et al., "Latency causes and reduction in optical metro networks," in *Proc. SPIE 9008, Optical Metro Networks and Short-Haul Systems VI*, 90080C, San Francisco (2013).

PAPER-7: Analog Radio-over-fiber WDM-PON Architecture for 5G Millimeter-wave Interface

T. Salgals, L. Skladova, J. Porins, V. Bobrovs and **S. Spolitis**, "Analog Radio-over-fiber WDM-PON Architecture for 5G Millimeter-wave Interface," *2019 PhotonIcs & Electromagnetics Research Symposium - Spring (PIERS-Spring)*, , pp. 2679-2686, Rome, Italy, June 17-20, (2019), DOI: [10.1109/PIERS-Spring46901.2019.9017431](https://doi.org/10.1109/PIERS-Spring46901.2019.9017431)

Analog Radio-over-fiber WDM-PON Architecture for 5G Millimeter-wave Interface

Toms Salgals, Laura Skladova, Jurgis Porins, Vjaceslavs Bobrovs, and Sandis Spolitis
Institute of Telecommunications, Riga Technical University, Azenes Street 12, LV-1048, Riga, Latvia

Abstract— Migration paths towards 5G require to increase network capacity and raise typical end-user data rates from 10 to 100 times. Wavelength division multiplexed passive optical network (WDM-PON) based third-generation fiber-to-the-x (FTTx) system architectures will be capable to provide solutions related to nowadays network problems with transmission capacity. Therefore, in our research paper we propose analog radio-over-fiber (A-RoF) system architecture with three hybrid photonic mm-wave generation techniques in WDM-PON network. In our developed model of A-RoF WDM-PON architecture, the baseband units are located on transmitter side in central office, by transporting intermediate frequencies along existing fiber optical distribution network and effectively performing signal up-conversion at the remote radio unit (RRU) located in receiver side. Investigated A-RoF WDM-PON transmission system model, created in the environment of OptSim simulation software, shows possible system types of A-RoF implementation for optimized generation of mm-wave signals that can be further used for data transmission between multiple-input and multiple-output (MIMO) antennas. The feasibility of A-RoF WDM-PON system is verified by the complexity of each mm-wave generation in optical transmitter side and the obtained quality of received signal.

1. INTRODUCTION

The fifth-generation (5G) is the latest generation of cellular mobile communications. Infrastructure for 5G needs to deliver solutions, architectures, technologies and standards for the ubiquitous 5G communication infrastructures of the next decade. The development of new communication networks depends on the emergence of globally accepted standards in order to achieve 1000 times the system capacity, 10 times the spectral efficiency and energy efficiency [1].

Traditional radio access network (RAN), which combines baseband processing and radio functions at each physical base station, are used also in long-term evolution (LTE) cellular 4G generation technology [2]. 5G is still under research and discussions, but it is already known, that baseband processing for many cells will be centralized and stands for Cloud RAN or Centralized RAN (C-RAN) with benefits of improved performance and cost reductions as result of pooling resources. Enabling C-RAN for the 5G front-haul architecture will evolve it to more complex network, where additional costs of the increase in capacity requirements is possible to be reduced. The basic front-haul is assumed to run over a common public radio interface (CPRI), processed in the Base-band units (BBU) and sent to the remote radio head (RRH). Functional split options of basic front-haul network is discussed in separate paper [3]. Nowadays it is being considered that 5G wireless communications will use backhaul section of existing optical fiber links between remote radio units (RRU) and BBUs located in central office (CO) side [3, 4].

Millimeter waves, compared to the spectrum below 6 GHz used for mobile communications, have enormous available bandwidths. Millimeter wave is a promising candidate to address the capacity demands of 5G. Integrated backhaul for 5G millimeter wave could be placed easily in urban areas, without additional effort, cost for wired backhaul and connection to the core network [5].

Currently, research and development of the 5G mobile systems at the higher frequency, such as 28 GHz band, has been considered for urban areas, as well vehicular communications [6]. At the moment two possible RF bands of 6 GHz and ka-band of 28 GHz are considered for 5G spectrum [6, 7]. Hybrid configuration of commercialized wavelength division multiplexing passive optical access network (WDM-PON) together with integration of radio-over-fiber (RoF) is an effective way to save construction costs, enhance flexibility and improve the capacity of RoF systems. Together with PON's segment the RoF provides unique solution for fiber optical infrastructure, that can be the next step for 5G wireless transmission implementation ensuring energy saving and cost reduction [8].

During the last decade several novel schemes, allowing transmitting 28 GHz RF carriers through optical modulation techniques for analog radio-over-fiber (A-RoF) links, are investigated. However, it is known that these solutions have mainly impact from linear (e.g., chromatic dispersion (CD)) and non-linear (e.g., nonlinear optical effects (NOE)) impairments for each sub-carrier signals in

fiber optical links that is the main distance-limiting factor for the high frequency transmission [9–12].

2. SIMULATION MODEL OF A-ROF WDM-PON ARCHITECTURE BASED ON NRZ-OOK MODULATED TRANSMISSION SYSTEM

The goal of this simulation model was to evaluate the performance and maximum reach for our investigated A-RoF WDM-PON transmission system with four 2.5 Gbit/s NRZ-OOK modulated channels, where BBUs are implemented in CO allowing transporting of intermediate frequencies along existing fiber optical distribution network (ODN) under condition that it is still possible to achieve pre-forward error correction (pre-FEC) BER of 10^{-3} or lower.

Displayed results in our research are obtained by OptSim simulation software with use of Time Domain Split-Step (TDSS) method to solve complex set of differential equations describing signal propagation through network components and estimate BER of received signals [13, 14]. Additional use of Matlab software was performed to display estimated results of received signals. In our research, we used forward-error-correction (FEC) with 10^{-3} BER performance threshold, which allows us to evaluate performance and determine maximal available reach of our investigated transmission system [12].

As it is shown in Fig. 1, our investigated A-RoF WDM-PON optical transmission system model consists of 4 channels operating at 2.5 Gbit/s bitrate each. According to ITU-T G.964.1 rec., dense WDM architecture with 100 GHz channel spacing and 193.1 THz central frequency is chosen [15]. Baseband units (BBUs) pool in our proposed model architecture is integrated in WDM-PON central office (CO) side, which consists of optical line terminal (OLT). CO includes optical line terminal (OLT) with four transmitters (OLT-Tx) modified for A-RoF system data containing 28 GHz carrier frequencies generation [16]. Electrical pseudo-random bit sequence (PRBS) data source and NRZ driver, which encodes the logical data form by using the non-return to zero (NRZ) technique are directly sent to low-pass filter (LPF) with 3 GHz 3-dB bandwidth in such a way generating widely used on-off keying non-return to zero (NRZ-OOK) modulated signal for all investigated system types of A-RoF implementation [17].

Three possible A-RoF system types for different generation of mm-wave inside transmitters (Tx) of our simulation environment model is investigated. Simulation model of first transmitter was designed by using two continuous wavelength (CW) light sources with linewidth of 50 MHz each, where one of them with output power of +10 dBm is directly connected to intensity Mach-Zehnder modulator (MZM). Second light source is operating as local oscillator (LO) and is used for generation of intermediate frequency (tone) with output power of +2.6 dBm. Such an output power of second CW laser is set to ensure equal power level of both optical tones afterwards being coupled by a power coupler. The frequency spacing between both above mentioned lasers is set to be 28 GHz, accordingly enabling to generate 28 GHz (ka-band) mm-wave.

By homodyne up-conversion channel interval between two laser sources are equal for necessary mm-wave generation, in our case for 28 GHz ka-band intermediate frequency generation. Second A-RoF transmitter for WDM-PON optical transmission system, was realized by use of two separately coupled continuous wavelength light sources with 28 GHz channel interval between two channels with related output power level of 10 dBm and sent to external MZM. In such way both optical tones are modulated in this scenario.

Third transmitter realization for intermediate frequency generation is more complex. CW laser source with 10 dBm output power is directly connected to first MZM which has 3 dB insertion loss and 20 dB extinction ratio, where modulator BIAS point is adjusted at its zero point. Sinusoidal signal generator with 14 GHz sinusoidal electrical signal (half of proposed IF frequency) is directly connected to first MZM electrical signal input. Output of first MZM with two 28 GHz spaced optical tones are amplified with EDFA amplifier and divided by 50% percent optical power splitter with 3.5 dB insertion loss. Afterwards each tone is filtered out by variable optical band-pass filter (BPF) with 20 GHz 3-dB bandwidth for each optical signal. Second optical signal is attenuated accordingly to optical power level of first modulated signal after MZM to ensure equal related power level for both optical signals. Finally coupled both optical signals are together and prepared for transmission in fiber optical part.

Optical signals from each OLT-Tx are coupled together by using arrayed waveguide grating (AWG) multiplexer with 3.5 dB insertion loss, 100 GHz channel interval where 3-dB bandwidth is 40 GHz. An optical signal pre-amplification by erbium doped amplifier (EDFA) with optimized gain accordingly to each A-RoF implementation type is realized before launching coupled optical signals

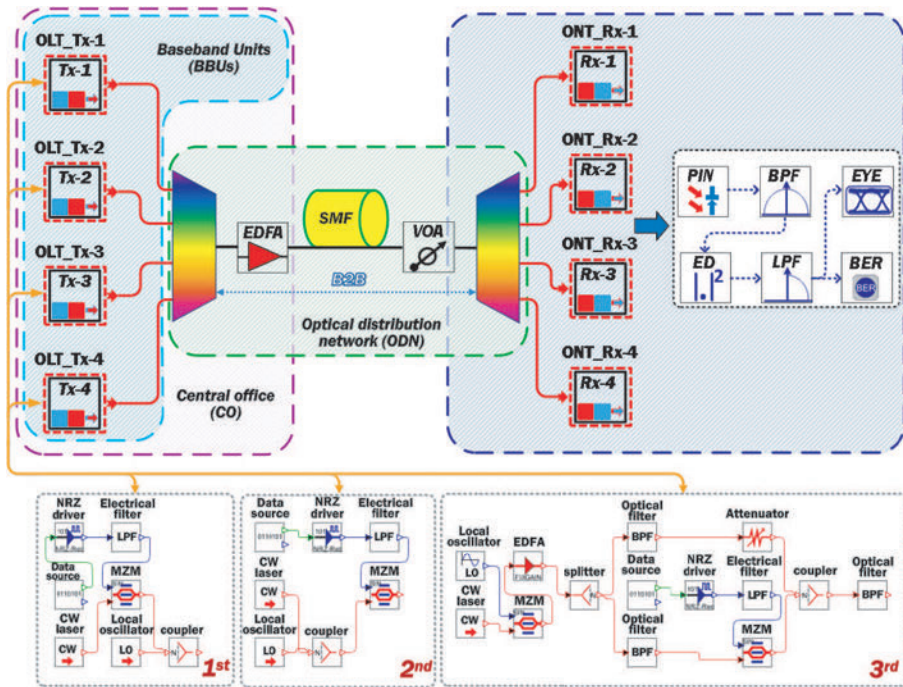


Figure 1: Simulation scheme of 4-channel 2.5 Gbit/s per channel NRZ-OOK modulated A-RoF WDM-PON optical transmission system with investigated A-RoF transmitters: (1st) using one laser source as LO, (2nd) use of two coupled light sources and (3rd) use of sinusoidal signal generator as LO for generation of 28 GHz mm-wave signal.

into ITU-T G.652 rec. single mode optical fiber (SMF) span, with 0.02 dB/km attenuation and 17 ps/nm/km dispersion coefficients at 1550 nm reference wavelength. Additional variable optical attenuator (VOA) is used to obtain BER in terms of received optical power. After transmission through ODN, intermediate frequency optical signals are separated by AWG de-multiplexer with 3.5 dB insertion loss, 100 GHz channel interval and of 40 GHz 3-dB bandwidth, located in optical network terminals (ONTs). After optical-to-electrical conversion the electrical data containing RF signals are sent through remote radio unit (RRU). The next containing step is to provide mm-wave transmission between multiple-input and multiple-output (MIMO) antennas.

Receiver side consists of optical network terminals (ONTs). Each ONT receiver (ONT-Rx) consists of PIN photoreceiver with 50 GHz 3-dB electrical bandwidth with sensitivity level +4 dBm for BER of 10^{-12} , dark current of 5 nA and responsivity of 0.65 A/W [18]. Electrical Bessel band-pass filter (BPF) with 3 GHz 3-dB electrical bandwidth tuned to 28 GHz central frequency is used for each containing channel carrier frequency pre-filtering. Filtered intermediate frequency signal down-conversion in our case is realized by homodyne signal processing technique using passive Schottky diode based envelope detector (ED) with video-bandwidth 28 GHz [19]. Afterwards received modulated baseband signal is filtered by electrical Bessel low-pass filter (LPF) with 3 GHz 3-dB electrical bandwidth. The scope and BER estimator based on statistical signal analysis was used for measurements of received signal, e.g., showing bit pattern and bit-error rate (BER).

3. RESULTS AND DISCUSSION

In our research, we implemented three different A-RoF system types for generation of mm-wave through the existing wavelength division multiplexed (DWDM) 100 GHz spaced 4-channel passive optical transmission system architecture. We show received signal with worst BER performance for middle channel, where the highest impact of crosstalk is observed. Obviously we conclude that

optical spectrum after transmission of 20 and 40 km long fiber span is mainly significant, therefore optical signal spectrum after B2B and 20 km long fiber transmission is shown. As one can see in Fig. 2(b), the 4-channel 100 GHz spaced by the NRZ signals spectrum of each channel in B2B and after 20 km transmission in our investigated DWDM-PON optical transmission system are shown.

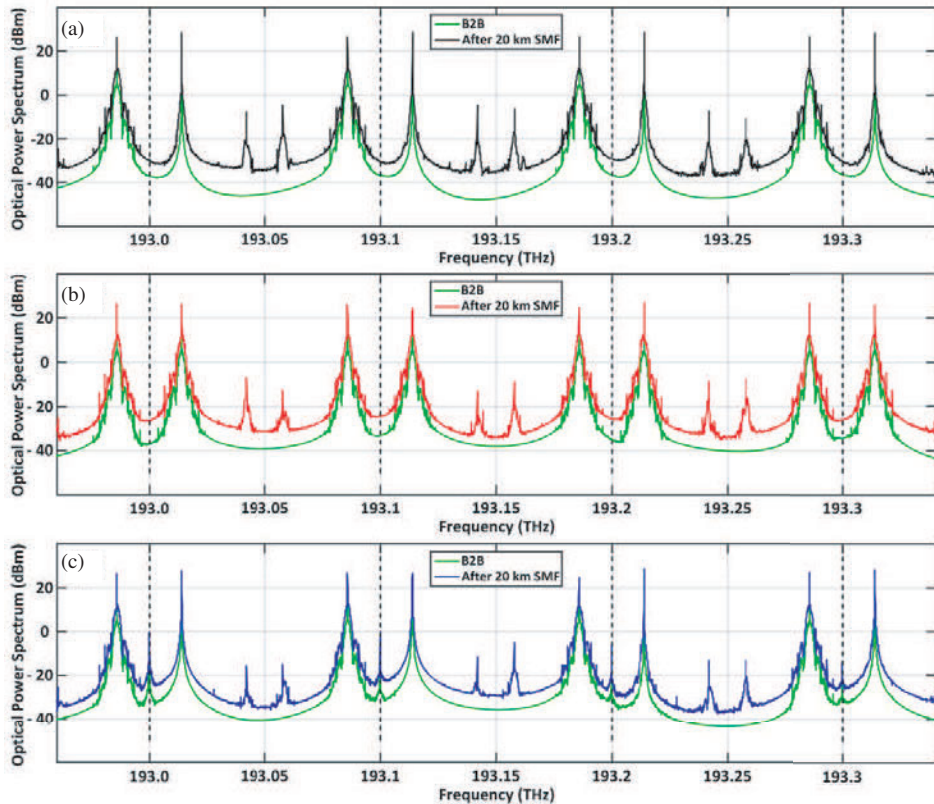


Figure 2: Optical spectrum of multiplexed 4-channel WDM-PON system before B2B and after 20 km transmission through ODN, for photonic up-conversion and generation of single 2.5 Gbit/s NRZ modulated 28 GHz carrier by different A-RoF implementation: (a) using one laser source as LO, (b) using two coupled light sources, (c) using sinusoidal signal generator as LO.

For homodyne up-conversion with one 2.5 Gbit/s NRZ modulated optical signal and CW local oscillator ensuring difference of 28 GHz between two sidebands in optical frequency domain for (1st) and (3rd) A-RoF designed transmitter in our investigated DWDM-PON optical transmission system B2B configuration and after 20 km transmission in ODN SMF part, please see Figs. 2(a) and 2(c).

The obtained BER of each A-RoF transmitter in response to received optical power at (PIN) photoreceiver is shown in Fig. 3. Results are obtained in two different scenarios, with 20 and 40 km ODN fiber length. The measured optical output power of 20 km ODN varied from 2.1 to 10.1 dBm, where the final 2.5 Gbit/s NRZ-OOK received and down-converted signal of 2nd implemented A-RoF transmitter BER was from 8.9×10^{-2} to 9.9×10^{-39} . But with 1st and 3rd A-RoF transmitter measured optical output power varied from 1.9 to 9.9 dBm and 1.7 to 9.7 dBm with estimated BER measurements of received signals from 2.2×10^{-1} to 4.9×10^{-38} and 1.9×10^{-1} to 3.4×10^{-33} . In such way second scenario with 40 km SMF fiber ODN link the measured optical output power varied from 2.5 to 10.5 dBm where the BER of received baseband signal of 2nd implemented A-RoF transmitter was from 1.7×10^{-2} to 2.6×10^{-22} but with 1st and 3rd A-RoF transmitter it varied

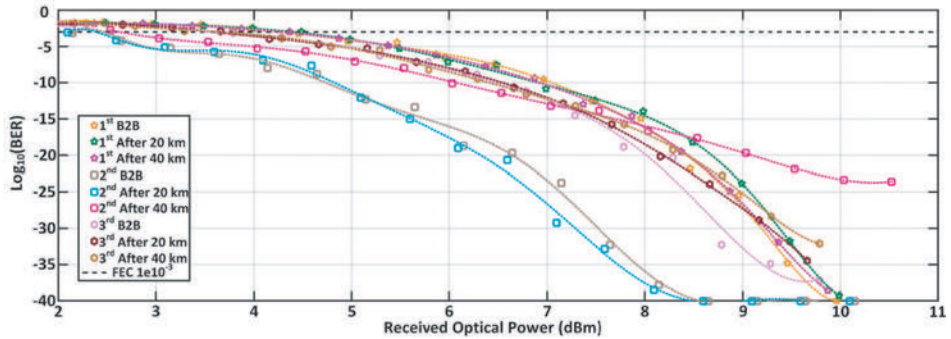


Figure 3: Comparison of measured BER after ED versus received optical power for 2.5 Gbit/s NRZ-OOK signals depending of A-RoF implementation realization type and use of photonics up-conversion method for 28 GHz carrier frequency.

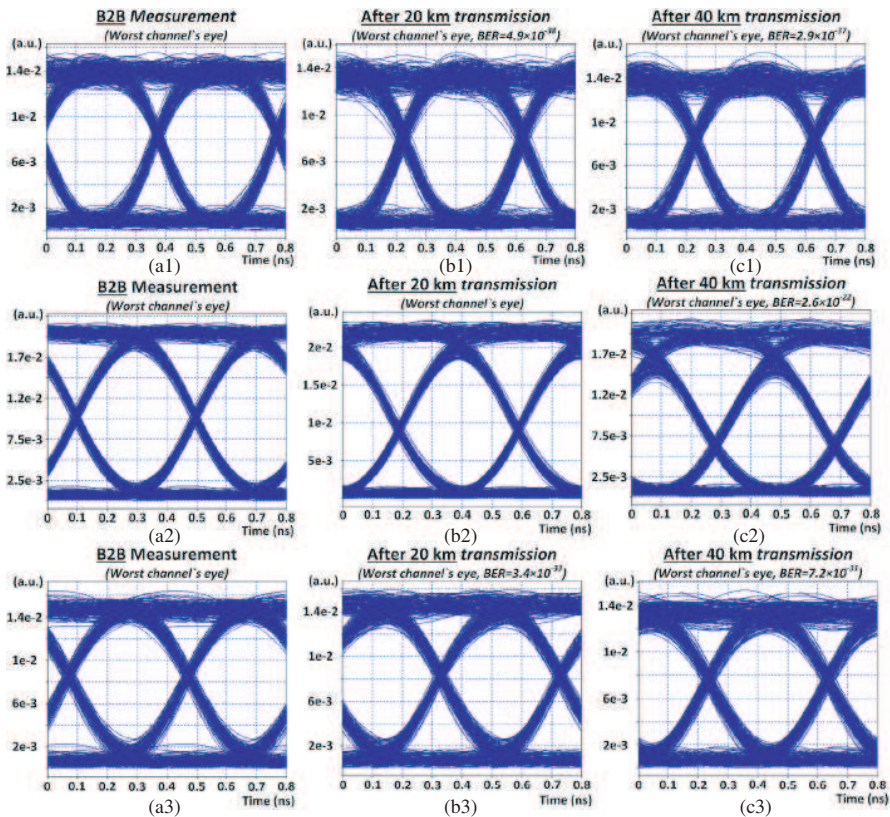


Figure 4: Eye diagrams of received 28 GHz carrier signal after ED detection: (a) after B2B transmission (b) after 20 km and (c) after 40 km for each type of A-RoF implemented transmitter: (1) transmission using one laser source as LO, (2) use of two coupled light sources and (3) use of sinusoidal signal generator as LO for 4-channel 2.5 Gbit/s 100 GHz spaced WDM-PON transmission system.

from 1.9 to 9.9 dBm and 1.8 to 9.8 dBm with estimated BER from 2.2×10^{-1} to 2.9×10^{-37} and 2.2×10^{-1} to 7.2×10^{-31} , respectively.

As one can see in Figs. 4(a1), 4(a2) and 4(a3) in B2B configuration the signal quality for all implemented A-RoF transmitter types is good, eye is open and error-free transmission of our investigated WDM-ROF system with 100 GHz channel spacing can be provided. After 20 km transmissions through ODN part from obtained results we conclude that use of 2nd implemented A-RoF transmitter error-free transmission is also provided, please see Fig. 4(b2). Implementation of 1st and 3rd A-RoF transmitters in high capacity WDM-PON transmission system shows acceptable performance, please see Figs. 4(b1) and 4(b3) where the BER of received signals was 4.9×10^{38} and 3.4×10^{33} , respectively.

Accordingly to Next generation PON standards (NG-PON2) ITU-T G.989.2 we chose ODN fiber distance classes with defined length of 20 and 40 km with equal differential optical path loss of maximum 8 dB for designed simulation model. By increasing length of distribution network up to 40 km, after transmission the BER of received signals with use of 2nd implemented A-RoF transmitter was 2.6×10^{-22} , please see Fig. 4(c2). Additional losses in optical fiber line and effect of CD after increasing length shows the relevance of WDM-PON transmission systems performance reduction, where the BER of implemented 1st and 3rd A-RoF transmitter after received signals was 2.9×10^{37} and 7.2×10^{31} please see Figs. 4(1c) and 4(3c) [20].

According to ITU-T G.989.2 recommendation, the specified valid optical link distances is up to 40 km, but it is also possible to support longer distances, which may require usage of extenders. We extend transmission distance of fiber optical link section up to 60 km. After extending the link section we conclude, that maximal possible reached distance for 2nd implemented A-RoF transmitter was 57 km with the BER of 3.6×10^4 , please see Fig. 5(b). As one can see in Figs. 5(a) and 5(c) with 1st implemented A-RoF transmitter using one laser source as LO and 3rd implemented A-RoF transmitter with use of sinusoidal signal generator as LO the BER of received signal was 3.3×10^{-4} and 5.1×10^{-4} , with maximum reached distance of 65 and 63 km, respectively.

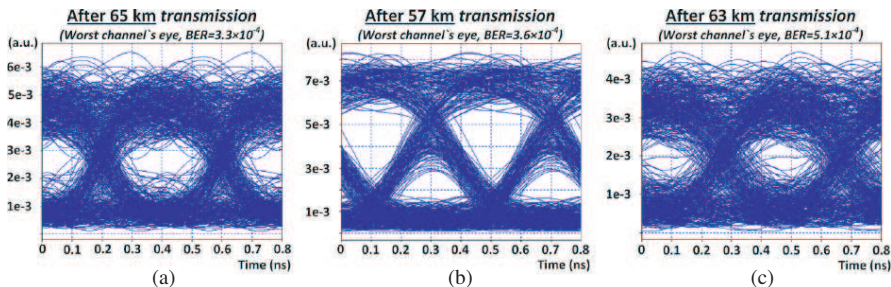


Figure 5: Eye diagrams of received 28 GHz carrier signal after ED detection by A-RoF implementation (a) after 65 km transmission using one laser source as LO, (b) after 57 km use two coupled light sources and (c) after 63 km use of sinusoidal wave generator as LO for 4-channel 100 GHz spaced WDM-PON transmission system with 2.5 Gbit/s transmission speed per channel.

4. CONCLUSION

The main goal of this work is to provide hybrid photonic A-RoF system integration in next-generation passive optical networks (NG-PON) represented by WDM-PON networks and find appropriate generation technique of mm-wave in these networks by providing unique solution and design of future fiber optical infrastructure that can be the next step to provide fifth-generation 5G wireless transmission with its technical requirements.

We have demonstrated wavelength division multiplexed passive optical network A-RoF based on third-generation FTTH architecture solution for next-step 5G telecommunication systems, by using different A-RoF implementation types and generation of mm-wave. Our investigated A-RoF based WDM-PON system is a viable solution for future high speed and high capacity communications. Proposed system model is realized in OptSim simulation environment based on traditional PON's segment with ITU-T G.694.1 rec. dense WDM frequency grid together with next-generation (NG-PON2) ITU-T G.989.2 rec. requirements (e.g., transmission reach, bitrate, etc.).

Our proposed 4-channel A-RoF WDM-PON transmission model and 1st implemented A-RoF transmitter, which showed the best performance in generation of mm-wave, is capable to provide data transmission over at least 65 km long standard ITU-T G.652 fiber span. Therefore, it is capable to increase capacity of data rate in fiber optical network accordingly to NG-PON2 and provide up to 128 channels in PON's segment, depending on MIMO system and centralized radio access networks (C-RANs) necessary requirements.

ACKNOWLEDGMENT

This work has been supported by the European Regional Development Fund within the Activity 1.1.1.2 “Post-doctoral Research Aid” of the Specific Aid Objective 1.1.1 “To increase the research and innovative capacity of scientific institutions of Latvia and the ability to attract external financing, investing in human resources and infrastructure” of the Operational Programme “Growth and Employment” (No. 1.1.1.2/VIAA/1/16/044).

REFERENCES

1. Anh, T., P., P. V. Trinh, V. V. Mai, N. T. Dang, and C. Truong, “Hybrid free-space optics/millimeter-wave architecture for 5G cellular backhaul networks,” *2015 Opto-Electronics and Communications Conference (OECC)*, 1–3, Shanghai, China, Jun. 28–Jul. 2, 2015, ISBN: 978-1-4673-7944-1, ISSN: 2166-8892.
2. Liu, C., J. Wang, L. Cheng, M. Zhu, and G. Chang, “Key microwave-photonics technologies for next-generation cloud-based radio access networks,” *Journal of Lightwave Technology*, Vol. 32, No. 20, 3452–3460, Oct. 15, 2014, ISSN: 1558-2213.
3. Jaber, M., M. A. Imran, R. Tafazolli, and A. Tukmanov, “5G backhaul challenges and emerging research directions: A survey,” *IEEE Access*, Vol. 4, 1743–1766, Apr. 20, 2016, ISSN: 2169-3536.
4. Gapeyenko, M., V. Petrov, D. Moltchanov, S. Andreev, N. Himayat, and Y. Koucheryavy, “Flexible and reliable UAV-assisted backhaul operation in 5G mmWave cellular networks,” *IEEE Journal on Selected Areas in Communications*, Vol. 36, No. 1, 2486–2496, Nov. 2018, ISSN: 1558-0008.
5. Berthold, P., “Scheduling conflicts in wireless in-band backhaul for 5G millimeter wave communications,” *2016 IEEE Conference on Computer Communications Workshops (INFOCOM WKSHPS)*, 1–2, San Francisco, CA, USA, Apr. 10–14, 2016, ISBN: 978-1-4673-9955-5.
6. Kawasaki, K., Y. Ito, H. Iwai, S. Nakano, Y. Suegara, M. Sibayama, and M. Umehara, “Analysis of diffraction characteristics at 28 GHz band in a vehicular communication environment,” *2018 International Symposium on Antennas and Propagation (ISAP)*, 1–2, Busan Korea (South), Oct. 23–26, 2018, ISBN: 978-89-5708-304-8.
7. Wang, G., Y. Liu, S. Li, X. Zhang, and Z. Chen, “Study on the outdoor wave propagation at 28 GHz by ray tracing method,” *2016 IEEE International Conference on Microwave and Millimeter Wave Technology (ICMMT)*, 1–3, Beijing, China, Jun. 5–8, 2016, ISBN: 978-1-4673-8983-9.
8. Liu, A., X. Wang, Q. Shao, T. Song, H. Yin, and N. Zhao, “A low cost structure of radio-over-fiber system compatible with WDM-PON,” *2016 25th Wireless and Optical Communication Conference (WOCC)*, 1–3, Chengdu, China, May 21–23, 2016, ISBN: 978-1-4673-9958-6, ISSN: 2379-1276.
9. Bobrovs, V., A. Udalcovs, S. Spolitis, and G. Ivanovs, “Schemes for compensation of chromatic dispersion in combined HDWDM systems,” *Latvian Journal of Physics and Technical Sciences*, Vol. 48, No. 5, 30–44, Jan. 1, 2011, ISSN: 08688257.
10. Olonkins, S., S. Spolitis, I. Lyashuk, and V. Bobrovs, “Cost effective WDM-AON with multicarrier source based on dual-pump FOPA,” *(2015) International Congress on Ultra Modern Telecommunications and Control Systems and Workshops*, 23–28, Art. No. 7002073, Jan. 6, 2015, ISSN: 21570221.
11. Giannoulis, G., N. Argyris, N. Iliadis, G. Pouloupoulos, K. Kanta, D. Apostolopoulos, and H. Avramopoulos, “Analog radio-over-fiber solutions for 5G communications in the beyond-CPRI era”, *2018 20th International Conference on Transparent Optical Networks (ICTON)*, 1–5, Bucharest Romania, Jul. 1–5, 2018, ISBN: 978-1-5386-6605-0, ISBN: 978-1-5386-6606-7.
12. Salgals, T., S. Spolitis, S. Olonkins, and V. Bobrovs, “Investigation of 4-PAM modulation format for use in WDM-PON optical access systems,” *Progress In Electromagnetics Research Symposium (PIERS 2017)*, 1–4, St. Petersburg, Russia, May 22–25, 2017.

13. Salgals, T., L. Skladova, K. Vilcane, J. Braunfelds, and S. Spolitis, “Evaluation of 4-PAM, NRZ and duobinary modulation formats performance for use in 20 Gbit/s DWDM-PON optical access systems,” *2018 Advances in Wireless and Optical Communications (RTUWO)*, 134–138, Riga Latvia, Nov. 15–16, 2018, ISBN: 978-1-5386-5558-0.
14. Spolitis, S., V. Bobrovs, and G. Ivanovs, “Reach improvement of spectrum-sliced dense WDM-PON system,” *2012 Seventh International Conference on Broadband, Wireless Computing, Communication and Applications (BWCCA 2012)*, 296–301, Art. No. 6363072,, Victoria, BC, Canada, Nov. 12–14, 2012, ISBN: 978-1-4673-2972-9.
15. ITU-T Recommendation G.694.1, “Transmission media and optical systems characteristics — Characteristics of optical systems: Spectral grids for WDM applications: DWDM frequency grid,” 7–12, 2012.
16. ITU-T Recommendation G.989.2, “Digital sections and digital line system – Optical line systems for local and access networks — 40-Gigabit-capable passive optical networks 2 (NG-PON2): Physical media dependent (PMD) layer specification,” 10–92, 2014.
17. Salgals, T., I. Kurbatska, S. Spolitis, V. Bobrovs, and G. Ivanovs, “Research of M-PAM and duobinary modulation formats for use in high-speed WDM-PON systems,” *Part of book: Telecommunication Systems*, 1–18, Feb. 22, 2019, DOI:10.5772/intechopen.84600.
18. Finisar “50 GHz DWDM single high-speed photodetector XPDV21x(RA),” *Technical Specification*, 1–5, 2015.
19. Hesler, J., K. Hui, and T. Crowe, “Ultrafast millimeter-wave and THz envelope detectors for wireless communications,” *2012 IEEE International Topical Meeting on Microwave Photonics*, 93–94, Noordwijk, Netherlands, Sept. 11–14, 2012, ISBN: 978-1-4673-2865-4.
20. Spolitis, S., V. Bobrovs, S. Berezins, and G. Ivanovs, “Optimal design of spectrally sliced ASE seeded WDM-PON system,” *2012 15th International Telecommunications Network Strategy and Planning Symposium (NETWORKS)*, Art. No. 6381687, 1–5, Oct. 15–18, 2012, ISBN: 978-1-4673-1391-9.

PAPER-8: Research of PAM-4 Modulated WDM-PON Architecture for 5G Millimeter-wave Hybrid Photonics-wireless Interface

T. Salgals, I. Kurbatska, V. Bobrovs and **S. Spolitis**, "Research of PAM-4 Modulated WDM-PON Architecture for 5G Millimeter-wave Hybrid Photonics-wireless Interface," *2019 Photonics & Electromagnetics Research Symposium - Fall (PIERS - Fall)*, pp. 728-734, Xiamen, China, Dec. 17-20, (2019), DOI: [10.1109/PIERS-Fall48861.2019.9021846](https://doi.org/10.1109/PIERS-Fall48861.2019.9021846)

Research of PAM-4 Modulated WDM-PON Architecture for 5G Millimeter-wave Hybrid Photonics-wireless Interface

Toms Salgals¹, Inna Kurbatska¹, Vjaceslavs Bobrovs¹, and Sandis Spolitis^{1,2}

¹Institute of Telecommunications, Riga Technical University, Riga, Latvia

²Communication Technologies Research Center, Riga Technical University, Riga, Latvia

Abstract— In this paper 4-level pulse amplitude modulation (PAM-4) analog radio over fiber (A-RoF) transmission through wavelength division multiplexed passive optical network (WDM-PON) architecture for future broadband fifth-generation (5G/5G+) cellular mobile communication networks is proposed. The goal of future cellular mobile communication infrastructures of the next decade is retaining at least one-third of global market share in Europe regarding future network equipment and support higher spectral efficiency providing ubiquitous access to wider spectrum applications in order to reduce the network energy consumption. An alternative solution that offers a good trade-off between performance and complexity is multi-level signaling formats such as PAM-M, where multiple digital bits are encoded into different signal amplitude levels or symbols. It is a relatively easy and effective way to double the bitrate of data transmission link by the implementation of PAM-4 modulation technique instead of well-known non-return-to-zero on-off-keying (NRZ-OOK). In this paper, we investigated the use of PAM-4 modulation format for A-RoF signals transmission through the passive optical network (PON), which is standardized to NGPON2. In our research, we show the possible A-RoF transmitter implementation into improved fiber-optical line terminals (OLT), enabling to generate PAM-4 modulated signal and perform mm-wave signal transmission over the WDM-PON optical distribution network.

1. INTRODUCTION

The Long Term Evolution (LTE) and latest fifth-generation (5G) mobile cellular technology introduce wireless technologies including multiple-input multiple-output (MIMO) transmission with carrier aggregation delivered to and from each radio unit (RU). Within deployment of 5G, it is expected to increase the transmission speed, improve the performance, capacity and area coverage keeping the power consumption low [1]. The demands of broadband wireless and fiber optical-line networks due to high data rate services (HDR), high resolution multimedia entertainment — live ultra-high quality video streaming (4K/8K), virtual reality (VR), daily increasing demand of Internet of Things (IoT) — sensor network, users required electrical gadgets etc., as well future perspective machine-to-machine (M2M) learning leads to challenge for cellular mobile networks requirements such as system capacity, transmission performance and spectrum efficiency [2–4].

It can be observed that the 5G mobile cellular technology instead of low-frequency, i.e., sub-6 GHz range wireless communication is going to adopt higher frequencies from the enormous available spectrum in the millimeter-wave (mm-wave) frequencies (30 to 300 GHz) and becomes one of the important development trends of communication technology for next decade [4–6]. In order to achieve ultra-high capacity and bring ubiquitous high-bitrate wireless connectivity per mobile user, the cost-effective hybrid photonics-wireless mm-wave interface communication systems are required [6]. At the same time, high capacity and low latency flexibility offered by passive optical access networks (PONs) have provided an obvious opportunity to facilitate 5G development by providing intermediate signals through optical fronthaul [7]. Passive optical network (PON) is a promising candidate to transmit both intermediate radio frequency (IF) and baseband signals by a single or multiple wavelengths per optical channel over a single fiber in a cost-efficient way. Traditionally widely used PON network architecture can be technologically modified to radio-over-fiber (RoF) link, which is seamlessly integrated into the PON segment, leaving the existing optical distribution network (ODN) part unchanged [3]. Transmission distances of PON access network (ODN link section length) are normally limited within 20 to 40 km for short-range application according to (NG-PON2) defined optical link section requirements with capability extending the network reach up to 60 km, more, e.g., 80 km for metro-access applications [8, 9].

Instead, to applying for more advanced modulation formats like multi-level quadrature amplitude modulation (M-QAM) and duobinary (DB), the M-PAM, where M is abbreviated as different signal amplitude levels, offers a simple way to enhance the spectral efficiency and at least double the bitrate per wavelength using the same optical bandwidth [5, 10]. Accordingly, the 4-level pulse

amplitude modulation format (PAM-4) attracted much attention to its relative ease of implementation which offers a good trade-off between performance and complexity allowing to double the bit rate in the channel without doubling the necessary bandwidth, if compared to the NRZ-OOK link [5, 10, 11]. In connection with this, the high-speed PAM-4 -based optical link for the common public radio interface (CPRI) in mobile fronthaul is still discussed [1].

According to ITU-T G. 9803 rec. describing RoF systems, the PONs network is desired for mobile fronthaul of latest 5G mobile systems with functions to provide the connection between the baseband units (BBU) pool and RU. It is enabling performing frequency up-conversion into necessary radio signals frequency band in optical line terminals (OLTs) located at the service provider's central office (CO), in such a way effectively allowing to transmit intermediate frequencies (IF) through ODN core network [1, 12]. Analog radio over fiber (A-RoF) as one of the promising solutions is considered for latest 5G mobile systems by transmitting intermediate signals through the fronthaul optical link [4]. Due to spectrum management and frequency allocation, the bands of sub-6 GHz, around 28 GHz (Ka-band) and up to 72 GHz (V-band) are considered for 5G [4, 13–16].

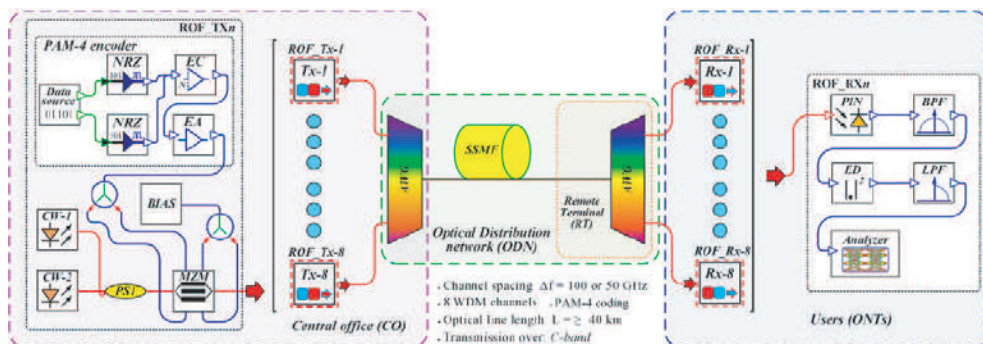
2. SIMULATION MODEL OF PAM-4 MODULATED AROF-WDM-PON TRANSMISSION SYSTEM

In the current research, we use VPI Photonics Design Suite software for design and simulation of 8-channel 2.5 Gbaud/s per channel PAM-4 modulated WDM-PON optical transmission system with investigated A-RoF transmission of 28 GHz mm-wave signal for 5G mm-wave hybrid photonics-wireless interface.

The goal of this hybrid photonics-wireless ARoF-WDM-PON system simulation model was to evaluate the performance and system reach up to 40 km according to NG-PON2 link section requirements, under condition that it is still possible to achieve pre-forward error correction (pre-FEC) BER level of 1×10^{-3} or lower [17]. According RoF ITU-T G.9803. rec., in our investigated 8-channel A-RoF-WDM-PON transmission system depicted in Fig. 1, the baseband units (BBUs) are located in the service provider's central office (CO) allowing to transport intermediate frequencies (IF) over optical front-haul network, and lastly performing signal up-conversion in radio units (RUs) located at the receiver side of the base station (BS) [12].

Passive optical access network (PON) architecture, standardized to NG-PON2 requirements can be technologically transformed into ARoF-WDM-PON transmission system through the A-RoF segment integration. The proposed ARoF-WDM-PON transmission system designed for the transmission of intermediate frequencies (IF) over commercially used optical core network is a perspective solution for the latest fifth-generation (5G/5G+) cellular mobile communication network.

According to the fundamental PONs architecture, we chose the frequency grid according to ITU-T G.694.1 rec (dense WDM systems) for our investigated 8-channel hybrid ARoF-WDM-PON system, where the central frequency is anchored on 193.1 THz and channel spacing is 50 or 100 GHz [18].



AWG: Arrayed-waveguide-grating multiplexer/de-multiplexer, Analyzer: Storage oscilloscope, BPF: Band-pass filter, BIAS: Bias voltage, CW: Continuous wavelength laser source, EA: Electrical amplifier, EC: electrical coupler, ED: Schottky diode, LPF: Low-pass filter, MZM: Differential Mach-Zehnder modulator, PIN: Photodiode, PS: Power splitter, SSMF: Standard single-mode fiber.

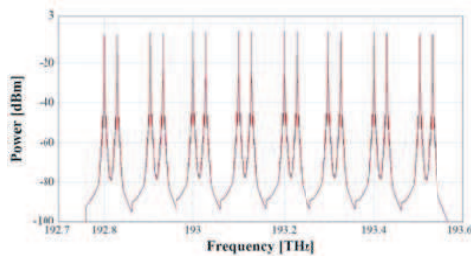
Figure 1: Simulation scheme of 8-channel 2.5 Gbaud/s per channel PAM-4 modulated AROF-WDM-PON optical transmission system with investigated A-RoF transmission of 28 GHz mm-wave signal for 5G mm-wave hybrid photonics-wireless interface.

As it is shown in Fig. 1, the CO includes OLT with eight transmitters modified as RoF transmitters (ROF_Tx) and designed for heterodyne A-RoF system, where 28 GHz intermediate frequencies are generated.

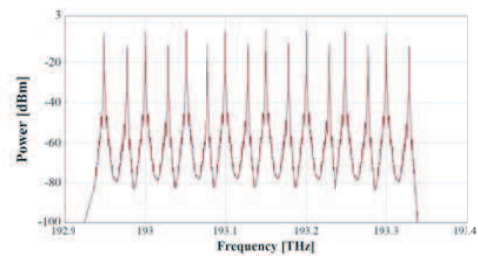
Each ROF_Tx transmitter based on heterodyne up-conversion technique by using two separately coupled continuous wave (CW) laser sources, with 28 GHz frequency difference for necessary mm-wave generation (in our case for 28 GHz (Ka-band)) with +9 dBm output power is directly connected to differential Mach-Zehnder modulator (MZM) resulting in +3.5 dBm optical transmitter average output power [16, 19]. The parameters of the MZM, including S_{21} frequency response, are set according to the specification of Photline MX-LN-10 intensity modulator [20].

The modulation of both optical signals is ensured as follows. Both arms of the differential MZM are driven by the same electrical PAM-4 signal, while bias voltage with opposite signs is ensured. The electrical PAM-4 signal is provided by dividing pseudo-random bit sequence (PRBS) from PRBS generator into two subsequences (sequence of most significant bits (MSBs) and the sequence of least significant bits (LSBs) with a bit rate of 2.5 Gbit/s each and generating electrical NRZ signals with appropriate amplitude levels. The NRZ signals are then combined into one PAM-4 signal with a bit rate of 5 Gbit/s (2.5 Gbaud/s), which is amplified by an electrical amplifier which parameters is set according to the specification of SHF 100 BP amplifier [21].

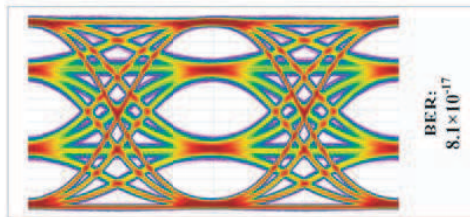
Optical signals from each ROF_Tx are coupled together by using an arrayed-waveguide-grating (AWG) multiplexer. The optical signal at the output of the multiplexer for 100 GHz and 50 GHz channel spacing is shown in Figs. 2(a) and 2(b), respectively.



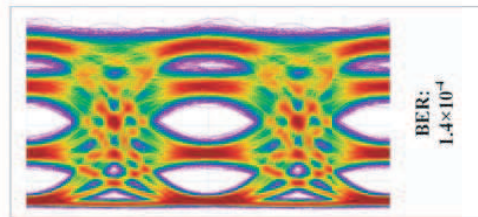
(a) Optical signal spectrum at the output of the AWG multiplexer for 100 GHz channel spacing



(b) Optical signal spectrum at the output of the AWG multiplexer for 50 GHz channel spacing



(c) Eye diagram after B2B transmission for 100 GHz channel spacing



(d) Eye diagram after B2B transmission for 50 GHz channel spacing

Figure 2: Optical spectra of multiplexed 8-channel hybrid photonics ARoF-WDM-PON system with (a) 100 GHz and (b) 50 GHz channel spacing and (c) received down-converted 2.5 Gbaud/s PAM-4 modulated 28 GHz mm-wave signal eye diagram after B2B transmission with 100 GHz channel spacing and (d) received down-converted 2.5 Gbaud/s PAM-4 modulated 28 GHz mm-wave signal eye diagram after B2B transmission with 50 GHz channel spacing.

At the receiver side, the signal is demultiplexed utilizing AWG demultiplexer, which corresponds to wavelength-routed WDM-PON (WR-WDM-PON) architecture. The 3-dB bandwidth of the each and every channel of AWGs was set to the 75 GHz for 100 GHz channel spacing and 35 GHz for 50 GHz channel spacing, respectively [22, 23]. Optical signals are transmitted through ODN link section in optical C-band via ITU-T G.652 standard-compliant single-mode optical fiber (SSMF).

The receiver side consists of optical network terminals (ONTs), where each ONT receiver

(ROF_Rx) consists of photoreceiver (PIN) with 3-dB bandwidth of 36 GHz, sensitivity of -18 dBm for BER of 10^{-12} , the dark current of 1 nA and responsivity of 0.7 A/W [24]. Pre-filtering of the received electrical signal after PIN is realized by the electrical Bessel band-pass filter (BPF), which has 28 GHz central frequency and 5 GHz 3-dB electrical bandwidth. Finally, down-conversion is realized by the envelope detector, which is emulated multiplying the signal by itself and filtering it using low-pass Bessel filter with the 3-dB bandwidth of 2.5 GHz [25–28]. The eye diagrams for the received and down-converted 100 GHz and 50 GHz spaced 2.5 Gbaud/s PAM-4 modulated 28 GHz mm-wave signal for B2B transmission are shown in Figs. 2(c) and 2(d), respectively.

3. RESULTS AND DISCUSSION

In our research, we implement PAM-4 modulated A-RoF transmission through PON's architecture to support higher spectral efficiency providing a good trade-off between performance and complexity for future broadband 5G/5G+ cellular mobile communication networks.

The feasibility of the designed hybrid photonics-wireless system is verified by the performance indicators as pre-forward-error-correction (pre-FEC) BER threshold $\text{BER} \leq 10^{-3}$ and eye diagrams of received and down-converted mm-wave radio signal. The obtained results of worst performing channel for transmission distances of up to 40 km over SMF ODN section for PAM-4 modulated 8-channel ARoF-WDM-PON transmission system with 100 GHz channel spacing are shown in Fig. 3.

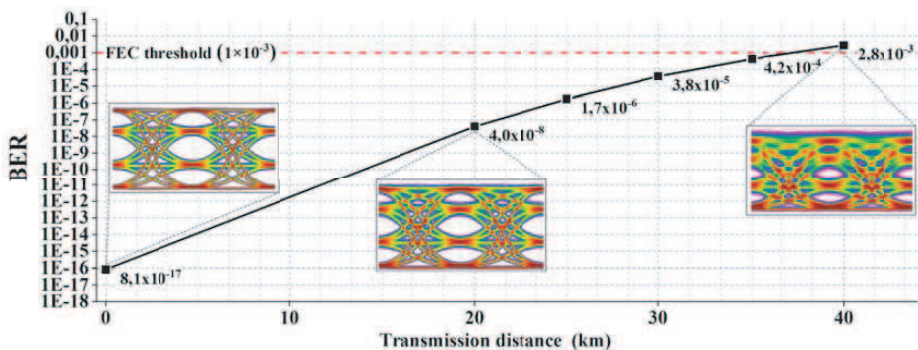


Figure 3: BER versus transmission distance for down-converted 2.5 Gbaud/s PAM-4 modulated 28 GHz mm-wave signal after ARoF-WDM-PON transmission over 20 and 40 km SSMF ODN distances. Insets show the received down-converted PAM-4 signal eye diagrams after B2B, 20 and 40 km transmission over SSMF for 2.5 Gbaud/s symbol rate with 100 GHz spacing.

After transmission through 20 km of ODN including SSMF fiber, the BER is significantly lower than the FEC threshold, where the BER of received signals was 4×10^{-8} . While after 40 km transmission through ODN the BER of received signals was 2.8×10^{-3} , which is slightly above FEC threshold. That means that it is technically difficult to ensure such transmission distance and more comprehensive future research on the limits of the parameters of the transmission system for the implementation of such a long transmission distance (40 km) is desirable.

Further, the utilization of twice narrower -50 GHz channel spacing was investigated. The optical spectrum of the 2.5 Gbaud/s PAM-4 modulated signal at the output of AWG de-multiplexer (original signal) and after AWG de-multiplexer (after transmission over 20 km ODN link section) for hybrid photonics ARoF-WDM-PON system obtained by use of AWG's with 50 GHz channel spacing and 3-dB bandwidth of the 35 GHz are shown at Fig. 4. While the eye diagram of the received signal and corresponding BER are shown at the inset of Fig. 4. As one can see in Fig. 4 (inset), with the 50 GHz channel spacing, it is not possible to ensure transmission with BER below FEC threshold for our investigated 2.5 Gbaud/s PAM-4 modulated 8-channel ARoF-WDM-PON transmission system even for 20 km long SSMF.

In this case the BER of received and down-converted 28 GHz mm-wave PAM4 modulated signal is 2.1×10^{-2} . It is worth to mention that even for B2B transmission the demonstrated BER is slightly below defined BER threshold (1.4×10^{-4} , please see Fig. 2(d)). This drop in the BER performance with applying the narrow (50 GHz) channel spacing can be explained by the small

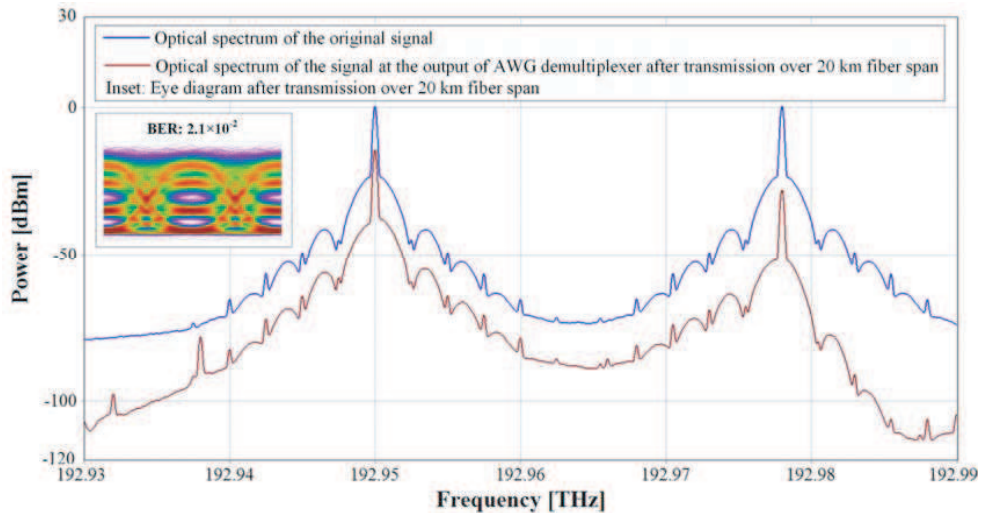


Figure 4: Optical spectra of the worst performing channel containing two 2.5 Gbaud/s PAM-4 modulated and 50 GHz spaced optical signals at the output of RoF transmitter (launched optical signal) and on the output of AWG demultiplexer after transmission over 20 km SMF fiber span. Insets show the corresponding eye diagram of the 2.5 Gbaud/s mm-wave signal received and down-converted after 20 km transmission.

cut-off frequency passband (3-dB bandwidth is 35 GHz) of commercially used AWG multiplexer/demultiplexer. Respectively, the signal at IF frequency is considerably affected by the bandwidth (3-dB bandwidth is 35 GHz) of 50 GHz spaced AWGs, as it is situated at 28 GHz inter-channel spacing relative to the main (baseband) frequency. The described effect can be observed by comparing the spectrums of the original and de-multiplexed signals as shown in Fig. 4. That is also confirmed with the relatively high BER value obtained for B2B transmission (please see Fig. 2(d)).

4. CONCLUSION

The main goal of this work is to provide PAM-4 analog radio over fiber A-RoF transmission through widely used PON's architecture to support higher spectral efficiency providing a good trade-off between performance and complexity for future broadband fifth-generation (5G/5G+) cellular mobile communication networks. We have demonstrated the perspective solution for latest fifth-generation (5G/5G+) cellular mobile communication network -passive optical access network (PON) architecture together with analog radio over fiber (A-RoF) segment integration, which is technologically transformed into ARoF-WDM-PON transmission system for transmission of intermediate frequencies (IF) over commercially used optical network. We show the use of PAM-4 modulation format with possible ARoF transmitter implementation into improved fiber-optical line terminals (OLT), enabling to generate PAM4 modulated signal and perform mm-wave signal transmission over the WDM-PON network allowing to support higher spectral efficiency and improve the performance, i.e., increase available transmission speed for the end-users.

In our research, we used VPI Photonics Design Suite software for design and simulation of 8-channel 2.5 Gbaud/s per channel PAM-4 modulated WDM-PON optical transmission system with investigated ARoF transmission of 28 GHz mm-wave signal for 5G mm-wave hybrid photonics-wireless interface. Our proposed 8-channel 2.5 Gbaud/s PAM-4 modulated ARoF-WDM-PON optical transmission system with 100 GHz channel spacing is capable to provide transmission through ODN over SSMF fiber for at least 20 km with BER significantly smaller than FEC threshold (BER is 4×10^{-8}), while after 40 km transmission the BER of received and down-converted mm-wave signal was 2.8×10^{-3} , which is slightly above FEC threshold. That means that it is technically difficult to ensure such a transmission distance of 40 km with the use of 100 GHz channel interval commercial AWG.

We also show that the use of 50 GHz channel spacing for such as hybrid system is limited. It is not possible to implement 50 GHz channel interval utilizing commercial AWG where 3-dB bandwidth is 35 GHz and, consequently, WR-WDM-PON architecture, due to the low cut-off frequency passband of AWG multiplexer/de-multiplexer, that leads to the considerable cut-off of the 28 GHz IF signal.

As a result, we conclude that our utilized WR-WDM-PON architecture can be utilized for the generation and transmission of 2.5 Gbaud/s PAM-4 modulated mm-wave signal ensuring channel spacing of 100 GHz, however for smaller channel spacing, e.g., 50 GHz and smaller, the use of wavelength-selective switch (WSS) with tunable bandwidth may be considered.

ACKNOWLEDGMENT

This work has been supported by the European Regional Development Fund within the Activity 1.1.1.2 “Post-doctoral Research Aid” of the Specific Aid Objective 1.1.1 “To increase the research and innovative capacity of scientific institutions of Latvia and the ability to attract external financing, investing in human resources and infrastructure” of the Operational Programme “Growth and Employment” (No. 1.1.1.2/VIAA/1/16/044).

REFERENCES

1. Lu, F., M. Xu, L. Cheng, J. Wang, S. Shen, H. J. Cho, and G. K. Chang, “Adaptive digitization and variable channel coding for enhancement of compressed digital mobile fronthaul in PAM-4 optical links,” *Journal of Lightwave Technology (JLT)*, ISSN:0733-8724, Vol. 35, No. 21, 4714–4720, November 1, 2017.
2. Li, H., X. Li, M. Luo, and S. Yu, “Digital mobile fronthaul employing enhanced noise shaping based pulse code modulation with nonuniform quantizer,” *2018 European Conference on Optical Communication (ECOC)*, 1–3, Rome Italy, September 23–27, 2018, ISBN: 978-1-5386-4862-9.
3. Noorani, R., L. Yi, P. Li, and W. Hu, “Demonstration of 25 Gbit/s PAM4 hybrid photonic-wireless transmission,” *2017 Asia Communications and Photonics Conference (ACP)*, 1–3, Guangzhou, China, November 10–13, 2017, ISBN: 978-1-943580-34-7.
4. Zeb, K., X. Zhang, and Z. Lu, “High capacity mode division multiplexing based MIMO enabled all-optical analog millimeter-wave over fiber fronthaul architecture for 5G and beyond,” *IEEE Access*, Vol. 7, 89522–89533, 2019.
5. Zhou, W., P. Gou, K. Wang, M. Kong, X. Li, L. Zhao, Z. Zhu, and J. Yu, “PAM-4 wireless transmission based on look-up-table pre-distortion and CMMA equalization at V-band,” *2018 Optical Fiber Communications Conference and Exposition (OFC)*, 1–3, San Diego, CA, USA, 2018, March 11–15, 2018, ISBN: 978-1-943580-38-5.
6. Zeb, K., Z. G. Lu, J. R. Liu, P. J. Poole, M. Rahim, G. Pakulski, Y. X. Mao, C. Y. Song, and X. Zhang, “Experimental demonstration of photonic MMW-over fiber system for next generation access networks,” *2019 Photonics North (PN)*, 1–1, Quebec City, QC, Canada, May 21–23, 2019, ISBN: 978-1-7281-3738-4.
7. Browning, C., A. Farhang, A. Saljoghei, N. Marchetti, V. Vujicic, L. E. Doyle, and L. P. Barry, “5G wireless and wired convergence in a passive optical network using UF-OFDM and GFDM,” *2017 IEEE International Conference on Communications Workshops (ICC Workshops)*, 386–392, Paris France, May 21–25, 2017, ISSN: 2474-9133.
8. Korra, A., T. Salgals, J. Porins, E. Kazoks, R. Miho, and S. Spolitis, “Performance analysis of cost-efficient high-speed up to 32 Gbit/s WDM-PON next-generation access network with dispersion compensation,” *Progress In Electromagnetics Research Symposium (PIERS 2019)*, 1–7, Rome, Italy, June 17–20, 2019.
9. ITU-T Recommendation G.989.2, “Digital sections and digital line system — Optical line systems for local and access networks – 40-Gigabit-capable passive optical networks 2 (NG-PON2): *Physical media dependent (PMD) layer specification*,” 1–122, 2019.
10. Salgals, T., L. Skladova, K. Vilcane, J. Braunfelds, and S. Spolitis, “Evaluation of 4-PAM, NRZ and duobinary modulation formats performance for use in 20 Gbit/s DWDM-PON optical access systems,” *Advances in Wireless and Optical Communications (RTUWO 2018)*, 134–138, Riga Latvia, November 15–16, 2018, ISBN: 978-1-5386-5558-0.
11. Salgals, T., S. Spolitis, S. Olonkins, and V. Bobrovs, “Investigation of 4-PAM modulation format for use in WDM-PON optical access systems,” *2017 Progress In Electromagnetics Research Symposium — Spring (PIERS)*, 1–4, St. Petersburg, Russia, May 22–25, 2017.

12. ITU-T Recommendation G.9803, “Transmission systems and media digital systems and networks — Access networks — *Optical line systems for local and access networks, internet of Radio over fibresystems*,” 1–50, 2018.
13. Kottkamp, M., A. Pandey, D. Raddino, A. Roessler, and R. Stuhlauff, *5G New Radio Fundamentals, Procedures, Testing Aspects*, 1–462, Rohde & Schwarz, July 1, 2019.
14. Tikhomirov, A., E. Omelyanchuk, and A. Semenova, “Recommended 5G frequency bands evaluation,” *2018 Systems of Signals Generating and Processing in the Field of on Board Communications*, 1–5, Moscow, Russia, March 14–15, 2018, ISBN: 978-1-5386-5622-8, doi: 10.1109/SOSG.2018.8350639.
15. Shinjo, S., K. Nakatani, J. Kamioka, R. Komaru, H. Noto, H. Nakamizo, S. Yamaguchi, S. Uchida, A. Okazaki, and K. Yamanaka, “A 28 GHz-band highly integrated GaAs RF front-end Module for Massive MIMO in 5G,” *2018 IEEE MTT-S International Microwave Workshop Series on 5G Hardware and System Technologies (IMWS-5G)*, 1–3, Dublin, Ireland, August 30–31, 2018, ISBN: 978-1-5386-1197-5.
16. Salgals, T., L. Skladova, J. Porins, V. Bobrovs, and S. Spolitis, “Analog radio-over-fiber WDM-PON architecture for 5G millimeter-wave interfac,” *Progress In Electromagnetics Research Symposium (PIERS 2019)*, 1–7, Rome, Italy, June 17–20, 2019.
17. Pang, X., O. Ozolins, S. Gaiarin, M. I. Olmedo, R. Schatz, U. Westergren, D. Zibar, S. Popov, and G. Jacobsen, “Evaluation of high-speed EML-based IM/DD links with PAM modulations and low-complexity equalization,” *ECOC 2016; 42nd European Conference on Optical Communication (ECOC)*, 1–3, Dusseldorf, Germany, September 18–22, 2016, ISBN: 978-3-8007-4274-5.
18. ITU-T Recommendation G.694.1, “Transmission media and optical systems characteristics — Characteristics of optical systems: *Spectral grids for WDM applications: DWDM frequency grid*,” 7–12, 2012.
19. Thomas, V. A., M. El-Hajjar, and L. Hanzo, “Millimeter-wave radio over fiber optical upconversion techniques relying on link nonlinearity,” *IEEE Communications Surveys & Tutorials*, Vol. 18, No. 1, 29–53, First quarter 2016, ISSN: 1553-877X, DOI: 10.1109/COMST.2015.2409154.
20. IXblue Photonics “MX-LN series 1550 nm band Intensity Modulators,” *Technical Specification*, 1–6, 2019.
21. SHF Communication Technologies AG “Datasheet SHF 100 BP Broadband Amplifier,” *Technical Specification*, 1–12, 2016
22. Breuer, D., E. Weis, S. Krauss, and M. Dueser, “5G converged transport in future access networks,” *Broadband Coverage in Germany; 11. ITG-Symposium*, 1–4, Berlin, Germany, March 29–30, 2017, ISBN: 978-3-8007-4397-1.
23. Behrens, C., E. Weis, and D. Breuer, “Technologies for convergence of fixed and mobile access: An operator’s perspective,” *2017 Optical Fiber Communications Conference and Exhibition (OFC)*, 1–3, Los Angeles, CA, USA, March 19–23, 2017, ISBN: 978-1-9435-8023-1.
24. Discovery Semiconductors Inc., “High optical power handling InGaAs photodiodes to 50 GHz,” *Technical Specification*, 1–4, 2003.
25. Yasir, M., M. Aldrigo, M. Dragoman, A. Dinescu, M. Bozzi, S. Iordanescu, and D. Vasilache, “Integration of antenna array and self-switching graphene diode for detection at 28 GHz,” *IEEE Electron Device Letters*, Vol. 40, No. 4, 628–631, February 13, 2019, ISSN: 1558-0563.
26. Hesler, J., K. Hui, and T. Crowe, “Ultrafast millimeter-wave and THz envelope detectors for wireless communications,” *2012 IEEE International Topical Meeting on Microwave Photonics*, 93–94, Noordwijk, Netherlands, September 11–14, 2012, ISBN: 9781-4673-2865-4.
27. Li, C. H., M. F. Wu, C. H. Lin, and C. T. Lin, “W-band OFDM RoF system with simple envelope detector down-conversion,” *2015 Optical Fiber Communications Conference and Exhibition (OFC)*, 1–3, Los Angeles, CA, USA, March 22–26, 2015, ISBN: 978-1-5575-2937-4.
28. Zhou, Y., G. Huang, S. Nam, and B. S. Kim, “A novel wide-band envelope detector,” *2008 IEEE Radio Frequency Integrated Circuits Symposium*, 219–222, Atlanta, GA, USA, June 15–17, 2008, ISBN: 978-1-4244-1808-4, ISSN: 2375-0995.

PAPER-9: Hybrid ARoF-WDM PON Infrastructure for 5G Millimeter-wave Interface and Broadband Internet Service

T. Salgals, A. Ostrovskis, A. Ipatovs, V. Bobrovs and **S. Spolitis**, "Hybrid ARoF-WDM PON Infrastructure for 5G Millimeter-wave Interface and Broadband Internet Service," *2019 Photonics & Electromagnetics Research Symposium - Fall (PIERS - Fall)*, pp. 2161-2168, Xiamen, China, Dec. 17-20, (2019), DOI: [10.1109/PIERS-Fall48861.2019.9021479](https://doi.org/10.1109/PIERS-Fall48861.2019.9021479)

Hybrid ARoF-WDM PON Infrastructure for 5G Millimeter-wave Interface and Broadband Internet Service

Toms Salgals¹, Armands Ostrovskis², Aleksandrs Ipatovs¹,
Vjaceslavs Bobrovs¹, and Sandis Spolitis^{1,2}

¹Institute of Telecommunications, Riga Technical University, Riga, Latvia

²Communication Technologies Research Center, Riga Technical University, Riga, Latvia

Abstract— In this paper, the architecture of hybrid analog radio over fiber (ARoF) and next-generation (NG) wavelength division multiplexed passive optical network (WDM-PON) infrastructure for broadband internet services and the latest fifth-generation (5G) cellular mobile communications is proposed. Investigated ARoF-WDM PON architecture is a trade-off between technology and cost for future 5G mobile cellular communications to meet the internet service requirements, allowing to increase system capacity ensuring higher spectral and energy efficiency. In our proposed infrastructure the widespread used passive optical access network (PON) architecture is technologically transformed to the AROF-WDM-PON transmission system without replacing existing network elements, by integrating baseband units (BBUs) or mobile radio transmitters located in optical line terminal (OLT) at the central office (CO) and the receiving radio unit (RU) part of mobile base stations, leaving the traditional WDM-PON broadband architecture unchanged. In our investigated ARoF-WDM PON transmission system model, designed in the simulation environment, we research the possible ARoF system implementation scenarios into the PON's segment, which has been now standardized to the 40 Gigabit-capable next-generation passive optical network (NG-PON2) standard providing an unique solution for hybrid fiber optical infrastructure serving as the next step for future 5G wireless communication networks.

1. INTRODUCTION

The past decades have seen mobile technologies indicated with several generations: 2G, 3G, 4G (LTE) and at the moment the latest generation (5G) [1]. Within the framework of new technology introduction and implementation for a comprehensive range of users, the previously used generations gradually will be evolved out. It is expected that the latest fifth-generation (5G) mobile communication networks will be capable to provide and fulfill service requirements to end-users, required services and daily used overflow of electrical gadgets [2]. The services within the scope of fifth-generation are categorized into three types: 1) High data rate services (HDR), 2) Internet of things (IoT) and 3) Ultra-reliable low-latency services (URLLC) [2–4].

Traditionally long-term evolution (LTE) cellular radio access network (RAN) combines basic bandwidth processing and radio functions in each physical base station and is still used for 4th generation (4G) mobile technology [5]. According to ITU-T G.9803 rec. it is proposed to implement analog radio over fiber (ARoF) into the passive optical network (PON) segment, coexisting with a 40-Gigabit-capable passive optical network (NG-PON2) supporting the international mobile telecommunication (IMT) systems over the fiber core network, e.g., optical distribution network (ODN) [6, 7]. The basic function of the radio over fiber (RoF) via optical line terminal (OLT) is to convert radio signals to optical signals and accommodate multiple (BBUs) to make efficient use of the ODN together with wavelength division multiplexing (WDM) technique wavelength grid [8]. The PON's core network functions are to provide connections between the RoF OLT and the RoF optical network terminals (ONU), where optical-to-electrical (O/E) conversion into radio signals at radio frequency band necessary for the base station (BS) is provided by ODN [9]. Connectivity between ODN and remote radio unit (RU) enables efficient frequency up/down conversion function for mm-wave up/down-stream data transmission between multiple-input and multiple-output (MIMO) antennas [9, 10]. To achieve the required capacity and end-user data rates across different regions, possible mm-wave frequency RF-bands of sub-6 GHz and above are considered [11, 12]. Due to management of frequency bands up to 28 GHz (Ka-band) in Europe, Japan, Korea, and Australia, as well as higher frequency bands in the US (≤ 72 GHz V-band), China (≤ 43.5 GHz V-band) are considered for deployment [2, 4, 9, 12].

2. SIMULATION MODEL OF HYBRID AROF-WDM PON TRANSMISSION SYSTEM

The goal is to design hybrid AROF-WDM-PON passive optical access communication system and evaluate the performance of such a data and radio signal transmission system, which implements

baseband radio processing in a service provider's central office (CO) part, allows the effective provision of broadband internet and cellular data transmission between the service provider's CO and end-users. As well, it allows reducing overall costs through a pooling of resources and providing end-users data rates.

The widespread used passive optical access network (PON) architecture can be technologically transformed into the AROF-WDM-PON transmission system without the need to replace existing network elements, by integrating mobile radio transmitters of baseband units BBUs and the receiving radio unit RU parts of mobile base stations, leaving the traditional WDM-PON broadband architecture the same. Developed and further investigated the 8-channel A-RoF-WDM-PON optical transmission system model is depicted in Fig. 1.

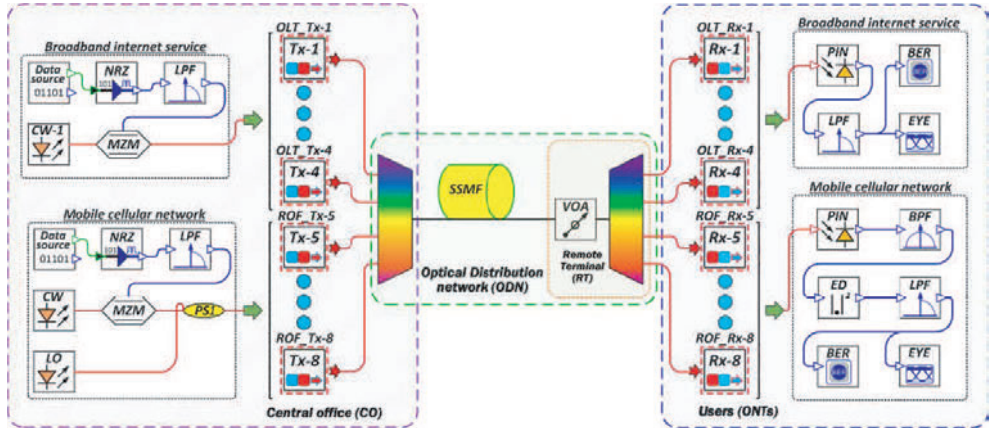


Figure 1: Simulation scheme of 8-channel hybrid AROF-WDM-PON transmission system which consists of two parts: (1st) 4-channel 10 Gbit/s per channel NRZ-OOK modulated signal transmission for broadband internet service and (2nd) 4-channel 2.5 Gbit/s per channel NRZ-OOK modulated multi-channel mobile cellular network — transmission of 28 GHz mm-wave signals for 5G mm-wave interface.

The hybrid AROF-WDM-PON system consists of cellular mobile and broadband internet transmission parts. The cellular mobile part consists of baseband units BBUs and mobile base station incoming receiver radio unit parts RUs, providing a radio signal transmission over optical fiber (RoF), while the broadband internet transmission part consists of an optical line terminal OLT, which houses optical transmitters (Tx) and a receiver or optical network terminal (ONT). Central office CO of our research model includes optical line terminal OLT, which consists of eight transmitters (OLT-Tx), where four of them are unchanged for commercial fiber optical broadband internet end-user data transmission and four of them are modified for A-RoF system data containing 28 GHz carrier frequencies (even more considered frequency bands depending on allocation of regional spectrum management) generation and transport of an intermediate frequencies through existing fiber optical distribution network ODN [6].

The cellular mobile transmission part is based on the principle, where the baseband radio signal processing is located in the CO part and performed by two carrier signals, used to transmit the radio signal through the optical fiber. The inter-channel frequency difference of the first data modulated optical carrier (F_1) and second local oscillator optical carrier (F_{LO1}) is equal to the necessary mm-wave radiofrequency (RF) for transmitting wireless signals at the receiver side. By transmitting the two carrier signals F_1 and F_{LO1} with an appropriate inter-channel interval through the ODN, providing backbone routing network operation, an uplink conversion of the transmitted signal to a carrier frequency (IF) is performed by a broadband semiconductor photodiode (PIN) within a single optical channel. Here $IF = F_{LO1} - F_1$, enabling the direct wireless transmission of data between remote base station radio units RU as well as multiple-input and multiple-output (MIMO) antennas [5, 13, 14].

Displayed results in our research are obtained by the newest RSoftOptSim simulation software with the use of the Time Domain Split-Step (TDSS) method to solve differential equations describing signal propagation. Additionally, Matlab software was used to estimate obtained quality of the

received signals, perform BER measurements and display them [5, 15]. In our research, we show the obtained performance of our investigated AROF-WDM-PON transmission system according to a commercially used BER threshold equal to 10^{-12} . Forward-error-correction (FEC) with a 10^{-3} BER performance threshold is shown to determine the system's performance and received signal capability after 20 and 40 km SSMF optical link transmission, in line with NG-PON requirements [16]. According to ITU-T G.964.1 recommendation, dense WDM architecture with 50 GHz and 100 GHz channel spacing with 193.1 THz central frequency is chosen for our investigated hybrid AROF-WDM-PON transmission system standardized to 40 G PON (NG-PON2) requirements. As it is shown in Fig. 1, our investigated 8-channel hybrid A-RoF-WDM-PON optical transmission system model consists of four channels operating at 2.5 Gbit/s for cellular mobile communication millimeter-wave (mm-wave) interface and four 10 Gbit/s channels for broadband internet connection.

The transmitter part of the cellular mobile communication mm-wave interface consists of base-band units (BBUs) integrated into the OLT of WDM-PON located on the CO side. According to the fundamental architecture of a typical RoF system for the case of downstream transmission, the CO includes OLT with four transmitters, where each of them has been modified to operate as RoF transmitter (ROF_Tx) designed for A-RoF system data containing 28 GHz intermediate frequencies IF generation. Trade-off radio communication service and requirements for the balance in radio signal frequency band, the necessary number of radio signals and optical path loss for various applications are achievable by investigated hybrid AROF-WDM-PON architecture taking into account ITU-T G. 9803 requirements [6]. Each of AROF transmitters located in OLT for generation of mm-wave IF signal bases on homodyne up-conversion principle and is designed by using two continuous wave (CW) laser sources with a linewidth of 30 MHz, where one of them (with +8 dBm output power) is directly connected to intensity Mach-Zehnder modulator (MZM) [5, 14]. Second light source with channel spacing equal to necessary intermediate frequency IF and mm-wave generation (in our case for 28 GHz (Ka-band)), by the inter-channel interval between two laser sources is operating as a local oscillator (LO) with a related output power of +1 dBm. The electrical pseudo-random bit sequence (PRBS) data source and non-return to zero (NRZ) driver encode the logical data into NRZ electrical signal [17, 18]. The MZM is driven at 2.5 Gbit/s bit rate by previously formed and Bessel low-pass filter (3-dB bandwidth is 3 GHz) filtered electrical NRZ signal.

The broadband internet transmitter part has an optical line terminal — OLT, which consists of four transmitters (OLT_Tx) located in a CO. Each OLT_Tx transmitter contains CW laser source (30 MHz linewidth, +9 dBm output power), which is directly connected to the intensity MZM modulator. The MZM is driven at 10 Gbit/s bit rate by previously formed and Bessel low-pass filter (3-dB bandwidth is 10 GHz) filtered electrical NRZ signal, passing from NRZ driver. MZM chirp factor, which guarantees the highest performances in terms of maximum achievable dispersion-tolerance in optical fiber links, was not observed. As a result, the transmitted optical signal was affected by the impact of chromatic dispersion (CD), which leads to inter-symbol interference. In such a way, it performs E/O conversion using one single carrier (optical tone) for transmission through ODN [5, 18, 19].

The mean launch power of +4 dBm and optical budget (OB) depending on optical path loss within range of 18 to 33 dB is provided for ROF_Tx and OLT_Tx transmitter optical output signals of our investigated hybrid AROF-WDM PON transmission system, which are compliant with the NG-PON2 defined E1 class optical distribution network ODN requirements [6, 7]. Optical signals from each RoF-Tx and OLT_Tx are coupled together by using arrayed waveguide grating (AWG) multiplexer with 3.5 dB insertion loss, and depending on the simulation model, 50 or 100 GHz channel interval (3-dB bandwidth is 30 GHz) is chosen. A single-mode optical fiber (SSMF) span with 0.2 dB/km attenuation and 16 ps/nm/km dispersion coefficients (at 1550 nm reference wavelength), according to ITU-T G.652 recommendation, is used for the ODN link sections with the length of 20 and 40 km [7]. After optical signal transmission through the ODN section, a variable optical attenuator (VOA) is used to obtain BER versus received optical power of the signal. After transmission through ODN and VOA, intermediate frequency (IF) and single-carrier are separated by AWG de-multiplexer located in the remote terminal (RT). AWG de-multiplexer has 3.5 dB insertion loss, 30 GHz 3-dB bandwidth, and depending on the simulation model, it has 50 GHz or 100 GHz channel spacing.

The receiver side consists of optical network terminals (ONTs) divided into two parts: 1st for broadband internet service (channels 1 to 4) and 2nd for a cellular mobile network (channels 5 to 8).

In the first scenario, each ONT receiver (ONT_Rx) of the broadband internet network consists of a semiconductor photoreceiver (PIN) with 50 GHz 3-dB bandwidth, the responsivity of 0.65 A/W, applicable to increase the total bitrate per wavelength up to 40 Gbit/s in line with ITU-T G.989.2 NGPON2 requirements [7, 20]. After O/E conversion by PIN photoreceiver, received electrical signal is pre-filtering by electrical Bessel low-pass filter (LPF) with 9 GHz 3-dB electrical bandwidth. In the second part, designed for the cellular mobile network, each ONT receiver (ROF_Rx) consists of the same 50 GHz photoreceiver (PIN) applicable in both scenarios with ITU-T G.989.2 [7]. After O/E conversion by PIN photoreceiver, pre-filtering of received electrical signal for each channel is realized by the electrical Bessel band-pass filter (BPF), which is tuned to 28 GHz central frequency and has 28 GHz 3-dB electrical bandwidth. Afterward, homodyne down-conversion is realized by the homodyne signal processing technique using a passive Schottky diode-based envelope detector (ED) [4, 10, 11, 21]. Received and down-converted modulated baseband signal is filtered by an electrical Bessel low-pass filter (LPF) with 3 GHz 3-dB electrical bandwidth.

3. RESULTS AND DISCUSSION

In our research we show A-RoF implementation and generation of 28 GHz mm-wave radio signals within the existing WDM-PON network without replacing its elements, leaving fiber-optical line terminals OLT as well as fiber optical network terminals ONT unchanged for end-user fiber optical

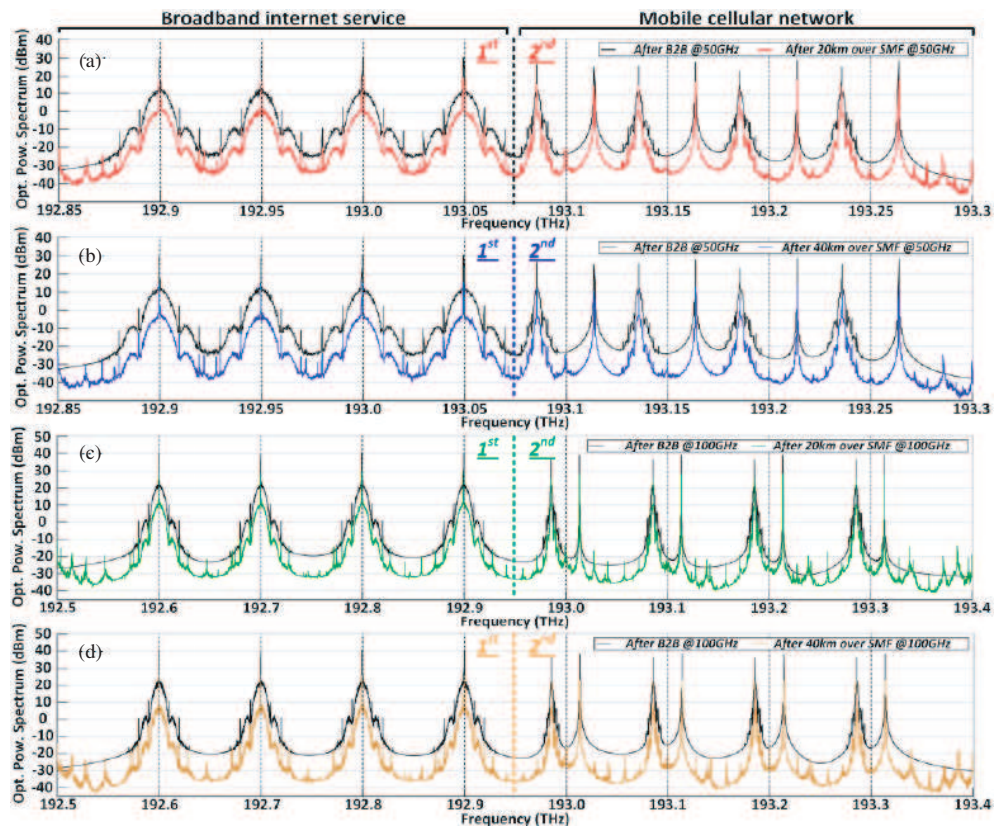


Figure 2: Optical spectra of multiplexed 8-channel hybrid ARoF-WDM PON transmission which consists of two parts: (1st) 4-channel 10 Gbit/s per channel NRZ modulated signal transmission for broadband internet service and (2nd) 4-channel 2.5 Gbit/s per channel NRZ modulated 28 GHz mm-wave signal transmission before B2B and after transmission through (a) 20 km long ODN (50 GHz ch. spacing), (b) 40 km ODN (50 GHz ch. spacing), (c) 20 km ODN (100 GHz ch. spacing), and (d) 40 km ODN (100 GHz ch. spacing).

broadband internet connections. Optical signal spectra after B2B and 20/40 km long ODN fiber span transmission are shown, please see Fig. 2.

As one can see in Figs. 2(c) and 2(d), the 8-channel 100 GHz spaced NRZ signals spectra of each channel in B2B and after 20 to 40 km long ODN fiber span transmission in our hybrid ARoF-WDM-PON transmission system are shown. In our research we applied also narrower channel spacing, therefore the second investigated channel spacing was 50 GHz. Spectra of 8-channel 50 GHz spaced hybrid ARoF-WDM-PON transmission system in B2B configuration and after transmission over 20 to 40 km long SSMF fiber spans is shown in Figs. 2(a) and 2(b).

The obtained BER versus received optical power at PIN photoreceiver in two different scenarios with 50 and 100 GHz channel spacing for (1st) 10 Gbit/s (broadband internet) NRZ signal and (2nd) down-converted 2.5 Gbit/s (28 GHz mm-wave 5G signal) after transmission over 20 to 40 km long ODN SSMF fiber span in 8-channel hybrid ARoF-WDM-PON transmission is shown in Fig. 3.

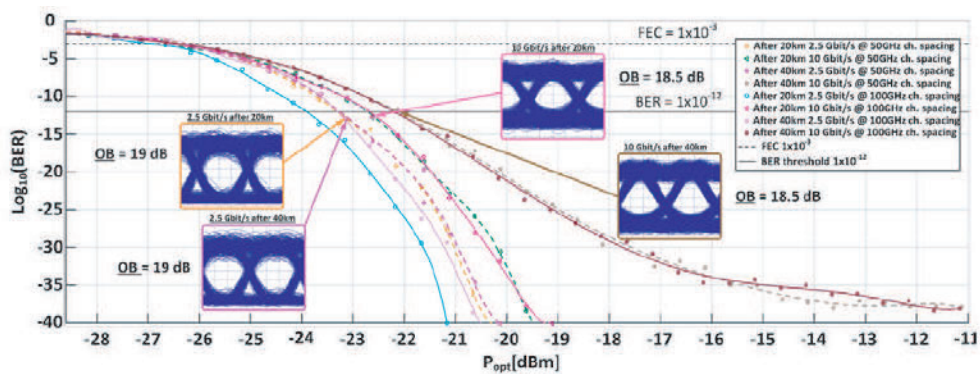


Figure 3: BER vs. received optical power for 1st down-converted 2.5 Gbit/s (28 GHz mm-wave 5G signal) and 2nd 10 Gbit/s (broadband internet) NRZ signal after hybrid ARoF-WDM PON transmission over 20 and 40 km SSMF fiber. Insets show the received signal eye diagrams after transmission over SSMF for 2.5 and 10 Gbit/s bitrates with 50 GHz ch. spacing.

The measured average optical output power after 20 km long ODN SSMF section for 1st received down-converted 2.5 Gbit/s 28 GHz mm-wave signal for 50 GHz spaced 8-channel hybrid ARoF-WDM PON transmission system varied from -20.15 dBm to -28.65 dBm, where the BER of received signal was from 9.8×10^{-39} to 2.2×10^{-1} . After a 40 km long ODN SSMF section, for 50 GHz spacing measured average optical output power varied from -20.12 dBm to 28.62 dBm, where the BER was 9.8×10^{-39} to 2.2×10^{-1} . In the case of 2nd down-converted 2.5 Gbit/s 28 GHz mm-wave received signal the error-free transmission was observed. In the first scenario with 10 Gbit/s NRZ signal (broadband internet) after 20 km long ODN SSMF section transmission for 50 GHz spaced 8-channel hybrid ARoF-WDM PON transmission system measured optical output power varied from -19.12 dBm to -27.12 dBm where the BER of received signal was 9.9×10^{-39} to 3.1×10^{-1} , respectively. Measured average optical power after 40 km long ODN SSMF section transmission at 50 and 100 GHz spacing varied from -11.12 to -28.62 dBm and -11.15 dBm to -28.65 dBm, where the BER of received signal was from 1.3×10^{-38} to 2.4×10^1 and 9.6×10^{-37} to 2.2×10^1 , respectively.

As one can see in Figs. 4(a), 4(b), 4(c), 4(d) and Figs. 5(a), 5(c) the signal quality after 20 and 40 km long ODN SSMF section transmission for cellular network mm-wave and end-user fiber optical broadband signal is good, the eye is open and error-free transmission is provided.

After 40 km transmission through the ODN section over standard SSMF fiber, we conclude that received signal for broadband internet with 10 Gbit/s bitrate is mainly affected by the impact of crosstalk and chromatic dispersion. As one can see in Figs. 5(b) and 5(d) after transmission for our investigated 8-channel hybrid ARoF-WDM PON transmission system with 50 and 100 GHz channel spacing through 40 km ODN in 1st scenario for (broadband internet service) the NRZ signal operating at 10 Gbit/s bitrate per channel was mainly affected by CD, where the BER was 1.3×10^{-38} and 9.6×10^{-37} .

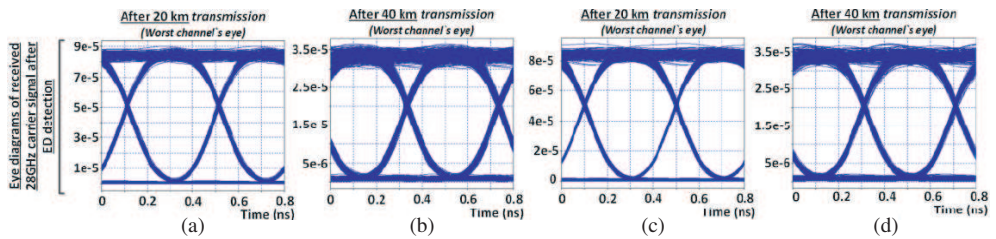


Figure 4: Eye diagrams of received 2.5 Gbit/s NRZ modulated 28 GHz mm-wave signal after ED detection: (a) after 20 km over SSMF transmission at 50 GHz spacing, (b) after 40 km over SSMF transmission at 50 GHz spacing, (c) after 20 km over SSMF transmission at 100 GHz spacing, (d) after 40 km over SSMF transmission at 100 GHz spacing for multiplexed 8-channel hybrid ARoF-WDM PON transmission system.

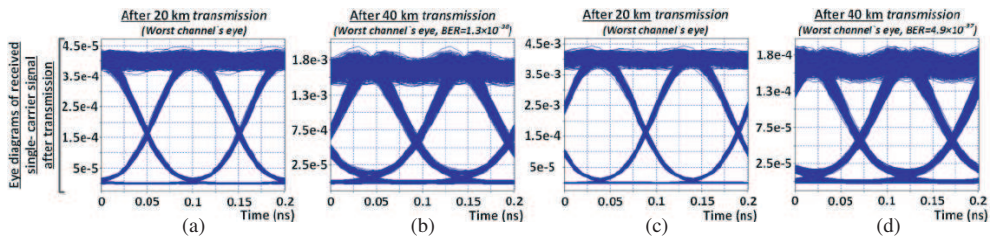


Figure 5: Eye diagrams of received 10 Gbit/s NRZ modulated broadband internet signal: (a) after 20 km over SSMF transmission at 50 GHz spacing, (b) after 40 km over SSMF transmission at 50 GHz spacing, (c) after 20 km over SSMF transmission at 100 GHz spacing, (d) after 40 km over SSMF transmission at 100 GHz spacing for multiplexed 8-channel hybrid ARoF-WDM PON transmission system.

4. CONCLUSION

In this paper, the architecture of hybrid analog radio over fiber (ARoF) and next-generation (NG) wavelength division multiplexed passive optical network (WDM-PON) infrastructure designed for broadband internet services and the latest fifth-generation (5G) cellular mobile communications is proposed. We have demonstrated the widespread used passive optical network (PON) architecture, which is technologically transformed to the ARoF-WDM-PON transmission system without replacing existing network elements, by integrating BBU's mobile radio transmitters and receiving parts of the mobile base stations RU, leaving the WDM-PON broadband architecture unchanged. The trade-off between radio communication services and requirements for a balance in radio signal frequency band, as well as the capability to increase the capacity of bitrate in the fiber optical networks, the necessary number of radio signals according to 40G NG-PON req. and optical path loss for various applications is achievable by investigated hybrid ARoF-WDM-PON architecture.

In our investigated transmission system model, designed in the environment of simulation software, we researched the possible A-RoF system implementations into PON's segment with dense WDM channel frequency grid (50 GHz), which has been standardized to next-generation (NG-PON2) standard, providing a unique solution for hybrid fiber optical infrastructure serving as the next step for future 5G wireless communication networks. The feasibility of the proposed system is verified by the obtained quality of the received signal, accordingly, eye diagrams and measurements of BER performance. Our proposed 8-channel ARoF-WDM-PON transmission system model is capable to provide data transmission over optical fiber distribution network with a length of up to 40 km with E1 class optical path loss using standardized ITU-T G.652 optical fiber as a signal transmission media.

ACKNOWLEDGMENT

This work has been supported by the European Regional Development Fund within the Activity 1.1.1.2 "Post-doctoral Research Aid" of the Specific Aid Objective 1.1.1 "To increase the research and innovative capacity of scientific institutions of Latvia and the ability to attract external financing, investing in human resources and infrastructure" of the Operational Programme "Growth and

Employment” (No. 1.1.1.2/VIAA/1/16/044).

REFERENCES

- Vij, S. and A. Jain, “5G: Evolution of a secure mobile technology,” *2016 3rd International Conference on Computing for Sustainable Global Development (INDIACom)*, 2192–2196, New Delhi, India, March 16–18, 2016, ISBN: 978-9-3805-4421-2.
- Kottkamp, M., A. Pandey, D. Raddino, A. Roessler, and R. Stuhlauffh, “5G new radio fundamentals, procedures, testing aspects,” *Rohde & Schwarz*, 1–462, July 1, 2019.
- Annaidh, B. Ó., P. Fitzgerald, H. Berney, R. Lakshmanan, N. Coburn, S. Geary, and B. Mulvey, “Devices and sensors applicable to 5G system implementations,” *2018 IEEE MTT-S International Microwave Workshop Series on 5G Hardware and System Technologies (IMWS-5G)*, 1–3, Dublin, Ireland, August 30–31, 2018, ISBN: 978-1-5386-1197-5.
- Yasir, M., M. Aldrigo, M. Dragoman, A. Dinescu, M. Bozzi, S. Iordanescu, and D. Vasilache, “Integration of antenna array and self-switching graphene diode for detection at 28 GHz,” *IEEE Electron Device Letters*, Vol. 40, No. 4, 628–631, February 13, 2019, ISSN: 1558-0563.
- Salgals, T., L. Skladova, J. Porins, V. Bobrovs, and S. Spolitis, “Analog radio-over-fiber WDM-PON architecture for 5G millimeter-wave interfac,” *Progress In Electromagnetics Research Symposium (PIERS 2019)*, 1–7, Rome, Italy, June 17–20, 2019.
- ITU-T Recommendation G.9803, “Transmission systems and media digital systems and networks — Access networks — Optical line systems for local and access networks, internet of Radio over fibresystems,” 1–50, 2018.
- ITU-T Recommendation G.989.2, “Digital sections and digital line system — Optical line systems for local and access networks — 40-Gigabit-capable passive optical networks 2 (NG-PON2): Physical media dependent (PMD) layer specification,” 1–122, 2019.
- ITU-T Recommendation G.694.1, “Transmission media and optical systems characteristics — Characteristics of optical systems: Spectral grids for WDM applications: DWDM frequency grid,” 7–12, 2012.
- Zeb, K., X. Zhang, and Z. Lu, “High capacity mode division multiplexing based MIMO enabled all-optical analog millimeter-wave over fiber fronthaul architecture for 5G and beyond,” *IEEE Access*, Vol. 7, 89522–89533, July 2, 2019, ISSN: 2169-3536.
- Hesler, J., K. Hui, and T. Crowe, “Ultrafast millimeter-wave and THz envelope detectors for wireless communications,” *2012 IEEE International Topical Meeting on Microwave Photonics*, 93–94, Noordwijk, Netherlands, September 11–14, 2012, ISBN: 978-1-4673-2865-4.
- Li, C. H., M. F. Wu, C. H. Lin, and C. T. Lin, “W-band OFDM RoF system with simple envelope detector down-conversion,” *2015 Optical Fiber Communications Conference and Exhibition (OFC)*, 1–3, Los Angeles, CA, USA, March 22–26, 2015, ISBN: 978-1-5575-2937-4.
- Tikhomirov, A., E. Omelyanchuk, and A. Semenova, “Recommended 5G frequency bands evaluation,” *2018 Systems of Signals Generating and Processing in the Field of on Board Communications*, 1–5, Moscow, Russia, March 14–15, 2018, ISBN: 978-1-5386-5622-8.
- Thomas, V. A., M. El-Hajjar, and L. Hanzo, “Millimeter-wave radio over fiber optical upconversion techniques relying on link nonlinearity,” *IEEE Communications Surveys & Tutorials*, Vol. 18, No. 1, 29–53, March 5, 2015, ISSN: 1553-877X.
- Latunde, A. T., M. Milosavljevic, P. Kourtessis, and J. Senior, “OQAM-OFDM RoF with IM-DD remote heterodyne 28 GHz upconversion for 5G millimeter RANs,” *2016 18th International Conference on Transparent Optical Networks (ICTON)*, 1–4, Trento, Italy, July 10–14, 2016, ISBN: 978-1-5090-1467-5.
- Spolitis, S., V. Bobrovs, and G. Ivanovs, “Reach improvement of spectrum-sliced dense WDM-PON system,” *2012 Seventh International Conference on Broadband, Wireless Computing, Communication and Applications (BWCCA 2012)*, 296–301, Victoria, BC, Canada, November 12–14, 2012, ISBN: 978-1-4673-2972-9.
- Salgals, T., S. Spolitis, S. Olonkins, and V. Bobrovs, “Investigation of 4-PAM modulation format for use in WDM-PON optical access systems,” *Progress In Electromagnetics Research Symposium (PIERS 2017)*, 1–4, St. Petersburg, Russia, May 22–25, 2017.
- Salgals, T., L. Skladova, K. Vilcane, J. Braunfelds, and S. Spolitis, “Evaluation of 4-PAM, NRZ and duobinary modulation formats performance for use in 20 Gbit/s DWDM-PON optical access systems,” *2018 Advances in Wireless and Optical Communications (RTUWO)*, 134–138, Riga, Latvia, November 15–16, 2018, ISBN: 978-1-5386-5558-0.

18. Korra, A., T. Salgals, J. Porins, E. Kazoks, R. Miho, and S. Spolitis, “Performance analysis of cost-efficient high-speed up to 32 Gbit/s WDM-PON next-generation access network with dispersion compensation,” *Progress In Electromagnetics Research Symposium (PIERS 2019)*, 1–7, Rome, Italy, June 17–20, 2019.
19. Bravetti, P., G. Ghislotti, and S. Balsamo, “Chirp-inducing mechanisms in Mach-Zehnder modulators and their effect on 10 Gb/s NRZ transmission studied using tunable-chirp single drive devices,” *Journal of Lightwave Technology (JLT)*, Vol. 22, No. 2, 605–611, March 30, 2004, ISSN: 1558-2213.
20. Finisar, “50 GHz DWDM single high-speed photodetector XPDV21x0(RA),” *Technical Specification*, 1–5, 2015.
21. Zhou, Y., G. Huang, S. Nam, and B. S. Kim, “A novel wide-band envelope detector,” *2008 IEEE Radio Frequency Integrated Circuits Symposium*, 219–222, Atlanta, GA, USA, June 15–17, 2008, ISBN: 978-1-4244-1808-4, ISSN: 2375-0995.

PAPER-10: Kerr Optical Frequency Combs With Multi-FSR Mode Spacing in Silica Microspheres

E. A. Anashkina, V. Bobrovs, **T. Salgals**, I. Brice, J. Alnis, and A. V. Andrianov, "Kerr Optical Frequency Combs With Multi-FSR Mode Spacing in Silica Microspheres," *IEEE Photon. Technol. Lett.* 33(9), 453–456, (2021), DOI: [10.1109/LPT.2021.3068373](https://doi.org/10.1109/LPT.2021.3068373)

Kerr Optical Frequency Combs With Multi-FSR Mode Spacing in Silica Microspheres

Elena A. Anashkina^{1b}, Vjaceslavs Bobrovs^{2b}, Toms Salgals^{2b}, Inga Brice^{2b}, Janis Alnis^{2b},
and Alexey V. Andrianov^{1b}

Abstract—We experimentally demonstrate Kerr optical frequency combs (OFCs) with mode spacing of 1, 2, 3, 5, 6, and 8 free spectral ranges (FSRs) corresponding to 0.4, 0.8, 1.2, 2, 2.4, and 3.2 THz, respectively, in silica microspheres pumped by CW C-band lasers in the anomalous dispersion range. Experimental realizations are based on using standard telecom equipment and components such as SMF-28e fiber for producing microspheres and fiber tapers for pump coupling and OFC outcoupling. Numerical simulation is performed to support the experimental results and explain the observed spectral asymmetry in OFCs by the influence of the 3rd-order dispersion.

Index Terms—Microsphere, whispering gallery mode (WGM), free spectral range (FSR), optical frequency comb (OFC).

I. INTRODUCTION

OPTICAL frequency combs (OFCs) generated in microresonators with whispering gallery modes (WGMs) are attractive for basic science and numerous applications (see, for example, the reviews [1], [2] and references therein). OFCs can be generated in manifold steady-state and dynamical regimes depending on system parameters in spherical, disk, ring, toroidal, and other microresonators made of glass or crystalline materials [1]. The spacing between OFC modes may correspond to microresonators' free spectral range (FSR), to multiples of FSR, or even to rational fractions of the FSR [1]–[6]. OFCs with multi-FSR mode spacing were observed in crystalline resonators [3], [4]. Detailed theoretical analysis in the framework of Lugiato-Lefever equation (LLE) in resonators with only a Kerr nonlinearity and constant 2nd-order dispersion was performed in [7]. A numerical

study of multi-FSR OFCs driven by a continuous wave (CW), cosine-modulated pump with allowance for 2nd-order and 3rd-order dispersion was presented in [8]. It was found that 3rd-order dispersion can modify OFC mode spacing and decrease the intensity of OFC modes, but for the considered parameters multi-FSR OFC spectra were almost symmetric relative to the pump frequency [8].

Silica microspheres with high Q -factors can be produced in an easy and cheap way by melting the end of a standard telecom fiber [9], and the observed nonlinear effects in them can be described by the LLE as for other types of microresonators. So, silica microspheres are a convenient platform for OFC generation and study of different regimes. Such microspheres can be pumped by telecom C-band CW lasers through a silica fiber taper, so the experimental realization can be based on using standard telecom components and equipment.

Here we generated single- and multi-FSR Kerr OFCs in silica microspheres in two experimental series and tested spectral long-term stability for up to 5 h. Numerical simulation of the LLE was performed to support the experimental results and explain the observed asymmetry in OFC spectra.

II. RESULTS

A. The First Experimental Series

The first experimental series was conducted according to the scheme shown in Fig. 1(a). The radiation of 'CW laser1' with a linewidth of 100 kHz and 6 dBm optical output power adjusted at a C-band wavelength of 1552 nm was amplified with an Er-doped fiber amplifier (EDFA) up to 23.5 dBm and after passing an optical Faraday isolator (ISO) and a polarization controller (PC) was coupled through a silica fiber taper to a silica microsphere. The fiber taper was manufactured by melting and stretching a silica fiber with a gas burner. A microsphere with a diameter of about 170 μm was produced from an SMF-28e telecom fiber by melting its end in a fiber splicer as described in [10]. Microphotos of the produced microsphere in two mutually orthogonal planes are presented in Fig. 1(b). Our microsphere was multimode, but we adjusted its position to the taper in such a way that only one WGM family (fundamental as we believe) was strongly excited (see Fig. 3(c)). The curve presented in Fig. 1(d) corresponds to the resonance from this family and gives Q -factor of $\sim 0.4 \cdot 10^8$. The dispersion for the fundamental WGMs was calculated by numerical solution of the characteristic equation as described in [11]. The calculated zero dispersion wavelength (ZDW) was 1545 nm. So, the microsphere was pumped in a slightly

Manuscript received February 5, 2021; revised March 9, 2021; accepted March 21, 2021. Date of publication March 24, 2021; date of current version March 31, 2021. This work was supported in part by the Center of Excellence «Center of Photonics» funded by the Ministry of Science and Higher Education of the Russian Federation under Contract 075-15-2020-906 (the study presented in Subsections II.B, II.C., and II.D) and in part by the European Regional Development Fund "The Development of Quantum Optics and Photonics in University of Latvia" under Project I.1.1.5/19/A/003 (the study presented in Subsections II.A). (Corresponding author: Elena A. Anashkina.)

Elena A. Anashkina and Alexey V. Andrianov are with the Institute of Applied Physics, Russian Academy of Sciences, 603950 Nizhny Novgorod, Russia (e-mail: elena.anashkina@ipfran.ru; andrian@ipfran.ru).

Vjaceslavs Bobrovs and Toms Salgals are with the Institute of Telecommunications, Riga Technical University, 1048 Riga, Latvia (e-mail: vjaceslavs.bobrovs@rtu.lv; toms.salgals@rtu.lv).

Inga Brice and Janis Alnis are with the Institute of Atomic Physics and Spectroscopy, University of Latvia, 1004 Riga, Latvia (e-mail: inga.brice@lu.lv; janis.alnis@lu.lv).

Color versions of one or more figures in this article are available at <https://doi.org/10.1109/LPT.2021.3068373>.

Digital Object Identifier 10.1109/LPT.2021.3068373

1041-1135 © 2021 IEEE. Personal use is permitted, but republication/redistribution requires IEEE permission. See <https://www.ieee.org/publications/rights/index.html> for more information.

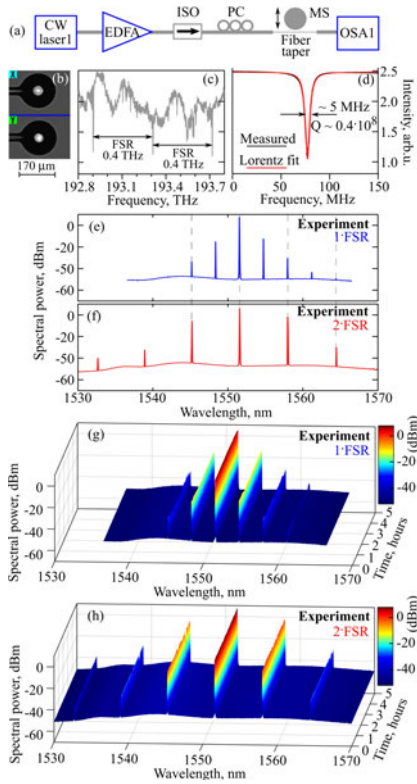


Fig. 1. (a) Simplified schematic for the first experimental series. (b) Microphotos of the produced silica microsphere in two mutually orthogonal planes. (c) Microsphere resonances. (d) Measured (black) and Lorentz fitted (red) single-resonant curve for Q -factor determination. (e) Spectrum with $1 \cdot \text{FSR}$ mode spacing. (f) Spectrum with $2 \cdot \text{FSR}$ mode spacing. Spectra as functions of time for OFCs with $1 \cdot \text{FSR}$ mode spacing (g) and $2 \cdot \text{FSR}$ mode spacing (h).

anomalous dispersion regime. The microsphere and the fiber taper were enclosed in a separate box for dust prevention and humidity control providing long-term stability of the generated OFCs. A piezo micro-positioner was used to control the relative position between the microsphere and the fiber taper as described in [9], [12]. The output spectra were recorded by a telecom Optical Spectrum Analyzer ‘OSA1’.

OFC generation was initiated by hard bumping the pump fiber which translated to abrupt changes in the pump power coupled to the microsphere (‘power kick method’ [13]). The process was not 100% successful, so that several attempts were needed to attain OFC generation. First, we generated an OFC with a single-FSR mode spacing of 0.4 THz which corresponds to the theoretical FSR estimation. The corresponding spectrum is plotted in Fig. 1(e). Next, by changing the relative position between the microsphere and the taper, we obtained an OFC with $2 \cdot \text{FSR}$ mode spacing of 0.8 THz with the spectrum plotted in Fig. 1(f). We tested the long-term stability of these OFCs for 5 h; the corresponding almost constant spectra as functions of time are shown in Fig. 1(g)

and (h) for mode spacings of $1 \cdot \text{FSR}$ and $2 \cdot \text{FSR}$, respectively. The recording time of 5 h for each measurement shown in Fig. 1(g,h) was chosen to obtain them in one day.

B. The Second Experimental Series

The second experimental series was conducted with a microsphere very similar to that described in the previous subsection but with another laser source pumping a microsphere in the anomalous dispersion regime at a longer wavelength farther from the ZDW. The spectrum demonstrating a Kerr OFC with $1 \cdot \text{FSR}$ mode spacing in the 1490–1630 nm range is plotted in Fig 2(a). This spectrum was used as a reference to find a mode spacing for multi-FSR OFCs demonstrated in Fig. 2 in the 1st column. A simplified experimental scheme is shown in Fig. 2(b). The microsphere was pumped through a fiber taper by ‘CW laser2’ (10 kHz linewidth, 18 dBm maximum power, 190.3–197.9 THz tuning range). Output spectra were registered by telecom ‘OSA2’.

To attain single- and multi-FSR OFCs, the regime of sweeping the frequency of ‘CW laser2’ near a resonant WGM at ~ 1570 nm was turned on. The laser frequency offset as a function of time is plotted in Fig. 2(c). When sweeping near a resonant WGM, OFC generation and its absence were observed dynamically and periodically. Next, we stopped the sweeping regime on the descending branch after 30 s (see Fig. 2(c)). A steady-state OFC with single- or multi-FSR mode spacing was often generated due to mode pulling [1], [2] for the pump power of about 13 dBm before the taper. The coupled pump power and the pump detuning from exact resonance are the key parameters governing the formation of different structures in a microresonator [7]. However, in the experiment it is difficult to access these parameters independently. We varied the distance between the taper and the microsphere that mainly affects the coupling coefficient and the pump wavelength. Due to mode pulling effect the effective detuning in the steady-state regime is also power-dependent and is not directly related to the shift of the pump wavelength from the cold resonance. By varying both parameters we could find the regimes corresponding to the generation of multi-FSR OFCs with a mode spacing of $3 \cdot \text{FSR}$, $5 \cdot \text{FSR}$, $6 \cdot \text{FSR}$, and $8 \cdot \text{FSR}$ (see Fig. 2, the 1st column), although these regimes were quite sensitive to the changes of any of the system parameters. The dotted gray lines through the left column in Fig. 2 show the correspondence between the modes generated in multi-FSR OFCs and in the single-FSR OFC. It is seen that the spectra are slightly asymmetric relative to the pump, and the short-wavelength harmonics have higher spectral intensities compared to the long-wavelength ones. The pedestals in the experimental spectra originate from the pump laser. Stability of OFC spectra with single- and multi-FSR mode spacing was tested for times of the order of 10 minutes. We did not observe operation in bistable regimes.

C. Numerical Simulation Supporting the Second Experimental Series

To support the experimental results and explain the observed spectral features, we performed a numerical simulation based

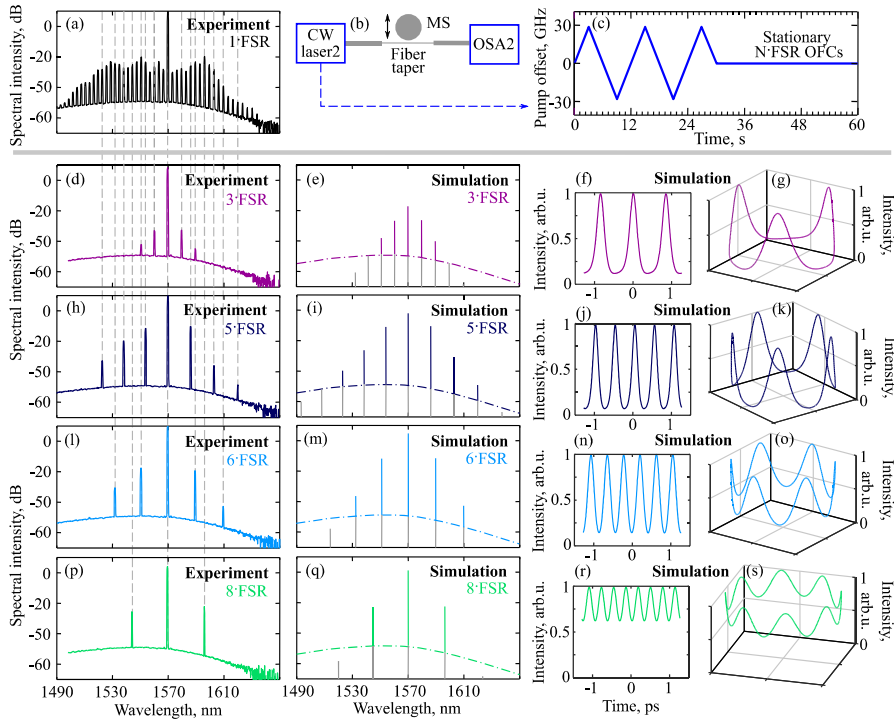


Fig. 2. (a) Spectrum with 1 · FSR mode spacing for the second experimental series. (b) Simplified schematic for the second experimental series. (c) Pump offset from the central frequency as a function of time. Results for OFCs with N · FSR mode spacing (under the horizontal gray bold line): experimental spectra (the 1st column), numerically simulated spectra (the 2nd column), numerically simulated intensity distribution in the time domain (the 3rd column), and the corresponding 3D representation (the 4th column) for 3 · FSR (d-g), for 5 · FSR (h-k), for 6 · FSR (l-o), and for 8 · FSR (p-s).

on the LLE. Home-made software based on the Split-step Fourier method was used for numerical modeling of the master equation written as [1], [14]:

$$\frac{\partial A}{\partial t} = -(1 + i\alpha)A + iA \int R(s) |A(t, \tau - s)|^2 ds - i \frac{b_2}{2} \frac{\partial^2 A}{\partial \tau^2} + \frac{b_3}{6} \frac{\partial^3 A}{\partial \tau^3} + F \quad (1)$$

where $A(t, \tau)$ is the intracavity dimensionless field; τ and t are the fast and slow dimensionless times; α is the phase detuning of the pump field F from the nearest resonance, b_2 and b_3 are the coefficients of 2nd-order and 3rd-order dispersion, and $R(t)$ is the Raman nonlinear response function [14]:

$$R(t) = (1 - f_R)\delta(t) + f_R(\tau_1^{-2} + \tau_2^{-2})\tau_1 \sin(t/\tau_1) \exp(-t/\tau_2) \quad (2)$$

where f_R is the Raman fraction; $\delta(t)$ is the Dirac delta function; $\tau_1 = 12.2$ fs, and $\tau_2 = 32$ fs.

It is known that multi-FSR (N · FSR) OFCs corresponding to the so-called Turing roll patterns (consisting of an integer number of rolls N in the microresonator) can be obtained in an anomalous dispersion range for certain areas of parameters [4], [7]. The analytical expression of this number N at a pump

threshold depending on α and b_2 is given in [7] for $b_3 = 0$ and $f_R = 0$. This expression is not valid above the threshold power with allowance for $b_3 \neq 0$, but we used it as the first guess in selecting the parameters for obtaining regimes with spectra similar to the experimental ones.

We took $b_2 = -0.05$, $b_3 = 0.002$ and varied α and $|F|^2$ to attain a good agreement between experimental and simulated spectra (compare Fig. 2, the 1st and 2nd columns under the horizontal gray, bold line). The presented numerical OFCs with mode spacings of 3 · FSR, 5 · FSR, 6 · FSR, and 8 · FSR were obtained for α equal to 1.7, 0.5, -1.5, and -6.5, respectively. The corresponding steady-state temporal structures with 3, 5, 6, and 8 rolls are plotted in the 3rd column and in 3D representation in the 4th column. The dashed-dotted lines shown in the 2nd column in the simulated spectra emulate the pedestal of ‘CW laser2’. So, Figs. 2(d, e, f, g) correspond to 3 · FSR OFC, Figs. 2(h, i, j, k) to 5 · FSR OFC, Figs. 2(l, m, n, o) to 6 · FSR OFC, and Figs. 2(p, q, r, s) to 8 · FSR OFCs. Thus, the experimental spectra coincide with the numerical ones obtained with allowance for the 2nd-order and 3rd-order dispersion, and Kerr and Raman nonlinearity. Note that our spectra are asymmetric relative to the pump (short-wavelength harmonics have higher intensities compared

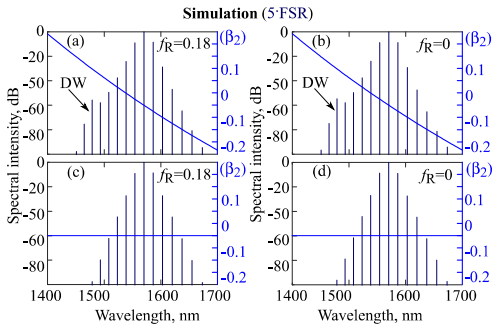


Fig. 3. Numerical spectra of OFCs with 5 · FSR mode spacing (dark-blue lines, left axes) simulated for $b_3 > 0$ and $f_R = 0.18$ (a), $b_3 > 0$ and $f_R = 0$ (b), $b_3 = 0$ and $f_R = 0.18$ (c), and $b_3 = 0$ and $f_R = 0$ (d). (a-d) Wavelength-dependent dispersion β_2 (blue curves, right axes).

to long-wavelength harmonics), but in the model without allowance for 3rd-order dispersion and Raman nonlinearity, the spectra are symmetric [7].

D. Numerical Study of Spectrum Asymmetry

To explain the asymmetry of the experimental spectra shown in Fig. 2(d, h, l), also observed for the numerical spectra in Fig. 2(e, i, m, q), we performed a more detailed simulation with switching on and switching off the 3rd-order dispersion and Raman response in Eq. (1). We considered the mode spacing of 5 · FSR corresponding to Fig. 2(i). The spectrum in the full model with allowance for $b_3 > 0$ and $f_R = 0.18$ in a wider range compared to Fig. 2(i) is shown in Fig. 3(a) together with the wavelength-dependent dispersion. In this case, short-wavelength harmonics have higher spectral intensities than long-wavelength ones. In addition, the dispersive wave (DW) generation in the normal dispersion region is observed. DW generation is a well-known effect for both optical fibers [14] and microresonators [2]. Then, we switched off the Raman response ($f_R = 0$) and obtained the spectrum shown in Fig. 3(b), which is very similar to the spectrum shown in Fig. 3(a). Therefore, the contribution of Raman nonlinearity was insignificant in this case. Then, we switched off the 3rd-order dispersion ($b_3 = 0$) and calculated the spectra with $f_R = 0.18$ (Fig. 3(c)) and $f_R = 0$ (Fig. 3(d)). In these cases, very similar symmetric spectra without DW were obtained. The same results were obtained when simulating OFCs with different mode spacings (3 · FSR, 6 · FSR, and 8 · FSR). Thus, the experimentally observed asymmetry of the spectra is explained by the influence of the 3rd-order dispersion. For the considered regimes, the effect of Raman nonlinearity is negligible.

III. CONCLUSION

We have experimentally attained single- and multi-FSR Kerr OFCs with mode spacings of 1 · FSR, 2 · FSR, 3 · FSR, 5 · FSR, 6 · FSR, and 8 · FSR corresponding to 0.4, 0.8, 1.2, 2, 2.4, and 3.2 THz, respectively, in 170- μm silica microspheres pumped by C-band CW lasers in the anomalous dispersion range and tested the spectral long-term stability for up to 5 hours. Numerical simulation based on the LLE was performed to support the experimental results and to explain the observed spectral asymmetry in OFCs by the influence of the 3rd-order dispersion. For the considered regimes, the Raman nonlinearity is negligible. Thus, multi-FSR OFC generation in a silica microsphere is a simple way to obtain steady-state long-term stable OFCs with a mode spacing of the order of 1 THz.

REFERENCES

- [1] A. Pasquazi *et al.*, "Micro-combs: A novel generation of optical sources," *Phys. Rep.*, vol. 729, pp. 1–81, Jan. 2018.
- [2] T. J. Kippenberg, A. L. Gaeta, M. Lipson, and M. L. Gorodetsky, "Dissipative Kerr solitons in optical microresonators," *Science*, vol. 361, no. 6402, Aug. 2018, Art. no. eaan8083.
- [3] I. S. Grudinin, N. Yu, and L. Maleki, "Generation of optical frequency combs with a CaF_2 resonator," *Opt. Lett.*, vol. 34, no. 7, pp. 878–880, Apr. 2009.
- [4] A. Coillet, Z. Qi, I. V. Balakireva, G. Lin, C. R. Menyuk, and Y. K. Chember, "On the transition to secondary Kerr combs in whispering-gallery mode resonators," *Opt. Lett.*, vol. 44, no. 12, pp. 3078–3081, Jun. 2019.
- [5] Y. Xu *et al.*, "Harmonic and rational harmonic driving of microresonator soliton frequency combs," *Optica*, vol. 7, no. 8, pp. 940–946, 2020.
- [6] Y. Xu, A. Sharples, J. Fatome, S. Coen, M. Erkintalo, and S. G. Murdoch, "Frequency comb generation in a pulse-pumped normal dispersion Kerr mini-resonator," *Opt. Lett.*, vol. 46, no. 3, pp. 512–515, 2021.
- [7] C. Godey, I. V. Balakireva, A. Coillet, and Y. K. Chember, "Stability analysis of the spatiotemporal Lugiato-Lefever model for Kerr optical frequency combs in the anomalous and normal dispersion regimes," *Phys. Rev. A, Gen. Phys.*, vol. 89, no. 6, Jun. 2014, Art. no. 063814.
- [8] X. Hu *et al.*, "Spatiotemporal evolution of a cosine-modulated stationary field and Kerr frequency comb generation in a microresonator," *Appl. Opt.*, vol. 54, no. 29, pp. 8751–8757 Oct. 2015.
- [9] A. Chiasera *et al.*, "Spherical whispering-gallery-mode microresonators," *Laser Photon. Rev.*, vol. 4, no. 3, pp. 457–482, Apr. 2010.
- [10] A. V. Andrianov and E. A. Anashkina, "Single-mode silica microsphere Raman laser tunable in the U-band and beyond," *Results Phys.*, vol. 17, Jun. 2020, Art. no. 103084.
- [11] E. A. Anashkina *et al.*, "Microsphere-based optical frequency comb generator for 200 GHz spaced WDM data transmission system," *Photonics*, vol. 7, no. 3, p. 72, Sep. 2020.
- [12] J. Braunfelds *et al.*, "Frequency comb generation in WGM microsphere based generators for telecommunication applications," *Quantum Electron.*, vol. 50, no. 11, pp. 1043–1049, Nov. 2020.
- [13] K. E. Webb, M. Erkintalo, S. Coen, and G. Stuart Murdoch, "Experimental observation of coherent cavity soliton frequency combs in silica microspheres," *Opt. Lett.*, vol. 41, no. 20, pp. 4613–4616, Oct. 2016.
- [14] G. P. Agrawal, *Nonlinear Fiber Optics*, 6th ed. Amsterdam, The Netherlands: Elsevier, 2019.

PAPER-11: Optical Frequency Combs Generated in Silica Microspheres in the Telecommunication C-, U-, and E-Bands

E. A. Anashkina, M. P. Marisova, **T. Salgals**, J. Alnis, I. Lyashuk, G. Leuchs, **S. Spolitis**, V. Bobrovs, and A. V. Andrianov, "Optical Frequency Combs Generated in Silica Microspheres in the Telecommunication C-, U-, and E-Bands", *Photonics* 8(9), 345, (2021), DOI: [10.3390/photonics8090345](https://doi.org/10.3390/photonics8090345)

Article

Optical Frequency Combs Generated in Silica Microspheres in the Telecommunication C-, U-, and E-Bands

Elena A. Anashkina^{1,2,*}, Maria P. Marisova^{1,2}, Toms Salgals³, Janis Alnis⁴, Ilya Lyashuk³, Gerd Leuchs^{1,5}, Sandis Spolitis³, Vjaceslavs Bobrovs³ and Alexey V. Andrianov¹

- ¹ Institute of Applied Physics of the Russian Academy of Sciences, 46 Ul'yanov Street, 603950 Nizhny Novgorod, Russia; marisova.mariya@rambler.ru (M.P.M.); gerd.leuchs@mpl.mpg.de (G.L.); andrianov@ipfran.ru (A.V.A.)
 - ² Advanced School of General and Applied Physics, Lobachevsky State University of Nizhny Novgorod, 23 Gagarin Ave., 603950 Nizhny Novgorod, Russia
 - ³ Institute of Telecommunications of Riga Technical University, 12 Azenes Street 1, 1048 Riga, Latvia; toms.salgals@rtu.lv (T.S.); ilja.lasuks@rtu.lv (I.L.); sandis.spolitis@rtu.lv (S.S.); vjaceslavs.bobrovs@rtu.lv (V.B.)
 - ⁴ Institute of Atomic Physics and Spectroscopy, University of Latvia, 3 Jelgavas Street, 1004 Riga, Latvia; janis.alnis@lu.lv
 - ⁵ Max Planck Institute for the Science of Light, Staudtstr. 2, D-91058 Erlangen, Germany
- * Correspondence: elena.anashkina@ipfran.ru

Abstract: Optical frequency combs (OFCs) generated in microresonators with whispering gallery modes are demanded for different applications including telecommunications. Extending operating spectral ranges is an important problem for wavelength-division multiplexing systems based on microresonators. We demonstrate experimentally three spectrally separated OFCs in the C-, U-, and E-bands in silica microspheres which, in principle, can be used for telecommunication applications. For qualitative explanation of the OFC generation in the sidebands, we calculated gain coefficients and gain bandwidths for degenerate four-wave mixing (FWM) processes. We also attained a regime when the pump frequency was in the normal dispersion range and only two OFCs were generated. The first OFC was near the pump frequency and the second Raman-assisted OFC with a soliton-like spectrum was in the U-band. Numerical simulation based on the Lugiato–Lefever equation was performed to support this result and demonstrate that the Raman-assisted OFC may be a soliton.

Keywords: silica microsphere; optical frequency comb (OFC); Raman OFC; soliton-like spectrum; four-wave mixing



Citation: Anashkina, E.A.; Marisova, M.P.; Salgals, T.; Alnis, J.; Lyashuk, I.; Leuchs, G.; Spolitis, S.; Bobrovs, V.; Andrianov, A.V. Optical Frequency Combs Generated in Silica Microspheres in the Telecommunication C-, U-, and E-Bands. *Photonics* **2021**, *8*, 345. <https://doi.org/10.3390/photonics8090345>

Received: 15 July 2021

Accepted: 19 August 2021

Published: 25 August 2021

Publisher's Note: MDPI stays neutral with regard to jurisdictional claims in published maps and institutional affiliations.



Copyright: © 2021 by the authors. Licensee MDPI, Basel, Switzerland. This article is an open access article distributed under the terms and conditions of the Creative Commons Attribution (CC BY) license (<https://creativecommons.org/licenses/by/4.0/>).

1. Introduction

Microresonators with whispering gallery modes (WGMs) are attractive for various applications, including classical and non-classical ones [1,2]. Sensing [3–5] and biosensing [6,7], optical filtering and switching [8–10], frequency stabilization, and linewidth narrowing [11,12] are just a few of them. A possibility of developing a new class of optical sources with a controllable number of robust soliton pulses operating in self-starting regimes based on coupled resonators is discussed in [13], where stabilization is implemented by linear coupling without saturable absorption. The OFC generation in microresonators, demonstrated for the first time in 2007 [14], has greatly expanded the application range of such photonic devices [1]. They are used in coherent communication [15,16], dual-comb spectroscopy [17], optical atomic clock [18], ultrafast optical ranging [19], and in many more areas.

Although on-chip microresonators belong to one of the most actively developing areas [20], silica microresonators are also of great interest, since they are a very convenient platform for the development of micro-photonic devices. For example, a four-port microdevice based on an SNAP (surface nanoscale axial photonics) microresonator produced on the surface of a silica fiber was demonstrated in [21]. The silica microresonator technologies

are easier and cheaper compared to the technologies of on-chip crystalline microresonators. The commonly used method of pump coupling into a microresonator through a tapered fiber also allows system parameters to be controlled in a wide range by varying the relative position between the resonator and the tapered fiber (while a similar adjustment is impossible for on-chip microresonators). To protect silica microresonators from air flows, dust, and high humidity, they are portably and robustly packaged [22].

Silica microresonators made of a standard optical fiber are suitable for application in the telecommunication range, since they can be pumped by narrow-linewidth C-band telecom lasers, and the corresponding experimental schemes are based on standard telecom components. Recently, we studied theoretically [23,24] and demonstrated experimentally [25] the implementation of wavelength division multiplexed-passive optical network (WDM-PON) in the C-band using an OFC generator based on a silica microsphere as a multiple light source. When several lasers (laser array) are replaced by a single OFC source, it improves the energy efficiency of the WDM fiber optical communication system, at the same time providing stable frequency spacing and strong phase relation between generated carriers (modes) [24–26]. Extending OFCs to the L-band is also a straightforward solution for WDM-PONs, when the use of the C-band is insufficient for satisfying the bandwidth demand. Particularly, it is of interest for next-generation passive optical network 2 (NG-PON2) or currently developing Super-PON networks, where frequencies of L-band are allocated for the downstream transmission [27]. U-band laser sources are mainly used for network monitoring purposes, so their development and investigation is also required.

It is known that, for Kerr OFC generation, the main mechanism is FWM, which can be readily applied for explanation of experiments. However, frequently, when generating OFCs, Raman nonlinearity plays an important role in silica microresonators. A Raman microsphere laser was demonstrated for the first time in [28]. Since then, Raman processes have been widely investigated. Many works were also devoted to study of Kerr–Raman OFCs (for example, [22,29–31]). However, the nonlinear dynamics of intracavity radiation can be so complex and diverse that it is still possible to discover new features or interesting regimes of nonlinear conversion of radiation.

Here, we demonstrate three experimental series on the generation of spectrally separated OFCs in silica microspheres. In the first series we obtained the first OFC near the pump frequency in the C-band, the second Stokes OFC in the U-band and beyond, and the third anti-Stokes OFC in the E-band. To give a qualitative explanation of OFC generation in the sidebands, we estimated gain coefficients and gain bandwidths for degenerate four-wave mixing (FWM) processes under the strong intracavity CW field approximation. To understand the opportunities for OFC generation in sidebands due to the degenerate FWM process within such an approximation, we analyzed in detail a pump frequency varying in the 190–198 THz range. In the second experimental series, by simple tuning of the pump frequency we attained frequency tunable Raman OFCs and E-band OFCs, as well as a C-band OFC. In the third experimental series, the pump frequency was in the normal dispersion range and we attained a Raman soliton-like spectrum without symmetric high-frequency sideband. To support this result, we performed numerical simulation based on the Lugiato–Lefever equation. We theoretically demonstrated Raman soliton generation in the anomalous dispersion range with the pump in the *normal* dispersion range, for the first time, to the best of our knowledge. Note that a Stokes (Raman-assisted) soliton co-existing with a fundamental dissipative Kerr soliton in the *anomalous* dispersion range was discovered in a silica on silicon microcavity [32], but this regime differs from ours.

2. Methods

2.1. Fabrication of Microspheres

Samples of silica microresonators were made of standard ITU-T G.652.D telecommunication fiber Corning SMF28e using the technology described in detail in [24]. In brief, it is based on repeated melting of a thinned fiber end with a fiber splicer. This fabrication process allows producing microspheres with reproducible and controllable diameters and

similar Q-factors. Within a few hours after manufacturing, the Q-factors, regardless of the microsphere diameter, exceeded 5×10^7 on average. Within a couple of days, the Q-factors dropped on the average to a value of 4×10^7 , and then this value remained unchanged for a long time. Two months after the preparation of the samples, the Q-factors were about 2×10^7 . Note that the record large value is $Q = 8 \times 10^9$ measured at 633 nm ~1 min after fabrication for a silica 750- μ m microsphere [33]. However, typical Q-factors for silica microspheres at 1.55 μ m used for OFC generation or Raman lasing are 10^7 – 10^8 [28,29,34,35], which agrees with our results. The reasons limiting Q-factors are discussed in [33].

We used microspheres with diameters $d \approx 165 \mu\text{m}$ and FSRs of about 400 GHz in all experiments and the corresponding numerical simulations. Note that the mode spacing 400 GHz = $M \times 100 \text{ GHz}$ ($M = 4$) satisfies the ITU-T recommendation G.694.1 [36], which specifies the spectral grid for WDM systems. To excite WGMs in a microsphere, we used tapered fibers made of Corning SMF28e with gas burners [24,25,37].

2.2. Numerical

2.2.1. Calculation of Dispersion and Nonlinear Coefficient

To find a free spectral range (FSR) and to calculate dispersion of a microsphere, we numerically solved the characteristic equation for a fundamental TE mode family [38]:

$$n \frac{\left[(kd/2)^{1/2} J_{l+1/2}(kd/2) \right]'}{(kd/2)^{1/2} J_{l+1/2}(kd/2)} = \frac{\left[(k_0d/2)^{1/2} H_{l+1/2}^{(1)}(k_0d/2) \right]'}{(k_0d/2)^{1/2} H_{l+1/2}^{(1)}(k_0d/2)}, \tag{1}$$

where the prime is the derivative with respect to the argument in parenthesis; $J_{l+1/2}$ and $H_{l+1/2}^{(1)}$ are the Bessel function and the Hankel function of the 1st kind of order $l + 1/2$, respectively; l is the azimuthal index; $k_0 = 2 \cdot \pi \cdot \nu / c$ is the light propagation constant in vacuum; ν is the frequency; $k = n(\nu) \cdot k_0$; $n(\nu)$ is the linear refractive index of the silica glass (calculated using the Sellmeier formula given in [39]). We selected the first roots of Equation (1) for the fundamental mode family. The roots were localized using a well-known approximation formula for the eigenfrequencies presented, for example, in [38]. These approximate eigenfrequencies were used as the initial values for finding the roots of Equation (1). The iterative algorithm was implemented with the dispersion of the silica glass taken into account [39]. After finding eigenfrequencies for the fundamental TE mode family, we calculated the 2nd-order dispersion [40]:

$$\beta_2 = -\frac{1}{2\pi^2 d} \frac{\Delta(\Delta\nu_l)}{(\Delta\nu_l)^3}, \tag{2}$$

where

$$\Delta\nu_l = \frac{\nu_{l+1} - \nu_{l-1}}{2}; \quad \Delta(\Delta\nu_l) = \nu_{l+1} - 2\nu_l + \nu_{l-1}. \tag{3}$$

The electric field $\tilde{E}(r)$ of the fundamental TE WGM was found as in [38], and after that, the effective WGM volume V_{eff} and nonlinear Kerr coefficient γ were calculated

$$V_{eff} = \frac{\int n^2 |\tilde{E}|^2 d^3r}{\max(n^2 |\tilde{E}|^2)}, \tag{4}$$

$$\gamma = \frac{2\pi}{\lambda} \frac{n_2}{V_{eff} / (\pi d)}, \tag{5}$$

where $n_2 = 2.2 \cdot 10^{-20} \text{ m}^2/\text{W}$ is the nonlinear refractive index of the silica glass [39]. We found $\gamma = 6.2 (\text{W} \cdot \text{km})^{-1}$ for $\nu \approx 193 \text{ THz}$ and neglected its frequency dependence in the simulations below.

2.2.2. Calculation of Intracavity CW Power

Nonlinear dynamics of the intracavity radiation neglecting Raman contribution can be described by the Lugiato–Lefever equation in the following form [1]:

$$t_R \frac{\partial E(t, \tau)}{\partial t} = \left[-\alpha - i\delta_0 + i\pi d \sum_{k \geq 2} \frac{\beta_k}{k!} \left(i \frac{\partial}{\partial \tau} \right)^k + i\gamma\pi d |E(t, \tau)|^2 \right] E(t, \tau) + \sqrt{\theta} E_{in} \quad (6)$$

where $E(t, \tau)$ is the intracavity field; t_R is the round trip time; t and τ are slow and fast times, respectively; α is the loss coefficient including intrinsic and coupling losses; β_k is the dispersion of the k -th order; θ is the coupling coefficient; and δ_0 is the frequency detuning of the pump field E_{in} from the exact resonance.

Further, to find the intracavity CW power, we applied the commonly used approach [39,41]. For the CW solution, Equation (6) is reduced to the following algebraic equation in the standard dimensionless form [41]:

$$Y^3 - 2\Delta Y^2 + (\Delta^2 + 1)Y = X. \quad (7)$$

Here, X and Y are the normalized pump and intracavity powers, respectively; Δ is the normalized detuning ($X = |E_{in}|^2(\pi \cdot d \cdot \gamma \cdot \theta / \alpha^3)$; $Y = |E|^2(\pi \cdot d \cdot \gamma / \alpha)$; and $\Delta = \delta_0 / \alpha$). We found $Y(\Delta)$ from Equation (7), and in the case when this equation had three roots, we took the maximum value corresponding to the upper stable branch.

2.2.3. Calculation of Gain Coefficients for the Degenerate FWM Processes under the Strong Intracavity CW Field Approximation

To estimate the possibility of generating sidebands via degenerate FWM under the strong intracavity field approximation, we followed the approach developed in [35,42] (which can be extended taking into account the dispersion of finesse [43]). We assumed that the total intracavity field can be approximated as the sum of a strong CW field E_0 found from Equation (7) and two small-amplitude sidebands ($|a_{\pm}| \ll |E_0|$) symmetrically shifted by $\pm\Omega$ from the pump frequency

$$E(t, \tau) \approx E_0 + a_+ \exp(i\Omega\tau) + a_- \exp(-i\Omega\tau). \quad (8)$$

Next, we rewrote Equation (6), taking into account the expression (8), and linearized this equation. After algebraic transforms, the following system of equations was obtained

$$t_R \frac{d}{dt} \begin{pmatrix} a_+ \\ a_-^* \end{pmatrix} = \begin{pmatrix} -\alpha + iB - i\pi d D_o(\Omega) & i\pi d \gamma (E_0^*)^2 \\ -i\pi d \gamma (E_0^*)^2 & -\alpha - iB - i\pi d D_o(\Omega) \end{pmatrix} \begin{pmatrix} a_+ \\ a_-^* \end{pmatrix}, \quad (9)$$

where $B = -\delta_0 + \pi d \cdot D_c(\Omega) + 2\pi d \gamma |E_0|^2$, $D_o(\Omega)$, and $D_e(\Omega)$ are odd and even dispersion, respectively

$$D_o(\Omega) = \sum_{k=1}^4 \beta_{2k+1} \Omega^{2k+1} / (2k+1)!. \quad (10)$$

$$D_e(\Omega) = \sum_{k=1}^4 \beta_{2k} \Omega^{2k} / (2k)!. \quad (11)$$

The eigenvalues of Equation (9) are

$$\lambda_{\pm}(\Omega) t_R = -\alpha + i\pi d D_o(\Omega) \pm \sqrt{4\pi d \gamma P (\delta_0 - \pi d D_e(\Omega)) - (\delta_0 - \pi d D_e(\Omega))^2 - 3\pi^2 d^2 \gamma^2 P^2} \quad (12)$$

Here, $P = |E_0|^2$ is the intracavity power.

The instability (exponential increase of a_{\pm}) is observed if $\text{Re}(\lambda_{\pm}(\Omega)) > 0$. For this case, the gain coefficient is $\text{Re}(\lambda_{\pm}(\Omega))$.

2.2.4. Numerical Simulation Based on Lugiato–Lefever Equation with the Raman Nonlinearity Taken into Account

To analyze the dynamics of the optical intracavity field taking the Raman nonlinearity into consideration, we used the generalized Lugiato–Lefever equation

$$t_R \frac{\partial E(t, \tau)}{\partial t} = \left[-\alpha - i\delta_0 + i\pi d \sum_{k \geq 2} \frac{\beta_k}{k!} \left(i \frac{\partial}{\partial \tau} \right)^k \right] E(t, \tau) + i\gamma\pi d \cdot E(t, \tau) \int R(s) |E(t, \tau - s)|^2 ds + \sqrt{\theta} E_{in}. \quad (13)$$

with the added Raman response function $R(t)$ [39]:

$$R(t) = (1 - f_R)\delta(t) + f_R(T_1^{-2} + T_2^{-2})T_1 \exp(-t/T_2) \sin(t/T_1), \quad (14)$$

where $\delta(t)$ is the Dirac delta function; $f_R = 0.18$ is the fraction of Raman contribution to the total nonlinear response; $T_1 = 12.2$ fs, and $T_2 = 32$ fs.

We used a home-made software based on the common symmetrized split-step Fourier method (SSFM) [39] for modeling intracavity light field dynamics.

3. Results

3.1. The 1st Experimental Series

In the 1st experimental series, we used the scheme shown in Figure 1a. The radiation from the output of a C-band tunable laser ‘CW pump laser (I)’ with a 4 mW power and a 100 kHz linewidth was amplified up to 220 mW using an erbium-doped fiber amplifier (EDFA). Next, the amplified signal passed a Faraday isolator (ISO), a polarization controller (PC), and was then coupled through a tapered fiber to a microsphere. Two CCD cameras were used for a rough control of the relative position between the tapered fiber and the microsphere and a piezo micro-positioner was used for precise control. We used a telecom Optical Spectrum Analyzer ‘OSA(I)’, which operates up to 1700 nm to record the output spectra. We varied the distance between the microsphere and the tapered fiber, thereby varying the effective coupling coefficient and the pump detuning from exact resonance (due to thermal mode pulling effect). It is well known that detuning is a very important parameter strongly affecting the nonlinear dynamics of intracavity radiation [44,45]. By changing the relative position between the tapered fiber and the microsphere, it is possible to obtain OFC in different regimes. Note that a similar scheme was previously used to generate a long-term stable OFC with 2-FSR mode spacing [46]. Here, in the 1st experimental series, we pumped the microsphere at 193.4 THz near the zero dispersion frequency of about 193.3 THz. The calculated dispersion of the microsphere is shown in Figure 1b. We attained the first relatively weak OFC near the pump frequency and two spectrally separated OFCs in the sidebands (Figure 1c). The second low-frequency OFC was near 180 THz and the third high-frequency OFC is located symmetrically to the second OFC.

To qualitatively explain the OFC generation in the sidebands (Figure 1c), we estimated gain coefficients and gain bandwidths as described in Section 2.2.3. We took the pump power before the microsphere $|E_{in}|^2 = 50$ mW, assumed $\alpha = \theta/2$, and set the finesse $\pi/\alpha = 5 \times 10^4$. Since detuning was not known for sure, we considered various values presented in Figure 1d. We found that the experimental sidebands shown in Figure 1c correspond to the gain bands for reasonable values of detuning. In addition, the Raman scattering may also affect the low-frequency OFC, but here we did not consider it for qualitative understanding of the FWM process.

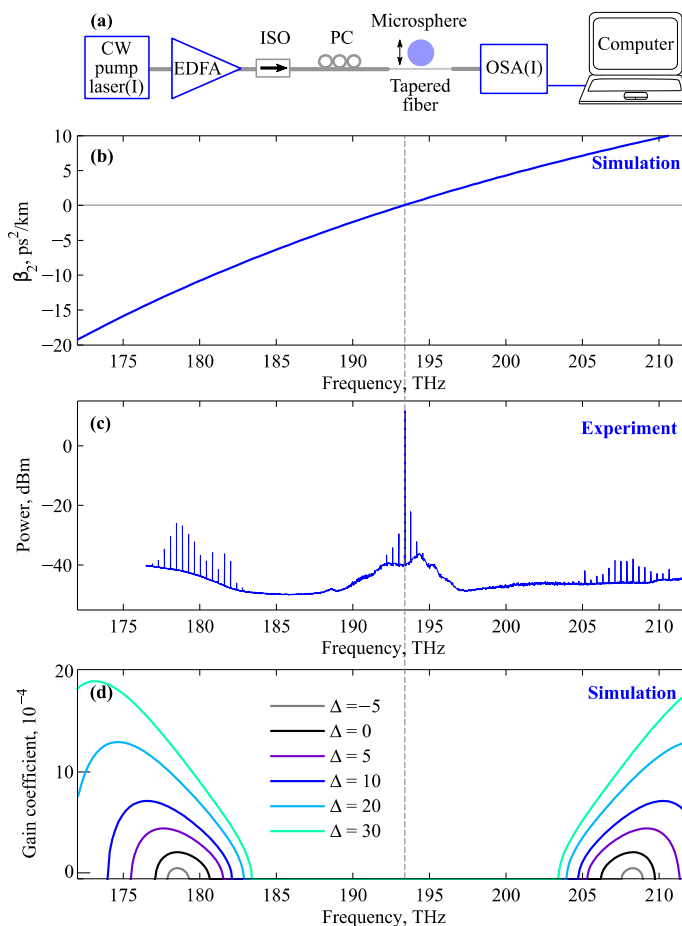


Figure 1. (a) Simplified experimental scheme for this series. (b) Numerically calculated dispersion for a silica microsphere with a diameter of 165 μm . (c) Experimental spectrum demonstrating three OFCs: near the pump and in two frequency-separated sidebands. (d) Numerically calculated gain coefficient under the strong pump approximation for a pump power of 50 mW. The dashed vertical line through (b–d) indicates zero dispersion.

3.2. Theoretical Study of FWM

To understand the potential of OFC generation in sidebands due to the degenerate FWM process for a strong intracavity pump field, we analyzed the pump frequency varying in the 190–198 THz range. This frequency range can be obtained with commercially available tunable narrow-line-width lasers. We considered a pump power $P_p = 10\text{ mW}$ and $\Delta = 0$ mW. We used the approach described in Section 2.2 for finding intracavity CW power and the approach described in Section 2.2.3 for finding gain coefficients for a FWM process.

The calculated intracavity CW powers are shown in Figure 2(a,b). For the marked points we calculated the gain coefficients as a function of the pump frequency and sideband frequency. The numerical results are shown in Figure 2(c). Figure 2(a,b) powers of 10 mW and 0 mW, respectively, are shown in the same color, regardless of $\Delta = 0$ or 15 (the corresponding points are marked in Figure 2(a)). Figure 2(c) after the same scale. The sidebands are wider and located closer to the pump frequency when it is in the

anomalous dispersion range. When the pump frequency is in the normal dispersion range, the sideband frequencies are shifted significantly from the pump frequency, which agrees with the results of the paper [3]. For the same sideband frequencies, the gain coefficients are slightly higher for $P_p = 50$ mW than for $P_p = 10$ mW. For the same detuning power (see Figure 2a), we also analyzed higher values of detuning $\Delta = 40, 60, 80$ mW and 50 mW (see also the corresponding marked points in Figure 1a). The calculated gain coefficients are given in Figure 2e (here, individual colormap scales are used for each value of detuning). The broadest gain-bands are obtained for the pump frequencies close to the zero dispersion frequency. Their spectral widths exceed 20 THz. The larger the detuning, the higher the gain coefficient.

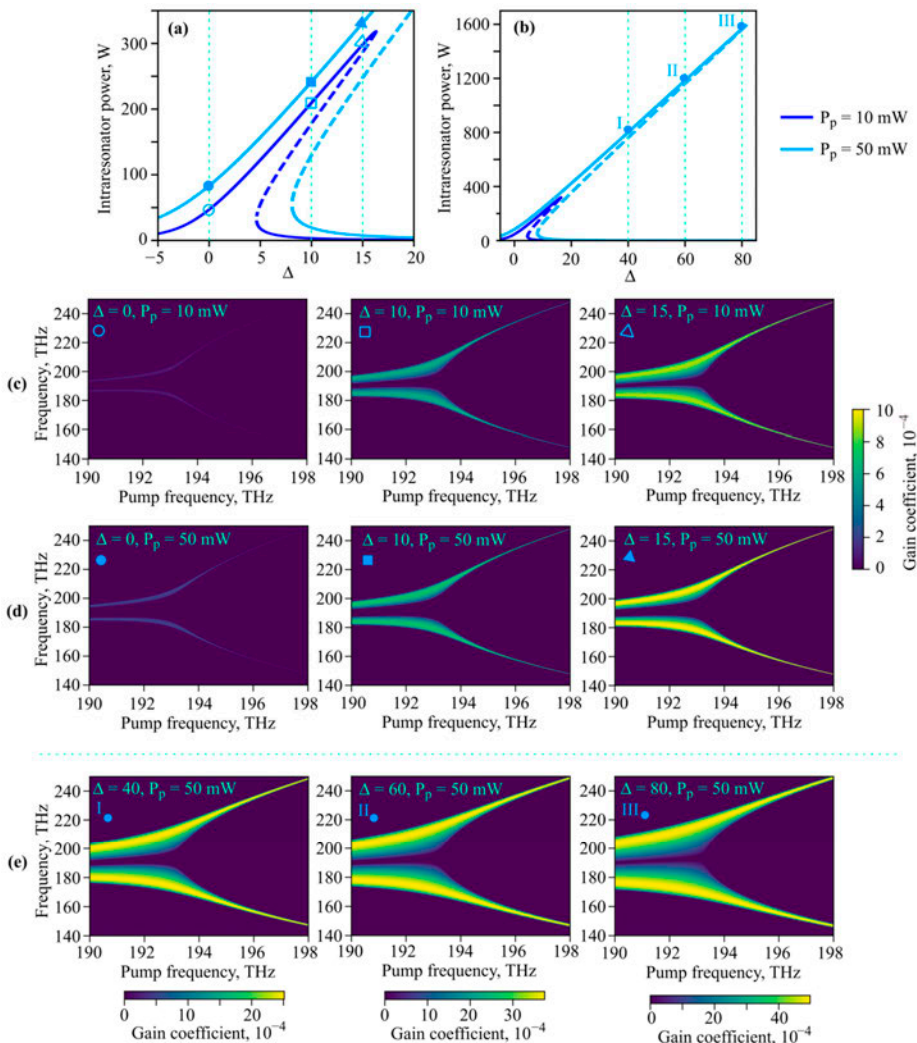


Figure 2. (a,b) Intracavity CW power versus normalized detuning calculated for pump powers of 10 and 50 mW ((a) is on a magnified scale). Numerically calculated gain coefficients under the strong pump approximation as functions of pump frequency and sideband frequency for pump powers $P_p = 10$ mW (c) and $P_p = 50$ mW (d,e). For (c,d) the same colormap scale is used. For (e) colormaps are individual for each subplot.

very weak (Figure 3c,d). In these cases, the Raman OFCs were not weak in comparison with the pump, so the simple method of calculating gain coefficients for the FWM process described in Section 2.2.3 and applied in Sections 3.1 and 3.2 could not be used.

It should be noted that in this experimental series, by simple tuning of the pump frequency we attained frequency tunable Raman soliton-like OFCs, which may be useful for applications.

3.4. The 3rd Experimental Series and Its Interpretation

Next, we removed the bandpass filter from the scheme plotted in Figure 3a and operated with the scheme shown in Figure 4a. We set the pump frequency $f_p = 197.7$ THz and attained only two OFCs: the first one was near the pump frequency, and the second was the Raman-assisted OFC (Figure 4b). In this case, the pump frequency was in the normal dispersion range, while the soliton-like Raman-assisted OFC was in the anomalous dispersion range.

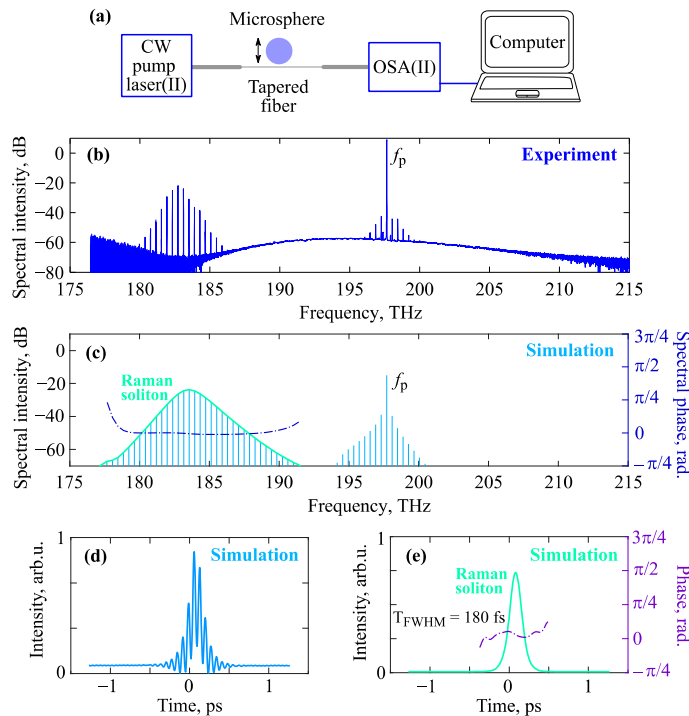


Figure 4. (a) A simplified experimental scheme for the 3rd series. (b) The experimental spectrum demonstrating Raman-assisted soliton-like OFCs. (c) The corresponding numerically simulated spectrum (vertical light blue lines, left axis), the spectral envelope of the Raman-assisted soliton (solid line, left axis), and the spectral phase of the Raman-assisted soliton (dash-dotted line, right axis). (d) Numerically simulated intensity distribution in the time domain. (e) Numerically simulated intensity (solid line, left axis) and its phase (dash-dotted line, right axis) of the Raman-assisted soliton. The OFC in the time domain (solid line, left axis) and its phase (dash-dotted line, right axis) on the pump band low intensity background in (b) is due to spontaneous emission from the pump laser.

4. Discussion

We demonstrate that the observed Raman OFC with a soliton-like spectral profile may correspond to a “true” soliton (with localized unchangeable temporal profile) as performed numerically simulation for the frame work of the Lugiato–Lefever equation with the Raman

In the first series, we have obtained the first OFC near the pump frequency in the C-band, the second Stokes OFC in the U-band and beyond, and the third anti-Stokes OFC in the E-band. The qualitative explanation of OFC generation in the sidebands is based on degenerate four-wave mixing (FWM) processes under the strong intracavity CW field approximation. Note that similar spectra were previously demonstrated in different mi-

nonlinearity taken into account as described in Section 2.2.4. We considered 2^9 modes. The numerically modeled stable spectrum and spectral phase of the Raman-assisted OFC are plotted in Figure 4c. Here, we set $\Delta = 6$ and $X = 25$ to attain a sufficiently good agreement between the experimental and the simulated spectra (compare Figure 4b,c). The measured spectral intensity at the pump frequency f_p is higher than the calculated spectral intensity at f_p because in the experiment the transmitted unconverted pump is also measured. The slight difference in the shape of the experimental and measured spectra is explained by the fact that we did not exactly know several experimental parameters (for example, detuning and coupling coefficient). The simulated intensity distribution in the time domain is shown in Figure 4d. Next, we filtered out the Raman-assisted OFC in the spectral domain (using the super-Gaussian filter for the complex spectral envelope: $\exp(-(\nu_p + \Delta f_R)^6 / \delta f^6)$, $\Delta f_R = 15$ THz, $\delta f = 7$ THz) and found its field distribution in the time domain. The temporal intensity and phase of the Raman soliton are plotted in Figure 4e. We indeed obtained the sech^2 -shape soliton demonstrated in Figure 4e. This soliton has almost flat spectral and temporal phases. Its duration is 180 fs (full width at half maximum, FWHM) and $\text{TBP} = 0.315$ (time-bandwidth product, TBP). Note that for the sech^2 -shape Fourier transform limited pulses, TBP is also 0.315.

4. Discussion

We have demonstrated three experimental series of spectrally separated OFC generation in different telecommunication bands in silica microspheres, with a diameter of about $165 \mu\text{m}$ and an FSR of about 400 GHz.

In the first series, we have obtained the first OFC near the pump frequency in the C-band, the second Stokes OFC in the U-band and beyond, and the third anti-Stokes OFC in the E-band. The qualitative explanation of OFC generation in the sidebands is based on degenerate four-wave mixing (FWM) processes under the strong intracavity CW field approximation. Note that similar spectra were previously demonstrated in different microresonators (for example, in [40,42,47]). We have also investigated the pump frequency varying in the 190–198 THz range. The sidebands are wider and are located closer to the pump frequency when the pump frequency is in the anomalous dispersion range. When the pump frequency is in the normal dispersion range, the sidebands' frequencies are shifted significantly from the pump frequency (which agrees with the results of the paper [35]). For the same detuning, maximum gain coefficients are slightly higher for a higher pump power due to a higher intracavity power. The broadest gainbands are obtained for pump frequencies close to the zero dispersion frequency. Their spectral widths exceed 20 THz. The larger the detuning, the higher the gain coefficient.

In the second experimental series, by simple tuning of the pump frequency, we have attained frequency tunable Raman OFCs in the U-band and anti-Stokes OFCs in the E-band, and also OFCs in the C-band. In these cases, the Raman OFCs are not weak in comparison with the pump, so the simple method of calculating gain coefficients for the FWM process applied for the first series cannot be used here.

In the third experimental series, the pump frequency was in the normal dispersion range and we have attained a Raman soliton-like spectrum without symmetric high-frequency sideband. To demonstrate that the observed Raman OFC with a soliton-like spectrum can indeed correspond to a soliton with a localized unchangeable temporal profile, we have performed numerical simulation in the framework of the Lugiato–Lefever equation, with the Raman nonlinearity taken into account. Note that experimental and theoretical studies of the generation of Raman OFCs with bell-shaped spectra from a silica rod microresonator with controlled center frequency via detuning and coupling optimization were presented in [30]. However, the possibility of Raman soliton formation was not investigated in the work [30]. A Stokes soliton co-existing with a fundamental dissipative Kerr soliton in the anomalous dispersion range was discovered in a silica on silicon microcavity [32]. However, we could not find works reporting a Raman soliton in microresonators (in the anomalous dispersion range) when the pump with a weak OFC

nearby was in the normal dispersion range (as in Figure 4). Therefore, we believe that this found regime of the Raman soliton generation is novel.

Author Contributions: Conceptualization, E.A.A. and A.V.A.; methodology, E.A.A., M.P.M., T.S., G.L., V.B. and A.V.A.; software, E.A.A., M.P.M., I.L. and A.V.A.; validation, E.A.A., M.P.M., T.S., J.A., V.B. and A.V.A.; formal analysis, E.A.A., M.P.M., T.S., J.A., S.S.; investigation, E.A.A., M.P.M., T.S., J.A. and A.V.A.; resources, I.L., S.S., V.B. and A.V.A.; data curation, E.A.A., M.P.M., T.S.; writing—original draft preparation, E.A.A.; writing—review and editing, M.P.M., T.S., I.L., S.S. and A.V.A.; visualization, E.A.A. and M.P.M.; supervision, E.A.A., S.S., V.B. and A.V.A.; project administration, E.A.A., G.L., V.B. and A.V.A.; funding acquisition, E.A.A., I.L., G.L., V.B. and A.V.A. All authors have read and agreed to the published version of the manuscript.

Funding: The 3rd experimental series presented in Section 3.4 and all theoretical studies are supported by the Russian Science Foundation, Grant No. 20-72-10188. The 2nd experimental series presented in Section 3.3 is supported by the Mega-grant of the Ministry of Science and Higher Education of the Russian Federation, contract No. 075-15-2021-633. The 1st experimental series presented in Section 3.1 is supported by the European Regional Development Fund (ERDF) postdoctoral research project, contract No. 1.1.1.2/VIAA/4/20/659 (COMBSYS).

Conflicts of Interest: The authors declare no conflict of interest.

References

- Pasquazi, A.; Peccianti, M.; Razzari, L.; Moss, D.J.; Coen, S.; Erkintalo, M.; Chembo, Y.K.; Hansson, T.; Wabnitz, S.; Del’Haye, P.; et al. Micro-combs: A novel generation of optical sources. *Phys. Rep.* **2018**, *729*, 1–81. [[CrossRef](#)]
- Strekalov, D.V.; Marquardt, C.; Matsko, A.B.; Schwefel, H.G.L.; Leuchs, G. Nonlinear and quantum optics with whispering gallery resonators. *J. Opt.* **2016**, *18*, 123002. [[CrossRef](#)]
- Reynolds, T.; Riesen, N.; Meldrum, A.; Fan, X.; Hall, J.M.; Monro, T.M.; François, A. Fluorescent and lasing whispering gallery mode microresonators for sensing applications. *Laser Photonics Rev.* **2017**, *11*, 1600265. [[CrossRef](#)]
- Brice, I.; Grundsteins, K.; Atvars, A.; Alnis, J.; Viter, R.; Ramanavicius, A. Whispering gallery mode resonator and glucose oxidase based glucose biosensor. *Sens. Actuators B Chem.* **2020**, *318*, 128004. [[CrossRef](#)]
- Zhivotkov, D.; Ristić, D.; Romanova, E.; Ivanda, M. Refractometric gas sensing using a whispering gallery mode microresonator coated with a supra-micron sol-gel layer. *Opt. Mater.* **2021**, *118*, 111286. [[CrossRef](#)]
- Soria, S.; Berneschi, S.; Brenci, M.; Cosi, F.; Nunzi Conti, G.; Pelli, S.; Righini, G.C. Optical Microspherical Resonators for Biomedical Sensing. *Sensors* **2011**, *11*, 785–805. [[CrossRef](#)] [[PubMed](#)]
- Toropov, N.; Cabello, G.; Serrano, M.P.; Gutha, R.R.; Rafti, M.; Vollmer, F. Review of biosensing with whispering-gallery mode lasers. *Light Sci. Appl.* **2021**, *10*, 42. [[CrossRef](#)]
- Peccianti, M.; Pasquazi, A.; Park, Y.; Little, B.E.; Chu, S.T.; Moss, D.J.; Morandotti, R. Demonstration of a stable ultrafast laser based on a nonlinear microcavity. *Nat. Commun.* **2012**, *3*, 765. [[CrossRef](#)]
- Xu, Q.; Soref, R. Reconfigurable optical directed-logic circuits using microresonator-based optical switches. *Opt. Express* **2011**, *19*, 5244–5259. [[CrossRef](#)]
- Han, Z.; Fast, S.S.; Klotz, E.; Vatik, I.D.; Churkin, D.V. Optical filtering with axial whispering gallery modes on the surface of tapered optical fibers. *Laser Phys. Lett.* **2020**, *17*, 066201. [[CrossRef](#)]
- Liang, W.; Ilchenko, V.S.; Savchenkov, A.A.; Matsko, A.B.; Seidel, D.; Maleki, L. Whispering-gallery-mode-resonator-based ultranarrow linewidth external-cavity semiconductor laser. *Opt. Lett.* **2010**, *35*, 2822–2824. [[CrossRef](#)]
- Kondratiev, N.M.; Lobanov, V.E.; Cherenkov, A.V.; Voloshin, A.S.; Pavlov, N.G.; Koptyaev, S.; Gorodetsky, M.L. Self-injection locking of a laser diode to a high-Q WGM microresonator. *Opt. Express* **2017**, *25*, 28167–28178. [[CrossRef](#)]
- Cutrona, A.; Hanzard, P.-H.; Rowley, M.; Totero-Gongora, J.S.; Peccianti, M.; Malomed, B.A.; Oppo, G.-L.; Pasquazi, A. Temporal cavity solitons in a laser-based microcomb: A path to a self-starting pulsed laser without saturable absorption. *Opt. Express* **2021**, *29*, 6629–6646. [[CrossRef](#)]
- Del’Haye, P.; Schliesser, A.; Arcizet, O.; Wilken, T.; Holzwarth, R.; Kippenberg, T.J. Optical frequency comb generation from a monolithic microresonator. *Nature* **2007**, *450*, 1214–1217. [[CrossRef](#)]
- Pfeifle, J.; Brasch, V.; Lauer, M.; Yu, Y.; Wegner, D.; Herr, T.; Hartinger, K.; Schindler, P.; Li, J.; Hillerkuss, D.; et al. Coherent terabit communications with microresonator Kerr frequency combs. *Nat. Photon.* **2014**, *8*, 375–380. [[CrossRef](#)]
- Fülöp, A.; Mazur, M.; Lorences-Riesgo, A.; Helgason, Ö.B.; Wang, P.-H.; Xuan, Y.; Leaird, D.E.; Qi, M.; Andrekson, P.A.; Weiner, A.M.; et al. High-order coherent communications using mode-locked dark-pulse Kerr combs from microresonators. *Nat. Commun.* **2018**, *9*, 1598. [[CrossRef](#)] [[PubMed](#)]
- Yu, M.; Okawachi, Y.; Griffith, A.G.; Picqué, N.; Lipson, M.; Gaeta, A.L. Silicon-chip-based mid-infrared dual-comb spectroscopy. *Nat. Commun.* **2018**, *9*, 1869. [[CrossRef](#)] [[PubMed](#)]
- Newman, Z.L.; Maurice, V.; Drake, T.; Stone, J.R.; Briles, T.C.; Spencer, D.T.; Fredrick, C.; Li, Q.; Westly, D.; Ilic, B.R.; et al. Architecture for the photonic integration of an optical atomic clock. *Optica* **2019**, *6*, 680–685. [[CrossRef](#)]

19. Trocha, P.; Karpov, M.; Ganin, D.; Pfeiffer, M.H.P.; Kordts, A.; Wolf, S.; Krockenberger, J.; Marin-Palomo, P.; Weimann, C.; Randel, S.; et al. Ultrafast optical ranging using microresonator soliton frequency combs. *Science* **2018**, *359*, 887–891. [[CrossRef](#)] [[PubMed](#)]
20. Gaeta, A.L.; Lipson, M.; Kippenberg, T.J. Photonic-chip-based frequency combs. *Nat. Photonics* **2019**, *13*, 158–169. [[CrossRef](#)]
21. Crespo-Ballesteros, M.; Yang, Y.; Toropov, N.; Sumetsky, M. Four-port SNAP microresonator device. *Opt. Lett.* **2019**, *44*, 3498–3501. [[CrossRef](#)] [[PubMed](#)]
22. Wang, M.; Yang, Y.; Lu, Z.; Wang, W.; Zhang, W.; Xie, C.; Zhong, H.; Wu, L.; Wu, T.; Tan, Q.; et al. Experimental demonstration of nonlinear scattering processes in a microbottle resonator based on a robust packaged platform. *J. Lightwave Technol.* **2021**. [[CrossRef](#)]
23. Anashkina, E.A.; Marisova, M.P.; Andrianov, A.V.; Akhmedzhanov, R.A.; Murnieks, R.; Tokman, M.D.; Skladova, L.; Oladyshkin, I.V.; Salgals, T.; Lyashuk, I.; et al. Microsphere-based optical frequency comb generator for 200 GHz spaced WDM data transmission system. *Photonics* **2020**, *7*, 72. [[CrossRef](#)]
24. Spolitis, S.; Murnieks, R.; Skladova, L.; Salgals, T.; Andrianov, A.V.; Marisova, M.P.; Leuchs, G.; Anashkina, E.A.; Bobrovs, V. IM/DD WDM-PON communication system based on optical frequency comb generated in silica whispering gallery mode resonator. *IEEE Access* **2021**, *9*, 66335–66345. [[CrossRef](#)]
25. Salgals, T.; Alnis, J.; Murnieks, R.; Brice, I.; Porins, J.; Andrianov, A.V.; Anashkina, E.A.; Spolitis, S.; Bobrovs, V. Demonstration of a fiber optical communication system employing a silica microsphere-based OFC source. *Opt. Express* **2021**, *29*, 10903–10913. [[CrossRef](#)]
26. Hu, H.; Oxenløwe, L.K. Chip-based optical frequency combs for high-capacity optical communications. *Nanophotonics* **2021**, *10*, 1367–1385. [[CrossRef](#)]
27. Spolitis, S.; Kurbatska, I.; Bobrovs, V. Comparison of C-band and L-band WDM-PON systems performance with PAM-4 modulation format. In Proceedings of the 2017 International Workshop on Fiber Optics in Access Network (FOAN), Munich, Germany, 6–8 November 2017; pp. 1–6. [[CrossRef](#)]
28. Spillane, S.M.; Kippenberg, T.J.; Vahala, K.J. Ultralow-threshold Raman laser using a spherical dielectric microcavity. *Nature* **2002**, *415*, 621–623. [[CrossRef](#)]
29. Zhu, S.; Shi, L.; Ren, L.; Zhao, Y.; Jiang, B.; Xiao, B.; Zhang, X. Controllable Kerr and Raman-Kerr frequency combs in functionalized microsphere resonators. *Nanophotonics* **2019**, *8*, 2321–2329. [[CrossRef](#)]
30. Suzuki, R.; Kubota, A.; Hori, A.; Fujii, S.; Tanabe, T. Broadband gain induced Raman comb formation in a silica microresonator. *J. Opt. Soc. Am. B* **2018**, *35*, 933–938. [[CrossRef](#)]
31. Andrianov, A.V.; Anashkina, E.A. Raman-assisted optical frequency combs generated in a silica microsphere in two whispering gallery mode families. *Laser Phys. Lett.* **2021**, *18*, 025403. [[CrossRef](#)]
32. Yang, Q.-F.; Yi, X.; Yang, K.Y.; Vahala, K. Stokes solitons in optical microcavities. *Nat. Phys.* **2017**, *13*, 53–57. [[CrossRef](#)]
33. Gorodetsky, M.L.; Savchenkov, A.A.; Ilchenko, V.S. Ultimate Q of optical microsphere resonators. *Opt. Lett.* **1996**, *21*, 453–455. [[CrossRef](#)]
34. Webb, K.E.; Erkintalo, M.; Coen, S.; Murdoch, S.G. Experimental observation of coherent cavity soliton frequency combs in silica microspheres. *Opt. Lett.* **2016**, *41*, 4613–4616. [[CrossRef](#)]
35. Sayson, N.L.B.; Webb, K.E.; Coen, S.; Erkintalo, M.; Murdoch, S.G. Widely tunable optical parametric oscillation in a Kerr microresonator. *Opt. Lett.* **2017**, *42*, 5190–5193. [[CrossRef](#)]
36. *ITU-T Recommendation G.694.1, Spectral Grids for WDM Applications: DWDM Frequency Grid*; Telecommunication Standardization Sector of ITU; International Telecommunication Union: Geneva, Switzerland, 2012; pp. 1–7.
37. Andrianov, A.V.; Anashkina, E.A. Single-mode silica microsphere Raman laser tunable in the U-band and beyond. *Results Phys.* **2020**, *17*, 103084. [[CrossRef](#)]
38. Oraevsky, A.N. Whispering-gallery waves. *Quantum Electron.* **2002**, *32*, 377–400. [[CrossRef](#)]
39. Agrawal, G.P. *Nonlinear Fiber Optics*, 6th ed.; Elsevier: London, UK, 2019.
40. Fujii, S.; Tanabe, T. Dispersion engineering and measurement of whispering gallery mode microresonator for Kerr frequency comb generation. *Nanophotonics* **2020**, *9*, 1087–1104. [[CrossRef](#)]
41. Coen, S.; Erkintalo, M. Universal scaling laws of Kerr frequency combs. *Opt. Lett.* **2013**, *38*, 1790–1792. [[CrossRef](#)] [[PubMed](#)]
42. Sayson, N.L.B.; Pham, H.; Webb, K.E.; Ng, V.; Trainor, L.S.; Schwefel, H.G.L.; Coen, S.; Erkintalo, M.; Murdoch, S.G. Origins of clustered frequency combs in Kerr microresonators. *Opt. Lett.* **2018**, *43*, 4180–4183. [[CrossRef](#)] [[PubMed](#)]
43. Puzyrev, D.N.; Skryabin, D.V. Finesse and four-wave mixing in microresonators. *Phys. Rev. A* **2021**, *103*, 013508. [[CrossRef](#)]
44. Godey, C.; Balakireva, I.V.; Coillet, A.; Chemo, Y.K. Stability analysis of the spatiotemporal Lugiato-Lefever model for Kerr optical frequency combs in the anomalous and normal dispersion regimes. *Phys. Rev. A* **2014**, *89*, 063814. [[CrossRef](#)]
45. Guo, H.; Karpov, M.; Lucas, E.; Kordts, A.; Pfeiffer, M.H.P.; Brasch, V.; Lihachev, G.; Lobanov, V.E.; Gorodetsky, M.L.; Kippenberg, T.J. Universal dynamics and deterministic switching of dissipative Kerr solitons in optical microresonators. *Nat. Phys.* **2017**, *13*, 94–102. [[CrossRef](#)]
46. Anashkina, E.A.; Bobrovs, V.; Salgals, T.; Brice, I.; Alnis, J.; Andrianov, A.V. Kerr optical frequency combs with multi-FSR mode spacing in silica microspheres. *IEEE Photonics Technol. Lett.* **2021**, *33*, 453–456. [[CrossRef](#)]
47. Jung, H.; Gong, Z.; Liu, X.; Guo, X.; Zou, C.; Tang, H.X. Stokes and anti-Stokes Raman scatterings from frequency comb lines in poly-crystalline aluminum nitride microring resonators. *Opt. Express* **2019**, *27*, 22246–22253. [[CrossRef](#)] [[PubMed](#)]

PAPER-12: Demonstration of a fiber optical communication system employing a silica microsphere-based OFC source

T. Salgals, J. Alnis, R. Murnieks, I. Brice, J. Porins, A. V. Andrianov, E. A. Anashkina, **S. Spolitis**, and V. Bobrovs, "Demonstration of a fiber optical communication system employing a silica microsphere-based OFC source," *Opt. Express* 29(7), 10903-10913, (2021), DOI: [10.1364/OE.419546](https://doi.org/10.1364/OE.419546)



Demonstration of a fiber optical communication system employing a silica microsphere-based OFC source

TOMS SALGALS,^{1,2,*}  JANIS ALNIS,³ RIHARDS MURNIEKS,^{1,4} INGA BRICE,³ JURGIS PORINS,¹ ALEXEY V. ANDRIANOV,⁵  ELENA A. ANASHKINA,⁵  SANDIS SPOLITIS,^{1,4}  AND VJACESLAVS BOBROVS¹

¹Institute of Telecommunications of the Riga Technical University, 12 Azenes Street, 1048 Riga, Latvia

²AFFOC Solutions Ltd., 17 Andrejostas Street, 1045 Riga, Latvia

³Institute of Atomic Physics and Spectroscopy, University of Latvia, 3 Jelgavas Street, 1004 Riga, Latvia

⁴Communication Technologies Research Center, Riga Technical University, 1048 Riga, Latvia

⁵Institute of Applied Physics of the Russian Academy of Sciences, 46 Ul'yanov Street, 603950 Nizhny Novgorod, Russia

*toms.salgals@rtu.lv

Abstract: The fabrication of microsphere resonators and the generation of optical frequency combs (OFC) have achieved a significant breakthrough in the past decade. Despite these advances, no studies have reported the experimental implementation and demonstration of silica microsphere OFCs for data transmission. In this work, to the best of our knowledge, we experimentally for the first time present a designed silica microsphere whispering-gallery-mode microresonator (WGMR) OFC as a C-band light source where 400 GHz spaced carriers provide data transmission of up to 10 Gbps NRZ-OOK modulated signals over the standard ITU-T G.652 telecom fiber span of 20 km in length. A proof-of-concept experiment is performed with two newly generated carriers (from 7-carrier OFC) having the highest peak power. The experimental realization is also strengthened by the modeling and simulations of the proposed system showing a strong match of the results. The demonstrated setup serves as a platform for the future experimental implementation of silica microsphere WGMR-OFC in more complex WDM transmission system realizations with advanced modulation schemes.

© 2021 Optical Society of America under the terms of the [OSA Open Access Publishing Agreement](#)

1. Introduction

Optical frequency combs (OFCs) have a high potential to replace tens of tunable continuous-wave (CW) lasers with a single laser source and a whispering-gallery-mode microresonator (WGMR) in modern wavelength-division multiplexing (WDM) optical communication systems to upgrade the architecture of the service provider's central office (CO). OFC can be generated in a controllable manner using different kinds of WGMRs – integrated microring resonators [1], microdisk resonators [2], and microtoroid resonators [3], spatial microdisk resonators [4], and microsphere resonators [5,6]. Even though integrated microresonators, providing Q-factor $\sim 10^6$, have been studied extensively, silica microspheres [7] have many advantages as more easily and quickly to manufacture by melting the end of standard optical fiber [8]. By using arc discharge of a fusion splicer, it is possible to quickly fabricate microspheres with repeatable diameter, and it is easy to control the free spectral range (FSR), which is inversely proportional to the diameter. Also, routinely reached Q-factor values in silica microspheres are higher 10^7 - 10^8 [9,10] compared to integrated resonators resulting in optical carriers with narrower linewidth [11]. The tapered fiber method of microsphere excitation allows to fine-tune the coupling conditions which is not possible for chip-based resonators with integrated waveguides. Considering these

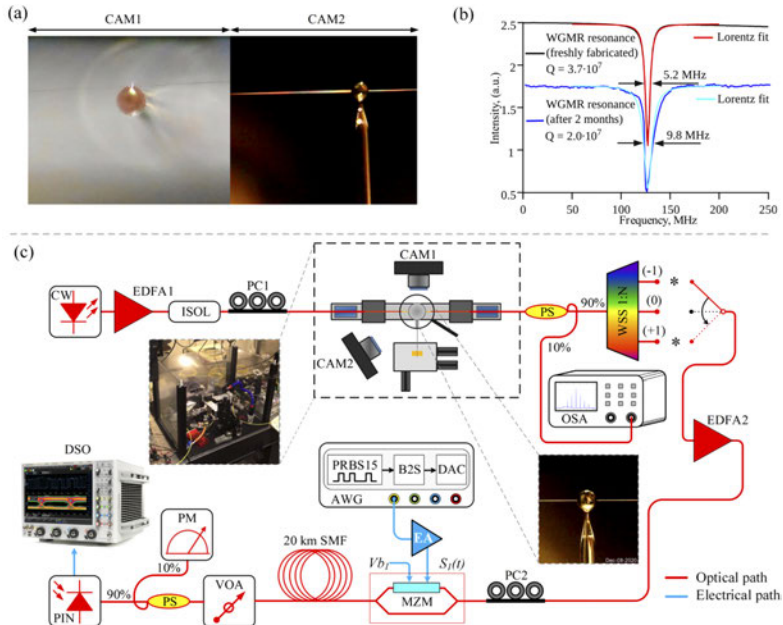
aspects of microsphere resonator advantages, we have chosen them for OFC generation in optical communication systems. While optical data transmission has been well studied and demonstrated employing OFC generated in integrated resonators showing even terabit communications [12–14], the experimental demonstration of data transmission based on OFC generated in microsphere resonator, to the best of our knowledge, has not been demonstrated until now. This research reports the first successful demonstration of experimental 2.5 and 10 Gbps non-return to zero (NRZ) on-off keying (OOK) WDM system based on optical carriers generated in fabricated silica microsphere resonator. We also integrated the experimentally obtained WGMR-OFC into the simulation model corresponding to the experimental system to support and verify the experimental results regarding the overall system operation and signal waveform quality in terms of the bit-error-ratio (BER) values. As a result, it enables the simulation environment to develop more complex WDM transmission systems with advanced modulation schemes.

The remainder of the manuscript is structured as follows: Section 2 describes the fabrication process of a microsphere resonator and an experimental process of coupling the light inside of a Kerr OFC in the produced WGMR. Section 3 presents the designed experimental setup of silica microsphere WGMR-OFC as a C-band light source providing data transmission of up to 10 Gbps/ λ NRZ-OOK modulated signals over 20 km the standard ITU-T G.652 telecom fiber using 400 GHz spaced carriers. This section also describes the performed setup for assessing the impact of pump source light polarization on the WGMR-OFC. Experimentally obtained results, spectra, received signal bit pattern, eye diagram, and system performance analysis are provided in section 4. Section 5 presents the integration of the experimental generated OFC comb into the simulation environment to verify the obtained experimental results regarding the overall system operation. The simulation model reproduces the data transmission part of the experimental setup as close as possible and enables the further development of more complex WDM transmission systems with advanced modulation schemes. Finally, section 6 gives a brief summary of the experimental and simulative results and concludes the paper.

2. Fabrication and characteristics of a designed silica WGMR-OFC microresonator

Microspheres with diameters of about 170 μm used in this research were fabricated from a standard ITU-T G.652 single-mode telecommunication fiber by a two-stage method using a specially developed program for a commercially available specialty optical fusion splicer. At the first stage, the fiber was tapered with a decrease in the diameter of the thinnest part by ~ 3 times. Then, as the arc discharge current increased, the fiber was divided into two parts. Then one of the parts was removed from the fiber splicer, and the remaining fiber end was melted several times by arc discharge. After that, a microresonator was formed under the action of surface tension. With each subsequent melting, the shape of the microresonator more and more approached a spherical one. Due to fiber tapering at the first stage, the fiber stem was obtained sufficiently thin at the point of contact with the microsphere, making it possible to minimize the effect of the stem on the microsphere's properties. This method of microsphere fabrication has been previously demonstrated by [9]. By varying the diameter of the microsphere, it is possible to control the distance between the eigenfrequencies and change the dispersion [5,8]. In our case, the calculated dispersion of the microsphere was slightly anomalous at 1550 nm (the zero dispersion wavelength was about 1540 nm). We experimentally optimized the number of fiber end melting cycles to form microspheres with 400 GHz spacing between fundamental eigenfrequencies for OFC generation suitable for WDM applications following the ITU-T frequency grid. It should be noted that the developed program for the fiber splicer provides the manufacturing of microspheres with reproducible parameters. The Q factor of produced microspheres is relatively persistent over at least 2 months, as we experimentally observed. A tapered fiber was used for coupling the light inside the microsphere resonator, please see Fig. 1(a). The jacket and coating were stripped from

ITU-T G.652 single-mode optical fiber (900 μm jacket) in the region of 1-2 cm where it was heated. A hydrogen flame was used to soften the fiber, and submicron microstepping motors were used to pull it in both directions with a constant speed of 80 $\mu\text{m/s}$. The burning temperature of the hydrogen flame is lower than the hydrogen-oxygen flame. It melted and softened the optical fiber slowly, which was more desirable as the time period for tapered fiber fabrication steps was more flexible. The optical fiber transmission spectrum was monitored during the tapering process to determine when it will return to the single-mode operation.



Acronyms: CW – Continuous wave laser, EDFA – erbium-doped fiber amplifier, ISOL – fiber optical isolator, PC – polarization controller, CAM – microscope with zoom camera, PS – power splitter, OSA – optical spectrum analyzer, WSS – wavelength selective switch, MZM – Mach-Zehnder modulator, AWG – arbitrary waveform generator, B2S – bits to symbol mapping, DAC – digital-to-analog converter, EA – electrical amplifier, SMF – single mode fiber, VOA – variable optical attenuator, PM – optical power meter, PIN – photodiode, DSO – digital storage oscilloscope, DSP – digital signal processing.

Fig. 1. (a) Silica microsphere and tapered fiber position state captured by microscopes with zoom cameras: side view and top view during the experiment where OFC carrier generation was observed. (b) Experimentally observed Q-factor degradation in terms of a 2-month life cycle (freshly fabricated and after 2 months) while it resided inside the cover box. (c) Experimental setup of the designed silica microsphere WGM-OFC as a light source where 400 GHz spaced carriers provide NRZ-OOK modulated 2.5 and 10 Gbps data transmission over 20 km SMF fiber. Insets show tapered fiber and silica microsphere resonator positions of coupling conditions and WGM-OFC reduced humidity and dust prevention cover box.

3. Experimental setup of the employed WGMR-OFC light source for a fiber optical communication system

The measured quality factor (Q) of the fresh microsphere resonator used for the comb generation in this research is 3.7×10^7 (5.2 MHz FWHM of the WGM resonance). After a two-month life cycle as the resonator ages, it is slightly reduced to 2.0×10^7 (9.8 MHz FWHM of the WGM resonance), please see Fig. 1(b). The setup for the generation of WGMR-OFC and the realized WDM communication system is shown in Fig. 1(c).

First, we search for stable combs on an optical spectrum analyzer by tuning external cavity CW semiconductor laser in wavelength steps of 10 pm and bumping light source output fiber. Such a kick method could possibly lead to soliton comb formation [15,16]. We found that the most appropriate wavelength, where a CW laser with a linewidth of about 100 kHz and +6 dBm optical output power can be used as an OFC comb pump source is 1552 nm. The light coming from the pump source is further amplified up to +23 dBm by the erbium-doped fiber amplifier (EDFA). The polarization state of the amplified signal is adjusted using the polarization controller (PC1) before coupling the signal into the microsphere through a tapered fiber. The isolator on the EDFA output is used to prevent back-scattered light from entering the output port of the CW laser, destabilizing its central frequency, therefore influencing the stability of the comb. Silica microsphere and tapered fiber are enclosed in a separate box for dust and air flow prevention, providing even further stability to the resulting OFC. The X, Y, and Z micro-translation stage is used to position the microsphere to touch the tapered fiber at a place slightly thicker than the taper waist, which changes such coupling conditions as coupled power and the Q factor of the resonances that we have demonstrated in our previous work [17].

The taper and microsphere are touching to improve WGMR-OFC stability, as maintaining a constant gap is challenging and minuscule changes considerably affect the intensity of the generated optical carriers. As shown in Fig. 1, an optical spectrum analyzer (OSA) with 0.01 nm resolution is used to measure OFC performance over 10 hours period (see Fig. 2(b)) and power stability and power distribution stability over the wavelength of the OFC carriers. After OFC generation the carriers (-1) and (+1) are similar but one can be a few dBm more intense than the other if multiple solitons are circling inside the resonator. We have observed that comb lines (-1) and (+1) have a different performance where power instability over a 10-hour period is within about a 3 dB margin due to the impact of resonator ability to support multiple spatial modes. As our experimental setup is located on an optical table with an active pneumatic vibration isolation system, the disturbance like small vibrations is not affecting the generated OFC and the rest of the transmission system. Setup temperature is not actively stabilized, while humidity inside the cover box is reduced using silica gel desiccant.

The optical carriers $\lambda = 1549$ nm depicted as (-1) and $\lambda = 1555$ nm depicted as (+1) are used further to demonstrate NRZ-OOK modulated 2.5 Gbps and 10 Gbps data transmission, please see Fig. 2(a). For a fair comparison, in this paper, we focus on newly generated carriers (-1) and (+1) having the highest achieved peak power levels. As shown in Fig. 1(a), the generated OFC signal is sent to the wavelength selective switch (WSS) used to filter out one optical carrier (-1) or (+1) at a time. The realization of an experimental setup corresponds to wavelength-selective (WS) fiber optical communication system architecture. Fully ITU flexible grid G.694.1 compliant WSS with dynamic channel width control provided by liquid crystal on silicon (LCoS) switching technology is set for 400 GHz OFCs channel spacing, where output optical channels bandwidth is 25 GHz (4×6.25 GHz).

The filtered output (-1) or (+1) carrier is amplified with EDFA2 pre-amplifier to the necessary optical power level. Polarization controller (PC2) is placed after EDFA2 to reduce the polarization-dependent loss. Bitrates of 2.5 Gbps and 10 Gbps by a 2^{15} long pseudo-random bit sequence (PRBS15) NRZ signal from 65 GSa/s and 25 GHz analog bandwidth arbitrary waveform generator (AWG) are modulated onto the optical carrier signal (-1) or (+1) using the Mach-Zehnder intensity

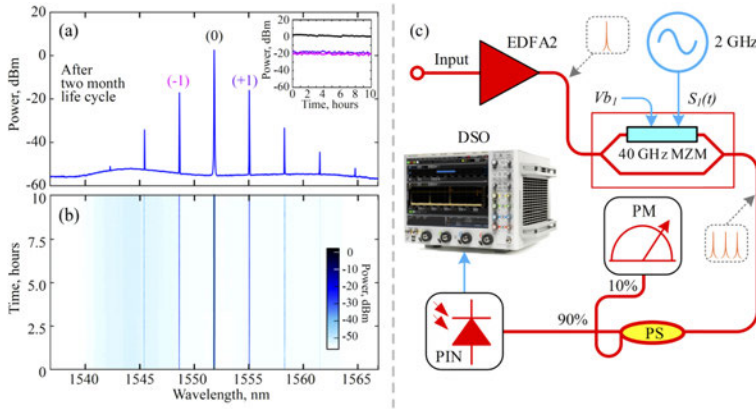


Fig. 2. Measured OFC performance over a 10-hour period: (a) optical spectrum with inset representing captured power stability, and (b) power distribution stability over the wavelength. (c) The experimental measurement setup, where one WGMR-OFC optical carrier (+1) is fed into an MZM modulator driven by a 2 GHz sinusoidal tone to assess the impact of optical signal polarization on the spectral purity of generated optical carriers

modulator (MZM) with an extinction ratio of 20 dB. Then the modulated signal is transmitted over 20 km of standard single-mode optical fiber (SMF), variable optical attenuator (VOA), and detected with 10 GHz photoreceiver (PIN), which sensitivity is equal to -18 dBm at BER of 10^{-10} and overload power 0 dBm for BER of 10^{-15} . An optical coupler (coupling ratio 10/90) and a power meter are used before PIN to monitor the optical power level falling on the PIN receiver. An 80 GSa/s and 33 GHz analog bandwidth digital storage oscilloscope (DSO) is used to sample the received electrical signal, filter it with an 8 GHz low-pass filter (LPF) in case of 10 Gbps and 2.3 GHz LPF in the case of 2.5 Gbps data transmission to measure the quality of the received signal (e.g., eye diagrams, waveform), and estimate its BER. Please note that the represented BER values are calculated from the DSO's estimated Q-factor values of the captured NRZ signal real-time eye diagrams.

We have also assessed the impact of the pump signal polarization state on the spectral purity of generated OFC carriers. An additional experimental measurement scheme is built for this purpose, as shown in Fig. 2(c). For this measurement, the optical heterodyning process of two optical carriers, where the frequency difference or intermediate frequency (IF) between them generates the desired carrier on the output of high-speed photodiode, is used [18]. RF peaks around DC can be masked by a photodetector flicker noise and low-frequency technical noise. For that reason, we are focusing on higher frequencies, which allows us to better evaluate the spectral purity of generated OFC carriers. For the polarization measurement, to prevent the IF frequency instability caused by laser phase noise we use (+1) WGMR-OFC optical carrier which is fed into an optical input of MZM modulator and modulated by the 2 GHz sinusoidal signal originating from a high-stability microwave signal generator, please see Fig. 2(c). Bias voltage V_{b1} of MZM is set to 3.33 VDC, which is near to its null-bias point. In such a way three optical carriers spaced by 2 GHz are obtained on the output of the 40 GHz analog bandwidth MZM.

The frequency spacing between the first and third carriers is 4 GHz. By changing the power of the 2 GHz sinusoidal signal applied to the $S_1(t)$ RF input of the MZM, an optimal RF drive voltage ($V_{\text{eff}} = 1.2$ V) ensuring almost equal peak powers of generated RF carriers is found. The

first RF peak located at DC is not seen in Fig. 3 as the DC blocker was attached to the electrical output of the PIN receiver. Accordingly, after directly receiving such an optical signal by the 10 GHz high-speed PIN photoreceiver, the optical heterodyne up-conversion process occurs. As a result, on the RF output of this PIN receiver, the electrical signal containing the DC-filtered baseband part and two RF carriers (2 GHz and 4 GHz) is generated. Here the 4 GHz RF tone originates from the heterodyning process of two outer optical carriers, while the 2 GHz RF tone originates from two neighboring optical carriers. An effect of polarization on signal quality is further discussed in the experimental results section of this paper.

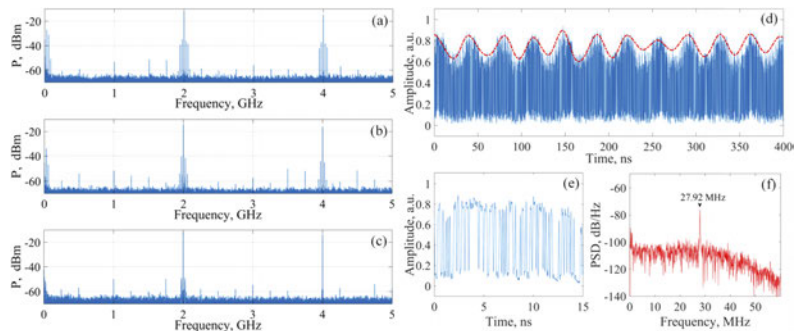


Fig. 3. Measured effect of polarization, by received electrical signal IF after optical heterodyne up-conversion on photodiode in different polarization states: (a) polarization state with large amplitude modulation, (b) intermediate state, and (c) the optimized polarization state for lowest amplitude modulation showing the highest spectral purity of the generated OFC optical carrier. (d) Part of the received and normalized 10 Gbps NRZ-OOK signal waveform after 20 km transmission with applied upper envelope function, highlighting the periodic waveform fluctuations, (e) 15 ns insight of the normalized waveform showing received bit sequence, and (f) power spectral density of the calculated envelope signal.

4. Experimental results

The setup displayed in Fig. 2(c) is used to determine the impact of light polarization of the input CW pump laser on generated OFC optical carriers. The effect of polarization is observed at three different scenarios; (1) polarization state with large amplitude modulation, (2) intermediate state, (3) polarization optimized for lowest amplitude modulation by adjusting PC1 before WGMR-OFC, see Figs. 3(a), 3(b) and 3(c).

Microsphere pump light polarization is adjusted by PC1 to minimize 27.92 MHz amplitude self-modulation of comb lines. Fast photodiode measure (+1) comb line to offset spectrum towards higher frequencies. The implemented heterodyne beating method enables to observe the effect of OFC input light polarization on the spectral purity of generated carriers. By the pump source first, and second polarization states, the generation of higher-order sub-carrier signals for 2 GHz and 4 GHz IF frequencies are observed, which lead to deterioration of the quality of our data signal, see Figs. 3(a) and 3(b).

An optimized polarization state, when the CW pump laser polarization coincides with the principal axes of the polarization, shows the best result and guarantees that equal amounts of optical power split to both the X/Y polarization states, see Fig. 3(c) [19]. We have set an optimized polarization state for the lowest amplitude modulation of PC1 during the data transmission of 2.5 and 10 Gbps NRZ-OOK modulated data over B2B and 20 km SMF transmission in both

cases using (-1) or (+1) optical carriers. As shown in Fig. 3(d), the waveform fluctuations with periodic nature are observed on the captured data signal waveforms. After 2.5 and 10 Gbps data transmission, we estimate that the period of these fluctuations for (+1) OFC optical carrier is 35.82 ns or 27.92 MHz in frequency, as it is confirmed by the spectral analysis of the applied upper envelope signal, see Figs. 3(e) and 3(f).

It should be noted that the fluctuations on the lowest part of the waveform are optically suppressed by intentionally adjusting the bias point of MZM closer to its null-point. For (-1) harmonic, the same fluctuations period is observed. As observed during the experimental measurements, a periodic intensity modulation often appears on the comb lines, always having the same frequency for the particular resonator.

This process has been previously studied in [20] where it was shown that mechanically driven oscillations occur due to radiation pressure force which subsequently causes microsphere deformation. By using COMSOL Multiphysics we calculate that for a silica microsphere with a diameter of 170 μm this resonance frequency corresponds to the strongest mechanical resonance of 27 ± 1 MHz, see Fig. 4.

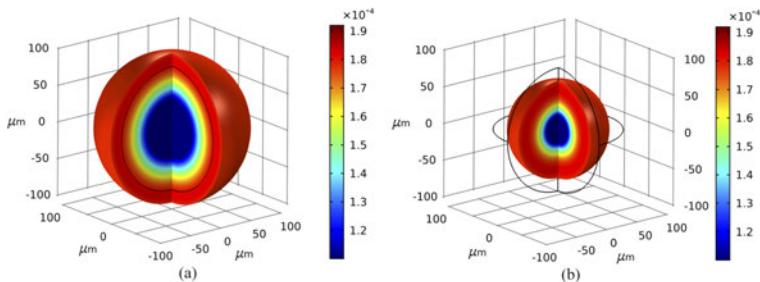


Fig. 4. COMSOL simulation of mechanical oscillations at nm scale for silica microsphere of 170 μm in diameter indicating the strongest eigenfrequency at about 27 ± 1 MHz that can be excited by a radiation pressure causing periodic detuning from resonance and back manifesting as an amplitude modulation of comb lines, where (a) represents microsphere at its diameter maximal expansion, and (b) represents the diameter maximal contraction. For a better visual representation, the deformation in simulation is exaggerated 100 000 times. The black surrounding line indicates the unperturbed microsphere size. Color scale represents the absolute value of deformation in micrometers.

We observe that an amplitude modulation depth of less than 30% is deteriorating telecom data demodulation. We can reduce this amplitude modulation by adjusting the polarization of the CW pump light, see Figs. 3(a) to 3(c). This reduction in amplitude modulation could be explained by the sideband cooling/heating effect of the mechanical resonance [21].

The performance indicators as eye diagrams and BER values of the received signal verify the feasibility of the fiber optical WGMR-OFC based transmission system. The worst-performing data channel based on the BER value is with the wavelength of 1549 nm, depicted as a carrier (-1), see Fig. 2(a). The BER of received 2.5 Gbps and 10 Gbps NRZ-OOK signals after 20 km transmission is 5.58×10^{-7} and 1.58×10^{-6} , please see Figs. 5(b) and 5(d). The best performing data channel based on the BER is the one with a wavelength of 1555 nm, denoted as a carrier (+1). In this case, the BER of received 2.5 Gbps and 10 Gbps NRZ-OOK signals after 20 km transmission is 1.39×10^{-15} and 3.64×10^{-10} , please see Figs. 5(a) and 5(c).

The error-free transmission is established during the experiment in both cases of 2.5 and 10 Gbps data rates for OFC comb pump source operating at 1552 nm wavelength. It allows to use

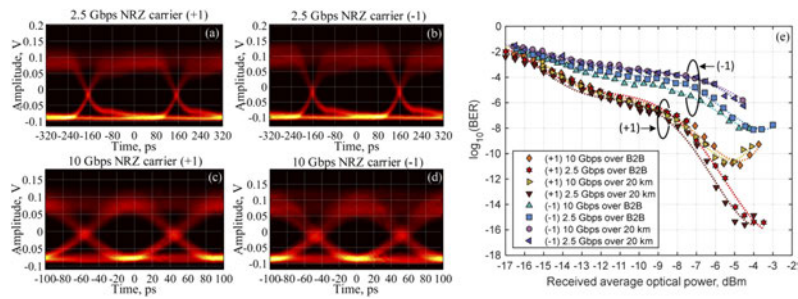


Fig. 5. Eye diagrams of the received signal after 20 km transmission over SMF fiber at a data rate of 2.5 Gbps for (a) carrier “+1” and (b) carrier “-1”, and at a data rate of 10 Gbps for (c) carrier “+1” and (d) carrier “-1”, and (e) the plots of BER vs. average received optical power in B2B and after 20 km transmission of the NRZ-OOK modulated signal with bitrates of 2.5 and 10 Gbps for “+1” and “-1” carriers.

WGMR-OFC as a light source where 400 GHz spaced carriers provide 2.5 and 10 Gbps NRZ modulated data transmission over 20 km SMF fiber. Please see the captured eye diagrams in Fig. 5(a) to 5(d). The BER versus received average optical power measurements are preferred for WGMR-OFC carrier signals (-1) and (+1) at 2.5 and 10 Gbps data rates to fully evaluate the quality of transmission characteristics, see Fig. 5(e).

We have chosen B2B transmission and a distance of 20 km corresponding to the NGPON2 requirements to measure the BER correlation diagrams. Figure 5(e) shows that the optical carrier denoted as (+1) provided the highest system performance, where the received optical power varies from -4 to -17.5 dBm, and the BER of 2.5 Gbps NRZ-OOK signal is in the range from 1.39×10^{-15} to 7.76×10^{-3} .

As one can see in Fig. 5, BER curves bending upwards are observed at relatively high detected power levels for WGMR-OFC comb carrier (+1) at 10 Gbps B2B and 10 Gbps 20 km transmission, as well as for (-1) carrier at 2.5 Gbps B2B transmission. It could be explained by detector saturation, nonlinear optical processes in the resonator or transmission fiber.

5. Results of mathematical modeling and discussion

The experimentally generated OFC is integrated into the simulation environment [22] to verify the obtained experimental results regarding the overall system operation, signal waveform quality in terms of eye diagrams, and the BER values. For this purpose, the VPI Photonics Transmission maker software is used, where the target is to reproduce the data transmission part of the experimental setup as close as possible, please see Fig. 6.

The developed simulation model (see Fig. 6) supports future research regarding fiber optical data transmission employing WGMR-OFC generated in silica microsphere, as the simulation environment enables the development of more complex WDM transmission systems with advanced modulation schemes, e.g., higher-order pulse amplitude modulation (M-PAM) or quadrature amplitude modulation (M-QAM) providing higher data rates per carrier. Figure 6 shows the developed simulation setup of a 400 GHz spaced WDM system used for the designed silica microsphere-based OFC comb spectrum implementation and performance assessment. The experimentally obtained silica microsphere-based OFC comb spectrum is implemented as a multiple laser source into the simulation model, shown in Fig. 6. Afterward, spectral lines from WGMR-OFC are filtered and de-multiplexed utilizing WSS, where the bandwidth of each

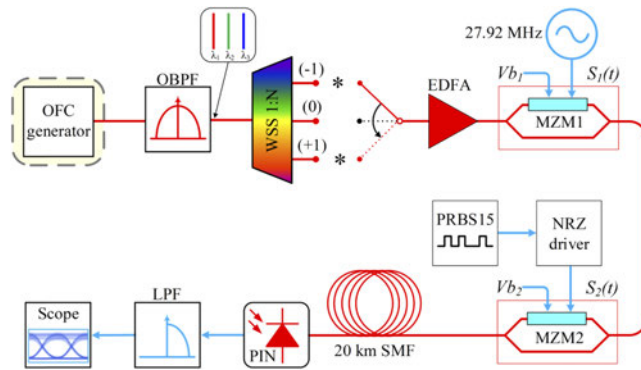


Fig. 6. Structure of simulation scheme corresponding to the experimental fiber optical data transmission system for data transmission of 2.5 Gbps and 10 Gbps NRZ-OOK modulated signals by 400 GHz spaced carriers generated in the experimental silica microsphere WGMR-OFC.

WSS channel for 400 GHz channel spacing is set to 25 GHz, and central frequencies correspond to the optical carriers (-1), (0), and (+1) shown in Fig. 2(a). Implemented OFC comb spectral lines are amplified by EDFA having 15.6 dB gain and fed to the optical input of the first MZM named MZM1. The circuit block, which consists of the electrical sinusoidal signal generator operating at 27.92 MHz frequency, is directly connected to the first MZM modulator (MZM1) to implement experimentally observed periodic oscillations.

The output of the MZM1 is connected to the output of MZM2, where the optical carriers are modulated by the 2.5 or 10 Gbps NRZ encoded bit sequence through the NRZ driver with a length of $2^{15}-1$ (PRBS15) originating from logical pseudo-random bit sequences (PRBS) source. Both MZMs have a 3-dB bandwidth of 12 GHz and a 20 dB extinction ratio. The modulated optical signals are transmitted over 20 km SMF spans.

The receiver consists of a PIN photodiode with 12 GHz of 3-dB bandwidth, -18 dBm sensitivity for BER of 10^{-10} , and responsivity of 0.65 A/W, electrical low-pass filter LPF, and electrical scope. In the case of 10 Gbps bitrate, the received, modulated signal is filtered by an LPF with 8 GHz 3-dB electrical bandwidth, while for 2.5 Gbps, the filter bandwidth of 2.3 GHz is used. The electrical signal analyzer is used to measure the received signal, e.g., showing a bit pattern for BER and eye diagram measurements. The parameters for all used elements are set according to the real equipment specifications used in the experiment. The same fluctuation period of 35.82 ns for 2.5 and 10 Gbps waveform fluctuations can be successfully emulated also in the simulation environment providing an experimentally observed effect of 27.92 MHz periodic oscillations, see Figs. 7(a) and 7(b). Received eye diagrams of the 2.5 and 10 Gbps NRZ-OOK modulated signals after transmission over 20 km SMF fiber span for implemented 400 GHz spaced (+1) and (-1) OFC carriers are displayed in Fig. 7.

The BER values corresponding to received eye diagrams in Fig. 7 are as follows. In the case of 2.5 Gbps data transmission over 20 km of SMF fiber, the BER value of simulated carrier (+1) is 2.39×10^{-16} (Fig. 7(c)), and the corresponding experimental value is 1.39×10^{-15} .

For simulative carrier (-1), the BER value is 3.7×10^{-10} (Fig. 7(d)), and the corresponding experimental value is 5.58×10^{-7} . In the case of 10 Gbps data transmission over 20 km of SMF fiber, the BER value for the simulated carrier (+1) is 1×10^{-9} (Fig. 7(e)), and the corresponding experimental value is 3.64×10^{-10} . For simulative carrier (-1), the BER value is 1.8×10^{-9}

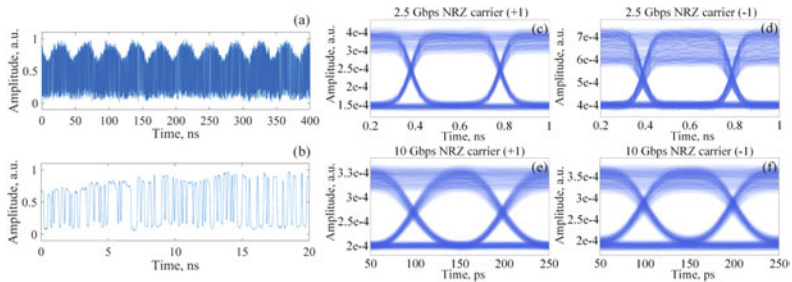


Fig. 7. Simulated and captured waveforms of (a) 10 Gbps NRZ-OOK signal waveform after 20 km transmission, and (b) 20 ns insight of the waveform showing received bit sequence. Simulative eye diagrams of the received signal after 20 km transmission over SMF fiber at a data rate of 2.5 Gbps for (c) carrier “+1” and (d) carrier “-1”, and data rate of 10 Gbps for (e) carrier “+1” and (f) carrier “-1”.

(Fig. 7(f)), and the corresponding experimental value is 1.58×10^{-6} . There is a strong correlation between the obtained BER results and eye diagrams of the realized experimental and simulative setups, indicating that the mathematical modeling following the experiment is performed correctly.

6. Conclusions

We have designed and demonstrated that the WGMR-OFC generated in silica microsphere with an FSR of 400 GHz can provide the stable operation of 2.5 and 10 Gbps NRZ-OOK modulated WDM data transmission over 20 km SMF link and have the potential to replace individual laser arrays as a multiple laser source. Modeling of the WDM data transmission system based on the experimentally measured parameters shows a high coincidence of results. The developed mathematical model reproduces the integration of generated OFC into the simulation environment and will support future research as the simulation platform. Note that lower spacing between comb carriers can be achieved by using a WGMR with a larger diameter. To obtain 200 GHz spacing, one can use ~ 330 μm diameter silica microsphere [22]. To obtain standard 100 GHz spacing, one can use ~ 660 μm diameter silica resonator. For operating with 100 GHz mode spacing, microspheres may be not a very optimal choice due to excitation of WGMs from not the fundamental mode family, so using silica microrod or microdisks [8] may be beneficial for this purpose. Moreover, when using larger WGMRs compared to our samples, the effective field areas of the fundamental modes will be larger, so the nonlinear Kerr coefficient γ will be smaller. The nonlinear processes leading to OFC generation depend on $\gamma \times P_{\text{pump}}$, so the pump power P_{pump} should be increased, which means that the power in each harmonic will grow too. This may be also beneficial for demonstrating advanced systems (with higher baud rate, coherent modulation formats, etc.). In addition, careful system optimization can help increase the efficiency of harmonic generation. Further, the application of WGMR-OFC is considered as potential to be used in more complex optical communication systems with advanced modulation formats, namely, M-PAM or M-QAM.

Funding. European Regional Development Fund (1.1.1.1/18/A/155); Ministry of Science and Higher Education of the Russian Federation (14.W03.31.0032); Russian Science Foundation (20-72-10188).

Acknowledgments. This research was funded by the European Regional Development Fund project No. 1.1.1.1/18/A/155 “Development of optical frequency comb generator based on a whispering gallery mode microresonator and its applications in telecommunications”. The development of the program for the optical fusion splicer was funded by the Mega-grant of

the Ministry of Science and Higher Education of the Russian Federation, Contract No.14.W03.31.0032. The fabrication of test samples of microspheres was funded by the Russian Science Foundation, Grant No. 20-72-10188.

Disclosures. The authors declare no conflicts of interest.

Data availability. Data underlying the results presented in this paper are not publicly available at this time but may be obtained from the authors upon reasonable request.

References

- J. Liu, A. S. Raja, M. Karpov, B. Ghadiani, M. H. P. Pfeiffer, B. Du, N. J. Engelsen, H. Guo, M. Zervas, and T. J. Kippenberg, "Ultralow-power chip-based soliton microcombs for photonic integration," *Optica* **5**(10), 1347–1353 (2018).
- S. H. Lee, D. Y. Oh, Q. Yang, B. Shen, H. Wang, K. Y. Yang, Y. Lai, X. Yi, X. Li, and K. Vahala, "Towards visible soliton microcomb generation," *Nat. Commun.* **8**(1), 1295 (2017).
- T. J. Kippenberg, S. M. Spillane, and K. J. Vahala, "Kerr-nonlinearity optical parametric oscillation in an ultrahigh-Q toroid microcavity," *Phys. Rev. Lett.* **93**(8), 083904 (2004).
- W. Liang, D. Eliyahu, V. S. Ilchenko, A. A. Savchenkov, A. B. Matsko, D. Seidel, and L. Maleki, "High spectral purity Kerr frequency comb radio frequency photonic oscillator," *Nat. Commun.* **6**(1), 7957 (2015).
- Z. Song, S. Lei, R. Linhao, Z. Yanjing, J. Bo, X. Bowen, and Z. Xinliang, "Controllable Kerr and Raman-Kerr frequency combs in functionalized microsphere resonators," *Nanophotonics* **8**(12), 2321–2329 (2019).
- G. Frigentini, D. Farnesi, G. N. Conti, and S. Soria, "Nonlinear Optics in Microspherical Resonators," *Micromachines* **11**(3), 303 (2020).
- I. H. Agha, Y. Okawachi, and A. L. Gaeta, "Theoretical and experimental investigation of broadband cascaded four-wave mixing in high-Q microspheres," *Opt. Express* **17**(18), 16209–16215 (2009).
- A. Pasquazi, M. Peccianti, L. Razzari, D. J. Moss, S. Coen, M. Erkintalo, Y. K. Chemo, T. Hansson, S. Wabnitz, P. Del'Haye, X. Xue, A. M. Weiner, and R. Morandotti, "Micro-combs: A novel generation of optical sources," *Phys. Rep.* **729**, 1–81 (2018).
- A. V. Andrianov and E. A. Anashkina, "Single-mode silica microsphere Raman laser tunable in the U-band and beyond," *Results Phys.* **17**, 103084 (2020).
- R. C. Beltrán, V. M. Diep, S. Soltani, E. Gungor, and A. M. Armani, "Plasmonically Enhanced Kerr Frequency Combs," *ACS Photonics* **4**(11), 2828–2834 (2017).
- W. Bogaerts, P. D. Heyn, T. V. Vaerenbergh, K. D. Vos, S. K. Selvaraja, T. Claes, P. Dumon, P. Bienstman, D. V. Thorhout, and R. Baets, "Silicon microring resonators," *Laser Photonics Rev.* **6**(1), 47–73 (2012).
- J. Pfeifle, Y. Yu, P. C. Schindler, V. Brasch, T. Herr, C. Weimann, K. Hartinger, R. Holzwarth, W. Freude, T. J. Kippenberg, and C. Koos, "Transmission of a 1.44 Tbit/s data stream using a feedback-stabilized SiN Kerr frequency comb source," *Optical Fiber Communication (OFC) Conference*, paper Th1A.6., (2014), <https://doi.org/10.1364/OFC.2014.Th1A.6>.
- J. Pfeifle, A. Kordts, P. Marin, M. Karpov, M. Pfeiffer, V. Brasch, R. Kemal, J. Rosenberger, S. Wolf, W. Freude, T. J. Kippenberg, and C. Koos, "Full C and L-Band Transmission at 20 Tbit/s Using Cavity-Soliton Kerr Frequency Comb Source," *Conference on Lasers and Electro-Optics (CLEO)*, paper JTh5C.8. (2015), https://doi.org/10.1364/CLEO_AT.2015.JTh5C.8
- P. M. Palomo, J. N. Kemal, M. Karpov, A. Kordts, J. Pfeifle, M. H. P. Pfeiffer, P. Trocha, S. Wolf, V. Brasch, M. H. Anderson, R. Rosenberger, K. Vijayan, W. Freude, T. J. Kippenberg, and C. Koos, "Microresonator-based solitons for massively parallel coherent optical communications," *Nature* **546**(7657), 274–279 (2017).
- K. E. Webb, M. Erkintalo, S. Coen, and S. G. Murdoch, "Experimental observation of coherent cavity soliton frequency combs in silica microspheres," *Opt. Lett.* **41**(20), 4613–4616 (2016).
- X. Yi, Q. F. Yang, K. Y. Yang, M. G. Suh, and K. Vahala, "Soliton frequency comb at microwave rates in a high-Q silica microresonator," *Optica* **2**(12), 1078–1085 (2015).
- J. Braunfelds, R. Murnieks, T. Salgals, I. Brice, T. Sharashidze, I. Lyashuk, A. Ostrovskis, S. Spolitis, J. Alnis, J. Porins, and V. Bobrovs, "Frequency Comb Generation in WGM Microsphere Based Generators for Telecommunication Applications," *Quantum Electron.* **50**(11), 1043–1049 (2020).
- T. Salgals, I. Kurbatska, V. Bobrovs, and S. Spolitis, "Research of PAM-4 Modulated WDM-PON Architecture for 5G Millimeter-wave Hybrid Photonics-wireless Interface," *2019 Photonics & Electromagnetics Research Symposium*, 728–734 (2019).
- Q. Wang and Y. Yue, "Accurate and Rigorous Calibration of Intradyne Coherent Receiver Using Polarization-Multiplexed Signal Generated within Intradyne Coherent Transmitter," *Appl. Sci.* **10**(10), 3467 (2020).
- R. Ma, A. Schliesser, P. Del'Haye, A. Dabirian, and T. J. Kippenberg, "Radiation pressure driven vibrational modes in ultra-high-Q silica microspheres," *Opt. Lett.* **32**(15), 2200–2202 (2007).
- A. Schliesser, R. Rivière, G. Anetsberger, O. Arcizet, and T. J. Kippenberg, "Resolved-sideband cooling of a micromechanical oscillator," *Nat. Phys.* **4**(5), 415–419 (2008).
- E. A. Anashkina, M. P. Marisova, A. V. Andrianov, R. A. Akhmedzhanov, R. Murnieks, M. D. Tokman, L. Skladova, I. V. Oladyskhin, T. Salgals, I. Lyashuk, A. Sorokin, S. Spolitis, G. Leuchs, and V. Bobrovs, "Microsphere-based optical frequency comb generator for 200 GHz spaced WDM data transmission system," *Photonics* **7**(3), 72 (2020).

PAPER-13: Silica microsphere WGMR-based Kerr-OFC light source and its application for high-speed IM/DD short-reach optical interconnects

T. Salgals, J. Alnis, **O. Ozolins**, A.V. Andrianov, E. Anashkina, I. Brice, R. Berkis, Z. Pang, A. Udalcovs, J. Porins, **S. Spolitis**, and V. Bobrovs, "Silica microsphere WGMR-based Kerr-OFC light source and its application for high-speed IM/DD short-reach optical interconnects", *Applied Sciences* 12(9), 4722, (2022), DOI: [10.3390/app12094722](https://doi.org/10.3390/app12094722)

Article

Silica Microsphere WGMR-Based Kerr-OFC Light Source and Its Application for High-Speed IM/DD Short-Reach Optical Interconnects

Toms Salgals^{1,2,*}, Janis Alnis³, Oskars Ozolins^{1,4,5}, Alexey V. Andrianov⁶, Elena A. Anashkina⁶, Inga Brice³, Roberts Berkis^{3,7}, Xiaodan Pang^{1,5}, Aleksejs Udalcovs¹, Jurgis Porins¹, Sandis Spolitis^{1,8} and Vjaceslavs Bobrovs¹

- ¹ Institute of Telecommunications, Riga Technical University, 12 Azenes Street, 1048 Riga, Latvia; ozolins@kth.se (O.O.); xiaodan@kth.se (X.P.); aleksejs.udalcovs@gmail.com (A.U.); jurgis.porins@rtu.lv (J.P.); sandis.spolitis@rtu.lv (S.S.); vjaceslavs.bobrovs@rtu.lv (V.B.)
 - ² AFFOC Solutions Ltd., 17 Andrejostas Street, 1045 Riga, Latvia
 - ³ Institute of Atomic Physics and Spectroscopy, University of Latvia, 3 Jelgavas Street, 1004 Riga, Latvia; janis.alnis@lu.lv (J.A.); inga.brice@lu.lv (I.B.); roberts.berkis@uibk.ac.at (R.B.)
 - ⁴ Networks Unit, RISE Research Institutes of Sweden, Kista, 164 40 Stockholm, Sweden
 - ⁵ Applied Physics Department, KTH Royal Institute of Technology, 106 91 Stockholm, Sweden
 - ⁶ Institute of Applied Physics, Russian Academy of Sciences, 46 Ul'yanov Street, 603950 Nizhny Novgorod, Russia; alex.v.andrianov@gmail.com (A.V.A.); elena.anashkina@gmail.com (E.A.A.)
 - ⁷ Institute for Experimental Physics, University of Innsbruck, Technikerstrasse 25, 6020 Innsbruck, Austria
 - ⁸ Communication Technologies Research Center, Riga Technical University, 12 Azenes Street, 1048 Riga, Latvia
- * Correspondence: toms.salgals@rtu.lv; Tel.: +371-278-36-269



Citation: Salgals, T.; Alnis, J.; Ozolins, O.; Andrianov, A.V.; Anashkina, E.A.; Brice, I.; Berkis, R.; Pang, X.; Udalcovs, A.; Porins, J.; et al. Silica Microsphere WGMR-Based Kerr-OFC Light Source and Its Application for High-Speed IM/DD Short-Reach Optical Interconnects. *Appl. Sci.* **2022**, *12*, 4722. <https://doi.org/10.3390/app12094722>

Academic Editors: (John) Xiupu Zhang and Gaoming Xu

Received: 18 March 2022
Accepted: 3 May 2022
Published: 7 May 2022

Publisher's Note: MDPI stays neutral with regard to jurisdictional claims in published maps and institutional affiliations.



Copyright: © 2022 by the authors. Licensee MDPI, Basel, Switzerland. This article is an open access article distributed under the terms and conditions of the Creative Commons Attribution (CC BY) license (<https://creativecommons.org/licenses/by/4.0/>).

Abstract: Kerr optical frequency combs (OFCs) based on silica microsphere whispering gallery mode resonator (WGMR) have various applications where they are used as a light source. For telecommunication purposes, WGMR-based Kerr-OFC comb generators can be physically realized using silica microsphere resonators and can be used to replace multiple laser arrays. In such a realization, these novel light sources have the potential to demonstrate an attractive solution for intra-datacenter interconnects (DCI). In this paper, we show an experimental demonstration of a silica microsphere WGMR-based Kerr OFC light source where newly generated 400 GHz spaced carriers together with powerful linear equalization techniques, such as a linear symbol-spaced adaptive decision-feedback equalizer (DFE) with feed-forward (FF) and feedback (FB) taps, provide an alternative to individual lasers ensuring low-cost and low-complexity IM/DD scheme for the transmission of NRZ-OOK modulated signals at data rates up to 50 Gbps/λ over 2 km SMF link. Finally, we demonstrate a record 50 Gbps per λ transmission of NRZ-OOK modulated signals with a novel silica microsphere WGMR-based Kerr-OFC as a light source operating in the optical C-band, surpassing the previously demonstrated data rate record by five times.

Keywords: Kerr optical frequency combs (OFC); silica microsphere; intra-datacenter interconnects (DCI); equalization

1. Introduction

Kerr optical frequency combs (OFC) based on whispering-gallery-mode microresonator (WGMR) with a single laser source have already shown different applications and especially its application in fiber optical communication systems replacing multiple laser arrays [1]. Accurate timing, low phase noise, and the narrow linewidth of generated harmonics allow achieving the ultimate performance desired from an optical comb-based system. In addition, OFC generators have applications in areas such as optical clocks [2], ultra-stable microwave generators [3], applications that require a precise and stable optical

frequency distribution via long fiber [4], spectroscopy [5], sensing [6], quantum applications [7], optical communications [8], etc. OFC sources for wavelength division multiplexed (WDM) systems cover use cases ranging from short reach fiber-optic links (e.g., as for data center interconnects (DCI)) to metro-access fiber-optic links interconnecting large geographic areas [9,10]. More specifically, the WGMR-based Kerr-OFC comb generators physically realized on silica microsphere demonstrate [9] a new concept able to provide an attractive solution to intra-DCIs due to low costs and energy consumption. The data centers (DCs) are the foundation of Internet applications such as cloud computing, where Big Data storage and large-scale high-performance computing (HPC) take place. The intra-DCI devices require not only large capacity but, most importantly, high scalability and low energy consumption. Therefore, these requirements require new transmission technologies for short-reach communications [10,11].

It can provide a lower energy consumption while ensuring improved spectral efficiency and a stable frequency spacing between OFC lines (carriers) thanks to the sustained strong phase relation between them [9,12,13]. OFCs have various realizations; among them, the realization by four-wave mixing (FWM) in highly nonlinear optical fiber (HNLF) [13], electro-optic phase modulation of a laser using, e.g., cascaded phase and amplitude modulators [1,14], chip-based mode-locked laser (MLL) combs [13], and silicon microring resonators [13,15]. Potentially cost-effective solutions for the realization of data transmission in optical WDM networks are OFC generation in silica whispering gallery mode resonator–microspheres manufactured from melted telecom fiber, e.g., from Corning SMF 28e (ITU-T G.652) [9,12,14], which is realized as the pumping of a high-quality (high Q factor) optical resonator with Kerr nonlinearity using a single continuous-wave (CW) laser. When optimal conditions are met, the intracavity pump photons are redistributed via the FWM to the neighboring cavity modes, thereby creating the so-called Kerr OFC. The exciting pump signal is launched into the Kerr-OFC resonator via a tapered fiber, and an OFC is generated at the output of this taper. In addition to being energy-efficient, conceptually simple and structurally robust Kerr comb generators are very compact devices (to micrometric size) that can be integrated on a chip [16,17]. Kerr microresonator OFCs can achieve bandwidths of hundreds of nanometers covering different (e.g., E-, S-, C-, and L-band) telecommunication bands (according to ITU-T G. 694.1 recommendation) [18,19].

Considering the findings of our previous works [9,12,20,21], here, we propose a silica microsphere WGMR-based Kerr-OFC as a light source operating in the C-band (1530–1565 nm) and having 400 GHz spaced comb lines. These comb lines are subsequently used as optical carriers for the data transmission using the intensity modulation direct detection (IM/DD). Data rates up to 50 Gbps/λ are employed in combination with the non-return to zero (NRZ) on-off keying (OOK) format for the transmission over a 2 km short fiber-optic link consisting of the standard ITU-T G.652 single-mode fiber. The aforementioned IM/DD signal format is chosen as it still dominates in short-reach optical interconnects due to its simplicity. Digital equalization techniques shown in our previous works [22], such as a linear equalizer with feed-forward (FF) and feedback (FB) taps, can improve the signal quality due to different system distortions, mainly caused by limited channel bandwidth and nonlinearities during the optical to electrical (O/E) and electrical to optical (E/O) conversions and the link induced inter-symbol interference (ISI). Therefore, we apply the use of the symbol-spaced adaptive decision-feedback equalizer (DFE) implemented at the receiver part to improve the pre-FEC bitrate and to achieve higher data rates in DCI with the optical carriers generated by the developed silica microsphere WGMR-based Kerr-OFC.

The rest of the paper is structured as follows. Section 2 describes the characteristics of the designed silica microsphere and shows the deterioration of its Q factor with time. Section 3 presents the experimental setup of the WGMR-based Kerr-OFC light source operating in the C-band and used for the generation of 400 GHz spaced optical carriers. This section also describes the fabrication process of a tapered fiber used for the coupling of light into and out of a silica microsphere and the experimental setup used to characterize

coupling conditions between the silica microsphere and the tapered fiber. Furthermore, Section 3 reveals the experimentally obtained characteristics of the designed WGMR-based Kerr-OFC light source, Q factor, and optical output spectra. Section 4 summarizes the conducted data transmission experiment by analyzing the received signal bit error rates (BER) and eye diagrams. The impact that digital post-equalization at the receiver has on system performance is provided in Section 5. Finally, Section 6 overviews the experimental results and concludes the paper.

2. Characteristics of Designed Silica Microsphere WGMR for Kerr-OFC

Silica (SiO_2) microspheres with a diameter of $D = 170 \mu\text{m}$ used for the Kerr-OFC were fabricated from a standard ITU-T G.652 single-mode telecommunication fiber by the melting method using a specially developed program for a commercially available optical fusion arc splicer, which has been previously demonstrated by authors in [9,23]. During the manufacturing process, by changing the diameter of the fabricated silica microsphere, we can obtain an OFC with a free spectral range (FSR) ranging from about 200 GHz (sphere $D = 320 \mu\text{m}$) [20] up to about 400 GHz (sphere $D = 170 \mu\text{m}$) [18] in addition to the possibility of finetuning the coupling conditions between the resonator and tapered fiber, which is not possible for chip-based resonators with integrated waveguides, and therefore can be considered to be a major advantage over other OFC technologies. Silica microsphere resonators also have advantages of fast and simple fabrication using commercially available fusion arc splicers, allowing the fabrication of silica microspheres with user-defined sphere diameter and high-quality factor ($Q \geq 10^7$) in a couple of minutes.

Most applications, especially silica microsphere-based Kerr-OFC, require the realization of the highest possible quality factor (so-called Q factor) microsphere resonators. In regular laboratory conditions, the microsphere's Q factor deteriorates within a 1 h time scale in the open environment due to the deposition of nanoscale particles or water vapors to the microsphere surface. The Q factor of the microsphere is determined by several aspects such as intrinsic radiative (curvature) losses, scattering losses on residual surface inhomogeneities, losses introduced by surface contaminants, and material losses [24]. For a more detailed illustration, see Figure 1 where newly fabricated and artificial degradations of the microsphere surface by water vapors are obtained using a scanning electron microscope (SEM, Hitachi S-4800) for $170 \mu\text{m}$ silica microsphere resonators. Scanned sphere illustrations with a focused beam of electrons (captured at: 3 kV (accelerating voltage) and 4.0 mm (surface scale) @ $\times 400$ to 45.0 k times and 2.9 mm @ $\times 180$ k times) for a particular micro-sphere resonator after 100% humidity exposure (resonator has been in humidity fog for 5 s) are shown in Figure 1a–d. The newly fabricated silica microsphere resonator obtained by SEM (captured at: 3 kV, 4.0 mm @ $\times 300$ to 50.0 k times) is shown in Figure 1e–h. White dots (see Figure 1f) for evaporated silica (cristobalite) from the arc fusion splicer discharge explain why the maximal Q factor of a newly fabricated microsphere is below 1×10^8 . We can observe that the evaporated silica dust from the arc fusion splicer (see Figure 1g) and nanoscale particles (see Figure 1h) are deposited on the surface of the silica microsphere.

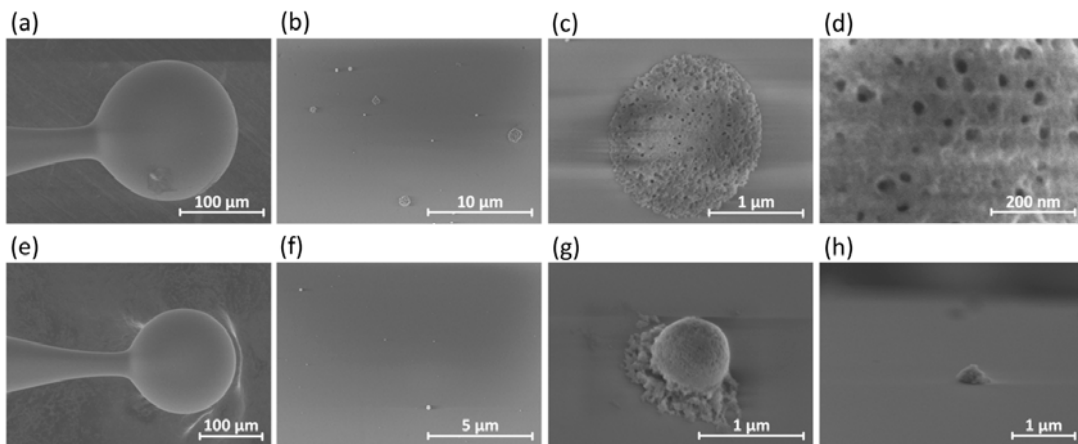


Figure 1. Illustration of 170- μm SiO_2 microsphere resonator scans captured by SEM at 3 kV after artificial degradation by 100% humidity, 100% relative humidity, and 100% humidity: (a) 170- μm SiO_2 microsphere resonator scan captured by SEM at 3 kV after artificial degradation by 100% humidity, 100% relative humidity, and 100% humidity; (b) 170- μm SiO_2 microsphere resonator scan captured by SEM at 3 kV after artificial degradation by 100% humidity, 100% relative humidity, and 100% humidity; (c) 170- μm SiO_2 microsphere resonator scan captured by SEM at 3 kV after artificial degradation by 100% humidity, 100% relative humidity, and 100% humidity; (d) 170- μm SiO_2 microsphere resonator scan captured by SEM at 3 kV after artificial degradation by 100% humidity, 100% relative humidity, and 100% humidity; (e) 170- μm SiO_2 microsphere resonator scan captured by SEM at 3 kV after artificial degradation by 100% humidity, 100% relative humidity, and 100% humidity; (f) 170- μm SiO_2 microsphere resonator scan captured by SEM at 3 kV after artificial degradation by 100% humidity, 100% relative humidity, and 100% humidity; (g) 170- μm SiO_2 microsphere resonator scan captured by SEM at 3 kV after artificial degradation by 100% humidity, 100% relative humidity, and 100% humidity; and (h) nanoscale particles at 4.0 mm @ $\times 30.0$ k times were observed.

It is important to note that, during the experiment, by testing samples of fabricated microspheres, we were able to significantly improve the degraded 4-month-old microsphere (added by water vapor) Q factor from $Q = 2.0 \times 10^6$ (96 MHz full width at half maximum (FWHM) of the WGM resonance) to $Q = 4.4 \times 10^6$ (44 MHz FWHM of the WGM resonance) using pure hydrogen (H_2) flame of a micro burner. Note that the Q factor of the newly fabricated microsphere was 3.7×10^7 (5.2 MHz FWHM of the WGM resonance). The built-up circulating intensity [25] was estimated to be 14 GW/cm^2 exceeding $\sim 2.0 \text{ GW/cm}^2$ [26] needed for OFC generation (see Table 1). No OFC was generated when it degraded below 2.0 GW/cm^2 . Microresonator with high Q factor can build up a significant internal circulating intensity when pumped with low laser power. The circulating intensity can be found using the following equation [25]:

$$P_{\text{circ}} = \frac{P_{\text{in}} Q_{\text{ext}}}{A_{\text{eff}}} \quad (1)$$

where P_{in} is the input power, and A_{eff} is the effective area of the mode area of the resonance. A_{eff} can be found by using simulations. As calculation parameters, resonator radius, refractive index, and resonance frequency at 1550 nm wavelength for fundamental mode were used. P_{circ} in the silica microsphere WGM can be found as follows [25]:

where P_{circ} is internal circulating power, and A_{eff} is the effective area of the mode area of the resonance. A_{eff} can be found by using simulations. As calculation parameters, resonator radius, refractive index, and resonance frequency at 1550 nm wavelength for fundamental mode were used. P_{circ} in the silica microsphere WGM can be found as follows [25]:

$$P_{\text{circ}} = \frac{P_{\text{in}} Q_{\text{ext}}}{A_{\text{eff}}} \quad (2)$$

where λ is the resonance wavelength, n is the refractive coefficient, R is the microsphere radius, P_{in} is the input power ($P_{\text{in}} = 100 \text{ mW}$), $\bar{K} = \frac{Q_{\text{ext}}}{Q_{\text{intr}}}$ or $K_c = \frac{Q_{\text{ext}}}{Q_{\text{intr}}}$ is the coupling parameter that shows the ratio between intrinsic and extrinsic Q-factors, and Q_{intr} is the intrinsic Q factor, which is limited by all losses defined by the resonator cavity. The coupling parameter can be estimated using transmission T at the resonance frequency [27].

where λ is the resonance wavelength, n is the refractive coefficient, R is the microsphere radius, P_{in} is the input power ($P_{\text{in}} = 100 \text{ mW}$), $\bar{K} = \frac{Q_{\text{ext}}}{Q_{\text{intr}}}$ or $K_c = \frac{Q_{\text{ext}}}{Q_{\text{intr}}}$ is the coupling parameter that shows the ratio between intrinsic and extrinsic Q-factors, and Q_{intr} is the intrinsic Q factor, which is limited by all losses defined by the resonator cavity. The coupling parameter can be estimated using transmission T at the resonance frequency [27].

Table 1. Results of characteristics calculations for 170 μm SiO₂ microsphere resonator versus life cycle.

Life Cycle	T	K	FWHM, MHz	Q	Q _{intr}	P _{circ} , W	I, GW/cm ²	Resulting OFC
Freshly fabricated	0.13	2.1	5.2	3.7×10^7	1.2×10^8	3327	13.8	yes
After 2 months	0.64	9.0	15.7	1.2×10^7	1.2×10^8	1458	6.0	yes
After 3.5 months	0.62	8.4	50	3.9×10^6	3.6×10^7	455	1.9	no
After 4 months	0.78	16.1	96	2.0×10^6	3.5×10^7	249	1.0	no
After 4 months (repaired by Hydrogen flame)	0.74	13.3	44	4.4×10^6	6.3×10^7	538	2.2	no

Several moisture and dust degradation methods of protection can be used to keep high Q factor of newly fabricated silica resonators, for instance, storage with ethanol drops or storage with dry nitrogen within hermetic enclosure boxes. The packaging technique utilized by UV-curable polymer for stabilizing both the microsphere and the tapered fiber could be preferred for long-term maintenance of silica microsphere WGMR-based Kerr-OFC light sources. While the use of a coating polymer significantly increases the stability of mechanical alignment between the microsphere and taper, accompanied by a relatively low absorption and insertion loss of polymer packaging [28]. An additional solution to keep a high Q factor for silica microresonators and taper satisfying coupling conditions and providing improved long-term frequency stability is packaging into modules that feature temperature control by integrated Peltier elements [29].

3. Experimental Setup of Designed Silica Microsphere WGMR-Based Kerr-OFC as A Light Source for Application in Optical Communications

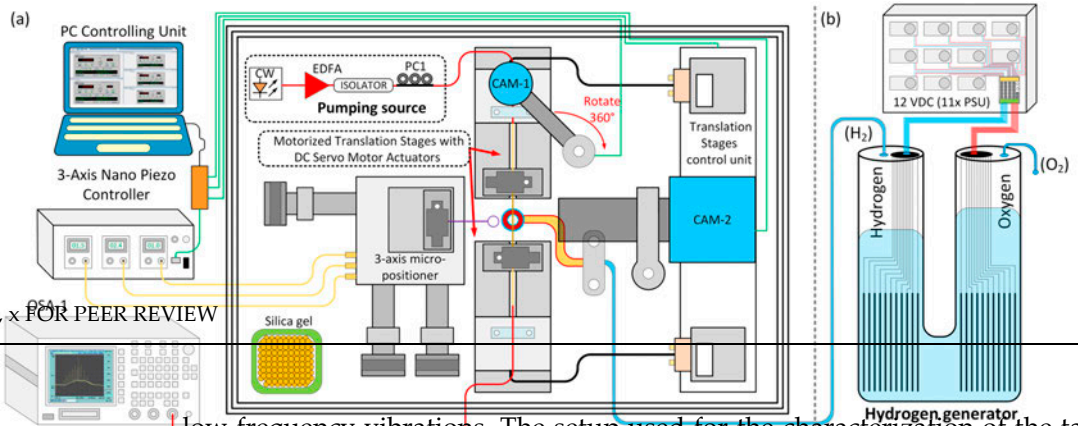
The setup used for the generation of WGMR-based Kerr-OFC is shown in Figure 2a,c. First, we prepare the tapered fiber for coupling the light into the silica microsphere. We used a non-zero dispersion-shifted fiber (NZ-DSF) patch-cable compliant with the ITU-T G.655 standard for the preparation of a tapered fiber pulling probe. In the process of the tapered fiber fabrication procedure, the tapered fiber probe was formed from two separate cut parts of an NZ-DSF compliant patch cable. The patch-cable fiber ends were cut using a fiber cleaver, cleaned, and spliced together with a commercial arc fusion splicer (Sumitomo, T-71C), ensuring a low insertion loss ≤ 0.01 dB. As a result, the jacket and coating of connectorized patch-cable were removed in the region of 3.8 cm, where it is intended for heat treatment.

Clamps of V-groove fiber holders located on the 50 mm compact, motorized translation stages with DC servo motor actuators (Thorlabs MTS50-Z8) were used to pull the tapered fiber in both directions with a constant speed of 100 $\mu\text{m}/\text{s}$ (see Figure 2a,e). Several techniques can be used to form tapered fiber through thermal heating, for instance, a ceramic tube microheater(s) consisting of a heat-resistant wire that is approximately 22 mm in length and 19 mm inner diameter and placed within the ceramic [30]; another option would be micro burners driven by propane–butane (30% propane and 70% butane) gas flows [23] or by pure hydrogen (H₂) [31], providing a high-temperature (≥ 1900 °C) flame. The latter setup was used in our experiments; specifically, a constant hydrogen flow of 50 mL/min from the hydrogen generator (see Figure 2b) was connected to a microburner placed between compact, motorized translation stages. For pure hydrogen generation, we use an in-house-built hydrogen generator (electrolyser) that operates by splitting the water into hydrogen and oxygen through electrolysis. The number of plates for cathode and anode is set to $\times 11$. Each plate was driven by 12 VDC (30 A) output voltage through an $11 \times$ high-speed Schottky diodes barrier using a (220 V~50 Hz 350 W) power supply unit (PSU). As shown in Figure 2b,f, sets of 11 cathode and 11 anode plates are located in separate tubes (D = 250 mm) where the electrolysis interconnection between them was made by water and potassium hydroxide (KOH) electrolyte through a round tube transition. For the microburner, we used an in-house-built micro torch that consists of 9 cylindrical

stainless-steel tubes of 0.9 mm inner diameter, allowing us to produce a low and wide flame of ~10 mm along the fiber axis [32]. The fiber position relative to the flame is a critical parameter. Therefore, the microtorch stainless-steel tube position is sprightly adjusted to the fiber's mid-point. To sustain transmission, the tapered fiber needs to be pulled adiabatically while not exceeding the delineation angle [33]. Using a ~7 mm wide hydrogen flame, we produced sub-wavelength nearly adiabatic tapers with an overall transmittance higher than 95%, as a very efficient adiabatic transfer from the single mode of the un-tapered fiber to the fundamental mode of the central part of the taper. The burning temperature of the hydrogen flame melted and softened the fiber slowly within the purified fiber section as a result of a tapered thicker section of 18 mm in length. It is important to mention that if the fiber ends are inclined (0.1 mrad) at the place of V-groove fiber holders, a curvature of 5 μm is intelligently formed in the melted location of the taper when the flame width is 1 mm. The angle exceeding 0.08 mrad is no longer good, as the allowable adiabatic angle is between 0.02 and 0.05 mrad [34]. Due to rapid assembly, a flame wider than 1 mm was used. The mounting of the fiber holders on one optical axis is adjusted under a microscope. The 3-axis X, Y, and Z micro-positioner stages with the built-in piezo controller were used to align the microsphere with the tapered fiber at a location slightly thicker than the taper waist to achieve the critical coupling and to minimize the coupler losses; see Figure 2d,e. Side and top view microscope cameras (CAM-1 and CAM-2) with 160 \times zoom lens (see Figure 2e) were used to monitor silica microsphere and tapered fiber positions to control the touchpoint of the resonator with the slightly thicker tapered fiber placed to excite the fundamental mode of the microsphere. Silica microsphere and tapered fibers, including integrated and developed components for fiber tapering and microsphere positioning, are included in an enclosure box to protect it from dust and airflows. Humidity inside the enclosure box is reduced and maintained at levels below 20% using a silica gel desiccant. The enclosure box together with pumping source components is located on a vibration isolation system breadboard table to minimize the impact of external low frequency vibrations. The setup used for the characterization of the taper fiber (see Figure 3) consists of InGaAs switchable gain amplified photo-detector (PD) $\lambda = 800\text{--}1700\text{ nm}$ (Thorlabs (Bergkirchen, Germany), PDA20CS2) connected with a digital signal analyzer (DSA) used to record the received electrical signal in time and to monitor the transmission spectra from the adiabatically tapered fiber for an overall transmittance analysis used also in further telecom data transmission. A tunable $\lambda = 1550\text{ nm}$ laser (Thorlabs SFL1550P) with a narrow linewidth of 50 kHz and 10 dBm output optical power is connected via a polarization controller (PC1) and used for transmission spectra measurements. The transmission spectrum was monitored during the tapering process to determine when it returns to the single-mode operation state (see Figure 4a). As shown in Figure 4a, the adiabatically tapered fiber spectrum presents single-mode (SM) operations in the beginning from 0 to 0.5 min mark and after pulling at around 3.3 min mark (represented in the red color) when the signal intensity becomes constant. SM fiber becomes multi-mode (MM) when the signal starts to propagate through the cladding (represented in the blue color).

Calculations show that the hot zone's width of exponentially pulled tapered fiber should be at least 7 mm long to satisfy the adiabaticity criteria at the middle of the pulling range and to maintain high final transmission [33]. Please see the calculations of the pulled length of tapered fiber hot zone to one side from center versus fiber diameter at the taper section in Figure 4b. The setup shown in Figure 3 also was used to determine the Q factor of the silica microsphere and to identify the best coupling condition region between the microsphere and tapered fiber used in OFC generation. The measured Q factor of the microsphere used for OFC comb generation and further telecom data transmission is 3.7×10^7 (5.2 MHz FWHM of the WGM resonance); please see Figure 4c. As shown in Figure 4c, resonances were obtained by scanning the laser over resonances while Kerr-OFC was generated with a single pumping wavelength. The silica microsphere resonator supports many modes inside the cavity, but not all modes in addition to the fundamental mode can support Kerr-OFC generation.

3.055 standard for the preparation of a tapered fiber using a flame brushing method. In the process of the tapered fiber fabrication procedure, the tapered fiber probe was formed from two separate cut parts of an NZ-DSF compliant patch cable. The patch-cable fiber ends were cut using a fiber cleaver, cleaned, and spliced together with a commercial arc fusion splicer (Sumitomo, T-71C), ensuring a low insertion loss ≤ 0.01 dB. As a result, the jacket and coating of connectorized patch-cable were removed in the region of 3.8 cm, where it is intended for heat treatment.



low frequency vibrations. The setup used for the characterization of the taper fiber

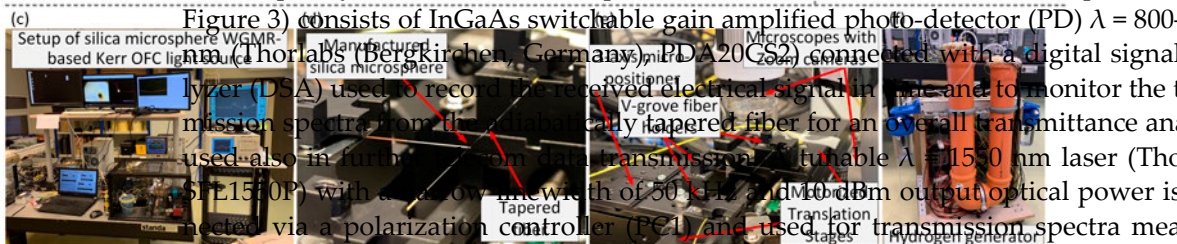


Figure 3 consists of InGaAs switchable gain amplified photo-detector (PD) $\lambda = 800$ nm (Thorlabs (Bergkirchen, Germany) PDA20GS2) connected with a digital signal analyzer (DSA) used to record the received electrical signal in real time and to monitor the transmission spectra from the tapered fiber. The tapered fiber is used for an overall transmittance analysis. The tapered fiber is used also in combination with a tunable $\lambda = 1550$ nm laser (Thorlabs (Munich, Germany) SFL1510P) with a narrow linewidth of 50 kHz and 10 dBm output optical power injected via a polarization controller (PC1) and used for transmission spectra measurements. The transmission spectrum was monitored during the tapering process to determine when it returns to the single mode operation state (see Figure 4a). As shown in Figure 4a, the adiabatically tapered fiber spectrum presents single mode (SM) operation the beginning from 0 to 0.5 min mark and after pulling at around 3.3 min mark (represented in the red color) when the signal intensity becomes constant. SM fiber becomes multi-mode (MM) when the signal starts to propagate through the cladding (represented in the blue color).

Figure 2: (a) Experimental setup illustrating the developed silica microsphere resonator based Kerr OFC as a light source for optical communications. (b) Schematic of a Hydrogen generator for pure generation of hydrogen (H_2) and oxygen (O_2) by electrolysis of water. (c) Captured setup of silica microsphere resonator, tapered fiber and microscopes with zoom microscopes. (d) Schematic of the silica microsphere resonator. (e) Schematic of the tapered fiber and microscopes with zoom microscopes. (f) Captured setup of the Hydrogen generator for pure hydrogen and oxygen production.

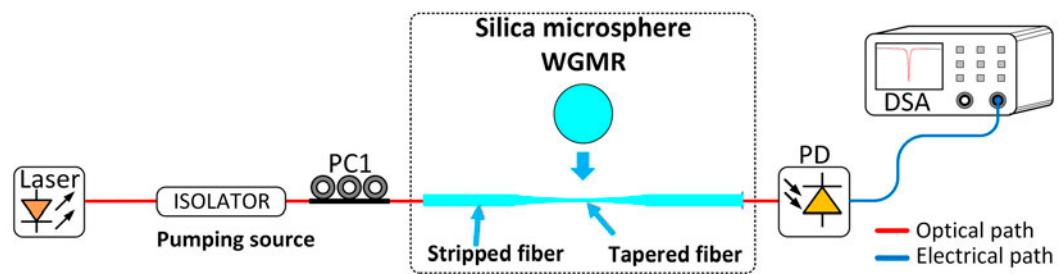
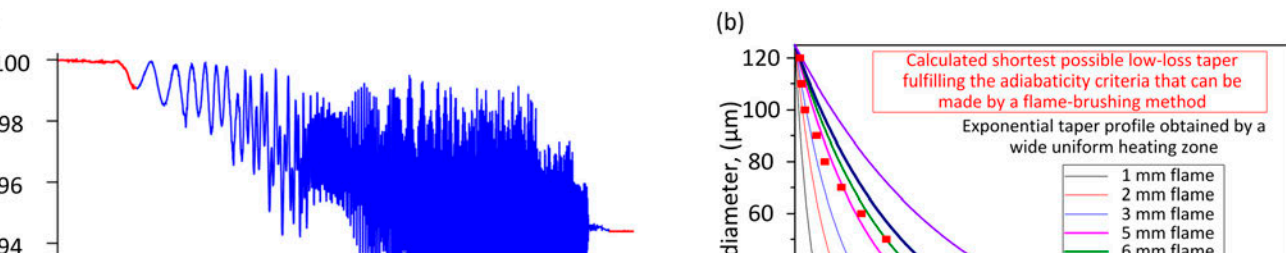


Figure 2. Experimental setup used for the characterization of the tapered fiber and silica microsphere.



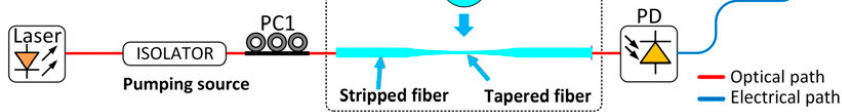


Figure 3. Experimental setup used for the characterization of the tapered fiber and silica microsphere.

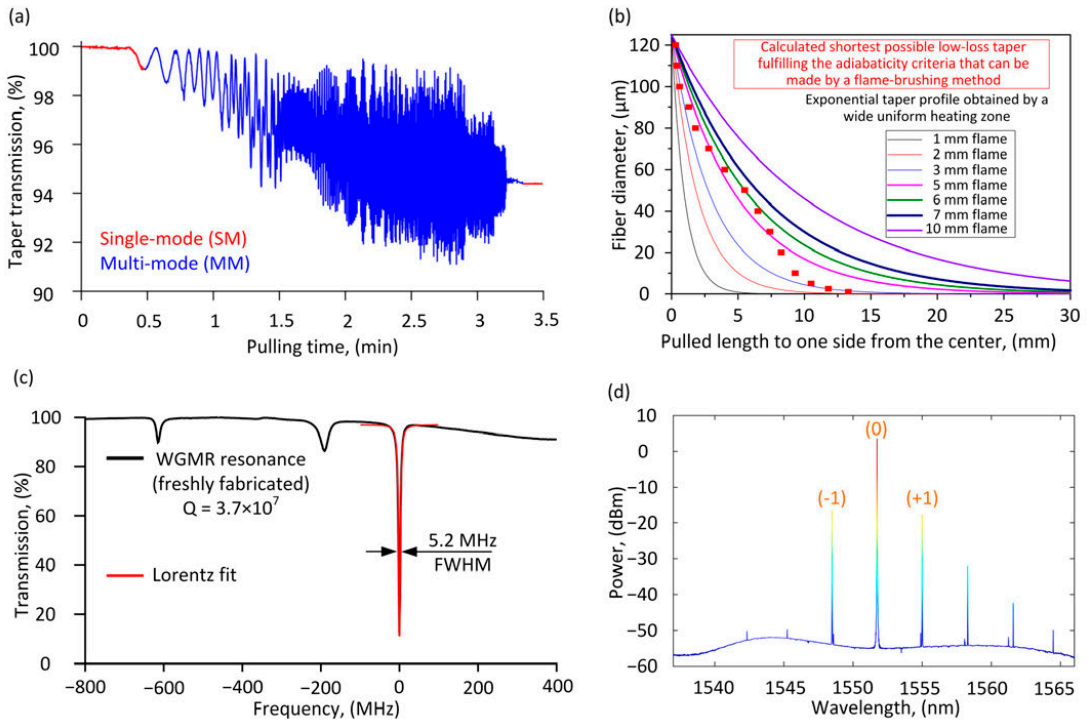


Figure 4. The characterization of the tapered fiber and its coupling conditions with the silica microsphere: (a) spectrum of the adiabatically tapered fiber recorded for the overall transmittance analysis and (b) the calculations of pulled one side fiber length at hot zone from center versus fiber diameter at tapered section. (c) Experimentally observed (from the microsphere excited by the tapered fiber) WGM resonances of the Kerr-OFC at the optical C-band used for the Q factor calculation and (d) optical spectra of the generated silica microsphere WGM-based Kerr-OFC comb source.

The pumping source for the Kerr-OFC generation consists of a continuous optical wavelength (CW) laser source (Agilent 81989A) with a linewidth of 100 kHz and +6 dBm optical output power at $\lambda = 1551.737$ nm wavelength that is directly connected to fixed output power (up to +23 dBm) erbium-doped fiber amplifier (EDFA). The light coming from the EDFA is passed through an optical isolator and PC1 to prevent back-scattering and to control the amplified signal's polarisation state before coupling it into the microsphere through the tapered fiber, providing further stability of the resulting OFC. An optical spectrum analyzer (OSA-1, Advantest Q8384) with 0.01 nm resolution and 1001 sampling points is used to monitor generated OFC as well as to measure the peak powers of generated (-1) and (+1) carriers and pumping source depicted as a carrier (0); see Figure 4d. The power instability and power distribution stability over the wavelength of the generated OFC comb carriers was not measured during this research. The generated comb carriers (-1) and (+1) over 10 h have a different performance within about a 3 dB margin; please see our previous work [9]. Silica microsphere WGM-based Kerr-OFC light source newly generated carriers (-1) and (+1) and comb carriers followed by (+1) carrier have additional sub-carriers generated under the influence of stimulated Brillouin scattering (SBS); see Figure 4d. The SBS effect occurs due to a relatively high pumping power launched from EDFA (up to +23 dBm) in the 170 μm silica microsphere. The SBS effect appears and then disappears in the time interval for both the pumping source and the newly generated carriers on the left or right side with a constant FSR of ~ 10 GHz and various power levels

within the time interval of about ~15 min (usually this is observed when the comb has been operated for some time). It is relatively hard to detect and predict those sub-carriers bursts because their phenomenon is unstable and changeable in time-lapse, as captured and shown in Figure 4d.

4. Experimental Setup of the Silica Microsphere WGMR-Based Kerr-OFC Light Source for Its Use in High-Speed IM/DD Short-Reach Optical Interconnects

The experimental setup is shown in Figure 5. The silica microsphere WGMR-based Kerr-OFC light source (i.e., Kerr-OFC) output 400 GHz spaced optical carriers at wavelengths $\lambda = 1548.485$ nm depicted as (-1), $\lambda = 1554.992$ nm depicted as (+1), and the pumping source at $\lambda = 1551.737$ nm depicted as (0) and having the highest achieved peak power levels (> 15 dBm) are used to demonstrate NRZ-OOK modulated data up to 50 Gbps λ over 2 km SMF link. As shown in Figure 5, the generated OFC carriers are sent to an optical bandpass filter (OBPF) used to capture the 0th, 1st, and 2nd order carriers using a 10/90 coupling ratio for monitoring purposes and to determine carriers' wavelength optical peak powers that are later used for data transmission. The filtered optical carrier is amplified by a pre-amplifier (EDFA2) that fixes the output power level for each carrier. A polarization controller (PC2) is placed before the intensity Mach-Zehnder modulator (MZM, Photonix (Paris, France), MX-LN40) to reduce the polarization-dependent loss. The high-speed NRZ signal is generated offline using a 2¹⁵-1 long pseudorandom binary sequence (PRBS). The high-speed NRZ signal is generated offline using a 2¹⁵-1 long pseudorandom binary sequence (PRBS).

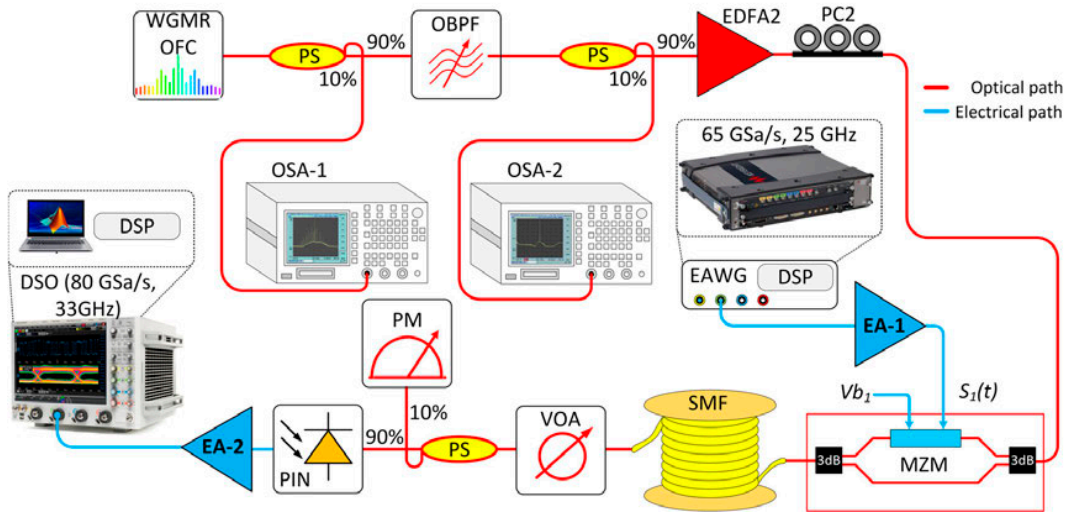


Figure 5. Experimental demonstration of the IM/DD optical interconnect relying on the in-house built silica microsphere WGMR-based Kerr-OFC as a light source generating 400 GHz spaced optical carriers that are used for up to 50 Gbps NRZ-OOK modulated signal transmission over a long SMF link.

The signal is up-sampled and filtered using a root-raised-cosine (RRC) filter having a roll-off factor of 0.1. At the next pre-processing stage, a frequency domain pre-equalization (FDE) filter is used to compensate for amplitude-frequency distortions and link bandwidths (BW) of a 65 GSa/s electrical arbitrary waveform generator (EAWG, Keysight M9502A, 25 GHz). Please observe (Figure 6) the response of an end-to-end system calibration for the optical back-to-back (OB2B) configuration.

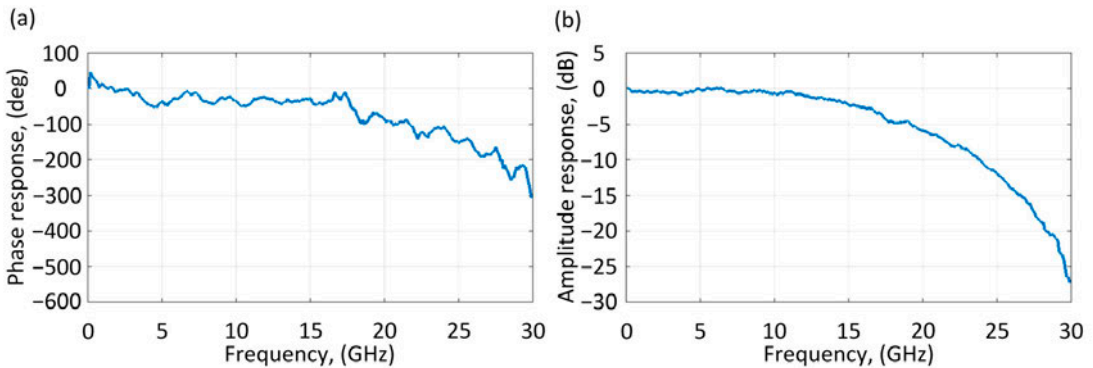


Figure 6. End-to-end system calibration using the EAWG for the OB2B configuration: (a) phase response and (b) amplitude response.

The high-speed NRZ encoded signal is loaded to the EAWG, pre-equalized, and transmitted. The generated output electrical signals are amplified by an electrical amplifier (EA-1, 38 GHz, and 29 dB gain) and fed into the S_1 input of the MZM with a null chirp factor and having 40 GHz 3 dB bandwidth, 20 dB extinction ratio, and 2 dB insertion loss. The high-speed NRZ encoded signal is loaded to the EAWG, pre-equalized, and transmitted. The generated output electrical signals are amplified by an electrical amplifier (EA-1, 38 GHz, and 29 dB gain) and fed into the S_1 input of the MZM with the MZM to 3.8 V. After MZM, the modulated optical signal is transmitted over a 2 km long SMF link and passed through a variable optical attenuator (VOA) located before a photoreceiver for the power control. The photoreceiver module (PIN, Lab Buddy, DSC10H-39) consists of high optical power 50 GHz InGaAs photodiode with a 3 dB bandwidth of 50 GHz, a sensitivity of +4 dBm at BER of 10^{-12} , and responsivity of 0.5 A/W. An optical coupler with a 10/90 coupling ratio and a power meter were used before PIN to monitor the optical power level at the receiver. After optical-to-electrical conversion, the electrical signal is amplified by an electrical amplifier (EA-2, 25 GHz, 16 dB gain). Thereafter, the signal is captured by a digital storage oscilloscope (DSO, Keysight DSAZ334A, 80 GSa/s, 33 GHz). The sampled signal is processed offline using digital signal processing (DSP) consisting of a low-pass filter (LPF), clock recovery, resampling, and linear post-equalization based on a symbol-spaced adaptive decision-feedback equalizer (DFE) and bit error rate (BER) counter. Please note that BER values are obtained using bit-by-bit comparison between the transmitted and received bit sequences.

5. Experimental Results

Using the experimental setup shown in Figure 5 and described in Section 4, we make a fair comparison, showing the performance limits in terms of achievable data rates for short-reach optical interconnect applications. Our goal is to achieve a data rate that is as high as possible, even up to 60 Gbps/λ in the system that uses the implemented Kerr-OFC generated optical carriers for carrying IM/DD data. The received and sampled signal is processed offline after the reception, using a DSP routine that consists of a low-pass filter (LPF), a maximum variance timing recovery, post-equalization, and a BER counter. The LPF has a bandwidth of 0.6 times the Baud rate. That value was identified using the results data shown in Figure 7. It ensures the best possible performance after further processing. In such a case, we obtain BER as a function of the LPF_{BW} /Baud rate from 0.4 to 0.8 for NRZ-OOK signals.

(LPF), a maximum variation timing recovery, and a BER counter. The LPF has a bandwidth of 0.6 times the Baud rate. That value was identified using the results data shown in Figure 7. It ensures the best possible performance after further processing. In such a case, we obtain BER as a function of the LPF_{BW}/Baud rate from 0.4 to 0.8 for NRZ-OOK signals.

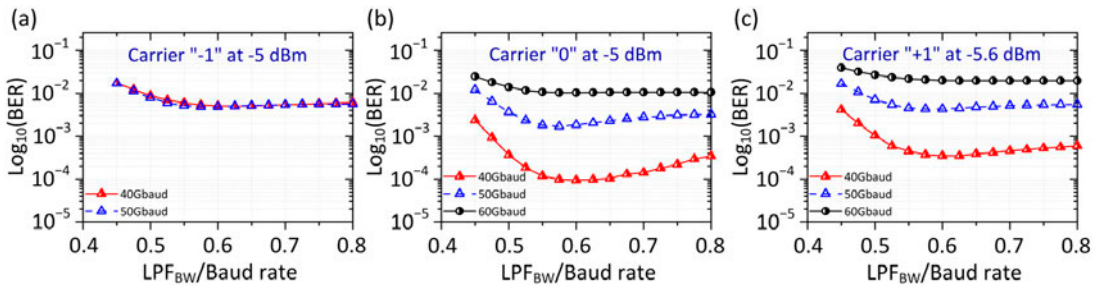


Figure 7. BER versus LPF_{BW}/Baud rate for the IM/DD communication system operating on 400 GHz spaced carriers generated by microsphere Kerr-OFC: (a) $\lambda = 1548.485$ depicted as carrier “-1”; (b) $\lambda = 1551.737$ depicted as carrier “0”; (c) $\lambda = 1554.992$ depicted as carrier “+1” provide NRZ-OOK signals up to 60 Gbps/λ.

The post-equalization was used to improve signal quality; we use a DFE configuration with 33 feed-forward taps (FFT) and 15 feedback taps (FBT), as well as 16 taps are used as a reference. The adaptive DFE helps to overcome the inter-symbol interference (ISI) in the presence of noise and bandwidth limitations. As shown in Figure 7a, 40 Gbaud and 50 Gbaud signals are almost overlapping because DFE with both feed-forward (FF) and feedback (FB) taps due to the intensity fluctuations (power instability) of carrier (-1) cannot show performance improvements in terms of high baud rate. The initial weights of the equalizer are obtained using the training data with the normalized least mean square (NLMS) algorithm before applying other data. A total number of 1.2 million bits are used for BER counting.

First, we analyze system performance without post-equalization. Afterward, we focus on diagrams of the received NRZ-OOK signals after the 2 km transmission over the SME link. In this paper, we consider the hard-decision forward error correction (HD-FEC) with 7% overheads (OH) with a pre-FEC BER threshold at 5×10^{-3} [35]. We use the conventional BER curves showing how pre-FEC BER values change with the received optical power (ROP). We assume that all errors can be corrected for the pre-FEC BER below that threshold. As one can see in Figure 8a, the worst-performing (based on the BER value) data channel is the carrier (-1) at 1548.485 nm, yet it is capable in providing the maximum bitrate of 50 Gbps. In this sub-figure, the 60 Gbps curve is not shown because due to extremely poor BER performance, i.e., it is way beyond our defined pre-FEC BER threshold of 5×10^{-3} . The best performing (based on the BER) data channel is the pumping source carrier with a wavelength of 1551.737 nm depicted as a carrier (0). Without the post-equalization, the received 40 Gbaud and 50 Gbaud NRZ-OOK signals are mostly below the 7% HD-FEC limit for the Kerr-OFC generated carriers (-1), (0), and (+1); see Figure 8a–c. In those cases, the main limitations are a relatively low effective bandwidth of the electrical components, ISI, and the implementation penalty itself.

remely poor BER performance), and a 5-way 50-Gbaud carrier channel is the pumping source carrier with a wavelength of 1551.737 nm depicted as a carrier (0). Without the post-equalization, the received 40 Gbaud and 50 Gbaud NRZ-OOK signals are mostly below the 7% HD-FEC limit for the Kerr-OFC generated carriers (-1), (0), and (+1); see Figure 8a–c. In those cases, the main limitations are a relatively low effective bandwidth of the electrical components, ISI, and the implementation penalty itself.

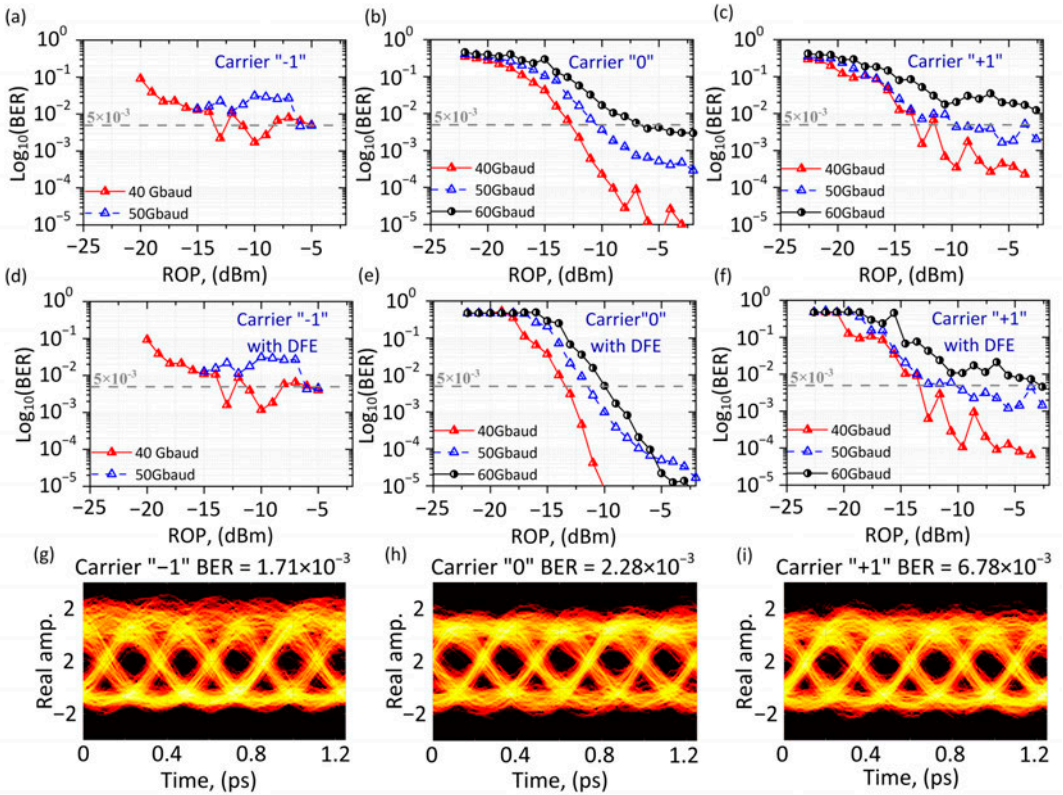


Figure 8. BER versus ROP for the IM/DD communication system where the Kerr-OFC light source carriers “-1”, “0”, and “+1” can be used for NRZ-OOK signals transmission with baud rates up to (a) 50 Gbaud, (b) 60 Gbaud, and (c) 50 Gbaud without any post-equalization. If the post-equalizer with 33-FF and 15-FB taps is used, the BER is significantly improved for carriers “-1”, “0”, and “+1” up to (d) 50 Gbaud, (e) 60 Gbaud, and (f) 60 Gbaud. Received signal eye diagrams for carriers: (g) “-1”, (h) “0”, and (i) “+1” captured at ROP of -10 dBm in the 40 Gbaud case.

To achieve higher data rates, a dispersion-induced power fading must be reduced, and signal equalization must be applied to reach the BER threshold of 5×10^{-3} . We have chosen a linear equalizer for which its structure consists of 33-FF and 15-FB taps. The number of taps is chosen in a manner that maximally improves performance by tackling the bandwidth limitations of electrical components and chromatic dispersion. The results show that such post-equalization significantly improves BER performance compared to the previous case without the post-equalization. As one can see in Figure 8e,f, post-equalization can significantly improve the signal quality for Kerr-OFC generated carriers (0) and (+1), or even enable new modulation format alternatives. However, the feed-forward equalizer, due to the intensity fluctuations of the (-1) carrier, cannot show visible performance improvement (see Figure 8a,d).

With the linear post-equalization (33-FF and 15-FB taps), BER performance is significantly improved for carrier (+1), which allows us to achieve the BER floor below the 7% HD-FEC limit for NRZ-OOK signals at 60 Gbaud. Figure 8g–i show the corresponding eye diagrams captured for modulated carriers (-1), (0), and (+1) at -10 dBm received optical power (ROP) that allows detecting signals with BER below 5×10^{-3} at 40 Gbaud.

6. Conclusions

This work is a significant achievement by experimentally demonstrating a data transmission record of 50 Gbps per λ with a silica microsphere WGMR-based Kerr-OFC light source. In this experiment, we have designed and demonstrated the silica microsphere WGMR-based Kerr-OFC built in-house and used as a light source for data center interconnects (DCIs). The Kerr-OFC consists of several carriers spaced 400 GHz apart together with powerful pre- and post-linear equalization techniques, such as a linear symbol-spaced adaptive decision-feedback equalizer (DFE) with feed-forward (FF), and feedback (FB) taps provide an alternative to ensure low-cost and low-complexity IM/DD schemes for the transmission of NRZ-OOK modulated signals over 2 km SMF links. The obtained results show that pre- and post-equalization techniques allow overcoming the ISI and help recover the signal from distortions caused by limited bandwidth, enabling higher data-rate alternatives to intra-DCIs. Without post-equalization, the received 40 Gbaud and 50 Gbaud NRZ-OOK signals are below the 7% HD-FEC limit for Kerr-OFC generated carriers (−1), (0), and (+1). The linear post-equalization, namely 33-FF and 15-FB taps, improves BER performance for carrier (+1), which allows us to achieve the BER floor below the 7% HD-FEC limit even for NRZ-OOK signals at 60 Gbaud.

Author Contributions: Conceptualization, T.S., J.A. and O.O.; methodology, T.S.; software, T.S., J.A., E.A.A., A.V.A., S.S., R.B., X.P. and V.B.; validation, A.U., E.A.A., S.S. and V.B.; formal analysis, A.U., E.A.A., S.S., I.B., R.B. and V.B.; investigation, T.S. and J.A.; resources, T.S., S.S., E.A.A., A.V.A., J.A. and V.B.; data curation, T.S.; writing—original draft preparation, T.S., A.U., S.S., I.B., J.A., E.A.A. and O.O.; writing—review and editing, T.S., J.A., O.O., A.V.A., E.A.A., I.B., R.B., X.P., A.U., J.P., S.S. and V.B.; visualization, T.S., I.B., J.A. and O.O.; supervision, J.A., S.S., O.O. and V.B.; project administration, T.S., S.S., J.A. and V.B.; funding acquisition, T.S., S.S., E.A.A., A.V.A. and V.B. All authors have read and agreed to the published version of the manuscript.

Funding: This research was funded by European Regional Development Fund (1.1.1.1/18/A/155); Ministry of Science and Higher Education of the Russian Federation (075-15-2021-633); Russian Science Foundation (20-72-10188).

Institutional Review Board Statement: Not applicable.

Informed Consent Statement: Not applicable.

Data Availability Statement: Not applicable.

Acknowledgments: This research was funded by the European Regional Development Fund project No. 1.1.1.1/18/A/155 “Development of optical frequency comb generator based on a whispering gallery mode microresonator and its applications in telecommunications”. The taper fiber preparation was supported by the European Social Fund within project number No. 8.2.2.0/20/1/008 and by the the Austrian Science Fund FWF within the DK-ALM W1259-N27. The development of the program for the optical fusion splicer was funded by the Mega-grant of the Ministry of Science and Higher Education of the Russian Federation, Contract No. 075-15-2021-633. The fabrication of test samples of microspheres was funded by the Russian Science Foundation, Grant No. 20-72-10188. Communication Technologies Research Center, Riga Technical University (RTU) acknowledges support from RTU Science Support Fund.

Conflicts of Interest: The authors declare no conflict of interest.

References

1. Torres-Company, V.; Weiner, A.M. Optical frequency comb technology for ultra-broadband radio-frequency photonics. *Laser Photonics Rev.* **2014**, *8*, 368–393. [[CrossRef](#)]
2. Ludlow, A.D.; Boyd, M.M.; Ye, J.; Peik, E.; Schmidt, P.O. Optical atomic clocks. *Rev. Mod. Phys.* **2015**, *87*, 637–701. [[CrossRef](#)]
3. Kwon, D.; Jeon, I.; Lee, W.K.; Heo, M.S.; Kim, J. Generation of multiple ultrastable optical frequency combs from an all-fiber photonic platform. *Sci. Adv.* **2020**, *6*, eaax4457. [[CrossRef](#)] [[PubMed](#)]
4. Predehl, K.; Grosche, G.; Raupach, S.M.F.; Droste, S.; Terra, O.; Alnis, J.; Legero, T.; Hänsch, T.W.; Udem, T.; Holzwarth, R.; et al. A 920-km optical fiber link for frequency metrology at the 19th decimal place. *Science* **2012**, *336*, 441–444. [[CrossRef](#)] [[PubMed](#)]
5. Adler, F.; Thorpe, M.J.; Cossel, K.C.; Ye, J. Cavity-enhanced direct frequency comb spectroscopy: Technology and applications. *Annu. Rev. Anal. Chem.* **2010**, *3*, 175–205. [[CrossRef](#)]

6. Guay, P.; Hébert, N.B.; Michaud-Belleau, V.; Lancaster, D.G.; Genest, J. Free-running optical frequency combs for remote sensing. In *Optical Sensors and Sensing Congress (ES, FTS, HISE, Sensors)*, OSA Technical Digest; Optica Publishing Group: Washington, DC, USA, 2019. [\[CrossRef\]](#)
7. Lu, H.H.; Weiner, A.M.; Lougovski, P.; Lukens, J.M. Quantum Information Processing with Frequency-Comb Qudits. *IEEE Photon. Technol. Lett.* **2019**, *31*, 1858–1861. [\[CrossRef\]](#)
8. Pfeifle, J.; Brasch, V.; Lauermaun, M.; Yimin, Y.; Wegner, D.; Herr, T.; Hartinger, K.; Schindler, P.; Li, J.; Hillerkuss, D.; et al. Coherent terabit communications with microresonator Kerr frequency combs. *Nat. Photon* **2014**, *8*, 375–380. [\[CrossRef\]](#)
9. Salgals, T.; Alnis, J.; Murnieks, R.; Brice, I.; Porins, J.; Andrianov, A.V.; Anashkina, E.A.; Spolitis, S.; Bobrovs, V. Demonstration of a fiber optical communication system employing a silica microsphere-based OFC source. *Opt. Express* **2021**, *29*, 10903. [\[CrossRef\]](#)
10. Kong, D.; Xin, H.; Kim, K.; Liu, Y.; Oxenløwe, L.K.; Dong, P.; Hu, H. Intra-Datcenter Interconnects With a Serialized Silicon Optical Frequency Comb Modulator. *J. Lightwave Technol.* **2020**, *38*, 4677–4682. [\[CrossRef\]](#)
11. Pang, X.; Udalcovs, A.; Schatz, R.; Bobrovs, V.; Jacobsen, G.; Popov, S.; Ozolins, O. Short Reach Communication Technologies for Client-Side Optics Beyond 400 Gbps. *IEEE Photon. Technol. Lett.* **2021**, *33*, 1046–1049. [\[CrossRef\]](#)
12. Spolitis, S.; Murnieks, R.; Skladova, L.; Salgals, T.; Andrianov, A.V.; Marisova, M.P.; Leuchs, G.; Anashkina, E.A.; Bobrovs, V. IM/DD WDM-PON Communication System Based on Optical Frequency Comb Generated in Silica Whispering Gallery Mode Resonator. *IEEE Access* **2021**, *9*, 66335–66345. [\[CrossRef\]](#)
13. Hu, H.; Oxenløwe, L.K. Chip-based optical frequency combs for high-capacity optical communications. *Nanophotonics* **2021**, *10*, 1367–1385. [\[CrossRef\]](#)
14. Wu, R.; Supradeepa, V.R.; Long, C.M.; Leaird, D.E.; Weiner, A.M. Generation of very flat optical frequency combs from continuous-wave lasers using cascaded intensity and phase modulators driven by tailored radio frequency waveforms. *Opt. Lett.* **2010**, *35*, 3234. [\[CrossRef\]](#) [\[PubMed\]](#)
15. Chembo, Y.K. Kerr optical frequency combs: Theory, applications and perspective. *Nanophotonics* **2016**, *5*, 214–230. [\[CrossRef\]](#)
16. Kippenberg, T.J.; Gaeta, A.L.; Lipson, M.; Gorodetsky, M.L. Dissipative Kerr solitons in optical microresonators. *Science* **2018**, *361*, eaan8083. [\[CrossRef\]](#)
17. Lee, S.H.; Oh, D.Y.; Yang, Q.-F.; Shen, B.; Wang, H.; Yang, K.Y.; Lai, Y.-H.; Yi, X.; Li, X.; Vahala, K. Towards visible soliton microcomb generation. *Nat. Commun.* **2017**, *8*, 1295. [\[CrossRef\]](#)
18. Anashkina, E.A.; Marisova, M.P.; Salgals, T.; Alnis, J.; Lyashuk, I.; Leuchs, G.; Spolitis, S.; Bobrovs, V.; Andrianov, A.V. Optical Frequency Combs Generated in Silica Microspheres in the Telecommunication C-, U-, and E-Bands. *Photonics* **2021**, *8*, 345. [\[CrossRef\]](#)
19. Salgals, T.; Ostrovskis, A.; Ipatovs, A.; Bobrovs, V.; Spolitis, S. Hybrid ARoF-WDM PON Infrastructure for 5G Millimeter-wave Interface and Broadband Internet Service. In Proceedings of the Photonics & Electromagnetics Research Symposium-Fall (PIERS-Fall), Xiamen, China, 17–20 December 2019. [\[CrossRef\]](#)
20. Anashkina, E.A.; Marisova, M.P.; Andrianov, A.V.; Akhmedzhanov, R.A.; Murnieks, R.; Tokman, M.D.; Skladova, L.; Oladyskhin, I.V.; Salgals, T.; Lyashuk, I.; et al. Microsphere-Based Optical Frequency Comb Generator for 200 GHz Spaced WDM Data Transmission System. *Photonics* **2020**, *7*, 72. [\[CrossRef\]](#)
21. Anashkina, E.A.; Bobrovs, V.; Salgals, T.; Brice, I.; Alnis, J.; Andrianov, A.V. Kerr Optical Frequency Combs With Multi-FSR Mode Spacing in Silica Microspheres. *IEEE Photon. Technol. Lett.* **2021**, *33*, 453. [\[CrossRef\]](#)
22. Udalcovs, A.; Salgals, T.; Zhang, L.; Pang, X.; Djupsjöbacka, A.; Spolitis, S.; Bobrovs, V.; Popov, S.; Ozolins, O. Optical Power Budget of 25+ Gbps IM/DD PON with Digital Signal Post-Equalization. *Appl. Sci.* **2020**, *10*, 6106. [\[CrossRef\]](#)
23. Andrianov, A.V.; Anashkina, E.A. Single-mode silica microsphere Raman laser tunable in the U-band and beyond. *Results Phys.* **2020**, *17*, 103084. [\[CrossRef\]](#)
24. Gorodetsky, M.L.; Savchenkov, A.A.; Ilchenko, V.S. Ultimate Q of optical microsphere resonators. *Opt. Lett.* **1996**, *21*, 453. [\[CrossRef\]](#)
25. Kovach, A.; Chen, D.; He, J.; Choi, H.; Dogan, A.H.; Ghasemkhani, M.; Taheri, H.; Armani, A.M. Emerging material systems for integrated optical Kerr frequency combs. *Adv. Opt. Photon.* **2020**, *12*, 135. [\[CrossRef\]](#)
26. Del’Haye, P.; Schliesser, A.; Arcizet, O.; Wilken, T.; Holzwarth, R.; Kippenberg, T.J. Optical frequency comb generation from a monolithic microresonator. *Nature* **2007**, *450*, 1214–1217. [\[CrossRef\]](#) [\[PubMed\]](#)
27. Spillane, S.M.; Kippenberg, T.J.; Painter, O.J.; Vahala, K.J. Ideality in a Fiber-Taper-Coupled Microresonator System for Application to Cavity Quantum Electrodynamics. *Phys. Rev. Lett.* **2003**, *91*, 043902. [\[CrossRef\]](#) [\[PubMed\]](#)
28. Wang, P.; Ding, M.; Murugan, G.S.; Bo, L.; Guan, C.; Semenova, Y.; Wu, Q.; Farrell, G.; Brambilla, G. Packaged, high-Q, microsphere-resonator-based add-drop filter. *Opt. Lett.* **2014**, *39*, 5208. [\[CrossRef\]](#) [\[PubMed\]](#)
29. Suh, M.; Wang, C.Y.; Johnson, C.; Vahala, K.J. Directly pumped 10 GHz microcomb modules from low-power diode lasers. *Opt. Lett.* **2019**, *44*, 1841. [\[CrossRef\]](#)
30. Yu, J.; Lewis, E.; Farrell, G.; Wang, P. Compound Glass Microsphere Resonator Devices. *Micromachines* **2018**, *9*, 356. [\[CrossRef\]](#)
31. Sveta, A.; Silver, J.; Del Bino, L.; Zhang, S.; Woodley, M.T.M.; Vanner, M.R.; Del’Haye, P. Coherent suppression of backscattering in optical microresonators. *Light Sci. Appl.* **2020**, *9*, 204. [\[CrossRef\]](#)
32. Orucevic, F.; Seguin, V.L.; Hare, J. Transmittance and near-field characterization of sub-wavelength tapered optical fibers. *Opt. Express* **2007**, *15*, 13624. [\[CrossRef\]](#)
33. Nagai, R.; Aoki, T. Ultra-low-loss tapered optical fibers with minimal lengths. *Opt. Express* **2014**, *22*, 28427. [\[CrossRef\]](#) [\[PubMed\]](#)

34. Tiecke, T.G.; Nayak, K.P.; Thompson, J.D.; Peyronel, T.; de Leon, N.P.; Vuletić, V.; Lukin, M.D. Efficient fiber-optical interface for nanophotonic devices. *Optica* **2015**, *2*, 70. [[CrossRef](#)]
35. Jian, Y.; Pfister, H.D.; Narayanan, K.R.; Raghu, R.; Mazahreh, R. In Iterative hard-decision decoding of braided BCH codes for high-speed optical communication. In Proceedings of the 2013 IEEE Global Communications Conference (GLOBECOM), Atlanta, GA, USA, 9–13 December 2013. [[CrossRef](#)]